IMAGING IN INFLAMMATORY RHEUMATIC DISEASES - RECENT ADVANCES

EDITED BY: Xenofon Baraliakos, Christian Dejaco and Raj Sengupta

PUBLISHED IN: Frontiers in Medicine

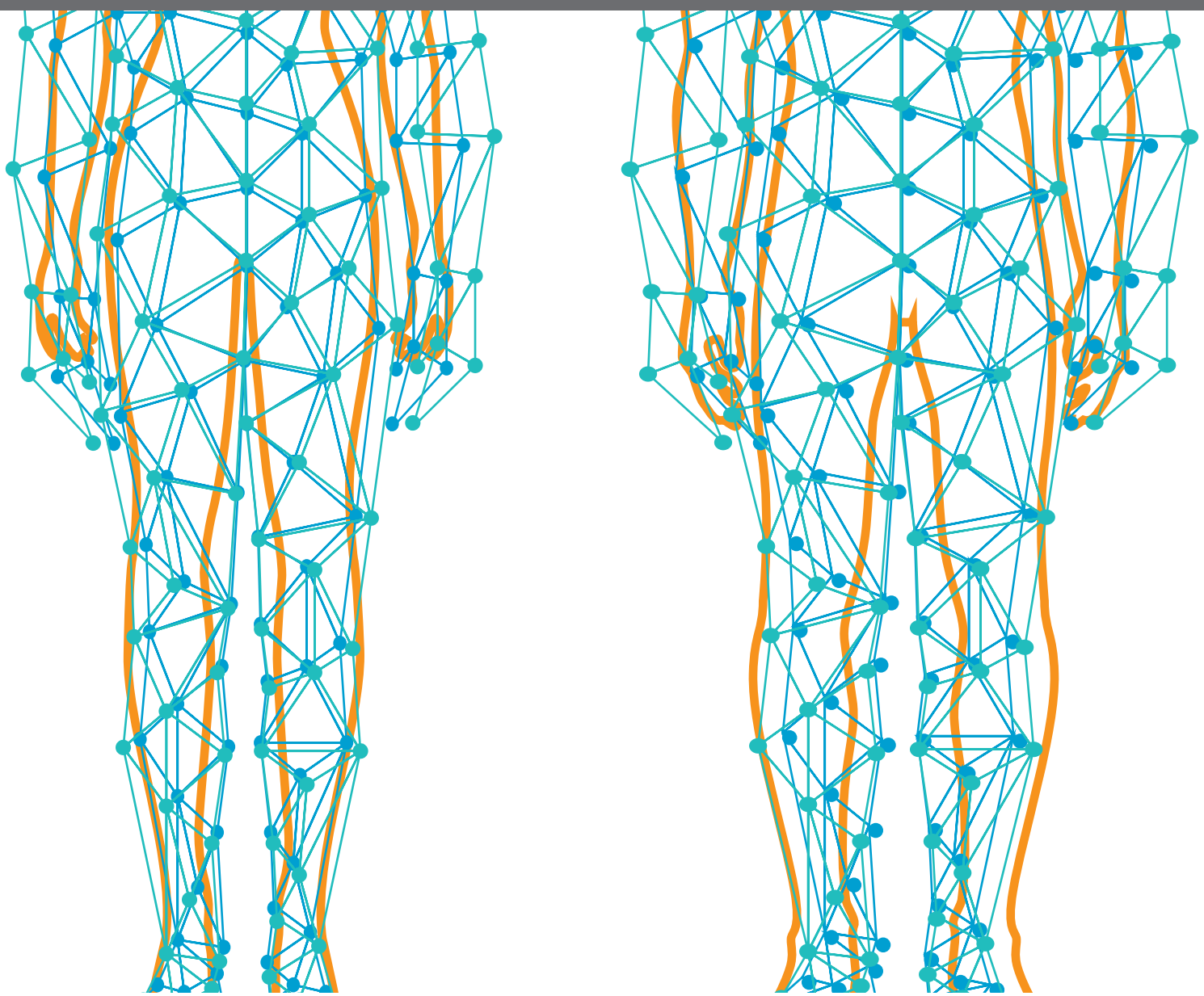

frontiers Research Topics

ISSN 1664-8714
ISBN 978-2-88974-273-8
DOI 10.3389/978-2-88974-273-8

About Frontiers

Frontiers is more than just an open-access publisher of scholarly articles: it is a pioneering approach to the world of academia, radically improving the way scholarly research is managed. The grand vision of Frontiers is a world where all people have an equal opportunity to seek, share and generate knowledge. Frontiers provides immediate and permanent online open access to all its publications, but this alone is not enough to realize our grand goals.

Frontiers Journal Series

The Frontiers Journal Series is a multi-tier and interdisciplinary set of open-access, online journals, promising a paradigm shift from the current review, selection and dissemination processes in academic publishing. All Frontiers journals are driven by researchers for researchers; therefore, they constitute a service to the scholarly community. At the same time, the Frontiers Journal Series operates on a revolutionary invention, the tiered publishing system, initially addressing specific communities of scholars, and gradually climbing up to broader public understanding, thus serving the interests of the lay society, too.

Dedication to Quality

Each Frontiers article is a landmark of the highest quality, thanks to genuinely collaborative interactions between authors and review editors, who include some of the world's best academicians. Research must be certified by peers before entering a stream of knowledge that may eventually reach the public - and shape society; therefore, Frontiers only applies the most rigorous and unbiased reviews.
Frontiers revolutionizes research publishing by freely delivering the most outstanding research, evaluated with no bias from both the academic and social point of view. By applying the most advanced information technologies, Frontiers is catapulting scholarly publishing into a new generation.

What are Frontiers Research Topics?

Frontiers Research Topics are very popular trademarks of the Frontiers Journals Series: they are collections of at least ten articles, all centered on a particular subject. With their unique mix of varied contributions from Original Research to Review Articles, Frontiers Research Topics unify the most influential researchers, the latest key findings and historical advances in a hot research area! Find out more on how to host your own Frontiers Research Topic or contribute to one as an author by contacting the Frontiers Editorial Office: frontiersin.org/about/contact

IMAGING IN INFLAMMATORY RHEUMATIC DISEASES - RECENT ADVANCES

Topic Editors:
Xenofon Baraliakos, Rheumazentrum Ruhrgebiet, Germany
Christian Dejaco, Medical University of Graz, Austria
Raj Sengupta, Royal National Hospital for Rheumatic Diseases, United Kingdom

Citation: Baraliakos, X., Dejaco, C., Sengupta, R., eds. (2022).
Imaging In Inflammatory Rheumatic Diseases - Recent Advances.
Lausanne: Frontiers Media SA. doi: 10.3389/978-2-88974-273-8

Table of Contents

frontiers in Medicine

SYSTEMATIC REVIEW
published: 07 May 2020
doi: 10.3389/fmed.2020.00141

Differential Diagnosis of Inflammatory Arthropathies by Musculoskeletal Ultrasonography: A Systematic Literature Review

Garifallia Sakellariou[1], Carlo Alberto Scirè[2,3], Antonella Adinolfi[4], Alberto Batticciotto[5], Alessandra Bortoluzzi[2], Andrea Delle Sedie[6], Orazio De Lucia[7], Christian Dejaco[8,9], Oscar Massimiliano Epis[4], Emilio Filippucci[10], Luca Idolazzi[11], Andrea Picchianti Diamanti[12], Alen Zabotti[13], Annamaria Iagnocco[14] and Georgios Filippou[2] on behalf of the Musculoskeletal Ultrasound Study Group of the Italian Society of Rheumatology*

[1] Division of Rheumatology, IRCCS Policlinico San Matteo Foundation, University of Pavia, Pavia, Italy, [2] UOC e Sezione di Reumatologia - Dipartimento di Scienze Mediche, Università degli Studi di Ferrara, Ferrara, Italy, [3] Società Italiana di Reumatologia, Unità Epidemiologica, Milan, Italy, [4] Rheumatology Unit, Grande Ospedale Metropolitano Niguarda, Milan, Italy, [5] Rheumatology Unit, Department of Internal Medicine, ASST-Settelaghi, "Ospedale di Circolo - Fondazione Macchi", Varese, Italy, [6] Rheumatology Unit, University of Pisa, Pisa, Italy, [7] Unit of Clinical Rheumatology, Department of Rheumatology and Clinical Sciences, ASST Centro Traumatologico Ortopedico G. Pini - CTO, Milan, Italy, [8] Department of Rheumatology, Medical University of Graz, Graz, Austria, [9] Department of Rheumatology, Hospital of Bruneck, Bruneck, Italy, [10] Rheumatology Unit, Department of Clinical and Molecular Sciences, Carlo Urbani Hospital, Polytechnic University of Marche, Ancona, Italy, [11] Rheumatology Unit, Ospedale Civile Maggiore, University of Verona, Verona, Italy, [12] Department of Clinical and Molecular Medicine, S. Andrea University Hospital, "Sapienza" University, Rome, Italy, [13] Department of Medical and Biological Science, Rheumatology Clinic, Azienda Sanitaria Universitaria Integrata, Udine, Italy, [14] Academic Rheumatology Centre, Università degli Studi di Torino, Turin, Italy

OPEN ACCESS

Edited by:
Helena Canhao,
New University of Lisbon, Portugal

Reviewed by:
Konstantinos Triantafyllias,
ACURA Rheumatology Clinic, Germany
Toby Helliwell,
Keele University, United Kingdom

***Correspondence:**
Carlo Alberto Sciré
c.scire@reumatologia.it

Specialty section:
This article was submitted to Rheumatology, a section of the journal Frontiers in Medicine

Received: 22 January 2020
Accepted: 31 March 2020
Published: 07 May 2020

Citation:
Sakellariou G, Scirè CA, Adinolfi A, Batticciotto A, Bortoluzzi A, Delle Sedie A, De Lucia O, Dejaco C, Epis OM, Filippucci E, Idolazzi L, Picchianti Diamanti A, Zabotti A, Iagnocco A and Filippou G (2020) Differential Diagnosis of Inflammatory Arthropathies by Musculoskeletal Ultrasonography: A Systematic Literature Review. Front. Med. 7:141. doi: 10.3389/fmed.2020.00141

Background: Differential diagnosis in early arthritis is challenging, especially early after symptom onset. Several studies applied musculoskeletal ultrasound in this setting, however, its role in helping diagnosis has yet to be clearly defined. The purpose of this work is to systematically assess the diagnostic applications of ultrasonography in early arthritis in order to summarize the available evidence and highlight possible gaps in knowledge.

Methods: In December 2017, existing systematic literature reviews (SLR) on rheumatoid arthritis (RA), osteoarthritis (OA), psoriatic arthritis (PsA), polymyalgia rheumatica (PMR), calcium pyrophosphate deposition disease (CPPD), and gout were retrieved. Studies on ultrasound to diagnose the target conditions and detecting elementary lesions (such as synovitis, tenosynovitis, enthesitis, bone erosions, osteophytes) were extracted from the SLRs. The searches of the previous reviews were updated and data from new studies fulfilling the inclusion criteria extracted. Groups of reviewers worked separately for each disease, when possible diagnostic accuracy (sensitivities, specificities) was calculated from primary studies. When available, the reliability of ultrasound to detect elementary lesions was extracted.

Results: For all the examined disease, recent SLRs were available. The new searches identified 27 eligible articles, with 87 articles included from the previous SLRs. The diagnostic performance of ultrasound in identifying diseases was addressed by 75 studies; in most of them, a single elementary lesion was used to define diagnosis, except

for PMR. Only studies on RA included consecutive patients with new onset of arthritis, while studies on gout and CPPD often focused on subjects with mono-arthritis. Most of the remaining studies enrolled patients with a defined diagnosis. Synovitis was the most frequently detected lesion; clinical diagnosis was the most common reference standard. The diagnostic performance of ultrasound across different conditions was extremely variable. Ultrasound to identify elementary lesions was assessed in 38 studies in OA, gout and CPPD. Its performance in OA was very variable, with better results in CPPD and gout. The reliability of ultrasound was moderate to good for most lesions.

Conclusions: Although a consistent amount of literature investigated the diagnostic application of ultrasound, in only a minority of cases its additional value over clinical diagnosis was tested. This SLR underlines the need for studies with a pragmatic design to identify the placement of ultrasound in the diagnostic pathway of new-onset arthritis.

Keywords: early arthritis, ultrasonography, diagnosis, systematic review, imaging

INTRODUCTION

With effective treatment strategies for inflammatory arthropathies becoming extensively available, in the last decade a prompt diagnosis, allowing intervention within the window of opportunity, has become a critical point in the management of early arthritis (1). However, in rheumatology diagnosis can be achieved with certainty in a minority of cases, and this is particularly true when patients are assessed at very early stages of diseases. While in some cases the presence of valuable biomarkers, such as anticyclic citrullinated peptides antibodies (ACPA), drives the diagnostic process, in seronegative early arthritis the degree of uncertainty remains high. Moreover, the current classification criteria for the main rheumatic diseases, which are often inappropriately used to help diagnosis, require differential diagnosis to be performed before they are applied (2). This difficulty in the correct definition of diagnoses at early stages might lead to inappropriate management, delaying the start of effective treatment but also exposing patients to useless and potentially toxic drugs. In addition, also in a research setting, an imprecise diagnosis implies the impossibility to measure reliably the effect of innovative treatments in early phases. In this context, there is a great interest in the research of new biomarkers and new tools to help the diagnostic process.

Musculoskeletal ultrasonography has been widely applied in rheumatic diseases, demonstrating to be a valid and reproducible tool in both inflammatory and non-inflammatory pathologies. The relevance of this instrument has also been recognized by the European League Against Rheumatism (EULAR), that recommends ultrasound among the imaging which can be considered to help the clinical management of several conditions (3–5). The applications of ultrasound cover the areas of diagnosis, assessment of prognosis, follow-up of diseases and guide for intra-articular and peri-tendinous procedures. In the field of diagnosis, most of the studies on ultrasound investigated the frequency of elementary lesions characteristics of diseases, thus providing information on the diagnostic performance of this tool to detect single abnormalities or on the performance of single lesions to diagnose a disease. On the other hand, only a minority of studies tests the diagnostic value of combinations of lesions, assessed at the same time. Moreover, in this context elementary lesions are not selected based on their diagnostic properties and specificity for a certain condition. Only a minority of studies, in which the added value of ultrasound is tested jointly with clinical evaluation (6, 7), apply a pragmatic design that reproduces the clinical context. The lack of information on the application of ultrasound in a realistic clinical process of diagnosis translates into the limited weight given to this imaging in classification criteria. For instance, the only role for ultrasound in Rheumatoid Arthritis (RA) classification is the possible confirmation of the presence of synovitis (2), while to date the only classification criteria including ultrasound are those for polymyalgia rheumatica (PMR) (8).

Given the limited availability of methodologically sound studies to address the diagnostic performance of ultrasound in a realistic clinical context of differential diagnosis of inflammatory arthropathies, the Ultrasound Study Group of the Italian Society for Rheumatology (SIR) prioritized its research on this subject. The present study represents the first step of such project. The aim of the present work was the evaluation of the available literature on the diagnostic application of ultrasound in inflammatory arthropathies.

MATERIALS AND METHODS

As a first step, the most relevant differential diagnoses in patients with suspected inflammatory arthropathies were identified, including also osteoarthritis (OA) as a relevant differential diagnosis. We afterwards individuated two research questions, rephrased following the PICOs (Patient, Intervention, Comparator, Outcome, Study type) methodology to provide inclusion and exclusion criteria (**Table 1**). On this basis, we planned separate systematic literature reviews (SLR) to assess the diagnostic performance of ultrasound to diagnose OA, RA, psoriatic arthritis (PsA), PMR, gout, calcium pyrophosphate deposition disease (CPPD). The SLRs were not registered, but a common protocol was available for all researchers before

TABLE 1 | Inclusion criteria for research questions.

	Population	Intervention	Comparators (reference standard)	Outcomes	Study type
What is the added value of ultrasound to diagnose the target diseases?	People presenting with joint symptoms	Ultrasound	Clinical diagnosis (without imaging) Other imaging	Confirmation of the diagnosis	Systematic literature reviews, meta-analyses, RCTs, controlled trials, non-controlled trials, diagnostic accuracy studies, cohort studies, cross-sectional studies, case-control studies
What is the accuracy of ultrasound for detecting elementary lesions of the target diseases?	Patients with confirmed diagnosis of the target disease	Ultrasound	Physical examination Surgery Other imaging	Sensitivity, specificity, Likelihood ratios, Diagnostic Odds Ratio, AUC, negative predictive value, positive predictive value Inter-reader and intra-reader reliability	Systematic literature reviews, meta-analyses, RCTs, controlled trials, non-controlled trials, diagnostic accuracy studies, cohort studies, cross-sectional studies, case-control studies

the beginning of the process. The diagnostic performance of ultrasound in detecting elementary lesions was also addressed. If studies on diagnostic performance reported also data on intra and inter-reader reliability on elementary lesions, that information was also extracted. Working groups composed by supervisors and fellows were created to work separately on each topic, participants were selected based on the expertise on the specific disease and on SLR methodology to create uniform groups. The most recent SLRs on ultrasound in the same diseases were first sought in electronic databases (5, 9–13). Some of the authors involved in the present project were also co-authors of these SLR and could provide background material (AA, ABa, AI, AZ, CS, EF, GF, GS). Since many of the existing SLR had a broader focus, only primary studies focusing on the diagnostic use of ultrasound were taken into account for the present work.

The search strategies of the previous SLR were applied in PubMed and Embase, starting from the date of the last search of the previous reviews (5, 9–13). Searches were last run on November 30th 2017. The search on PubMed and Embase was selected because we expected that all the relevant literature would be retrieved, and we did not expect to find further evidence including other databases. The records retrieved from the new searches were transferred into a bibliographic manager software (Zotero, RRID:SCR_013784) and libraries shared with each working group. The titles and abstracts of the retrieved records were evaluated by pairs of reviewers to assess the eligibility for full-text review according to the pre-specified criteria. Full-texts were afterwards evaluated by the same criteria and data from the included studies extracted into a standardized form, including 2 × 2 tables of diagnostic performance. A flow-chart describing the selection process was separately generated for each SLR. Results were summarized through summary of findings tables, describing both studies included in the previous reviews and those identified by the present ones.

RESULTS

In total, all search strategies retrieved 943 references since the date of the last search of the previous SLRs. The higher number of references belonged to the fields of PsA and gout (Additional Online File). After reviewing the abstracts, 27 papers were finally included, together with 87 articles from previous SLRs meeting the inclusion criteria, for a total of 114 papers included in the present SLR (**Table 2**). The PRISMA flow-chart of the SLR for each disease is available in the Additional Online File, as well as the full results, presented through summary of findings tables.

Ultrasound for the Clinical Diagnosis of Inflammatory Arthropathy

Information regarding the value of ultrasound to diagnose diseases could be extracted from 75 studies. The greatest amount of evidence was available for PsA, with 29 studies assessing the diagnostic performance of ultrasound.

There were meaningful differences in terms of enrolled populations across different diseases. In fact, in studies addressing PsA and OA, the primary aim was mostly to report the prevalence of different lesions. The frequency of each lesion was compared in patients with already known PsA or OA and healthy controls or patients with other definite diseases. A realistic clinical scenario of consecutive patients referred for suspicion of inflammatory arthropathy was rarely available (6).

Conversely, studies on RA evaluated the added value of ultrasound over classification criteria (14–17), the added value for diagnosis on top of clinical findings (18–20) or its prognostic value over the future development of RA (21–25) by cross-sectional or longitudinal study design.

Studies dealing with PMR mostly included populations of consecutive patients with shoulder pain (8, 13, 26) and some of them evaluated the additional value of ultrasound on the diagnostic performance of the 2012 classification criteria (8, 26, 27).

In the fields of both gout and CPPD, most of the studies included patients presenting with mono-arthritis and with suspect crystal-related arthritis.

Despite these discrepancies across different conditions, there were only a few studies, mainly focused on RA, that enrolled a population of consecutive patients with joint pain (6, 16–20, 22, 24, 28).

TABLE 2 | Features of the SLRs used as a basis for the present work.

Target disease	References	Aim of the SLR	Last searches	Number of studies included in the present SLR
RA	(12)	To evaluate the added value of ultrasound over clinical findings to the diagnosis of RA in patients with suspected arthritis	November 2015	11
OA	(5)	To provide evidence for the development of the EULAR recommendations for the use of imaging for the clinical management of OA. The SLR does not focus only on ultrasound	December 2015	18
PsA	(9)	To provide evidence for the selection and design of an observational study of the Ultrasound Study Group of the SIR. The SLR focuses on ultrasound	September 25th 2015	24
CPPD	(10)	To provide evidence on the diagnostic performance of ultrasound to diagnose CPPD and to retrieve all the ultrasound definitions of CPPD. The SLR focuses on ultrasound.	31 December 2014	18
PMR	(13)	To review the accuracy of imaging to diagnose PMR	October 2nd 2013	10
Gout	(11)	To provide evidence on the diagnostic performance of ultrasound to help clinicians in the choice of imaging. The SLR does not focus only on ultrasound	February 2016	6

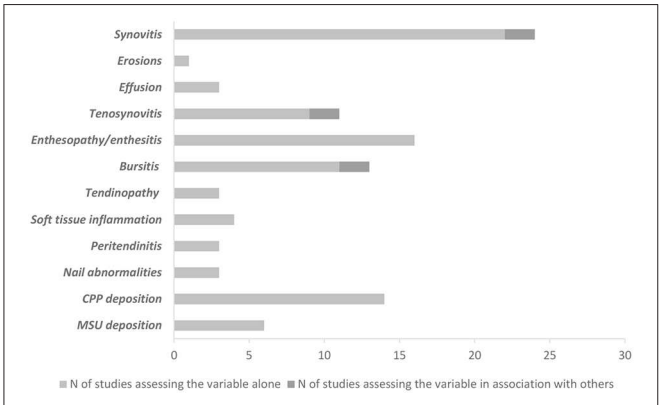

GRAPH 1 | Number of studies using each single elementary lesion to establish diagnoses, alone or in combination. CPP, calcium pyrophosphate; MSU, monosodium urate.

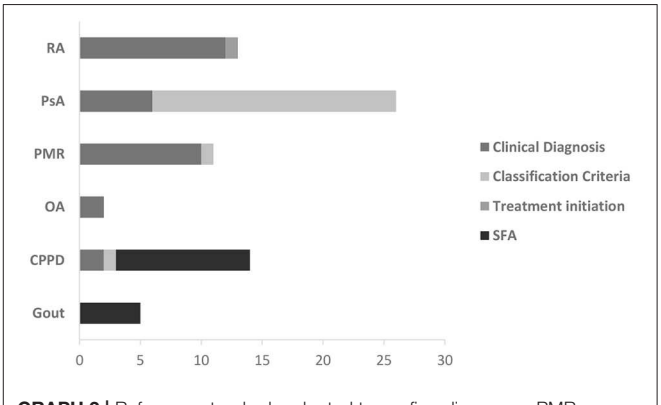

GRAPH 2 | Reference standards adopted to confirm diagnoses. PMR, polymyalgia rheumatica; CPPD, calcium pyrophosphate deposition disease; OA, osteoarthritis; PsA, psoriatic arthritis; RA, rheumatoid arthritis; SFA, synovial fluid analysis.

The interventions used to help diagnosis were also variable. Since most of the studies did not have diagnostic accuracy as primary objective, data on the diagnosis of disease were based on single elementary lesions. A relevant exception was represented by PMR, for which some studies addressed different lesions (tenosynovitis, bursitis and synovitis) in combination (8, 26, 27). **Graph 1** summarizes all the different lesions used to define diagnosis.

The confirmation of the diagnosis was based on a variety of reference standards, which depended on the diagnostic suspicion, as expected. While clinical diagnosis was frequently considered in RA and PMR, for PsA the confirmation of diagnosis mostly relied on clinical diagnosis and classification criteria, while synovial fluid analysis was frequently considered in crystal-related arthropathies (**Graph 2**).

The study design adopted to define diagnostic accuracy was also widely variable. While studies aiming to diagnose RA were mainly cohort studies (15–24, 28), in the field of PsA emerged a significant prevalence of studies with a case-control design; controls were represented mostly by patients with RA (29–37), while in some studies also healthy controls were included (29, 31, 33, 38–43). For the remaining diseases, the type of study was more variable (**Graph 3**).

In OA, adding ultrasound information to the clinical evaluation increased the certainty of the diagnosis made by the clinician (6), while the likelihood of OA, compared to being healthy, increased with the finding of bone erosions (44).

In the field of RA, some studies supported the possibility to integrate clinical and ultrasound findings to reclassify undifferentiated arthritis (14–17, 21), while in other studies ultrasound information was applied to confirm a diagnosis of RA

or tested against a clinical diagnosis (18–20), leading in general to an increase in diagnostic performance. The prognostic value of ultrasound in predicting the future development of the disease or the need for specific treatment has also been tested, once again with positive results supporting this application (22–24, 28) (**Tables 3**, **4**). The most specific lesion to diagnose RA were bone erosions, with the specificity of 1 reported by a single study (19), although also the specificity of PD positive synovitis was high (ranging from 0.88 to 0.93).

Despite a higher number of studies with a focus on PsA, in this area there was a greater variability, due to many different lesions, tissues and sites assessed. Many studies (14 studies) focused on the assessment of entheseal abnormalities (30, 34, 35, 39, 40, 42, 45–52) and the joints (6 studies) (29, 32, 33, 38, 41, 53), while only a few studies assessed the fingers (considering joints, tendons, soft tissues and entheses) (31, 36, 37) or the nails (43, 54, 55). The primary aim of the included studies rarely addressed the diagnostic accuracy. In fact, most of the studies compared the prevalence of lesions in PsA and other diseases. Also, for this, the diagnostic performance of ultrasound findings, which were usually considered alone and not in combination or in addition to clinical findings, was extremely variable across lesions and sites (**Table 5**). Among the tested lesions, those proving to be more specific to detect PsA were those at the level of the entheses. In fact, the specificity of entheseal PD ranged from 0.33 to 0.99, of enthesophytes from 0.52 to 1 and of calcifications from 0.86 to 0.97. Peritenonitis was also very specific (from 0.95 to 1 when PD signal was present).

Studies focusing on ultrasound of the hips and the shoulders in PMR had a more variable design. In fact, along with some older studies with a case-control design (8, 56–59) several cohort studies, including that on which the current classification criteria are based (8), included consecutive patients with shoulder pain (34, 60). Moreover, several recent studies provided external validation for the classification criteria (26). Again, in terms of accuracy, studies yielded very heterogeneous results (**Table 6**). In general, bilateral findings seemed to be more specific for PMR. The specificity of bilateral subacromiodeltoid bursitis ranged from 0.68 to 0.99, while for bilateral long head of the biceps tenosynovitis ranged from 0.62 to 0.98.

Studies in CPPD evaluated several different sites, including the knees (61–68), the wrist (69, 70), the affected joint or all joints (71). Study design was variable, including both case-control and cohort studies. The diagnosis of CPPD was confirmed more frequently by synovial fluid analysis, while in some cases a clinical diagnosis (70, 71) or histology (68) were used as references. In general, ultrasound seemed to perform well in identifying this condition, especially at the knee and the wrist. The specificity to confirm CPPD at the knee (considering all the assessed sites) ranged from 0.66 to 1, while at the wrist from 0.81 to 0.91.

In the field of gout, the type of joint under investigation was widely variable, all studies (72–74) but two (75, 76) adopted synovial fluid analysis as reference standard to diagnose the

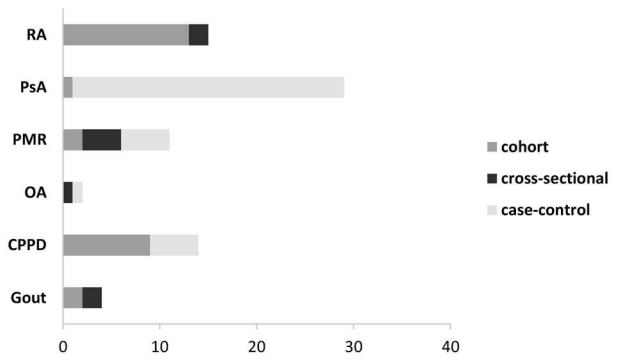

GRAPH 3 | Study design of the included studies, depending on the assessed disease. PMR, polymyalgia rheumatica; CPPD, calcium pyrophosphate deposition disease; OA, osteoarthritis; PsA, psoriatic arthritis; RA, rheumatoid arthritis; SFA: synovial fluid analysis.

TABLE 4 | Performance of ultrasound to predict RA by elementary lesions by site.

	Sensitivity	
GS SYNOVITIS	**Sensitivity**	**Specificity**
Wrist	0.79	0.69
MCP	0.9	0.48
PIP	0.79	0.66
PD SYNOVITIS		
Wrist	0.9	0.48
MCP	0.9	0.66
PIP	0.66	0.76

Summary of sensitivities, specificities across studies assessing the performance of ultrasound to predict RA by elementary lesions by site. Only Filer reports sensitivity and sensitivity for every joint. Gray Scale and power Doppler ≥ 2. MCP, Metacarpophalangeal; PIP, Proximal interphalangeal.

TABLE 3 | Performance of ultrasound to detect RA by elementary lesions and reliability.

Lesion*	Sensitivity		Specificity		Intra-reader kappa		Inter-reader kappa	
	Min	**Max**	**Min**	**Max**	**Min**	**Max**	**Min**	**Max**
Erosions	–	0.38	–	1	–	0.93	–	–
GS synovitis	0.69	0.94	0.5	0.86	0.83	0.94	0.56	0.86
PD synovitis	0.72	0.89	0.88	0.93	0.87	0.99	0.64	0.89

*Summary of sensitivities, specificities and reliability across studies assessing the performance of ultrasound to diagnose RA elementary lesions. Of the 13 papers included,only four reported sensibility-sensitivity by using gray scale (GS) and/or power Doppler (PD) ≥ 2. *Hands (including proximal interphalangeal joints) and wrists.*

TABLE 5 | Performance of ultrasound lesions to detect PsA and reproducibility.

Lesion	Sensitivity		Specificity		Intra-reader kappa		Inter-reader kappa	
	Min	Max	Min	Max	Min	Max	Min	Max
Synovial hypertrophy	0.16	0.76	0	1	–	–	0.78–1	–
Joint effusion	0.07	0.61	0.33	0.82	–	–	–	–
Erosions	0.04	0.58	0.40	1	–	–	–	–
Enthesopathy	0.22	1	0.20	1	–	–	–	–
Entheseal PD	0.05	0.3	0.30	0.99	0.91	0.97	–	–
Entheseal erosions	0.05	0.20	0.96	1	–	–	–	–
Enthesophytes	0.15	0.55	0.52	1	–	–	–	–
Entheseal calcifications	0.02	0.19	0.86	0.97	–	–	–	–
Peritenonitis PD	0.36	0.65	0.95	1.00	–	–	–	–
Peritenonitis GS	0.54	0.60	0.95	0.97	–	–	–	–
Soft tissue oedema	0.29	0.42	0.90	1	–	–	–	–
Bursitis	0.02	0.10	0.90	0.99	0.96	–	0.87	–

Summary of sensitivities, specificities and reliability across studies assessing the performance of ultrasound to diagnose PsA. Min, minimal; Max, maximal; PD, power Doppler; GS, gray scale.

TABLE 6 | Performance of ultrasound lesions to detect PMR.

Lesion	Sensitivity		Specificity	
	Min	Max	Min	Max
SAD bursitis at least monolateral	0.09	0.96	0.59	0.90
SAD bursitis bilateral	0.32	0.93	0.68	0.99
LHB tenosynovitis at least monolateral	0.14	0.81	0.47	0.59
LHB tenosynovitis bilateral	0.30	0.37	0.62	0.98
GH synovitis at least monolateral	0.20	0.77	0.34	0.78
GH synovitis bilateral	0.03	0.52	0.66	0.90
Hip synovitis at least monolateral	0.24	0.45	0.55	0.88
Hip synovitis bilateral	0.18	0.38	0.83	0.92
Trochanteric bursitis at least monolateral	0.21	0.98	0.70	0.91

Summary of sensitivities, specificities across studies assessing the performance of ultrasound to diagnose PMR. Min, minimal; Max, maximal; SAD, subacromiodeltoid; LHB, long head of the biceps; GH, gleno-humeral.

disease. 4/6 studies had a cross-sectional design, while the two remaining were a prospective (73) and a retrospective (72) study. While 4 studies reported a satisfactory performance of ultrasound (73–75, 77), for 2 studies sensitivity was low (72, 76). Considering the combination of all possible elementary lesions (e.g., double contour, aggregates, tophi), the specificity of ultrasound to diagnose gout ranged from 0.42 to 0.87.

Ultrasound to Diagnose Elementary Lesions

Data on the accuracy of ultrasound to detect elementary lesions were extracted only for OA, CPPD and gout, with 20 (78–96), 12 (68–70, 97–104), and 6 (105–110) studies addressing this aspect, respectively (**Tables 7**–**10**).

The typical population enrolled was represented by subjects with confirmed disease, in which ultrasound was compared to a reference standard to confirm the presence of a lesion.

As expected, also the reference standard was variable, in particular for OA. For CPPD, the only assessed target lesion was CPP deposition, which was evaluated by conventional radiography (2 studies), synovial fluid analysis (6 studies), microscopic analysis (2 studies). All studies on gout but one (107), in which conventional radiography was used, adopted synovial fluid analysis as reference standard.

Most of the studies assessing ultrasound to detect elementary lesions had a cross-sectional design, in particular, all the studies on OA, 4 (74–77) and 9 (62, 69, 70, 99–101, 103) studies for gout and CPPD, respectively, while the remaining studies for these two conditions had a cohort design.

In OA, results on the performance of ultrasound were once again widely variable across studies. This was also due to the variability of the reference standards adopted to define each separate lesion and the assessment of different anatomical areas.

Most of the studies on CPPD reported good performance of ultrasound to detect deposits, and this was true especially for specificity. The same conclusions can be drawn from the included articles on gout.

Reliability

Most of the studies on OA in which reliability data were presented reported good reliability for the assessment of osteophytes, erosions, effusion, cartilage damage, synovitis and cysts (**Table 7**).

In RA, the available evidence supported a good intra-reader and inter-reader reliability for erosions, GS and PD synovitis across all the assessed sites (**Tables 3**, **4**).

There was less information about reliability in the ultrasound assessment of PsA; entheseal PD, synovial hypertrophy and bursitis were the only lesions for which reliability was available. Inter-reader reliability was good for synovial hypertrophy and bursitis, as well as intra-reader for entheseal PD and bursitis (**Table 5**).

TABLE 7 | Performance of ultrasound to detect osteoarthritis elementary lesions and reliability.

Site/lesion	Sensitivity		Specificity		Intra-reader kappa		Inter-reader kappa	
	Min	Max	Min	Max	Min	Max	Min	Max
Knee osteophytes								
Vs CR	0.95	0.99	0.57	0.94	0.82	0.87	–	–
Vs hist.	0.7	0.9	–	–				
Hand osteophytes								
Vs CR	0.83	0.96	0.65	0.76	0.087	1	0.53	0.69
Vs MRI	0.82	0.9	0.75	0.95				
Vs PE	0.89	–	0.68	–				
Foot osteophytes								
Vs CR	0.62	–	0.86	–	–	–	–	–
Hand JSN								
Vs CR	0.82	–	0.72	–	–	–	–	–
Knee cartilage damage								
Vs CR	1	–	1	–	–	–		–
Vs hist.	0.78	0.89	–	–			0.67	
Hand erosions								
Vs CR	0.73	0.94	0.90	1	0.81	–	0.69	0.90
Vs MRI	0.65	0.88	0.90	0.96				
Knee erosions								
Vs CR	0.33	–	0.99	–	–	–	–	–
Foot erosions								
Vs CR	0.33	–	0.98	–	–	–	–	–
Knee effusion								
Vs PE	0.74	1	0	0.52	–	–	–	–
Vs JA	1	–	0	–				
Vs MRI	0.81	–	–	–				
Hand effusion								
Vs PE	1	–	–	–	0.81	–	0.69	–
Vs MRI	0.92	–	0.98	–				
Popliteal cyst								
Vs PE	0.36	0.67	0.89	0.98	–	–	–	–
Vs scint.	0.29	–	0.90	–				
Hand cysts								
Vs MRI	0.87	–	0.97	–	0.81	–	0.69	–
Hand synovitis								
Vs PE	0.15	–	0.96	–	0.81	–	0.69	–
Vs MRI	0.84	–	0.96	–				
Knee synovitis								
Vs PE	0.67	–	0.50	–	–	–	–	–
Pes anserinus bursitis								
Vs PE	0.50	–	0.96	–	–	–	–	–

Summary of sensitivities, specificities and reliability across studies assessing the performance of ultrasound to diagnose OA elementary lesions. Min, minimal; Max, maximal; CR, conventional radiography; hist, histology; MRI, magnetic resonance imaging; PE, physical examination; JA, joint aspiration; scint, scintigraphy.

Among the included studies on PMR, none reported information on the reliability for the assessed lesions.

For CPPD, some studies reported a good inter-reader reliability to assess both the meniscal fibrocartilage and the hyaline cartilage at the level of the knee (**Table 8**). In gout during acute attacks, very good intra-reader reliability was reported for double contour, aggregates, erosions and hypervascularisation. Inter-reader reliability was assessed for tophi, erosions, double contour, hypervascularisation and aggregates, still with good values (**Table 9**). The reliability on the same lesions was also assessed in the intercritical phases, with still good, although in general lower, results (**Table 10**).

TABLE 8 | Performance of ultrasound to detect CPPD elementary lesions and reproducibility.

Site/lesion	Sensitivity		Specificity		Intra-reader kappa		Inter-reader kappa	
	Min	Max	Min	Max	Min	Max	Min	Max
Knee FC	0.007	0.96	0.50	1.00	–	–	0.68	0.81
Knee HC	0.59	1.00	0.00	1.00	–	–	0.55	0.81
Wrist TFCC	0.78	0.81	0.85	0.91	–	–	–	–

Summary of sensitivities, specificities and reliability across studies assessing the performance of ultrasound to diagnose CPPD elementary lesions. FC, fibrocartilage; HC, Hyaline Cartilage; TFCC, Triangular Fibrocartilage Complex.

TABLE 9 | Performance of ultrasound to detect gout elementary lesions and reproducibility (acute attack).

Site/lesion	Sensitivity		Specificity		Intra-reader kappa		Inter-reader kappa	
	Min	Max	Min	Max	Min	Max	Min	Max
Knee/DC	–	0.75	–	–	–	–	–	–
Knee/tophi	—	0.62	–	–	–	–	–	–
1st MTP/DC	0.62	0.87	–	–	–	–	–	–
1st MTP/tophi	0.71	0.87	–	–	–	–	–	0.82
1st MTP/erosion	0.52	–	–	–	–	–	–	0.83
1st MTP/effusion	0.29	–	–	–	–	–	–	–
Knee/1st MTP erosion	0.31	0.48	0.53	0.79	–	–	–	–
Knee/1st MTP DC	0.34	0.51	0.91	0.99	–	–	–	0.87
Knee/1st MTP tophi	0.21	0.65	0.96	1.0	–	–	0.47	0.83
Knee/1st MTP echogenic foci	0.71	0.85	0.56	0.73	–	–	–	–
Symptomatic joint or tendon/erosion	0.11	0.33	0.03	0.81	1.0	–	0.86	–
Symptomatic joint or tendon/hypervascularization	0.88	0.98	0.39	0.66	0.83	-	0.67	–
Symptomatic joint or tendon/HCA	0.25	0.87	0.18	0.99	0.81	–	0.58	0.71
Symptomatic joint or tendon/DC	0.36	0.52	0.83	0.96	1.0	–	0.63	0.71
Symptomatic joint or tendon/tophi	0.29	0.52	0.95	1.0	–	–	0.74	–

Summary of sensitivities, specificities and reliability across studies assessing the performance of ultrasound to diagnose gouty elementary lesions (acute attack). Min, minimal; Max, maximal; MTP, metatarsophalangeal; DC, double contour; HCA, hyperechoic cloudy area.

DISCUSSION

The aim of our SLR was that of retrieving all the available evidence to support future studies on the integration of the information provided by ultrasound in the diagnostic process. Several groups had already focused on this aspect, since recent SLRs were available for all of the conditions of our interest (5, 9, 11, 13, 104). The existing reviews presented a summary of the diagnostic use of ultrasound deriving from a relevant number of studies for each considered disease. Despite all the reviews being relatively recent, we found additional studies in the subsequent literature from which we could retrieve further evidence. The number of SLRs and eligible studies represents a clue of the interest that ultrasound as diagnostic tool has raised. The easier availability of high-end ultrasound equipment, the accessibility to training and the possibility to apply directly the information provided by ultrasound during a routine visit are likely the features that have driven the enthusiasm about the technique. However, when analyzing in depth the available literature, there is an evident gap between the interest in the diagnostic applications of ultrasound and the quality of the studies produced so far in this field. In fact, with some important exceptions, the main objective of the studies was that of describing the prevalence of different lesions and comparing groups of patients in terms of ultrasound findings. Although information on diagnostic accuracy can be retrieved also from such study design, these results cannot be generalized to external populations, since a realistic clinical setting is not reproduced.

Many studies, in fact, included patients with definite and longstanding diagnosis and adopted a case-control design, with controls that were unlikely to be very similar to the true differential diagnoses of disease. This is particularly true for PsA, for which most of the studies had a case-control design.

There was limited evidence regarding the diagnosis of OA (6), while for RA and PMR the studies reproduced a more pragmatic context. In fact, in RA, some studies evaluated patients with new-onset arthralgia and tested the ability of ultrasound to help confirm diagnosis (19), while some others integrated ultrasound on top of classification criteria (16, 17). There were also some studies testing the prognostic value of ultrasound on the future development of RA (22).

In the context of PMR, some older studies still adopted a case-control design (56), however, since the development of the new classification criteria (8), the interest has shifted to the

TABLE 10 | Performance of ultrasound to detect gout elementary lesions and reproducibility (intercritic phase).

Site/lesion	Sensitivity		Specificity		Intra-reader kappa		Inter-reader kappa	
	Min	Max	Min	Max	Min	Max	Min	Max
Knee effusion	0.92	1.0	0.77	0.95	–	–	–	–
Knee synovial hypertrophy	0.49	0.74	0.92	1.0	–	–	–	–
Knee intra-articular PD	0.20	0.45	0.92	1.0	–	–	–	–
Midtarsal joints /effusion, synovial hypertrophy, erosion, tophi	0.91	0.94	0.93	0.96	–	–	–	–
MTP joints/effusion, synovial hypertrophy, erosion, tophi	0.90	0.95	0.78	0.85	–	–	–	–
Multiple sites/intra-articular or intrabursal HAG	0.78	0.91	0.65	0.91	–	0.67	0.50	0.54
Tendon/ligament HAG	0.55	0.72	0.84	0.95	–	0.67	0.50	0.54
Tendon/hyperechoic linear band	0.47	0.64	0.65	0.91	–	0.70	0.35	0.36
Cartilage/DC	0.66	0.82	0.76	0.89	–	0.88	0.69	0.74
1st MTP erosion	0.51	0.77	0.84	0.98	–	–	0.29	0.74
1st MTP DC	0.53	0.84	0.59	1.0	–	–	0.37	0.61
1st MTP tophi	0.26	0.77	0.88	1.0	–	–	0.26	0.78
1st MTP effusion	0.09	0.30	0.51	0.77	–	–	0.23	0.60
1st MTP synovial hypertrophy	0.03	0.19	0.92	1.0	–	–	0.36	0.81
1st MTP synovitis	0.01	0.14	0.73	0.93	–	–	0.48	0.83

Summary of sensitivities, specificities and reliability across studies assessing the performance of ultrasound to diagnose gouty elementary lesions (intercritic phase). Min, minimal; Max, maximal; PD, power Doppler; MTP, metatarsophalangeal; DC, double contour; HAG, hyperechoic aggregate.

evaluation of the additional impact of ultrasound on classification (26). The performance of US in this context was highly variable. Such heterogeneous results might be due to the disease, which may present with variable abnormalities, thus affecting the US sensitivity. Bilateral pathologic conditions appear to be the most specific US findings.

In the field of crystal-related arthropathies, several studies evaluated both patients during the acute presentation and the inter-critical periods. The population of interest was that of patients presenting with monoarthritis, representing a realistic clinical scenario for this diagnostic suspicion, although quite specific.

The ability of ultrasound to correctly identify elementary lesions typical of each disease seemed to be good, and this was especially true for inflammatory lesions. When a suboptimal performance was achieved, it must be kept in mind that in several studies the reference standard adopted to define a lesion (e.g., physical examination) could not be considered the optimal one for the specific lesion.

Although this was not the primary objective of this SLR, we extracted information on intra and inter-reader reliability, if available. The information from the primary studies supported good reliability of ultrasound to identify inflammatory lesions, as well as signs of damage, at the level of joints and entheses, as well as deposition of crystals. It must however be considered that rheumatologists taking part in ultrasound studies might have greater expertise on a specific lesion or disease than average, so that such reliabilities could not be reproduced in a clinical setting.

The present SLR has some limitations. First, only two databases were searched, and, although probably the greatest part of the literature has been covered, we cannot exclude the presence of further studies, even among gray literature. Due to the clinical heterogeneity of the results, we did not perform a pooled estimate of the diagnostic performance. Moreover, a formal assessment of quality and risk of bias was not performed. However, the present work is, to our knowledge, the first one to provide a comprehensive overview on the diagnostic use of ultrasound in arthritis, with a focus on the general question and without concentrating on a single disease.

What emerges from the overview of the results of our SLR is that a very few studies (6, 16, 19, 22, 24) investigated the additional impact of ultrasound findings in making a diagnosis in consecutive patients presenting with joint symptoms, which is indeed the typical scenario of every day's rheumatologist work.

In most studies, clinical and ultrasound assessments were performed separately, and ultrasound findings were not evaluated on top of clinical findings but validated against clinical diagnosis. With this being almost the only evidence available today, it is of no surprise that so far, the relevance of ultrasound in recommendations on the diagnosis and management of rheumatic diseases and in classification criteria is so limited. This happens despite ultrasound being an ideal tool in this context: adequate ultrasound equipment can now be easily accessible, they can be used during scheduled visits and provide immediately helpful information. Multiple sites can be assessed at the same time with good acceptability by the patients. Several other modern imaging have been applied in the setting of early arthritis, such as magnetic resonance imaging (MRI), positron emission tomography (PET) od dual energy CT (DECT), however they present a limited feasibility compared to ultrasound, limited availability, higher costs and, in some cases, limited data in the clinical setting. Since the accuracy of ultrasound in detecting elementary lesions has been established and the increasing ultrasound expertise across

rheumatologists allows at least some findings to be detected reliably, the time has come to test the real potentialities of ultrasound during the first evaluation for the suspicion of inflammatory arthropathy. The Musculoskeletal ultrasound Study Group of the Italian Society for Rheumatology has recently focused on the design of such study, which implies the definition of the ideal combination of joints to be assessed based on the clinical suspicion and confirming diagnoses after a follow-up. Before the application of ultrasound, an initial set of differential diagnoses should be defined for each patient, based on clinical features. The additional value of an ultrasound examination, targeted on the clinical suspicion, would afterwards be tested in terms of correct and timely diagnosis. We expect that these results will help clarify the real role of ultrasound through the process of diagnosis and help giving a new insight into its correct placement in the management of inflammatory arthropathies.

DATA AVAILABILITY STATEMENT

The datasets generated for this study are available on request to the corresponding author.

AUTHOR CONTRIBUTIONS

GS, SC, GF, and AI conceived the study and supervised its conduction. SC performed the searches in the electronic databases. AA, ABa, ABo, AD, OD, CD, OE, EF, LI, AP, AZ, and GS performed the systematic literature review. GS drafted the manuscript. All authors revised critically the article, read and approved its final version for submission.

FUNDING

This work was supported by the Italian Society of Rheumatology by affording the open access fees.

ACKNOWLEDGMENTS

The Authors would like to thank Cecilia Agnes, Irene Azzolin, Emanuela Bellis, Nicola Boffini Marco Canzoni, Marta Caprioli, Linda Carli, Francesco Cavatorta, Giovanni Ciancio, Giovanna Cuomo, Andrea Di Matteo, Ilaria Farina, Matteo Filippini, Valentina Foschi, Alessandra Gabba, Ariela Hoxha, Federica Martinis, Claudio Mastaglio, Augusta Ortolan, Simone Parisi, Marco Piras, Francesco Porta, Bernd Raffeiner, Roberta Ramonda, Daniela Rossi, Silvia Rossi, Crescenzio Scioscia, Palma Scolieri, Teodora Serban, Riccardo Terenzi, Giulia Tesei, Ilaria Tinazzi, Carmela Toscano, Carlo Venditti, and Gentiana Vukatana for contributing to the SLR.

SUPPLEMENTARY MATERIAL

The Supplementary Material for this article can be found online at: https://www.frontiersin.org/articles/10.3389/fmed.2020.00141/full#supplementary-material

REFERENCES

1. Smolen JS, Breedveld FC, Burmester GR, Bykerk V, Dougados M, Emery P, et al. Treating rheumatoid arthritis to target: 2014 update of the recommendations of an international task force. *Ann Rheum Dis*. (2016) 75:3–15. doi: 10.1136/annrheumdis-2015-207524
2. Aletaha D, Neogi T, Silman AJ, Funovits J, Felson DT, Bingham CO, et al. 2010 rheumatoid arthritis classification criteria: an American College of Rheumatology/European League Against Rheumatism collaborative initiative. *Ann Rheum Dis*. (2010) 69:1580–8. doi: 10.1136/ard.2010.138461
3. Mandl P, Navarro-Compan V, Terslev L, Aegerter P, van der Heijde D, D'Agostino MA, et al. EULAR recommendations for the use of imaging in the diagnosis and management of spondyloarthritis in clinical practice. *Ann Rheum Dis*. (2015) 74:1327–39. doi: 10.1136/annrheumdis-2014-206971
4. Colebatch AN, Edwards CJ, Østergaard M, van der Heijde D, Balint PV, D'Agostino M-A, et al. EULAR recommendations for the use of imaging of the joints in the clinical management of rheumatoid arthritis. *Ann Rheum Dis*. (2013) 72:804–14. doi: 10.1136/annrheumdis-2012-203158
5. Sakellariou G, Conaghan PG, Zhang W, Bijlsma JWJ, Boyesen P, D'Agostino MA, et al. EULAR recommendations for the use of imaging in the clinical management of peripheral joint osteoarthritis. *Ann Rheum Dis*. (2017) 76:1484–94. doi: 10.1136/annrheumdis-2016-210815
6. Matsos M, Harish S, Zia P, Ho Y, Chow A, Ioannidis G, et al. Ultrasound of the hands and feet for rheumatological disorders: influence on clinical diagnostic confidence and patient management. *Skeletal Radiol*. (2009) 38:1049–54. doi: 10.1007/s00256-009-0738-2
7. D'Agostino M-A, Saraux A, Chary-Valckenaere I, Marcelli C, Guis S, Gaudin P, et al. Can we improve the diagnosis of spondyloarthritis in patients with uncertain diagnosis? The EchoSpA prospective multicenter French cohort. *Joint Bone Spine Rev Rhum*. (2012) 79:586–90. doi: 10.1016/j.jbspin.2012.02.007
8. Dasgupta B, Cimmino MA, Maradit-Kremers H, Schmidt WA, Schirmer M, Salvarani C, et al. 2012 Provisional classification criteria for polymyalgia rheumatica: a European League Against Rheumatism/American College of Rheumatology collaborative initiative. *Ann Rheum Dis*. (2012) 71:484–92. doi: 10.1016/j.ymed.2012.09.009
9. Zabotti A, Bandinelli F, Batticciotto A, Scirè CA, Iagnocco A, Sakellariou G, et al. Musculoskeletal ultrasonography for psoriatic arthritis and psoriasis patients: a systematic literature review. *Rheumatology*. (2017) 56:1518–32. doi: 10.1093/rheumatology/kex179
10. Filippou G, Adinolfi A, Iagnocco A, Filippucci E, Cimmino M.A, Bertoldi I, et al. Ultrasound in the diagnosis of calcium pyrophosphate dihydrate deposition disease. a systematic literature review and a meta-analysis. *Osteoarthr Cartil*. (2016) 24:973–81. doi: 10.1016/j.joca.2016.01.136
11. Chen J, Liao M, Zhang H, Zhu D. Diagnostic accuracy of dual-energy CT and ultrasound in gouty arthritis: a systematic review. *Z Rheumatol*. (2017) 76:723–9. doi: 10.1007/s00393-016-0250-8
12. Lage-Hansen PR, Lindegaard H, Chrysidis S, Terslev L. The role of ultrasound in diagnosing rheumatoid arthritis, what do we know? an updated review. *Rheumatol Int*. (2017) 37:179–87. doi: 10.1007/s00296-016-3587-z
13. Mackie SL, Koduri G, Hill CL, Wakefield RJ, Hutchings A, Loy C, et al. Accuracy of musculoskeletal imaging for the diagnosis of polymyalgia rheumatica: systematic review. *RMD Open*. (2015) 1:e000100. doi: 10.1136/rmdopen-2015-000100
14. Filer A, De Pablo P, Allen G, Nightingale P, Jordan A, Jobanputra P, et al. Utility of ultrasound joint counts in the prediction of rheumatoid arthritis in patients with very early synovitis. *Ann Rheum Dis*. (2011) 70:500–7. doi: 10.1136/ard.2010.131573
15. Kawashiri SY, Suzuki T, Okada A, Yamasaki S, Tamai M, Nakamura H, et al. Musculoskeletal ultrasonography assists the diagnostic performance of the

2010 classification criteria for rheumatoid arthritis. *Mod Rheumatol*. (2013) 23:36–43. doi: 10.3109/s10165-012-0628-7
16. Nakagomi D, Ikeda K, Okubo A, Iwamoto T, Sanayama Y, Takahashi K, et al. Ultrasonographic assessment of synovitis improves the accuracy of 2010 american college of rheumatology/European league against rheumatism classification criteria for rheumatoid arthritis to predict development of a methotrexate-requiring disease. *Ann Rheum Dis*. (2013) 65:890–8.
17. Ji L, Deng X, Geng Y, Song Z, Zhang Z. The additional benefit of ultrasonography to 2010 ACR/EULAR classification criteria when diagnosing rheumatoid arthritis in the absence of anti-cyclic citrullinated peptide antibodies. *Clin Rheumatol*. (2017) 36:261–7. doi: 10.1007/s10067-016-3465-9
18. Minowa K, Ogasawara M, Murayama G, Gorai M, Yamada Y, Nemoto T, et al. Predictive grade of ultrasound synovitis for diagnosing rheumatoid arthritis in clinical practice and the possible difference between patients with and without seropositivity. *Mod Rheumatol*. (2015) 3:1–6. doi: 10.3109/14397595.2015.1069457
19. Broll M, Albrecht K, Tarner I, Müller-Ladner U, Strunk J. Sensitivity and specificity of ultrasonography and low-field magnetic resonance imaging for diagnosing arthritis. *Clin Exp Rheumatol*. (2012) 30:543–7.
20. Rezaei H, Torp-Pedersen S, Af Klint E, Backheden M, Kisten Y, Györi N, et al. Diagnostic utility of musculoskeletal ultrasound in patients with suspected arthritis–a probabilistic approach. *Arthritis Res Ther*. (2014) 16:448. doi: 10.1186/s13075-014-0448-6
21. Salaffi F, Ciapetti A, Gasparini S, Carotti M, Filippucci E, Grassi W. A clinical prediction rule combining routine assessment and power doppler ultrasonography for predicting progression to rheumatoid arthritis from early-onset undifferentiated arthritis. *Clin Exp Rheumatol*. (2010) 28:686–94.
22. Navalho M, Resende C, Rodrigues AM, Alberto Pereira DSJ, Fonseca JE, Campos J, et al. Bilateral evaluation of the hand and wrist in untreated early inflammatory arthritis: A comparative study of ultrasonography and magnetic resonance imaging. *J Rheumatol*. (2013) 40:1282–92. doi: 10.3899/jrheum.120713
23. Ozgul A, Yasar E, Arslan N, Balaban B, Taskaynatan MA, Tezel K, et al. The comparison of ultrasonographic and scintigraphic findings of early arthritis in revealing rheumatoid arthritis according to criteria of American College of Rheumatology. *Rheumatol Int*. (2009) 29:765–8. doi: 10.1007/s00296-008-0765-7
24. Platt PN, Pratt A. The predictive value of musculoskeletal ultrasound in unselected early arthritis clinic patients with polyarthralgia. *Rheumatology*. (2013) 52:i65.
25. Tămaş MM, Rednic N, Felea I, Rednic S. Ultrasound assessment for the rapid classification of early arthritis patients. *J Investig Med*. (2013) 61:1184–91. doi: 10.2310/JIM.0000000000000005
26. Macchioni P, Boiardi L, Catanoso M, Pazzola G, Salvarani C. Performance of the new 2012 EULAR/ACR classification criteria for polymyalgia rheumatica: Comparison with the previous criteria in a single-centre study. *Ann Rheum Dis*. (2014) 73:1190–3. doi: 10.1136/annrheumdis-2013-204167
27. Weigand S, Ehrenstein B, Fleck M, Hartung W. Joint involvement in patients with early polymyalgia rheumatica using high-resolution ultrasound and its contribution to the EULAR/ACR 2012 classification criteria for polymyalgia rheumatica. *J Rheumatol*. (2014) 41:730–4. doi: 10.3899/jrheum.130946
28. Zufferey P, Rebell C, Benaim C, Ziswiler HR, Dumusc A, So A. Ultrasound can be useful to predict an evolution towards rheumatoid arthritis in patients with inflammatory polyarthralgia without anticitrullinated antibodies. *Joint Bone Spine*. (2017) 84:299–303. doi: 10.1016/j.jbspin.2016.05.011
29. Gutierrez M, Filippucci E, Salaffi F, Di Geso L, Grassi W. Differential diagnosis between rheumatoid arthritis and psoriatic arthritis: the value of ultrasound findings at metacarpophalangeal joints level. *Ann Rheum Dis*. (2011) 70:1111–4. doi: 10.1136/ard.2010.147272
30. Iagnocco A, Spadaro A, Marchesoni A, Cauli A, de Lucia O, Gabba A, et al. Power doppler ultrasonographic evaluation of enthesitis in psoriatic arthritis. a multi-center study. *Joint Bone Spine*. (2012) 79:324–5. doi: 10.1016/j.jbspin.2011.10.005
31. Lin Z, Wang Y, Mei Y, Zhao Y, Zhang Z. High-Frequency ultrasound in the evaluation of psoriatic arthritis: a clinical study. *Am J Med Sci*. (2015) 350:42–6. doi: 10.1097/MAJ.0000000000000504
32. Melchiorre D, Calderazzi A, Maddali Bongi S, Cristofani R, Bazzichi L, Eligi C, et al. A comparison of ultrasonography and magnetic resonance imaging in the evaluation of temporomandibular joint involvement in rheumatoid arthritis and psoriatic arthritis. *Rheumatology*. (2003) 42:673–6. doi: 10.1093/rheumatology/keg181
33. Wiell C, Szkudlarek M, Hasselquist M, Moller JM, Vestergaard A, Norregaard J, et al. Ultrasonography, magnetic resonance imaging, radiography, and clinical assessment of inflammatory and destructive changes in fingers and toes of patients with psoriatic arthritis. *Arthritis Res Ther*. (2007) 9:R119. doi: 10.1186/ar2327
34. Falsetti P, Frediani B, Fioravanti A, Acciai C, Baldi F, Filippou G, et al. Sonographic study of calcaneal entheses in erosive osteoarthritis, nodal osteoarthritis, rheumatoid arthritis and psoriatic arthritis. *Scand J Rheumatol*. (2003) 32:229–34. doi: 10.1080/03009740310003721
35. Falsetti P, Frediani B, Filippou G, Acciai C, Baldi F, Storri L, et al. Enthesitis of proximal insertion of the deltoid in the course of seronegative spondyloarthritis. an atypical enthesitis that can mime impingement syndrome. *Scand J Rheumatol*. (2002) 31:158–62. doi: 10.1080/713798352
36. Fournié B, Margarit-Coll N, Champetier de Ribes TL, Zabraniecki L, Jouan A, Vincent V, et al. Extrasynovial ultrasound abnormalities in the psoriatic finger. Prospective comparative power-doppler study versus rheumatoid arthritis. *Joint Bone Spine*. (2006) 73:527–31. doi: 10.1016/j.jbspin.2006.01.019
37. Zabotti A, Salvin S, Quartuccio L, De Vita S. Differentiation between early rheumatoid and early psoriatic arthritis by the ultrasonographic study of the synovio-entheseal complex of the small joints of the hands. *Clin Exp Rheumatol*. (2016) 34:459–65.
38. Turner DE, Hyslop E, Barn R, McInnes IB, Steultjens MPM, Woodburn J. Metatarsophalangeal joint pain in psoriatic arthritis: a cross-sectional study. *Rheumatology*. (2014) 53:737–40. doi: 10.1093/rheumatology/ket435
39. Woodburn J, Hyslop E, Barn R, McInnes IB, Turner DE. Achilles tendon biomechanics in psoriatic arthritis patients with ultrasound proven enthesitis. *Scand J Rheumatol*. (2013) 42:299–302. doi: 10.3109/03009742.2012.747626
40. Eder L, Jayakar J, Thavaneswaran A, Haddad A, Chandran V, Salonen D, et al. Is the madrid sonographic enthesitis index useful for differentiating psoriatic arthritis from psoriasis alone and healthy controls? *J Rheumatol*. (2014) 41:466–72. doi: 10.3899/jrheum.130949
41. Ciancio G, Volpinari S, Fotinidi M, Furini F, Farina I, Bortoluzzi A, et al. Involvement of the inconstant bursa of the fifth metatarsophalangeal joint in psoriatic arthritis: a clinical and ultrasonographic study. *BioMed Res Int*. (2014) 2014:174841 doi: 10.1155/2014/174841
42. Bandinelli F, Prignano F, Bonciani D, Bartoli F, Collaku L, Candelieri A, et al. Ultrasound detects occult entheseal involvement in early psoriatic arthritis independently of clinical features and psoriasis severity. *Clin Exp Rheumatol*. (2013) 31:219–24.
43. Aydin SZ, Castillo-Gallego C, Ash ZR, Abignano G, Marzo-Ortega H, Wittmann M, et al. Potential use of optical coherence tomography and high-frequency ultrasound for the assessment of nail disease in psoriasis and psoriatic arthritis. *Dermatol Basel Switz*. (2013) 227:46–51. doi: 10.1159/000351702
44. Zayat AS, Ellegaard K, Conaghan PG, Terslev L, Hensor EM, Freeston JE, et al. The specificity of ultrasound-detected bone erosions for rheumatoid arthritis. *Ann Rheum Dis*. (2015) 745:897–903. doi: 10.1136/annrheumdis-2013-204864
45. Freeston JE, Coates LC, Helliwell PS, Hensor EM, Wakefield RJ, Emery P, et al. Is there subclinical enthesitis in early psoriatic arthritis? A clinical comparison with power doppler ultrasound. *Arthritis Care Res*. (2012) 64:1617–21. doi: 10.1002/acr.21733
46. Marchesoni A, de Lucia O, Rotunno L, de Marco G, Manara M. Entheseal power doppler ultrasonography: a comparison of psoriatic arthritis and fibromyalgia. *J Rheumatol*. (2012) 39:29–31. doi: 10.3899/jrheum.120238
47. Acquacalda E, Albert C, Montaudie H, Fontas E, Danre A, Roux CH, et al. Ultrasound study of entheses in psoriasis patients with or without musculoskeletal symptoms: a prospective study. *Joint Bone Spine*. (2015) 82:267–71. doi: 10.1016/j.jbspin.2015.01.016

48. Falcao S, de Miguel E, Castillo-Gallego C, Peiteado D, Branco J, Martín Mola E. Achilles enthesis ultrasound: the importance of the bursa in spondyloarthritis. *Clin Exp Rheumatol*. (2013) 31:422–7.
49. Ezzat Y, Gaber W, Abd ELRSF, Ezzat M, El Sayed M. Ultrasonographic evaluation of lower limb enthesis in patients with early spondyloarthropathies. *Egypt Rheumatol*. (2013) 35:29–35. doi: 10.1016/j.ejr.2012.09.004
50. Aydin SZ, Ash ZR, Tinazzi I, Castillo-Gallego C, Kwok C, Wilson C, et al. The link between enthesitis and arthritis in psoriatic arthritis: a switch to a vascular phenotype at insertions may play a role in arthritis development. *Ann Rheum Dis*. (2013) 72:992–5. doi: 10.1136/annrheumdis-2012-201617
51. Farouk HM, Mostafa AAA, Youssef SS, Elbeblawy MMS, Assaf NY, Elokda ESE. Value of entheseal ultrasonography and serum cartilage oligomeric matrix protein in the preclinical diagnosis of psoriatic arthritis. *Clin Med Insights Arthritis Musculoskelet Disord*. (2010) 3:7–14. doi: 10.4137/CMAMD.S4461
52. Groves C, Chandramohan M, Chew NS, Aslam T, Helliwell PS. Clinical examination, ultrasound and MRI imaging of the painful elbow in psoriatic arthritis and rheumatoid arthritis: which is better, ultrasound or MR, for imaging enthesitis? *Rheumatol Ther*. (2017) 4:71–84. doi: 10.1007/s40744-017-0053-7
53. De Simone C, Caldarola G, D'Agostino M, Carbone A, Guerriero C, Bonomo L, et al. Usefulness of ultrasound imaging in detecting psoriatic arthritis of fingers and toes in patients with psoriasis. *Clin Dev Immunol*. (2011) 2011:390726. doi: 10.1155/2011/390726
54. Aydin SZ, Castillo-Gallego C, Ash ZR, Marzo-Ortega H, Emery P, Wakefield RJ, et al. Ultrasonographic assessment of nail in psoriatic disease shows a link between onychopathy and distal interphalangeal joint extensor tendon enthesopathy. *Dermatology*. (2012) 225:231–5. doi: 10.1159/000343607
55. Mendonça JA. [Differences of spectral doppler in psoriatic arthritis and onychomycosis]. *Rev Bras Reumatol*. (2014) 54:490–3. doi: 10.1016/j.rbre.2014.03.028
56. Ruta S, Rosa J, Navarta DA, Saucedo C, Catoggio LJ, Monaco RG, et al. Ultrasound assessment of new onset bilateral painful shoulder in patients with polymyalgia rheumatica and rheumatoid arthritis. *Clin Rheumatol*. (2012) 31:1383–7. doi: 10.1007/s10067-012-2016-2
57. Cantini F, Salvarani C, Olivieri I, Niccoli L, Padula A, Macchioni L, et al. Shoulder ultrasonography in the diagnosis of polymyalgia rheumatica: a case-control study. *J Rheumatol*. (2001) 28:1049–55.
58. Cantini F, Niccoli L, Nannini C, Padula A, Olivieri I, Boiardi L, et al. Inflammatory changes of hip synovial structures in polymyalgia rheumatica. *Clin Exp Rheumatol*. (2005) 23:462–8.
59. Coari G, Paoletti F, Iagnocco A. Shoulder involvement in rheumatic diseases. sonographic findings. *J Rheumatol*. (1999) 26:668–73.
60. Lange U, Piegsa M, Teichmann J, Neeck G. Ultrasonography of the glenohumeral joints–a helpful instrument in differentiation in elderly onset rheumatoid arthritis and polymyalgia rheumatica. *Rheumatol Int*. (2000) 19:185–9. doi: 10.1007/s002960000051
61. Catay E, Ruta S, Rosa J, Navarta DA, Scolnik M, Garcia-Monaco R, et al. Knee effusion: Sensitivity and specificity of ultrasound for the identification of calcium pyrophosphate crystals. *Arthritis Rheum*. (2013) 65:S367.
62. Juge PA, Ottaviani S, Aubrun A, Palazzo E, Dieudé P. Sensitivity and reproducibility of ultrasonography in calcium pyrophosphate crystal deposition: a case-control study. *Ann Rheum Dis*. (2014) 73:492–509. doi: 10.1136/annrheumdis-2014-eular.3849
63. Ottaviani S, Juge PA, Aubrun A, Palazzo E, Dieudé P. Sensitivity and reproducibility of ultrasonography in calcium pyrophosphate crystal deposition in knee cartilage: a cross-sectional study. *J Rheumatol*. (2015) 42:1511–3. doi: 10.3899/jrheum.141067
64. Salcion A, Kozyreff-Meurice M, Richette P, Avenel G, Bisson-Vaivre A, Trouvin A.-P, et al. Assessment of the ultrasonography's efficiency as a diagnostic tool for calcium pyrophosphate crystal deposition disease. *Ann Rheum Dis*. (2015) 74:538. doi: 10.1136/annrheumdis-2015-eular.4964
65. Adinolfi A, Picerno V, Scanu A, Toscano C, Scirè C, Carrara G, et al. Diagnostic performance of the new omeract criteria for CPPD identification by us: correlation with synovial fluid analysis. *Ann Rheum Dis*. (2017) 2017:730–1. doi: 10.1136/annrheumdis-2017-eular.5164
66. Filippou G, Frediani B, Gallo A, Menza L, Falsetti P, Baldi F, et al. A 'new' technique for the diagnosis of chondrocalcinosis of the knee: sensitivity and specificity of high-frequency ultrasonography. *Ann Rheum Dis*. (2007) 66:1126–8. doi: 10.1136/ard.2007.069344
67. Ellabban AS, Kamel SR, Abo Omar HAS, El-Sherif AMH, Abdel-Magied RA. Ultrasonographic diagnosis of articular chondrocalcinosis. *Rheumatol Int*. (2012) 32:3863–8. doi: 10.1007/s00296-011-2320-1
68. Filippou G, Bozios P, Gambera D, Lorenzini S, Bertoldi I, Adinolfi A, et al. Ultrasound detection of calcium pyrophosphate dihydrate crystal deposits in menisci: a pilot *in vivo* and *ex vivo* study. *Ann Rheum Dis*. (2012) 71:1426–7. doi: 10.1136/annrheumdis-2011-201001
69. Forien M, Combier A, Gardette A, Palazzo E, Dieudé P, Ottaviani S. Comparison of ultrasonography and radiography of the wrist for diagnosis of calcium pyrophosphate deposition. *Joint Bone Spine*. (2018) 85:615–8. doi: 10.1016/j.jbspin.2017.09.006
70. Di Matteo A, Filippucci E, Salaffi F, Carotti M, Carboni D, Di Donato E, et al. Diagnostic accuracy of musculoskeletal ultrasound and conventional radiography in the assessment of the wrist triangular fibrocartilage complex in patients with definite diagnosis of calcium pyrophosphate dihydrate deposition disease. *Clin Exp Rheumatol*. (2017) 35:647–52.
71. Contant E, Ornetti P, Bohm A, Fortunet C, Maillefert JF. Interest of musculoskeletal ultrasound in the diagnosis of calcium pyrophosphate dihydrate deposition disease. *Ann Rheum Dis*. (2014) 73:775 doi: 10.1136/annrheumdis-2014-eular.3533
72. Lai KL, Chiu YM. Role of ultrasonography in diagnosing gouty arthritis. *J Med Ultrasound*. (2011) 19:7–13. doi: 10.1016/j.jmu.2011.01.003
73. Huppertz A, Hermann KGA, Diekhoff T, Wagner M, Hamm B, Schmidt WA. Systemic staging for urate crystal deposits with dual-energy CT and ultrasound in patients with suspected gout. *Rheumatol Int*. (2014) 34:763–71. doi: 10.1007/s00296-014-2979-1
74. Elsaman AM, Muhammad EMS, Pessler F. Sonographic findings in gouty arthritis: diagnostic value and association with disease duration. *Ultrasound Med Biol*. (2016) 42:1330–6. doi: 10.1016/j.ultrasmedbio.2016.01.014
75. Basaric MM, Radunovic G, Damjanov N, Perovic-Radak M. Sensitivity and specificity of ultrasound score for the diagnosis of gout. *Ann Rheum Dis*. (2016) 75:863–4. doi: 10.1136/annrheumdis-2016-eular.3750
76. Gruber M, Bodner G, Rath E, Supp G, Weber M, Schueller-Weidekamm C. Dual-energy computed tomography compared with ultrasound in the diagnosis of gout. *Rheumatol*. (2014) 53:173–9. doi: 10.1093/rheumatology/ket341
77. Pascal Z, Valcov R, Fabreguet I, Dumusc A, Omoumi P, So A. A prospective evaluation of ultrasound as a diagnostic tool in acute microcrystalline arthritis. *Arthritis Res Ther*. (2015) 17:188 doi: 10.1186/s13075-015-0701-7
78. Iagnocco A, Filippucci E, Ossandon A, Ciapetti A, Salaffi F, Basili S, et al. High resolution ultrasonography in detection of bone erosions in patients with hand osteoarthritis. *J Rheumatol*. (2005) 32:2381–3.
79. Keen HI, Lavie F, Wakefield RJ, D'Agostino MA, Berner Hammer H, Hensor EMA, et al. The development of a preliminary ultrasonographic scoring system for features of hand osteoarthritis. *Ann Rheum Dis*. (2008) 67:651–5. doi: 10.1136/ard.2007.077081
80. Koutroumpas AC, Alexiou IS, Vlychou M, Sakkas LI. Comparison between clinical and ultrasonographic assessment in patients with erosive osteoarthritis of the hands. *Clin Rheumatol*. (2010) 29:511–6. doi: 10.1007/s10067-009-1348-z
81. Hammer HB, Mathiessen A, Iagnocco A, Filippucci E, Gandjbakhch F, Kortekaas MC, et al. High reliability was found for ultrasound scoring of osteophytes in patients with hand osteoarthritis using an atlas as reference; an omeract initiative. *Arthritis Rheum*. (2013) 65:S728–9.
82. Vlychou M, Koutroumpas A, Malizos K, Sakkas LI. Ultrasonographic evidence of inflammation is frequent in hands of patients with erosive osteoarthritis. *Osteoarthr Cartil*. (2009) 17:1283–7. doi: 10.1016/j.joca.2009.04.020
83. Vlychou M, Koutroumpas A, Alexiou I, Fezoulidis I, Sakkas LI. High-resolution ultrasonography and 3.0 T magnetic resonance imaging in erosive and nodal hand osteoarthritis: high frequency of erosions in nodal osteoarthritis. *Clin Rheumatol*. (2013) 32:755–62. doi: 10.1007/s10067-013-2166-x

84. Wittoek R, Carron P, Verbruggen G. Structural and inflammatory sonographic findings in erosive and non-erosive osteoarthritis of the interphalangeal finger joints. *Ann Rheum Dis*. (2010) 69:2173–6. doi: 10.1136/ard.2010.128504
85. Wittoek R, Jans L, Lambrecht V, Carron P, Verstraete K, Verbruggen G. Reliability and construct validity of ultrasonography of soft tissue and destructive changes in erosive osteoarthritis of the interphalangeal finger joints: a comparison with MRI. *Ann Rheum Dis*. (2011) 70:278–83. doi: 10.1136/ard.2010.134932
86. Iagnocco A, Coari G. Usefulness of high resolution US in the evaluation of effusion in osteoarthritic first carpometacarpal joint. *Scand J Rheumatol*. (2000) 29:170–3. doi: 10.1080/030097400750002049
87. Akgul O, Guldeste Z, Ozgocmen S. The reliability of the clinical examination for detecting Baker's cyst in asymptomatic fossa. *Int J Rheum Dis*. (2014) 17:204–9. doi: 10.1111/1756-185X.12095
88. Chatzopoulos D, Moralidis E, Markou P, Makris V, Arsos G. Baker's cysts in knees with chronic osteoarthritic pain: a clinical, ultrasonographic, radiographic and scintigraphic evaluation. *Rheumatol Int*. (2008) 29:141–6. doi: 10.1007/s00296-008-0639-z
89. Eşen S, Akarirmak U, Aydin FY, Unalan H. Clinical evaluation during the acute exacerbation of knee osteoarthritis: the impact of diagnostic ultrasonography. *Rheumatol Int*. (2013) 33:711–7. doi: 10.1007/s00296-012-2441-1
90. Ike RW, Somers EC, Arnold EL, Arnold WJ. Ultrasound of the knee during voluntary quadriceps contraction: a technique for detecting otherwise occult effusions. *Arthritis Care Res*. (2010) 62:725–9. doi: 10.1002/acr.20047
91. Pendleton A, Millar A, O'Kane D, Wright GD, Taggart AJ. Can sonography be used to predict the response to intra-articular corticosteroid injection in primary osteoarthritis of the knee? *Scand J Rheumatol*. (2008) 37:395–7. doi: 10.1080/03009740802050738
92. Song IH, Althoff CE, Hermann KG, Scheel AK, Knetsch T, Burmester GR, et al. Contrast-enhanced ultrasound in monitoring the efficacy of a bradykinin receptor 2 antagonist in painful knee osteoarthritis compared with MRI. *Ann Rheum Dis*. (2009) 68:75–83. doi: 10.1136/ard.2007.080382
93. Yoon CH, Kim HS, Ju JH, Jee WH, Park SH, Kim HY. Validity of the sonographic longitudinal sagittal image for assessment of the cartilage thickness in the knee osteoarthritis. *Clin Rheumatol*. (2008) 27:1507–16. doi: 10.1007/s10067-008-0956-3
94. Okano T, Filippucci E, Carlo M.D, Draghessi A, Carotti M, Salaffi F, et al. Ultrasonographic evaluation of joint damage in knee osteoarthritis: Feature-specific comparisons with conventional radiography. *Rheumatol UK*. (2016) 55:2040–9. doi: 10.1093/rheumatology/kew304
95. Camerer M, Ehrenstein B, Hoffstetter P, Fleck M, Hartung W. High-resolution ultrasound of the midfoot: sonography is more sensitive than conventional radiography in detection of osteophytes and erosions in inflammatory and non-inflammatory joint disease. *Clin Rheumatol*. (2017) 36:2145–9. doi: 10.1007/s10067-017-3658-x
96. Mortada M, Zeid A, Abd El-Hamid Al-Toukhy M, Ezzeldin N, Elgawish M. Reliability of a proposed ultrasonographic grading scale for severity of primary knee osteoarthritis. *Clin Med Insights Arthritis Musculoskelet Disord*. (2016) 9:161–6. doi: 10.4137/CMAMD.S38141
97. Ellabban AS, Kamel SR, Omar HASA, El-Sherif AMH, Abdel-Magied RA. Ultrasonographic findings of Achilles tendon and plantar fascia in patients with calcium pyrophosphate deposition disease. *Clin Rheumatol*. (2012) 31:697–704. doi: 10.1007/s10067-011-1911-2
98. Ottaviani S. Ultrasonography in crystal-related diseases. *Rev Rhum Monogr*. (2015) 82:181–6. doi: 10.1016/j.monrhu.2015.04.005
99. Foldes K. Knee chondrocalcinosis: an ultrasonographic study of the hyalin cartilage. *Clin Imaging*. (2002) 26:194–6. doi: 10.1016/S0899-7071(01)00385-0
100. Falsetti P, Frediani B, Acciai C, Baldi F, Filippou G, Prada EP, et al. Ultrasonographic study of achilles tendon and plantar fascia in chondrocalcinosis. *J Rheumatol*. (2004) 31:2242–50.
101. Filippucci E, Gutierrez Riveros M, Georgescu D, Salaffi F, Grassi W. Hyaline cartilage involvement in patients with gout and calcium pyrophosphate deposition disease. *An ultrasound study. Osteoarthritis Cartilage*. (2009) 17:178–81. doi: 10.1016/j.joca.2008.06.003
102. Barskova VG, Kudaeva FM, Bozhieva LA, Smirnov AV, Volkov AV, Nasonov EL. Comparison of three imaging techniques in diagnosis of chondrocalcinosis of the knees in calcium pyrophosphate deposition disease. *Rheumatology*. (2013) 52:1090–4. doi: 10.1093/rheumatology/kes433
103. Gutierrez M, Di Geso L, Salaffi F, Carotti M, Girolimetti R, de Angelis R, et al. Ultrasound detection of cartilage calcification at knee level in calcium pyrophosphate deposition disease. *Arthritis Care Res*. (2014) 66:69–73. doi: 10.1002/acr.22190
104. Filippou G, Adinolfi A, Lorenzini S, Bertoldi I, Di Sabatino V, Picerno V, et al. Ultrasound versus X-rays versus synovial fluid analysis for the diagnosis of calcium pyrophosphate dihydrate deposition disease: Is it CPPD? *Arthritis Rheumatol*. (2014) 66:S77–8.
105. de Miguel E, Puig JG, Castillo C, Peiteado D, Torres RJ, Martín-Mola E. Diagnosis of gout in patients with asymptomatic hyperuricaemia: a pilot ultrasound study. *Ann Rheum Dis*. (2012) 71:157–8. doi: 10.1136/ard.2011.154997
106. Rettenbacher T, Ennemoser S, Weirich H, Ulmer H, Hartig F, Klotz W, et al. Diagnostic imaging of gout: comparison of high-resolution US versus conventional X-ray. *Eur Radiol*. (2008) 18:621–30. doi: 10.1007/s00330-007-0802-z
107. Naredo E, Uson J, Jiménez-Palop M, Martínez A, Vicente E, Brito E, et al. Ultrasound-detected musculoskeletal urate crystal deposition: which joints and what findings should be assessed for diagnosing gout? *Ann Rheum Dis*. (2014) 73:1522–8. doi: 10.1136/annrheumdis-2013-203487
108. Lamers-Karnebeek FBG, van Riel PLCM, Jansen TL. Additive value for ultrasonographic signal in a screening algorithm for patients presenting with acute mono-/oligoarthritis in whom gout is suspected. *Clin Rheumatol*. (2014) 33:555–9. doi: 10.1007/s10067-014-2505-6
109. Pattamapaspong N, Vuthiwong W, Kanthawang T, Louthrenoo W. Value of ultrasonography in the diagnosis of gout in patients presenting with acute arthritis. *Skeletal Radiol*. (2017) 46:759–67. doi: 10.1007/s00256-017-2611-z
110. Das S, Ghosh A, Ghosh P, Lahiri D, Sinhamahapatra P, Basu K. Sensitivity and specificity of ultrasonographic features of gout in intercritical and chronic phase. *Int J Rheum Dis*. (2017) 20:887–93. doi: 10.1111/1756-185X.12928

Conflict of Interest: The authors declare that the research was conducted in the absence of any commercial or financial relationships that could be construed as a potential conflict of interest.

frontiers in Medicine

BRIEF RESEARCH REPORT
published: 05 June 2020
doi: 10.3389/fmed.2020.00204

Power Doppler Ultrasound Assessment of A1 Pulley. A New Target of Inflammation in Psoriatic Arthritis?

Gianluca Smerilli[1*†], *Edoardo Cipolletta*[1†], *Marco Di Carlo*[1†], *Andrea Di Matteo*[1,2†], *Walter Grassi*[1] and *Emilio Filippucci*[1†]

[1] Rheumatology Unit, Department of Clinical and Molecular Sciences, Polytechnic University of Marche, "Carlo Urbani" Hospital, Jesi, Ancona, Italy, [2] Leeds Institute of Rheumatic and Musculoskeletal Medicine, University of Leeds, Leeds, United Kingdom

OPEN ACCESS

Edited by:
Christian Dejaco,
Medical University of Graz, Austria

Reviewed by:
Hilde Berner Hammer,
Diakonhjemmet Hospital, Norway
Sibel Zehra Aydin,
University of Ottawa, Canada

***Correspondence:**
Gianluca Smerilli
smerilli.gianluca@gmail.com

†ORCID:
Gianluca Smerilli
orcid.org/0000-0002-3972-4458
Edoardo Cipolletta
orcid.org/0000-0002-6881-8197
Marco Di Carlo
orcid.org/0000-0002-0906-4647
Andrea Di Matteo
orcid.org/0000-0003-0867-7051
Emilio Filippucci
orcid.org/0000-0002-7251-7784

Specialty section:
This article was submitted to Rheumatology, a section of the journal Frontiers in Medicine

Received: 11 March 2020
Accepted: 27 April 2020
Published: 05 June 2020

Citation:
Smerilli G, Cipolletta E, Di Carlo M, Di Matteo A, Grassi W and Filippucci E (2020) Power Doppler Ultrasound Assessment of A1 Pulley. A New Target of Inflammation in Psoriatic Arthritis? Front. Med. 7:204. doi: 10.3389/fmed.2020.00204

Objective: To determine the prevalence of grey scale and power Doppler (PD) ultrasound (US) features of A1 pulley inflammation in a cohort of psoriatic arthritis (PsA) patients compared with rheumatoid arthritis (RA) patients.

Methods: Sixty patients (30 with PsA and 30 with RA) were consecutively enrolled. The main clinimetric indexes were recorded, and US assessment of A1 pulleys from second to fifth fingers bilaterally was carried out. The presence of A1 pulley inflammation, defined as PD signal within a thickened pulley, was registered.

Results: A1 pulley inflammation was found in 15 of 240 fingers (6.3%) of eight PsA patients (26.7%) and in one of 240 fingers (0.4%) of one RA patient (3.3%) ($p < 0.01$ and $p = 0.03$, respectively). Seven of eight PsA patients (88%) with at least one inflamed A1 pulley had a moderate/high disease activity score. The regression linear analysis ($R^2 = 0.36$, adjusted $R^2 = 0.31$) showed that A1 pulley inflammation was correlated with Disease Activity Index for Psoriatic Arthritis (DAPSA) ($\beta = 0.43$, $p = 0.03$).

Conclusion: US A1 pulley inflammation appears to be relatively common at patient level in PsA, seems to be a characteristic feature of PsA compared to RA, and correlates with DAPSA.

Keywords: ultrasonography, psoriatic arthritis, rheumatoid arthritis, diagnostic imaging, annular pulley

INTRODUCTION

Finger flexor tendons and their surrounding synovial sheaths are located in osteofibrous channels, which are composed by the palmar aspect of the phalanges and metacarpal heads and by the digital fibrous tendon sheaths made by the digital pulleys (1). These structures are divided into annular pulleys (A1–A5) and cruciform pulleys, and their main function is to stabilize the tendons during finger flexion (1).

While feasibility of high-frequency ultrasound (US) assessment of annular pulleys has been well documented (2, 3), cruciform pulleys are not easily depictable with US because of their small size (3).

A1 pulley thickening has been recognized having a key role in the pathogenesis of "trigger finger," and US has proven to be useful in depicting this morphostructural abnormality (4).

In 2015, a magnetic resonance imaging (MRI) study turned the attention to the annular pulleys, demonstrating that these are common targets of inflammation in psoriatic arthritis (PsA) patients with dactylitis (5). Since then, two US studies evaluated the thickness of annular pulleys in chronic arthropathies, and both concluded that this is increased in PsA patients compared to rheumatoid arthritis (RA) patients and healthy subjects (6, 7). A possible link between A1 pulley thickening and dactylitis through a "deep Koebner" phenomenon was hypothesized because of the correlation between this finding and previous dactylitis (7). In a case report, inflammatory involvement of annular pulleys was depicted by US in a PsA patient (8), and power Doppler (PD) enhancement of annular pulleys was found in active psoriatic dactylitis (9). Moreover, in a very recent article, MRI signs of inflammatory involvement of annular pulleys were more often encountered in a small cohort of PsA patients compared to RA patients and healthy controls (10).

Thus, we believe that PD US potential in the assessment of A1 pulley involvement in PsA has not been adequately investigated yet.

The main aim of the present study was to determine the prevalence of PD US findings indicative of A1 pulley inflammation in PsA patients and in controls with RA.

MATERIALS AND METHODS

Patients

Consecutive patients with PsA according to the Classification Criteria for Psoriatic Arthritis criteria (11) and controls with RA fulfilling the American College of Rheumatology/European League Against Rheumatism (ACR/EULAR) criteria (12) were enrolled at the Rheumatology Unit of "Carlo Urbani" Hospital, in Jesi (Ancona, Italy). Patients younger than 18 years were excluded.

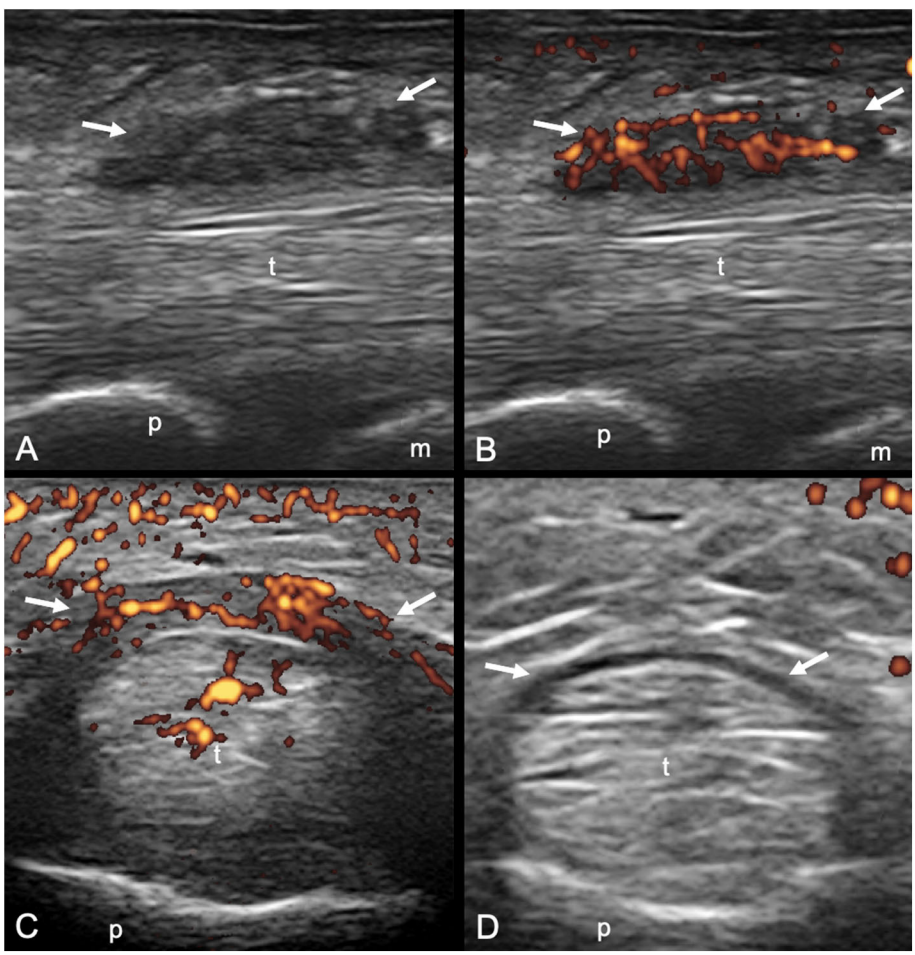

FIGURE 1 | Psoriatic arthritis. Longitudinal **(A,B)** and transverse **(C,D)** scans of the annular pulley A1 using a 22-MHz probe. In **(A,B)** a markedly thickened and inflamed A1 pulley (arrows) is depicted without and with power Doppler mode, respectively. In **(C,D)** a right–left comparison of the A1 pulley (arrows) of the third finger of another patient is illustrated. Note the thickening of the inflamed pulley and the presence of power Doppler within it in **(C)** compared to **(D)**. In **(C)** concomitant intratendinous power Doppler signal can be appreciated. m, metacarpal head; p, proximal phalanx; t, finger flexor tendons.

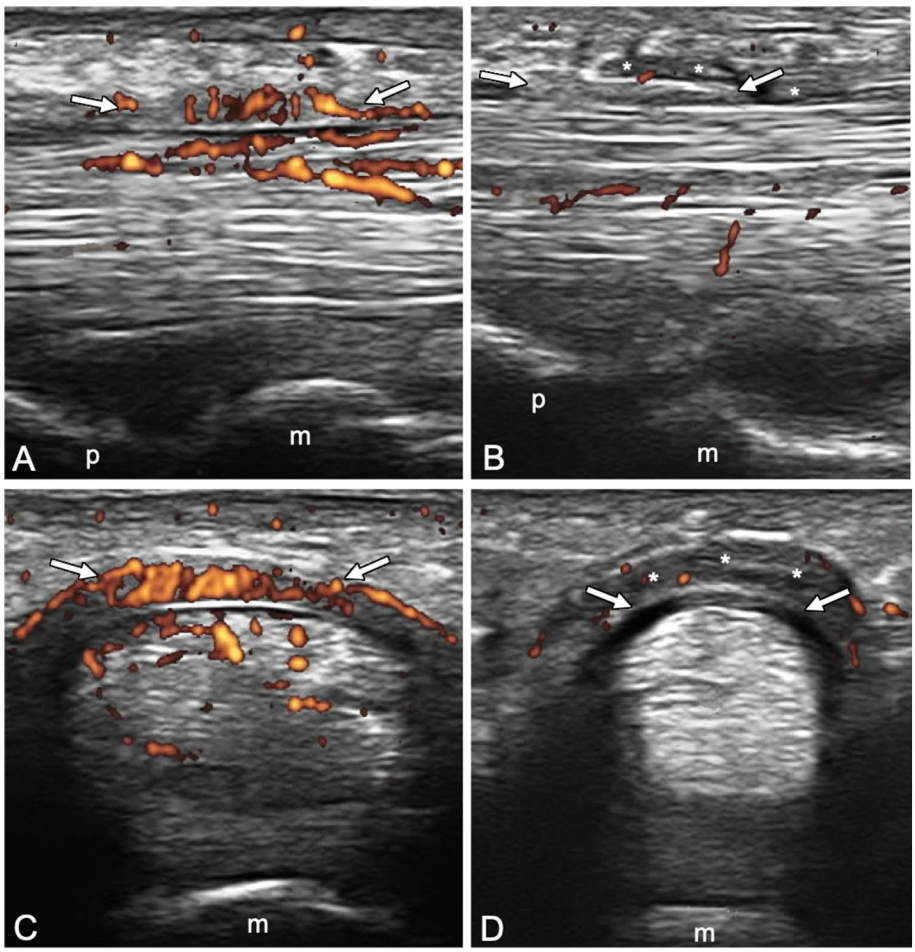

FIGURE 2 | Longitudinal **(A,B)** and transverse **(C,D)** scans of the annular pulley A1 using a 22-MHz probe in psoriatic arthritis **(A,C)** and rheumatoid arthritis **(B,D)** patients. In **(A,C)**, A1 pulley (arrows) inflammation is depicted (power Doppler signal inside a thickened pulley). Power Doppler signal is also noticeable within the superficial flexor tendon in the portion closest to the pulley. In **(B,D)**, A1 pulley (arrows) is not inflamed. The presence of synovial proliferation in the tendon sheath spilling over the normal pulley is shown (asterisks), representing a potential diagnostic pitfall. m, metacarpal head; p, proximal phalanx.

The study was conducted in accordance with the Helsinki Declaration and was approved by the local ethics committee. All patients signed informed consent.

Clinical Examination

A rheumatologist (E.C.) recorded for each patient the presence of "trigger finger", current or previous dactylitis (second to fifth fingers bilaterally), and tenderness in the A1 pulley region (second to fifth fingers bilaterally). The main clinimetric indexes (Disease Activity Index for PSoriatic Arthritis [DAPSA] in PsA patients and 28-joint Disease Activity Score [DAS28-C reactive protein (CRP)] in RA patients) were calculated.

Disease activity was interpreted according to the following cutoff values: DAPSA >28 and DAS28 >5.1 correspond to high disease activity, 28 ≥ DAPSA > 14 and 5.1 ≥ DAS28 ≥ 3.2 to moderate disease activity, 14 ≥ DAPSA > 4 and 3.2 > DAS28 ≥ 2.6 to low disease activity, and DAPSA ≤4 and DAS28 <2.6 to a remission status.

US Assessment

On the same day, another rheumatologist (G.S.) blinded to clinical data performed all the US examinations using a MyLabClassC (Esaote, Genova, Italy) equipped with a 10- to 22-MHz linear transducer. Patients were asked not to talk about their clinical condition with the sonographer.

A1 pulley from second to fifth fingers were assessed bilaterally adopting longitudinal and transverse scans as indicated by the 2017 EULAR standardized procedures for US imaging in rheumatology (13). The following pathological US findings were recorded: inflammation of the pulley (defined as the presence of PD signal within a thickened pulley) and tenosynovitis of the digital flexor tendons at finger level according to OMERACT definition (14). Thickening of the pulley was defined comparing the assessed structure with the adjacent and contralateral fingers (2). Particular attention was paid to the correct distinction between inflammatory involvement of the A1 pulley and tenosynovitis of flexor tendons (**Figures 1**, **2**). A thorough US examination with dynamic

TABLE 1 | Demographic and clinical characteristics of PsA and RA patients.

	PsA ($n = 30$)	RA ($n = 30$)
Age, mean ± SD (years)	58.6 ± 10.8	58.5 ± 13.6
Female/male	14/16	23/7
BMI, mean ± SD (kg/m^2)	25.9 ± 2.9	25.0 ± 5.4
R/L dominant hand	27/3	30/0
Trigger fingers (%)	2 (6.7)	2 (6.7)
Previous hand dactylitis (%)	8 (26.6)	0 (0)
Current hand dactylitis (%)	1 (3.3)	0 (0)
WORKING CONDITION		
Blue collar workers (%)	16 (53.3)	7 (23.3)
White collar workers (%)	5 (16.7)	5 (16.7)
Retired/unoccupied (%)	9 (30.0)	18 (60.0)
DISEASE ACTIVITY		
Disease duration, mean ± SD (years)	7.5 ± 10.1	6.0 ± 7.3
Disease activity (DAPSA/DAS28), mean ± SD	14.2 ± 11.2	3.4 ± 1.3
Remission/low disease activity	16 (53.3)	16 (53.3)
Moderate/high disease activity	14 (46.7)	14 (46.7)
TREATMENT		
cDMARDs (%)	13 (43.3)	17 (56.7)
bDMARDs (%)	17 (56.7)	8 (26.7)
Steroid (%)	2 (6.7)	13 (43.3)

bDMARDs, biologic disease-modifying antirheumatic drugs; BMI, body mass index; cDMARDs, conventional disease-modifying antirheumatic drugs; DAPSA, Disease Activity in PSoriatic Arthritis score; DAS28, Disease Activity Score in 28 joints for rheumatoid arthritis; L, left; PsA, psoriatic arthritis; R, right; RA, rheumatoid arthritis; SD, standard deviation.

assessment during passive finger flexion and extension was conducted to distinguish the pulley, which stays still, from the tendons and the tenosynovial proliferation, which move with the finger.

Statistical Analysis

The association between the sonographic findings and clinical–demographic data was tested using Cramer's V (V), point-biserial correlation (Rpb), and Spearman correlation coefficient (R). Stepwise linear regression analysis was performed to define predictive values of A1 pulley inflammation. DAPSA was used as the dependent variable, whereas independent variables were the presence of pulley inflammation and the presence of tenosynovitis. Statistical analysis was performed using SPSS (Chicago, IL, USA).

RESULTS

Sixty patients were enrolled in this cross-sectional and monocentric study: 30 with PsA and 30 with RA. **Table 1** reports the demographic and clinical characteristics of PsA and RA patients.

Tenderness of the volar side of the metacarpophalangeal joint was reported in 28 fingers (11.7%) of 13 PsA patients (43.3%) and in 13 fingers (4.6%) of six RA patients (20.0%).

US Findings

Inflammation of A1 pulley was found in 15 of 240 fingers (6.3%) of eight PsA patients (26.7%) and in one of 240 fingers (0.4%) of one RA patient (3.3%) ($p < 0.01$ and $p = 0.03$, respectively). Inflammation of A1 pulley in the absence of tenosynovitis was reported in six A1 pulleys (2.5%) of six PsA patients (20.0%).

No significant difference was reported regarding the prevalence of flexor finger flexor tendons between PsA [22 fingers (9.2%) in 10 PsA patients (33.3%)] and RA patients [21 fingers (8.8%) in six RA patients (20.0%)] ($p = 1.0$ and $p = 0.24$, respectively).

Correlation Between Demographic, Clinical, and Sonographic Data

Both pulley inflammation and tenosynovitis were correlated with DAPSA (Rpb = 0.56, $p < 0.01$, and Rpb = 0.48, $p < 0.01$). In fact, seven of eight PsA patients (88%) with at least one inflamed A1 pulley had a moderate/high disease activity score.

The regression linear analysis ($R^2 = 0.36$, adjusted $R^2 = 0.31$) showed that A1 pulley inflammation was predictive of higher DAPSA scores ($\beta = 0.43$, $p = 0.03$), whereas tenosynovitis did not reach statistical significance ($\beta = 0.25$, $p = 0.18$).

Both A1 pulley inflammation and flexor tendons tenosynovitis were associated with tenderness ($V = 0.55$, $p < 0.01$, and $V = 0.38$, $p < 0.01$).

No significant association was reported between A1 pulley inflammation and past or current episodes of dactylitis ($p = 0.09$). However, the only current dactylitis assessed showed A1 pulley inflammation. No significant correlations were found between A1 pulley inflammation and other demographic variables.

No significant association was found between the presence of at least one inflamed A1 pulley and working condition ($p = 0.84$).

DISCUSSION

The identification of the pathophysiological processes underlying the inflammatory involvement of periarticular structures during PsA is still a fascinating area of research, and US is capable of providing a clear depiction of finger pathology in PsA (15–19).

Annular pulleys are functional entheses, being subjected to very high shear stress provoked by continuous friction with adjacent tendons (7). The repetitive microtrauma makes them an ideal target for PsA inflammation, which can often be triggered mechanically. On the other hand, RA has a predilection for synovial structures; thus, we hypothesized that A1 pulley could be relatively spared.

To the best of our knowledge, this is the first study that compared PD US findings indicative of inflammation at A1 pulley level in PsA and RA patients. As expected, inflammation of A1 pulley was relatively common in PsA patients, whereas it was found in only one of 240 RA fingers examined. Moreover, the only inflamed A1 pulley in RA was found in a clinically diagnosed trigger finger and may therefore not be a RA manifestation in that patient. Indeed, an increased PD signal within the pulley has been described in trigger finger (4). However,

according to our preliminary data, A1 pulley inflammation is only rarely associated with trigger finger symptoms in PsA [one of 15 (6.6%)].

This finding, in our PsA cohort, was correlated with a higher disease activity (DAPSA), and this is an interesting aspect to be explored in future research.

The link between pulleys involvement and psoriatic dactylitis is currently a topic of growing interest. In fact, pulleys are thicker in fingers previously affected by dactylitis, and recently PD signal within pulleys has been found to be common in dactylitic fingers, with a prevalence reaching 51% for A1 pulley (7, 9). The absence of a clear correlation in our cohort between A1 pulley inflammation and previous dactylitis raises an interesting question about the chronological relationship of pulley inflammation with dactylitis, and a prospective study may shed light on this possibly crucial pathogenetic moment.

The main limitations of our study were the small number of patients assessed and the fact that we only assessed A1 pulley. Another limitation of our study was that the two groups were not matched for working condition. However, no significant association was found between the presence of A1 pulley inflammation and working condition at patient level, and five of nine patients (55.5%) with at least one A1 pulley inflamed were not blue collar workers.

One of the limitations acknowledged by the authors in a recent article (9) was that the presence digital flexor tendons tenosynovitis could be misinterpreted as pulley inflammation. However, high-frequency US probes allow an excellent anatomical resolution of small structures such as A1 pulley, and a detailed and dynamic US examination with longitudinal and transverse scans allows distinguishing tenosynovitis from inflammation of the pulley with great accuracy, avoiding this potential pitfall.

To summarize, in the present pilot study, we found that A1 pulley inflammatory involvement is not uncommon in PsA at patient level, seems to be a characteristic feature of PsA compared to RA, and correlates with disease activity.

DATA AVAILABILITY STATEMENT

The datasets generated for this study are available on request to the corresponding author.

ETHICS STATEMENT

The studies involving human participants were reviewed and approved by CERM MARCHE. The patients/participants provided their written informed consent to participate in this study.

AUTHOR CONTRIBUTIONS

GS, EC, and EF substantially contributed to study conception and design, acquisition of data, and analysis and interpretation of data. MD substantially contributed to acquisition of data, and analysis and interpretation of data. WG and AD substantially contributed to study conception and design. All the authors revised the paper and approved the final version of the article to be published.

REFERENCES

1. Doyle JR. Anatomy of the finger flexor tendon sheath and pulley system. *J Hand Surg Am.* (1988) 13:473–84. doi: 10.1016/S0363-5023(88)80082-0
2. Bianchi S, Martinoli C, de Gautard R, Gaignot C. Ultrasound of the digital flexor system: Normal and pathological findings. *J Ultrasound.* (2007) 10:85–92. doi: 10.1016/j.jus.2007.03.002
3. Boutry N, Titécat M, Demondion X, Glaude E, Fontaine C, Cotten A. High-frequency ultrasonographic examination of the finger pulley system. *J Ultrasound Med.* (2005) 24:1333–9. doi: 10.7863/jum.2005.24.10.1333
4. Guerini H, Pessis E, Theumann N, Le Quintrec JS, Campagna R, Chevrot A, et al. Sonographic appearance of trigger fingers. *J Ultrasound Med.* (2008) 27:1407–13. doi: 10.7863/jum.2008.27.10.1407
5. Tan AL, Fukuba E, Halliday NA, Tanner SF, Emery P, McGonagle D. High-resolution MRI assessment of dactylitis in psoriatic arthritis shows flexor tendon pulley and sheath-related enthesitis. *Ann Rheum Dis.* (2015) 74:185–9. doi: 10.1136/annrheumdis-2014-205839
6. Furlan A, Stramare R. The thickening of flexor tendons pulleys: a useful ultrasonographical sign in the diagnosis of psoriatic arthritis. *J Ultrasound.* (2018) 21:309–14. doi: 10.1007/s40477-018-0325-2
7. Tinazzi I, McGonagle D, Aydin SZ, Chessa D, Marchetta A, Macchioni P. "Deep Koebner" phenomenon of the flexor tendon-associated accessory pulleys as a novel factor in tenosynovitis and dactylitis in psoriatic arthritis. *Ann Rheum Dis.* (2018) 77:922–5. doi: 10.1136/annrheumdis-2017-212681
8. Zabotti A, Idolazzi L, Batticciotto A, De Lucia O, Scirè CA, Tinazzi I, et al. Enthesitis of the hands in psoriatic arthritis: an ultrasonographic perspective. *Med Ultrason.* (2017) 19:438–43. doi: 10.11152/mu-1172
9. Tinazzi I, McGonagle D, Macchioni P, Aydin SZ. Power Doppler enhancement of accessory pulleys confirming disease localization in psoriatic dactylitis. *Rheumatology (Oxford).* (2019). doi: 10.1093/rheumatology/kez549
10. Abrar DB, Schleich C, Nebelung S, Frenken M, Radke KL, Vordenbäumen S, et al. High-resolution MRI of flexor tendon pulleys using a 16-channel hand coil: disease detection and differentiation of psoriatic and rheumatoid arthritis. *Arthritis Res Ther.* (2020) 22:40. doi: 10.1186/s13075-020-2135-0
11. Taylor W, Gladman D, Helliwell P, Marchesoni A, Mease P, Mielants H. Classification criteria for psoriatic arthritis: development of new criteria from a large international study. *Arthritis Rheum.* (2006) 54:2665–73. doi: 10.1002/art.21972
12. Aletaha D, Neogi T, Silman AJ, Funovits J, Felson DT, Bingham CO 3rd, et al. Rheumatoid arthritis classification criteria: an American College of Rheumatology/European League against Rheumatism collaborative initiative. *Arthritis Rheum.* (2010) 62:2569–81. doi: 10.1136/ard.2010.138461
13. Möller I, Janta I, Backhaus M, Ohrndorf S, Bong DA, Martinoli C, et al. The 2017 EULAR standardised procedures for ultrasound imaging in rheumatology. *Ann Rheum Dis.* (2017) 76:1974–79.
14. Naredo E, D'Agostino MA, Wakefield RJ, Möller I, Balint PV, Filippucci E, et al. Reliability of a consensus-based ultrasound score for tenosynovitis in rheumatoid arthritis. *Ann Rheum Dis.* (2013) 72:1328–34. doi: 10.1136/annrheumdis-2012-202092
15. Tinazzi I, McGonagle D, Zabotti A, Chessa D, Marchetta A, Macchioni P. Comprehensive evaluation of finger flexor tendon

entheseal soft tissue and bone changes by ultrasound can differentiate psoriatic arthritis and rheumatoid arthritis. *Clin Exp Rheumatol.* (2018) 36:785–90.
16. Delle Sedie A, Riente L. Psoriatic arthritis: what ultrasound can provide us. *Clin Exp Rheumatol.* (2015) 33(5 Suppl 93):S60–5.
17. Ficjan A, Husic R, Gretler J, Lackner A, Graninger WB, Gutierrez M, et al. Ultrasound composite scores for the assessment of inflammatory and structural pathologies in Psoriatic Arthritis (PsASon-Score). *Arthritis Res Ther.* (2014) 16:476. doi: 10.1186/s13075-014-0476-2
18. Lackner A, Duftner C, Ficjan A, Gretler J, Hermann J, Husic R, et al. The association of clinical parameters and ultrasound verified inflammation with patients' and physicians' global assessments in psoriatic arthritis. *Semin Arthritis Rheum.* (2016) 46:183–9. doi: 10.1016/j.semarthrit.2016.05.010
19. Zabotti A, Mandl P, Zampogna G, Dejaco C, Iagnocco A. One year in review 2018: ultrasonography in rheumatoid arthritis and psoriatic arthritis. *Clin Exp Rheumatol.* (2018) 36:519–25. doi: 10.1136/annrheumdis-2017-211585

Conflict of Interest: EF has received speaking fees from AbbVie, Bristol - Myers Squibb, Novartis, Pfizer, Roche, and Union Chimique Belge Pharma. WG has received speaking fees from AbbVie, Celgene, Grünenthal, Pfizer, and Union Chimique Belge Pharma. This study was conducted while AD was an ARTICULUM fellow.

The remaining authors declare that the research was conducted in the absence of any commercial or financial relationships that could be construed as a potential conflict of interest.

frontiers in Medicine

ORIGINAL RESEARCH
published: 19 June 2020
doi: 10.3389/fmed.2020.00285

Whole-Body Magnetic Resonance Imaging Assessment of Joint Inflammation in Rheumatoid Arthritis—Agreement With Ultrasonography and Clinical Evaluation

*Sin Ngai Ng[1,2], Mette B. Axelsen[1], Mikkel Østergaard[1,3], Susanne Juhl Pedersen[1], Iris Eshed[4], Merete L. Hetland[1,3], Jakob M. Møller[3,5] and Lene Terslev[1,3]**

[1] Copenhagen Center for Arthritis Research, Center for Rheumatology and Spine Diseases, Rigshospitalet, Glostrup, Denmark, [2] Department of Medicine, Queen Elizabeth Hospital, Kowloon, Hong Kong, [3] Department of Clinical Medicine, Faculty of Health Sciences, University of Copenhagen, Copenhagen, Denmark, [4] Department of Diagnostic Imaging, Sheba Medical Center, Tel Giborim Affiliated With Tel Aviv University, Tel Aviv, Israel, [5] Department of Radiology, Herlev-Gentofte Hospital, Copenhagen, Denmark

OPEN ACCESS

Edited by:
Raj Sengupta,
Royal National Hospital for Rheumatic Diseases, United Kingdom

Reviewed by:
Mihir D. Wechalekar,
Flinders Medical Centre, Australia
Florian Berghea,
Carol Davila University of Medicine and Pharmacy, Romania
Ingrid Möller,
University of Barcelona, Spain

***Correspondence:**
Lene Terslev
terslev@dadlnet.dk;
lene.terslev.01@regionh.dk

Specialty section:
This article was submitted to Rheumatology, a section of the journal Frontiers in Medicine

Received: 05 November 2019
Accepted: 21 May 2020
Published: 19 June 2020

Citation:
Ng SN, Axelsen MB, Østergaard M, Pedersen SJ, Eshed I, Hetland ML, Møller JM and Terslev L (2020) Whole-Body Magnetic Resonance Imaging Assessment of Joint Inflammation in Rheumatoid Arthritis—Agreement With Ultrasonography and Clinical Evaluation. Front. Med. 7:285. doi: 10.3389/fmed.2020.00285

Objective: To compare joint inflammation seen by whole-body magnetic resonance imaging (WBMRI), with "whole-body" ultrasound and clinical assessments, in patients with active rheumatoid arthritis (RA) before and during tumor necrosis factor-inhibitor (TNF-I, adalimumab) treatment.

Methods: In 18 patients with RA, clinical assessment for joint tenderness and swelling, WBMRI, and ultrasound were obtained at baseline and week 16. Wrist, metacarpophalangeal (MCP) and proximal interphalangeal (PIP), elbow (except for WBMRI), shoulder, knee, ankle, and metatarsophalangeal joints were examined. Joint inflammation was defined by WBMRI as the presence of synovitis and/or osteitis and by ultrasound as gray-scale synovial hypertrophy grade >2 and/or color Doppler grade >1. On patient level, agreement was assessed by Spearman correlation coefficients (rho) for sum scores for 28 joints (i.e., wrists, MCPs, PIPs, elbows, shoulders, and knees) between clinical examination (DAS28CRP), ultrasound (US28), and WBMRI (WBMRI26; elbows not included). On joint level, agreement on inflammation between WBMRI, ultrasound, and clinical findings was calculated with Cohen's kappa (κ).

Results: At patient level, WBMRI26 and US28 sum scores showed good correlation (rho = 0.72; $p < 0.01$) at baseline, but not at follow-up (rho = 0.25; $p = 0.41$). At joint level, moderate agreement was seen for hand joints (κ = 0.41–0.44); for other joints κ < 0.40. No correlation with DAS28CRP was seen. No statistically significant correlations were observed between changes in WBMRI26, US28, and DAS28CRP during treatment.

Conclusions: WBMRI and ultrasound joint inflammation sum scores at patient level showed good agreement in clinically active RA patients before TNF-I initiation, whereas agreement was poorer at joint level, and after treatment.

Keywords: ultrasound, WBMRI, rheumatoid arhtritis, inflammation, agreement

INTRODUCTION

Suppression of joint inflammation is essential in modern management of rheumatoid arthritis (RA) and is a key element in clinical trials (1, 2) and is traditionally assessed by clinical joint examination, but magnetic resonance imaging (MRI) and ultrasound have been demonstrated to be more sensitive than clinical assessment for detecting joint involvement (3–6) and have been shown to be sensitive to change during treatment with TNF inhibitors (7–10). While, conventional MRI is limited to assessing one or a few joint regions per examination whole-body (WB) MRI has been introduced as a potential method for accurately assessing joint inflammation in the entire body in one session, covering both axial and peripheral joints. Its potential use for monitoring disease activity has been indicated in studies demonstrating a decrease in inflammation scores after biologic treatment in RA (11, 12), psoriatic arthritis (13), and axial spondyloarthritis (14); however, the sensitivity has not been assessed.

Ultrasound can assess multiple joints in one session and several studies have shown that ultrasound has good agreement with conventional MRI for detecting synovitis (3, 4) and is, consequently, a well-suited comparator for the ability of WBMRI for detecting joint inflammation.

The aim of the current study was to assess the agreement between WBMRI findings of joint inflammation with "whole-body" ultrasound joint inflammation and clinical joint assessment and the ability to assess change during treatment with adalimumab in a cohort of clinically active RA patients.

METHODS

Study Design

The current study was undertaken as a sub-study related to an investigator-initiated clinical trial (EudraCT number NCT01029613), of 37 patients with clinically active (DAS28CRP>3.2) RA, fulfilling the 1987 American College of Rheumatology classification criteria for RA (15) with the aim to use WBMRI to visualize inflammation and structural lesions during treatment with Adalimumab (see Axelsen et al. (11) for details). The patients had to be naïve to biological therapy and initiated treatment with adalimumab 40 mg subcutaneous every other week. The patients were not allowed to receive glucocorticoids or any synthetic Disease Modifying antirheumatic Drugs other than methotrexate from 4 weeks before inclusion and throughout the study. The patients included in the main study were invited to participate in the sub-study and 19 of these patients accepted to participate. However, one patient were subsequently excluded due technical problems with the baseline WBMRI.

At each clinical visit bilateral wrist, metacarpophalangeal joints (MCPs) 1–5, proximal interphalangeal joints (PIPs) 1–5, elbow, shoulder and knee joints, ankles, and metatarsal-phalangeal joints (MTPs) 1–5 were assessed for swelling and tenderness. Visual analog scale (VAS, 0–100 mm) assessments of pain and patients and physician's global assessment, Health Assessment Questionnaire (HAQ), and C-reactive protein (CRP) were determined, and the DAS28CRP was calculated. The ultrasound examination was performed prior to the WBMRI with an average of 2 days in between. The clinical examination, the ultrasound examination, and WBMRI were performed at baseline before initiation of treatment and at week 16.

All the patients were seen by the same clinician throughout the study. At 16 weeks, the clinical response was evaluated applying the EULAR response criteria.

The study was approved by the local ethical committee and the Danish Medicines Agency, following the Helsinki Declaration and the Good Clinical Practice guidelines.

MRI Methodology

All WBMRI scans were performed in the same 3T MRI unit (Achieva, Philips, Best, the Netherlands). Short tau inversion recovery (STIR) and pre-contrast T1-weighted spin-echo images were obtained for six imaging stations, assessing the following anatomical areas: cervical spine, shoulder/thoracic spine, lumbar spine, hips/hands, knees, and feet. The field of view was 470 × 253–287 mm, slice thickness 3 mm for hips/hands and feet, while 5 mm for the other locations. The T1-weighted sequences of hips/hands and feet were repeated after intravenous gadolinium-contrast injection (16).

Joints within the field of view, were read and scored separately for the presence/absence of synovitis and bone marrow edema (BME), respectively, using the validated OMERACT definitions developed for conventional MRI (17).

The examined joints included 26 of the 28 peripheral joints used in DAS28 (elbows were not examined by WBMRI as they were outside the field of view). In addition, ankles metatarsophalangeal joint 1–5 were examined bilaterally. MRI synovitis and BME were separately scored as present/absent (0–1) applying the aforementioned OMERACT definitions and an WBMRI joint inflammation score (range 0–2) was calculated per joint. To assess the inflammation at patient level the score per joint was used for calculating total WBMRI scores per patient (WBMRI26; range 0–52) by summing up the joint score in 26 joints. At joint level, joint inflammation was considered present if either synovitis or BME was present.

The WBMRIs were evaluated by one experienced WBMRI radiologist (IE), who was blinded to time point, clinical and biochemical data. Average duration of the WBMRI examination was 60 min and with similar average duration for evaluation and scoring the WBMRI.

Ultrasound Methodology

All ultrasound examinations were performed with a General Electric Logiq 9 ultrasound machine equipped with a high-frequency linear probe ML 6–15 MHz. Doppler setting was adjusted for slow flow according to published recommendations (18). The examined joints were the same as for MRI plus the elbows.

Applying the validated OMERACT definition for synovitis (19) all joints were scored using a semi-quantitative score (0–3) for gray scale (GS) and color Doppler (CD) (20). Each component (GS and CD, respectively) was scored separately and subsequently converted to a binary score (presence/absence,

0–1, as follows: positive GS synovitis was defined as a score >2, and positive CD was defined as a score >*1*. Based on these binary scores for GS synovitis and CD an ultrasound joint inflammation score (range 0–2) was calculated per joint, and to assess the inflammation on patient level the joint scores for 28 joints were added to calculate a total US inflammation score per patient (US28 score; range 0–56). At joint level, joint inflammation was considered present if either GS synovitis (>2) or CD (>1) was present. All ultrasound examinations were performed by one experienced sonographer (LT) blinded to clinical and biochemical data, but not to time point. Each ultrasound examination and scoring of the joints for joint inflammation lasted ∼60 min.

Assessment of Agreement at Joint Level

At joint level, the agreement between WBMRI and ultrasound was evaluated using presence vs absence of joint inflammation for the wrists, MCP and PIP 1–5, elbows, shoulders, knees, ankles, and MTP 1–5. In addition, the agreement between clinical SJ and TJ and WBMRI and ultrasound, respectively, was assessed on data from baseline and week16 follow-up, i.e., data from both baseline and follow-up were pooled and analyzed together.

Assessment of Agreement at Patient Level

To assess the total inflammatory burden at patient level, composite scores were established including only the joints necessary to establish DAS28CRP (wrists, MCP, and PIP1–5, elbows, shoulders, knees). For clinical assessment a DAS28CRP were calculated and 28 tender (TJC28) and 28 swollen (SJC28) joint counts. For ultrasound and MRI the US28 and MRI26 (described above) were used. The correlation between US28 and WBMRI26 and with DAS28CRP was assessed as were the correlation to TJC28 and SJC28.

Statistics

Agreement between clinical assessment, ultrasound, and WBMRI at joint level was assessed with Cohen's kappa (κ) where κ values 0–0.20 indicates slight, 0.21–0.40 fair, 0.41–0.60 moderate, 0.61–0.80 substantial, and 0.81–1 perfect agreement) (21). Percentages of observed agreement (i.e., percentage of observations that obtained the same score) were also calculated. At patient level, sum scores were compared using the Spearman correlation analyses (rho). $P < 0.05$ was considered statistically significant. Statistical analyses were performed by IBM SPSS program version 20.0 (SPSS Incorporated, Chicago, USA).

RESULTS

Clinical Characteristics

Baseline characteristics are shown in **Table 1**. Eighteen patients were included in the study; 89% women, median age 54.4 years (range 26–73), and median disease duration 4.5 years (range 1–28). Thirteen patients were seen at 16 week-follow-up, whereas 5 were lost to follow up due to lack of treatment effect (2 patients), side effects to medication (1 patient), fracture (1 patient), and patient's cancellation of ultrasound appointment (1 patient).

TABLE 1 | Patient characteristics at baseline and follow up.

n	Baseline	Week 16
	18 patients	13 patients
Gender (female) (%)	89%	85%
Age (years)	54.5 (26–73)	55 (29–73)
Disease duration	4.5 (1–28)	5.5 (1–28)
DAS28 CRP (mg/dl)	4.52 (3.48–6.66)	3.26 (1.97–4.76)
Tender joint count (0–28)	6.5 (2–19)	3 (0–11)
Swollen Joint (0–28)	5.5 (1–13)	1 (0–5)
WBMRI26 inflammation (0–52)	8 (0–26)	5 (1–21)
US28 inflammation (0–56)	4 (0–29)	3 (0–26)

Values are median (range) if not otherwise indicated. N, number of patients; WBMRI26, whole body magnetic resonance imaging sum score for 26 joints; US28, ultrasound sum score for 28 joints.

Overall, the cohort had low inflammatory activity at baseline at patient level by both US28 and WBMRI26 with a median (range) US28 score of 4 (0–29) and a WBMRI26 score of 8 (0–26).

Correlation at Patient Level at Baseline and Follow-Up

The correlation between WBMRI26 and US28 was good at baseline (rho = 0.78; $p < 0.01$), while there was no correlation at 16 weeks (rho = 0.25; $p = 0.41$). Neither WBMRI26 nor US28 correlated with DAS28CRP at baseline (rho = 0.05, $p = 0.86$, and rho = −0.28, $p = 0.26$, respectively) or at week 16 (rho = 0.13, $p = 0.67$; rho = −0.26, $p = 0.39$, respectively).

WBMRI26 did not correlate with TJC28 at baseline (rho = −0.24, $p = 0.34$) nor at week 16 (rho = 0.39, $p = 0.19$). No correlation was found with SJC28 at baseline (rho = 0.37, $p = 0.13$) nor at week 16 (rho = −0.07, $p = 0.83$).

US28 had a negative correlation with TJC28 at baseline and week 16 (rho = −0.53, $p = 0.02$ and rho = −0.36, $p = 0.23$) and no correlation was found for SJC28 at baseline (rho = 0.42, $p = 0.09$) nor at week 16 (rho = 0.23, $p = 0.46$).

Agreement at Joint Level

In the pooled joint analysis, a moderate agreement was found between WBMRI and ultrasound for the wrist, MCP and PIP joints (κ = 0.41, 0.41, and 0.44, respectively)—**Figure 1**, whereas the agreement was fair-poor for other joints (κ < 0.40), **Table 2**.

The agreement between WBMRI and clinical TJ and SJ was fair-poor with κ < 0.40 for all joints (**Table 2**).

The agreement between ultrasound and clinical SJC in shoulders was moderate (κ = 0.48), while fair-poor (κ < 0.40) for other joints. Poor agreement was found with TJC (κ < 0.23).

The percent agreement between WBMRI and ultrasound was generally low for ankle, MTP, and knee joints (30, 59, and 6%, respectively) and high for shoulder, MCP, and PIP joints (80, 70, and 76%, respectively).

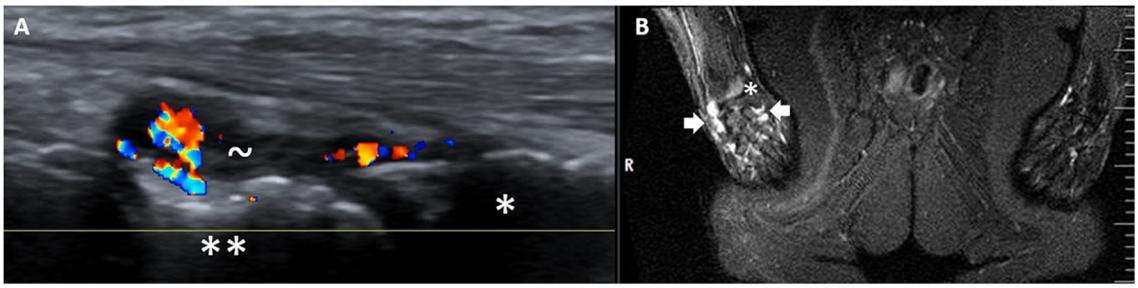

FIGURE 1 | Inflammatory activity in the right (R) wrist as shown by ultrasound **(A)** and WBMRI (STIR) **(B)**. * = radius, ** = schaphoid bone, ∼ = synovial hypertrophy with Doppler activity, white thick arrows = high signal intensity in the wrist compatible with inflammation.

TABLE 2 | Agreement between ultrasound, WBMRI, and clinical evaluation at joint level.

Sites	Ultrasound inflammation			MRI inflammation	
Kappa *P*-value % agreement *N*	MRI inflammation	Clinically tender joints	Clinically swollen joints	Clinically tender joints	Clinically swollen joints
Shoulders	0.20 0.01 80% 59	0.10 0.247 81% 59	0.48 0.000 97% 59	0.08 0.504 67% 64	0.05 0.485 72% 64
Elbows	– 	0.08 0.514 76% 59	0.37 0.000 90% 59	– 	–
Wrists	0.41 0.000 69% 59	0.26 0.037 64% 61	0.13 0.309 57% 61	0.14 0.163 52% 62	−0.01 0.908 42% 62
MCP1–5 joints	0.41 0.001 70% 60	0.10 0.362 52% 61	0.27 0.026 62% 61	0.06 0.645 54% 63	0.07 0.955 51% 63
PIP1–5 joints	0.44 0.001 76% 58	0.22 0.067 62% 61	0.30 0.019 74% 61	0.33 0.007 67% 61	0.36 0.003 74% 61
Knees	0.12 0.298 61% 57	0.15 0.198 69% 59	0.13 0.309 80% 59	0.15 0.223 60% 60	0.07 0.433 58% 60
Ankles	−0.06 0.246 30% 61	0.10 0.325 68% 59	0.18 0.110 76% 59	0.16 0.092 52% 62	0.07 0.395 40% 62
MTP1–5 joints	0.11 0.265 59% 61	0.01 0.918 53% 59	−0.12 0.259 41% 59	0.08 0.418 63% 62	0.08 0.102 35% 62

Values are kappa (1st row), p-values for kappa statistic (2nd row), Percent agreement (3rd row) and number on observations (n, 4th row).
WBMRI, whole body magnetic resonance imaging; MCP, metacarpophalangeal; PIP, proximal interphalangeal; MTP, metatarsophalangeal.

Correlation Between Changes During Treatment

After 16 weeks of treatment, median DAS28CRP had decreased from median 4.52 to 3.26, the tender joint count from 7 to 3 and the swollen joint count from 6 to 1, WBMRI26 from 8 to 5 and US28 from 4 to 3—showing a numerical decline for all parameters (**Table 1**). Six patients (46%) had achieved a good EULAR response, and 7 patients (54%) a moderate response.

The change in WBMRI26 during treatment did not correlate with the change in US28 (rho = 0.38; $p = 0.21$). Neither WBMRI26 nor US28 correlated with the change in DAS28CRP (rho = −0.07, $p = 0.82$ and rho = 0.10, $p = 0.76$, respectively).

DISCUSSION

This study is the first study to compare whole body assessment of joint inflammation as detected by both WBMRI and ultrasound in clinically active RA patients initiating a biological Disease Modifying anti-rheumatic Drug (DMARD) due to persistent elevated DAS28CRP despite conventional DMARD treatment. We found a good correlation between WBMRI26 and US28 at baseline at patient level, while the agreement at joint level was moderate for the hands and poor for the other joints. Both modalities correlated poorly with the DAS28CRP and clinical joint evaluation.

The strong correlation between WBMRI26 and US28 at baseline (at patient level) combined with the moderate-poor correlation at joint level suggest that ultrasound and MRI both provide measures of the overall inflammatory burden, but take different aspects into account. This could be explained by very different image acquisitions techniques, e.g., ultrasound cannot visualize bone marrow edema. The lack of correlation between the two imaging modalities for changes during treatment and at week 16 may partly be explained by the low level of inflammation in a small patient cohort, particular at follow-up, leaving a narrow disease severity spectrum, which will give small variations in the detected joint inflammation between the two modalities a larger impact on the correlation coefficient. Another contributing factor may be the overall low degree of peripheral inflammation by imaging in the cohort, even at baseline, and hence a lesser potential to improve during treatment.

With the ability to assess multiple joints in a single session ultrasound appeared a well-suited comparator to WBMRI for peripheral inflammatory changes in RA patients. Previous studies comparing conventional MRI and ultrasound have reported a relatively good agreement for synovitis in small peripheral joints (3, 4), i.e., a better agreement than in the present study. When obtaining WBMRI, more anatomical areas are scanned than by conventional MRI and to shorten the imaging time, the image slices are typically thicker and in-plane resolution reduced compared with conventional MRI. Together with the lack of dedicated receiver coils larger voxels and less optimal positioning the image quality is generally lower as compared to conventional MRI with the same field strength. As an example, the hand will at conventional MRI be positioned in a dedicated hand coil in the isocenter of the MRI unit, where the magnetic field is most homogenous, while during WBMRI the hand will have no specific coil and will be positioned below the buttocks, more distant from the isocenter of the magnet. This probably contributed to the observed lower agreement on the individual joint level. It should be emphasized, that the image quality has markedly improved since the study was performed in 2012 and is still undergoing continuous improvements which may positively influence the agreement in the future. Another factor that could have impaired the concordance at joint level is the fact that ultrasound cannot visualize bone marrow edema.

In our study, WBMRI and ultrasound sum scores did not correlate with DAS28CRP at baseline nor at follow-up and the agreement with clinical examination at joint level was generally poor. This is in line with previous studies (22, 23) and may be related to the lower sensitivity of clinical examination for synovitis as compared to ultrasound and MRI (3–6). Furthermore, joint inflammation by imaging was not an inclusion criterion. The low number of patients and the low degree of peripheral inflammation in the investigated cohort may also have contributed to the contra-intuitive findings such as the negative correlation between ultrasound and TJC. WBMRI has the potential, with technical improvements, to become a well-suited tool for clinical trials but is currently not suggested as a clinical tool due to generally lower availability and delay in information to the clinician about the inflammatory status as compared to ultrasound examination.

In conclusion, WBMRI and ultrasound showed good correlation for joint inflammation at patient level indicating that WBMRI is a potential tool for assessing the overall inflammatory burden in RA patients. Further studies implementing recent technical improvements in WBMRI, are needed.

DATA AVAILABILITY STATEMENT

All datasets generated for this study are included in the article/supplementary material.

ETHICS STATEMENT

The studies involving human participants were reviewed and approved by De Videnskabsetiske Komiteer, Kongens Vænge 2, 3400 Hilleroed, Denmark and the Danish Medicines Agency (EudraCT number NCT01029613). The patients/participants provided their written informed consent to participate in this study.

AUTHOR CONTRIBUTIONS

SN has performed data analysis and interpretation and written the manuscript. MA has conducted patient examination, performed data analysis and corrected the proof. MØ has performed data analysis, read WBMRIs, and written the manuscript. SP has performed data interpretation, read WBMRIs, and contributed to the manuscript. IE has read all the WBMRI images and contributed to the manuscript. MH conducted patient examination, contributed to the manuscript. JM has performed all the WBMRIs and contributed to the manuscript. LT has performed all the ultrasound examinations, performed data analysis, and written the manuscript. All authors contributed to the article and approved the submitted version.

FUNDING

This work was supported by AbbVie A/S Denmark who provided financial support and the study drug adalimumab for this investigator-initiated study.

ACKNOWLEDGMENTS

The authors acknowledge AbbVie A/S Denmark for providing financial support for this investigator-initiated study and for adalimumab during the study period. AbbVie A/S Denmark was not involved in study set-up, data collection, analysis or interpretation, and had no influence on the publication of data.

REFERENCES

1. Smolen JS, Aletaha D, Bijlsma JW, Breedveld FC, Boumpas D, Burmester G, et al. T2T Expert Committee. Treating rheumatoid arthritis to target: recommendations of an international task force. *Ann Rheum Dis.* (2010) 69:631–7. doi: 10.1136/ard.2009.123919
2. Haavardsholm EA, Aga AB, Olsen IC, Lillegraven S, Hammer HB, Uhlig T, et al. Ultrasound in management of rheumatoid arthritis: ARCTIC randomised controlled strategy trial. *BMJ.* (2016) 354:i4205. doi: 10.1136/bmj.i4205
3. Terslev L, Torp-Pedersen S, Savnik A, von der Recke P, Qvistgaard E, Danneskiold-Samsøe B, et al. Doppler ultrasound and magnetic resonance imaging of synovial inflammation of the hand in rheumatoid arthritis: a comparative study. *Arthritis Rheum.* (2003) 48:2434–41. doi: 10.1002/art.11245
4. Szkudlarek M, Klarlund M, Narvestad E, Court-Payen M, Strandberg C, Jensen KE, et al. Ultrasonography of the metacarpophalangeal and proximal interphalangeal joints in rheumatoid arthritis: a comparison with magnetic resonance imaging, conventional radiography and clinical examination. *Arthritis Res Ther.* (2006) 8:R52. doi: 10.1186/ar1904

5. Conaghan PG, Emery P, Østergaard M, Keystone EC, Genovese MC, Hsia EC, Xu W, et al. Assessment by MRI of inflammation and damage in rheumatoid arthritis patients with methotrexate inadequate response receiving golimumab: results of the GO-FORWARD trial. *Ann Rheum Dis.* (2011) 70:1968–74. doi: 10.1136/ard.2010.146068
6. Wakefield RJ, Green MJ, Marzo-Ortega H, Conaghan PG, Gibbon WW, McGonagle D, et al. Should oligoarthritis be reclassified? Ultrasound reveals a high prevalence of subclinical disease. *Ann Rheum Dis.* (2004) 63:382–5. doi: 10.1136/ard.2003.007062
7. Filippucci E, Iagnocco A, Salaffi F, Cerioni A, Valesini G, Grassi W. Power Doppler sonography monitoring of synovial perfusion at the wrist joints in patients with rheumatoid arthritis treated with adalimumab. *Ann Rheum Dis.* (2006) 65:1433–7. doi: 10.1136/ard.2005.044628
8. Hammer HB, Kvien TK. Ultrasonography shows significant improvement in wrist and ankle tenosynovitis in rheumatoid arthritis patients treated with adalimumab. *Scand J Rheumatol.* (2011) 40:178–82. doi: 10.3109/03009742.2010.517549
9. Døhn UM, Ejbjerg B, Boonen A, Hetland ML, Hansen MS, Knudsen LS, et al. No overall progression and occasional repair of erosions despite persistent inflammation in adalimumab-treated rheumatoid arthritis patients: results from a longitudinal comparative MRI, ultrasonography, CT and radiography study. *Ann Rheum Dis.* (2011) 70:252–8. doi: 10.1136/ard.2009.123729
10. Østergaard M, Emery P, Conaghan PG, Fleischmann R, Hsia EC, Xu W, Rahman MU.Significant improvement in synovitis, osteitis, and bone erosion following golimumab and methotrexate combination therapy as compared with methotrexate alone: a magnetic resonance imaging study of 318 methotrexate-naive rheumatoid arthritis patients. *Arthritis Rheum.* (2011). 63:3712–22. doi: 10.1002/art.30592
11. Axelsen MB, Eshed I, Østergaard M, Hetland ML, Møller JM, Jensen DV, et al. Monitoring total-body inflammation and damage in joints and entheses: the first follow-up study of whole-body magnetic resonance imaging in rheumatoid arthritis. *Scand J Rheumatol.* (2017) 46:253–62. doi: 10.1080/03009742.2016.1231338
12. Kono M, Kamishima T, Yasuda S, Sakamoto K, Abe S, Noguchi A, et al. Effectiveness of whole-body magnetic resonance imaging for the efficacy of biologic anti-rheumatic drugs in patients with rheumatoid arthritis: a retrospective pilot study. *Mod Rheumatol.* (2017) 27:953–60. doi: 10.1080/14397595.2016.1276425
13. De Marco G, Helliwell P, McGonagle D, Emery P, Coates LC, Hensor EMA, et al. The GOLMePsA study protocol: an investigator-initiated, double-blind, parallel-group, randomised, controlled trial of GOLimumab and methotrexate versus methotrexate in early diagnosed psoriatic arthritis using clinical and whole body MRI outcomes. *BMC Musculoskelet Disord.* (2017) 18:1–13. doi: 10.1186/s12891-017-1659-1
14. Krabbe S, Østergaard M, Eshed I, Sørensen IJ, Jensen B, Møller JM, et al. Whole-body magnetic resonance imaging in axial spondyloarthritis: reduction of sacroiliac, spinal, and entheseal inflammation in a placebo-controlled trial of adalimumab. *J Rheumatol.* (2018) 45:621–9. doi: 10.3899/jrheum.170408
15. Arnett FC, Edworthy SM, Bloch DA, McShane DJ, Fries JF, Cooper NS, et al. The American Rheumatism Association 1987 revised criteria for the classification of rheumatoid arthritis. *Arthritis Rheum.* (1988) 31:315–24. doi: 10.1002/art.1780310302
16. Poggenborg RP, Eshed I, Østergaard M, Sørensen IJ, Møller JM, Madsen OR, et al. Enthesitis in patients with psoriatic arthritis, axial spondyloarthritis and healthy subjects assessed by 'head-to-toe' whole-body MRI and clinical examination. *Ann Rheum Dis.* (2015) 74:823–9. doi: 10.1136/annrheumdis-2013-204239
17. Østergaard M, Peterfy C, Conaghan P, McQueen F, Bird P, Ejbjerg B, et al. OMERACT rheumatoid arthritis magnetic resonance imaging studies. Core set of MRI acquisitions, joint pathology definitions, and the OMERACT RA-MRI scoring system. *J Rheumatol.* (2003) 30:1385–6.
18. Torp-Pedersen S, Terslev L. Settings and artefacts relevant in colour/power Doppler ultrasound in rheumatology. *Ann Rheum Dis.* (2008) 67:143–9. doi: 10.1136/ard.2007.078451
19. Wakefield RJ, Balint PV, Szkudlarek M, Filippucci E, Backhaus M, D'Agostino MA, et al. Musculoskeletal ultrasound including definitions for ultrasonographic pathology. *J Rheumatol.* (2005) 32:2485–7.
20. Szkudlarek M, Court-Payen M, Jacobsen S, Klarlund M, Thomsen HS, Østergaard M. Interobserver agreement in ultrasonography of the finger and toe joints in rheumatoid arthritis. *Arthritis Rheum.* (2003) 48:955–62. doi: 10.1002/art.10877
21. Landis JR, Koch G. The measurement of observer agreement for categorical data. *Biometrics.* (1977) 33:159–74. doi: 10.2307/2529310
22. Gandjbakhch F, Haavardsholm EA, Conaghan PG, Ejbjerg B, Foltz V, Brown AK, et al. Determining a magnetic resonance imaging inflammatory activity acceptable state without subsequent radiographic progression in rheumatoid arthritis: Results from a followup MRI Study of 254 patients in clinical remission or low disease activity. *J Rheumatol.* (2014) 41:398–406. doi: 10.3899/jrheum.131088
23. Brown AK, Conaghan PG, Karim Z, Quinn MA, Ikeda K, Peterfy CG, et al. An explanation for the apparent dissociation between clinical remission and continued structural deterioration in rheumatoid arthritis. *Arthritis Rheum.* (2008) 58:2958–67. doi: 10.1002/art.23945

Conflict of Interest: MØ: research support, consultancy fees, and/or speaker fees form AbbVie, BMS, Boehringer-Ingelheim, Celgene, Eli-Lilly, Hospira, Janssen, Merck, Novartis, Novo, Orion, Pfizer, Regeneron, Roche, Sandoz, Sanofi and UCB. SP: speakers fee from MSD, Pfizer, AbbVie, Novartis, and UCB. Advisory board member for AbbVie and Novartis, research support from AbbVie, MSD, and Novartis. MH: funding for research from AbbVie, Biogen, BMS, CellTrion; MSD, Novartis, Orion, Pfizer, Samsung, and UCB. LT: Speakers fee from AbbVie, Janssen, Roche, Novartis, Pfizer, MSD, BMS, and GE.

The remaining authors declare that the research was conducted in the absence of any commercial or financial relationships that could be construed as a potential conflict of interest.

frontiers in Medicine

REVIEW
published: 30 June 2020
doi: 10.3389/fmed.2020.00296

Magnetic Resonance Imaging of Enthesitis in Spondyloarthritis, Including Psoriatic Arthritis—Status and Recent Advances

Ashish J. Mathew [1,2,3,4]* *and Mikkel Østergaard* [1,2]

[1] *Copenhagen Center for Arthritis Research (COPECARE), Center for Rheumatology and Spine Diseases, Glostrup, Denmark,* [2] *Department of Clinical Medicine, Faculty of Health and Medical Sciences, University of Copenhagen, Copenhagen, Denmark,* [3] *Clinical Immunology and Rheumatology, Christian Medical College, Vellore, India,* [4] *Centre for Prognosis Studies in the Rheumatic Diseases, Krembil Research Institute, University Health Network, University of Toronto, Toronto, ON, Canada*

Enthesitis, inflammation at the attachment sites of tendons, ligaments, fascia, and joint capsules to bones plays a critical role in the pathogenesis of spondyloarthritis (SpA), including psoriatic arthritis (PsA). Magnetic resonance imaging (MRI) has aided in a better understanding of pathophysiology, early diagnosis, prognostication, therapeutic outcomes, and follow up of enthesitis. The concept of enthesitis as a focal insertional pathology has transformed over the past decade, with the help of MRI, to a more widespread entity involving both bone and surrounding soft tissues. The utility of MRI in the differential diagnosis of suspected enthesitis has recently been explored. With the emergence of the treat-to-target concept, and a domain-based approach in the management of SpA, objective and sensitive monitoring of response to targeted therapy becomes prudent. Properties like high sensitivity, ability to image intra-osseous pathology along with surrounding structures exemplify the utility of MRI technology. Considering the lack of a comprehensive, validated MRI score the Outcome Measures in Rheumatology (OMERACT) MRI in Arthritis Working Group, informed by a systematic literature review, developed the first international, consensus-based MRI-scoring system, combined with MRI definitions of pathologies for enthesitis in patients with spondyloarthritis (SpA) and PsA. An atlas with representative images of each grade of the scoring system was subsequently developed by the group to aid readers interested in using the heel enthesitis MRI scoring system (HEMRIS). The HEMRIS can find utility in clinical trials targeting enthesitis as the primary outcome. MRI also finds value for global assessment of the total burden of enthesitis. The concept of whole-body MRI (WBMRI), enabling visualization of entheses throughout the body using a single image is relatively new. The MRI whole-body score for inflammation in peripheral joints and entheses (MRI-WIPE) is a promising scoring system, which is undergoing further testing in clinical trials and longitudinal cohorts evaluating global measures of inflammation at entheses. This review discusses the role of MRI in diagnosis and monitoring of enthesitis in SpA and PsA, along with recent advances in the field, based on published literature.

Keywords: magnetic resonance imaging (MRI), enthesitis, spondyloarthritis, psoriatic arthritis, inflammation

OPEN ACCESS

Edited by:
Christian Dejaco,
Medical University of Graz, Austria

Reviewed by:
Alen Zabotti,
Università degli Studi di Udine, Italy
Lennart Jans,
Ghent University, Belgium

***Correspondence:**
Ashish J. Mathew
ashishjacobmathew@gmail.com

Specialty section:
This article was submitted to Rheumatology, a section of the journal Frontiers in Medicine

Received: *27 March 2020*
Accepted: *26 May 2020*
Published: *30 June 2020*

Citation:
Mathew AJ and Østergaard M (2020) Magnetic Resonance Imaging of Enthesitis in Spondyloarthritis, Including Psoriatic Arthritis—Status and Recent Advances. Front. Med. 7:296. doi: 10.3389/fmed.2020.00296

INTRODUCTION

The entheses are insertion sites of tendon, ligament, fascia, or joint capsule into bone. Enthesopathy refers to involvement of entheses due to trauma, degeneration, or in pathological conditions including metabolic syndrome, endocrine disorders, and inflammatory arthritis (1). Inflammation at the entheseal sites, enthesitis plays a cardinal role in the pathophysiology of spondyloarthritis (SpA), including psoriatic arthritis (PsA) (2). Initially thought to be just a focal insertional site, enthesis is better known currently as being part of an "enthesis organ," with intricate immune-pathogenetic relationship with synovium, substantiated by McGonagle and colleagues as the concept of synovio-entheseal complex (3). Biomechanical stress induced micro-injuries in the synovio-entheseal complex lead to a cascade of inflammatory process in the adjoining fibrocartilage, bursae, synovium, and trabecular bone by interleukin (IL)-23 from macrophages, dendritic cells and innate lymphoid cells—type 3 (ILC3) (4).

The prevalence of enthesitis in SpA, including PsA from various studies has been reported to be 13.6–35%, with Achilles tendon, plantar fascia, and lateral epicondyle insertion being the most common sites (5, 6). Presence of enthesitis has shown to be associated with higher disease activity, disability and incapacity to work, ultimately leading to poor quality of life (6–8). Clinical enthesitis measures including the Leeds enthesitis index (LEI), the Spondyloarthritis Research Consortium of Canada (SPARCC) enthesitis index and the Maastricht Ankylosing Spondylitis Enthesitis Score (MASES) offer poor reliability and sensitivity compared to advanced imaging techniques like ultrasound and magnetic resonance imaging (MRI) (9, 10).

By providing sensitive visualization of the extent of disease, MRI and ultrasound (US) in patients with PsA have shown utility in diagnosis, prognostication, and monitoring of treatment response. (11) The European League Against Rheumatism (EULAR) recommendations for the use of imaging in SpA, built on research-based evidence and expert opinion highlight the role of MRI in diagnosis and monitoring peripheral enthesitis, acknowledging the need for further research to optimize the use of imaging in clinical practice (12).

This review aims at elucidating the role of magnetic resonance imaging (MRI) in better understanding of enthesitis in SpA, including PsA, highlighting the recent advances in this field.

HOW HAS MRI CONTRIBUTED TO THE UNDERSTANDING OF PATHOGENESIS OF ENTHESITIS IN SPA?

Based on their structure and location two types of entheses have been described – fibrous and fibrocartilaginous, with the latter being affected more commonly in SpA (13, 14). MRI, with its potential to visualize both soft tissue and intra-osseous abnormalities has fostered our understanding of the entheseal organ concept by demonstrating extension of enthesitis to adjacent bone and surrounding structures, including fibrocartilage, bursa, fat pad and deeper fascia (15, 16). McGonagle and colleagues described the correlation of HLA-B27 with the degree of MRI bone marrow edema surrounding the entheses in patients with SpA, compared to those with mechanically induced disease (17). The close link between enthesitis and synovitis in swollen peripheral joints, as demonstrated by MRI studies in PsA and SpA has invoked the possibility of enthesitis inciting an inflammatory response within the closely located synovial tissue (18, 19). This augments the hypothesis that enthesitis is a critical lesion in SpA.

The importance of enthesitis in explaining the relationship between the nail and distal interphalangeal joint disease in PsA was studied by Tan et al. using high-resolution MRI and histology, comparing patients with osteoarthritis (OA) and PsA. The MRI inflammation observed over the entire nail bed region was shown to be anatomically associated with an enthesitis organ apparatus, providing a novel explanation for distal interphalangeal joint (DIP) arthritis in PsA patients with nail involvement (20). Yet another study from the same group applying high resolution MRI to explore flexor tenosynovitis in PsA patients with dactylitis observed microscopic enthesitis in miniature pulleys around the flexor tendon, explaining the tenosynovitis, and also the concept of enthesitis in PsA (21). In a recent study Abrar et al. compared high resolution MRI of hands using a 3 T scanner and dedicated 16-channel hand coil in patients with PsA, rheumatoid arthritis (RA) and healthy controls. Compared to the other groups, PsA patients had significantly thicker A1 and A2 flexor tendon pulleys. This study corroborates the role of enthesitis in the pathogenesis of SpA (22).

UTILITY OF MRI IN THE DIAGNOSIS OF ENTHESITIS IN SPA

Given the avascular nature of the entheses at bony attachment sites and low density of vessels in the surrounding ligaments and tendons, diagnosis of enthesitis with imaging can be demanding (14). MRI has the unique advantage of identifying peri-entheseal inflammation with adjacent bone marrow edema, potentially facilitating early diagnosis in SpA (23) (**Figures 1a–d**). Fat-suppressed MRI with or without gadolinium enhancement is the most sensitive method of visualizing active enthesitis (24, 25). The European Society of Musculoskeletal Imaging (ESSR) arthritis subcommittee for the use of MRI has suggested specific sequences based on the area to be examined for inflammatory changes (26). The OMERACT MRI in enthesitis initiative proposes T1weighted post gadolinium sequence for entheseal soft tissue inflammation, STIR/T2weighted fat suppressed sequence for entheseal osteitis, and T1 weighted pre-gadolinium sequence for entheseal structural changes (27). MRI is useful in diagnosing enthesitis in the appendicular and axial skeleton. Bone marrow edema (BME) in PsA is often located close to the entheses, as compared to capsular attachments and subchondral areas in RA and OA, respectively (28).

An MRI and power doppler ultrasound (PDUS) study at the heel region compared SpA patients with current heel pain and those with no pain or past history of heel pain. MRI

FIGURE 1 | MR images of the knee and elbow depicting enthesitis. **(a)** Sagittal STIR image of the knee showing soft tissue high signal intensity (intra- and peritendinous) at the insertions of the quadriceps tendon (long arrows) and the patellar ligament (short arrows) at the patella, suggesting enthesitis. **(b)** Sagittal T2-weighted fat suppressed image of the knee showing high signal intensity (intra- and peritendinous) in the soft tissues of the pes anserine (short arrows), indicating pes anserine enthesitis, as well as bone marrow edema (long arrows) close to the insertion of the medial patellar retinaculum at medial tibial plateau. **(c,d)** Coronal (c) and axial (d) STIR images of the elbow showing bone marrow edema (mild, short arrow) and soft tissue high signal intensity (long arrows) at the common extensor tendon insertion at the lateral epicondyle, indicating enthesitis. Images courtesy of Professor Iris Eshed, Sackler School of Medicine, Tel Aviv University, Tel Aviv, Israel.

lesions considered to depict early injury included Achilles tendon (tendonitis) or aponeurosis hypersignal, peri-tendon or peri-aponeurosis hypersignal, retrocalcaneal bursitis, inferior or posterior BME, and thickening of the tendon, and those depicting chronic injury included enthesophytes and bone erosions. MRI pathologies of enthesitis were noted in 81% of SpA patients with current heel pain, compared to 56% of SpA patients without heel pain or with history of heel pain. Intra- or peri-aponeurosis MRI signal abnormalities were the most useful features, while only BME in calcaneum was specific to distinguish patients with SpA from controls (29). A similar study including SpA patients with heel or ankle pain compared high-field and low-field MRI to evaluate the hindfoot. Retrocalcaneal bursitis and plantar fasciitis were the commonest lesions in this study, which inferred an acceptable diagnostic quality for both the units (30). Enthesitis of the rotator cuff, with intense acromial BME at the deltoid origin is described as a highly specific feature of ankylosing spondylitis (AS) (31). According to a recent study erosive changes at the heel entheses seem to be more frequent in peripheral SpA patients compared to non-SpA individuals with painful heels or knees (32).

High resolution MRI with specialized "microscopy coils" have been used for detecting enthesitis at insertions of flexor and extensor tendons to the phalanges. Tan et al. investigated the microanatomic basis for localization of hand disease at the DIP joints in patients with PsA and OA using a high-resolution MRI. More severe changes at the DIP joint entheseal insertions, and marked extracapsular enhancement were noted in patients with PsA as compared to those with OA (33). Another MRI study comparing small joints of hands in RA and SpA patients demonstrated enthesitis and extracapsular changes adjacent to synovial joints more commonly in the latter (34).

MRI is the imaging method of choice for diagnosing axial enthesitis. The revised definition of MRI enthesitis in sacroiliac joints of patients with SpA excludes the inter-osseous soft tissues in the ligamentary portion of the SI joint (35). Pelvic enthesitis on MRI of sacroiliac joints is highly specific for the diagnosis of SpA, and the specificity increases with the number of sites with enthesitis. Enthesitis at the iliac crest and retroarticular ligaments have high positive predictive value for diagnosis of SpA (36). Spinal enthesitis may be seen on spine MRIs as increased signal intensity over inter-spinal ligaments extending between the transverse or spinous processes, supra-spinal ligaments and osteitis of adjacent bone marrow in the spinous process on short tau inversion recovery (STIR) images, T2-weighted fat-suppressed images and contrast enhanced T1-weighted fat-suppressed images (37). The vertebral corners (or edges) are often inflamed in axial SpA and PsA, and this finding represents enthesitis at the insertions of the anterior and posterior longitudinal ligaments (38) (**Figures 2a–f**).

Conventional MRI methods generally allow assessment of only one or few selected areas of the human body. Enthesitis in SpA, especially PsA can be widespread, and capturing the extent of disease can be challenging using conventional MRIs (39). Whole-body MRI (WBMRI), with recent technical advancements allows visualization of the entire body in one imaging session. WBMRI may, in the future clinical practice aid in diagnosis of early forms of SpA, enabling evaluation of both axial and peripheral entheses and joints. (40–42) Readability and reproducibility of WBMRI were high in spine and SI joints, but lower in the peripheral joints in earlier studies (43). However, a more recent study has found good reliability in peripheral entheses too (41). Poggenborg et al. investigated the ability of WBMRI to assess axial and peripheral enthesitis in patients with PsA and axial SpA, and observed moderate agreement between clinical examination and WBMRI. The most frequent sites of enthesitis included greater femoral trochanter, supraspinatus and Achilles tendon insertions (10). Weckbach et al. reported enthesitis in 68% of the hip regions among 30 patients with PsA using WBMRI (44). Althoff et al. compared MRI findings in patients with radiographic and non-radiographic axial SpA (nr-axSpA) using WBMRI. Enthesitis, mostly multilocular was significantly more in the SpA group as compared to the nr-axSpA group (45). Weber et al., assessed inflammation at the anterior chest wall using WBMRI in 122 patients, and reported

FIGURE 2 | Sagittal MR images of the spine, showing enthesitis at different locations (T1-weighted images on the left, short tau inversion recovery (STIR) *(Continued)*

FIGURE 2 | images on the right). **(a,b)** Several anterior and posterior corner inflammatory lesions (arrows) are seen in the thoracic spine, representing enthesitis at the insertion of the anterior and posterior longitudinal ligaments. **(c,d)** Bone marrow edema is seen at several spinous processes, particularly at the L3 spinous process (arrow), representing enthesitis. **(e,f)** Bone marrow edema is seen in two upper thoracic transverse processes (arrows), representing enthesitis. Images are from University of Copenhagen, Denmark.

inflammation in 49.5 and 25.9% of patients with SpA and nr-axSpA, respectively as opposed to 26% by clinical assessment using the Maastricht Ankylosing Spondylitis Enthesitis Score (MASES) (46). Though fairly sensitive in its diagnostic capacity, further studies are warranted to demonstrate the ability of MRI in distinguishing inflammatory enthesitis from other forms.

ROLE OF MRI IN MONITORING INFLAMMATORY AND STRUCTURAL ENTHESITIS IN SPA AND PSA

Monitoring of disease progression and treatment response is dependent on the responsiveness of the applied measure. MRI has found utility in following up patients with SpA and PsA on treatment. Marzo-Ortega et al., determining the efficacy of etanercept on axial and peripheral entheseal lesions in patients with SpA using MRIs noted improvement or regression in 86% of MRI detected entheseal lesions between baseline and 6 months (47). A similar study by the same group ascertained the efficacy of anakinra on spinal enthesitis in patients with active ankylosing spondylitis (AS) using MRI. There was complete regression or improvement in 23 of the 38 regions of enthesitis (61%) determined by MRI at baseline following 3 months of treatment (48).

Karpitschka et al. demonstrated significant reduction in enthesitis using WBMRI with gadolinium enhancement at week 52 in patients with active AS being treated with etanercept. MRI enthesitis lesions showed reduction during therapy by 94% at week 52 (49). In an investigator initiated randomized controlled trial of adalimumab in patients with axSpA, Krabbe et al. demonstrated the resolution of inflammation at multiple entheseal sites. A higher frequency of clinical resolution was observed in the joints which were tender with MRI inflammation compared to those which were tender without MRI inflammation. This supports the utility of MRI in differentiating inflammatory from non-inflammatory causes of tenderness in patients with SpA (50). Another randomized, double-blind, placebo-controlled trial on adalimumab investigated the responsiveness of WBMRI in axial and peripheral joints and entheses in patients with axSpA. The authors could demonstrate significant reductions in the WBMRI enthesis inflammation index after 6 weeks of adalimumab therapy. The WBMRI total inflammation index, covering both axial and peripheral joints and entheses, could also distinguish treatment from placebo groups (51). Further development and validation of WBMRI inflammation index may be efficacious in assessing

responsiveness to treatment of the global entheseal inflammatory burden in future clinical trials.

EVIDENCE ON MRI ENTHESITIS IN PROGNOSTICATION OF SPA AND PSA

Existence of a pre-clinical phase in PsA characterized by nonspecific arthralgias, stiffness and fatigue has been established in a prospective cohort study (52). Ultrasound studies have noted baseline sonographic evidence of enthesitis being associated with future development of clinical PsA (53, 54). MRI may aid in detection of the pre-clinical phase of PsA. However, there is scarcity of MRI studies on this topic. Whether pre-clinical MRI enthesitis can predict subsequent development of PsA remains to be established. Enthesitis presumably precedes synovitis in SpA and PsA (3, 55). Peri-entheseal BME at the tibial plateau and bony attachments of patellar tendon and posterior cruciate ligament, detected by McGonagle et al. in SpA and PsA patients with knee swelling of recent onset, indicates subclinical enthesitis near the swollen joint and suggests enthesitis as the primary lesion (18). Emad et al. studied the entheseal changes at knee joints in patients with psoriasis and SpA, including axSpA, inflammatory bowel disease (IBD) and PsA. Subclinical enthesitis was noted in patients with psoriasis and IBD. The authors concluded that enthesitis at the knee joint may be an early and pathognomonic MRI finding in patients with SpA (56). Erdem et al. determined MRI changes of foot in psoriasis patients with no clinical arthritis and healthy controls. Achilles tendonitis and retrocalcaneal bursitis were observed in more than half of the psoriasis patients, with none in the healthy control group having similar findings (57).

These studies, although with significant limitations did provide insight into the possibility of MRI enthesitis being the initial subclinical pathology in SpA. In a recent study Simon et al., scanning psoriasis patients without clinical arthritis from a longitudinal cohort have established the role of structural enthesitis at the 2nd and 3rd metacarpophalangeal joints of the dominant hand in prediction of PsA (58). Another study evaluating MRI inflammation in the hand joints of patients with psoriasis without PsA and healthy controls noted a 55.5% likelihood of developing PsA in psoriasis patients with arthralgia and evidence of MRI synovitis. This observation should, nevertheless be interpreted in the background of a 29.6% conversion rate to PsA in this cohort within the short follow up period of 1 year. Moreover, osteitis, periarticular inflammation and tenosynovitis were comparable in psoriasis patients and controls (59).

HOW HAVE CLINICAL TRIALS APPLIED MRI FOR ASSESSING ENTHESITIS?

With the advent of treat-to-target strategies in SpA and domain specific treatment approach in PsA, a subset of future clinical trials with novel molecules are expected to focus on enthesitis as their primary outcome (60–62). Inclusion of enthesitis as a core domain by the outcome measures in rheumatology (OMERACT)

FIGURE 3 | Sagittal MR images of the heel region depicting enthesitis at Achilles tendon and plantar fascia attachments. **(a)** STIR image showing bone marrow edema at the plantar fascia insertion to the calcaneum, intrafascia high signal intensity and perifascia high signal intensity. **(b)** Corresponding T1-weighted image showing probable mild thickening of a part of the Achilles tendon (arrow). **(c)** STIR image showing bone marrow edema (short arrows) close to the plantar fascia insertion to calcaneum and severe perifascia high signal intensity (long arrows). **(d)** STIR image showing bone marrow edema (long thick arrow) at the Achilles tendon insertion to calcaneum, intratendonous (long thin arrow) and, peritendonous (short thin arrow) high signal intensity, as well as retrocalcaneal bursitis (short thick arrow). **(a,b)** Courtesy of Professor Iris Eshed, Sackler School of Medicine, Tel Aviv University, Tel Aviv, Israel. **(c,d)** have been taken from the OMERACT MRI heel enthesitis exercises (27, 80).

PsA group warrants its assessment in all clinical trials and observational studies (63). MRI, despite being an objective and sensitive adjunct to clinical examination for monitoring response of enthesitis to therapy, has not been employed in clinical trials distinctly. One of the early placebo-controlled, randomized clinical trials of etanercept to determine its efficacy in patients with refractory heel enthesitis used MRI as an adjunct to clinical examination. No statistically significant differences were noted between the placebo and etanercept groups among the 19 patients who presented with positive MRI heel enthesitis, defined by BME at calcaneus insertions of Achilles tendon and plantar fascia (64). The ACHILLES trial is a randomized, quadruple-blind study (NCT02771210) evaluating the efficacy of secukinumab in resolution of Achilles tendon enthesitis in patients with active PsA and axSpA in which MRI is applied as a secondary outcome measure. The recruitment of this trial has been completed and the results are awaited (65).

Improvement in overall enthesitis in the body, as assessed by WBMRI, have been studied in few clinical trials. A randomized clinical trial compared etanercept and sulphasalazine on active bony inflammation in patients with early axSpA using WBMRI.

Reduction of peripheral enthesitis on MRI was a secondary endpoint. The authors demonstrated a 58% reduction in MRI enthesitis in patients on etanercept at week 48, as compared to no reduction in the comparator arm (66). Another randomized, placebo-controlled trial to investigate efficacy of adalimumab on WBMRI indices of inflammation at entheses in patients with axSpA demonstrated significant reduction of both BME and soft tissue indices in the treatment group compared to placebo at week 6 (51).

For MRI assessment of enthesitis in clinical trials, it is recommended to apply validated assessment methods, such as the OMERACT MRI scoring systems (27, 41). More studies are needed to validate and optimize the existing MRI outcome measures. Different aspects of validity, including criterion validity (comparison with gold standard reference, such as histopathology) and discriminant validity (reproducibility and sensitivity to change) should preferably be investigated.

UTILITY OF MRI IN ENTHESITIS IN JUVENILE ARTHRITIS

Active enthesitis and arthritis in patients with enthesitis related arthritis (ERA) at baseline has been reported to predict sacroiliitis at follow up (67). Enthesitis detected by MRI of the pelvis has been described as a specific finding in juvenile spondyloarthritis (68). Herregods et al. determined the diagnostic value of enthesitis on pelvic MRIs in patients with ERA, and noted high correlation between pelvic enthesitis and sacroiliitis (69). WBMRI is increasingly being used in the pediatric population to determine the overall inflammatory and structural burden of synovitis and enthesitis (70). Enthesitis has been included in the inflammatory MRI components of the recently developed OMERACT juvenile idiopathic arthritis MRI score (71).

LIMITATIONS OF IMAGING ENTHESITIS IN SPA AND PSA USING MRI

Notwithstanding all these benefits, MRI has certain limitations which curtails its application in routine clinical settings. Practical impediments for clinical practice like cost, referrals to specialist facilities, and some contraindications, such as claustrophobia, pacemakers, or certain metal implants, cannot be overlooked. The avascular nature and limited water accumulation in structures that make up the entheses contribute to technical difficulties, with MR signals often being low (72). A major limitation with MRI enthesitis until recently was the lack of a comprehensive, generally accepted, validated scoring system with proper definition of pathologies to be scored, which can be applied uniformly in all clinical trials and longitudinal observational studies. Most scoring methods and lesions adapted in studies of MRI enthesitis display poor content and construct validity, and lack responsiveness (73).

Limitations with WBMRI include the examination time, low resolution of images and attainable spatial resolution compared to conventional MRI (74, 75). The total scan time for WBMRI, including peripheral and axial joints, and entheses is generally around 60 min (41, 43). Patients with active arthritis may find it challenging to remain stationary in the same position for long periods of time, which may result in motion artifacts. Image resolution with current acquisition techniques could be compromised, especially in the distal small joints. With advances in technology these limitations could be addressed to a great extent. Experience of the reader also plays a pivotal role with WBMRI. Reliability among experienced readers has been shown to be good, while poorer among less experienced ones (41).

For use in clinical trials, however, MRI has the major advantage of allowing fully standardized image acquisition across all study sites, storage of the entire examination for later review and centralized reading. This makes MRI the ideal method for objective assessment of entheseal inflammation in future clinical trials.

RECENT ADVANCES IN THE FIELD OF MRI ENTHESITIS IN SPA

Expected advancements countering the technical shortcomings of MRI in imaging entheses have recently been reported. Diffusion-weighted imaging (DWI), known to have a high signal to noise ratio has been analyzed as an encouraging alternative to STIR and T2 weighted fat suppressed sequences for sacroiliac joint assessment (76–78). Lecouvet et al. compared the diagnostic accuracy of DWI and STIR sequences in WBMRI of SpA patients. DWI was found to offer higher sensitivity for detection of inflammatory lesions compared to STIR sequences, and to differentiate inflammatory from degenerative changes (78). Ultrashort echo time (UTE) sequences have been explored for better visualization of entheses. Chen et al. demonstrated higher resolution of enthesis at the Achilles tendon in healthy volunteers and patients with PsA using three-dimensional UTE-cones sequences, compared to gradient recalled echo (GRE) and fast spine echo (FSE) sequences. The authors stressed the utility of this sequence in morphological and quantitative evaluation of enthesitis in PsA patients (79). The same group recently explored the MRI morphology of Achilles tendons and entheses using high resolution MRI UTE sequences, and described its utility as biomarkers of biomechanical degradation of entheses in SpA (80).

The OMERACT MRI in arthritis Working Group, informed by a systematic review has developed consensus-based definitions and reader rules for enthesitis in patients with SpA and PsA. Through a series of multi-reader scoring exercises focusing on the heel region using an intuitive web-based image platform and data entry the group developed the OMERACT heel enthesitis in MRI scoring system (HEMRIS). HEMRIS exhibited good reliability and responsiveness among trained readers (27). This was followed by an atlas of the OMERACT HEMRIS, with detailed definitions and reader rules (**Box 1**), which could be used as a guide while scoring Achilles tendon and plantar fascia enthesitis (**Figures 3a–d**) in future clinical trials and longitudinal studies using MRI (81). Applying a similar methodology the group also developed a WBMRI scoring system (MRI-WIPE) for

BOX 1 | OMERACT HEMRIS recommendations for MRI acquisition, definitions and scoring of inflammatory and structural pathologies at the entheses (Adapted from Box 1, Mathew et al. (81)).

A. Core set of basic MRI sequences and imaging planes

MRI studies that intend to assess inflammatory and structural changes at entheses should include at least the following sequences:

- Short tau inversion recovery (STIR)/T2-weighted fat suppressed (T2wFS) images or, alternatively, gadolinium-enhanced T1-weighted fat suppressed images
- T1-weighted images without contrast injection (not mandatory if only inflammation is being assessed)

Suggested imaging planes for the heel region:

- Achilles tendon—Sagittal and preferably also axial
- Plantar fascia—Sagittal and preferably also coronal

B. Definitions and grades of inflammatory and structural pathologies at the Achilles tendon insertion and the plantar fascia insertion to the calcaneum

(Adapted from **Box 1**, Mathew et al. (81))

1. Intratendon/intrafascia hypersignal (STIR/T2FS)

Definition

Signal characteristics consistent with increased water content/inflammation within the tendon/fascia, close to its insertion[¥].

Grades

0: No intratendon/intrafascia hypersignal. ∗

1: Minimal intratendon/intrafascia hypersignal spots ∗ (≤25% of the tendon volume).

2: Moderate intratendon/intrafascia hypersignal ∗ (>25% and ≤50% of the tendon volume).

3: Severe intratendon/intrafascia hypersignal ∗ (>50% of the tendon volume).

[¥] For Achilles tendon: From the tendon insertion up to 2 cm proximal to the posterosuperior corner of calcaneum on all the available images. For Plantar fascia: From the fascia insertion up to 2 cm proximal to the anterior margin of the plantar tuberosity on all the available images.

2. Peritendon/perifascia hypersignal (STIR/T2FS)

Definition

Signal characteristics consistent with increased water content/inflammation in the soft tissues surrounding the tendon or fascia, close to its insertion.

Grades

0: No hypersignal. ∗

1: Minimal[†] (or mild) focal hypersignal. ∗

2: Moderate[†] hypersignal. ∗

3: Severe[†] hypersignal. ∗

[†] *By comparison with reference images (see Mathew et al. (81))*

∗ For Achilles tendon: From tendon insertion up to 2 cm proximal to the posterosuperior corner of calcaneum. For Plantar fascia: From fascia insertion up to 2 cm proximal to the anterior margin of the plantar tuberosity on all the available images.

3. Achilles tendon/plantar fascia calcaneal bone marrow edema

Definition

Bone marrow edema (BME) should be assessed in the bone from the entheseal insertion to a depth of 1 cm on all available images.

Grades:

The scale is 0-3, based on the proportion of bone with edema, compared to the "assessed bone volume", judged on all available images:

0: no edema.

1: 1–33% of the bone is edematous (i.e. BME occupying 1–33% of the assessed bone volume).

2: 34–66% of the bone is edematous.

3: 67–100% of the bone is edematous.

If the lesion is judged borderline, i.e., 1 vs. 2 or 2 vs. 3, lesion intensity may be considered. For example, if a lesion is borderline between 1 (mild) and 2 (moderate), it may be scored 1 (mild) if not judged intense. Similarly, if a lesion is borderline between 2 (moderate), and 3 (severe), it may be scored 3 (severe) if judged intense.

4. Retrocalcaneal bursitis (only relevant at Achilles tendon insertion)

Definition

Signal characteristics consistent with increased water content/inflammation in an above-normal sized bursa.

Grades

0: No hypersignal or maximal diameter of hyper-signal in the shorter of two perpendicular dimensions to be <0.25 cm.

1: Maximal diameter of hypersignal in the shorter of two perpendicular dimensions to be ≥0.25 cm to <0.5 cm.

2: Maximal diameter of hypersignal in the shorter of two perpendicular dimensions to be 0.5 cm to <1.0 cm.

3: Maximal diameter of hypersignal in the shorter of two perpendicular dimensions to be ≥1.0 cm.

5. Tendon/fascia thickening

Definition

Abnormal thickening of the tendon/fascia close to its insertion. ∗

Grades

0: None.

1: Mild.[†] ∗

2: Moderate.[†] ∗

3: Severe.[†] ∗

[†] *By comparison with reference images (see Mathew et al. (81))*

BOX 1 | Continued

∗ For Achilles tendon: Maximally 2 cm proximal from the postero-superior corner of calcaneum. For plantar fascia: Maximally 2 cm proximal to the anterior margin of the plantar tuberosity.

6. Achilles tendon/plantar fascia calcaneal enthesophyte

Definition

Abnormal bone formation at the insertion of tendon/fascia into the bone

Grades

0: None.
1: Small.†
2: Medium-sized.†
3: Large.†

† *By comparison with reference images (see Mathew et al. (81))*

7. Achilles tendon/plantar fascia calcaneal bone erosion

Definition

A sharply marginated bone lesion, with typical signal characteristics and a visible cortical break, located close to the tendon/fascia insertion.

Grades

0: None.
1: Small.†
2: Medium-sized.†
3: Large.†

† *By comparison with reference images (see Mathew et al. (81))*

peripheral arthritis and enthesitis, which depicted good reliability among the experienced readers (41, 42).

FUTURE PERSPECTIVES

Technical Advancements

New and potentially better MRI sequences have been described in SpA, but they need validation in longitudinal studies and clinical trials, applying novel and established MRI enthesitis measures in the same studies, to document validity and additional value as outcome measures. Also, their utility in assessing axial and peripheral entheses, and differentiating inflammatory from degenerative and other causes of enthesitis needs to be appraised in larger number of patients. The UTE sequence in high resolution MRI may help in better understanding of pathogenesis of different forms of enthesitis. There seems to be a window of opportunity in patients with SpA and PsA wherein early diagnosis and prompt initiation of therapy will be key in curtailing long-term damage (82). The utility of pre-clinical enthesitis visualized by MRI in prognostication of future PsA or SpA needs validation.

Refinement and Further Validation of MRI Scoring Systems

The recently developed MRI enthesitis indices should be further tested in clinical trials. Refinements may further improve their utility. Development of detailed MRI scoring systems for other regions than the heel may be relevant, even though it seems likely that clinical trials aiming to document the effect of a new drug on enthesitis will choose either a detailed evaluation of the most common region, like the heel, or an overall measure of enthesitis in the entire body, by WBMRI. Image resolution in WBMRI needs further enhancement for better visualization of peripheral entheses. The OMERACT MRI in arthritis Working Group is currently endeavoring on a modular approach in WBMRI to assess the overall inflammation burden at individual sites, thus further validating the WIPE-MRI scoring system. Based on the definitions laid out by the Working Group scoring systems for other regions need to be developed.

Role of MRI in Disease Prediction and Interception

In the transition phase toward the development of PsA, a subclinical phase with soluble biomarkers and imaging findings but no clinical sign is well recognized (83). Longitudinal studies with high-resolution MRI of hand or foot at baseline in psoriasis patients at risk of developing PsA are warranted to further validate the role of imaging in predicting PsA. For instance, WBMRI could be utilized in quantification of the global inflammatory burden of enthesitis in psoriasis patients at risk of developing PsA, and it could be investigated if this overall enthesitis burden is closely related with future development of PsA in the "at risk" patients.

Effect of treatment strategies to impede the development of PsA in psoriasis patients at risk may also be estimated. In the Interception in very early PsA (IVEPSA) study, MRI was used to assess inflammatory and structural changes in the joints at baseline and 24 weeks following secukinumab therapy (84). Most of the intervention studies with this objective focus on imaging synovitis in the hand joints. Nevertheless, technical advancements and validated scoring systems like the HEMRIS and WIPE-MRI can pave the way for harnessing MRI enthesitis as an outcome in future clinical trials targeting disease interception.

CONCLUSION

MRI has aided in understanding the pathogenesis, assessment of inflammatory and structural pathologies, monitoring, and prognostication of enthesitis in patients with SpA, including PsA. There is robust evidence for MRI as an adjunct to clinical examination in the assessment and follow up of enthesitis. Having a sound knowledge of its strengths and weaknesses, as compared to other imaging modalities, will facilitate optimal application of MRI in clinical trials, longitudinal studies and clinical practice.

AUTHOR'S NOTE

All the figures in this manuscript are unpublished, and original. These figures are based on the "MRI definitions of key entheseal pathologies" as described by the OMERACT MRI in arthritis Working Group in Table 1 of Mathew et al. (27).

AUTHOR CONTRIBUTIONS

AM prepared the first draft of the manuscript, and MØ critically reviewed and modified the manuscript. All authors contributed to the article and approved the submitted version.

FUNDING

AM is supported partly by a National Psoriasis Foundation Psoriatic Disease Research Fellowship.

ACKNOWLEDGMENTS

The authors would like to acknowledge Professor Iris Eshed, Sackler School of Medicine, Tel Aviv University, Tel Aviv, Israel for kindly providing images for **Figures 1**, **3**.

REFERENCES

1. Benjamin M, McGonagle D. The enthesis organ concept and its relevance to the spondyloarthropathies. *Adv Exp Med Biol.* (2009) 649:57–70. doi: 10.1007/978-1-4419-0298-6_4
2. Schett G, Lories RJ, D'Agostino MA, Elewaut D, Kirkham B, Soriano ER, et al. Enthesitis: from pathophysiology to treatment. *Nat Rev Rheumatol.* (2017) 13:731–41. doi: 10.1038/nrrheum.2017.188
3. McGonagle D, Lories RJU, Tan AL, Benjamin M. The concept of a 'synovio-entheseal complex' and its implications for understanding joint inflammation and damage in psoriatic arthritis and beyond. *Arthritis Rheum.* (2007) 56:2482–91. doi: 10.1002/art.22758
4. McGonagle D, Stockwin L, Isaacs J, Emery P. An enthesitis based model for the pathogenesis of spondyloarthropathy, additive effects of microbial adjuvant and biomechanical factors at disease sites. *J Rheumatol.* (2001) 28:2155–59.
5. de Winter JJ, van Mens LJ, van der Heijde D, Landewé R, Baeten DL. Prevalence of peripheral and extra-articular disease in ankylosing spondylitis versus non-radiographic axial spondyloarthritis: a meta-analysis. *Arthritis Res Ther.* (2016) 18:196. doi: 10.1186/s13075-016-1093-z
6. Polachek A, Li S, Chandran V, Gladman DD. Clinical enthesitis in a prospective longitudinal psoriatic arthritis cohort: incidence, prevalence, characteristics and outcome. *Arthritis Care Res (Hoboken).* (2017) 69:1685–91. doi: 10.1002/acr.23174
7. Carneiro S, Bortoluzzo A, Gonçalves C, da Silva JAB, Ximenes AC, Bertolo M, et al. Effect of enthesitis on 1505. Brazilian patients with spondyloarthritis. *J Rheumatol.* (2013) 40:1719–25. doi: 10.3899/jrheum.121145
8. Rezvani A, Bodur H, Ataman S, Kaya T, Bugdayci DS, Demir SE, et al. Correlations among enthesitis, clinical, radiographic and quality of life parameters in patients with ankylosing spondylitis. *Mod Rheumatol.* (2014) 24:651–56. doi: 10.3109/14397595.2013.850182
9. Bakewell C, Aydin SZ, Ranganath VK, Eder L, Kaeley GS. Imaging techniques: options for the diagnosis and monitoring of treatment of enthesitis in psoriatic arthritis. *J Rheumatol.* (2019). doi: 10.3899/jrheum.190512. [Epub ahead of print].
10. Poggenborg RP, Eshed I, Østergaard M, Sørensen IJ, Møller JM, Madsen OR, et al. Enthesitis in patients with psoriatic arthritis, axial spondyloarthritis and healthy subjects assessed by 'head-to-toe'whole body MRI and clinical examination. *Ann Rheum Dis.* (2015) 74:823–29. doi: 10.1136/annrheumdis-2013-204239
11. Baraliakos X, Conaghan PG, D'Agostino MA, Maksymowych W, Naredo E, Østergaard M, et al. Imaging in rheumatoid arthritis, psoriatic arthritis, axial spondyloarthritis, and osteoarthritis: an international viewpoint on the current knowledge and future research priorities. *Eur J Rheumatol.* (2019) 6:38–47. doi: 10.5152/eurjrheum.2018.18121
12. Mandl P, Navarro-Compán V, Terslev L, Aegerter P, van der Heijde D, D'Agostino MA, et al. EULAR recommendations for the use of imaging in the diagnosis and management of spondyloarthritis in clinical practice. *Ann Rheum Dis.* (2015) 74:1327–39. doi: 10.1136/annrheumdis-2014-206971
13. Rufai A, Ralphs JR, Benjamin M. Structure and histopathology of the insertional region of the human Achilles tendon. *J Orthop Res.* (1995) 13:585–93. doi: 10.1002/jor.1100130414
14. Benjamin M, McGonagle D. The anatomical basis for disease localisation in seronegative spondyloarthropathy at entheses and related sites. *J Anat.* (2001) 199:503–26. doi: 10.1046/j.1469-7580.2001.19950503.x
15. Benjamin M, Moriggl B, Brenner E, Emery P, McGonagle D, Redman S. The 'enthesitis organ' concept: why enthesopathies may not present as focal insertional disorders. *Arthritis Rheum.* (2004) 50:3306–13. doi: 10.1002/art.20566
16. McGonagle D. Imaging the joint and enthesis: insights into pathogenesis of psoriatic arthritis. *Ann Rheum Dis.* (2005) 64(Suppl II):ii58-ii60. doi: 10.1136/ard.2004.034264
17. McGonagle D, Marzo-Ortega H, O'Connor P, Gibbon W, Pease C, Reece R, et al. The role of biomechanical factors and HLA-B27 in magnetic resonance imaging-determined bone changes in plantar fascia enthesopathy. *Arthritis Rheum.* (2002) 46:489–93. doi: 10.1002/art.10125
18. McGonagle D, Gibbon W, O'Connor P, Green M, Pease C, Emery P. Characteristic magnetic resonance imaging entheseal changes in knee synovitis in spondyloarthropathy. *Arthritis Rheum.* (1998) 41:694–700. doi: 10.1002/1529-0131(199804)41:4<694::AID-ART17>3.0.CO;2-#
19. McGonagle D, Gibbon W, Emery P. Classification of inflammatory arthritis by enthesitis. *Lancet.* (1998) 352:1137–40. doi: 10.1016/S0140-6736(97)12004-9
20. Tan AL, Benjamin M, Toumi H, Grainger AJ, Tanner SF, Emery P, et al. The relationship between the extensor tendon enthesis and the nail in distal interphalangeal joint disease in psoriatic arthritis - a high-resolution MRI and histological study. *Rheumatology.* (2007) 46:253–56. doi: 10.1093/rheumatology/kel214
21. Tan AL, Fukuba E, Halliday NA, Tanner SF, Emery P, McGonagle D. High-resolution MRI assessment of dactylitis in psoriatic arthritis shows flexor tendon pulley and sheath-related enthesitis. *Ann Rheum Dis.* (2015) 74:185–89. doi: 10.1136/annrheumdis-2014-205839
22. Abrar DB, Schleich C, Nebelung S, Frenken M, Radke KL, Vordenbäumen S, et al. High-resolution MRI of flexor tendon pulleys using a 16-channel hand coil: disease detection and differentiation of psoriatic and rheumatoid arthritis. *Arthritis Res Ther.* (2020) 22:40. doi: 10.1186/s13075-020-2135-0
23. Mathew AJ, Coates LC, Danda D, Conaghan PG. Psoriatic arthritis: lessons from imaging studies and implications for therapy. *Exp Rev Clin Immunol.* (2017) 13:133–42. doi: 10.1080/1744666X.2016.1215245

24. Watad A, Eshed I, McGonaghle D. Lessons learned from imaging of enthesitis in psoriatic arthritis. *IMAJ.* (2017) 19:703–07.
25. Eshed I, Bollow M, McGonagle DG, Tan AL, Althoff CE, Asbach P, et al. MRI of enthesitis of the appendicular skeleton in spondyloarthritis. *Ann Rheum Dis.* (2007) 66:1553–59. doi: 10.1136/ard.2007.070243
26. Sudol-Szopinska I, Jurik AG, Eshed I, Lennart J, Grainger A, Østergaard M, et al. Recommendations of the ESSR arthritis subcommittee for the use of magnetic resonance imaging in musculoskeletal rheumatic diseases. *Semin Musculoskelet Radiol.* (2015) 19:396–411. doi: 10.1055/s-0035-1564696
27. Mathew AJ, Krabbe S, Eshed I, Gandjbakhch F, Bird P, Pedersen SJ, et al. The OMERACT MRI in enthesitis initiatives: definitions of key pathologies, suggested MRI sequences, and a novel heel enthesitis scoring system. *J Rheumatol.* (2019) 46:1232–38. doi: 10.3899/jrheum.181093
28. Poggenborg RP, Terslev L, Pedersen SJ, Østergaard M. Recent advances in imaging in psoriatic arthritis. *Ther Adv Musculoskel Dis.* (2011) 3:43–53. doi: 10.1177/1759720X10394031
29. Feydy A, Lavie-Brion M-C, Gossec L, Laive F, Guerini H, Nguyen C, et al. Comparative study of MRI and power Doppler ultrasonography of the heel in patients with spondyloarthritis with and without heel pain and in controls. *Ann Rheum Dis.* (2012) 71:498–503. doi: 10.1136/annrheumdis-2011-200336
30. Eshed I, Althoff CE, Feist E, Minden K, Schink T, Hamm B, et al. Magnetic resonance imaging of hindfoot involvement in patients with spondyloarthritides: comparison of low-field and high-field strength units. *Eur J Radiol.* (2008) 65:140–47. doi: 10.1016/j.ejrad.2007.03.009
31. Lambert RGW, Dhillon SS, Jhangri GS, Sacks J, Sacks H, Wong B, et al. High prevalence of symptomatic enthesopathy of the shoulder in ankylosing spondylitis: deltoid origin involvement constitutes a hallmark of disease. *Arthritis Rheum.* (2004) 51:681–90. doi: 10.1002/art.20681
32. Baraliakos X, Kiltz U, Appel H, Dybowski F, Igelmann M, Kalthoff L, et al. Chronic but not inflammatory changes at the Achilles' tendon differentiate patients with peripheral spondyloarthritis from other diagnoses - results from a prospective clinical trial. *RMD Open.* (2017) 3:e000541. doi: 10.1136/rmdopen-2017-000541
33. Tan AL, Grainger AJ, Tanner SF, Emery P, McGonagle D. A high-resolution magnetic resonance imaging study of distal interphalangeal joint arthropathy in psoriatic arthritis and osteoarthritis. Are they same? *Arthritis Rheumatol.* (2006) 54:1328–33. doi: 10.1002/art.21736
34. Jevtic V, Watt I, Rozman B, Kos-Golja M, Demsar F, Jarh O. Distinctive radiological features of small hand joints in rheumatoid arthritis and seronegative spondyloarthritis demonstrated by contrast-enhanced (Gd-DTPA) magnetic resonance imaging. *Skeletal Radiol.* (1995) 24:351–55. doi: 10.1007/BF00197064
35. Maksymowych WP, Lambert RGW, Østergaard M, Pedersen SJ, Machado PM, Weber U, et al. MRI lesions in the sacroiliac joints of patients with spondyloarthritis: an update of definitions and validation by the ASAS MRI working group. *Ann Rheum Dis.* (2019) 78:1550–58. doi: 10.1136/annrheumdis-2019-215589
36. Jans L, van Langenhove C, Van Praet L, Carron P, Elewaut D, van den Bosch F, et al. Diagnostic value of pelvic enthesitis on MRI of the sacroiliac joints in spondyloarthritis. *Eur Radiol.* (2014) 24:866–71. doi: 10.1007/s00330-013-3074-9
37. Hermann K-G A, Althoff CE, Schneider U, Zühlsdorf S, Lembcke A, Hamm B, et al. Spinal changes in patients with spondyloarthritis: comparison of MR imaging and radiographic appearances. *Radiographics.* (2005) 25:559–70. doi: 10.1148/rg.253045117
38. Lambert RGW, Pedersen SJ, Maksymowych WP, Chiowchanwisawakit P, Østergaard M. Active inflammatory lesions detected by magnetic resonance imaging in the spine of patients with spondyloarthritis - definitions, assessment system, and reference imaging set. *J Rheumatol.* (2009) 36 Suppl 84:3–17. doi: 10.3899/jrheum.090616
39. Eder L, Aydin SZ, Kaeley GS, Maksymowych WP, Østergaard M. Options for assessing joints and entheses in psoriatic arthritis by ultrasonography and magnetic resonance imaging: How to move forward. *J Rheumatol Suppl.* (2018) 94:44–7. doi: 10.3899/jrheum.180140
40. Mager A-K, Althoff CE, Sieper J, Hamm B, Hermann K-GA. Role of whole-body magnetic resonance imaging in diagnosing early spondyloarthritis. *Eur J Radiol.* (2009) 71:182–88. doi: 10.1016/j.ejrad.2009.04.051
41. Krabbe S, Eshed I, Gandjbakhch F, Pedersen SJ, Bird P, Mathew AJ, et al. Development and validation of an OMERACT MRI whole-body score for inflammation in peripheral joints and entheses in inflammatory arthritis (MRI-WIPE). *J Rheumatol.* (2019) 46:1215–21. doi: 10.3899/jrheum.181084
42. Østergaard M, Eshed I, Althoff CE, Poggenborg RP, Diekhoff T, Krabbe S, et al. Whole-body magnetic resonance imaging in inflammatory arthritis: systematic literature review and first steps toward standardization and an OMERACT scoring system. *J Rheumatol.* (2017) 44:1699–705. doi: 10.3899/jrheum.161114
43. Poggenborg RP, Pedersen SJ, Eshed I, Sørensen IJ, Møller JM, Madsen OR, et al. Head-to-toe whole-body MRI in psoriatic arthritis, axial spondyloarthritis and healthy subjects: first steps towards global inflammation and damage scores of peripheral and axial joints. *Rheumatology.* (2015) 54:1039–40. doi: 10.1093/rheumatology/keu439
44. Weckbach S, Schewe S, Michaely HJ, Steffinger D, Reiser MF, Glaser C. Whole-body MR imaging in psoriatic arthritis: additional value of therapeutic decision. *Eur J Radiol.* (2011) 77:149–55. doi: 10.1016/j.ejrad.2009.06.020
45. Althoff CE, Sieper J, Song I-H, Haibel H, Weiß A, Diekhoff T, et al. Active inflammation and structural change in early active axial spondyloarthritis as detected by whole-body MRI. *Ann Rheum Dis.* (2013) 72:967–73. doi: 10.1136/annrheumdis-2012-201545
46. Weber U, Lambert RGW, Rufibach K, Maksymowych WP, Hodler J, Zejden A, et al. Anterior chest wall inflammation by whole-body magnetic resonance imaging in patients with spondyloarthritis: lack of association between clinical and imaging findings in a cross-sectional study. *Arthritis Res Ther.* (2012) 14:R3. doi: 10.1186/ar3551
47. Marzo-Ortega H, McGonagle D, O'Connor P, Emery P. Efficacy of etanercept in the treatment of the entheseal pathology in resistant spondyloarthropathy. *Arthritis Rheum.* (2001) 44:2112–17. doi: 10.1002/1529-0131(200109)44:9<2112::AID-ART363>3.0.CO;2-H
48. Tan AL, Marzo-Ortega H, O'Connor P, Fraser A, Emery P, McGonagle D. Efficacy of anakinra in active ankylosing spondylitis: a clinical and magnetic resonance imaging study. *Ann Rheum Dis.* (2004) 63:1041–45. doi: 10.1136/ard.2004.020800
49. Karpitschka M, Godau-Kellner P, Kellner H, Horng A, Theisen D, Glaser C, et al. Assessment of therapeutic response in ankylosing spondylitis patients undergoing anti-tumour necrosis factor therapy by whole-body magnetic resonance imaging. *Eur Radiol.* (2013) 23:1773–84. doi: 10.1007/s00330-013-2794-1
50. Krabbe S, Eshed I, Sørensen IJ, Jensen B, Møller JM, Balding L, et al. Whole-body magnetic resonance imaging inflammation in peripheral joints and entheses in axial spondyloarthritis: distribution and changes during adalimumab treatment. *J Rheumatol.* (2020) 47:50–8. doi: 10.3899/jrheum.181159
51. Krabbe S, Østergaard M, Eshed I, Sørensen IJ, Jensen B, Møller JM, et al. Whole-body magnetic resonance imaging in axial spondyloarthritis: reduction of sacroiliac, spinal and entheseal inflammation in a placebo-controlled trial of adalimumab. *J Rheumatol.* (2018) 45:621–29. doi: 10.3899/jrheum.170408
52. Eder L, Polachek A, Rosen CF, Chandran V, Cook R, Gladman DD. The development of psoriatic arthritis in patients with psoriasis is preceded by a period of nospecific musculoskeletal symptoms. A prospective cohort study. *Arthritis Rheumatol.* (2017) 69:622–29. doi: 10.1002/art.39973
53. Zabotti A, McGonagle DG, Giovannini I, Errichetti E, Zuliani F, Zanetti A, et al. Transition phase towards psoriatic arthritis: clinical and ultrasonographic characterization of psoriatic arthralgia. *RMD Open.* (2019) 5:e001067. doi: 10.1136/rmdopen-2019-001067
54. Elnady B, El Shaarawy NK, Dawoud NM, Elkhouly T, Desouky DE, El Shafey EN, et al. Subclinical synovitis and enthesitis in psoriasis patients and controls by ultrasonography in Saudi Arabia: incidence of psoriatic arthritis during two years. *Clin Rheumatol.* (2019) 38:1627–35. doi: 10.1007/s10067-019-04445-0
55. Takata T, Takahashi A, Taniguchi Y, Terada Y, Sano S. Detection of asymptomatic enthesitis in psoriasis patients: an onset of psoriatic arthritis? *J Dermatol.* (2016) 43:650–54. doi: 10.1111/1346-8138.13212
56. Emad Y, Ragab Y, Bassyouni I, Moawayh O, Fawzy M, Saad A, et al. Enthesitis and related changes in knees in seronegative spondyloarthropathies and skin psoriasis: magnetic resonance imaging case-control study. *J Rheumatol.* (2010) 37:1709–17. doi: 10.3899/jrheum.100068

57. Erdem CZ, Tekin NS, Sarikaya S, Erdem LO, Gulec S. MR imaging features of foot involvement in patients with psoriasis. *Eur J Radiol.* (2008) 67:521–25. doi: 10.1016/j.ejrad.2007.08.005
58. Simon D, Tascilar K, Kleyer A, Bayat S, Kampylafka E, Sokolova M, et al. Structural enthesitis lesions in patients with psoriasis are associated with an increased risk of progression to psoriatic arthritis. *Arthritis Rheumatol.* (2020). doi: 10.1002/art.41239. [Epub ahead of print].
59. Faustini F, Simon D, Oliveira I, Kleyer A, Haschka J, Englbrecht M, et al. Subclinical joint inflammation in patients with psoriasis without concomitant psoriatic arthritis: a cross-sectional and longitudinal analysis. *Ann Rheum Dis.* (2016) 75:2068–74. doi: 10.1136/annrheumdis-2015-208821
60. Smolen JS, Schöls M, Braun J, Dougados M, FitzGerald O, Gladman DD, et al. Treating axial spondyloarthritis and peripheral spondyloarthritis, especially psoriatic arthritis, to target: 2017 update of recommendations by an international task force. *Ann Rheum Dis.* (2018) 77:3–17. doi: 10.1136/annrheumdis-2017-211734corr1
61. Coates LC, Kavanaugh A, Mease PJ, Soriano ER, Laura Acosta-Felquer M, Armstrong AW, et al. Group for research and assessment of psoriasis and psoriatic arthritis 2015 treatment recommendations for psoriatic arthritis. *Arthritis Rheumatol.* (2016) 68:1060–71. doi: 10.1002/art.39573
62. Gossec L, Smolen JS, Ramiro S, de Wit M, Cutolo M, Dougados M, et al. European league against rheumatism (EULAR) recommendations for the management of psoriatic arthritis with pharmacological therapies: 2015 update. *Ann Rheum Dis.* (2016) 75:499–510. doi: 10.1136/annrheumdis-2015-208337
63. Orbai AM, de Wit M, Mease PJ, Callis Duffin K, Elmamoun M, Tillet W, et al. Updataing the psoriatic arthritis (PsA) core domain set: a report from the PsA workshop at OMERACT (2016). *J Rheumatol.* (2017) 44:1522–28. doi: 10.3899/jrheum.160904
64. Dougados M, Combe B, Braun J, Landewè R, Sibilia J, Cantagrel A, et al. A randomised, multicentre, double-blind, placebo-controlled trial of etanercept in adults with refractory heel enthesitis in spondyloarthritis: the HEEL trial. *Ann Rheum Dis.* (2010) 69:1430–35. doi: 10.1136/ard.2009.121533
65. ClinicalTrials.gov. *Study of Efficacy and Safety of Secukinumab in Psoriatic Arthritis and Axial Spondyloarthritis Patients With Active Enthesitis Including One Achilles Tendon Site (ACHILLES)*. Available online at: https://clinicaltrials.gov/ct2/show/record/NCT02771210?term=NCT02771210&rank=1
66. Song IH, Hermann KG, Haibel H, Althoff CE, Listing J, Burmester GR, et al. Effects of etanercept versus sulfasalazine in early axial spondyloarthritis on active inflammatory lesions as detected by whole-body MRI (ESTHER): a 48-week randomised controlled trial. *Ann Rheum Dis.* (2011) 70:590–96. doi: 10.1136/ard.2010.139667
67. Pagnini I, Savelli S, Matucci-Cerinic M, Fonda C, Cimaz R, Simonini G. Early predictors of juvenile sacroiliitis in enthesitis-related arthritis. *J Rheumatol.* (2010) 37:2395–401. doi: 10.3899/jrheum.100090
68. Lin C, MacKenzie JD, Courtier JL, Gu JT, Milojevic D. Magnetic resonance imaging findings in juvenile spondyloarthropathy and effects of treatment observed on subsequent imaging. *Pediatr Rheumatol Online J.* (2014) 12:25. doi: 10.1186/1546-0096-12-25
69. Herregods N, Dehoorne J, Pattyn E, Jaremko JL, Baraliakos X, Elewaut D, et al. Diagnostic value of pelvic enthesitis on MRI of the sacroiliac joints in enthesitis related arthritis. *Pedatr Rheumatol Online J.* (2015) 13:46. doi: 10.1186/s12969-015-0045-5
70. Panwar J, Patel H, Tolend M, Akikusa J, Herregods N, Highmore K, et al. Toward developing a semiquantitative whole body-MRI scoring for juvenile idiopathic arthritis: critical appraisal of the state of the art, challenges, and opportunities. *Acad Radiol.* (2020). doi: 10.1016/j.acra.2020.01.022. [Epub ahead of print].
71. Otobo TM, Conaghan PG, Maksymowych WP, van der Heijde D, Weiss P, Sudol-Szopinska I, et al. Preliminary definitions for sacroiliac joint pathologies in the OMERACT juvenile idiopathic arthritis MRI score (OMERACT JAMRIS-SIJ). *J Rheumatol.* (2019) 46:1192–97. doi: 10.3899/jrheum.181115
72. Kehl AS, Corr M, Weisman MH. Enthesitis: new insights into pathogenesis, diagnostic modalities, and treatment. *Arthritis Rheumatol.* (2016) 68:312–22. doi: 10.1002/art.39458
73. Mathew AJ, Krabbe S, Kirubakaran R, Barr AJ, Conaghan PG, Bird P, et al. Utility of magnetic resonance imaging (MRI) in diagnosing and monitoring enthesitis in patients with spondyloarthritis: a systametic literature review. *J Rheumatol.* (2019) 46:1207–14. doi: 10.3899/jrheum.181083
74. Østergaard M, Eder L, Christiansen SN, Kaeley GS. Imaging in the diagnosis and management of peripheral psoriatic arthritis - the clinical utility of magnetic resonance imaging and ultrasonography. *Best Pract Res Clin Rheumatol.* (2016) 30:624–37. doi: 10.1016/j.berh.2016.08.012
75. Kwee TC. Can whole-body MRI replace (18)F-fluorodeoxyglucose PET/CT? *Lancet Oncol.* (2014) 15:243–44. doi: 10.1016/S1470-2045(14)70037-3
76. Gezmis E, Donmez FY, Agildere M. Diagnosis of early sacroiliitis in seronegative spondyloarthropathies by DWI and correlation of clinical and laboratory findings with ADC values. *Eur J Radiol.* (2013) 82:2316–21. doi: 10.1016/j.ejrad.2013.08.032
77. Vendhan K, Bray TJ, Atkinson D, Punwani S, Fisher C, Sen D, et al. A diffusion-based quantification technique for assessment of sacroiliitis in adolescents with enthesitis-related arthritis. *Br J Radiol.* (2016) 89:20150775. doi: 10.1259/bjr.20150775
78. Lecouvet FE, Maren NV, Collette L, Michoux N, Triqueneaux P, Stoenoiu M, et al. Whole-body MRI in spondyloarthritis (SpA): preliminary results suggest that DWI outperforms STIR for lesion detection. *Eur Radiol.* (2018) 28:4163–73. doi: 10.1007/s00330-018-5377-3
79. Chen B, Zhao Y, Cheng X, Ma Y, Chang EY, Kavanaugh A, et al. Three-dimensional ultrashort echo time cones (3D UTE-Cones) magnetic resonance imaging of entheses and tendons. *Magn Reson Imaging.* (2018) 49:4–9. doi: 10.1016/j.mri.2017.12.034
80. Chen B, Cheng X, Dorthe EW, Zhao Y, D'Lima D, Bydder GM, et al. Evaluation of normal cadaveric achilles tendon and enthesis with ultrashort echo time (UTE) magnetic resonance imaging and indentation testing. *NMR Biomed.* (2019) 32:e4034. doi: 10.1002/nbm.4034
81. Mathew AJ, Krabbe S, Eshed I, Lambert RGW, Laredo JD, Maksymowych WP, et al. Atlas of the OMERACT heel enthesitis MRI scoring system (HEMRIS). *RMD Open.* (2020) 6:e001150. doi: 10.1136/rmdopen-2019-001150
82. Haroon M, Gallagher P, Fitzgerald O. Diagnostic delay of more than 6 months contributes to poor radiographic and functional outcome in psoriatic arthritis. *Ann Rheum Dis.* (2015) 74:1045–50. doi: 10.1136/annrheumdis-2013-204858
83. Scher JU, Ogdie A, Merola JF, Ritchlin C. Preventing psoriatic arthritis: focusing on patients with psoriasis at increased risk of transition. *Nat Rev Rheumatol.* (2019) 15:153–56. doi: 10.1038/s41584-019-0175-0
84. Kampylafka E, Simon D, d'Oliveira I, Linz C, Lerchen V, Englbrecht M, et al. Disease interception with interleukin-17 inhibition in high-risk psoriasis patients with subclinical joint inflammation - data from the prospective IVEPSA study. *Arthritis Res Ther.* (2019) 21:178. doi: 10.1186/s13075-019-1957-0

Conflict of Interest: The authors declare that the research was conducted in the absence of any commercial or financial relationships that could be construed as a potential conflict of interest.

frontiers in Medicine

BRIEF RESEARCH REPORT
published: 03 July 2020
doi: 10.3389/fmed.2020.00319

Performance of Ultrasonography Compared to Conventional Radiography for the Diagnosis of Osteoarthritis in Patients With Knee Pain

Martin Brom[1], Ignacio J. Gandino[1], Johana B. Zacariaz Hereter[1], Marina Scolnik[1], Florencia B. Mollerach[1], Leandro G. Ferreyra Garrott[1], Josefina Marin[1], Santiago O. Ruta[1], Javier E. Rosa[1], Ricardo D. García-Mónaco[2] and Enrique R. Soriano[1]*

[1] Rheumatology Department, Hospital Italiano de Buenos Aires, Buenos Aires, Argentina, [2] Radiology Department, Hospital Italiano de Buenos Aires, Buenos Aires, Argentina

OPEN ACCESS

Edited by:
Raj Sengupta, Royal National Hospital for Rheumatic Diseases, United Kingdom

Reviewed by:
Paul Studenic, Medical University of Vienna, Austria
Filipa Farinha, University College London, United Kingdom

***Correspondence:**
Martin Brom
martin.brom@hospitalitaliano.org.ar

Specialty section:
This article was submitted to Rheumatology, a section of the journal Frontiers in Medicine

Received: *22 March 2020*
Accepted: *01 June 2020*
Published: *03 July 2020*

Citation:
Brom M, Gandino IJ, Zacariaz Hereter JB, Scolnik M, Mollerach FB, Ferreyra Garrott LG, Marin J, Ruta SO, Rosa JE, García-Mónaco RD and Soriano ER (2020) Performance of Ultrasonography Compared to Conventional Radiography for the Diagnosis of Osteoarthritis in Patients With Knee Pain. Front. Med. 7:319. doi: 10.3389/fmed.2020.00319

Purpose: To investigate the performance of ultrasonography (US) for the detection of knee osteoarthritis (OA) in patients suffering from knee pain, compared to conventional radiographs.

Methods: Cross-sectional study performed at a university teaching hospital. Consecutive patients complaining of unilateral or bilateral mechanical knee pain who signed an informed consent were included. All patients underwent simultaneously an ultrasonographic and a radiographic evaluation of the knee. Exclusion criteria were age under 18 years, prior diagnosis of knee OA, diagnosis of inflammatory arthritis, history of knee surgery or trauma, severe knee deformities, and corticosteroid injection within the last 2 months. The diagnostic properties of US for the detection of knee OA were evaluated using radiological data as the reference method. Evaluated test properties were sensitivity, specificity, positive predictive value (PPV), negative predictive value (NPV), and the positive and negative likelihood ratio (LR+ and LR–).

Results: Three-hundred twenty-two knees (281 patients) were included. Radiographic degenerative changes were present in 56.8% (183) of the evaluated knees. Regarding the diagnostic properties of the US, the presence of either osteophytes or the compromise of the femoral hyaline cartilage had the best sensitivity to detect OA (95%), with a NPV of 92% and a LR– of 0,07, while the combined identification of osteophytes and compromise of the femoral hyaline cartilage had the best specificity (94%), with 94% PPV and a LR+ of 13.

Conclusion: US demonstrated an excellent sensitivity with an adequate specificity for the detection of radiographic knee OA.

Keywords: radiography (D011859), ultrasonography (D014463), osteoarthritis (D010003), knee osteoarthritis (D020370), diagnostic imaging (D003952)

INTRODUCTION

Osteoarthritis (OA) is the most prevalent joint disorder, with a global age-standardized prevalence of knee OA of 3.8% (1), and it is one of the leading causes of global disability (2). It is characterized by mechanical joint pain and stiffness, and the most frequently affected joints are knees, hips, hands, and spine (3).

Although OA may be diagnosed merely by the presence of typical symptoms and signs in the at-risk group of patients (2, 4, 5), additional testing might be needed to rule out alternative diagnoses and especially, to stratify the degree of joint structural damage. The most frequently used imaging tool is conventional radiography since it is a widely available and cheap method that allows the detection of OA's classical features: marginal osteophytes, joint space narrowing, subchondral sclerosis, and cysts (5–7).

On the other hand, the use of X-Rays in OA has several limitations. Early diagnosis of OA cannot be achieved by this method since X-Rays can only identify late, non-reversible joint damage. Previous studies demonstrated that among patients with knee pain suspicious of OA, only 50% will have radiographic changes of OA (3), and moreover, there is only a moderate association between the degree of knee OA and the level of pain (4, 8) and only about 50% of the patients with knee OA experience pain (9). Pain in knee OA is multifactorial and it is influenced by mechanical, structural, inflammatory, bone-related, neurological and psychological factors (10, 11).

Considering the previously listed limitations of conventional radiography, it is important to have more sensitive tools for the diagnosis and assessment of knee OA. The most sensitive and specific diagnostic tool up to date is Magnetic Resonance Imaging (MRI), since it can evaluate all articular and periarticular structures—including bone marrow, and even biochemical composition of the articular tissues—but its use is limited to research due to the high cost and unavailability of MRI, and its contraindication on certain patients such as those with cardiac pacemakers (12).

Ultrasonography (US) is an attractive tool since, in contrast to conventional radiography, it can evaluate periarticular soft tissue structures and the presence of synovitis, and compared to MRI, it is a safe, inexpensive and less time-consuming method (13). Although US is an operator-dependent method, several studies demonstrated that the use of US in knee OA has good construct validity and moderate to good interobserver reliability (14–17).

In this context, we decided to investigate the properties and performance of US for the detection of knee OA in patients suffering from knee pain, compared to the conventional radiographic study of the knee.

PATIENTS AND METHODS

Cross-sectional study performed at a university teaching hospital in Buenos Aires, Argentina. Consecutive patients complaining of unilateral or bilateral mechanical knee pain who signed an informed consent were included. All patients underwent US and X-Ray evaluation of the knee. Exclusion criteria were age under 18 years, prior diagnosis of knee OA, diagnosis of inflammatory arthritis, history of knee surgery or trauma, severe knee deformities, and corticosteroid injection within the last 2 months. All procedures were in accordance with the ethical standards of the institutional research committee, and with the 1964 Helsinki declaration and its later amendments or comparable ethical standards.

US examinations were performed by 2 experienced rheumatologist ultrasonographists (SOR and JER), blinded to clinical and radiological data, using a MyLab 70 machine (Esaote) provided with a multi-frequency linear transducer (4–13 MHz). Patients were not allowed to speak to the ultrasonographist about their clinical condition. A standardized scanning method was adopted in order to evaluate the presence of osteophytes and degenerative femoral hyaline cartilage involvement. Patients were placed in supine position, and knees were evaluated in extension and in 30° flexion. Osteophytes were defined as protrusions at the joint margin seen in two planes. The degenerative femoral hyaline cartilage was defined by the presence of at least two of the following: loss of sharpness of the cartilage margins, loss of homogeneity of the cartilage layer or cartilage thinning (<2 mm) focal or extend to the entire cartilaginous layer.

Weight-bearing anteroposterior and lateral knee radiographs, acquired simultaneously to the US, were read by an experienced rheumatologist, blinded to the clinical and US data, who determined the presence or absence of radiological degenerative changes and classified the severity of knee OA using Kellgren-Lawrence (KL) grading scale (18).

Statistical analysis was performed using STATA V.14.1. Continuous variables were reported as mean and standard deviation (SD), according to the variable distribution. The Chi^2 Test was used for the comparison of the US features (osteophytes and hyaline cartilage involvement) with the radiographic KL grades, with a $p < 0.05$ considered significant. The diagnostic properties of US for the detection of osteophytes and degenerative cartilage involvement in the knee were evaluated using radiological data as the reference method. Evaluated test properties were sensitivity, specificity, positive predictive value (PPV), negative predictive value (NPV), and the positive and negative likelihood ratio (LR+ and LR–).

RESULTS

Two-hundred eighty-one patients were included, with a female-to-male ratio of 3:1 and a mean age of 64 years (*SD* 17). A total of 322 knees were evaluated since 41 patients complained of bilateral knee pain.

Table 1 shows the frequency of the US abnormal findings stratified by the radiographic extent of knee damage according to KL grading. Radiographic degenerative changes were present in 56.8% (183) of the evaluated knees, being KL 3 the most frequently observed grade. Regarding the US assessment, the presence of osteophytes or femoral hyaline cartilage involvement was more frequent in those knees with radiographic changes of OA, regardless of the severity according to the KL grading scale ($p < 0.001$ both for hyaline cartilage and osteophytes between

TABLE 1 | Frequency of the US abnormal findings according to radiographic features of knee OA.

	Presence of radiological degenerative changes, *n*: 183				Absence of radiological degenerative changes
	KL 1, *n*: 34	**KL 2, *n*: 20**	**KL 3, *n*: 115**	**KL 4, *n*: 14**	**KL 0, *n*: 139**
US femoral hyaline cartilage involvement, % (CI 95%)	77 (64–92)	70 (49–90)	97 (93–99)	100	24 (17–31)
US osteophytes, % (CI 95%)	62 (44–73)	90 (76–100)	85 (79–92)	100	14 (8–20)
US femoral hyaline cartilage involvement or US osteophytes, % (CI 95%)	92 (82–100)	100	95 (91–99)	100	24 (16–31)

US, ultrasound; OA, osteoarthritis; KL, Kellgren-Lawrence.

TABLE 2 | Diagnostic test properties of the US abnormal findings for the detection of knee OA using radiological data as the reference method.

	Sensitivity	**Specificity**	**PPV**	**NPV**	**LR+**	**LR-**
US femoral hyaline cartilage involvement, % (CI 95%)	90 (86–95)	75 (68–83)	84 (79–89)	85 (78–91)	3.6	0.13
US osteophytes, % (CI 95%)	82 (77–88)	86 (80–92)	89 (84–94)	78 (71–84)	5.85	0.21
US femoral hyaline cartilage involvement or US osteophytes, % (CI 95%)	95 (92–98)	76 (69–83)	85 (80–90)	92 (87–97)	3.96	0.07
US femoral hyaline cartilage and US osteophytes, % (CI 95%)	75 (68–81)	94 (89–97.5)	94 (89–97.6)	74 (67–80)	13	0.27

US, ultrasonography; PPV, positive predictive value; NPV, negative predictive value; CI, confidence interval; LR+, positive likelihood ratio; LR–, negative likelihood ratio.

all KL grades with radiographic damage and KL0, respectively). The damage of the femoral hyaline cartilage was significantly more frequently found in knees with radiographic knee OA KL 3 and 4 (97 and 100%, respectively; $p < 0.001$ between KL3 and KL4 compared with KL1), while the frequency of osteophytes detected by US was lowest in KL 1 (62%) compared to the other grades ($p = 0.0067$, and 0.0027 vs. KL3 and KL4, respectively). Noteworthy, 24% of the evaluated knees didn't show radiographic degenerative changes (KL 0) but did have ultrasonographic findings of knee OA. On the other hand, none of the patients with radiographic degenerative changes (KL $\geq$1) had a normal US.

Diagnostic test properties of the US abnormal findings for the detection of knee OA using radiological data as the reference method are shown in **Table 2**. The presence of osteophytes or the compromise of the femoral hyaline cartilage had the best sensitivity to detect OA (95%), with a NPV of 92% and a LR– of 0.07. The identification of osteophytes and compromise of the femoral hyaline cartilage the best specificity (94%), with 94% PPV and a LR+ of 13.

DISCUSSION

This cross-sectional study shows that US has very good diagnostic properties compared to the standard method, conventional radiography, for the diagnosis of knee OA. The definition and diagnosis of osteoarthritis has changed over time, driven by an increased understanding of the disease and the development of new technologies, which led to the appearance of concepts such as early OA (19). Ultrasonography has growing evidence as an alternative imaging method for the assessment of OA (14). Unlike conventional radiography, US has the ability to visualize articular and periarticular soft tissue structures such as cartilage thickness and soft tissues alterations such as joint effusion, synovitis, Baker's cyst, tendinopathy, bursitis, and meniscal lesions (8, 20–22). On the other hand, and in contrast to MRI, it is a widely available and inexpensive imaging method (13). Additionally, US features such as joint space narrowing and synovitis have been found to better correlate with pain than structural damage (23, 24), and US might be good tool to measure changes in clinical trials (13, 14, 25).

In this context we decided to perform a study to evaluate the diagnostic properties of US for the detection of knee OA in patients who sought medical attention due to knee pain. Although US allows the assessment of many soft tissue structures, the ultrasonographic evaluation of the knees in this cohort was limited to the presence of osteophytes and hyaline cartilage involvement since these are the only joint changes that can be observed both by US and conventional radiography, and therefore, these are the features that allow the comparison of the diagnostic properties of these 2 imaging methods.

Several studies have shown US to be reliable and valid for the evaluation of cartilage pathology in OA, and especially for large joints such as the knee (26–29), and US has demonstrated strong criterion validity with cartilage histology (25). The knee's hyaline

cartilage has a normal thickness of 2 mm, and superficial regions can easily be evaluated by US (26, 27).

In this cohort, 56.8% of the patients with knee pain had radiological degenerative changes, and in concordance with previous studies (20, 30), KL 3 was the most frequently identified group. Interestingly, 24% of the patients without radiographic degenerative changes presented ultrasonographic findings of OA. Whether this represents a false positive result of US or the diagnosis of early OA can only be elucidated by following these knees in time, and cannot be answer by this study.

Previous studies demonstrated that US is as sensitive as MRI and more sensitive than conventional radiography for the detection of osteophytes (25, 26, 31–34), and showed a high intra and inter-reader agreement (26–28, 35). In this cohort, ultrasonography had a sensitivity of 95% (CI95% 92–98) for the detection of hyaline cartilage involvement or osteophytes, and a specificity of 86% (CI95% 80–92) for the identification of osteophytes, compared to conventional radiography. Using both features, as expected, increased specificity but decreased sensitivity (**Table 2**). On the other hand, if we had used US as gold standard, conventional radiography would have shown sensitivity of 83% and specificity of 93%.

There are some limitations that need mentioning. First, there are limitations that are inherent to the method: The visualization of the cartilage may be hindered by the acoustic window, which depends on the patient's joint anatomy, and US is an operator-dependent method (15). Second, inter and intraobserver agreement was not evaluated, which might affect reliability. Nevertheless, the participating ultrasonographists are part of the same group and share the same concepts on acquisition and reading of images. In addition, they have demonstrated a very good level of agreement (85%) in a previous studies (36). Third, although we are aware that looking for a correlation between the images and pain or clinical characteristics such as Body Mass Index (BMI), etc. would enrich the study, since the objective was the comparison of the diagnostic properties of US and radiographs and patients did not undergo an *ad hoc* physical examination, this was not possible. Finally, since this is a cross-sectional study, we cannot know if the changes found by US in knees with normal radiographs (KL 0) are false positive results or if it is an early diagnosis of OA.

On the other hand, this study has several strengths. This is a large cohort of patients, who were included consecutively and unselected. All patients were evaluated by 2 rheumatologists expert in ultrasonography, who were blinded to the KL grading. Likewise, the radiographic evaluators were expert rheumatologists, blinded to the US findings.

In conclusion, US demonstrated an excellent sensitivity with an adequate specificity for the detection of radiographic knee OA. The identification by US of femoral hyaline cartilage involvement or osteophytes showed the best sensitivity while the presence of both osteophytes and femoral hyaline cartilage showed the best specificity. We believe that ultrasonography is a valid method for the evaluation of patients with knee pain when OA is suspected. Its capability to identify early knee OA in patients with non-radiographic knee OA (KL 0) should be evaluated using as a more sensitive method, such as MRI, as the comparator group.

DATA AVAILABILITY STATEMENT

The raw data supporting the conclusions of this article will be made available by the authors, without undue reservation.

ETHICS STATEMENT

The studies involving human participants were reviewed and approved by Hospital Italiano de Buenos Aires. The patients/participants provided their written informed consent to participate in this study.

AUTHOR'S NOTE

This study was previously published as an abstract after being presented at an ACR meeting (37) (https://acrabstracts.org/abstract/radiographic-knee-osteoarthritis-in-patients-complaining-of-knee-pain-ultrasound-features/) and a PANLAR meeting (38) (https://journals.lww.com/jclinrheum/Fulltext/2018/04001/Abstracts_20th_PANLAR_Meeting__Buenos_Aires,0.1.aspx).

AUTHOR CONTRIBUTIONS

MB, IG, JZ, MS, FM, LF, JM, SR, JR, RG-M, and ES meet the ICMJE 4 criteria and the journal authorship criteria, and the final manuscript has been read and approved by all the authors.

REFERENCES

1. Cross M, Smith E, Hoy D, Nolte S, Ackerman I, Fransen M, et al. The global burden of hip and knee osteoarthritis: estimates from the Global Burden of Disease 2010 study. *Ann Rheum Dis.* (2014) 73:1323–30. doi: 10.1136/annrheumdis-2013-204763
2. Hunter DJ, Bierma-Zeinstra S. Osteoarthritis. *Lancet.* (2019) 393:1745–59. doi: 10.1016/S0140-6736(19)30417-9
3. Arden N, Nevitt MC. Osteoarthritis: epidemiology. *Best Pract Res Clin Rheumatol.* (2006) 20:3–25. doi: 10.1016/j.berh.2005.09.007
4. Bedson J, Croft PR. The discordance between clinical and radiographic knee osteoarthritis: a systematic search and summary of the literature. *BMC Musculoskelet Disord.* (2008) 9:116. doi: 10.1186/1471-2474-9-116
5. National Clinical Guideline Centre (UK). *Osteoarthritis: Care and Management in Adults*. National Institute for Health and Care Excellence (2014).
6. Hayashi D, Roemer FW, Guermazi A. Imaging for osteoarthritis. *Ann Phys Rehabil Med.* (2016) 59:161–9. doi: 10.1016/j.rehab.2015.12.003
7. Roemer FW, Eckstein F, Hayashi D, Guermazi A. The role of imaging in osteoarthritis. *Best Pract Res Clin Rheumatol.* (2014) 28:31–60. doi: 10.1016/j.berh.2014.02.002
8. Bevers K, Bijlsma JW, Vriezekolk JE, van den Ende CH, den Broeder AA. Ultrasonographic features in symptomatic osteoarthritis of the knee and relation with pain. *Rheumatology.* (2014) 53:1625–9. doi: 10.1093/rheumatology/keu030

9. Salaffi F, Ciapetti A, Carotti M. The sources of pain in osteoarthritis: a pathophysiological review. *Reumatismo.* (2014) 66:57–71. doi: 10.4081/reumatismo.2014.766
10. Claessens AAMC, Schouten JSAG, van den Ouweland FA, Valkenburg HA. Do clinical findings associate with radiographic osteoarthritis of the knee? *Ann Rheum Dis.* (1990) 49:771–4. doi: 10.1136/ard.49.10.771
11. Bijlsma JWJ, Berenbaum F, Lafeber FPJG. Osteoarthritis: an update with relevance for clinical practice. *Lancet.* (2011) 377:2115–26. doi: 10.1016/S0140-6736(11)60243-2
12. Hayashi D, Roemer FW, Guermazi A. Recent advances in research imaging of osteoarthritis with focus on MRI, ultrasound and hybrid imaging. *Clin Exp Rheumatol.* (2018) 36(Suppl. 1):43–52.
13. Bevers K, Bijlsma JWJ, Vriezekolk JE, van den Ende CHM, den Broeder AA. The course of ultrasonographic abnormalities in knee osteoarthritis: 1 year follow up. *Osteoarthr Cartil.* (2014) 22:1651–6. doi: 10.1016/j.joca.2014.06.012
14. Keen HI, Wakefield RJ, Conaghan PG. A systematic review of ultrasonography in osteoarthritis. *Ann Rheum Dis.* (2009) 68:611–9. doi: 10.1136/ard.2008.102434
15. Möller I, Bong D, Naredo E, Filippucci E, Carrasco I, Moragues C, et al. Ultrasound in the study and monitoring of osteoarthritis. *Osteoarthr Cartil.* (2008) 16(Suppl. 3):S4–7. doi: 10.1016/j.joca.2008.06.005
16. Bevers K, Zweers MC, van den Ende CHM, Martens HA, Mahler E, Bijlsma JWJ, et al. Ultrasonographic analysis in knee osteoarthritis: evaluation of inter-observer reliability. *Clin Exp Rheumatol.* (2012) 30:673–8.
17. Iagnocco A, Perricone C, Scirocco C, Ceccarelli F, Modesti M, Gattamelata A, et al. The interobserver reliability of ultrasound in knee osteoarthritis. *Rheumatology.* (2012) 51:2013–9. doi: 10.1093/rheumatology/kes161
18. Kellgren JH, Lawrence JS. Radiological assessment of osteo-arthrosis. *Ann Rheum Dis.* (1957) 16:494–502. doi: 10.1136/ard.16.4.494
19. Magnusson K, Kumm J, Turkiewicz A, Englund M. A naturally aging knee, or development of early knee osteoarthritis? *Osteoarthr Cartil.* (2018) 26:1447–52. doi: 10.1016/j.joca.2018.04.020
20. de Miguel Mendieta E, Cobo Ibáñez T, Usón Jaeger J, Bonilla Hernán G, Martín Mola E. Clinical and ultrasonographic findings related to knee pain in osteoarthritis. *Osteoarthr Cartil.* (2006) 14:540–4. doi: 10.1016/j.joca.2005.12.012
21. Mermerci BB, Garip Y, Uysal RS, Dogruel H, Karabulut E, Özoran K, et al. Clinic and ultrasound findings related to pain in patients with knee osteoarthritis. *Clin Rheumatol.* (2011) 30:1055–62. doi: 10.1007/s10067-011-1701-x
22. Meenagh G, Filippucci E, Delle Sedie A, Iagnocco A, Scirè CA, Riente L, et al. Ultrasound imaging for the rheumatologist XXX. Sonographic assessment of the painful knee. *Clin Exp Rheumatol.* (2010) 28:803–5.
23. Neogi T, Felson D, Niu J, Nevitt M, Lewis CE, Aliabadi P, et al. Association between radiographic features of knee osteoarthritis and pain: results from two cohort studies. *BMJ.* (2009) 339:b2844. doi: 10.1136/bmj.b2844
24. Torres L, Dunlop DD, Peterfy C, Guermazi A, Prasad P, Hayes KW, et al. The relationship between specific tissue lesions and pain severity in persons with knee osteoarthritis. *Osteoarthr Cartil.* (2006) 14:1033–40. doi: 10.1016/j.joca.2006.03.015
25. Oo WM, Linklater JM, Daniel M, Saarakkala S, Samuels J, Conaghan PG, et al. Clinimetrics of ultrasound pathologies in osteoarthritis: systematic literature review and meta-analysis. *Osteoarthr Cartil.* (2018) 26:601–11. doi: 10.1016/j.joca.2018.01.021
26. Mathiessen A, Cimmino MA, Hammer HB, Haugen IK, Iagnocco A, Conaghan PG. Imaging of osteoarthritis (OA): what is new? *Best Pract Res Clin Rheumatol.* (2016) 30:653–69. doi: 10.1016/j.berh.2016.09.007
27. Bruyn GAW, Naredo E, Damjanov N, Bachta A, Baudoin P, Hammer HB, et al. An OMERACT reliability exercise of inflammatory and structural abnormalities in patients with knee osteoarthritis using ultrasound assessment. *Ann Rheum Dis.* (2016) 75:842–6. doi: 10.1136/annrheumdis-2014-206774
28. Razek AAKA, El-Basyouni SR. Ultrasound of knee osteoarthritis: interobserver agreement and correlation with Western Ontario and McMaster Universities Osteoarthritis. *Clin Rheumatol.* (2016) 35:997–1001. doi: 10.1007/s10067-015-2990-2
29. Podlipská J, Guermazi A, Lehenkari P, Niinimäki J, Roemer FW, Arokoski JP, et al. Comparison of diagnostic performance of semi-quantitative knee ultrasound and knee radiography with MRI: Oulu Knee Osteoarthritis study. *Sci Rep.* (2016) 6:22365. doi: 10.1038/srep22365
30. Castaño Carou A, Pita Fernández S, Pértega Díaz S, de Toro Santos FJ. Clinical profile, level of affection and therapeutic management of patients with osteoarthritis in primary care: the spanish multicenter study EVALÚA. *Reumatol Clínica.* (2015) 11:353–60. doi: 10.1016/j.reumae.2015.03.007
31. Vlychou M, Koutroumpas A, Alexiou I, Fezoulidis I, Sakkas LI. High-resolution ultrasonography and 3.0 T magnetic resonance imaging in erosive and nodal hand osteoarthritis: high frequency of erosions in nodal osteoarthritis. *Clin Rheumatol.* (2013) 32:755–62. doi: 10.1007/s10067-013-2166-x
32. Roemer FW, Nevitt MC, Felson DT, Niu J, Lynch JA, Crema MD, et al. Predictive validity of within-grade scoring of longitudinal changes of MRI-based cartilage morphology and bone marrow lesion assessment in the tibio-femoral joint – the MOST study. *Osteoarthr Cartil.* (2012) 20:1391–8. doi: 10.1016/j.joca.2012.07.012
33. Wittoek R, Jans L, Lambrecht V, Carron P, Verstraete K, Verbruggen G. Reliability and construct validity of ultrasonography of soft tissue and destructive changes in erosive osteoarthritis of the interphalangeal finger joints: a comparison with MRI. *Ann Rheum Dis.* (2011) 70:278–83. doi: 10.1136/ard.2010.134932
34. Mathiessen A, Haugen IK, Slatkowsky-Christensen B, Bøyesen P, Kvien TK, Hammer HB. Ultrasonographic assessment of osteophytes in 127 patients with hand osteoarthritis: exploring reliability and associations with MRI, radiographs and clinical joint findings. *Ann Rheum Dis.* (2013) 72:51–6. doi: 10.1136/annrheumdis-2011-201195
35. Hammer HB, Iagnocco A, Mathiessen A, Filippucci E, Gandjbakhch F, Kortekaas MC, et al. Global ultrasound assessment of structural lesions in osteoarthritis: a reliability study by the OMERACT ultrasonography group on scoring cartilage and osteophytes in finger joints. *Ann Rheum Dis.* (2016) 75:402–7. doi: 10.1136/annrheumdis-2014-206289
36. Rosa JE, Ruta S, Bravo M, Pompermayer L, Marin J, Ferreyra-Garrot L, et al. Value of color Doppler ultrasound assessment of sacroiliac joints in patients with inflammatory low back pain. *J Rheumatol.* (2019) 46:694–700. doi: 10.3899/jrheum.180550
37. Gandino IJ, Ruta S, Scolnik M, Zacariaz J, Marin J, Rosa J, et al. Radiographic knee osteoarthritis in patients complaining of knee pain: ultrasound features [abstract]. *Arthritis Rheumatol.* (2016) 68(Suppl. 10). Available online at: https://acrabstracts.org/abstract/radiographic-knee-osteoarthritis-in-patients-complaining-of-knee-pain-ultrasound-features/ (accessed June 22, 2020).
38. Gandino IJ, Brom M, Ruta SO, Scolnik M, Zacariaz JB, Marin J, et al. Radiographic knee osteoarthritis in patients complaining of knee pain: ultrasound features. *JCR J Clin Rheumatol.* (2018) 24:S1–174. doi: 10.1097/RHU.0000000000000802

Conflict of Interest: The authors declare that the research was conducted in the absence of any commercial or financial relationships that could be construed as a potential conflict of interest.

frontiers in Medicine

BRIEF RESEARCH REPORT
published: 15 July 2020
doi: 10.3389/fmed.2020.00341

Peripheral Enthesitis Detected by Ultrasonography in Patients With Axial Spondyloarthritis—Anatomical Distribution, Morphology, and Response to Tumor Necrosis Factor-Inhibitor Therapy

Sengul Seven[1,2]*, *Susanne Juhl Pedersen*[1,2], *Mikkel Østergaard*[1,2], *Sara Kamp Felbo*[1,2], *Inge Juul Sørensen*[1], *Uffe Møller Døhn*[1] and *Lene Terslev*[1,2]

[1] Copenhagen Center for Arthritis Research and Center for Rheumatology and Spine Diseases, Centre of Head and Orthopaedics, Rigshospitalet, Glostrup, Denmark, [2] Department of Clinical Medicine, University of Copenhagen, Copenhagen, Denmark

OPEN ACCESS

Edited by:
Raj Sengupta,
Royal National Hospital for Rheumatic Diseases, United Kingdom

Reviewed by:
Antonis Fanouriakis,
University General Hospital Attikon, Greece
Filipa Farinha,
University College London, United Kingdom
Philippe Carron,
Ghent University, Belgium

***Correspondence:**
Sengul Seven
sengul.seven@dadlnet.dk

Specialty section:
This article was submitted to Rheumatology, a section of the journal Frontiers in Medicine

Received: 23 March 2020
Accepted: 08 June 2020
Published: 15 July 2020

Citation:
Seven S, Pedersen SJ, Østergaard M, Felbo SK, Sørensen IJ, Døhn UM and Terslev L (2020) Peripheral Enthesitis Detected by Ultrasonography in Patients With Axial Spondyloarthritis—Anatomical Distribution, Morphology, and Response to Tumor Necrosis Factor-Inhibitor Therapy. Front. Med. 7:341. doi: 10.3389/fmed.2020.00341

Objectives: To investigate the anatomical distribution, morphological abnormalities and response to adalimumab therapy of ultrasound(US)-detected peripheral enthesitis in patients with axial spondyloarthritis (SpA).

Methods: In a randomized, placebo-controlled, double-blinded, investigator-initiated trial (NCT01029847), patients with axial SpA according to the Assessment of Spondyloarthritis International Society criteria were randomized to subcutaneous adalimumab 40 mg every other week or placebo from baseline to week 6. From week 6 to 24, all patients received adalimumab 40 mg every other week. Of 49 patients enrolled, 21 patients participated in our observational US sub-study. US assessment applying the OMERACT US definitions for enthesitis of 10 peripheral entheseal regions of the upper and lower extremities and clinical examination were performed at baseline, weeks 6 and 24. US was performed by one experienced investigator. Hypo-echogenicity, increased thickness and Doppler activity of the enthesis were considered signs of active inflammation, whereas insertional bone erosions, intratendinous calcifications, and enthesophytes were regarded as signs of structural lesions.

Results: Enthesitis on US was mostly present in the lower limbs, especially in the Achilles tendon (81%), the quadriceps tendon (62%), and the greater femoral trochanter (52%). Structural lesions were predominant (38 vs. 12% of examined entheses with inflammatory changes), particularly in the entheses of the lower limbs, and exhibited no change during treatment.

Conclusion: US-detected structural lesions were common while inflammatory lesions were relatively rare in patients initiating adalimumab due to axial SpA. Structural lesions did not appear to change during 24 weeks follow-up, suggesting that these lesions may not be helpful outcome measures in short-term clinical trials.

Keywords: imaging, ultrasound, enthesitis, spondyloarthritis, inflammation

INTRODUCTION

Enthesitis is typically defined as inflammation of the insertion of tendons, ligaments, aponeurosis, and capsules into the bone, and it is considered a pathological, clinical, and imaging hallmark of the spondyloarthritis (SpA) group, including psoriatic arthritis (PsA) (1–3). The Assessments in the SpondyloArthritis International Working Group (ASAS) and the Group for Research and Assessment of Psoriasis and Psoriatic Arthritis (GRAPPA) have recommended enthesitis as one of the key domains for assessing disease activity and response in SpA (axial and peripheral) and PsA (4, 5). The Outcome Measures in Rheumatology (OMERACT) Ultrasound (US) Working Group (WG), has developed and validated consensus-based US definitions for enthesitis lesions in SpA including PsA (1, 2) of which some are related to inflammation and some to inactive structural lesions.

Enthesitis lesions may be detected by US at clinically asymptomatic entheses and with a greater sensitivity than clinical examination (3–5). Since 1994, US has been used for evaluating peripheral enthesitis in SpA patients in both lower and upper limb entheses (6–9). B-mode and Doppler US (color and power) both depict the morphological features and vascularity of the enthesis and may aid in the diagnosis and evaluation of treatment effect (10–12), however, in most studies the inclusion criterion was symptomatic entheses in addition to US verified Doppler activity in the entheses. Different clinical enthesitis scores (13–15) and US enthesitis scores (5, 16, 17) exist in literature, but currently there is no consensus on which clinical scores and US scores to apply. Additionally, little is known about the presence and response to treatment of US-detected enthesitis (inflammatory lesions and/or structural lesions) in axial SpA patients initiating TNF-I therapy due to axial inflammatory activity.

The aim of the study was to investigate the anatomical distribution, morphological abnormalities and response to Tumor Necrosis Factor-inhibitor (TNF-I) therapy of US-detected peripheral enthesitis lesions in a cohort of patients with axial SpA, with or without symptomatic peripheral enthesitis, initiating adalimumab therapy, applying the OMERACT US definitions for enthesitis lesions.

PATIENTS AND METHODS

Study Design

The main study (the ASIM study) was a randomized, double-blinded, placebo-controlled investigator-initiated, 52 weeks longitudinal trial (ClinicalTrials.gov, NCT01029847) conducted in Denmark at five rheumatology outpatient clinics from 2010 to 2014. Fifty patients were included and randomized to receive subcutaneous adalimumab 40 mg every other week or placebo from baseline to week 6. From week 6 to 24, all patients received adalimumab 40 mg every other week. Participants in our observational US sub-study were recruited among patients in the main study. The US sub-study was conducted at Rigshospitalet, Glostrup. The study was approved by the local ethical committee, approval number H1-2013-118, and conducted according to the Declaration of Helsinki V and the Danish legislation. All participants gave written informed consent before study inclusion.

Inclusion and Exclusion Criteria

All patients had axial SpA according to the Assessment of Spondyloarthritis International Society (ASAS) classification criteria, sacroiliitis on X-ray or MRI, disease activity assessed by BASDAI >4 (0–10) despite NSAID treatment and a clinical indication for TNF-I treatment. Treatment with glucocorticoids and/or initiation or changes in csDMARD were not allowed 4 weeks prior to inclusion. Entheseal involvement was not an inclusion criterion.

Patient Evaluation

Patient demographics, clinical and biochemical data were obtained for all participants at every visit. The clinical examination included 66/68 joint count, the Bath Ankylosing Spondylitis Metrology Index (BASMI) and assessment of entheses according to the Leeds enthesitis index (LEI) (13), Maastricht Ankylosing Spondylitis Enthesitis Score (MASES) (15) and the Spondyloarthritis Research Consortium of Canada (SPARCC) enthesitis index (14). A standardized approach to clinical examination of entheses based on a predefined illustrated set of instructions was developed (18). Blood samples were analyzed for serum C-reactive protein (CRP) and Human Leukocyte Antigen B27 (HLA-B27). US assessments were performed at baseline, and weeks 6 and 24.

Ultrasound

All US scans were performed with General Electric Logiq 9 US machine. A ML 12 high-frequency linear probe was used with a center frequency of 14 megahertz (MHz). Doppler setting was adjusted for slow flow according to published recommendations (19). US was performed blinded to clinical and biochemical data according to a standardized protocol by an experienced investigator (LT), who has previously participated in reliability exercises on patients with enthesitis showing high inter- and intrareader reliability (2). Twenty entheseal sites were examined by greyscale and color Doppler; the common extensor, and flexor tendons of the elbow, insertions of supraspinatus tendon, triceps, greater femoral trochanter, quadriceps, proximal, and distal patellar and Achilles tendon, and plantar fascia. Enthesitis was defined according to the OMERACT definitions (2). Hypo-echogenicity, increased thickness (morphologic abnormalities) and Doppler activity of the enthesis were considered signs of active inflammation, whereas insertional bone erosions, intra-tendinous calcifications, and enthesophytes were regarded as signs of structural lesions (2). All lesions were scored dichotomously. US enthesitis was scored according to the Glasgow Ultrasound Enthesitis Scoring System (GUESS) (5), Spanish Enthesitis Index (SEI) (16) and the Madrid Sonography Enthesitis Index (MASEI) (17).

TABLE 1 | Demographic, clinical, and laboratory characteristics of the study population.

	All patients	Placebo	Adalimumab	*P*-value*
Number of participants	21	10	11	
Demographics				
Age, years	39.4 (9.4)	34.3 (5.5)	44.1 (10.0)	**0.02**
Female sex, *N* (%)	9 (42.9)	5 (50.0)	4 (36.4)	0.5
Symptom duration, years	14.1 (12.8)	11.1 (6.8)	16.8 (16.4)	0.9
Biochemical characteristics				
HLA-B27 positive, *N* (%)	15 (71.4)	8 (80.0)	7 (63.6)	0.4
C-reactive protein (mg/L)	8.5 (15.9)	3.8 (3.5)	12.8 (21.3)	0.3
Clinical characteristics				
Physician VAS global (0–10)[a]	6.8 (2.0)	7.7 (1.4)	5.9 (2.2)	0.2
SJC66	0.2 (0.6)	0.2 (0.6)	0.3 (0.7)	0.6
TJC68	3.6 (7.0)	3.6 (4.3)	3.6 (9.0)	0.4
MASES (0–13)	3.9 (3.8)	4.6 (4.0)	2.9 (3.7)	0.3
LEI (0–6)	0.9 (1.0)	0.7 (1.0)	1.1 (1.1)	0.5
SPARCC enthesitis index (0–16)	3.0 (3.2)	3.2 (3.8)	2.6 (2.9)	1.0
Patient reported outcomes				
HAQ	1.0 (0.5)	1.1 (0.7)	1.0 (0.4)	0.6
VAS pain (0–10)[a]	7.3 (2.0)	7.7 (1.8)	6.9 (2.1)	0.4
VAS patient global (0–10)[a]	7.2 (2.1)	7.6 (2.2)	6.8 (2.1)	0.3
BASDAI (0–10)	6.6 (1.6)	7.0 (1.9)	6.3 (1.3)	0.4
BASFI (0–10)	5.9 (2.1)	5.9 (2.5)	5.8 (1.9)	0.9
BASMI (0–10)	3.2 (2.1)	2.7 (2.0)	3.7 (2.2)	0.2

*N (%) for female sex and HLA-B27 status, mean (SD) for all others. Chi²-test for female gender and HLA-B27, Mann-Whitney U-tests for all others. *P < 0.05 is considered significant and indicated in bold.*

[a]*According to Bath Ankylosing Spondylitis Questionnaire.*

BASDAI, Bath Ankylosing Spondylitis Disease Activity Index; BASFI, Bath Ankylosing Spondylitis Functional Index; BASMI, Bath Ankylosing Spondylitis Metrology Index; HAQ, Health Assessment Questionnaire; HLA-B27, Human Leukocyte Antigen B27; LEI, Leeds Enthesitis Index; MASES, Maastricht Ankylosing Spondylitis Enthesitis Score; SJC, Swollen Joint Count; SPARCC, Spondyloarthritis Research Consortium of Canada; TJC, Tender Joint Count; VAS, Visual Analog Scale.

STATISTICS

Descriptive statistics were applied for analysis of demographics, clinical, biochemical, and US data. Statistical analyses were performed using non-parametric tests. Differences in the two study populations were analyzed by applying Chi²-test and Mann-Whitney *U*-test, and the Wilcoxon Rank test was used to analyze differences in treatment effect over time. To determine the agreement between clinical enthesitis vs. US enthesitis and US inflammation, respectively, Cohen's Kappa was calculated, and Spearman's Rho was performed to calculate correlations between clinical scores vs. US enthesitis scores at baseline. We considered Kappa values of <0 as indicating no agreement, 0–0.20 as slight, 0.21–0.40 fair, 0.41–0.60 moderate, 0.61–0.80 good, and 0.81–1 as excellent agreement. A $p < 0.05$ was considered statistically significant. All statistical analyses were performed in IBM SPSS version 22.0.

RESULTS

Demographics, Clinical, and Biochemical Characteristics

Of the 49 patients enrolled in the main study, 21 participated in the US sub-study. The number of patients randomized to receive adalimumab and placebo were 11 and 10, respectively. The patients were 57% males with a mean age of 39.4 years, and 71% were HLA-B27 positive. Baseline demographics, clinical and biochemical characteristics are shown in **Table 1**. The two randomization groups were comparable in baseline characteristics apart from age where patients in the adalimumab group were statistically significantly older than in the placebo group.

The Distribution of US Enthesitis at Baseline

The distribution of clinical and US signs of enthesitis in all 21 patients at baseline is provided in **Table 2**, including the Kappa agreement between clinical enthesitis vs. US enthesitis (i.e., inflammatory lesions and/or structural lesions) and clinical enthesitis vs. US inflammatory lesions alone. Overall, enthesitis (inflammatory lesions and/or structural lesions) was found in 95% of patients. Inflammatory lesions were found in 52% of patients (12% of examined entheses—2% with Doppler activity), while 95% of patients (38% of examined entheses) had structural lesions perceived to be inactive. In comparison 67% of patients had clinical signs of enthesitis. The US-inflammatory lesions in the lower extremities were most frequently found in the insertions of the Achilles tendon (19%) and plantar fascia (19%), while in the upper extremities in the insertion of triceps tendon (5%) and the common extensor tendon of the elbow (5%). Inflammatory lesions were not seen at the greater femoral trochanter and at the insertion of the common flexor tendon.

US enthesitis (inflammation and/or structural US changes) was predominantly found in the lower extremities, especially in the Achilles tendon (81%), the quadriceps tendon (62%) and at the insertion onto the greater femoral trochanter (52%), and these were mostly structural lesions (76, 62, 52%, respectively). In the upper extremities US enthesitis was mostly recorded in the supraspinatus tendon insertion (29%) and at the insertion of the common extensor tendon of the elbow (24%).

When evaluating the different types of inflammatory and structural lesions (**Table 3**), at the upper extremities we observed the presence of erosion only at the insertion of the supraspinatus tendon (18%) and the common extensor tendon of the elbow (5%), while erosions were recorded at nearly all entheses of the lower extremities, especially at the greater femoral trochanter (33%), although never in the distal insertion of the patellar tendon. Calcifications and/or enthesophytes were present across all entheseal regions, except for the common flexor tendon of the elbow and the plantar fascia. Increased thickness and/or

TABLE 2 | Distribution of clinical and US entheseal findings and enthesitis scores at baseline ($n = 21$).

Entheseal region	US			Clinical enthesitis[c]
	Inflammatory lesions[a]	Structural lesions[b]	Enthesitis (inflammatory and/or structural lesions)	
Supraspinatus tendon	0	6 (28.6)	6 (28.6)[##]	8 (38.1)
Triceps tendon	1 (4.8)	1 (4.8)	2 (9.5)	NA
Common extensor tendon, elbow	1 (4.8)[$]	5 (23.8)	5 (23.8)[#]	3 (14.3)
Common flexor tendon, elbow	0	0	0	6 (28.6)
Greater femoral trochanter	0	11 (52.4)	11 (52.4)[##]	12 (57.1)
Quadriceps tendon	3 (14.3)[$]	13 (61.9)	13 (61.9)[#]	3 (14.3)
Proximal insertion of the patellar tendon	1 (4.8)[$]	2 (9.5)	3 (14.3)[#]	4 (19.0)
Distal insertion of the patellar tendon	2 (9.5)[$]	2 (9.5)	3 (14.3)[#]	2 (9.5)
Achilles tendon	4 (19.0)[$$$]	16 (76.2)	17 (81.0)[#]	4 (19.0)
Plantar fascia	4 (19.0)[$]	0	4 (19.0)[#]	6 (28.6)
US enthesitis score				
GUESS (0–36)			3.1 (1.9)	
SEI (0–76)			1.8 (2.1)	
MASEI (0–136)			6.7 (4.6)	

N (%) participants with lesions.

[a]Inflammation: Doppler activity, hypo-echogenicity or increased thickness.

[b]Chronic lesions: Erosions, calcifications or enthesophytes.

[c]Entheses with tenderness.

Kappa agreement was calculated for US enthesitis vs. clinical enthesitis. Kappa value<0 no[#], 0–0.20 slight[##], 0.21–0.40 fair, 0.41–0.60 moderate, 0.61–0.80 good, 0.81–1 excellent agreement, respectively.

Kappa agreement was calculated for US inflammatory lesion vs. clinical enthesitis. Kappa value<0 no[$], 0–0.20 slight[$$], 0.21–0.40 fair[$$$], 0.41–0.60 moderate, 0.61–0.80 good, 0.81–1 excellent agreement, respectively.

GUESS, The Glascow Ultrasound Enthesitis Scoring System; LEI, Leeds Enthesitis Index; MASEI, Madrid Sonography Enthesitis Index; MASES, Maastricht Ankylosing Spondylitis Enthesitis Score; NA, not applicable; SEI, Spanish Enthesitis Index; SPARCC, Spondyloarthritis Research Consortium of Canada; US, ultrasound.

TABLE 3 | US findings at baseline ($n = 21$).

Entheseal region	Erosion	Calcifications / enthesophytes	Increased thickness / hypoechoic	Doppler
Supraspinatus tendon	7 (18)	2 (5)	0	0
Triceps tendon	0	1 (3)	1 (2)	0
Common extensor tendon, elbow	2 (5)	6 (14)	2 (5)	0
Common flexor tendon, elbow	0	0	0	0
Greater femoral trochanter	14 (33)	6 (14)	0	0
Quadriceps tendon	3 (7)	20 (48)	2 (5)	3 (7)
Proximal insertion of the patellar tendon	3 (7)	2 (5)	1 (2)	0
Distal insertion of the patellar tendon	0	3 (7)	1 (2)	1 (2)
Achilles tendon	3 (7)	28 (67)	6 (14)	0
Plantar fascia ($n = 20$)	1 (3)	0	6 (15)	0

N (%) of entheses with lesions.

hypoechoic features were mostly seen at the Achilles tendon insertion and the plantar fascia (14 and 15%, respectively), while completely absent at the supraspinatus tendon, common flexor tendon of the elbow, and the greater femoral trochanter. Doppler was only recorded at the quadriceps tendon (7%) and the distal insertion of the patellar tendon (2%).

Agreement Between US Enthesitis and Clinical Assessment

A fair agreement for US inflammatory lesions vs. clinical enthesitis was seen at the Achilles tendon insertion, while none to poor agreement was found between US structural lesions and inflammatory lesions vs. clinical enthesitis for all other entheses (**Table 2**). Overall, 10% of non-tender entheses showed US signs of inflammation and on the contrary 18% of tender entheses did not show US signs of inflammation. The different clinical scores of enthesitis and the different US enthesitis scores at baseline are also seen in **Table 2**. When performing the Spearmann's rho, we only found a statistically significant correlation between the LEI clinical enthesitis score vs. SEI US enthesitis score.

US and Clinical Enthesitis Changes During Treatment

The clinical findings and US enthesitis (inflammatory and/or structural lesions) scores in the two randomization groups at weeks 0, 6, and 24 are provided in **Table 4**. A statistically significant decrease in BASDAI was seen at both weeks 6 and 24 in the adalimumab group, while only at week 24 in in the placebo group. The SPARCC enthesitis index had decreased significantly from baseline at weeks 6 and 24. No other changes in clinical indices was observed in either of the groups. Regarding the US findings, the only statistically significant changes were for the common extensor tendon of the elbow from baseline to weeks 6 and 24 in the adalimumab group, and for the SEI US score from baseline to week 24 in the placebo group.

DISCUSSION

In this observational US sub-study of axial SpA patients who initiated TNF-I treatment based on axial inflammation, a high prevalence of structural lesions was observed in peripheral entheses (95% of patients, 38% of examined entheses), whereas the prevalence of inflammatory entheseal changes was fairly low (52% of patients, 12% of examined entheses, and 2% with Doppler activity). US signs of enthesitis were mainly identified in the lower extremities, mostly as structural lesions. No change in structural lesions were found during treatment, indicating a low ability to change and supporting the perception of being inactive lesions.

TABLE 4 | Clinical and US findings during study period.

	Placebo			Adalimumab		
	Week 0	**Week 6**	**Week 24**	**Week 0**	**Week 6**	**Week 24**
Number of patients	10	9	10	11	11	10
Clinical enthesitis scores						
MASES (0–13)	4.6 (4.0)	4.0 (3.3)	2.2 (3.7)	3.0 (3.7)	2.1 (2.5)	2.0 (3.0)
LEI (0–6)	0.7 (0.9)	0.9 (1.0)	0.6 (0.9)	1.1 (1.1)	0.7 (0.9)	0.3 (0.7)
SPARCC enthesitis index (0–16)	3.2 (3.8)	3.6 (2.6)	2.2 (2.8)	2.6 (2.9)	1.6 (1.9)**	0.8 (1.1)***
BASDAI	7.0 (1.9)	6.4 (2.5)	4.3 (2.7)***	6.3 (1.3)*	4.2 (2.3)**	2.9 (2.5)***
US findings[a]						
Supraspinatus tendon	3 (30)	2 (22)	1 (10)	3 (27)	2 (18)	1 (10)
Common extensor tendon, elbow	0	0	0	5 (46)*	0	1 (10)***
Common flexor tendon, elbow	0	0	0	0	0	0
Triceps tendon, elbow	1 (10)	0	1 (10)	1 (9)	0	2 (20)
Greater femoral trochanter	6 (60)	6 (67)	6 (60)	5 (46)	6 (55)	6 (60)
Quadriceps tendon	4 (40)	1 (11)	4 (40)	9 (82)	8 (73)	6 (60)
Proximal insertion of the patellar tendon	1 (10)	0	0	2 (18)	1 (9)	1 (10)
Distal insertion of the patellar tendon	2 (20)	1 (11)	1 (10)	1 (9)	1 (9)	0
Achilles tendon	7 (70)	7 (78)	8 (80)	10 (91)	7 (64)	7 (70)
Plantar fascia	1 (10)	0	0	3 (27)	3 (27)	2 (20)
US enthesitis scores						
GUESS (0–36)	2.90 (2.33)	2.56 (1.59)	2.22 (1.39)	3.18 (1.60)	3.09 (1.92)	2.56 (1.81)
SEI (0–76)	2.10 (2.13)	1.22 (1.30)	0.89 (1.54)***	1.55 (2.16)	1.18 (0.98)	0.89 (1.05)
MASEI (0–136)	6.00 (4.92)	4.89 (3.06)	5.00 (3.87)	7.36 (4.46)	7.36 (4.59)	6.89 (5.13)

Mean (SD) for clinical and US enthesitis scores, n (%) participants with US findings.

[a]*Inflammatory and/or structural lesions.*

Wilcoxon Rank test was applied. $P < 0.05$ is considered significant. $^{*}p < 0.05$ week 0–6; $^{**}P < 0.05$ week 6–24; $^{***}P < 0.05$ week 0–24.

BASDAI, Bath Ankylosing Spondylitis Disease Activity Index; GUESS, The Glascow Ultrasound Enthesitis Scoring System; LEI, Leeds Enthesitis Index; MASEI, Madrid Sonography Enthesitis Index; MASES, Maastricht Ankylosing Spondylitis Enthesitis Score; SEI, Spanish Enthesitis Index; SPARCC, Spondyloarthritis Research Consortium of Canada; US, Ultrasound.

The high frequency of US structural lesions in our population with long-standing disease is in line with previous US studies of enthesitis in SpA patients by Naredo et al. (3) and D'Agostino et al. (20) and in AS patients by Wink et al. (6) and Spadaro et al. (7) Calcifications/enthesophytes can also be seen in healthy subjects (8–11), with the highest frequency in the lower limbs, possibly increasing with increasing age, but with a lower prevalence than in SpA patients.

Regarding US signs of entheseal inflammation, the study by Wink et al. (6), which included AS patients, found Doppler activity in 55% of examined entheses, (i.e., more frequently compared with our study). Wink et al. did not include the insertions of triceps or supraspinatus but included the pes anserine. The latter may explain the high frequency of Doppler findings, as this was the most frequent site for Doppler activity. The proximity of the pes anserine to the inferior geniculate artery might increase the risk of overestimation of the inflammation. Since this study also looked at combinations of inflammatory lesions and included adjacent bursitis and effusion in this definition, results are therefore not comparable. Spadaro et al. (7) found a frequency of entheseal Doppler activity (6%) more similar to ours. However, Naredo et al. (20) also found a high prevalence of inflammatory changes with morphologic abnormalities in 61% of the SpA patients and intra-entheseal Doppler activity in 47% of the patients, both most commonly at the Achilles tendon insertion (29 and 16%, respectively). Our population, however, was selected based on axial manifestations, while peripheral findings were not required. This explains the low frequency of inflammatory US findings. The frequently registered high frequency of structural changes in peripheral entheses documents that most patients with axial SpA at some stage in their disease course get entheseal affection which is severe enough to leave recognizable structural damage.

Entheseal Doppler activity has been found in healthy subjects (8, 12, 21), also at the quadriceps insertion, where most Doppler activity was also found in our population. Other studies did not find any entheseal Doppler activity in healthy subjects (9, 22).

Although not an inclusion criterion, the patients in our study had clinically peripheral enthesis involvement with a MASES index of 3.9 (3.8), however, there were none to poor agreement between clinical entheses assessment and US findings of enthesitis. Further, no agreement was seen when evaluating different clinical enthesis scores and different US enthesitis scores. This is in line with several previous studies that have found US to be more sensitive than clinical evaluation for detection of inflammation (4). The tenderness at the clinically tender entheses that did not show US signs of inflammation may originate from other tender structures close to the entheses.

An outcome measure needs to possess ability to change during effective therapies (23). Wink et al. found no statistically significant decrease in inflammatory lesions (6). In the present study US enthesitis was not sensitive to change during adalimumab therapy, which is probably at least partially explained by the low number of inflammatory lesions. The lack of documented responsiveness supports that future studies should both test the current US measures in more actively inflamed cohorts and investigate new and potentially more sensitive measures.

The strength of this study is the placebo-controlled study design applying a standardized clinical and US protocol performed by an experienced sonographer. However, the study was observational and included axial SpA patients regardless of the presence of US enthesitis findings. Additionally, the low number of patients and low number of inflammatory lesions are the primary limitation, since the statistical power to show significant changes over time and differences between the groups was low.

In conclusion, we found by US a high prevalence of structural lesions and a very low prevalence of inflammatory lesions in a population of axial SpA patients with or without clinical peripheral enthesitis. In our study US structural lesions did not appear to have ability to change during 24 weeks of TNF-I treatment, suggesting that US-structural enthesitis lesions may not be helpful outcome measures in short-term clinical trials.

DATA AVAILABILITY STATEMENT

The raw data supporting the conclusions of this article will be made available by the authors, without undue reservation.

ETHICS STATEMENT

The studies involving human participants were reviewed and approved by the Videnskabsetiske Komiteer in the Capital Region of Denmark. The patients/participants provided their written informed consent to participate in this study.

AUTHOR CONTRIBUTIONS

LT, SP, and MØ contributed to the conception and design of the study. SS, SF, and LT wrote sections of the manuscript. SS and LT wrote the first draft of the manuscript. SS, LT, SF, and SP performed the statistical analysis and interpretation. SS organized the database. LT, IS, SP, and UD contributed to the acquisition of data. All authors contributed to manuscript revision, read, and approved the submitted version.

FUNDING

The authors acknowledge Abbvie A/S Denmark for providing financial support for this investigator-initiated study and for adalimumab during the study period. Abbvie A/S Denmark was not involved in study set-up, data collection, analysis or interpretation, and had no influence on the publication of data.

ACKNOWLEDGMENTS

The abstract has previously been presented at the EULAR conference [abstract no. OP0287 (24)].

REFERENCES

1. Terslev L, Naredo E, Iagnocco A, Balint PV, Wakefield RJ, Aegerter A. et al. Defining enthesitis in spondyloarthritis by ultrasound: results of a Delphi process and of a reliability reading exercise. *Arthritis Care Res.* (2014) 66:741–8. doi: 10.1002/acr.22191
2. Balint PV, Terslev L, Aegerter P, Bruyn GW, Valckenaere IC, Gandjbakhch F, et al. Reliability of a consensus-based ultrasound definition and scoring for enthesitis in spondyloarthritis and psoriatic arthritis: an OMERACT US initiative. *Ann Rheum Dis.* (2018) 77:1730–35. doi: 10.1136/annrheumdis-2018-213609
3. D'Agostino M-A, Said-Nahal R, Hacquard-Bouder C, Brasseur JL, Dougados M, Bredan M. Assessment of peripheral enthesitis in the spondylarthropathies by ultrasonography combined with power aoppler: a cross-sectional study. *Arthritis Rheum.* (2003) 48:523–33. doi: 10.1002/art.10812
4. Lehtinen A, Taavitsainen M, Leirisalo-Repo M. Sonographic analysis of enthesopathy in the lower extremities of patients with spondylarthropathy. *Clin Exp Rheumatol.* (1994) 12:143–8.
5. Balint PV, Kane D, Wilson H, McInnes IB, Sturrock RD. Ultrasonography of entheseal insertions in the lower limb in spondyloarthropathy. *Ann Rheum Dis.* (2002) 61:905–10. doi: 10.1136/ard.61.10.905
6. Wink F, Bruyn GA, Maas F, Griep EN, van der Veer E, Bootsma H, et al. Ultrasound evaluation of the entheses in daily clinical practice during tumor necrosis factor-alpha blocking therapy in patients with ankylosing spondylitis. *J Rheumatol.* (2017) 44:587–93. doi: 10.3899/jrheum.160584
7. Spadaro A, Iagnocco A, Perrotta FM, Modesti M, Scarno A, Valesini G. Clinical and ultrasonography assessment of peripheral enthesitis in ankylosing spondylitis. *Rheumatology.* (2011) 50:2080–6. doi: 10.1093/rheumatology/ker284
8. Guldberg-Moller J, Terslev L, Nielsen SM, Kønig MJ, Torp-Pedersen ST, Torp-Pedersen A, et al. Ultrasound pathology of the entheses in an age and gender stratified sample of healthy adult subjects: a prospective cross-sectional frequency study. *Clin Exp Rheumatol.* (2019) 37:408–13.
9. Queiro R, Alonso S, Alperi M, Fernández M, Tejón P, Riestra JL, et al. Entheseal ultrasound abnormalities in patients with SAPHO syndrome. *Clin Rheumatol.* (2012) 31:913–9. doi: 10.1007/s10067-012-1959-7
10. Gutierrez M, Luccioli F, Salaffi F, Bartoloni E, Bertolazzi C, Bini V, et al. Ultrasound revealing subclinical enthesopathy at the greater trochanter level in patients with spondyloarthritis. *Clini Rheumatol.* (2012) 31:463–8. doi: 10.1007/s10067-011-1875-2
11. Jaen-Diaz JI, Cerezo-Lopez E, Lopez-de Castro F, Mata-Castrillo M, Barceló-Galíndez, JP, de la Fuente J, et al. Sonographic findings for the common extensor tendon of the elbow in the general population. *J Ultrasound Med.* (2010) 29:1717–24. doi: 10.7863/jum.2010.29.12.1717
12. Lin C, Diab M, Milojevic D. Grey-scale ultrasound findings of lower extremity entheses in healthy children. *Pediatr Rheumatol Online J.* (2015) 13:14. doi: 10.1186/s12969-015-0012-1
13. Healy PJ, Helliwell PS. Measuring clinical enthesitis in psoriatic arthritis: assessment of existing measures and development of an instrument specific to psoriatic arthritis. *Arthritis Rheum.* (2008) 59:686–91. doi: 10.1002/art.23568
14. Maksymowych WP, Mallon C, Morrow S, Shojania K, Olszynski WP, Wong RL, et al. Development and validation of the spondyloarthritis research consortium of Canada (SPARCC) enthesitis index. *Ann Rheum Dis.* (2009) 68:948–53. doi: 10.1136/ard.2007.084244

15. Heuft-Dorenbosch L, Spoorenberg A, van Tubergen A, Landewé R, van ver Tempel H, Mielants H, et al. Assessment of enthesitis in ankylosing spondylitis. *Ann Rheum Dis.* (2003) 62:127–32. doi: 10.1136/ard.62.2.127
16. Alcalde M, Acebes JC, Cruz M, González-Hombrado L, Herrero-Beaumont G, Sánchez-Pernaute O. A sonographic enthesitic index of lower limbs is a valuable tool in the assessment of ankylosing spondylitis. *Ann Rheum Dis.* (2007) 66:1015–9. doi: 10.1136/ard.2006.062174
17. de Miguel E, Cobo T, Munoz-Fernandez S, Naredo E, Usón J, Acebes JC, et al. Validity of enthesis ultrasound assessment in spondyloarthropathy. *Ann Rheum Dis.* (2009) 68:169–74. doi: 10.1136/ard.2007.084251
18. Poggenborg RP, Eshed I, Ostergaard M, Sørensen IJ, Møller JM, Madsen OK, et al. Enthesitis in patients with psoriatic arthritis, axial spondyloarthritis and healthy subjects assessed by 'head-to-toe' whole-body MRI and clinical examination. *Ann Rheum Dis.* (2015) 74:823–9. doi: 10.1136/annrheumdis-2013-204239
19. Torp-Pedersen ST, Terslev L. Settings and artefacts relevant in colour/power Doppler ultrasound in rheumatology. *Ann Rheum Dis.* (2008) 67:143–49. doi: 10.1136/ard.2007.078451
20. Naredo E, Batlle-Gualda E, Garcia-Vivar ML, García-Aparicio AM, Fernández-Sueiro JL, Fernández-Prada M, et al. Power doppler ultrasonography assessment of entheses in spondyloarthropathies: response to therapy of entheseal abnormalities. *J Rheumatol.* (2010) 37:2110–7. doi: 10.3899/jrheum.100136
21. Krogh TP, Fredberg U, Ammitzbol C, Ellingsen T. Ultrasonographic characteristics of the common extensor tendon of the elbow in asymptomatic individuals: thickness, color doppler activity, and bony spurs. *Orthop J Sports Med.* (2017) 5:2325967117704186. doi: 10.1177/2325967117704186
22. Jousse-Joulin S, Morvan J, Devauchelle-Pensec V, Saraux A. Ultrasound assessment of the entheses in primary Sjogren syndrome. *Ultrasound Med Biol.* (2013) 39:2485–7. doi: 10.1016/j.ultrasmedbio.2013.05.013
23. Terslev L, Naredo E, Keen HI, Bruyn GAW, Iagnocco A, Wakefield RJ, et al. The OMERACT stepwise approach to select and develop imaging outcome measurement instruments: the musculoskeletal ultrasound example. *J Rheumatol.* (2019) 46:1394–400. doi: 10.3899/jrheum.181158
24. Seven S, Pedersen SJ, Østergaard M, Sørensen IJ. OP0287 ultrasonography-detected peripheral enthesitis in patients with axial spondyloarthritis – anatomical distribution, morphology and response to anti-tnf therapy. *Ann Rheum Dis*. (2017) 76:175.1–75. doi: 10.1136/annrheumdis-2017-eular.2781

Conflict of Interest: SS: research support from Novartis, Honoraria from Sanofi, UCB, and Abbvie. SP: speakers fee from MSD, Pfizer, AbbVie, Novartis, and UCB. Advisory board member for AbbVie and Novartis, research support from AbbVie, MSD, and Novartis. MØ: research support, consultancy fees and/or speaker fees form Abbvie, BMS, Boehringer-Ingelheim, Celgene, Eli-Lilly, Hospira, Janssen, Merck, Novartis, Novo, Orion, Pfizer, Regeneron, Roche, Sandoz, Sanofi, and UCB. SF: research support from Celgene. UD: speaker and consulting fees from Eli-Lilly, Pfizer, Novartis, Roche, and Abbvie. LT: speakers fee from AbbVie, Janssen, Roche, Novartis, Pfizer, MSD, BMS, and GE.

The remaining author declares that the research was conducted in the absence of any commercial or financial relationships that could be construed as a potential conflict of interest.

frontiers in Medicine

SYSTEMATIC REVIEW
published: 15 July 2020
doi: 10.3389/fmed.2020.00337

High-Resolution Peripheral Quantitative Computed Tomography for Bone Evaluation in Inflammatory Rheumatic Disease

Rasmus Klose-Jensen[1,2], *Justin J. Tse*[3,4], *Kresten Krarup Keller*[5], *Cheryl Barnabe*[3,6], *Andrew J. Burghardt*[7], *Stephanie Finzel*[8,9], *Lai-Shan Tam*[10], *Ellen-Margrethe Hauge*[1,2], *Kathryn S. Stok*[11] *and Sarah L. Manske*[3,4]*

[1] Department of Rheumatology, Aarhus University Hospital, Aarhus, Denmark, [2] Department of Clinical Medicine, Faculty of Health, Aarhus University, Aarhus, Denmark, [3] Cumming School of Medicine, McCaig Institute for Bone and Joint Health, University of Calgary, Calgary, AB, Canada, [4] Department of Radiology, Cumming School of Medicine, University of Calgary, Calgary, AB, Canada, [5] Diagnostic Centre, Silkeborg Regional Hospital, Silkeborg, Denmark, [6] Department of Medicine, Cumming School of Medicine, University of Calgary, Calgary, AB, Canada, [7] Department of Radiology and Biomedical Imaging, University of California, San Francisco, San Francisco, CA, United States, [8] Department of Rheumatology and Clinical Immunology, Medical Centre - University of Freiburg, Freiburg, Germany, [9] Faculty of Medicine, University of Freiburg, Freiburg, Germany, [10] Department of Medicine and Therapeutics, The Chinese University of Hong Kong, Hong Kong, China, [11] Department of Biomedical Engineering, The University of Melbourne, Parkville, VIC, Australia

OPEN ACCESS

Edited by:
Christian Dejaco, Medical University of Graz, Austria

Reviewed by:
Tobias De Zordo, Brixsana Private Clinic, Italy
Arnd Kleyer, University Hospital Erlangen, Germany

***Correspondence:**
Sarah L. Manske
smanske@ucalgary.ca

Specialty section:
This article was submitted to Rheumatology, a section of the journal Frontiers in Medicine

Received: *25 March 2020*
Accepted: *05 June 2020*
Published: *15 July 2020*

Citation:
Klose-Jensen R, Tse JJ, Keller KK, Barnabe C, Burghardt AJ, Finzel S, Tam L-S, Hauge E-M, Stok KS and Manske SL (2020) High-Resolution Peripheral Quantitative Computed Tomography for Bone Evaluation in Inflammatory Rheumatic Disease. Front. Med. 7:337. doi: 10.3389/fmed.2020.00337

High resolution peripheral quantitative computed tomography (HR-pQCT) is a 3-dimensional imaging modality with superior sensitivity for bone changes and abnormalities. Recent advances have led to increased use of HR-pQCT in inflammatory arthritis to report quantitative volumetric measures of bone density, microstructure, local anabolic (e.g., osteophytes, enthesiophytes) and catabolic (e.g., erosions) bone changes and joint space width. These features may be useful for monitoring disease progression, response to therapy, and are responsive to differentiating between those with inflammatory arthritis conditions and healthy controls. We reviewed 69 publications utilizing HR-pQCT imaging of the metacarpophalangeal (MCP) and/or wrist joints to investigate arthritis conditions. Erosions are a marker of early inflammatory arthritis progression, and recent work has focused on improvement and application of techniques to sensitively identify erosions, as well as quantifying erosion volume changes longitudinally using manual, semi-automated and automated methods. As a research tool, HR-pQCT may be used to detect treatment effects through changes in erosion volume in as little as 3 months. Studies with 1-year follow-up have demonstrated progression or repair of erosions depending on the treatment strategy applied. HR-pQCT presents several advantages. Combined with advances in image processing and image registration, individual changes can be monitored with high sensitivity and reliability. Thus, a major strength of HR-pQCT is its applicability in instances where subtle changes are anticipated, such as early erosive progression in the presence of subclinical inflammation. HR-pQCT imaging results could ultimately impact decision making to uptake aggressive treatment strategies and prevent progression of joint damage. There are several potential areas where HR-pQCT evaluation of inflammatory arthritis still requires development. As a highly sensitive imaging technique, one of the major challenges has been motion artifacts;

motion compensation algorithms should be implemented for HR-pQCT. New research developments will improve the current disadvantages including, wider availability of scanners, the field of view, as well as the versatility for measuring tissues other than only bone. The challenge remains to disseminate these analysis approaches for broader clinical use and in research.

Keywords: HR-pQCT (high-resolution peripheral quantitative computed tomography), arthritis, joint space, erosions, osteophytes, bone mineral density, bone microstructure

INTRODUCTION

Imaging is playing an increasing role in the diagnosis and monitoring of inflammatory disease. For many years the only imaging modality for joint assessment was conventional radiographs (CR); however, newer technologies have revolutionized the diversity of medical imaging capabilities in rheumatic diseases. Magnetic resonance imaging (MRI) and ultrasound (US) are now used regularly in both research and clinical practice for investigating joint diseases, particularly for the identification of soft tissue pathology and inflammation. In contrast, computed tomography (CT) capitalizes on the ability of bone to attenuate x-rays, thus providing excellent bone contrast in three dimensions with high spatial resolution but is limited by poor soft-tissue contrast. High-resolution peripheral quantitative computed tomography (HR-pQCT) imaging was designed to examine volumetric bone mineral density and microstructure of the radius and tibia and has been used extensively in osteoporosis research. HR-pQCT uses the same principles as traditional CT but can achieve a much higher spatial resolution and still has a very low radiation dose. The total effective dose for the metacarpophalangeal (MCP) joint and wrist scans is ∼0.025 mSv (1). For comparison, the radiation dose for a conventional chest X-ray is 0.1 mSv. Still, HR-pQCT has a smaller field of view. Isotropic voxel sizes of 61 or 82 μm lead to spatial resolutions of 100 or 142 μm, respectively, approximately the thickness of an individual human trabecula. The high resolution allows segmentation of the bone at the microstructural level, permitting quantification of architecture and micro-scale pathological features, such as erosions. Initially limited by a gantry size that limited imaging to distal joints in the hands (**Figure 1**), wrist, foot, and ankles only, the newest generation HR-pQCT permits more proximal imaging of the elbows and knee, expanding capabilities to important anatomic sites in the context of inflammatory arthritis.

In 2011 the Study grouP for x-trEme Computed Tomography in Rheumatoid Arthritis (SPECTRA) was formed to facilitate the worldwide collaboration of periarticular image acquisition standards, image interpretation and analysis guides, and applications in clinical research. A systematic review was published in 2016, detailing the published research of HR-pQCT imaging and arthritis (2). Since then, the number of published papers has more than doubled, suggesting the importance of this review to update the current knowledge and expanded uses of this technology. We have structured this review to summarize pathological findings observed at the metacarpophalangeal (MCP) and wrist joints in different types of peripheral inflammatory arthritis using HR-pQCT, compare HR-pQCT imaging outcomes with other modalities in terms of erosions, joint space width, bony proliferations, bone density and microstructure, summarize the reproducibility of the quantitative outcome measures assessed with HR-pQCT imaging, investigate early detection of arthritis, the longitudinal changes over time for the quantitative outcome measures, and finally discuss the implications of the use of HR-pQCT in inflammatory arthritis and future directions.

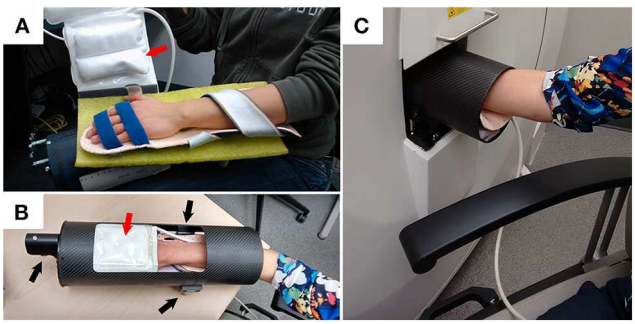

FIGURE 1 | Example demonstrating how a participant is positioned for XtremeCTII scanning. **(A)** Participant's hand is positioned on a rigid-formed mold, with straps securing the distal and proximal ends of the forearm. An additional x-ray compatible, inflatable, pad-based positioning system (red arrows) is positioned above the hand to further reduce accidental motion during scan acquisitions. **(B)** The secured appendage is then placed within a cylindrical, annular, carbon-fiber molded sample holder. Using three spherical landmarks (black arrows), and with the participant resting comfortably, the supported participants' hand and sample holder is then securely and accurately placed within the scanner **(C)**.

MATERIALS AND METHODS

Search Strategy

US National Library of Medicine Medical Subject Heading (MeSH) terms, keywords, and acronyms for HR-pQCT were selected. We combined this search with MeSH terms, keywords, and acronyms for the metacarpophalangeal joints (MCP) and/or radius and/or wrist, to specify the periarticular regions of interest, and MeSH terms and keywords for arthritis (search terms available in **Appendix 1** in Supplementary Material). PubMed (1966–January 2020) and Embase (1980–January 2020) searches were conducted to identify potentially relevant studies. Filters were applied to eliminate animal studies and identify English language studies and full-length articles. Web of Science was used

to identify articles which referenced the articles found through PubMed and Embase. References from identified articles were checked manually. Authors from the SPECTRA Collaboration aided in identifying any potential studies we did not find through the other searches.

Inclusion Criteria

Any studies reporting original results of HR-pQCT imaging of the MCP and/or wrist joints were selected through the title/abstract search. These studies could report on the normal state or any arthritis conditions [including RA, osteoarthritis (OA), PsA], as well as "pre-arthritis" states [e.g., persons positive for anticitrullinated protein antibodies (ACPA) with arthralgia]. At the full-text review stage, we selected articles for data extraction if they reported on any of the following outcomes: (1) pathology findings, determined a priori to include bone mineral architecture, bone mineral density (BMD), erosions, vascular channels, cortical breaks, joint space, bony proliferations, or surface changes; (2) comparison to other imaging modalities; and (3) reproducibility. Article selection and data extraction were performed by one author (RKJ).

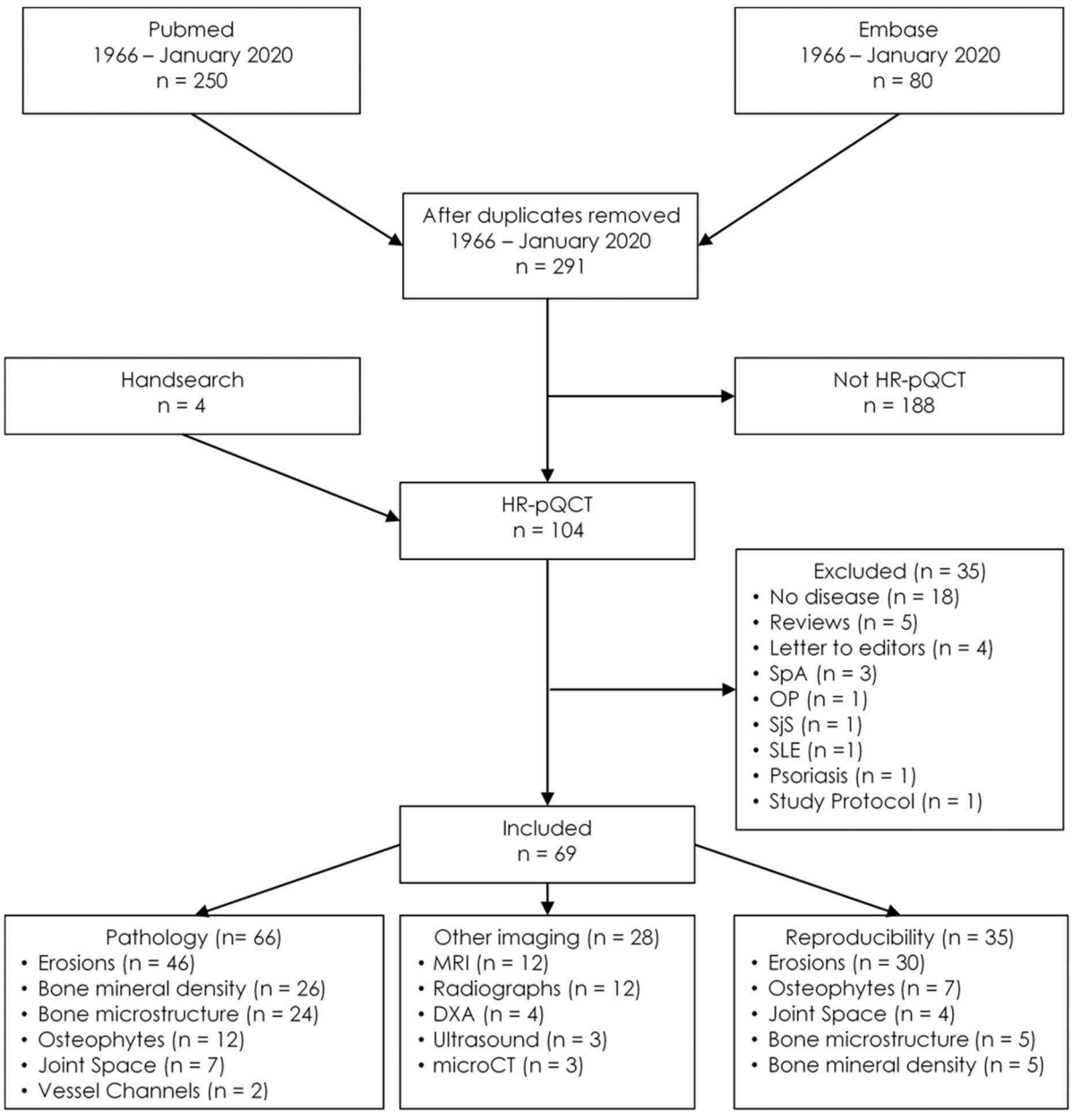

FIGURE 2 | Flow diagram for study inclusion. DXA, Dual x-ray absorptiometry; HR-pQCT, High-resolution peripheral quantitative computed tomography; OP, Osteoporosis; SjS, Sjogren's syndrome; SpA, Spondyloarthritis; SLE, Systemic lupus erythematosus; microCT, Micro-computed tomography.

Analysis

Owing to the heterogeneity of case definitions for different pathologies, variations in analysis techniques, and the identification of studies in a variety of normal and disease states, it was not possible to perform a meta-analysis. Therefore, a narrative summary of the work was performed following pathology descriptions and comparisons to other imaging modalities and reproducibility.

PATHOLOGY

A total of 291 unique publications were identified, each subject to selection based on the title and abstract. One hundred and three met eligibility for full-text review, with 69 selected for data extraction (**Figure 2**). Of these 69 articles, 66 described pathology findings, 28 related comparisons of HR-pQCT findings to another imaging modality, and 35 described precision or reproducibility. All the studies meeting inclusion criteria are detailed in **Table 1**.

Erosion Detection by HR-pQCT

Bone erosions were originally defined radiographically as breaks in the cortical bone surface, typically accompanied by loss of underlying trabecular bone (71–73).

Erosions on HR-pQCT have been defined in a diverse manner; the early studies simply defined erosion as a clear juxta-articular break of the cortical shell (4, 5) while others stated that the break had to be seen in a minimum number of consecutive slices (3). Not until 2016 was a clear definition proposed by the SPECTRA Collaboration following a consensus exercise (63). Erosions were defined as (1) a definite break in the cortical bone; (2) the cortical break must extend over at least two consecutive slices; (3) the cortical break must be detectable in two perpendicular planes; (4) the cortical interruption must have a loss of underlying trabecular bone, and (5) the cortical interruption must be non-linear in shape to differentiate from vascular channels penetrating the cortices (**Figure 3**). In contrast, cortical breaks or interruptions have been defined as a clear interruption of the cortex, seen on two consecutive slices on two orthogonal planes but without the need to demonstrate loss of trabecular bone or shape (34). Such, cortical breaks or interruptions have not been incorporated in the SPECTRA definition of erosions.

The high spatial resolution of HR-pQCT images has allowed deeper investigation into the role of these erosions in the inflammatory arthritis disease course. Forty-six publications characterizing erosions or cortical breaks/interruptions were found. Erosions have been assessed in a variety of arthritic conditions including early inflammatory arthritis (3, 33, 37, 53, 58, 59, 67), RA (1, 3–7, 9, 10, 12, 15, 23, 26, 28–30, 34, 39, 40, 44, 46–48, 52, 54, 55, 61, 64, 65, 67), PsA (5, 7, 14, 49, 61, 66, 69), and erosive hand OA (21), as well as healthy controls (3, 5, 7, 16, 33, 39, 40, 44, 45, 52, 54, 55, 60, 61, 64, 67) and subjects with ACPA antibodies but no features of arthritis (32, 50, 62).

Erosions are most abundant in patients with RA (3, 4, 16, 33, 52, 54, 55, 57, 64, 65, 69), especially ACPA and rheumatoid factor (RF) positive RA patients (26). The erosions exhibit a clear predilection for the radial and ulnar quadrant of the 2nd and 3rd MCP joints. Erosions are most common in the metacarpal head but are also prevalent in the proximal interphalangeal (PIP) bases (4, 15). Although patients with PsA also exhibited a high degree of erosive damage (69), erosions are not as prevalent in PsA patients when compared with RA patients (5, 7, 61). For patients with PsA, erosions are most common in the radial quadrant. However, PsA erosions were also found to a high degree in the dorsal and palmar quadrant of the MCP joint (5, 69). Differences in erosion morphology have also been described in RA compared with PsA patients. In one study, erosions in RA patients were typically U-shaped in appearance, while erosions in PsA patients are more often tubule and Ω-shaped (5); these findings have not been confirmed in other studies. The possible differences in shape may reflect different pathophysiological mechanisms, leading to greater erosion repair in PsA than RA, or alternatively, these morphological phenotypes may reflect differences in disease severity. Further investigation is needed to explore differences between morphologies observed in RA and PsA.

Typically, erosion presence has been assessed manually by an experienced reader. However, manual scoring is laborious and requires substantial training and standardization. An automated detection algorithm has been developed, named the Cortical Interruption Detection Algorithm (39, 40, 52, 53, 64). The Cortical Interruption Detection Algorithm detects the presence of cortical interruptions, directing the reader to lesion locations to verify that they meet the erosion definition as opposed to those that merely represent physiological breaks in the cortical bone, i.e., vascular channels (**Figure 4A**) or stack misalignment (**Figure 4B**) and osteophyte formation (**Figure 4C**). This algorithm also captures very small cortical breaks (>0.246 mm in diameter) that can be challenging to detect through visual inspection (39, 40).

Comparison of Erosion Detection With Other Imaging Modalities

Erosion detection by HR-pQCT has been compared with other pre-clinical and clinical imaging modalities. An image review showing erosions on HR-pQCT, MRI, and CR have also been published for patients with RA (33).

Micro-computed tomography (microCT) applies the same technology as HR-pQCT for pre-clinical investigations but uses a smaller field of view to acquire even higher spatial resolution images (<10 μm, depending on the size of the sample and scanner characteristics) that can be performed on *ex vivo* samples only. Two studies compared cortical interruption detection using HR-pQCT with microCT as a gold standard. The sensitivity of HR-pQCT in detecting cortical interruptions was 82% (34). MicroCT has also been used as a gold standard in order to investigate the ability of the Cortical Interruption Detection Algorithm to find the minimum diameter to detect and quantify cortical interruptions on HR-pQCT. This algorithm performed best for the detection of cortical interruptions with a minimum diameter of 0.16 mm (40).

Additional research has been performed comparing clinical CR and MRI with HR-pQCT, as a gold standard, for the detection of erosions (**Figure 5**). In a clinical setting, CR is still the gold standard. The sensitivity of erosion detection by CR was 61 to 68% when HR-pQCT was considered as a reference (1, 12). Face validity of HR-pQCT identification of erosions

TABLE 1 | Studies included in the systematic review.

Author, year (ref)	Participants	Type of study	Joints included	Outcomes	Other modalities
Fouque-Aubert, 2010 (3)	RA ($n = 57$); eRA ($n = 36$); control ($n = 43$)	Cross-sectional	MCP	Erosions, BMD, microstructure	
Stach, 2010 (4)	RA ($n = 58$); control ($n = 30$)	Cross-sectional	MCP; Radius	Erosions, Osteophyte	
Finzel, 2011 (5)	RA ($n = 58$); PsA ($n = 30$)	Cross-sectional	MCP	Erosions, Osteophyte	
Finzel, 2011 (6)	RA ($n = 30$)	Cohort	MCP	Erosions	
Finzel, 2011 (7)	RA ($n = 14$); PsA ($n = 6$); control ($n = 6$)	Cross-sectional	MCP	Erosions	US
Zhu, 2012 (8)	RA ($n = 100$)	Cross-sectional	MCP; Radius	BMD, microstructure	DXA
Albrech, 2013 (9)	RA ($n = 50$)	Cross-sectional	MCP	Erosions	MRI
Aschenberg, 2013 (10)	RA ($n = 40$)	Cohort	MCP	Erosions, Osteophyte	
Barnabe, 2013 (11)	eRA ($n = 10$)	Cross-sectional	MCP	JSW	
Barnabe, 2013 (12)	RA ($n = 15$); control ($n = 15$)	Cross-sectional	MCP; PIP	Erosions, JSW, BMD, microstructure	CR
Burghardt, 2013 (13)	RA ($n = 16$); control ($n = 7$)	Cross-sectional	MCP; Radius	JSW	CR
Finzel, 2013 (14)	PsA [($n = 41$) TNFi/MTX $n = 28/13$]	Cohort	MCP	Erosions, Osteophyte	
Finzel, 2013 (15)	RA ($n = 20$)	Cohort	MCP	Erosions	
Srikhum, 2013 (16)	RA ($n = 16$); control ($n = 7$)	Cross-sectional	MCP; Radius	Erosions	MRI
Zhu, 2013 (17)	RA ($n = 66$); control ($n = 66$)	Cross-sectional	Radius	BMD, microstructure	DXA
Kleyer, 2014 (18)	ACPA+ ($n = 15$); ACPA– ($n = 15$)	Cross-sectional	MCP	BMD, microstructure	
Kocijan, 2014 (19)	RA ($n = 90$); control ($n = 70$)	Cross-sectional	Radius	BMD, microstructure	
Kocijan, 2014 (20)	RA ($n = 60$); PsA ($n = 50$)	Cross-sectional	Radius	BMD, microstructure	
Finzel, 2014 (21)	PsA ($n = 25$); HOA ($n = 25$); control ($n = 20$)	Cross-sectional	MCP	Osteophyte	
Teruel, 2014 (22)	RA ($n = 16$)	Cross-sectional	Radius	BMD, microstructure	MRI
Töpfer, 2014 (23)	RA ($n = 18$)	Cross-sectional	MCP	Erosions	
Zhu, 2014 (24)	RA ($n = 50$); control ($n = 50$)	Cross-sectional	Radius	BMD, microstructure	
Zhu, 2015 (25)	PsA ($n = 53$); control ($n = 53$)	Cross-sectional	Radius	BMD, microstructure	DXA
Hecht, 2015 (26)	RA ($n = 242$)	Cross-sectional	MCP	Erosions	
Kocijan, 2015 (27)	PsA ($n = 50$); PsO ($n = 30$); control ($n = 70$)	Cross-sectional	Radius	BMD, microstructure	
Lee, 2015 (1)	RA ($n = 16$)	Cross-sectional	MCP; Radius	Erosions	MRI; CR
Regensburger, 2015 (28)	RA ($n = 103$)	Cross-sectional	MCP; Radius	Erosions	MRI
Töpfer, 2015 (29)	RA ($n = 22$)	Cohort	MCP	Erosions, BMD	
Barnabe, 2016 (30)		Cross-sectional	MCP	Erosions	
Figueriredo, 2016 (31)	ACPA+ RA ($n = 202$)	Cohort	MCP	Erosions, Osteophytes	
Kleyer, 2016 (32)	ACPA+ ($n = 20$); ACPA– ($n = 13$)	Cross-sectional	MCP	Erosions	MRI
Scharmga, 2016 (33)	RA ($n = 34$); eRA ($n = 10$); control ($n = 38$)	Cross-sectional	MCP	Erosions	MRI; CR
Scharmga, 2016 (34)	Cadaver ($n = 10$)	Cross-sectional	MCP; PIP	Erosions	μCT
Shen, 2016 (35)	PsA ($n = 80$)	Cross-sectional	Radius	BMD, BMS	DXA
Tom, 2016 (36)	Cadaver ($n = 7$)	Cross-sectional	MCP	JSW	
Feehan, 2017 (37)	eRA ($n = 30$); control ($n = 30$)	Cohort	MCP; Radius	BMD, BMS	
Kleyer, 2017 (38)	RA ($n = 15$); PsA ($n = 15$); control ($n = 15$)	Cross-sectional	MCP	3D printing	
Peters, 2017 (39)	RA ($n = 7$); control ($n = 3$)	Cross-sectional	MCP	Erosions	
Peters, 2017 (40)	RA ($n = 32$); control ($n = 32$)	Cohort	MCP	Erosions	μCT
Scharmga, 2017 (41)	Cadaver ($n = 7$)	Cross-sectional	MCP	Erosions, VC	
Shimizu, 2017 (42)	RA [($n = 27$) TNFi/MTX $n = 17/10$]	Cohort	MCP; Radius	Erosions, JSW, BMD	MRI; CR
Simon, 2017 (43)	RA ($n = 106$); control ($n = 108$); Cadaver ($n = 6$)	Cross-sectional	MCP; Radius	BMD, BMS	
Werner, 2017 (44)	RA ($n = 107$); control ($n = 105$); Cadaver ($n = 6$)	Cross-sectional	MCP; Radius	Erosions, VC	μCT

(Continued)

TABLE 1 | Continued

Author, year (ref)	Participants	Type of study	Joints included	Outcomes	Other modalities
Yang, 2017 (45)	RA ($n = 12$); control ($n = 20$)	Cross-sectional	MCP; Radius	BMD, microstructure	
Yue, 2017 (46)	RA ($n = 20$); RA ($n = 20$)	Cohort	MCP	Erosions	
Figueriredo, 2018 (47)	RA ($n = 65$)	Cross-sectional	MCP	Erosions	
Ibrahim-Nasser, 2018 (48)	RA ($n = 29$)	Cross-sectional	MCP	Erosions, BMD, microstructure	CR
Kampylafka, 2018 (49)	PsA [($n = 20$) IL17 = 20)	Cohort	MCP; PIP; Radius	Erosions, Osteophytes, BMD, microstructure	MRI; US
Keller, 2017 (50)	Control [ACPA+ ($n = 29$); ACPA– ($n = 29$)]	Cross-sectional	MCP	Erosions, BMD, microstructure	
Kong, 2018 (51)	RA [($n = 32$) US+/– $n = 20/12$]	Cross-sectional	MCP	BMD, microstructure	US
Peters, 2018 (52)	RA ($n = 41$); control ($n = 38$)	Cross-sectional	MCP; PIP	Erosions	MRI; CR
Peters, 2018 (53)	eRA ($n = 17$); undifferentiated arthritis ($n = 4$)	Cross-sectional	MCP	Erosions	
Scharmga, 2018 (54)	RA ($n = 39$); control ($n = 38$)	Cross-sectional	MCP; PIP	Erosions	MRI; CR
Scharmga, 2018 (55)	RA ($n = 20$); control ($n = 10$)	Cross-sectional	MCP; PIP	Erosions	CR
Simon, 2018 (56)	RA ACPA + ($n = 106$); RA ACPA – ($n = 30$); CD ($n = 43$); UC ($n = 27$); PsO ($n = 74$); PsA ($n = 88$); control ($n = 108$)	Cross-sectional	MCP	BMD, microstructure	
Simon, 2018 (57)	PsA ($n = 55$); PsO ($n = 55$); control ($n = 47$)	Cross-sectional	MCP	Erosions, Osteophytes	
Yue, 2018 (58)	eRA ($n = 63$); Remission/not remission	Cohort	MCP	Erosions, BMD, microstructure	
Finzel, 2019 (59)	eRA ($n = 66$ TOC/TNFi $n = 33/33$)	Cohort	MCP; Radius	Erosions	
Berlin, 2019 (60)	Control ($n = 120$)	Cross-sectional	MCP; PIP	Erosions, Osteophytes	
Henchie, 2019 (61)	RA ($n = 17$); PsA ($n = 17$); control ($n = 12$)	Cross-sectional	MCP	Erosions, Osteophytes	
Keller, 2019 (62)	Control [ACPA+ ($n = 22$); ACPA– ($n = 23$)]	Cohort	MCP; Radius	Erosions	
Manske, 2019 (63)	RA ($n = 43$)	Cross-sectional	MCP	JSW	CR
Peters, 2019 (64)	RA ($n = 32$); control ($n = 32$)	Cohort	MCP; PIP	Erosions, BMD, microstructure	CR
Shimizu, 2019 (65)	RA [($n = 28$) TNFi+/– $n = 18/10$]	Cohort	Radius	Erosions	MRI
Wu, 2019 (66)	PsA ($n = 60$)	Cohort	MCP	Erosions, Osteophytes.	
Yue, 2019 (67)	eRA ($n = 117$)	Cohort	MCP	Erosions	
Simon, 2019 (68)	PsA [($n = 165$) None/MTX/bDMARD $n = 79;52;34$]	Cross-sectional	Radius	BMD, microstructure	
Wu, 2020 (69)	PsA ($n = 62$); control ($n = 62$)	Cross-sectional	MCP	Erosions, Osteophytes, BMD, microstructure	
Stok, 2020 (70)	RA ($n = 30$)	Cross-Sectional	MCP	JSW	

RA, Rheumatoid arthritis; PsA, Psoriasis arthritis; PSO, Psoriasis; ACPA, Anticitrullinated protein antibodies; US, Ultrasound; IL, interleukin; TNFi, Tumor necrosis factor inhibitors; TOC, tocilizumab; UC, Ulcerative colitis; CD, Crohn's disease; MTX, Methotrexate; bDMARD, biological Disease-modifying antirheumatic drug; BMD, Bone mineral density; MCP, Metacarpophalangeal; PIP, proximal interphalangeal.

was supported by one study that reported that the Sharp/van der Heijde (SvH) score based on MCP and PIP joints using CR were significantly associated with the number and size of erosions by HR-pQCT (52). However, the HR-pQCT scanner has a much smaller field of view, and it remains unknown if the added benefit of the greater sensitivity can make up for the fewer joints examined.

Twelve studies have compared erosion detection by HR-pQCT and MRI, with HR-pQCT as the gold standard, in patients with RA, PsA as well as ACPA positive arthralgia patients without arthritis. The sensitivity for MRI erosion detection ranged from 60 to 86% (1, 9, 16, 28), while the specificity was 97 to 100% (1, 9, 28, 32). HR-pQCT was superior at detecting erosions of less than 10 mm^3 (9).

HR-pQCT has also been used as a reference for erosion detection in order to compare it with US (7). US and HR-pQCT were consistent in the measurement of the width of erosions. However, there was a 10% false-negative rate, and 29% false-positive rate for erosion detection by US. False-negative

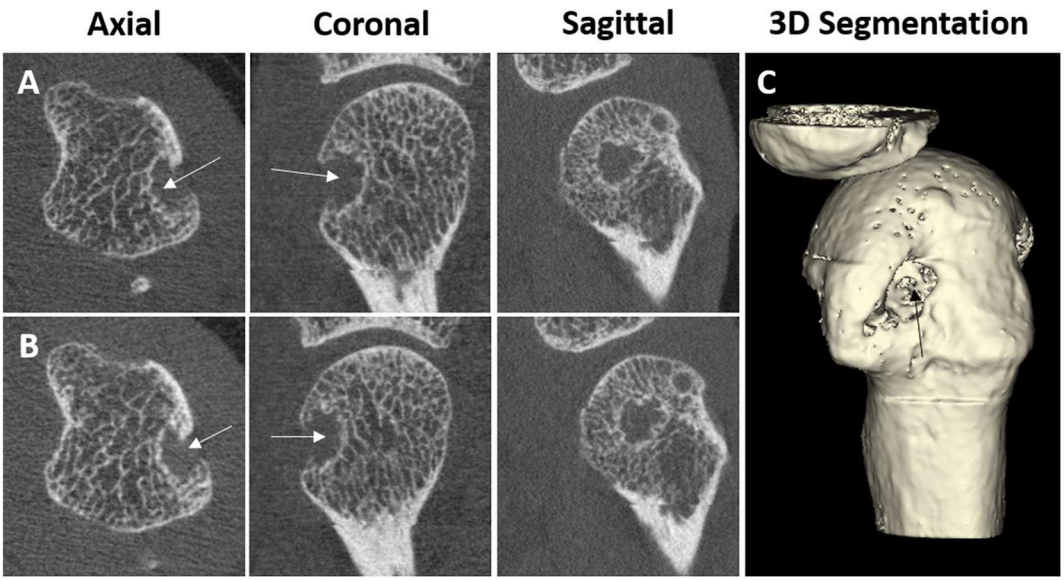

FIGURE 3 | Example of a cortical break meeting the SPECTRA definition of erosion by high-resolution peripheral quantitative computed tomography imaging in the radial quadrant of the second metacarpophalangeal joint from a 54-year-old female patient with rheumatoid arthritis. Arrows indicate the cortical break. **(A,B)** Are the grayscale, consecutive slices. **(C)** Is the 3D segmentation, performed using thresholding (3D Slicer, http://www.slicer.org). Images provided courtesy of Aarhus University (RKJ, KKK, EMH).

results recorded with US were due to its limited resolution to detect cortical lesions <2 mm in width. It was interpreted that the false-positive results occurred because of surface irregularities suggestive of bone erosions on US (7). US has a crucial drawback, as some quadrants of the joints are hard to visualize due to the acoustic window, e.g., radial or ulnar quadrant of the 3rd MCP.

Overall, these findings indicate that HR-pQCT detects more erosions and cortical interruptions than any other clinical imaging modality. However, with increased spatial resolution, more cortical interruptions are observed; this likely includes more physiological cortical interruptions, i.e., vascular channels. However, the higher resolution could also help distinguish pathological from physiological cortical interruptions.

Quantitative Evaluation of Erosions From HR-pQCT Imaging

As a result of the high spatial resolution and 3D imaging, accurate quantification of erosion size is possible. Several published methods exist, including semiquantitative scores (1, 4, 16), manual measures of the maximal dimension of width and depth (5, 7, 15, 30, 46, 48, 58), sphericity (23, 29), and surface area (23, 52, 64). Erosion volume is the most commonly used method due to the ability to detect changes (progression or repair) in three dimensions. However, there is presently no consensus on how to quantify erosion volume. Erosion width and depth have been manually assessed using OsiriX medical imaging software (Pixmeo, Bernex, Switzerland) (48, 50, 62, 65). The erosion volume can then be estimated from a half-ellipsoid formula (9, 23, 26, 28, 47, 57) or ellipsoid formula (**Figure 6A**) (42). More recently, semi-automated and automated algorithms have been introduced. These include Medical Image Analysis Framework (MIAF) (custom software developed at the University of Erlangen; **Figure 6B**) (23, 29), modified Evaluation Script for Erosions (mESE; using Image Processing Language, Scanco Medical) (47), Cortical Interruption Detection Algorithm (custom analysis developed at Maastricht University and Eindhoven University of Technology using Image Processing Language, Scanco Medical; **Figure 7**) (39, 40, 52, 53, 64) and a surface transformation algorithm (custom software developed at Worcester Polytechnic Institute; **Figure 8**) (61). MIAF, mESE, and the Cortical Interruption Detection Algorithm perform a segmentation of the bone and an estimation of the location of the cortical break. Based on this segmentation, the number of voxels in the erosion are counted, producing a true volumetric measure of erosion size. In contrast, the surface transformation algorithm uses statistical shape modeling to compare surface deformities of inflammatory arthritis joints with healthy joints, producing measurements of erosion depth (**Figure 8**) (61).

A single study compared erosion volumes measured manually (estimated from width and depth and calculated assuming the erosion approximated a half-ellipsoid) and using MIAF and mESE. While erosion volumes were similar when measured with the semi-automated methods, manual measurements yield significantly lower absolute volume measures compared with semi-automated methods, particularly for irregularly shaped erosions, illustrating that the erosions should not be assumed to be shaped like a half-ellipsoid (47). To date, no other studies have compared other erosion measurement algorithms.

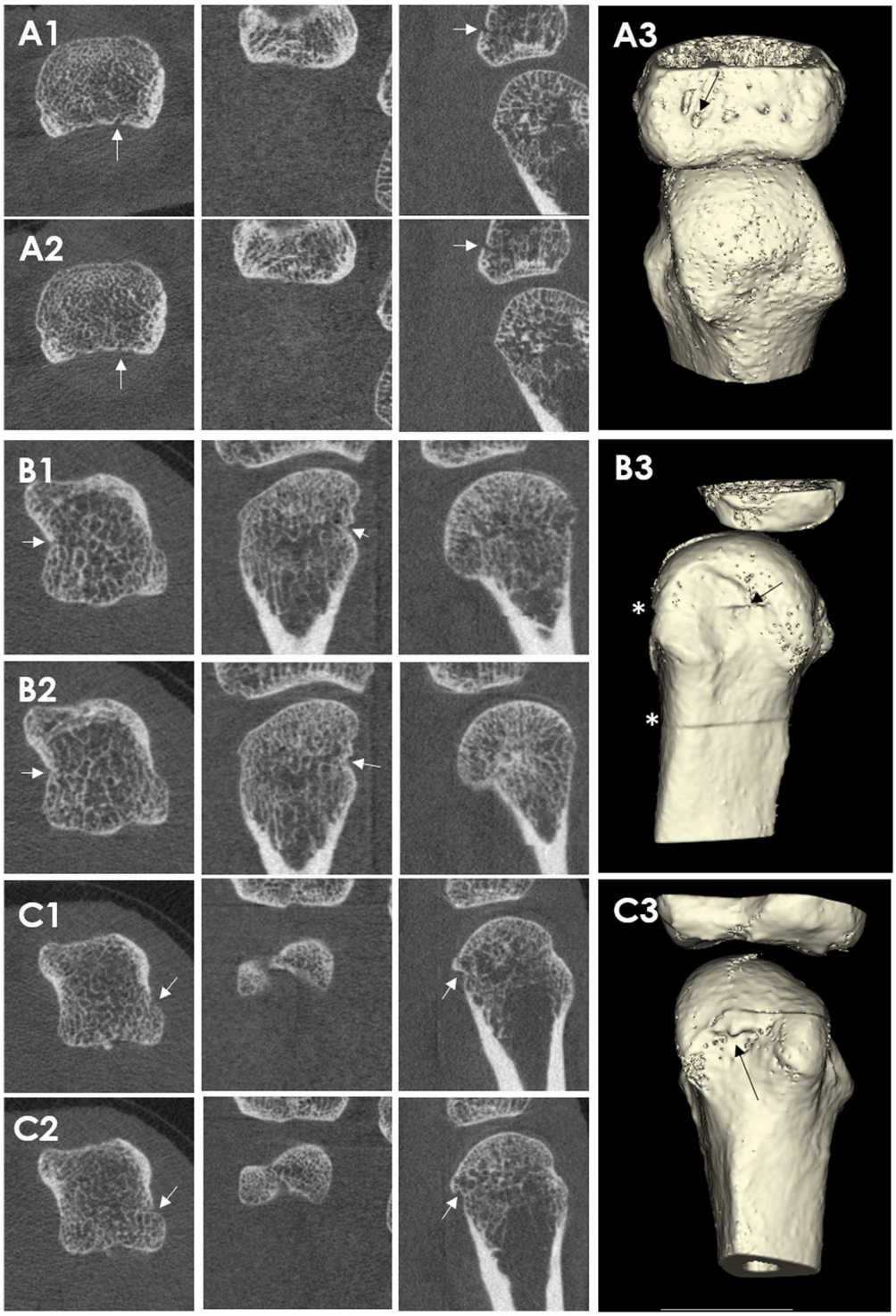

FIGURE 4 | HR-pQCT images of cortical breaks, which do not meet the SPECTRA definition for erosions. Arrows indicate the cortical break. Patient A, where **(A1,A2)** are consecutive slices and **(A3)** is the 3D segmentation. Third MCP Joint from a 67-year-old male patient with rheumatoid arthritis. The cortical break is linear in shape. Therefore, the cortical break is defined as a vascular channel Patient B, where **(B1,B2)** are consecutive slices, and **(B3)** is the 3D segmentation. Second MCP Joint from a 51-year-old female patient with rheumatoid arthritis. Cortical break in relation to stack misalignment represented by *. Patient C, where **(C1,C2)** are consecutive slices and **(C3)** are 3D segmentation. Second MCP Joint from a 51-year-old female patient with rheumatoid arthritis. Cortical break in relation to a bony proliferation. Images provided courtesy of Aarhus University (RK-J, KK, and E-MH).

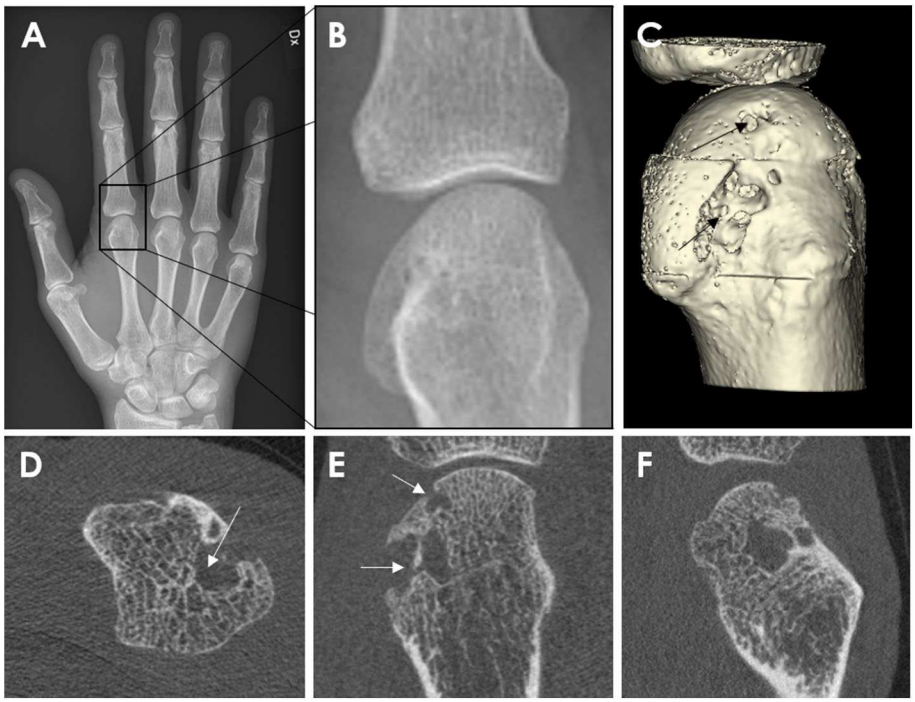

FIGURE 5 | Conventional Radiography **(A,B)** and HR-pQCT imaging **(C–E)** from a 62-year-old male patient with rheumatoid arthritis. Anterior-posterior view of the right hand **(A)**. Enlargement of the second metacarpophalangeal joint **(B)**. High-resolution peripheral quantitative computed tomography images of the second MCP joint as 3D segmentations performed using thresholding **(C)** (3D Slicer, http://www.slicer.org) and the axial **(D)**, coronal **(E)**, and sagittal **(F)** plane, congruent with the corresponding radiograph. The arrow demonstrates the erosion location. Images provided courtesy of Aarhus University (RKJ, KKK, EMH).

Vascular Channels and Cortical Micro-Channels

The high resolution of HR-pQCT not only reveals cortical interruptions meet the definition of erosions but also interruptions which have been hypothesized to be vascular channels. According to the SPECTRA erosion definition, the cortical interruption was suspected to be vascular channels if the interruption was characterized by a parallel cortical lining seen on two consecutive slices and two orthogonal planes (41).

Efforts have been made to test this hypothesis. One study investigated 10 cadaveric fingers, not necessarily affected by inflammatory arthritis, imaged by HR-pQCT with subsequent histological evaluation. Fifty-two vascular channels were identified by histology, and 11 of these fulfilled the definition of erosions on HR-pQCT. Seven cortical breaks which fulfilled the SPECTRA definition of vascular channels were located. Five could be evaluated with histology, and only one of these was a true vascular channel. While they are not vascular channels, these microchannels may provide a link between the synovium and the bone marrow (41). Another approach for investigating vascular channels was to inject the contrast agent Imeron into the ulnar and radial artery of six cadaveric hands prior to HR-pQCT scanning (44). This technique detected very small intraarticular vascular channels. The vascular channels, however, were located proximal to the cortical micro-channels. With both studies, it is possible that very small vascular channels escaped detection due to the challenges of visualizing by perfusion and casting, microCT contrast or standard histological stains (44).

These findings do support the suggestion that bone has a large number of channels passing from the inside to the outside of the bone that is not necessarily linked to erosions, nor do all channels contain vessels. The shape of cortical interruptions cannot be used to accurately decide if cortical breaks contain vessels, as many cortical interruptions, that do not have a classic linear shape, contain vessels (41). Understanding the role of these various channels may be important to understand RA pathology. Traditionally, it has been postulated that synovitis is an initial process that is succeeded by bone involvement known as the "outside-in hypothesis." Conversely, it has been suggested that RA is primarily a bone marrow disease which subsequently affects the synovial membrane; this is known as the "inside-out hypothesis" (74). The cortical micro-channels connect the synovial compartment with the bone marrow and might be important in investigating whether bone damage begins from the inside-out or outside-in (75, 76). HR-pQCT will be useful in combination with other imaging techniques to understand some of these pathological mechanisms.

Bony Proliferations

Bony proliferation is another common pathologic feature of many arthritic diseases, including PsA, primary hand OA and secondary OA due to inflammatory arthritis. There is currently

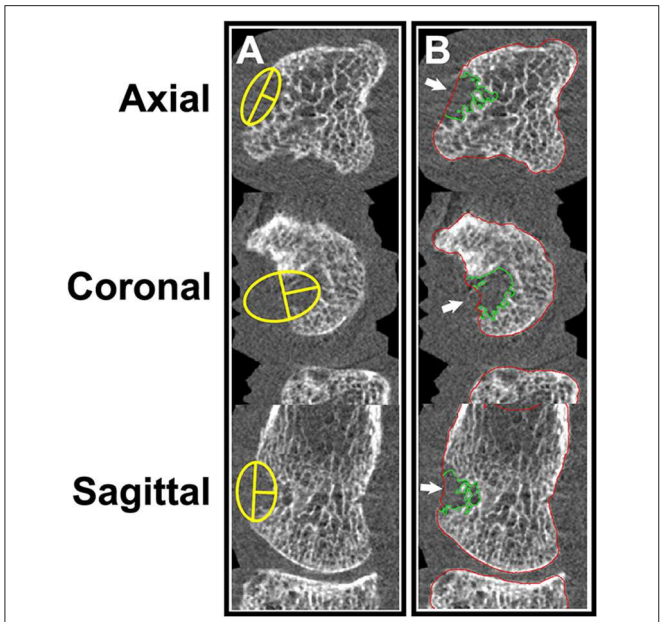

FIGURE 6 | (A) Manual measurement of erosion width and depth. **(B)** Semi-automated erosion volume assessment using MIAF (University of Erlangen). Images provided courtesy of the University of Calgary (JJT, CB, SLM).

no consensus on how to define or quantify the assessment of bony proliferations. However, most studies have defined osteophytes and enthesophytes in a similar fashion; these include bony protrusions from the juxta-articular cortical shell (4, 5, 10, 14, 21, 57) (**Figure 9**), bony proliferation at specific anatomical sites (57), or bone formation arising from the periosteal bone cortex at the insertion sites of the capsule, ligament, or tendons (66, 69). Thirteen publications characterizing osteophytes or enthesophytes with HR-pQCT were found; 8 of which were cross-sectional studies. In three of the studies, the osteophytes or enthesophytes were graded on a semi-quantitative scale (0–3) according to the height measured as the maximum distance between the original and the new cortical lining (4, 5, 21). Two of these three studies also presented direct measurements of the height. The remaining five studies measured osteophyte or enthesophyte height directly (5, 14, 21, 57), and one of these also segmented the osteophyte volume (69). Two studies found that chronic RA patients had a greater number and larger osteophytes than healthy subjects (4, 61); these osteophytes were found mostly in the palmar and dorsal quadrant of the joints. PsA patients had a greater number and size of osteophytes relative to RA patients (5, 61). The highest number of osteophytes in PsA patients was observed in the radial quadrant, closely followed by the dorsal and palmar quadrants. Enthesophytes in patients with PsA is more abundant and greater in size compared to healthy subjects. The majority of enthesophytes in patients with PsA were found at the palmar and dorsal quadrants of the metacarpal heads (57). The volume of enthesophytes is also significantly greater in patients with PsA compared to healthy controls (69). Patients with PsA had a similar number and size of osteophytes compared to those with hand OA. The osteophytes of patients with hand OA were seen predominantly in the palmar and dorsal quadrant, while the distribution of osteophytes in patients with PsA was more widespread (21). In addition, patients with PsA have significantly taller and more abundant bony proliferations (5). There have also been attempts to study bony proliferations according to age. In healthy subjects, the number of osteophytes in the 2nd and 3rd MCP and PIP joints were found to increase with age (60). The number and height of enthesophytes also increase with age; these have been observed not only in patients with PsA but also in healthy subjects. Therefore, the progression of osteophytes may not solely signify disease severity but may also indicate normal age-related change (57). Like erosions, the sensitivity for enthesophyte detection by HR-pQCT is far higher than MRI as 89% of PsA patients had enthesophytes by HR-pQCT, while they were observed in only 30% of the PsA patients on MRI (49). Presently, it is unknown whether there is a benefit of HR-pQCT imaging for tracking the progression of bony proliferation compared to conventional radiographs since no studies have compared the sensitivity and osteophytes seem to progress despite therapy.

Joint Space Width

HR-pQCT images can also be used to quantify joint space width and volume based on the 3D volume between the bones rather than the 2D analysis that is typically applied to conventional radiographs. Seven publications with joint space analysis were found; all but one has investigated the validity of proposed semi-automatic scripts. Three different algorithms were developed using a similar methodology (11, 13). A consensus method has recently been published by the SPECTRA Collaboration (**Figure 10**), this method is proposed for universal use in ongoing and future clinical trials of arthritic conditions (70). The established joint space width (JSW) metrics include mean, minimum and maximum JSW as well as standard deviation, asymmetry (maximum/minimum) and joint space volume. A single study has investigated the validity of a JSW script on cadaveric MCP joints at different flexion angles. The study found in order to have reliable joint space measures, the acquisition of the joints had to be < 10 degrees flexion for longitudinal studies (36). Whether the joint space analysis is affected by other factors such as joint swelling, is currently under investigation.

Lastly, two studies evaluated relationships between joint space narrowing assessed from CR and 3D joint space analysis on HR-pQCT. Minimum JSW, JSW standard deviation, and JSW asymmetry assessed by HR-pQCT were associated with SvH joint space score (13, 63).

The minimum joint space width has been shown to be significantly smaller in patients with RA compared to healthy subjects, which is suggestive of a loss of cartilage thickness in the affected patients (13). However, larger studies are needed to reliably investigate group differences.

Bone Mineral Density and Microstructure

HR-pQCT provides 3D images, so volumetric bone mineral density (vBMD, g/cm^3) is assessed rather than areal BMD (aBMD) that is reported by dual-energy x-ray absorptiometry (DXA). Microstructural features of trabecular bone, including

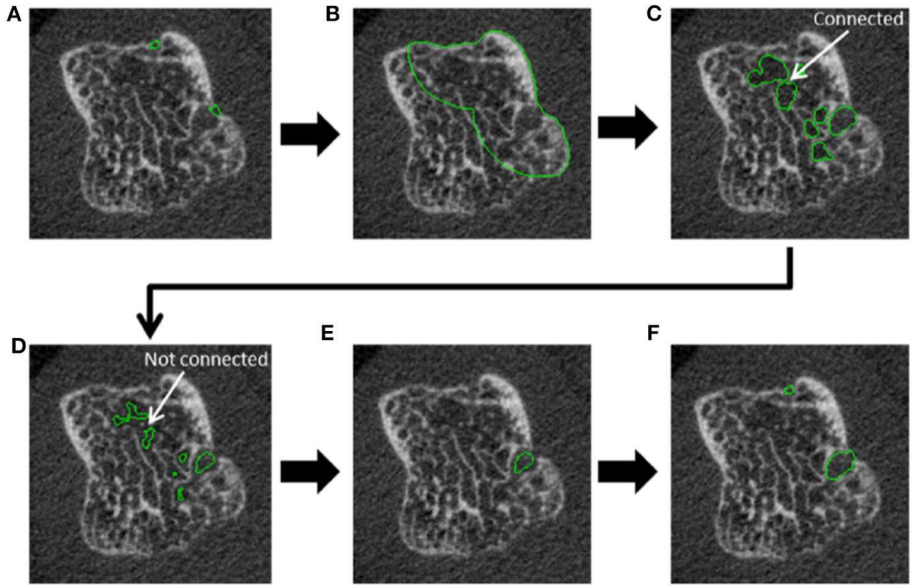

FIGURE 7 | Steps incorporated in the automated cortical interruption detection algorithm and measurement of underlying loss of trabecular bone, as visualized on a 2D grayscale image. **(A)** Detection of two cortical interruptions ≥0.41 mm. **(B)** Region of interest (ROI) identified by dilating the cortical interruptions by 48 voxels (corresponding to 3.936 mm), and masking with the periosteal contour. **(C)** Only voids that are ≥0.738 in diameter are selected by performing a distance transformation within the ROI. **(D)** Voids are eroded by 2 voxels to detach connections of ≤0.328 mm and prevent leakage into the trabecular bone. **(E)** Inclusion of voids that remain connected to a cortical interruption after erosion. **(F)** Dilation of voids to the original size, and inclusion of cortical interruptions that were originally detected. Reproduced with permission from (53).

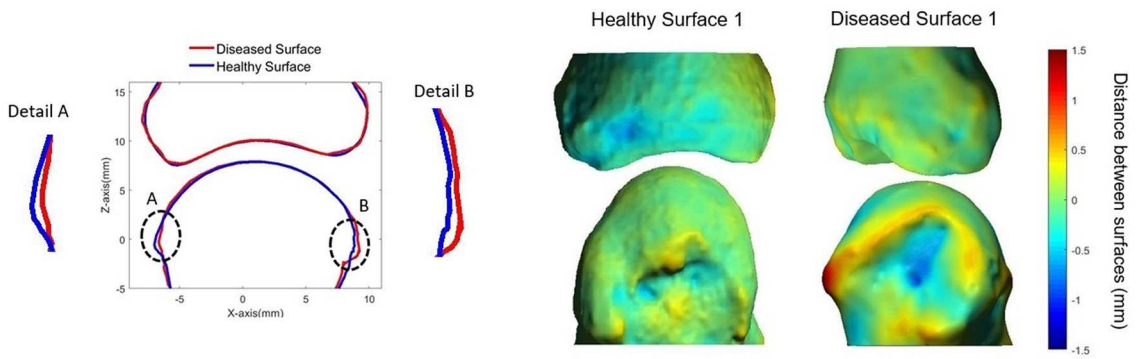

FIGURE 8 | Surface deformation model (61) showing: **(Left)** cross-section of MCP joint with the diseased surface (red) overlaid on the average healthy surface (blue). **(Right)** 3D heat map representing distances between diseased (top) and healthy (bottom) surfaces. Positive distances reflect bony proliferations, while negative distances represent erosive damage. Image provided courtesy of Worcester Polytechnic Institute (Kyle Murdock and Karen Troy).

trabecular thickness, number and separation, have been measured directly and with greater accuracy using the second-generation scanners compared to the first-generation scanner (77). BMD and microstructure imaged by HR-pQCT have been investigated in several different groups of patients and with focus on different joints of interest as well as the typical measurements of the distal radius and distal tibia applied in osteoporosis studies. Most of these studies were cross-sectional, and the majority of studies were done with either RA or PsA patients. One study assessed the relationship of periarticular osteoporosis in the wrist and MCP joint by HR-pQCT imaging with BMD in axial skeletal sites by DXA. Areal BMD in the axial skeleton was moderately correlated with vBMD assessed by HR-pQCT in both the radius and 2nd metacarpal head while microarchitecture only had a weak to moderate correlation in patients with RA (8). Finally, one study investigated the correlation between bone density and bone microstructure parameters measured at the MCP joint and SvH score in patients with RA, but only found a significant correlation between trabecular separation and SvH score (3).

Six cross-sectional studies compared RA patients with healthy subjects. Cortical and trabecular vBMD was significantly lower in female and male patients with RA when compared to healthy subjects at the distal radius, even though no difference in axial

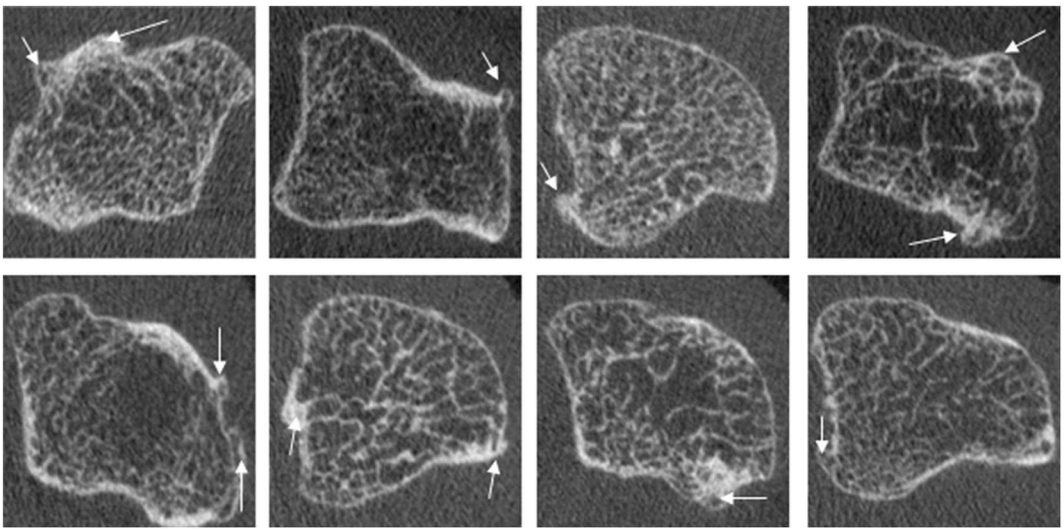

FIGURE 9 | Examples of osteophytes in the metacarpal head of PsA patients, which commonly show widespread involvement of the cortical bone. Images provided courtesy of The Chinese University of Hong Kong (L-ST).

aBMD measured by DXA could be observed (17, 24). In the same population, the cortical porosity and trabecular separation were significantly greater, and bone volume fraction significantly lower, in the RA patients (17, 19, 24). Volumetric BMD and microarchitecture were similarly different at the MCP joints in three of four studies. The trabecular vBMD, bone volume fraction and thickness was significantly lower, while trabecular separation was significantly higher in patients with RA compared to healthy subjects (3, 12, 43, 45).

Five cross-sectional studies have investigated bone density and microarchitecture in patients with PsA. At the radius, cortical vBMD was significantly lower, while cortical porosity was significantly higher in PsA patients compared to healthy subjects. By DXA, the PsA patients had significantly higher aBMD at the lumbar spine compared to healthy subjects; this difference, however, became insignificant after adjusting for Body Mass Index (BMI), suggesting BMI may have confounded the relationship (4). Other studies have found a significant loss of periarticular trabecular bone in PsA patients compared to healthy subjects with regards to both vBMD (69) and bone structure (27). Compared to treatment naïve PsA patients, patients with a history of biological disease-modifying anti-rheumatic drugs (DMARD) treatment had significantly higher vBMD, BV/TV as well as greater trabecular number and thickness. No significant differences in bone density or microarchitecture outcomes were observed in patients previously treated with MTX compared to treatment naïve PsA patients (68).

The trabecular number and vBMD were significantly lower, while trabecular separation was significantly higher for PsA patients when compared with RA patients. However, this difference was only seen between ACPA positive RA patients and PsA patients. The ACPA positive RA patients had a significantly longer disease duration. Therefore, this difference is more likely attributed to disease duration rather than the underlying condition (20). In contrast, when comparing patients with various chronic inflammatory diseases (ACPA-positive RA, ACPA-negative RA, Crohn's Disease, ulcerative colitis, psoriasis and PsA) and healthy participants, vBMD differed only between ACPA-positive RA and healthy subjects (56). Together these findings suggest that to date, the bone density and microstructure seems to be affected in different kinds of inflammatory diseases, but the nature of these findings are unclear as the periarticular bone density and microstructure are influenced by other factors independent of the inflammatory nature of the disease, such as genetic factors, sex, physical activity, height, weight, BMI, smoking and alcohol consumption, and daily calcium intake.

Reproducibility of the Pathological Measures

Reproducibility has been reported for erosion measurements, osteophytes, joint space width, bone mineral density and microstructure (**Table 2**). Reproducibility is most often presented as Intraclass correlation coefficients (ICC), root mean square coefficient of variance (CV_{RMS}%), but also as the coefficient of variation. The reproducibility for bone mineral density, microstructure, and most joint space width metrics are excellent (**Table 2**). Reproducibility for erosion measures is generally good but does show some variation. Due to the distinct methods used for erosion quantification, these values are hard to compare. Osteophyte assessment has the lowest values for reproducibility (69).

When compared with reproducibility for semi-quantitative scoring systems on MRI (RAMRIS) (78) and CR (SvH) (79), HR-pQCT offers many advantages by using quantitative tools for outcome measurement that require fewer operator inputs. The reliability for erosion count was higher for HR-pQCT than MRI. However, the ICC was excellent for both modalities (9, 28), while only moderate for CR (55). The semi-automated or fully-automated assessments of bone mineral density, microstructure, joints space width and cortical interruptions result in intra-reader and inter-reader differences that are non-existent, or

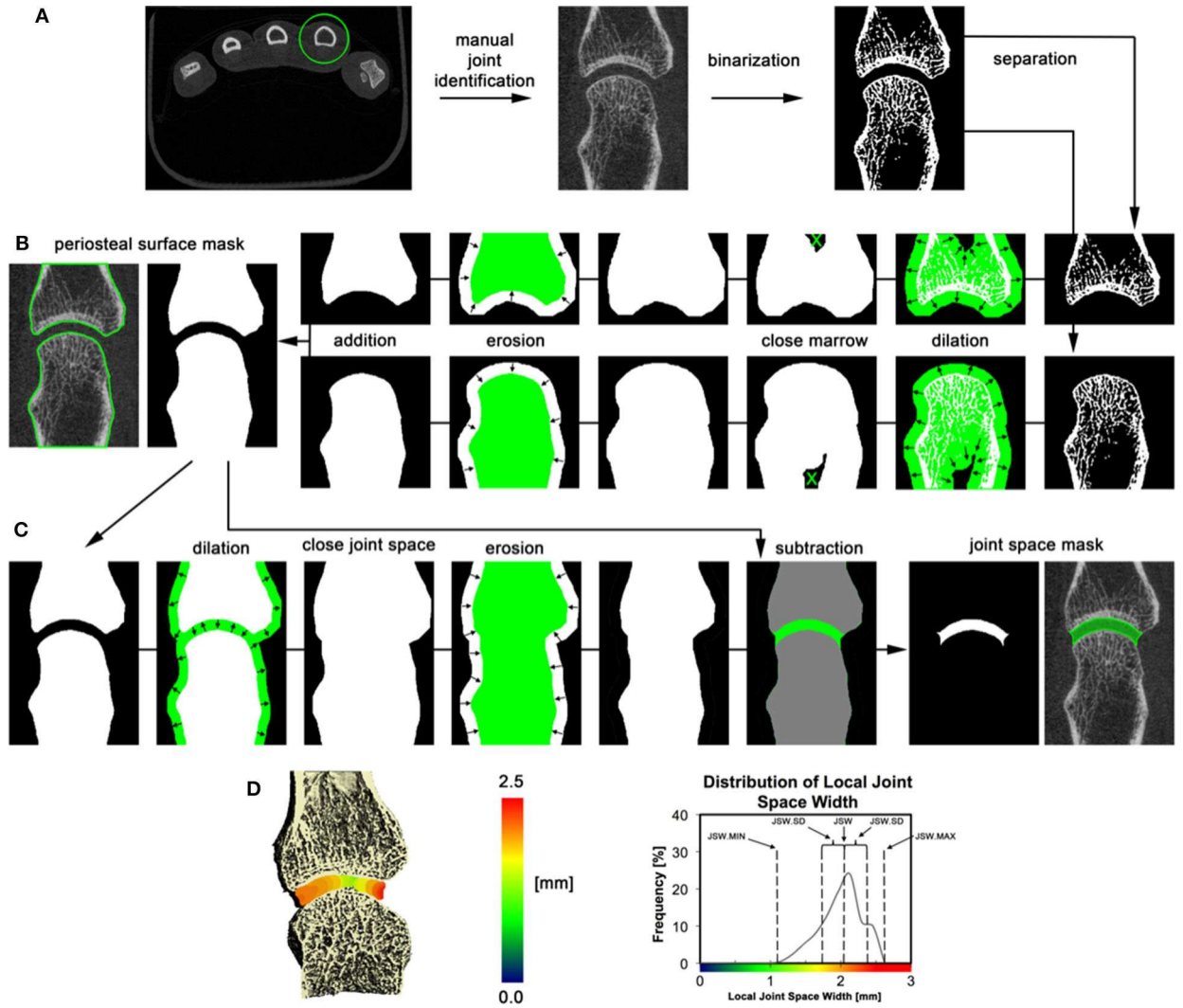

FIGURE 10 | 3D volumetric joint space width analysis by HR-pQCT. **(A)** The relevant joint is identified; bone is segmented by thresholding, and bones are separated based on their relevant position (distal and proximal). **(B)** Periosteal surfaces for each bone in the joint are identified using an automated process. **(C)** Joint space volume is identified through a series of morphological operations and subtraction of the original bone volumes. **(D)** Joint space metrics are derived from the 3D map of local joint space widths. The 3D map is shown in pseudo color (left), and as a distribution (right) for the 2nd metacarpal of an RA patient. Reproduced with permission from (13).

nearly negligible because the analyses are automated, with the exception of an allowance for corrections of bone segmentation. Scan-rescan reproducibility for JSW minimum is similar to that obtained with inter-reader ratings on 2D radiographs (RMSSD 0.18 mm) but far superior for mean JSW (RMSSD 0.05 mm) (80). Intra- and inter-reader reproducibility and reliability for erosion detection and volume are comparable to reproducibility and reliability reported for the erosion domain of the RAMRIS scoring system (9, 28, 81, 82).

Longitudinal Changes of the Pathological Measures

While the diagnostic uses of HR-pQCT might be limited at present, the research applications are vast. Several clinical trials have been conducted using erosion volume by HR-pQCT as an outcome measure. One of the major advantages is the potential for shorter monitoring times to evaluate erosion progression or repair. Fifteen studies have reported longitudinal changes in the number and/or size of erosions. Of these, three investigated PsA (14, 49, 66), 10 investigated patients with RA (6, 10, 15, 29, 42, 46, 58, 59, 64, 65), and one study examined ACPA+ individuals without arthritis (62). Seven studies investigated intervention with different therapies either as an open-label study or secondary analysis in a randomized controlled trial. Five of the seven studies were done on patients with RA (12, 19, 43, 55, 69), and two in PsA (21, 60). In patients with established RA, two studies of patients with mean disease duration more than 5 years did not detect any change in erosions at 1-year follow-up (10, 64). However, longitudinal changes are diverse.

Studies which traced changes of individual erosions in patients receiving care according to treat-to-target strategy over a 1-year period have shown that 15–31% of erosions progress in size, 48–65% were stable in size and 20–21% show partial repair after 1 year (29, 58, 67).

The shortest time interval over which significant changes have been evaluated is 3 months. This study was conducted enrolling patients with RA and a mean disease duration of more than 5 years who were receiving either a TNF inhibitor (TNFi) in combination with methotrexate or methotrexate alone. While no significant changes in MRI outcome measures were observed, a significant increase in erosion volume assessed by HR-pQCT was observed for the methotrexate-treated patients, and those on combination therapy with treatment response had a demonstrated decrease in erosion volume (42). In this same study, joint space did decrease significantly in patients in combination therapy only. Paradoxically, this was not seen in methotrexate-treated patients. However, methotrexate-treated patients had smaller joint space at baseline, which may explained why no change was seen after the 3-month follow-up (42). Change in erosion volume after 3 and 6 months has also been investigated for patients with RA and a mean disease duration of roughly 10 years receiving either alendronate or denosumab together with their regular DMARD treatment (46). No significant change was observed after 3 months. Conversely, erosion volume increased significantly in patients receiving alendronate, while decreasing significantly in patients receiving denosumab after 6 months. While these represent the shortest time interval over which changes in erosion volume and JSW have been observed, two studies have shown decreases in erosion volume in response to tocilizumab in combination with methotrexate for both patients with newly diagnosed RA (59) and established RA (15); this has also been observed for patients with established RA treated with TNFi in combination with methotrexate (6) over a 1-year follow-up. Stabilization in erosion size with therapy has also been demonstrated, in newly diagnosed patients with RA on treatment with a TNFi in combination with methotrexate (59). PsA studies have shown slower erosion changes than RA; no significant progression in erosions was seen in patients with established PsA after 24 weeks (49) or 1-year (14). However, one study found progression of erosion number and size after 5-years in patients with established PsA and a mean disease duration of 14 years (66).

While the measurement of erosion size has been the most commonly used outcome metric, osteophytes and bone quality have also been assessed. Five longitudinal studies investigated changes in osteophytes over time. In RA patients, no significant change in osteophyte number or score was seen after a year (10). However, an 18-month follow-up study did find an increase in both osteophytes number and volume in RA patients in open-label treatment (31). No change in osteophyte size was observed in PsA patients treated with secukinumab for 24 weeks (49). However, in patients treated with MTX and TNFi osteophyte height increased over 1 year (14), and volume increased over 5 years in patients in open-label treatment (66).

Only six longitudinal studies of bone density and microarchitecture in the MCP joint or the radius have been reported. In longitudinal studies of RA or PsA patients without a healthy control group, conducted with 3-month or 1-year follow-up, no significant changes in vBMD or microstructure were observed (42, 49, 58). In one study, greater decreases in vBMD and microstructure over 1 year were observed in RA patients compared to healthy controls (64), while two other studies found comparable decreases in both early RA patients and healthy controls (37, 62). Differences in disease duration, treatment status, and the anatomic site measured may explain the variable findings across studies. More extensive longitudinal studies are needed to reveal the critical anatomic locations, time course, and mechanisms of bone loss that should be strategically targeted for observation.

Combined with advances in image processing and image registration, individual spatially localized changes can be monitored with high sensitivity and reliability (**Table 2**) (64). To date, the published studies report data for the joint region captured in the field of view, and not for the local changes such as the peri-articular region. Furthermore, these techniques can be applied where only subtle changes are anticipated, such as understanding bony damage progression in the presence of subclinical inflammation.

Early Detection of Articular Damage in Inflammatory Arthritis by HR-pQCT Imaging

The sensitive detection of erosive damage and bony proliferation suggests that HR-pQCT may have utility in the early detection of articular damage in inflammatory arthritis. For conventional radiographs, erosions have been observed to be prevalent in ∼50% of RA patients at clinical diagnosis, and up to 60% of patients have erosions after 1 year (83). Therefore, the higher sensitivity of HR-pQCT compared to conventional radiographs is promising not only in assessing longitudinal changes but may also be useful for early detection in patients where the diagnosis is suspected but cannot be made clinically. However, the ability to image multiple joints is limited by the acquisition speed. Although many erosions occur in the standard scan sites of the 2nd and 3rd metacarpals of the dominant hand, other joints will be missed. Further, the contrast is insufficient to detect inflammation (synovitis and osteitis, also referred to as bone marrow oedema in RA patients) believed to be key precursors to clinical disease. Nonetheless, two cross-sectional studies found a significantly thinner trabecular bone in the MCP joints of ACPA positive individuals with arthralgia compared with ACPA negative healthy individuals (18, 50). Kleyer et al. also observed significantly lower trabecular number, bone volume fraction and vBMD in ACPA positive individuals with arthralgia compared with ACPA negative healthy individuals (18), suggesting that periarticular bone loss may be an early sign of clinical disease. Changes to bone mineral density and microstructure, however, is very non-specific to arthritis, as possible changes can be attributed to many other factors. Therefore, the use of bone mineral density and microstructure for early detection of articular damage in inflammatory arthritis

TABLE 2 | Reproducibility measures.

Author, year (ref)	Participants	Reproducibility feature	Method	Findings
Erosion count				
Albrecht, 2013 (9)	RA ($n = 50$)	Inter-reader reliability	Erosion count	ICC range: metacarpal head: 0.936–1.00. ICC range: phalangeal Base: 0.948–1.00.
Aschenberg, 2013 (10)	RA ($n = 40$)	Inter-reader reliability	Erosion score	ICC (range): 0.79 (0.57–0.95)
Hecht, 2015 (26)	RA ($n = 242$)	Inter-reader agreement	Erosion count	ICC: [0.87–1.00]
Regensburger, 2015 (28)	RA ($n = 103$)	Inter-reader reliability	Erosion count	ICC [95% CI]: 0.98 [0.98–0.98]
Scharmga, 2016 (34)	RA ($n = 44$); control ($n = 38$)	Intra- and inter-reader reliability	Cortical break count	ICC [95% CI]: 0.61 [0.49–0.70] ICC [95% CI]: 0.55 [0.43–0.65]
Peters, 2017 (40)	RA ($n = 32$); control ($n = 32$)	Inter-reader reliability	Cortical break count 1>0.16 mm, 2>0.33 mm 3>0.53 mm	ICC [95% CI]: 0.91 [0.65–0.97] ICC [95% CI]: 0.81 [0.52–0.92] ICC [95% CI]: 0.52 [0.11–0.78]
Scharmga, 2017 (41)	Cadaver ($n = 7$)	Intra- and inter-reader reliability	Cortical break count	ICC range: 0.52–0.75 ICC range: 0.37–0.55
Peters, 2017 (39)	RA ($n = 7$); control ($n = 3$)	Inter-reader reliability	Cortical break count	ICC [95%CI]: 0.97 [0.90–0.99]
Peters, 2018 (53)	eRA ($n = 17$); undifferentiated arthritis ($n =4$)	Inter-reader reliability and reproducibility	Cortical interruptions count	ICC [95%CI]: 0.96[0.89–0.97] ICC [95%CI]: 0.94[0.89–0.97] ICC [95%CI]: 0.96[0.92–0.98] ICC [95%CI]: 0.94[0.89–0.97]
Scharmga, 2018 (54)	RA ($n = 39$); control ($n = 38$)	Intra- and inter-reader reliability	Cortical interruptions	ICC [95%CI]: 0.69[0.65–0.73] ICC [95%CI]: 0.56[0.49–0.62]
Scharmga, 2018 (55)	RA ($n = 20$); control ($n = 10$)	Intra- and inter-reader reliability	Cortical interruptions	ICC [95%CI]: 0.88 [0.83–0.92] ICC [95%CI]: 0.48 [0.20–0.67]
Simon, 2018 (57)	PsA ($n = 55$); PsO ($n = 55$); control ($n = 47$)	Inter-reader agreement	Erosions number	ICC: 0.96
Berlin, 2019 (60)	Control ($n = 120$)	Inter-reader agreement	Erosion count	ICC [95%CI]: 0.76 [0.62–0.86]
Erosion score				
Aschenberg, 2013 (10)	RA ($n = 40$)	Inter-reader reliability	Erosion and osteophyte count and score	ICC (range): 0.79 (0.57–0.95)
Erosions width and depth				
Finzel, 2013 (15)	RA ($n = 20$)	Intra- and inter-reader reproducibility	Width and depth	ICC: 0.99 ICC: 0.99 ICC: 0.93 ICC: 0.94
Lee, 2015 (1)	RA ($n = 16$)	Intra- and inter-reader reproducibility	Sum maximum dimension.	ICC: 0.89 ICC: 0.99
Barnabe, 2016 (30)		Inter-reader reliability	Width and depth	CV_{RMS}%: 12.3–20.6 CV_{RMS}%: 22.2–24.0
Yue, 2017 (46)	RA ($n = 20$); RA ($n = 20$)	Intra- and inter-reader reliability	Width and depth	ICC [95%CI]: 0.99 [0.94–1.00] ICC [95%CI]: 0.99 [0.96–1.00] ICC [95%CI]: 0.98 [0.96–0.99] ICC [95%CI]: 0.98 [0.97–0.99
Keller, 2017 (50)	Control [ACPA+ ($n = 29$); ACPA– ($n = 29$)]	Intrareader reproducibility	Width and depth	CV%: 14.9 CV%:10.8%
Ibrahim-Nasser, 2018 (48)	RA ($n = 29$)	Inter-reader precision	Width and depth	CV_{RMS}%: 16.0–20 CV_{RMS}%: 17.5–23.4
Yue, 2018 (58)	eRA ($n = 63$); Remission/not remission	Intra- and inter-reader reliability	Width and depth	ICC [95%CI]: 0.97 [0.93–0.99] ICC [95%CI]: 1.00 [0.99–1.00] ICC [95%CI]: 0.98 [0.93–0.99] ICC [95%CI]: 0.92 [0.70– 0.98]
Henchie, 2019 (61)	RA ($n = 17$); PsA ($n = 17$); control ($n = 12$)	Inter-reader precision	Depth.	RMSE: 4+/−3% Precision error: 50 μm
Erosion volume				
Töpfer, 2014 (23)	RA ($n = 18$)	Inter-reader precision	Volume (Half-ellipsoid). Volume. (MIAF).	CV_{RMS}%: 15.4 CV_{RMS}%: 7.78
Regensburger, 2015 (28)	RA ($n = 103$)	Inter-reader reliability	Volume (Half-ellipsoid).	ICC [95% CI]: 0.95 [0.94–0.96]

(Continued)

TABLE 2 | Continued

Author, year (ref)	Participants	Reproducibility feature	Method	Findings
Töpfer, 2015 (29)	RA ($n = 22$)	Inter-reader precision	Volume. (MIAF).	CV_{RMS}%: 6 – 8.3
Figueriredo, 2016 (31)	ACPA+ RA ($n = 202$)	Inter-reader reliability	Volume (Half-ellipsoid).	ICC [95%CI]: 0.96 [0.94–0.97]
Shimizu, 2017 (42)	RA [($n = 27$) TNFi/MTX $n =$ 17/10)	Intra- and inter reader agreement	Volume	CV_{RMS}%: 3.43 CV_{RMS}%: 3.92
Yue, 2017 (46)	RA ($n = 20$); RA ($n = 20$)	Intra- and inter-reader reliability	Volume	ICC [95%CI]: 0.98 [0.87–1.00] ICC [95%CI]: 0.96 [0.73–1.00]
Keller, 2017 (50)	Control [ACPA+ ($n = 29$); ACPA– ($n = 29$)]	Intrareader reproducibility	Volume (Osirix)	CV%20.6%,
Figueriredo, 2018 (47)	RA ($n = 65$)	Inter-reader reliability	Volume (Half-ellipsoid) Volume (MIAF) Volume (mESE)	ICC [95%CI]: 0.95 [0.92–0.97] ICC [95%CI]: 0.92 [0.79–0.97] ICC [95%CI]: 0.99 [0.99–0.99]
Ibrahim-Nasser, 2018 (48)	RA ($n = 29$)	Inter-reader precision error	Volume (Osirix)	CV_{RMS}%: 16.0–20 CV_{RMS}%: 17.5–23.4 CV_{RMS}%: 14.0–21.2
Peters, 2018 (53)	eRA ($n = 17$); undifferentiated arthritis (n =4)	Intra- Inter-reader reliability and Intra- Inter-reader reproducibility	Cortical interruptions (CIDA)	ICC [95%CI]: 0.99[0.99–1.00] ICC [95%CI]: 0.91[0.81–0.96] ICC [95%CI]: 1.00[0.99–1.00] ICC [95%CI]: 0.91[0.81–0.96]
Simon, 2018 (57)	PsA ($n = 55$); PsO ($n = 55$); control ($n = 47$)	Inter-reader agreement	Volume	ICC: 0.90
Yue, 2018 (58)	eRA ($n = 63$); Remission/not remission	Intra- and inter-reader reliability	Volume	ICC [95%CI]: 0.95 [0.79–0.99] ICC [95%CI]: 0.98 [0.83–1.00]
Shimizu, 2019 (65)	RA [($n = 28$) TNFi+/– $n =$ 18/10]	Intra- and Inter-reader reproducibility	Volume (Osirix)	ICC: 0.93 ICC: 0.80
Wu, 2020 (69)	PsA ($n = 62$); control ($n =$ 62)	Inter-reader reliability	Volume	ICC [95%CI]: 1.00 [0.99–1.00]
Erosion surface area				
Töpfer, 2014 (23)	RA ($n = 18$)	Inter-reader precision	Surface Area (MIAF)	CV_{RMS}%: 9.89
Peters, 2017 (40)	RA ($n = 32$); control ($n = 32$)	Inter-reader reliability	Cortical interruptions 1>0.16 mm, 2>0.33 mm 3>0.53 mm	1.ICC [95% CI]:0.93 [0.82–0.97 2.ICC [95% CI]:0.86 [0.67–0.94] 3.ICC [95% CI]:0.21 [−0.15–0.56]
Peters, 2017 (39)	RA ($n = 7$); control ($n = 3$)	Inter-reader reliability	Cortical break Surface area	ICC [95%CI]: 0.98 [0.92–1.00]
Peters, 2018 (53)	eRA ($n = 17$); undifferentiated arthritis (n =4)	Intra- Inter-reader reliability and Intra- Inter-reader reproducibility	Cortical interruptions surface area (CIDA)	ICC [95%CI]: 0.95[0.92–0.98] ICC [95%CI]: 0.70[0.41–0.84] ICC [95%CI]: 0.95[0.92–0.98] ICC [95%CI]: 0.70[0.41–0.86]
Erosion sphericity				
Töpfer, 2014 (23)	RA ($n = 18$)	Inter-reader precision	Sphericity. (MIAF).	CV_{RMS}%: 5.46
Erosion marginal osteosclerosis				
Yue, 2017 (46)	RA ($n = 20$); RA ($n = 20$)	Intra- and inter-reader reliability	Marginal osteosclerosis	ICC [95%CI]: 0.98 [0.96–0.99] ICC [95%CI]: 0.97 [0.90–0.99]
Yue, 2018 (58)	eRA ($n = 63$); Remission/not remission	Intra- and inter-reader reliability	Marginal osteosclerosis	ICC [95%CI]: 0.99 [0.91–1.00] ICC [95%CI]: 0.94 [0.73–0.99]
Osteophyte count				
Aschenberg, 2013 (10)	RA ($n = 40$)	Inter-reader reliability	Count	ICC (range): 0.79 (0.57–0.95)
Finzel, 2013 (21)	PsA ($n = 25$); HOA ($n = 25$); control ($n = 20$)	Intra- Inter-reader reproducibility	Count	Spearman's rho (0.95–1.00) ICC 0.91
Simon, 2018 (57)	PsA ($n = 55$); PsO ($n = 55$); control ($n = 47$)	Inter-reader agreement	Count	ICC: 0.95
Berlin, 2019 (60)	Control ($n = 120$)	Inter-reader agreement	Count	ICC [95%CI]: 0.96 [0.92–0.98]
Osteophyte score				
Aschenberg, 2013 (10)	RA ($n = 40$)	Inter-reader agreement	Score	ICC (range): 0.79 (0.57–0.95)
Finzel, 2013 (21)	PsA ($n = 25$); HOA ($n = 25$); control ($n = 20$)	Intra- and Inter-reader reproducibility	Score	Spearman's rho (0.95–1.00) ICC 0.92

(Continued)

TABLE 2 | Continued

Author, year(ref)	Participants	Reproducibility feature	Method	Findings
Osteophyte height				
Finzel, 2013 (14)	PsA [($n = 41$) TNFi/MTX $n = 28/13$]; RA ($n = 43$)	Inter-reader reproducibility Intra-reader reliability	Height	$r = 0.9692$ $r = 0.9722$
Finzel, 2013 (21)	PsA ($n = 25$); HOA ($n = 25$); control ($n = 20$)	Inter-reader reproducibility	Height	ICC 0.96
Simon, 2018 (57)	PsA ($n = 55$); PsO ($n = 55$); control ($n = 47$)	Inter-reader agreement	Height	ICC: 0.94
Henchie, 2019 (61)	RA (n = 17); PsA (n = 17); control (n = 12)	Inter-reader precision	Periosteal bone growth height	RMSE: 20+/−13% Precision error:210 μm
Wu, 2020 (69)	PsA ($n = 62$); control ($n = 62$)	Inter-reader reliability	Entesophyte height	ICC [95%CI]: 0.74 [0.42–0.89]
Osteophyte volume				
Wu, 2020 (69)	PsA ($n = 62$); control ($n = 62$)	Inter-reader reliability	Entesophyte volume	ICC [95%CI]: 0.99 [0.97–0.99]
Bone mineral density				
Fouque-Aubert, 2010 (3)	RA ($n = 14$); control ($n = 14$)	Repositioning and scan/rescan	BMD	CV%: ≤ 1.8
Barnabe, 2013 (12)	RA ($n = 15$); control ($n = 15$)	Intrareader reproducibility	BMD	CV_{RMS}%: < 0.83
Keller, 2017 (50)	Control [ACPA+ ($n = 29$); ACPA– ($n = 29$)]	Intrareader reproducibility	BMD	CV%: 0.6–3.53
Peters, 2018 (53)	eRA ($n = 17$); undifferentiated arthritis ($n = 4$)	Inter-reader reliability and Intra- Inter-reader reproducibility	BMD	ICC [95%CI]: 0.99[0.99–1.00] ICC [95%CI]: 0.99[0.99–1.00] ICC [95%CI]: 0.99[0.99–1.00] ICC [95%CI]: 1.00[1.00–1.00]
Wu, 2020 (69)	PsA ($n = 62$); control ($n = 62$)	Inter-reader reliability	BMD	CV%: 0.38–1.03
Bone microstructure				
Fouque-Aubert, 2010 (3)	RA ($n = 14$); control ($n = 14$)	Repositioning and scan/rescan	Microstructure	CV%: ≤ 12.5
Barnabe, 2013 (12)	RA ($n = 15$); control ($n = 15$)	Intrareader reproducibility	Microstructure	CV_{RMS}%: < 0.83
Keller, 2017 (50)	Control [ACPA+ ($n = 29$); ACPA– ($n = 29$)]	Intrareader reproducibility	Microstructure	CV%: 0.6–3.53
Peters, 2018 (53)	eRA ($n = 17$); undifferentiated arthritis ($n =4$)	Inter-reader reliability and Intra- and inter-reader reproducibility	Microstructure	ICC [95%CI]: 0.99[0.99–1.00] ICC [95%CI]: 0.99[0.99–1.00] ICC [95%CI]: 1.00[1.00–1.00] ICC [95%CI]: 1.00[1.00–1.00]
Wu, 2020 (69)	PsA ($n = 62$); control ($n = 62$)	Inter-reader reliability	Microstructure	CV%: 0.38–1.03
Joint space				
Barnabe, 2013 (12)	RA ($n = 15$); control ($n = 15$)	Intrareader	JSW	CV_{RMS}%: 17.1
Burghardt, 2013 (13)	RA ($n = 16$); control ($n = 7$)	Repositioning and scan/rescan	JSV JSW JSW.SD JSW.Min JSW.MAX JSW.AS	CV_{RMS}%: 3.5 CV_{RMS}%: 2.1 CV_{RMS}%: 10.4 CV_{RMS}%: 12.5 CV_{RMS}%: 2.2 CV_{RMS}%: 13.9
Tom, 2016 (36)	Cadaver ($n = 7$)	Repositioning and scan/rescan	JSV JSW JSW.Min JSW.Max	CV_{RMS}%: 2.2 CV_{RMS}%: 3.8 CV_{RMS}%: 8.0 CV_{RMS}%: 4.4
Stok, 2020 (70)	RA ($n = 30$)	Repositioning and scan/rescan	JSV JSW JSW.Minimum JSW.Maximum JSW.Asymmetry	ICC [95%CI]: 0.99 [0.98–0.99] ICC [95%CI]: 0.95 [0.91–0.97] ICC [95%CI]: 0.66 [0.36–0.82] ICC [95%CI]: 0.73 [0.50–0.86] ICC [95%CI]: 0.75 [0.54–0.87]

ACPA, Anti-citrullinated protein antibodies; BMD, Bone mineral density; CV, coefficient of variance; CIDA, Cortical interruption detection algorithm; eRA, Early Rheumatoid arthritis; ICC, Intra-class correlation coefficient; JSW, Joint space width; JSV, Joint space volume; MTX, Methotrexate; MIAF-finger, Medical Image Analysis Framework – Finger; mESE, modified Evaluation Script for Erosions; PsO, Psoriasis; PsA, Psoriatic arthritis; RA, Rheumatoid arthritis; RMSE, root-mean-square error; $CV_{RMS\%}$, root mean square coefficient of variance; TNFi, Tumor necrosis factor inhibitors.

is still limited. The number and volume of erosions have been shown to increase over a 1-year period in ACPA positive individuals with arthralgia but with no sign of arthritis and when compared with an ACPA negative control group (62). Therefore, erosion number and size may be a sensitive measure for early RA progression.

CURRENT LIMITATIONS AND FUTURE DIRECTIONS FOR IMPROVEMENT

Availability of an Accessible Tool for Erosion Quantification

Clinical studies have been successfully performed using HR-pQCT and a variety of custom software packages for analysis. The detection of clinical erosive features is demonstrated, as well as the reproducibility and sensitivity to measure change. However, while erosion volume quantification shows clear promise as an outcome measure, one of the challenges has been the heterogeneity of approaches to identify erosions and measure their size. This also includes distinguishing erosions from other physiological features. An ideal tool would require minimal operator input but allow corrections when necessary. Furthermore, current approaches have been built with a variety of proprietary and/or custom software packages which are typically only accessible to individual research groups. To improve reproducibility and consistency of definitions, as well as the widespread adoption of semi-automated techniques, a new approach must be developed in an open-source, user-friendly software platform. Machine learning approaches may also better automate erosion detection (84).

Segmentation to Assess the Cortical and Trabecular Bone Density and Microstructure

The current standard approach for segmentation to assess bone mineral density and microstructure is a semi-automated slice-by-slice hand contouring approach or semi-automated edge detection algorithm (85). The algorithms were developed for the distal radius and tibia with the assumption that cortical bone is thicker and denser than trabecular bone, which is not necessarily appropriate for the MCP and PIP joints (86). As well, joints with low bone mineral density and high cortical porosity, such as seen in advanced RA, have proven problematic for the algorithms. The presence of cortical breaks and erosions is also problematic for the existing segmentation approaches, i.e., there exists no consensus as to whether the site of an erosion should be included or excluded. Another important consideration for the examined joint is how much of the bone should be segmented, some have used a volume of interest that spans the majority of the metaphysis, and is standardized to be 10% of the metacarpal length (45). However, presently, there is no consensus on this matter.

To date, significant differences in bone mineral density and microstructure between patients with inflammatory arthritis and healthy controls were primarily reported for the trabecular bone compartment. It is possible that further development of the segmentation algorithms and the imaging resolution could improve segmentation accuracy and might reveal greater differences in the cortical bone of inflammatory arthritis patients.

Motion Compensation

One disadvantage of HR-pQCT imaging is that the lengthy, but highly sensitive acquisition process renders it susceptible to motion artifacts, which can impair the ability to accurately and precisely quantify bone and joint outcomes (87, 88). To date, the number of scans excluded for patient motion is rarely reported with sufficient detail, and as such, it is challenging to know the impact of motion on outcomes.

Motion artifact is particularly problematic for longitudinal studies or when implementing more advanced analyses, such as quantifying bone structure, formation, and resorption (89, 90). While this technique holds promise to identify erosions undergoing repair or progression (64), the technique is currently limited to cross-sectional studies because motion artifact typically occurs in the multi-acquisition scan (multi-stack) for joints, and might falsely detect repair or progression. A partial solution to this problem has been implemented by overlapping the acquisitions. However, this simply serves to smooth the effects of motion on scan quality rather than eliminate it (90). Ideally, existing motion compensation algorithms could be implemented in HR-pQCT image reconstruction software to reduce data loss and maximize the utility of acquired data (91, 92).

Joints of Interest

Conventional radiographs assess erosions in 16 joints in each hand and six joints in each foot. Presently, the image acquisition protocol recommended by the SPECTRA Collaboration for the MCP joints specifies that at a minimum, both the 2nd and 3rd MCP should be imaged (93). There is currently no standard image acquisition protocol for the PIP joints. In spite of this, a limited number of published studies have investigated the PIP joint in a similar fashion as the MCP joints (12, 34, 49, 52, 54, 55, 60, 64). The wrist is also examined in multiple studies with the intention of evaluation of bone mineral density and microstructure of the radius, and JSW in the wrist (13). Still, no protocol for assessing erosions in the radius have been published. Whether there is any benefit to include other joints such as the knee, elbow, ankle or foot remains unclear, but are accessible for HR-pQCT imaging. For the HR-pQCT to be a viable modality for assessing progression in clinical practice, further research to explicitly investigate the number and which specific joints needed for the HR-pQCT scanner to have an added benefit compared to CR are needed.

Disadvantages of HR-pQCT Scanning and the Limited Field of View

The HR-pQCT scanner is not widely available to most researchers or clinicians. Presently, HR-pQCT scanners are only developed by Scanco Medical (Bruttisellen, Switzerland). Worldwide only 93 HR-pQCT scanners are installed (46 of the first-generation and 47 of the second-generation), and about 20 research groups use the technology in rheumatological research, this limits the

feasibility of implementing the method in clinical practice at this time. However, the existing HR-pQCT models use cone-beam configurations (conical x-ray beam which projects onto a flat panel detector), the term "cone-beam CT" has been adopted in reference to scanners with a very large detector that commonly uses this hardware configuration. Cone-beam CT provides higher spatial resolution at lower costs than conventional multi-detector CT systems (94). Acquisition times can be much faster (<1 min vs. 6 to 9 min) than HR-pQCT due to the larger detector sizes. Improvements to image reconstruction can advance the accuracy of bone microarchitectural measurement to be comparable with HR-pQCT (95, 96). Therefore, cone-beam CT could be a viable modality to complement HR-pQCT imaging, thereby increasing access. The outcome measures described throughout this review could be widely implemented for cone-beam CT. Another limitation of exclusively using HR-pQCT for inflammatory arthritis is the inability to visualize soft tissue and inflammation. Dual-energy CT scans acquire projections at two different energy levels to take advantage of differing attenuation coefficients for different tissues at each energy (97–99). Approaches have been implemented in commercial multi-detector CT scanners (100) and have been used to identify tophi and other crystal arthropathies (101–103), as well as more recently to identify bone marrow edema (104, 105). While not currently available in HR-pQCT scanners, there is the potential that future extremity CT scanners will additionally be able to quantify soft tissue and inflammatory abnormalities.

Using Multi-Modal Imaging to Link Erosive Damage to Inflammatory Markers

Investigators have proceeded with evaluating if HR-pQCT images and findings can be used in conjunction with those obtained using US or MRI to provide a comprehensive overview of soft tissue and bone in the same joint. A complimentary paper on this topic is included in this issue (Tse et al., submitted). In particular, the presence of hyperintense signals on MRI linked to inflammation in RA patients, such as osteitis (106) and synovitis is associated with more pronounced erosive damage in patients with RA (52, 54). In the radius of patients with RA, bone mineral density, trabecular thickness and number were significantly higher, while trabecular separation was lower in regions with MRI-defined osteitis than without (22). Similarly, US Doppler-positive RA patients identified with ultrasound had a lower trabecular number and vBMD alongside higher trabecular separation and distribution of trabecular separation in the MCP joints compared to Doppler negative patients (51).

Education for Patients and Students

Lastly, the use of HR-pQCT imaging as possible pedagogical tool should not be overlooked. The spatial and high-resolution imaging are useful for developing 3D models of the periarticular changes of the joint. 3D printed prototypes of arthritic and healthy joints from HR-pQCT data have been investigated as a tool to demonstrate joint disease to address an eventual gap in patient education and disease understanding (38). The HR-pQCT data have also been used with Virtual Reality application for student training (107).

CONCLUSIONS

In conclusion, owing to the ability to detect change over time periods as short as 3 months, there is a great capacity to utilize HR-pQCT measurements as outcomes in future clinical trials. In addition, HR-pQCT provides uniquely high *in-vivo* sensitivity for erosion detection compared to other modalities. The erosion measures, joint space narrowing, bone density and microstructure have high to excellent reproducibility, whereas osteophytes measure only showed moderate to high reproducibility. The highly sensitive assessment of bone microstructure and damage has the potential to better understand bone changes, particularly in the early stages of inflammatory diseases. Finally, new research developments will improve the accessibility of scanners, the field of view of the imaging, analysis tools such as automatic methods for longitudinally evaluating distinct erosions, as well as the versatility for measuring tissues other than only bone.

DATA AVAILABILITY STATEMENT

The original contributions presented in the study are included in the article/**Supplementary Material**, further inquiries can be directed to the corresponding author/s.

AUTHOR CONTRIBUTIONS

RK-J performed the systematic literature review. RK-J and SM drafted the manuscript. All authors contributed conception and design of the review and contributed to manuscript revision, and read and approved the submitted version.

FUNDING

Funding to support the review was provided by a grant from the University of Calgary and Canadian Institutes for Health Research (Planning and Dissemination). JT received salary support from the T. Chen Fong Postdoctoral Fellowship; SM received support from the Arthritis Society Stars Early Career Investigator Award. RK-J received support from Aarhus University, The Danish Rheumatism Association and A.P. Møller Fonden. E-MH received support from the Danish Rheumatism Association and the Novo Nordic Foundation.

SUPPLEMENTARY MATERIAL

The Supplementary Material for this article can be found online at: https://www.frontiersin.org/articles/10.3389/fmed.2020.00337/full#supplementary-material

REFERENCES

1. Lee CH, Srikhum W, Burghardt AJ, Virayavanich W, Imboden JB, Link TM, et al. Correlation of structural abnormalities of the wrist and metacarpophalangeal joints evaluated by high-resolution peripheral quantitative computed tomography, 3 Tesla magnetic resonance imaging and conventional radiographs in rheumatoid arthritis. *Int J Rheum Dis.* (2015) 18:628–39. doi: 10.1111/1756-185X.12495
2. Nagaraj S, Finzel S, Stok KS, Barnabe C. High-resolution peripheral quantitative computed tomography imaging in the assessment of periarticular bone of metacarpophalangeal and wrist joints. *J Rheumatol.* (2016) 43:1921–34. doi: 10.3899/jrheum.160647
3. Fouque-Aubert A, Boutroy S, Marotte H, Vilayphiou N, Bacchetta J, Miossec P, et al. Assessment of hand bone loss in rheumatoid arthritis by high-resolution peripheral quantitative CT. *Ann Rheum Dis.* (2010) 69:1671–76. doi: 10.1136/ard.2009.114512
4. Stach CM, Bäuerle M, Englbrecht M, Kronke G, Engelke K, Manger B, et al. Periarticular bone structure in rheumatoid arthritis patients and healthy individuals assessed by high resolution computed tomography. *Arthritis Rheum.* (2010) 62:330–9. doi: 10.1002/art.27252
5. Finzel S, Englbrecht M, Engelke K, Stach C, Schett G. A comparative study of periarticular bone lesions in rheumatoid arthritis and psoriatic arthritis. *Ann Rheum Dis.* (2011) 70:122–27. doi: 10.1136/ard.2010.132423
6. Finzel S, Rech J, Schmidt S, Engelke K, Englbrecht M, Stach C, et al. Repair of bone erosions in rheumatoid arthritis treated with tumour necrosis factor inhibitors is based on bone apposition at the base of the erosion. *Ann Rheum Dis.* (2011) 70:1587–93. doi: 10.1136/ard.2010.148395
7. Finzel S, Ohrndorf S, Englbrecht M, Stach C, Messerschmidt J, Schett G, et al. A detailed comparative study of high-resolution ultrasound and micro-computed tomography for detection of arthritic bone erosions. *Arthritis Rheum.* (2011) 63:1231–6. doi: 10.1002/art.30285
8. Zhu TY, Griffith JF, Qin L, Hung VWY, Fong TN, Kwok AW, et al. Bone density and microarchitecture: relationship between hand, peripheral, and axial skeletal sites assessed by HR-pQCT and DXA in rheumatoid arthritis. *Calcif Tissue Int.* (2012) 91:343–55. doi: 10.1007/s00223-012-9644-z
9. Albrecht A, Finzel S, Englbrecht M, Rech J, Hueber A, Schlechtweg P, et al. The structural basis of MRI bone erosions: An assessment by microCT. *Ann Rheum Dis.* (2013) 72:1351–7. doi: 10.1136/annrheumdis-2012-201982
10. Aschenberg S, Finzel S, Schmidt S, Kraus S, Engelke K, Englbrecht1 M, et al. Catabolic and anabolic periarticular bone changes in patients with rheumatoid arthritis: a computed tomography study on the role of age, disease duration and bone markers. *Arthritis Res Ther.* (2013) 15:R62. doi: 10.1186/ar4235
11. Barnabe C, Buie H, Kan M, Szabo E, Barr SG, Martin L, et al. Reproducible metacarpal joint space width measurements using 3D analysis of images acquired with high-resolution peripheral quantitative computed tomography. *Med Eng Phys.* (2013) 35:1540–44. doi: 10.1016/j.medengphy.2013.04.003
12. Barnabe C, Szabo E, Martin L, Boyd SK, Barr SG. Quantification of small joint space width, periarticular bone microstructure and erosions using high-resolution peripheral quantitative computed tomography in rheumatoid arthritis. *Clin Exp Rheumatol.* (2013) 31:243–50. doi: 10.1016/j.bone.2010.05.034
13. Burghardt AJ, Lee CH, Kuo D, Majumdar S, Imboden JB, Link TM, et al. Quantitative *in vivo* HR-pQCT imaging of 3D wrist and metacarpophalangeal joint space width in rheumatoid arthritis. *Ann Biomed Eng.* (2013) 41:2553–64. doi: 10.1007/s10439-013-0871-x
14. Finzel S, Kraus S, Schmidt S, Hueber A, Rech J, Engelke K, et al. Bone anabolic changes progress in psoriatic arthritis patients despite treatment with methotrexate or tumour necrosis factor inhibitors. *Ann Rheum Dis.* (2013) 72:1176–81. doi: 10.1136/annrheumdis-2012-201580
15. Finzel S, Rech J, Schmidt S, Engelke K, Englbrecht M, Schett G. Interleukin-6 receptor blockade induces limited repair of bone erosions in rheumatoid arthritis: a micro CT study. *Ann Rheum Dis.* (2013) 72:396–400. doi: 10.1136/annrheumdis-2011-201075
16. Srikhum W, Virayavanich W, Burghardt AJ, Yu A, Link TM, Imboden JB, et al. Quantitative and semiquantitative bone erosion assessment on high-resolution peripheral quantitative computed tomography in rheumatoid arthritis. *J Rheumatol.* (2013) 40:408–16. doi: 10.3899/jrheum.120780
17. Zhu TY, Griffith JF, Qin L, Hung VWY, Fong TN, Au SK, et al. Structure and strength of the distal radius in female patients with rheumatoid arthritis: a case-control study. *J Bone Miner Res.* (2013) 28:794–806. doi: 10.1002/jbmr.1793
18. Kleyer A, Finzel S, Rech J, Manger B, Krieter M, Faustini F, et al. Bone loss before the clinical onset of rheumatoid arthritis in subjects with anticitrullinated protein antibodies. *Ann Rheum Dis.* (2014) 73:854–60. doi: 10.1136/annrheumdis-2012-202958
19. Kocijan R, Finzel S, Englbrecht M, Engelke K, Rech J, Schett G, et al. Decreased quantity and quality of the periarticular and nonperiarticular bone in patients with rheumatoid arthritis: a cross-sectional HR-pQCT study. *J Bone Miner Res.* (2014) 29:1005–14. doi: 10.1002/jbmr.2109
20. Kocijan R, Finzel S, Englbrecht M, Engelke K, Rech J, Schett G. Differences in bone structure between rheumatoid arthritis and psoriatic arthritis patients relative to autoantibody positivity. *Ann Rheum Dis.* (2014) 73:2022–28. doi: 10.1136/annrheumdis-2013-203791
21. Finzel S, Sahinbegovic E, Kocijan R, Engelke K, Englbrecht M, Schett G. Inflammatory bone spur formation in psoriatic arthritis is different from bone spur formation in hand osteoarthritis. *Arthritis Rheumatol.* (2014) 66:2968–75. doi: 10.1002/art.38794
22. Teruel JR, Burghardt AJ, Rivoire J, Srikhum W, Noworolski SM, Link TM, et al. Bone structure and perfusion quantification of bone marrow edema pattern in the wrist of patients with rheumatoid arthritis: a multimodality study. *J Rheumatol.* (2014) 41:1766–73. doi: 10.3899/jrheum.131564
23. Töpfer D, Finzel S, Museyko O, Schett G, Engelke K. Segmentation and quantification of bone erosions in high-resolution peripheral quantitative computed tomography datasets of the metacarpophalangeal joints of patients with rheumatoid arthritis. *Rheumatology.* (2014) 53:65–71. doi: 10.1093/rheumatology/ket259
24. Zhu TY, Griffith JF, Qin L, Hung VW, Fong TN, Au SK, et al. Alterations of bone density, microstructure, and strength of the distal radius in male patients with rheumatoid arthritis: a case-control study with HR-pQCT. *J Bone Miner Res.* (2014) 29:2118–29. doi: 10.1002/jbmr.2221
25. Zhu TY, Griffith JF, Qin L, Hung VWY, Fong TN, Au SK, et al. Density, structure, and strength of the distal radius in patients with psoriatic arthritis: the role of inflammation and cardiovascular risk factors. *Osteoporos Int.* (2014) 26:261–72. doi: 10.1007/s00198-014-2858-3
26. Hecht C, Englbrecht M, Rech J, Schmidt S, Araujo E, Engelke K, et al. Additive effect of anti-citrullinated protein antibodies and rheumatoid factor on bone erosions in patients with RA. *Ann Rheum Dis.* (2015) 74:2151–6. doi: 10.1136/annrheumdis-2014-205428
27. Kocijan R, Englbrecht M, Haschka J, Simon D, Kleyer A, Finzel S, et al. Quantitative and qualitative changes of bone in psoriasis and psoriatic arthritis patients. *J Bone Miner Res.* (2015) 30:1775–83. doi: 10.1002/jbmr.2521
28. Regensburger A, Rech J, Englbrecht M, Finzel S, Kraus S, Hecht K, et al. A comparative analysis of magnetic resonance imaging and high-resolution peripheral quantitative computed tomography of the hand for the detection of erosion repair in rheumatoid arthritis. *Rheumatology.* (2015) 54:1573–81. doi: 10.1093/rheumatology/kev031
29. Töpfer D, Gerner B, Finzel S, Kraus S, Museyko O, Schett G, et al. Automated three-dimensional registration of high-resolution peripheral quantitative computed tomography data to quantify size and shape changes of arthritic bone erosions. *Rheumatology.* (2015) 54:2171–80. doi: 10.1093/rheumatology/kev256
30. Barnabe C, Toepfer D, Marotte H, Hauge EM, Scharmga A, Kocijan R, et al. Definition for rheumatoid arthritis erosions imaged with high resolution peripheral quantitative computed tomography and interreader reliability for detection and measurement. *J Rheumatol.* (2016) 43:1935–40. doi: 10.3899/jrheum.160648
31. Figueiredo CP, Simon D, Englbrecht M, Haschka J, Kleyer A, Bayat S, et al. Quantification and impact of secondary osteoarthritis in patients with anti-citrullinated protein antibody-positive rheumatoid arthritis. *Arthritis Rheumatol.* (2016) 68:2114–21. doi: 10.1002/art.39698
32. Kleyer A, Krieter M, Oliveira I, Faustini F, Simon D, Kaemmerer N, et al. High prevalence of tenosynovial inflammation before

onset of rheumatoid arthritis and its link to progression to RA—A combined MRI/CT study. *Semin Arthritis Rheum.* (2016) 46:143–50. doi: 10.1016/j.semarthrit.2016.05.002
33. Scharmga A, Peters M, van Tubergen A, van den Bergh J, Barnabe C, Finzel S, et al. Heterogeneity of cortical breaks in hand joints of patients with rheumatoid arthritis and healthy controls imaged by high-resolution peripheral quantitative computed tomography. *J Rheumatol.* (2016) 43:1914–20. doi: 10.3899/jrheum.160646
34. Scharmga A, Peters M, van Tubergen A, Van Den Bergh J, De Jong J, Loeffen D, et al. Visual detection of cortical breaks in hand joints: reliability and validity of high-resolution peripheral quantitative CT compared to microCT. *BMC Musculoskelet Disord.* (2016) 17:271. doi: 10.1186/s12891-016-1148-y
35. Shen J, Shang Q, Wong C-K, Li EK, Kun EW, Cheng IT, et al. Carotid plaque and bone density and microarchitecture in psoriatic arthritis: the correlation with soluble ST2. *Sci Rep.* (2016) 6:32116. doi: 10.1038/srep32116
36. Tom S, Frayne M, Manske SL, Burghardt AJ, Stok KS, Boyd SK, et al. Determining metacarpophalangeal flexion angle tolerance for reliable volumetric joint space measurements by high-resolution peripheral quantitative computed tomography. *J Rheumatol.* (2016) 43:1941–4. doi: 10.3899/jrheum.160649
37. Feehan LM, Li LL, McKay HA. Micro-structural bone changes in early rheumatoid arthritis persist over 1-year despite use of disease modifying anti-rheumatic drug therapy. *BMC Musculoskelet Disord.* (2017) 18:521. doi: 10.1186/s12891-017-1888-3
38. Kleyer A, Beyer L, Simon C, Stemmler F, Englbrecht M, Beyer C, et al. Development of three-dimensional prints of arthritic joints for supporting patients' awareness to structural damage. *Arthritis Res Ther.* (2017) 19:34. doi: 10.1186/s13075-017-1234-z
39. Peters M, Scharmga A, De Jong J, van Tubergen A, Geusens P, Arts JJ, et al. An automated algorithm for the detection of cortical interruptions on high resolution peripheral quantitative computed tomography images of finger joints. *PLoS ONE.* (2017) 12:e0175829. doi: 10.1371/journal.pone.0175829
40. Peters M, Scharmga A, van Tubergen A, Arts J, Loeffen D, Weijers R, et al. The reliability of a semi-automated algorithm for detection of cortical interruptions in finger joints on high resolution CT compared to microct. *Calcif Tissue Int.* (2017) 101:132–40. doi: 10.1007/s00223-017-0264-5
41. Scharmga A, Keller KK, Peters M, Van Tubergen A, Van Den Bergh JP, Van Rietbergen B, et al. Vascular channels in metacarpophalangeal joints: a comparative histologic and high-resolution imaging study. *Sci Rep.* (2017) 7:8966. doi: 10.1038/s41598-017-09363-2
42. Shimizu T, Choi HJ, Heilmeier U, Tanaka M, Burghardt AJ, Gong J, et al. Assessment of 3-month changes in bone microstructure under anti-TNFα therapy in patients with rheumatoid arthritis using high-resolution peripheral quantitative computed tomography (HR-pQCT). *Arthritis Res Ther.* (2017) 19:222. doi: 10.1186/s13075-017-1430-x
43. Simon D, Kleyer A, Stemmler F, Simon C, Berlin A, Hueber AJ, et al. Age- and sex-dependent changes of intra-articular cortical and trabecular bone structure and the effects of rheumatoid arthritis. *J Bone Miner Res.* (2017) 32:722–30. doi: 10.1002/jbmr.3025
44. Werner D, Simon D, Englbrecht M, Stemmler F, Simon C, Berlin A, et al. Early changes of the cortical micro-channel system in the bare area of the joints of patients with rheumatoid arthritis. *Arthritis Rheumatol.* (2017) 69:1580–87. doi: 10.1002/art.40148
45. Yang H, Yu A, Burghardt AJ, Virayavanich W, Link TM, Imboden JB, et al. Quantitative characterization of metacarpal and radial bone in rheumatoid arthritis using high resolution- peripheral quantitative computed tomography. *Int J Rheum Dis.* (2017) 20:353–62. doi: 10.1111/1756-185X.12558
46. Yue J, Griffith JF, Xiao F, Shi L, Wang D, Shen J, et al. Repair of bone erosion in rheumatoid arthritis by denosumab: a high-resolution peripheral quantitative computed tomography study. *Arthritis Care Res.* (2017) 69:1156–63. doi: 10.1002/acr.23133
47. Figueiredo CP, Kleyer A, Simon D, Stemmler F, D'Oliveira I, Weissenfels A, et al. Methods for segmentation of rheumatoid arthritis bone erosions in high-resolution peripheral quantitative computed tomography (HR-pQCT). *Semin Arthritis Rheum.* (2018) 47:611–18. doi: 10.1016/j.semarthrit.2017.09.011
48. Ibrahim-Nasser N, Marotte H, Valery A, Salliot C, Toumi H, Lespessailles E. Precision and sources of variability in the assessment of rheumatoid arthritis erosions by HRpQCT. *Jt Bone Spine.* (2018) 85:211–17. doi: 10.1016/j.jbspin.2017.02.011
49. Kampylafka E, D'Oliveira I, Linz C, Lerchen V, Stemmler F, Simon D, et al. Resolution of synovitis and arrest of catabolic and anabolic bone changes in patients with psoriatic arthritis by IL-17A blockade with secukinumab: results from the prospective PSARTROS study. *Arthritis Res Ther.* (2018) 20:153. doi: 10.1186/s13075-018-1653-5
50. Keller KK, Thomsen J, Stengaard-Pedersen K, Nielsen A, Schiøttz-Christensen B, Svendsen L, et al. Local bone loss in patients with anti-citrullinated peptide antibody and arthralgia, evaluated with high-resolution peripheral quantitative computed tomography. *Scand J Rheumatol.* (2018) 47:110–16. doi: 10.1080/03009742.2017.1333629
51. Kong S, Locrelle H, Amouzougan A, Denarie D, Collet P, Pallot-Prades B, et al. Remaining local subclinical joint inflammation is associated with deteriorated metacarpeal head bone microarchitecture in rheumatoid arthritis patients low disease activity. *Joint Bone Spine.* (2018) 85:569–72. doi: 10.1016/j.jbspin.2017.11.010
52. Peters M, van Tubergen A, Scharmga A, Driessen A, van Rietbergen B, Loeffen D, et al. Assessment of cortical interruptions in the finger joints of patients with rheumatoid arthritis using HR-pQCT, radiography, and MRI. *J Bone Miner Res.* (2018) 33:1676–85. doi: 10.1002/jbmr.3466
53. Peters M, de Jong J, Scharmga A, van Tubergen A, Geusens P, Loeffen D, et al. An automated algorithm for the detection of cortical interruptions and its underlying loss of trabecular bone; a reproducibility study. *BMC Med Imaging.* (2018) 18:13. doi: 10.1186/s12880-018-0255-7
54. Scharmga A, Geusens P, Peters M, van den Bergh JP, Loeffen D, Schoonbrood T, et al. Structural damage and inflammation on radiographs or magnetic resonance imaging are associated with cortical interruptions on high-resolution peripheral quantitative computed tomography: a study in finger joints of patients with rheumatoid arthritis and h. *Scand J Rheumatol.* (2018) 47:431–9. doi: 10.1080/03009742.2018.1424234
55. Scharmga A, Peters M, van den Bergh JP, Geusens P, Loeffen D, van Rietbergen B, et al. Development of a scoring method to visually score cortical interruptions on high-resolution peripheral quantitative computed tomography in rheumatoid arthritis and healthy controls. *PLoS ONE.* (2018) 13:e0200331. doi: 10.1371/journal.pone.0200331
56. Simon D, Kleyer A, Englbrecht M, Stemmler F, Simon C, Berlin A, et al. A comparative analysis of articular bone in large cohort of patients with chronic inflammatory diseases of the joints, the gut and the skin. *Bone.* (2018) 116:87–93. doi: 10.1016/j.bone.2018.07.017
57. Simon D, Kleyer A, Faustini F, Englbrecht M, Haschka J, Berlin A, et al. Simultaneous quantification of bone erosions and enthesiophytes in the joints of patients with psoriasis or psoriatic arthritis - effects of age and disease duration. *Arthritis Res Ther.* (2018) 20:203. doi: 10.1186/s13075-018-1691-z
58. Yue J, Griffith JF, Xu J, Xiao F, Shi L, Wang D, et al. Effect of treat-to-target strategies on bone erosion progression in early rheumatoid arthritis: An HR-pQCT study. *Semin Arthritis Rheum.* (2018) 48:374–83. doi: 10.1016/j.semarthrit.2018.05.001
59. Finzel S, Kraus S, Figueiredo CP, Regensburger A, Kocijan R, Rech J, et al. Comparison of the effects of tocilizumab monotherapy and adalimumab in combination with methotrexate on bone erosion repair in rheumatoid arthritis. *Ann Rheum Dis.* (2019) 78:1186–91. doi: 10.1136/annrheumdis-2018-214894
60. Berlin A, Simon D, Tascilar K, Figueiredo C, Bayat S, Finzel S, et al. The ageing joint-standard age- and sex-related values of bone erosions and osteophytes in the hand joints of healthy individuals. *Osteoarthr Cartil.* (2019) 27:1043–47. doi: 10.1016/j.joca.2019.01.019
61. Henchie TF, Gravallese EM, Bredbenner TL, Troy KL. An image-based method to measure joint deformity in inflammatory arthritis: development and pilot study. *Comput Methods Biomech Biomed Eng.* (2019) 22:942–52. doi: 10.1080/10255842.2019.1607315
62. Keller KK, Thomsen JS, Stengaard-Pedersen K, Therkildsen J, Nielsen AW, Schiøtz-Christensen B, et al. One-year progression of erosive disease in patients with anti-citrullinated peptide antibodies and arthralgia. *Joint Bone Spine.* (2019) 87:181–3. doi: 10.1016/j.jbspin.2019.09.006

63. Manske SL, Brunet SC, Finzel S, Stok KS, Conaghan PG, Boyd SK, et al. The SPECTRA collaboration OMERACT working group: construct validity of joint space outcomes with high-resolution peripheral quantitative computed tomography. *J Rheumatol.* (2019) 46:1369–73. doi: 10.3899/jrheum.180870
64. Peters M, van den Bergh JP, Geusens P, Scharmga A, Loeffen D, Weijers R, et al. Prospective follow-up of cortical interruptions, bone density, and micro-structure detected on HR-pQCT: a study in patients with rheumatoid arthritis and healthy subjects. *Calcif Tissue Int.* (2019) 104:571–81. doi: 10.1007/s00223-019-00523-2
65. Shimizu T, Cruz A, Tanaka M, Mamoto K, Pedoia V, Burghardt AJ, et al. Structural changes over a short period are associated with functional assessments in rheumatoid arthritis. *J Rheumatol.* (2019) 46:676–84. doi: 10.3899/jrheum.180496
66. Wu D, Griffith JF, Lam SHM, Wong PCH, Shi L, Li EK, et al. Progressive structural bone changes and their relationship with treatment in patients with psoriatic arthritis: a longitudinal HR-pQCT study. *Arthritis Res Ther.* (2019) 21:265. doi: 10.1186/s13075-019-2043-3
67. Yue J, Lau TCK, Griffith JF, Xu J, Xiao F, Shi L, et al. Circulating miR-99b-5p as a novel predictor of erosion progression on high-resolution peripheral quantitative computed tomography in early rheumatoid arthritis: a prospective cohort study. *Int J Rheum Dis.* (2019) 22:1724–33. doi: 10.1111/1756-185X.13644
68. Simon D, Kleyer A, Bayat S, Tascilar K, Kampylafka E, Meinderink T, et al. Effect of disease-modifying anti-rheumatic drugs on bone structure and strength in psoriatic arthritis patients. *Arthritis Res Ther.* (2019) 21:162. doi: 10.1136/annrheumdis-2019-eular.7249
69. Wu D, Griffith JF, Lam SHM, Wong P, Yue J, Shi L, et al. Comparison of bone structure and microstructure in the metacarpal heads between patients with psoriatic arthritis and healthy controls: an HR-pQCT study. *Osteoporos Int.* (2020) 31:941–50. doi: 10.1007/s00198-020-05298-z
70. Stok KS, Burghardt AJ, Boutroy S, Peters MPH, Manske SL, Stadelmann VA, et al. Consensus approach for 3D joint space width of metacarpophalangeal joints of rheumatoid arthritis patients using high-resolution peripheral quantitative computed tomography. *Quant Imaging Med Surg.* (2020) 10:314–325. doi: 10.21037/qims.2019.12.11
71. Sharp JT, Lidsky MD, Collins LC, Moreland J. Methods of scoring the progression of radiologic changes in rheumatoid arthritis. Correlation of radiologic, clinical and laboratory abnormalities. *Arthritis Rheum.* (1971) 14:706–20. doi: 10.1002/art.1780140605
72. Schett G, Gravallese E. Bone erosion in rheumatoid arthritis: mechanisms, diagnosis and treatment. *Nat Rev Rheumatol.* (2012) 8:656–64. doi: 10.1038/nrrheum.2012.153
73. Geusens P, Van den Bergh J. Bone erosions in rheumatoid arthritis. *Rheumatology.* (2014) 53:4–5. doi: 10.1093/rheumatology/ket358
74. Ten Brinck RM, Van Steenbergen HW, Van Der Helm-Van Mil AHM. Sequence of joint tissue inflammation during rheumatoid arthritis development. *Arthritis Res Ther.* (2018) 20:1–8. doi: 10.1186/s13075-018-1756-z
75. Hetland ML, Ejbjerg B, Hørslev-Petersen K, Jacobsen S, Vestergaard A, Jurik AG, et al. MRI bone oedema is the strongest predictor of subsequent radiographic progression in early rheumatoid arthritis. Results from a 2-year randomised controlled trial (CIMESTRA). *Ann Rheum Dis.* (2009) 68:384–90. doi: 10.1136/ard.2008.088245
76. McInnes IB, Schett G. The pathogenesis of rheumatoid arthritis. *N Engl J Med.* (2011) 365:2205–19. doi: 10.1056/NEJMra1004965
77. Manske SL, Zhu Y, Sandino C, Boyd SK. Human trabecular bone microarchitecture can be assessed independently of density with second generation HR-pQCT. *Bone.* (2015) 79:213–21. doi: 10.1016/j.bone.2015.06.006
78. Conaghan P, Bird P, Ejbjerg B, O'Connor P, Peterfy C, McQueen F, et al. The EULAR-OMERACT rheumatoid arthritis MRI reference image atlas: the metacarpophalangeal joints. *Ann Rheum Dis.* (2005) 64:i11–21. doi: 10.1136/ard.2004.031815
79. Van Der Heijde D. How to read radiographs according to the sharp/van der heijde method. *J Rheumatol.* (2000) 27:261–3. doi: 10.1097/00002281-200007000-00005
80. Neumann G, DePablo P, Finckh A, Chibnik LB, Wolfe F, Duryea J. Patient repositioning reproducibility of joint space width measurements on hand radiographs. *Arthritis Care Res.* (2011) 63:203–7. doi: 10.1002/acr.20374
81. Døhn UM, Conaghan PG, Eshed I, Boonen A, Boyesen P, Peterfy CG, et al. The OMERACT-RAMRIS rheumatoid arthritis magnetic resonance imaging joint space narrowing score: Intrareader and interreader reliability and agreement with computed tomography and conventional radiography. *J Rheumatol.* (2014) 41:392–7. doi: 10.3899/jrheum.131087
82. Crowley AR, Dong J, McHaffie A, Clarke AW, Reeves Q, Williams M, et al. Measuring bone erosion and edema in rheumatoid arthritis: a comparison of manual segmentation and RAMRIS methods. *J Magn Reson Imaging.* (2011) 33:364–71. doi: 10.1002/jmri.22425
83. Hørslev-Petersen K, Hetland ML, Ørnbjerg LM, Junker P, Pødenphant J, Ahlquist P, et al. Clinical and radiographic outcome of a treat-to-target strategy using methotrexate and intra-articular glucocorticoids with or without adalimumab induction: A 2-year investigator-initiated, double-blinded, randomised, controlled trial (OPERA). *Ann Rheum Dis.* (2016) 75:1645–53. doi: 10.1136/annrheumdis-2015-208166
84. Lauze FB, Ren J, Moaddel HA, Hauge EM, Keller KK, Jensen RK. Automatic detection and localization of bone erosion in hand HR-pQCT. In: Hahn HK, Mori K, editors. *Medical Imaging 2019: Computer-Aided Diagnosis (SPIE)*, (San Diego, CA), 74. doi: 10.1117/12.2512876
85. Burghardt AJ, Buie HR, Laib A, Majumdar S, Boyd SK. Reproducibility of direct quantitative measures of cortical bone microarchitecture of the distal radius and tibia by HR-pQCT. *Bone.* (2010) 47:519–28.
86. Buie HR, Campbell GM, Klinck RJ, MacNeil JA, Boyd SK. Automatic segmentation of cortical and trabecular compartments based on a dual threshold technique for *in vivo* micro-CT bone analysis. *Bone.* (2007) 41:505–15. doi: 10.1016/j.bone.2007.07.007
87. Pauchard Y, Liphardt AM, Macdonald HM, Hanley DA, Boyd SK. Quality control for bone quality parameters affected by subject motion in high-resolution peripheral quantitative computed tomography. *Bone.* (2012) 50:1304–10. doi: 10.1016/j.bone.2012.03.003
88. Sode M, Burghardt AJ, Pialat J-B, Link TM, Majumdar S. Quantitative characterization of subject motion in HR-pQCT images of the distal radius and tibia. *Bone.* (2011) 48:1291–7. doi: 10.1016/j.bone.2011.03.755
89. Christen P, Boutroy S, Ellouz R, Chapurlat R, Van Rietbergen B. Least-detectable and age-related local *in vivo* bone remodelling assessed by time-lapse HR-pQCT. *PLoS ONE.* (2018) 13:e0191369. doi: 10.1371/journal.pone.0191369
90. Brunet SC, Kuczynski MT, Bhatla JL, Sophie L, Pauchard Y, Salat P, et al. The utility of multi-stack alignment and 3D longitudinal image registration to assess bone remodeling in rheumatoid arthritis patients from second generation HR-pQCT scans. *BMC Med Imaging.* (2020) 20:36. doi: 10.1186/s12880-020-00437-8
91. Sisniega A, Stayman JW, Yorkston J, Siewerdsen JH, Zbijewski W. Motion compensation in extremity cone-beam CT using a penalized image sharpness criterion. *Phys Med Biol.* (2017) 62:3712–34. doi: 10.1088/1361-6560/aa6869
92. Sisniega A, Thawait GK, Shakoor D, Siewerdsen JH, Demehri S, Zbijewski W. Motion compensation in extremity cone-beam computed tomography. *Skeletal Radiol.* (2019) 48:1999–2007. doi: 10.1007/s00256-019-03241-w
93. Barnabe C, Feehan L. High-resolution peripheral quantitative computed tomography imaging protocol for metacarpophalangeal joints in inflammatory arthritis: the SPECTRA collaboration. *J Rheumatol.* (2012) 39:1494–5. doi: 10.3899/jrheum.120218
94. Posadzy M, Desimpel J, Vanhoenacker F. Cone beam CT of the musculoskeletal system: clinical applications. *Insights Imaging.* (2018) 9:35–45. doi: 10.1007/s13244-017-0582-1
95. Mys K, Varga P, Gueorguiev B, Hemmatian H, Stockmans F, van Lenthe GH. Correlation between cone-beam computed tomography and high-resolution peripheral computed tomography for assessment of wrist bone microstructure. *J Bone Miner Res.* (2019) 34:867–74. doi: 10.1002/jbmr.3673
96. Mys K, Stockmans F, Vereecke E, van Lenthe GH. Quantification of bone microstructure in the wrist using cone-beam computed tomography. *Bone.* (2018) 114:206–14. doi: 10.1016/j.bone.2018.06.006
97. Granton PV, Pollmann SI, Ford NL, Drangova M, Holdsworth DW. Implementation of dual- and triple-energy cone-beam micro-CT for postreconstruction material decomposition. *Med Phys.* (2008) 35:5030–42. doi: 10.1118/1.2987668

98. Patino M, Prochowski A, Agrawal MD, Simeone FJ, Gupta R, Hahn PF, et al. Material separation using dual-energy CT: current and emerging applications. *Radiographics*. (2016) 36:1087–105. doi: 10.1148/rg.2016150220
99. Johnson TRC. Dual-energy CT: general principles. *AJR Am J Roentgenol.* (2012) 199:3–8. doi: 10.2214/AJR.12.9116
100. Graser A, Johnson TRC, Bader M, Staehler M, Haseke N, Nikolaou K, et al. Dual energy CT characterization of urinary calculi: initial *in vitro* and clinical experience. *Invest Radiol.* (2008) 43:112–9. doi: 10.1097/RLI.0b013e318157a144
101. Diekhoff T, Kiefer T, Stroux A, Pilhofer I, Juran R, Mews J, et al. Detection and characterization of crystal suspensions using single-source dual-energy computed tomography: a phantom model of crystal arthropathies. *Invest Radiol.* (2015) 50:255–60. doi: 10.1097/RLI.0000000000000099
102. Davies J, Riede P, van Langevelde K, Teh J. Recent developments in advanced imaging in gout. *Ther Adv Musculoskelet Dis.* (2019) 11:1759720X19844429. doi: 10.1177/1759720X19844429
103. McQueen FM, Doyle A, Dalbeth N. Imaging in gout - what can we learn from MRI, CT, DECT and US? *Arthritis Res Ther.* (2011) 13:246. doi: 10.1186/ar3489
104. Diekhoff T, Scheel M, Hermann S, Mews J, Hamm B, Hermann KGA. Osteitis: a retrospective feasibility study comparing single-source dual-energy CT to MRI in selected patients with suspected acute gout. *Skeletal Radiol.* (2017) 46:185–90. doi: 10.1007/s00256-016-2533-1
105. Jans L, De Kock I, Herregods N, Verstraete K, Van den Bosch F, Carron P, et al. Dual-energy CT: a new imaging modality for bone marrow oedema in rheumatoid arthritis. *Ann Rheum Dis.* (2018) 77:958–60. doi: 10.1136/annrheumdis-2018-213152
106. McQueen FM. Bone marrow edema and osteitis in rheumatoid arthritis: the imaging perspective. *Arthritis Res Ther.* (2012) 14:224. doi: 10.1186/ar4035
107. Kleyer A, Simon D, Hartmann F, Schuster L, Hueber AJ. "Virtual rheumatology": a new teaching concept for rheumatology of the future? *Z Rheumatol.* (2019) 78:112–15. doi: 10.1007/s00393-019-0594-y

Conflict of Interest: The authors declare that the research was conducted in the absence of any commercial or financial relationships that could be construed as a potential conflict of interest.

The reviewer AK declared a past collaboration with one of the authors SF to the handling editor.

frontiers in Medicine

PERSPECTIVE
published: 12 August 2020
doi: 10.3389/fmed.2020.00434

Novel Muscle Imaging in Inflammatory Rheumatic Diseases—A Focus on Ultrasound Shear Wave Elastography and Quantitative MRI

Matthew Farrow[1,2,3], *John Biglands*[2,4], *Abdulrahman M. Alfuraih*[5], *Richard J. Wakefield*[1,2] *and Ai Lyn Tan*[1,2]*

[1] Leeds Institute of Rheumatic and Musculoskeletal Medicine, Chapel Allerton Hospital, University of Leeds, Leeds, United Kingdom, [2] NIHR Leeds Biomedical Research Centre, Leeds Teaching Hospitals NHS Trust, Leeds, United Kingdom, [3] School of Pharmacy and Medical Sciences, University of Bradford, Bradford, United Kingdom, [4] Medical Physics and Engineering, Leeds Teaching Hospitals NHS Trust, Leeds, United Kingdom, [5] Radiology and Medical Imaging Department, Prince Sattam Bin Abdulaziz University, Al-Kharj, Saudi Arabia

OPEN ACCESS

Edited by:
Christian Dejaco,
Medical University of Graz, Austria

Reviewed by:
Garifallia Sakellariou,
University of Pavia, Italy
Philipp Sewerin,
Heinrich Heine University of Düsseldorf, Germany

***Correspondence:**
Ai Lyn Tan
a.l.tan@leeds.ac.uk

Specialty section:
This article was submitted to Rheumatology, a section of the journal Frontiers in Medicine

Received: 22 May 2020
Accepted: 06 July 2020
Published: 12 August 2020

Citation:
Farrow M, Biglands J, Alfuraih AM, Wakefield RJ and Tan AL (2020) Novel Muscle Imaging in Inflammatory Rheumatic Diseases—A Focus on Ultrasound Shear Wave Elastography and Quantitative MRI. Front. Med. 7:434. doi: 10.3389/fmed.2020.00434

In recent years, imaging has played an increasing role in the clinical management of patients with rheumatic diseases with respect to aiding diagnosis, guiding therapy and monitoring disease progression. These roles have been underpinned by research which has enhanced our understanding of disease pathogenesis and pathophysiology of rheumatology conditions, in addition to their key role in outcome measurement in clinical trials. However, compared to joints, imaging research of muscles is less established, despite the fact that muscle symptoms are very common and debilitating in many rheumatic diseases. Recently, it has been shown that even though patients with rheumatoid arthritis may achieve clinical remission, defined by asymptomatic joints, many remain affected by lingering constitutional systemic symptoms like fatigue, tiredness, weakness and myalgia, which may be attributed to changes in the muscles. Recent improvements in imaging technology, coupled with an increasing clinical interest, has started to ignite new interest in the area. This perspective discusses the rationale for using imaging, particularly ultrasound and MRI, for investigating muscle pathology involved in common inflammatory rheumatic diseases. The muscles associated with rheumatic diseases can be affected in many ways, including myositis—an inflammatory muscle condition, and myopathy secondary to medications, such as glucocorticoids. In addition to non-invasive visual assessment of muscles in these conditions, novel imaging techniques like shear wave elastography and quantitative MRI can provide further useful information regarding the physiological and biomechanical status of the muscle.

Keywords: muscle, myositis, myopathy, MRI, ultrasound, shear wave elastography, imaging, rheumatic

INTRODUCTION

Advances in diagnostic imaging in rheumatology, particularly in the area of arthritis, have contributed to significant clinical benefits to patients and improved knowledge in disease pathogenesis. Despite the usefulness of ultrasound and magnetic resonance imaging (MRI) in diagnosing arthritis and monitoring disease progression in joints and related joint structures, the role of muscle imaging has conventionally been centered around the diagnosis of inflammatory muscle diseases. However, with an increasing appreciation of the impact and prevalence of muscular symptoms in rheumatic diseases (1), and as a result of technological developments, recent attention has been directed toward the utility of imaging for the assessment of muscle pathology in rheumatic diseases.

The impact of muscle weakness is significant for the health of patients and is associated with disease activity (2). There is an unmet need for further understanding of more generalized muscle pathology observed in rheumatic diseases. This is required to develop effective future strategies to target this under-researched area. In addition to ultrasound and MRI, positron emission tomography combined with computed tomography (PET-CT) is increasingly used in clinical practice to aid the diagnosis of myositis, with the added advantage that this technique can screen for malignancy and evaluate related pulmonary pathologies (3, 4). This perspective will discuss recent novel imaging developments in ultrasound and MRI for the assessment of muscles in common inflammatory rheumatic diseases, with a particular focus on research applicability of shear wave elastography and quantitative MRI in improving the knowledge of muscle pathology in rheumatic diseases. The potential application of these novel techniques will be explored in the context of three common inflammatory rheumatology conditions where the muscle is of interest. The first is in myositis, a primary inflammatory condition of the muscle; the second is in glucocorticoid-induced myopathy, where patients with giant cell arteritis and polymyalgia rheumatica are at risk from the complications of prolonged high dose steroid therapy; and the third is rheumatoid arthritis where patients often complain of muscle related symptoms in addition to their joints.

MUSCLE IMAGING TECHNIQUES

Ultrasound

Due to recent innovations, ultrasonography has evolved from demonstrating mainly anatomical details to elucidating the physical properties of tissues. Although B-mode ultrasonography has been shown to be reliable in assessing muscle mass and quality (5–7), and muscle fibers during dynamic scanning (8, 9), recent interest has been directed to a new type of ultrasound called elastography (10). This technique provides a measure of the stiffness of tissue (11). The first generation machines, developed in the 1990's utilized "strain elastography," where a mechanical ultrasound pulse was generated by repeated probe compressions on the skin by the operator. The returned waves could be used to qualitatively estimate stiffness by comparing the pre- and post-compression tissue deformations. The images were represented as a color map, superimposed on a B-mode image (blue—hard, and red—soft). Shear wave elastography (SWE) has more recently been introduced to offer quantitative measurements by monitoring the velocity of the shear waves generated by strong acoustic pulses. The physics behind shear waves is complex and beyond the scope of this article, but essentially, the velocity of the shear wave increases proportionally with Young's elasticity modulus. SWE is less operator dependent than strain elastography, and offers more objective outcomes. Hence, this perspective will focus on the potential uses of SWE, which has more commonly been established for examining breast, liver, thyroid and prostate tissues (12–14).

In the musculoskeletal setting, SWE has largely been used to study tendinopathies (15, 16). More recently however, SWE has been extended to examining muscles, and has been shown to be a reliable tool to measure muscle stiffness (17–19). The technique has been used in the sports and exercise scenarios, to assess muscle injuries and the effect of exercise interventions on muscles (20, 21). Clinically, SWE of muscles, such as of the rotator cuff muscles that are commonly susceptible to tears, has been shown to inform appropriate management strategies (22). In the hospital setting, it has shown good reliability for monitoring the muscles of critically ill patients (23). Other clinical uses of SWE are in the assessment of the muscles in neuromuscular conditions including Parkinson's disease, Duchene muscular dystrophy, and in post-stroke spasticity (24–26). Insight into the potential of using SWE in assessing muscle elasticity has prompted recommendations into standardizing the technique for optimal data acquisition (27–29). It is known that muscles change with age, which is apparent in the structure and the function of the muscles (30, 31). Although some studies using SWE have shown that there is a decline in muscle stiffness with age (32–35), this observation was not corroborated by others (36–38). These studies looked at different muscles, which may have influenced the final outcomes, as it has been found that SWE findings may be muscle-dependent (39).

MRI

MRI offers the ability to examine deeper tissue structures compared to ultrasound. Although MRI can also measure the elasticity of muscles using magnetic resonance elastography (40–44), the cost of the technique is more prohibitive when compared to SWE; thus far, the utility of MRI in assessing muscle elasticity is still debatable (45).

Due to its excellent spatial and contrast resolution, MRI can evaluate a wide array of muscle pathologies including muscle injury (46) and soft tissue masses (47). MRI is beginning to have a role in the diagnosis and monitoring of muscle disease and in guiding muscle biopsy (48, 49). Whole-body MRI can help identify muscular involvement over large anatomical regions (50, 51). Aside from conventional MRI there is also an important role for quantitative MRI (qMRI) measurements, such as fat fraction, T2 measurement and diffusion tensor imaging (DTI), in muscle imaging. Quantitative MRI can provide information about tissue microstructure that may not be apparent in conventional MRI. It provides objective measurements, as opposed to a qualitative

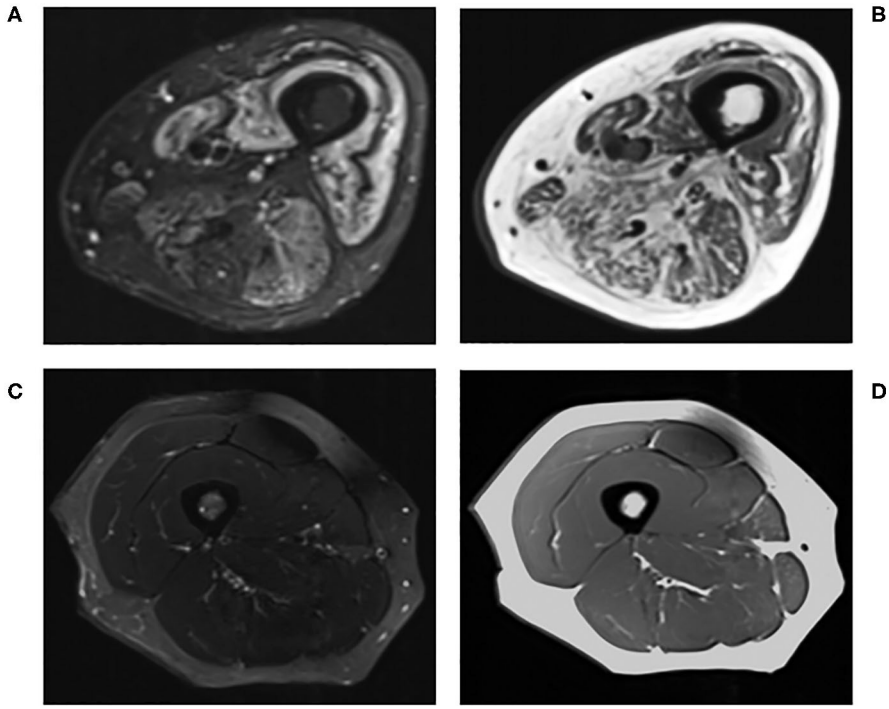

FIGURE 1 | Conventional MRI of the right thigh in **(A)** T2-STIR and **(B)** T1-weighted images of a 60-years-old male with active myositis, compared to **(C)** T2-STIR and **(D)** T1-weighted images of a 45-years-old healthy female.

assessment and has been shown to be reliable and reproducible in the muscle (52, 53).

Fat fraction measurements exploit the differences in the resonant frequencies between the MR signals of fat and water in order to generate a measurement of the proportion of fat in each voxel in the image (54). These measurements provide an objective assessment of fatty infiltration in muscle, which is a common pathology in muscle disease.

Measurements of the T2-relxation time also have applications in the muscle. T2, or the spin-spin relaxation time, is one of the fundamental contrast mechanisms in MRI. By measuring the signal at multiple echo times, measurements of T2 can be made within the muscle. Raised T2 is often interpreted as increased fluid due to edema or inflammation. However, care must be taken in the interpretation of T2. Fat can also increase T2 values and fat suppression is challenging in T2 measurements (55, 56), with some papers arguing that T2 may actually decrease with disease activity (57).

Diffusion MRI is able to measure water diffusion in the muscle. Diffusion measurements in inflamed muscle may be greater due to increased fluid in the extracellular space. Diffusion tensor imaging (DTI) allows the anisotropy of the diffusion to be assessed. As muscle is made up of long fibers, or fibrils, muscle diffusion is highly anisotropic and ordered. As muscle diameters are relatively wide, long diffusion times are necessary if the measurements are to be sensitive to restricted diffusion across the fiber. Fiber disorganization and deterioration through trauma or disease can be detected by DTI measurements, such as fractional anisotropy (FA) (26). However, the interpretation of what a change in diffusion measurement means is difficult. Fiber disorder, fiber density, fiber diameter (58, 59) and changes in extracellular water (60) can all affect diffusion parameters. There is on-going research into the use of modeling to analyse DTI acquisitions at multiple diffusion times to separate out different properties of the muscle microstructure from diffusion measurements (61–63).

In the clinical setting, qMRI of various tissues including muscles shows potential as a promising biomarker for assessing and monitoring a range of neuromuscular and musculoskeletal diseases (57, 64–68). In general, these patients show higher muscle fat fractions, smaller muscle volume, and increased T2 measures, which also correlate with muscle function (69).

MUSCLE IMAGING IN INFLAMMATORY RHEUMATIC DISEASES

Myositis

The idiopathic inflammatory myopathies (IIM) are the commonest inflammatory muscle diseases seen by rheumatologists. They are a heterogeneous group of autoimmune inflammatory muscle conditions comprising mainly of dermatomyositis and polymyositis, which present with muscle weakness, raised muscle enzymes, abnormal electromyography (EMG), abnormal muscle biopsies and myositis-related antibodies (70).

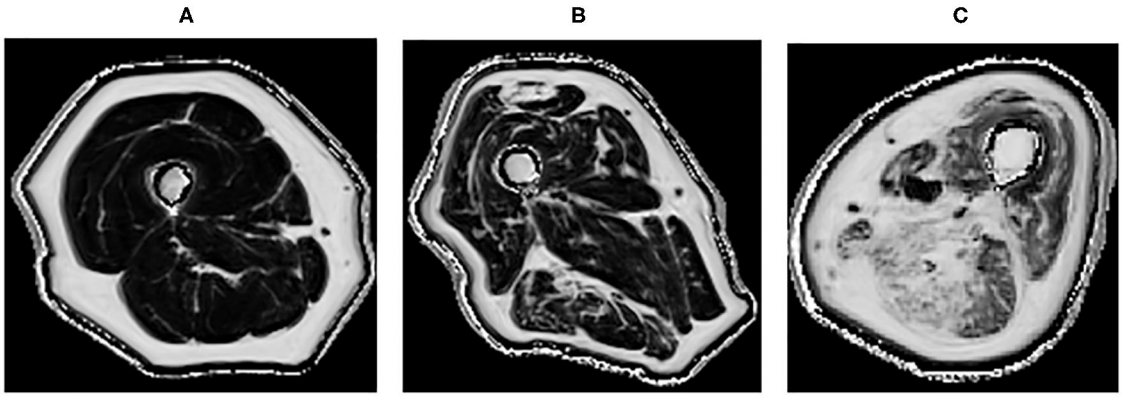

FIGURE 2 | Quantitative MRI fat fraction measurement in the quadriceps and hamstrings, respectively in the thigh in **(A)** 45-years-old healthy female with a fat fraction of 1.9 and 2.7%, respectively, **(B)** 83-years-old healthy male presenting with fatty infiltration associated with healthy aging with a fat fraction of 9.6 and 13.4%, respectively, **(C)** 60-years-old male with active myositis presenting with fatty infiltration with a fat fraction of 19.6 and 28.5%, respectively.

MRI has become an integral imaging tool in the clinical diagnosis and monitoring of disease activity of myositis due to its ability to non-invasively detect abnormal muscles and identify the most suitable site for muscle biopsies (**Figure 1**) (45, 71–74). Reassuringly, MRI findings in myositis correlate well with biopsy results (75), and whole body MRI can be more sensitive than muscle enzymes and EMG in diagnosing myositis (76). Nevertheless, the image interpretation can be subjective (77), there is no validated MRI protocol for assessing myositis (45) and MRI findings in isolation may not be specific enough for diagnostic purposes (78).

Quantitative MRI, which allows further characterization of the muscle structure at a microscopic level, can provide a more precise description of muscle pathology (55, 73, 79). It could potentially be used in longitudinal monitoring of disease (80). It has been demonstrated that T2 and fat fraction increase in myositis patients (**Figure 2**), demonstrating that MRI is sensitive enough to quantitatively detect muscle edema (55, 81) and myosteatosis (82). These measures could be used to more accurately guide muscle biopsies. This may be of greater importance in patients with low grade inflammation, where there are subtle muscle changes that might go undetected by conventional MRI. DTI measurements are sensitive to subtle changes in the muscle, and have been used to detect differences in muscle due to diseases including myositis (83). However, muscle DTI is far from standardized. The optimal methods and parameters for performing diffusion in muscle have not been established and larger studies are necessary to establish whether diffusion will be a useful tool for monitoring muscle disease in clinical practice.

One of the drawbacks of MRI as an imaging tool is its cost. Often, this is the deciding factor in choosing ultrasonography over MRI as a more feasible modality in assessing articular joints. But does this cost consideration translate to examining muscles or in patients with myositis? In addition to the more favorable cost compared to MRI, ultrasound also has a greater acceptability by patients. Although there is greater operator dependence for ultrasound, there is the possibility to apply the ultrasound information directly in the clinical setting. There is a suggestion that ultrasound elastography of muscles may be able to aid diagnosis of myositis and its follow-up (84), but the impression is that ultrasound is unlikely to replace MRI in the clinical setting in myositis just yet, because the current evidence is not strong, due to small sample sized studies that results in inconclusive findings (85).

Nevertheless, the current evidence suggests that SWE shows less muscle stiffness in myositis compared to healthy individuals (**Figure 3**), and can distinguish myositis from normal muscles (86). The loss of muscle stiffness in myositis patients was also observed using magnetic resonance elastography (87). SWE measurements also correlate with muscle strength and MRI grades of edema and atrophy (86, 88). All of these findings appear to only manifest when the muscles are under no passive or active loading.

IIM can be a very disabling condition. The potential to use promising non-invasive diagnostic and monitoring tools like qMRI and SWE could facilitate prompt diagnosis and treatment for patients. In the diagnosis of giant cell arteritis (GCA) (89), ultrasound can now reliably replace invasive temporal artery biopsies in GCA diagnosis. Similarly, the continuing development of qMRI and SWE of muscle could 1 day replace muscle biopsy in the diagnosis of IIM.

Steroid Myopathy

Glucocorticoids are powerful anti-inflammatory agents and have a variety of uses in rheumatology, most commonly as bridging therapy before other longer term treatments are started. Polymyalgia rheumatic (PMR) and the related GCA are two examples where high doses of steroids are prescribed. As a result, many often develop a proximal myopathy, without typical inflammatory laboratory markers, such as muscle enzyme abnormalities or myositis-related antibodies. These patients are often disabled by muscle weakness from the disease process. It would, therefore, be reasonable to hypothesize that, despite

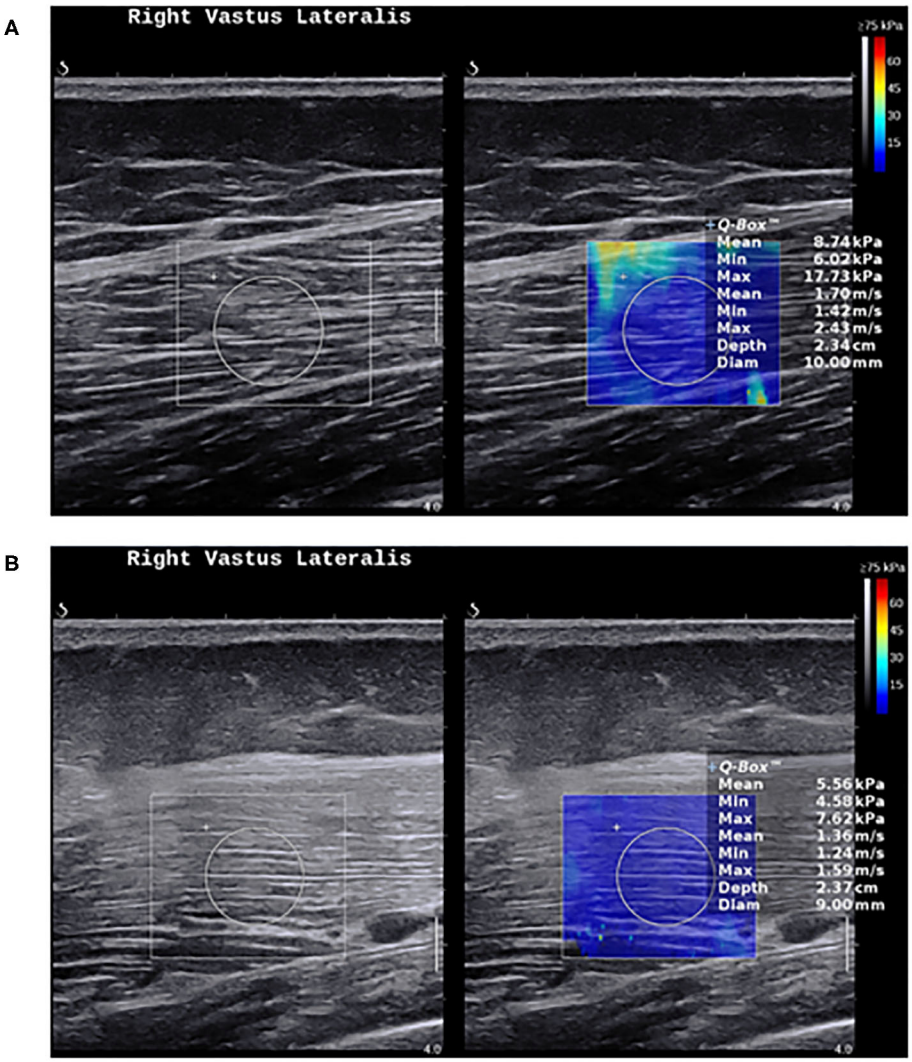

FIGURE 3 | Shear wave elastography in healthy muscles and myositis. **(A)** Shows a normal muscle stiffness (8.7 kPa) in a 50-year-old healthy female person. **(B)** Shows a low muscle stiffness (5.5 kPa) in a 49-year-old male with active polymyositis.

not demonstrating a classical myositic picture with abnormal blood markers, muscles in PMR and GCA are likely to be abnormal.

There may be a fine line between the effects of inflammation from disease (PMR and GCA) and the catabolic effects of therapy (steroids) on muscle in patients. Amongst the many adverse effects of glucocorticoids, they trigger muscle atrophy, with a particular affinity for the atrophy of fast-twitch or type II muscle fibers (90, 91). This will often present as myopathy or muscle weakness, but due to the lack of a standardized definition of glucocorticoid-induced myopathy, reporting of myopathy due to therapy in PMR and GCA can prove inconsistent (92). Therefore, the management of steroid-induced myopathy can be challenging due to the difficulty in identifying myopathy before any clinical symptoms with the current means of investigation (93).

Can imaging help in characterizing the myopathy in this group of patients? Very little research in this area has been performed. Most studies have been focused on the diagnosis of PMR and GCA and responses to steroid therapy, based mainly on joint findings (94–97). Certainly, studies have demonstrated that quantitative ultrasound was able to show muscle changes associated to chronic use of steroids, but was unable to tell if the observed changes could be due to other causes including cachexia or sarcopenia (98, 99). A recent study showed that SWE detected a higher reduction in muscle stiffness over time in GCA patients on long term glucocorticoid who were also weaker (100). However, as patients with GCA (and PMR) tend to be older, and therefore more likely to be sarcopenic, these observed muscle changes have to be interpreted cautiously. If future research shows that SWE changes could potentially be evident before patients present with signs of weakness, then we may have an imaging tool that can direct appropriate management of steroid-induced myopathy, including preventative strategies to preserve muscle function.

The fact that type II muscle fibers tend to be affected by steroid therapy suggests that techniques like MRI diffusion tensor imaging that are sensitive to changes in muscle microstructure could be potentially useful in understanding the pathogenesis of steroid-induced myopathy and its diagnosis (80, 101). Due to the inflammatory nature of PMR and GCA, T2 MRI could be able to identify the edema within the muscle itself, which could be contributing to pain and fatigue. The muscle atrophy due to the catabolic effects of glucocorticoids could be quantitatively measured to monitor muscle change over time. The challenge will be interpreting the findings and to tease out if the observed imaging changes are due to therapy (glucocorticoids), or to the inflammatory disease process. Previously, when patients with RA were treated with long term steroids, it was possible to tell when they had weaker strength compared to patients who did not receive steroid therapy (102, 103). This would have provided a useful cohort to compare imaging findings of the muscle, and changes could be attributed to the steroid therapy independent of the disease process. However, due to the complexities of modern therapy and the ethical limitations, such direct comparison studies may not be feasible. Another iatrogenic cause of myopathy is in IIM treated with glucocorticoids, which presents another challenging dilemma in differentiating between muscle changes due to therapy and that due to the inflammatory muscle disease *per se*. This proposes an unmet need for means to identify the exact cause of the myopathy to optimize management—an area for further exploration of imaging as a potential tool for this purpose.

Nevertheless, qMRI can differentiate the muscle properties between the ages and has been shown to correlate with muscle outcome measures. Therefore, it shows potential promise as a tool to help understand the varying factors that can affect muscle in rheumatic diseases (104).

Rheumatoid Arthritis

The predominant site of pathology in rheumatoid arthritis is in the joints. The articular joints are therefore the most commonly imaged structure in RA. However, there are many reasons for patients with RA to have weaker muscles, including impaired physical function and a greater tendency toward physical inactivity (105, 106). RA patients often present with lower muscle mass (107), which remains apparent in remission (105). A large proportion of RA patients report experiencing muscle problems or myopathy (108, 109). Histologically, RA is also associated with atrophy of type II muscle fibers, similar to the effects of glucocorticoids on muscle (110, 111). In addition, the pro-inflammatory state in inflammatory arthritis predisposes patients to a cachectic body composition—another reason for abnormal muscles in inflammatory arthritis (112, 113).

Despite the many causes of muscle involvement in inflammatory arthritis, there are relatively little muscle imaging data in RA. Reduced muscle strength is associated with disease activity in RA, and muscle function and physical activity are modifiable factors (2). Preliminary SWE of the muscles in RA shows some indication that muscles are less stiff compared to healthy individuals, but the results do not show statistical significance despite the fact that RA patients show reduced strength (114). The lack of differential findings from SWE studies suggests that muscle pathology in RA is less likely to be due to biomechanical properties of muscle. Quantitative MRI offers a different imaging perspective of muscle, and can provide further insight into the pathogenesis of muscle pathology in RA. Indeed, qMRI could be used to identify if rheumatic patients in remission still have muscle pathology, such as inflammation or fatty infiltration. This would identify whether effective treatment is improving muscle health, or if additional interventions, such as exercise, should be developed for a more holistic approach in patients with inflammatory arthritis.

Fatigue is a common symptom in many rheumatic conditions including inflammatory arthritis with significant impact on patients' lives (115). Although treatment including biological therapy can help improve symptoms of fatigue, they are not effective in all patients (116). Of note is that exercise has also been shown to reduce fatigue levels in RA (117); this suggests that modifying the muscles in inflammatory arthritis is a potential route to improving symptoms in patients. This is an area where the mechanism of action needs clarifying—an important cue for imaging, such as SWE and qMRI to help provide some insights.

FUTURE PERSPECTIVES AND CONCLUSIONS

The capabilities of novel imaging in muscle continue to be stretched to better understand the significance of the observations. Quantitative ultrasonographic techniques, such as muscle echo-intensity may reveal useful imaging biomarkers beyond the mechanical properties of SWE (88). The use of both SWE and qMRI in assessing muscles are relatively recent imaging advances. Due to the heterogeneous nature of muscle involvement in rheumatic diseases, a multi-parametric imaging approach may offer a clearer picture of the varying disease processes (118). Combining both techniques could result in a more powerful imaging combination that provides complementary understanding of muscle changes (119). The application of artificial intelligence (AI) in imaging in rheumatology has enhanced efficacy and efficiency in image interpretation (120). Unsurprisingly, AI in rheumatology imaging is currently confined to assessing the common joint abnormalities like joint synovitis, tenosynovitis, bone erosions and cartilage loss. Deep learning involving qMRI and SWE may accelerate the knowledge and application of these imaging techniques.

This perspective highlights that the involvement of muscle is widespread in many rheumatic diseases, which can also affect other conditions including the connective tissue diseases like systemic lupus erythematosus, Sjogren's syndrome and systemic sclerosis (1). Imaging, in particular the more recent novel techniques like SWE and qMRI, shows potential to improve the understanding of how muscle is affected in rheumatic diseases. Imaging has an important role in assessing potential interventions on preserving muscle function. Imaging has improved our knowledge of joint abnormalities, but it is now timely for a call to action for a more anatomically-holistic

approach toward the understanding of the pathogenesis of rheumatic diseases, with due attention to the muscle.

DATA AVAILABILITY STATEMENT

This research is funded by the NIHR infrastructure at Leeds. The views expressed are those of the authors and not necessarily those of the NHS, the NIHR or the Department of Health.

AUTHOR CONTRIBUTIONS

MF and AT wrote the first draft of the manuscript. JB, RW, and AA edited and revised the manuscript. MF, JB, and AA contributed the figures. All authors revised the manuscript critically and approved the final version of the manuscript. All authors contributed to the article and approved the submitted version.

REFERENCES

1. Altabas-Gonzalez I, Perez-Gomez N, Pego-Reigosa JM. How to investigate: suspected systemic rheumatic diseases in patients presenting with muscle complaints. *Best Pract Res Clin Rheumatol.* (2019) 33:101437. doi: 10.1016/j.berh.2019.101437
2. Uutela TI, Kautiainen HJ, Hakkinen AH. Decreasing muscle performance associated with increasing disease activity in patients with rheumatoid arthritis. *PLoS ONE.* (2018) 13:e0194917. doi: 10.1371/journal.pone.0194917
3. Kubínová K, Dejthevaporn R, Mann H, Machado PM, Vencovský J. The role of imaging in evaluating patients with idiopathic inflammatory myopathies. *Clin Exp Rheumatol.* (2018) 36:74–81. Available online at: https://www.clinexprheumatol.org/abstract.asp?a=13317
4. Selva-O'Callaghan A, Gil-Vila A, Simó-Perdigó M, Trallero-Araguás E, Alvarado-Cárdenas M, Pinal-Fernandez I. PET scan: nuclear medicine imaging in myositis. *Curr Rheumatol Rep.* (2019) 21:64. doi: 10.1007/s11926-019-0864-3
5. Mourtzakis M, Parry S, Connolly B, Puthucheary Z. Skeletal muscle ultrasound in critical care: a tool in need of translation. *Ann Am Thorac Soc.* (2017) 14:1495–503. doi: 10.1513/AnnalsATS.201612-967PS
6. Scott JM, Martin DS, Ploutz-Snyder R, Caine T, Matz T, Arzeno NM, et al. Reliability and validity of panoramic ultrasound for muscle quantification. *Ultrasound Med Biol.* (2012) 38:1656–61. doi: 10.1016/j.ultrasmedbio.2012.04.018
7. Berger J, Bunout D, Barrera G, de la Maza MP, Henriquez S, Leiva L, et al. Rectus femoris (RF) ultrasound for the assessment of muscle mass in older people. *Arch Gerontol Geriatr.* (2015) 61:33–8. doi: 10.1016/j.archger.2015.03.006
8. van Hooren B, Teratsias P, Hodson-Tole EF. Ultrasound imaging to assess skeletal muscle architecture during movements: a systematic review of methods, reliability, and challenges. *J Appl Physiol.* (2020) 128:978–99. doi: 10.1152/japplphysiol.00835.2019
9. Drakonaki EE, Sudol-Szopinska I, Sinopidis C, Givissis P. High resolution ultrasound for imaging complications of muscle injury: is there an additional role for elastography? *J Ultrasonogr.* (2019) 19:137–44. doi: 10.15557/JoU.2019.0020
10. Li Y, Snedeker JG. Elastography: modality-specific approaches, clinical applications, and research horizons. *Skeletal Radiol.* (2011) 40:389–97. doi: 10.1007/s00256-010-0918-0
11. Sigrist RMS, Liau J, Kaffas AE, Chammas MC, Willmann JK. Ultrasound elastography: review of techniques and clinical applications. *Theranostics.* (2017) 7:1303–29. doi: 10.7150/thno.18650
12. Barr RG, Nakashima K, Amy D, Cosgrove D, Farrokh A, Schafer F, et al. WFUMB guidelines and recommendations for clinical use of ultrasound elastography: part 2: breast. *Ultrasound Med Biol.* (2015) 41:1148–60. doi: 10.1016/j.ultrasmedbio.2015.03.008
13. Ferraioli G, Filice C, Castera L, Choi BI, Sporea I, Wilson SR, et al. WFUMB guidelines and recommendations for clinical use of ultrasound elastography: Part 3: liver. *Ultrasound Med Biol.* (2015) 41:1161–79. doi: 10.1016/j.ultrasmedbio.2015.03.007
14. Cosgrove D, Barr R, Bojunga J, Cantisani V, Chammas MC, Dighe M, et al. WFUMB guidelines and recommendations on the clinical use of ultrasound elastography: part 4. Thyroid. *Ultrasound Med Biol.* (2017) 43:4–26. doi: 10.1016/j.ultrasmedbio.2016.06.022
15. Domenichini R, Pialat JB, Podda A, Aubry S. Ultrasound elastography in tendon pathology: state of the art. *Skeletal Radiol.* (2017) 46:1643–55. doi: 10.1007/s00256-017-2726-2
16. Dirrichs T, Quack V, Gatz M, Tingart M, Kuhl CK, Schrading S. Shear wave elastography (SWE) for the evaluation of patients with tendinopathies. *Acad Radiol.* (2016) 23:1204–13. doi: 10.1016/j.acra.2016.05.012
17. Sarabon N, Kozinc Z, Podrekar N. Using shear-wave elastography in skeletal muscle: a repeatability and reproducibility study on biceps femoris muscle. *PLoS ONE.* (2019) 14:e0222008. doi: 10.1371/journal.pone.0222008
18. Phan A, Lee J, Gao J. Ultrasound shear wave elastography in assessment of skeletal muscle stiffness in senior volunteers. *Clin Imaging.* (2019) 58:22–6. doi: 10.1016/j.clinimag.2019.06.006
19. Maslarska M, Weis C, Bode C, Hehrlein C. Shear wave elastography of peripheral muscle weakness in patients with chronic congestive heart failure. *Ultrasound Med Biol.* (2018) 44:2531–9. doi: 10.1016/j.ultrasmedbio.2018.08.011
20. Akagi R, Takahashi H. Effect of a 5-week static stretching program on hardness of the gastrocnemius muscle. *Scand J Med Sci Sports.* (2014) 24:950–7. doi: 10.1111/sms.12111
21. Zhang ZJ, Ng GYF, Lee WC, Fu SN. Increase in passive muscle tension of the quadriceps muscle heads in jumping athletes with patellar tendinopathy. *Scand J Med Sci Sports.* (2017) 27:1099–104. doi: 10.1111/sms.12749
22. Itoigawa Y, Sperling JW, Steinmann SP, Chen Q, Song P, Chen S, et al. Feasibility assessment of shear wave elastography to rotator cuff muscle. *Clin Anat.* (2015) 28:213–8. doi: 10.1002/ca.22498
23. Flatres A, Aarab Y, Nougaret S, Garnier F, Larcher R, Amalric M, et al. Real-time shear wave ultrasound elastography: a new tool for the evaluation of diaphragm and limb muscle stiffness in critically ill patients. *Crit Care.* (2020) 24:34. doi: 10.1186/s13054-020-2745-6
24. Du LJ, He W, Cheng LG, Li S, Pan YS, Gao J. Ultrasound shear wave elastography in assessment of muscle stiffness in patients with Parkinson's disease: a primary observation. *Clin Imaging.* (2016) 40:1075–80. doi: 10.1016/j.clinimag.2016.05.008
25. Lacourpaille L, Hug F, Guevel A, Pereon Y, Magot A, Hogrel JY, et al. Non-invasive assessment of muscle stiffness in patients with Duchenne muscular dystrophy. *Muscle Nerve.* (2015) 51:284–6. doi: 10.1002/mus.24445
26. Gao J, He W, Du LJ, Chen J, Park D, Wells M, et al. Quantitative ultrasound imaging to assess the biceps brachii muscle in chronic post-stroke spasticity: preliminary observation. *Ultrasound Med Biol.* (2018) 44:1931–40. doi: 10.1016/j.ultrasmedbio.2017.12.012
27. Alfuraih AM, O'Connor P, Hensor E, Tan AL, Emery P, Wakefield RJ. The effect of unit, depth, and probe load on the reliability of muscle shear wave elastography: variables affecting reliability of SWE. *J Clin Ultrasound.* (2018) 46:108–15. doi: 10.1002/jcu.22534
28. Alfuraih AM, O'Connor P, Tan AL, Hensor E, Emery P, Wakefield RJ. An investigation into the variability between different shear wave elastography systems in muscle. *Med Ultrasonogr.* (2017) 19:392–400. doi: 10.11152/mu-1113
29. Kot BC, Zhang ZJ, Lee AW, Leung VY, Fu SN. Elastic modulus of muscle and tendon with shear wave ultrasound elastography: variations with different technical settings. *PLoS ONE.* (2012) 7:e44348. doi: 10.1371/journal.pone.0044348

30. Faulkner JA, Larkin LM, Claflin DR, Brooks SV. Age-related changes in the structure and function of skeletal muscles. *Clin Exp Pharmacol Physiol.* (2007) 34:1091–6. doi: 10.1111/j.1440-1681.2007.04752.x
31. Kragstrup TW, Kjaer M, Mackey AL. Structural, biochemical, cellular, and functional changes in skeletal muscle extracellular matrix with aging. *Scand J Med Sci Sports.* (2011) 21:749–57. doi: 10.1111/j.1600-0838.2011.01377.x
32. Alfuraih AM, Tan AL, O'Connor P, Emery P, Wakefield RJ. The effect of ageing on shear wave elastography muscle stiffness in adults. *Aging Clin Exp Res.* (2019) 31:1755–63. doi: 10.1007/s40520-019-01139-0
33. Akagi R, Yamashita Y, Ueyasu Y. Age-related differences in muscle shear moduli in the lower extremity. *Ultrasound Med Biol.* (2015) 41:2906–12. doi: 10.1016/j.ultrasmedbio.2015.07.011
34. Yoshida K, Itoigawa Y, Maruyama Y, Saita Y, Takazawa Y, Ikeda H, et al. Application of shear wave elastography for the gastrocnemius medial head to tennis leg. *Clin Anat.* (2017) 30:114–9. doi: 10.1002/ca.22788
35. Sendur HN, Cindil E, Cerit MN, Kiliç P, Gültekin II, Oktar SÖ. Evaluation of effects of aging on skeletal muscle elasticity using shear wave elastography. *Eur J Radiol.* (2020) 128:109038. doi: 10.1016/j.ejrad.2020.109038
36. Eby SF, Cloud BA, Brandenburg JE, Giambini H, Song P, Chen S, et al. Shear wave elastography of passive skeletal muscle stiffness: influences of sex and age throughout adulthood. *Clin Biomech.* (2015) 30:22–7. doi: 10.1016/j.clinbiomech.2014.11.011
37. Wang CZ, Guo JY, Li TJ, Zhou Y, Shi W, Zheng YP. Age and sex effects on the active stiffness of vastus intermedius under isometric contraction. *BioMed Res Int.* (2017) 2017:9469548. doi: 10.1155/2017/9469548
38. Baumer TG, Dischler J, Davis L, Labyed Y, Siegal DS, van Holsbeeck M, et al. Effects of age and pathology on shear wave speed of the human rotator cuff. *J Orthopaedic Res.* (2018) 36:282–8. doi: 10.1002/jor.23641
39. Chodock E, Hahn J, Setlock CA, Lipps DB. Identifying predictors of upper extremity muscle elasticity with healthy aging. *J Biomech.* (2020) 103:109687. doi: 10.1016/j.jbiomech.2020.109687
40. Dresner MA, Rose GH, Rossman PJ, Muthupillai R, Manduca A, Ehman RL. Magnetic resonance elastography of skeletal muscle. *J Magn Reson Imaging.* (2001) 13:269–76. doi: 10.1002/1522-2586(200102)13:2<269::AID-JMRI1039>3.0.CO;2-1
41. Uffmann K, Maderwald S, Ajaj W, Galban CG, Mateiescu S, Quick HH, et al. *In vivo* elasticity measurements of extremity skeletal muscle with MR elastography. *NMR Biomed.* (2004) 17:181–90. doi: 10.1002/nbm.887
42. Bensamoun SF, Ringleb SI, Littrell L, Chen Q, Brennan M, Ehman RL, et al. Determination of thigh muscle stiffness using magnetic resonance elastography. *J Magn Reson Imaging.* (2006) 23:242–7. doi: 10.1002/jmri.20487
43. Zonnino A, Smith DR, Delgorio PL, Johnson CL, Sergi F. MM-MRE: a new technique to quantify individual muscle forces during isometric tasks of the wrist using MR elastography. *IEEE Int Conf Rehabil Robot.* (2019) 2019:270–5. doi: 10.1109/ICORR.2019.8779562
44. Creze M, Soubeyrand M, Yue JL, Gagey O, Maitre X, Bellin MF. Magnetic resonance elastography of the lumbar back muscles: a preliminary study. *Clin Anat.* (2018) 31:514–20. doi: 10.1002/ca.23065
45. Day J, Patel S, Limaye V. The role of magnetic resonance imaging techniques in evaluation and management of the idiopathic inflammatory myopathies. *Semin Arthritis Rheum.* (2017) 46:642–9. doi: 10.1016/j.semarthrit.2016.11.001
46. Nealon AR, Docking SI, Lucas PE, Connell DA, Koh ES, Cook JL. MRI findings are associated with time to return to play in first class cricket fast bowlers with side strain in Australia and England. *J Sci Med Sport.* (2019) 22:992–6. doi: 10.1016/j.jsams.2019.05.020
47. Crombe A, Marcellin PJ, Buy X, Stoeckle E, Brouste V, Italiano A, et al. Soft-tissue sarcomas: assessment of MRI features correlating with histologic grade and patient outcome. *Radiology.* (2019) 291:710–21. doi: 10.1148/radiol.2019181659
48. Mercuri E, Jungbluth H, Muntoni F. Muscle imaging in clinical practice: diagnostic value of muscle magnetic resonance imaging in inherited neuromuscular disorders. *Curr Opin Neurol.* (2005) 18:526–37. doi: 10.1097/01.wco.0000183947.01362.fe
49. Mercuri E, Pichiecchio A, Allsop J, Messina S, Pane M, Muntoni F. Muscle MRI in inherited neuromuscular disorders: past, present, and future. *J Magn Reson Imaging.* (2007) 25:433–40. doi: 10.1002/jmri.20804
50. Schmidt GP, Reiser MF, Baur-Melnyk A. Whole-body imaging of the musculoskeletal system: the value of MR imaging. *Skeletal Radiol.* (2007) 36:1109–19. doi: 10.1007/s00256-007-0323-5
51. Leung DG, Carrino JA, Wagner KR, Jacobs MA. Whole-body magnetic resonance imaging evaluation of facioscapulohumeral muscular dystrophy. *Muscle Nerve.* (2015) 52:512–20. doi: 10.1002/mus.24569
52. Farrow M, Grainger AJ, Tan AL, Buch MH, Emery P, Ridgway JP, et al. Normal values and test-retest variability of stimulated-echo diffusion tensor imaging and fat fraction measurements in the muscle. *Br J Radiol.* (2019) 92:20190143. doi: 10.1259/bjr.20190143
53. Schlaffke L, Rehmann R, Rohm M, Otto LAM, de Luca A, Burakiewicz J, et al. Multi-center evaluation of stability and reproducibility of quantitative MRI measures in healthy calf muscles. *NMR Biomed.* (2019) 32:e4119. doi: 10.1002/nbm.4119
54. Ma J. Dixon techniques for water and fat imaging. *J Magn Reson Imaging.* (2008) 28:543–58. doi: 10.1002/jmri.21492
55. Yao L, Yip AL, Shrader JA, Mesdaghinia S, Volochayev R, Jansen AV, et al. Magnetic resonance measurement of muscle T2, fat-corrected T2 and fat fraction in the assessment of idiopathic inflammatory myopathies. *Rheumatology.* (2015) 55:441–9. doi: 10.1093/rheumatology/kev344
56. Burakiewicz J, Hooijmans MT, Webb AG, Verschuuren J, Niks EH, Kan HE. Improved olefinic fat suppression in skeletal muscle DTI using a magnitude-based dixon method. *Magn Reson Med.* (2018) 79:152–9. doi: 10.1002/mrm.26655
57. Schlaeger S, Weidlich D, Klupp E, Montagnese F, Deschauer M, Schoser B, et al. Decreased water T2 in fatty infiltrated skeletal muscles of patients with neuromuscular diseases. *NMR Biomed.* (2019) 32:e4111. doi: 10.1002/nbm.4111
58. Scheel M, Prokscha T, von Roth P, Winkler T, Dietrich R, Bierbaum S, et al. Diffusion tensor imaging of skeletal muscle–correlation of fractional anisotropy to muscle power. *RoFo.* (2013) 185:857–61. doi: 10.1055/s-0033-1335911
59. Sinha S, Sinha U, Edgerton VR. *In vivo* diffusion tensor imaging of the human calf muscle. *J Magn Reson Imaging.* (2006) 24:182–90. doi: 10.1002/jmri.20593
60. Kermarrec E, Budzik JF, Khalil C, Le Thuc V, Hancart-Destee C, Cotten A. *In vivo* diffusion tensor imaging and tractography of human thigh muscles in healthy subjects. *AJR Am J Roentgenol.* (2010) 195:W352–6. doi: 10.2214/AJR.09.3368
61. Fieremans E, Lemberskiy G, Veraart J, Sigmund EE, Gyftopoulos S, Novikov DS. *In vivo* measurement of membrane permeability and myofiber size in human muscle using time-dependent diffusion tensor imaging and the random permeable barrier model. *NMR Biomed.* (2017) 30:3612. doi: 10.1002/nbm.3612
62. Sigmund EE, Novikov DS, Sui D, Ukpebor O, Baete S, Babb JS, et al. Time-dependent diffusion in skeletal muscle with the random permeable barrier model (RPBM): application to normal controls and chronic exertional compartment syndrome patients. *NMR Biomed.* (2014) 27:519–28. doi: 10.1002/nbm.3087
63. Malis V, Sinha U, Csapo R, Narici M, Smitaman E, Sinha S. Diffusion tensor imaging and diffusion modeling: application to monitoring changes in the medial gastrocnemius in disuse atrophy induced by unilateral limb suspension. *J Magn Reson Imaging.* (2019) 49:1655–64. doi: 10.1002/jmri.26295
64. Barendregt AM, Bray TJP, Hall-Craggs MA, Maas M. Emerging quantitative MR imaging biomarkers in inflammatory arthritides. *Eur J Radiol.* (2019) 121:108707. doi: 10.1016/j.ejrad.2019.108707
65. Maggi L, Moscatelli M, Frangiamore R, Mazzi F, Verri M, de Luca A, et al. Quantitative muscle MRI protocol as possible biomarker in Becker muscular dystrophy. *Clin Neuroradiol.* (2020). doi: 10.1007/s00062-019-00875-0. [Epub ahead of print].
66. Nunez-Peralta C, Alonso-Perez J, Llauger J, Segovia S, Montesinos P, Belmonte I, et al. Follow-up of late-onset Pompe disease patients with muscle magnetic resonance imaging reveals increase in fat replacement in skeletal muscles. *J Cachexia Sarcopenia Muscle.* (2020). doi: 10.1002/jcsm.12555. [Epub ahead of print].

67. D'Souza A, Bolsterlee B, Herbert RD. Architecture of the medial gastrocnemius muscle in people who have had a stroke: a diffusion tensor imaging investigation. *Clin Biomech.* (2020) 74:27–33. doi: 10.1016/j.clinbiomech.2020.02.004
68. Heskamp L, van Nimwegen M, Ploegmakers MJ, Bassez G, Deux JF, Cumming SA, et al. Lower extremity muscle pathology in myotonic dystrophy type 1 assessed by quantitative MRI. *Neurology.* (2019) 92:e2803–14. doi: 10.1212/WNL.0000000000007648
69. Barnard AM, Willcocks RJ, Finanger EL, Daniels MJ, Triplett WT, Rooney WD, et al. Skeletal muscle magnetic resonance biomarkers correlate with function and sentinel events in Duchenne muscular dystrophy. *PLoS ONE.* (2018) 13:e0194283. doi: 10.1371/journal.pone.0194283
70. Chinoy H, Lilleker JB. Pitfalls in the diagnosis of myositis. *Best Pract Res Clin Rheumatol.* (2020) 34:101486. doi: 10.1016/j.berh.2020.101486
71. van de Vlekkert J, Maas M, Hoogendijk JE, de Visser M, van Schaik IN. Combining MRI and muscle biopsy improves diagnostic accuracy in subacute-onset idiopathic inflammatory myopathy. *Muscle Nerve.* (2015) 51:253–8. doi: 10.1002/mus.24307
72. Pipitone N. Value of MRI in diagnostics and evaluation of myositis. *Curr Opin Rheumatol.* (2016) 28:625–30. doi: 10.1097/BOR.0000000000000326
73. Kubinova K, Mann H, Vencovsky J. MRI scoring methods used in evaluation of muscle involvement in patients with idiopathic inflammatory myopathies. *Curr opin Rheumatol.* (2017) 29:623–31. doi: 10.1097/BOR.0000000000000435
74. Connor A, Stebbings S, Anne Hung N, Hammond-Tooke G, Meikle G, Highton J. STIR MRI to direct muscle biopsy in suspected idiopathic inflammatory myopathy. *J Clin Rheumatol.* (2007) 13:341–5. doi: 10.1097/RHU.0b013e31815dca0a
75. Milisenda JC, Collado MV, Pinal-Fernandez I, Hormaza Jaramillo A, Faruch Bilfeld M, Cano MD, et al. Correlation between quantitative and semiquantitative magnetic resonance imaging and histopathology findings in dermatomyositis. *Clin Exp Rheumatol.* (2019) 37:633–40. Available online at: https://www.clinexprheumatol.org/abstract.asp?a=13003
76. Huang ZG, Gao BX, Chen H, Yang MX, Chen XL, Yan R, et al. An efficacy analysis of whole-body magnetic resonance imaging in the diagnosis and follow-up of polymyositis and dermatomyositis. *PLoS ONE.* (2017) 12:e0181069. doi: 10.1371/journal.pone.0181069
77. Filli L, Maurer B, Manoliu A, Andreisek G, Guggenberger R. Whole-body MRI in adult inflammatory myopathies: do we need imaging of the trunk? *Eur Radiol.* (2015) 25:3499–507. doi: 10.1007/s00330-015-3783-3
78. Kadoba K, Mizukawa K, Nishimura K, Murabe H. Large vessel giant cell arteritis suggested by magnetic resonance imaging of the thigh: a potential mimicker of myositis, fasciitis and skeletal muscle vasculitis. *Rheumatology (Oxford).* (2019) 58:2211. doi: 10.1093/rheumatology/kez138
79. Ran J, Ji S, Morelli JN, Wu G, Li XM. The diagnostic value of T2 maps and rs-EPI DWI in dermatomyositis. *Br J Radiol.* (2019) 92:20180715. doi: 10.1259/bjr.20180715
80. Qi J, Olsen NJ, Price RR, Winston JA, Park JH. Diffusion-weighted imaging of inflammatory myopathies: polymyositis and dermatomyositis. *J Magn Reson Imaging.* (2008) 27:212–7. doi: 10.1002/jmri.21209
81. Kim HK, Laor T, Horn PS, Racadio JM, Wong B, Dardzinski BJ. T2 mapping in Duchenne muscular dystrophy: distribution of disease activity and correlation with clinical assessments. *Radiology.* (2010) 255:899–908. doi: 10.1148/radiol.10091547
82. Gaeta M, Scribano E, Mileto A, Mazziotti S, Rodolico C, Toscano A, et al. Muscle fat fraction in neuromuscular disorders: dual-echo dual-flip-angle spoiled gradient-recalled MR imaging technique for quantification—a feasibility study. *Radiology.* (2011) 259:487–94. doi: 10.1148/radiol.10101108
83. Sigmund EE, Baete SH, Luo T, Patel K, Wang D, Rossi I, et al. MRI assessment of the thigh musculature in dermatomyositis and healthy subjects using diffusion tensor imaging, intravoxel incoherent motion and dynamic DTI. *Eur Radiol.* (2018) 28:5304–15. doi: 10.1007/s00330-018-5458-3
84. Botar-Jid C, Damian L, Dudea SM, Vasilescu D, Rednic S, Badea R. The contribution of ultrasonography and sonoelastography in assessment of myositis. *Med Ultrasonogr.* (2010) 12:120–6. Available online at: https://www.medultrason.ro/medultrason/index.php/medultrason/article/view/212
85. Berko NS, Hay A, Sterba Y, Wahezi D, Levin TL. Efficacy of ultrasound elastography in detecting active myositis in children: can it replace MRI? *Pediatr Radiol.* (2015) 45:1522–8. doi: 10.1007/s00247-015-3350-8
86. Alfuraih AM, O'Connor P, Tan AL, Hensor EMA, Ladas A, Emery P, et al. Muscle shear wave elastography in idiopathic inflammatory myopathies: a case-control study with MRI correlation. *Skeletal Radiol.* (2019) 48:1209–19. doi: 10.1007/s00256-019-03175-3
87. McCullough MB, Domire ZJ, Reed AM, Amin S, Ytterberg SR, Chen Q, et al. Evaluation of muscles affected by myositis using magnetic resonance elastography. *Muscle Nerve.* (2011) 43:585–90. doi: 10.1002/mus.21923
88. Bachasson D, Dubois GJR, Allenbach Y, Benveniste O, Hogrel JY. Muscle shear wave elastography in inclusion body myositis: feasibility, reliability and relationships with muscle impairments. *Ultrasound Med Biol.* (2018) 44:1423–32. doi: 10.1016/j.ultrasmedbio.2018.03.026
89. Ponte C, Martins-Martinho J, Luqmani RA. Diagnosis of giant cell arteritis. *Rheumatology (Oxford).* (2020) 59:iii5–16. doi: 10.1093/rheumatology/kez553
90. Schakman O, Kalista S, Barbe C, Loumaye A, Thissen JP. Glucocorticoid-induced skeletal muscle atrophy. *Int J Biochem Cell Biol.* (2013) 45:2163–72. doi: 10.1016/j.biocel.2013.05.036
91. Lofberg E, Gutierrez A, Wernerman J, Anderstam B, Mitch WE, Price SR, et al. Effects of high doses of glucocorticoids on free amino acids, ribosomes and protein turnover in human muscle. *Eur J Clin Invest.* (2002) 32:345–53. doi: 10.1046/j.1365-2362.2002.00993.x
92. Harris E, Tiganescu A, Tubeuf S, Mackie SL. The prediction and monitoring of toxicity associated with long-term systemic glucocorticoid therapy. *Curr Rheumatol Rep.* (2015) 17:513. doi: 10.1007/s11926-015-0513-4
93. Minetto MA, Rainoldi A, Jabre JF. The clinical use of macro and surface electromyography in diagnosis and follow-up of endocrine and drug-induced myopathies. *J Endocrinol Invest.* (2007) 30:791–6. doi: 10.1007/BF03350820
94. Mackie SL, Pease CT, Fukuba E, Harris E, Emery P, Hodgson R, et al. Whole-body MRI of patients with polymyalgia rheumatica identifies a distinct subset with complete patient-reported response to glucocorticoids. *Ann Rheum Dis.* (2015) 74:2188–92. doi: 10.1136/annrheumdis-2015-207395
95. McGonagle D, Pease C, Marzo-Ortega H, O'Connor P, Gibbon W, Emery P. Comparison of extracapsular changes by magnetic resonance imaging in patients with rheumatoid arthritis and polymyalgia rheumatica. *J Rheumatol.* (2001) 28:1837–41. Available online at: https://www.jrheum.org/content/28/8/1837.long
96. Mori S, Koga Y, Ito K. Clinical characteristics of polymyalgia rheumatica in Japanese patients: evidence of synovitis and extracapsular inflammatory changes by fat suppression magnetic resonance imaging. *Mod Rheumatol.* (2007) 17:369–75. doi: 10.3109/s10165-007-0595-6
97. Matteson EL, Maradit-Kremers H, Cimmino MA, Schmidt WA, Schirmer M, Salvarani C, et al. Patient-reported outcomes in polymyalgia rheumatica. *J Rheumatol.* (2012) 39:795–803. doi: 10.3899/jrheum.110977
98. Martucci MG, McIlduff CE, Shin C, Gutierrez HV, Nam JY, Greenstein P, et al. Quantitative ultrasound of muscle can detect corticosteroid effects. *Clin Neurophysiol.* (2019) 130:1460–4. doi: 10.1016/j.clinph.2019.04.709
99. Webster JM, Fenton CG, Langen R, Hardy RS. Exploring the interface between inflammatory and therapeutic glucocorticoid induced bone and muscle loss. *Int J Mol Sci.* (2019) 20:5768. doi: 10.3390/ijms20225768
100. Alfuraih AM, Tan AL, O'Connor P, Emery P, Mackie S, Wakefield RJ. Reduction in stiffness of proximal leg muscles during the first 6 months of glucocorticoid therapy for giant cell arteritis: a pilot study using shear wave elastography. *Int J Rheum Dis.* (2019) 22:1891–9. doi: 10.1111/1756-185X.13667
101. Damon BM, Froeling M, Buck AK, Oudeman J, Ding Z, Nederveen AJ, et al. Skeletal muscle diffusion tensor-MRI fiber tracking: rationale, data acquisition and analysis methods, applications and future directions. *NMR Biomed.* (2017) 30:e3563. doi: 10.1002/nbm.3563
102. Danneskiold-Samsoe B, Grimby G. Isokinetic and isometric muscle strength in patients with rheumatoid arthritis. The relationship to clinical parameters and the influence of corticosteroid. *Clin Rheumatol.* (1986) 5:459–67.
103. Rothstein JM, Delitto A, Sinacore DR, Rose SJ. Muscle function in rheumatic disease patients treated with corticosteroids. *Muscle Nerve.* (1983) 6:128–35. doi: 10.1002/mus.880060208
104. Farrow M, Biglands J, Tanner SF, Clegg A, Brown L, Hensor EMA, et al. The effect of ageing on skeletal muscle as assessed by quantitative MR imaging: an association with frailty and muscle

strength. *Aging Clin Exp Res*. (2020). doi: 10.1007/s40520-020-01530-2. [Epub ahead of print].
105. Lemmey AB, Wilkinson TJ, Clayton RJ, Sheikh F, Whale J, Jones HS, et al. Tight control of disease activity fails to improve body composition or physical function in rheumatoid arthritis patients. *Rheumatology (Oxford)*. (2016) 55:1736–45. doi: 10.1093/rheumatology/kew243
106. Hanaoka BY, Ithurburn MP, Rigsbee CA, Bridges SL Jr., Moellering DR, et al. Chronic inflammation in rheumatoid arthritis and mediators of skeletal muscle pathology and physical impairment: a review. *Arthritis Care Res.* (2019) 71:173–7. doi: 10.1002/acr.23775
107. Baker JF, Von Feldt J, Mostoufi-Moab S, Noaiseh G, Taratuta E, Kim W, et al. Deficits in muscle mass, muscle density, and modified associations with fat in rheumatoid arthritis. *Arthritis Care Res.* (2014) 66:1612–8. doi: 10.1002/acr.22328
108. Ekdahl C, Andersson SI, Svensson B. Muscle function of the lower extremities in rheumatoid arthritis and osteoarthrosis. A descriptive study of patients in a primary health care district. *J Clin Epidemiol.* (1989) 42:947–54. doi: 10.1016/0895-4356(89)90159-5
109. Miro O, Pedrol E, Casademont J, Garcia-Carrasco M, Sanmarti R, Cebrian M, et al. Muscle involvement in rheumatoid arthritis: clinicopathological study of 21 symptomatic cases. *Semin Arthritis Rheum.* (1996) 25:421–8. doi: 10.1016/S0049-0172(96)80007-2
110. Brooke MH, Kaplan H. Muscle pathology in rheumatoid arthritis, polymyalgia rheumatica, and polymyositis: a histochemical study. *Arch Pathol.* (1972) 94:101–18.
111. Edstrom L, Nordemar R. Differential changes in type I and type II muscle fibres in rheumatoid arthritis. A biopsy study. *Scand J Rheumatol.* (1974) 3:155–60. doi: 10.3109/03009747409097142
112. Roubenoff R, Roubenoff RA, Cannon JG, Kehayias JJ, Zhuang H, Dawson-Hughes B, et al. Rheumatoid cachexia: cytokine-driven hypermetabolism accompanying reduced body cell mass in chronic inflammation. *J Clin Invest.* (1994) 93:2379–86. doi: 10.1172/JCI117244
113. Engvall IL, Elkan AC, Tengstrand B, Cederholm T, Brismar K, Hafstrom I. Cachexia in rheumatoid arthritis is associated with inflammatory activity, physical disability, and low bioavailable insulin-like growth factor. *Scand J Rheumatol.* (2008) 37:321–8. doi: 10.1080/03009740802055984
114. Alfuraih AM, Tan AL, O'Connor P, Emery P, Wakefield RJ. Muscle stiffness in rheumatoid arthritis is not altered or associated with muscle weakness: a shear wave elastography study. *Mod Rheumatol.* (2020) 30:617–25. doi: 10.1080/14397595.2019.1645374
115. Seifert O, Baerwald C. Impact of fatigue on rheumatic diseases. *Best Pract Res Clin Rheumatol.* (2019) 33:101435. doi: 10.1016/j.berh.2019.101435
116. Almeida C, Choy EH, Hewlett S, Kirwan JR, Cramp F, Chalder T, et al. Biologic interventions for fatigue in rheumatoid arthritis. *Cochrane Database Syst Rev*. (2016) 2016:CD008334. doi: 10.1002/14651858.CD008334.pub2
117. Azeez M, Clancy C, O'Dwyer T, Lahiff C, Wilson F, Cunnane G. Benefits of exercise in patients with rheumatoid arthritis: a randomized controlled trial of a patient-specific exercise programme. *Clin Rheumatol*. (2020) 39:1783–92. doi: 10.1007/s10067-020-04937-4
118. Bryant ND, Li K, Does MD, Barnes S, Gochberg DF, Yankeelov TE, et al. Multi-parametric MRI characterization of inflammation in murine skeletal muscle. *NMR Biomed.* (2014) 27:716–25. doi: 10.1002/nbm.3113
119. Giambini H, Hatta T, Rezaei A, An KN. Extensibility of the supraspinatus muscle can be predicted by combining shear wave elastography and magnetic resonance imaging-measured quantitative metrics of stiffness and volumetric fat infiltration: a cadaveric study. *Clin Biomech.* (2018) 57:144–9. doi: 10.1016/j.clinbiomech.2018.07.001
120. Stoel B. Use of artificial intelligence in imaging in rheumatology–current status and future perspectives. *RMD Open.* (2020) 6:e001063. doi: 10.1136/rmdopen-2019-001063

Conflict of Interest: The authors declare that the research was conducted in the absence of any commercial or financial relationships that could be construed as a potential conflict of interest.

frontiers in Medicine

MINI REVIEW
published: 25 August 2020
doi: 10.3389/fmed.2020.00487

Ultrasound Imaging in Psoriatic Arthritis: What Have We Learnt in the Last Five Years?

Sayam R. Dubash[1,2†‡], *Gabriele De Marco*[1,2†‡], *Richard J. Wakefield*[1,2‡], *Ai Lyn Tan*[1,2‡], *Dennis McGonagle*[1,2] *and Helena Marzo-Ortega*[1,2*‡]

[1] NIHR Leeds Biomedical Research Centre, Leeds Teaching Hospitals Trust, Leeds, United Kingdom, [2] Leeds Institute of Rheumatic and Musculoskeletal Medicine, University of Leeds, Leeds, United Kingdom

Psoriatic arthritis (PsA) is a complex heterogeneous disease with multiple inter-related pathologies such as synovitis, enthesitis, tendinopathy, and dactylitis. Clinical assessment is limited in its detail to assess pathology, thus in recent years, ultrasound (US) has become more popular, given its high sensitivity to detect inflammatory arthritis and ability to inform clinical decisions. Although a qualitative technique, US findings can be graded semi-quantitatively for grayscale (GS) and power Doppler (PD). Synovitis is frequently present in inflammatory arthritis pathologies, and in PsA, recent evidence shows a propensity for tendon and entheseal lesions. The presence of flexor tenosynovitis and flexor tendon insertional enthesopathy at accessory pulleys is supportive of the "Deep Koebner" concept. Peri-tendinous inflammation—mutual to PsA or rheumatoid arthritis (RA), is associated with soft tissue oedema with PD signal frequently at the flexor tendon compartments in PsA. Research on enthesitis in PsA/PsO has improved understanding in subclinical and clinical PsA, explored associations with progression to PsA, and investigated links to prognosis assessment. Dactylitis is a pathognomonic PsA lesion where US has enhanced knowledge of the disease course and pathology of lesions such as: flexor tenosynovitis; synovitis; and soft tissue oedema. Increased US sensitivity has also brought innovation including promising automated ultrasound scanning techniques. So, what have we learnt in recent years and what are the unmet needs to focus future research initiatives in this disabling disease? This narrative review article assesses the neoteric evidence, bringing into context the knowledge gained and highlighting potential areas of research.

Keywords: spondyloarthritis (including psoriatic arthritis), enthesitis, dactylitis, synovitis tendon inflammation, peri-tendon inflammation, tenosynovitis, ultrasonography

OPEN ACCESS

Edited by:
Raj Sengupta,
Royal National Hospital for Rheumatic Diseases, United Kingdom

Reviewed by:
Sandra Salvador Falcao,
New University of Lisbon, Portugal
Rafael Chakr,
Federal University of Rio Grande do Sul, Brazil

***Correspondence:**
Helena Marzo-Ortega
medhmo@leeds.ac.uk

† These authors have contributed equally to this work

‡ORCID:
Sayam R. Dubash
orcid.org/0000-0002-9303-7122
Gabriele De Marco
orcid.org/0000-0003-2406-161X
Richard J. Wakefield
orcid.org/0000-0001-5352-8683
Ai Lyn Tan
orcid.org/0000-0002-9158-7243
Helena Marzo-Ortega
orcid.org/0000-0002-9683-3407

Specialty section:
This article was submitted to Rheumatology, a section of the journal Frontiers in Medicine

Received: *04 June 2020*
Accepted: *17 July 2020*
Published: *25 August 2020*

Citation:
Dubash SR, De Marco G, Wakefield RJ, Tan AL, McGonagle D and Marzo-Ortega H (2020) Ultrasound Imaging in Psoriatic Arthritis: What Have We Learnt in the Last Five Years? Front. Med. 7:487. doi: 10.3389/fmed.2020.00487

INTRODUCTION

Psoriatic arthritis (PsA) is a heterogeneous disease characterized by joint, tendon, and entheseal inflammation in both the peripheral and axial skeleton. At these sites, inflammation gives rise to pain, tenderness and swelling which is either localized around a joint or more diffuse e.g., along a whole digit (dactylitis). Categorized as one of the main disorders under the umbrella term Spondyloarthritis (SpA), PsA incorporates associated extra-articular manifestations including cutaneous psoriasis (PsO), related onychodystrophy, inflammatory bowel disease and uveitis.

The musculoskeletal burden is comparable to rheumatoid arthritis (RA), with joint related damage, functional impairment and reduced quality of life over time (1).

The challenges of diagnosis in early PsA are not confined to the heterogeneity of disease, which is evident from the variety of outcome measures available (2). In contrast to RA, there are no biomarkers such as anti-citrullinated peptide antibody (ACPA) or rheumatoid factor (RF) to identify early PsA and therefore diagnosis is dependent upon identification of specific clinical features. In addition, elevation of acute phase markers such as C-reactive protein (CRP) only occurs in up to half of patients and is therefore of limited value in early PsA (3). Lastly, the absence of PsO in the presence of arthritis may lead to a label of undifferentiated arthritis. Reflecting these shortcomings, imaging has been increasingly utilized for PsA evaluation and therapy assessment.

Plain film radiographs of joints are feasible, quick to perform and low in cost, with the ability to assess progressive damage reasonably well. However, when compared to ultrasound (US) or magnetic resonance imaging (MRI), they lack sensitivity for detecting early inflammatory arthritis and associated damage (4, 5). Ultrasonography (US) has various advantages over MRI, including greater accessibility, overall reduced cost, lack of contraindications, and its availability in the clinic. However, MRI has the advantage of allowing access to sites where US has a limited acoustic window e.g., axial skeleton and all osseous based pathology. Given the mounting evidence on early treatment of active inflammation for optimal outcomes, the need for adopting sensitive imaging tools into routine practice has never been greater. The aim of this review was to evaluate the recent research literature on US use in PsA with relevance to clinical practice.

METHODS

A panel of rheumatologists undertook this project. Although no systematic search was performed as such, the Patient-Intervention-Comparison-Outcome (PICO) standard was adhered to. Intervention: the search strategy focused on scientific publications reporting on the use of US for diagnosis, management and assessment of PsA. Population: the target group included adults ($\geq$ 18 years of age) with a diagnosis of PsA of any disease duration. Specific PsA musculoskeletal manifestations explored were synovitis, dactylitis, and enthesitis. PsA-related spondylitis was not included due to unfeasible accessibility of axial skeleton structures to US imaging techniques. Comparator: the imaging techniques appraised, whenever available, were conventional radiography, computed tomography (CT), and MRI. Outcome: no pre-set outcome measures were chosen, as the panel felt that a restricted approach would narrow the focus of the review excessively. Whenever available, measures of diagnostic accuracy (sensitivity, specificity, positive/negative predictive values, and likelihood ratios) were retrieved (**Table 1**).

The search strategy encompassed clinical trials, well-designed cohorts and systematic reviews published in Pubmed from 2015 onwards and was performed by two members of the working party (SRD, GDM). Only publications in English were considered. Key papers before 2015 were included if considered relevant to the review.

RESULTS

Ultrasound for Diagnosis

Synovitis

Grayscale (GS) US findings in PsA are similar to those of RA in morphology with synovial hypertrophy, intra-articular effusion, enhanced power Doppler (PD) signal, and erosions (**Figure 1A**). However, the literature shows a trend to higher severity in RA synovitis as compared to PsA (6, 7). In these studies focussing on synovitis in PsA, US showed more prominent tendinous/entheseal involvement adjacent to synovial joints in the PsA groups (8, 9). Absence of PD signal over the hypertrophic tissues, however, did not rule out active intra-articular synovitis (6). Preliminary data suggested that the pathologic processes in the intra-articular synovia may follow – not precede- inflammation at the level of soft tissues surrounding extensor tendons in the hands (9, 10). One limitation of US, in the context of the evaluation of psoriatic polyarthritis, could be the amount of time needed to perform such investigation, as compared to clinical evaluation. However, automated US scanning techniques showed 2-fold higher sensitivity in detecting synovitis of the hands, when compared to clinical examination, and have potential for improving the current standard of care in rheumatology clinics (10).

Subclinical Synovitis: What Does it Mean?

Attribution of articular swelling to synovitis is better performed by US as compared to clinical examination, especially at a sub-clinical stage. Subclinical synovitis as detected by US is frequent in subjects with psoriasis and healthy individuals (up to 49.6% may show at least one abnormality, in at least one site investigated). Although less common, PD signal suggestive of subclinical synovitis was present in 24% of healthy subjects (11). It is interesting to note that in the healthy subjects recruited in this cross-sectional study, PD signal showed mild alteration (grading 1 out of 3) and lesions scoring 2 or 3 were uncommon or absent, respectively. Of note, PsA patients recruited in this study had subclinical synovitis more frequently, affecting more sites and with more severe PD signal alterations. Frequent findings of subclinical synovitis in healthy subjects (55%) and psoriatic patients (85%) were confirmed by another cross-sectional study (12). However, in this report, "active synovitis" (that is, the combination of synovial hypertrophy with PD signal) was found exclusively in psoriatic subjects (27.5%) (12). Histological evaluation would ideally be needed to disentangle the meaning of these imaging findings in pre-clinical PsA and in normal.

Subclinical synovitis -with or without subclinical enthesitis- at baseline is more frequent in psoriatic patients who develop PsA over a follow-up of 2 years (13). In PsA patients who are in clinical remission/minimal disease activity, US detection (using associated PD) of non-clinically noticeable synovitis is a predictor of short-term (6 months) flare (14).

TABLE 1 | References appraised and selected for inclusion.

Ultrasound for diagnosis

- Synovitis
  Records evaluated: 80;
  Records included: 6 (2 relevant references from > 5 years included)
- Subclinical synovitis
  Records evaluated: 65;
  Records included 4
- Tendon pathologies
  Records evaluated: 97;
  Records included 10 (of which 2 are also cited in "synovitis") (3 relevant references from > 5 years included)
- Entheseal pathology
  Records evaluated: 126;
  Records included 13 (of which 1 already cited in tendon pathologies) (1 relevant reference from > 5 years included)
- Dactylitis
  Records evaluated: 38;
  Records included 5 (0 references from > 5 years)
- US in differential diagnosis of PsA
  Records evaluated: 134;
  Records included 4 (of which 1 already cited in tendon)
- Limitations of US in clinical practice
  Records evaluated: 43;
  Records included 1 (0 references from > 5 years)
- Comparison of US with clinical examination and composite clinical scores
  Records evaluated: 101;
  Records included 5 (of which 1 is already cited in "dactylitis"); (1 relevant reference from > 5 years included).

Ultrasound for management

- US for management
  Records evaluated: 59;
  Records included: 2 (0 references from > 5 years)
- Monitoring of PsA
  Records evaluated: 280;
  Records included 2 (0 references from > 5 years)
- Remission assessment
  Records evaluated: 120;
  Records included 3 (of which 2 already cited in subclinical synovitis and comparison of US with clinical examination) (1 relevant reference from > 5 years included)
- Prognosis
  Records evaluated: 87;
  Records included 4 (of which 1 already cited in tendon)
- Composite US scores (joints, entheses)
  Records evaluated: 19;
  Records included 9 (of which 1 is also cited in "tendon pathologies"), (3 relevant references from > 5 years duration).
- Guided injections
  Records evaluated: 116;
  Records included 4 (2 relevant references from >5 years).

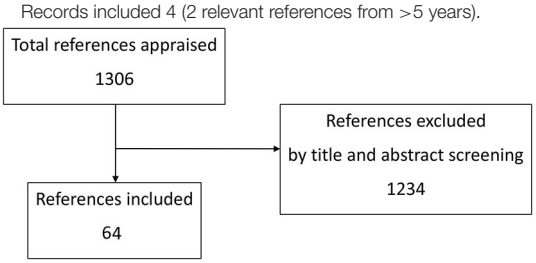

Tendon Pathologies

Tendinopathic pathologies can exist in both PsA and RA but can be difficult to attribute specifically to either disease. Benjamin et al. (15) described the concept of a "functional enthesis," an anatomical, biomechanical, and pathological feature that share fibrocartilaginous entheses proximal to regions of attachment to allow tendons or ligament to wrap around bony pulleys. It is at these sites that there is a propensity for disease in PsA which has been confirmed through US (16). Flexor tenosynovitis can be detected by high-resolution US of the hand flexor tendons as illustrated in **Figure 1B**. Peri-tendinous soft tissue oedema and PD signal have been reported in the 2nd−4th flexor tendon compartments of the dominant hand in one third of PsA vs. no RA patients (8, 17). Additionally, flexor tendon insertional enthesopathy occurs at accessory pulleys including new bone formation, significantly more common in PsA, supporting the "Deep Koebner" phenomenon (18). A much higher percentage of peritendinous extensor digitorum tendon inflammation was

observed in PsA compared to RA (9). Soft tissue oedema was detected almost exclusively in PsA when the most clinically involved finger was assessed. Further, central slip enthesitis at the PIP joints was exclusively found in early PsA. Ultrasound detection of extra-synovial features and at the synovio-entheseal complex may be helpful in the differential diagnosis between early RA and early PsA (9).

There is some expert based consensus that the most useful anatomical sites for identifying disease at tendons (with sheaths) are at the hand flexor tendons, extensor tendon compartment of the wrist, and for peri-tendonitis (inflamed tendons without sheath) hand extensor tendons are favored over the feet extensor tendons (19).

Further recent studies have also added to the literature on significantly greater tendon sheath synovial thickening and tendon sheath PD signal observed in PsA compared to PsO without PsA (20). On a practical level, a previous study demonstrated greater peritendon extensor tendon inflammation at the MCP level in PsA than RA, indicating that it is a key characteristic of PsA, valuable in differential diagnosis (10). Importantly in PsA, the most recent evidence indicates that MCP swelling is actually attributable to not only synovitis, but also peri-tendonitis (**Figure 1A**), and are detectable at similar frequencies (21).

Entheseal Pathology

Enthesitis is considered characteristic of PsA and an early lesion throughout disease progression (22). The clinical assessment of the entheses can be impaired by lack of sensitivity and overlap with pain amplification syndromes (23, 24). Moreover, data suggest a disconnection between arthritis severity and enthesitis severity (25). Although recent studies found no correlation between the clinical and the US assessments of entheses in PsA there is potential for increased accuracy of enthesitis assessment using US scan (26, 27).

OMERACT proposed (28) a definition for the elementary lesions that characterize enthesopathy: (1) "hypoechogenicity at the enthesis"; (2) "thickened enthesis"; (3) "calcification/enthesophyte at enthesis"; (4) "erosion at enthesis"; (5) "Doppler signal at enthesis" (**Figures 1C–E**). Some of these lesions are structural and commonly seen in people not affected by PsA, although in PsA they tend to be more severe (29–31). Moreover, the definition of PD alterations within 2 mm from the enthesis is not accepted by the whole scientific community. Furthermore, body weight and other mechanical factors and metabolic conditions are considered confounders for enthesopathic structural lesions (17, 32). However, US-detected active enthesitis (that is, the combination of elementary lesions 1 and 5) is related to older age and higher levels of physical activity in PsA patients (33). Interestingly, inflammatory entheseal changes are commonly found in people who have psoriasis or arthralgia and psoriasis, preceding the clinical onset of PsA. In the study by Zabotti et al. (32) the presence of US evidence of enthesitis was associated with progression to PsA.

Dactylitis

The use of US has added to the understanding of pathologies involved in dactylitis that extend beyond the presence of synovitis and flexor tenosynovitis. In a recent study of dactylitis in PsA patients, joint synovitis was detected by US in 40% of dactylitic digits and was associated with longer duration of dactylitis and the asymptomatic "cold" type characterized by swelling but not pain or tenderness (34). Another study of psoriatic dactylitis identified PD at the accessory pulleys of affected digits, suggesting that these sites of mechanical stress may be more important in the disease process than previously thought (35). Moreover, flexor tenosynovitis is most prevalent in the majority of PsA imaged dactylitis and over half of patients also display subcutaneous oedema and synovitis (36). Unlike the OMERACT US definitions aforementioned for synovitis and enthesitis, no widely accepted ultrasound definition was present for dactylitis. Just recently, Zabotti et al. (37) have developed an US score for dactylitis, namely the DACTylitis glObal Sonographic score in PsA (DACTOS). Dactylitis elementary lesions were reviewed via a Delphi exercise of 12 experts to reach a consensus on scoring which resulted in moderate/excellent reliability for US scored lesions (37). Imaging scores of such may assist in the diagnosis and evaluation of the response of tissue compartments to therapies (38).

US in Differential Diagnosis in PsA

The morphological similarities between PsA synovium and that of RA leave open substantial issues related to the differential diagnosis of inflammatory arthritides. Narrowing the view on synovitis, the integration of contrast enhancement technique to US scans may assist in distinguishing across different diseases. Some evidence points to the potential of different software for quantitative analysis of the kinetic parameters of the synovial vascular perfusion pattern. In one study, this sophisticated technique has shown discriminatory ability in the assessment of RA vs. other forms of arthritis, including PsA (39). However, such advanced analysis tool would be available only in research centers for now.

Beyond synovitis, the available evidence supports the concept that PsA is mainly differentiated from RA by the involvement of non-synovial articular and peri-articular structures/tissues (17, 40). Key findings are enthesitis, peritendonitis of the extensor tendons of the hands, thickening of the pulleys of the flexor tendons of the hands, peri-tendineal dermal soft tissue oedema and bone proliferation associated with erosions (usually smaller than RA). The presence of extra-synovial features on US of the hands showed sensitivity of 68% and specificity of 88.1% for early PsA (16). Some limitations apply, since most studies were performed on limited parts of the musculoskeletal system (hands and wrists mainly). Moreover, the comparisons were made between RA, seronegative SpA and PsA (leaving out crystal-caused arthropathies, especially the chronic forms).

The Limitations of US in Clinical Practice

On a practical level, clinical examination, which is subjective and not anatomically nor pathology specific, is complemented by the high sensitivity of US to detect inflammatory and structural lesions, clearly advantageous to identify characteristic PsA-related pathologies. Despite these significant benefits, a recent systematic review reported variable diagnostic accuracy for US in PsA, in fact confirmation of a PsA diagnosis was heavily

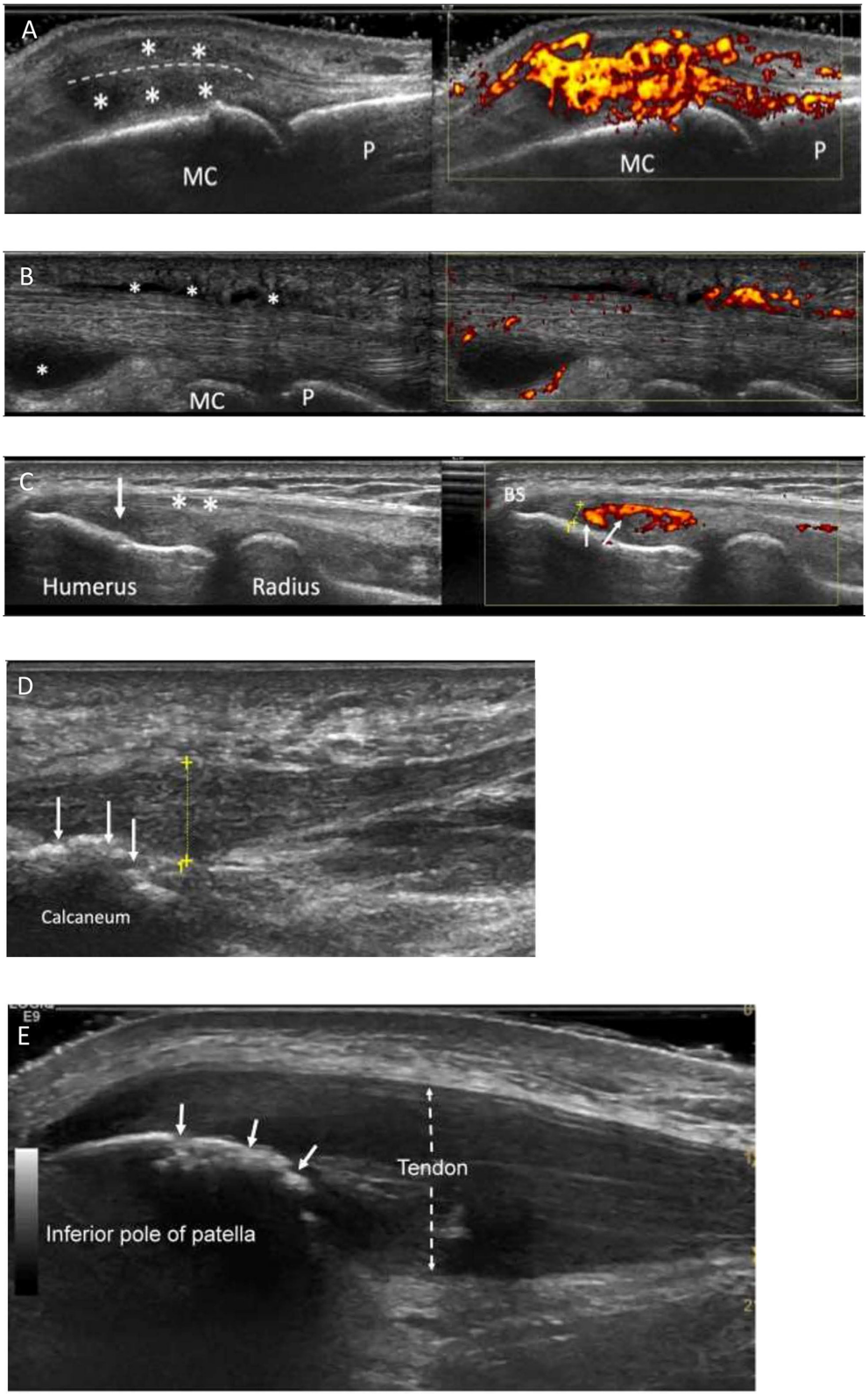

FIGURE 1 | Characteristic ultrasound appearances in Psoriatic arthritis. **(A)** Longitudinal view through a metacarpophalangeal joint with synovitis. There is gray scale

(Continued)

FIGURE 1 | thickening (*between joint and extensor tendon-dotted line) and marked increased power Doppler signal (grade 3, right image) consistent with "active" synovitis and peri-tendonitis (*above tendon). MC, metacarpal; P, phalanx. **(B)** Longitudinal view through the flexor tendon on a finger. It demonstrates fluid and synovial thickening within the tendon sheath (*). There is also marked power Doppler signal within the tendon sheath (right image). MC, metacarpal; P, phalanx. **(C)** Enthesitis of common extensor origin (CEO): Longitudinal view through the common extensor origin. Hypoechogenicity (arrow/left), loss of fibrillary pattern (*), Bone spur (BS), increased Doppler signal (small arrows/right) within 2 mm (dotted line) of bone surface. **(D)** Longitudinal view through the plantar fascia of a patient with PsA. There is thickening of the fascia (dotted yellow line measuring 8.3 mm; normal < 5 mm). Power Doppler signal is rarely seen at the plantar fascia insertion. Bone irregularity is suggestive of erosive change (arrows). **(E)** Longitudinal section through the proximal patellar tendon. The tendon is markedly thickened (dotted arrow), hypoechogenic (compared to normal tendon more distally) and has lost its fibrillary pattern. The bone surface of the patella shows bone irregularity consistent with erosive change (white arrows). This was confirmed on transverse view.

based on clinical diagnosis and classification criteria (CASPAR) (41). One should also be cognizant that the objectivity of US is dependent upon having a skilled operator for scanning and image interpretation, and a sensitive US machine/ transducer, particularly relevant for PD signal detection. Further, it is unfeasible to scan 68 joints and numerous entheses for every patient in routine clinical practice due to time constraints, therefore comprehensive US assessments of this nature occur mostly in a research setting. There are also costs to be considered involving the purchase, running, and servicing of the equipment.

Comparison of US With Clinical Examination and Composite Clinical Scores

A recent study has confirmed that in fact there is a significant association between clinical and US assessment of the large entheses when assessing Achilles and Patellar tendon origins (42). Furthermore, digital pain and tenderness in dactylitis was linked to US tenosynovitis GS $\geq$ 2 (34). However, large discrepancies have been reported between clinical examination and US findings for synovitis and enthesitis (43). In the same study, the DAPSA composite scores partially reflected Boolean's remission criteria and correlated with GS and PD synovitis but not the CPDAI (43). In another longitudinal study of 47 PsA patients, the SJC66, CRP, ESR, DAS28, and the physician global assessment were associated with PD, whereas the DAPSA was not (44). Therefore, the discordance between clinical examination and US synovitis needs further research. However, a recent report on clinical low disease activity (LDA) states, (determined by DAPSA, PASDAS, CPDAI, or MDA) suggests they are able to differentiate between high and low (MUDA) US determined disease activity (45). The unmet needs and suggested areas to focus US research in diagnosis and management of PsA are summarized in **Table 2**.

MANAGEMENT

Ultrasound for Management

The EULAR recommendations for the use of imaging in the diagnosis and management of SpA in clinical practice suggest that US has a place in providing "additional information" on top of clinical examination and laboratory investigation for monitoring the activity of peripheral SpA, including PsA (46). Perhaps surprising is that in RA, recent data showed a dichotomy between the relationship of the clinical TJC and SJC with US synovitis suggesting TJC is not associated with US synovitis, but data from similarly large cohorts for PsA is missing (47). The complex relationship between clinical and US examination is poorly understood in PsA and would suggest the inclusion of US can aid the assessment of disease where clinical assessment may have missed underlying occult PsA disease activity. As well as for disease monitoring, remission status, and disease activity measures, we evaluated data for the value of US in prognostication and targeted therapeutic interventions (intra-articular injections).

Monitoring of PsA

One study on PsA looking at the utility of US in the clinic showed that PD signal detected at baseline was not associated with response to treatment at 4 months [either biologic or conventional synthetic disease-modifying anti-rheumatic drugs (bDMARDs, csDMARDs, respectively)] in the routine care setting (48). These findings contrast with those from studies in RA, so Højgaard et al. (48) argued that one possible explanation could be the different presentation of the two diseases (that is, RA is more symmetric/uniform than PsA). The possibility remained that PD signal grading continuum, not merely its presence, would be more relevant for prognosis. In the TICOPA imaging substudy US inflammation scores were based on summation of GS and PD and both these features were graded 0–3. In this underpowered substudy, the US-based measure demonstrated responsiveness, was aligned to clinical outcome measures at baseline, and was aligned to the change detected by clinical outcome measures between two different time-points (49).

Remission Assessment

In PsA patients who are in clinical remission/minimal disease activity, US detection of subclinical synovitis using PD was a predictor of short-term (6 months) PsA flare (14). There is however, evidence of poor correlation between levels of clinical PsA activity (as measured by composite outcome measures) and US inflammatory findings (above all, PD signal) (50). US remission was found in 49.6% of the patients in this cross-sectional study, while clinical remission was achieved by 5.7–9.9% of the patients (depending on the composite outcome measure used). In this study, patient-reported-outcome-measures, a component of many clinical composite outcome measure, correlated with US findings worse than swollen joint count.

In another study, in 20% of PsA patients with clinically active disease (as measured by clinical composite outcome measures such as DAPSA, PASDAS, CPDAI, MDA) US assessment resulted in minimal inflammatory activity (MUDA) (43). In this study,

TABLE 2 | Unmet needs in ultrasound imaging in Psoriatic arthritis.

Topic of interest in PsA	Unmet needs: suggested research focus, by clinical phenotype	
	Psoriatic oligo/polyarthritis	**Psoriatic dactylitis**
Diagnosis:		
Sensitivity and specificity:	• PsA is frequently underdiagnosed or misdiagnosed. Can US improve the PsA diagnostic yield? • The specificity of US features to PsA is an area where further knowledge may improve clinical diagnosis given that overlapping pathologies exist between diseases. • Larger sized prospective cohorts may provide further insight into the characterisation of US features useful to differentiate different inflammatory arthritides (e.g., RA, PsA/SpA, crystal arthropathies).	• Dactylitis is a unique lesion in PsA. Yet the significance of dactylitis is still unclear in terms of the overall burden of disease in PsA. Further research on this lesion and US in PsA will drive further knowledge and understanding of this pathognomonic lesion in PsA/SpA. • The nature of dactylitis from early disease onset into chronic PsA is not fully understood. More research from large PsA cohorts may explain this further. • High sensitivity US may be useful in detection of small entheseal tissue in dactylitis research.
Synovial Synovitis:	• Disparity between clinical examination and US findings in PsA is still not well-understood. The relationship between clinical examination and US for identifying synovitis (and enthesitis below) is poorly understood and requires further research to clarify and inform clinical practice and decision making. • The large number of joints in the Psoriatic joint clinical/US assessment is time limiting and impractical in the clinic. A condensed, time-sensitive, but valid and reliable US tool that can be easily implementable is required for practicality in clinical practice and research. • More work on longitudinal PsA/PsO cohorts needed on the subject of subclinical synovitis and its prognostic value in the short and medium term (up to 5 years of follow-up).	• What is the relationship between dactylitis and synovitis? Does this differ depending upon disease course or treatment type? • Are there any ultrasound predictors that determine why some people with dactylitis may be affected by worse outcomes? • PsA cohorts with dactylitis may provide more insight into future dactylitis research. • Is there a risk from dactylitis to overall disease related affliction and treatment in early disease? • Does synovitis represent risk of dactylitis relapse/recurrence?
Extra-synovial Enthesitis:	• Discordance between clinical an US enthesitis suggests further studies may inform the differentiation between PsA and non-PsA. • Is an enthesitis US composite research score needed? If so, how many entheses should be included and which ones?	• The enthesis organ concept is highly implicated in PsA, yet we do not know whether dactylitis results in more clinical/US enthesitis? • Does dactylitis represent an intermediary lesion in the disease spectrum, developing from enthesitis and next into synovitis, or could it be a more significant clinical marker of disease severity in early PsA? These are questions that future US research may be able to answer using US at time-points in PsA evolution.
Tendon related pathologies:	• Research to improve differentiation of tendon pathologies in early PsA from RA or Palindromic rheumatism is where US may inform clinical practice. • Further research is needed on imaging of tendon pulleys and sheaths in early PsA which may hold early diagnostic value. • Identification of flexor/extensor tendons, peritendinous regions: where, when, and which should we scan? Is there a significance in terms of the disease overall burden?	• Tendon pathologies are key pathological features in dactylitis and correspond to the anatomical concept of swelling across the whole digit. Further understanding of tendinopathy in this lesion may improve targeted PsA therapy per patient based upon lesion. • Flexor tenosynovitis and flexor tendon sheath and pulley pathologies are key components of dactylitis. • Peritendon inflammation: US vs. MRI, disease course and response to therapy. • Scoring is a "hot" topic: Validation of scoring methods can permit use in research and clinical settings. • Hot and cold differentiation and active pathologies: clinical examination findings could be included to encompass the best representation of dactylitis status.
Management: US disease activity scores/composite outcome measures for monitoring	• How should overall US disease activity be measured per patient? • Which composite measure should be used?	• Isolated US vs. combined clinical and US features of dactylitis should be considered to assess dactylitis disease activity and monitor treatment response. • Clinical trials and longitudinal cohort studies may provide further clues into this arena where the data is sparse.
Disease remission:	• Clinical vs. US remission: which should be used? How should US remission/low disease activity be defined? More research in this area is needed.	
Pragmatic, additional issues:	• Advancing technologies are emerging which allow automated and simplified assessment of joints in less time. Can they be reliably and validly implemented and with cost-effectiveness?	

the pain-related items, as part of the clinical composite outcome measures, were the components conditioning higher disease activity scores. The authors postulated that the evaluation of clinical treatment targets can benefit from US evaluation.

Prognosis

In PsA patients clinically classified as oligoarthritis, US scanning has uncovered synovial hypertrophy of polyarticular distribution (51). Similar findings are relevant for the assessment of PsA prognosis. Baseline US findings of synovitis (upon GS and

PD assessment) were identified as risk factors for additional articular damage in one study (52). In this study, the presence of baseline enthesopathy/enthesitis also accounted as a risk factor for articular damage.

Another study found that 26 PsA patients who were in clinical remission had low levels of PD signal on US scan. Once csDMARD or bDMARD therapy was stopped the clinical recurrence rate of PsA was high (90%). One predictor of PsA relapse was synovial hypertrophy on US scan at the time of therapy cessation (53). Further data on the assessment of remission and prognosis are expected from the UPSTREAM study (19).

Composite US Scores

Just as there are several clinical composite scores for the assessment of PsA, US disease activity may be scored using a number of validated methods for the joints and entheses in clinical and research practice.

Joints

Two composite scores have been specifically developed to monitor disease activity in PsA: the 5TPD and PsA-Son composite scores with good sensitivity to detect inflammation and feasibility, but not yet validated in any other series (19).

Following the suit of many rheumatology clinical composite scores, Ficjan et al. (54) proposed two US scoring methods to assess inflammatory and structural PsA lesions, the PsA-Son13, (unilateral joints), and PsA-Son22 score (bilateral joints). They reported sufficient construct validity, reliability, and sensitivity to change for both scores. The reduced number of joints included may be considerably time saving, however there is potential to miss involved joints leading to a false reflection of overall disease activity, especially relevant for oligo/monoarticular phenotypes.

The "5 targets Power Doppler for Psoriatic disease" (5TDP) was based on joints, tendons, entheses, skin and nails scoring the highest expression of PD signal (55). The limitations were that the score does not consider multiple joint involvement from single joint involvement and may lead to under estimation of disease activity in polyarticular disease (55). A further drawback is that nail and skin US assessment is not commonplace in routine practice and therefore not practical outside of a research setting. Finally, it is notable that large joint involvement is frequent in PsA, therefore a tool initially developed for validation in RA, SOnography in LArge joints in Rheumatology (SOLAR), has been reported for its suitability for PsA (56).

Entheses

In a recent study, the Madrid Sonographic Enthesitis Index (MASEI), a scoring tool designed for enthesitis in SpA/PsA, failed to distinguish between enthesitis in PsA from healthy controls (57). It was found that by excluding the knee enthesis thickness and refining PD severity, marked differences could be shown between PsA patients and healthy controls, indicating that given considerable overlap of features exists between groups, setting the best discriminative thresholds for detecting pathology is imperative (57). On the contrary, a recent systematic literature review concluded that the MASEI was feasible, reliable and a valid ultrasound score for assessing enthesitis, but did not find any articles assessing MASEI as an outcome for treatment response (58). Whether clinical tenderness is derived from enthesitis or fibromyalgia can be difficult to assess, but has recently been studied using US and scored via the Glasgow enthesitis scoring system (GUESS) (59). It was found that US enthesitis was more prevalent in PsA and PsA with fibromyalgia compared to fibromyalgia alone, and clinical entheseal scores (LEI, MASES) were shown to potentially overestimate active enthesitis in fibromyalgia (59). A further preliminary enthesitis score developed in a recent GRAPPA study has reported the ability to differentiate between PsA and healthy controls (60). However, this has led to further discussion/debate on whether a further enthesitis score is actually needed, and if so, how many entheses should be included, and the suggestion that a study to prioritize differentiation of PsA from PsO and osteoarthritis/mechanical pain should be prioritized (61).

Guided Interventions (Injections)

Ultrasound provides the ability to visualize the needle for injection procedures and therefore optimize placement accuracy. There are no specific recent studies on PsA and the effectiveness of US guided routine intra-articular injections. However, previous randomized controlled trials (RCT) in inflammatory arthritis reported significantly better accuracy of joint injection by US over the blind/palpation approach (62). In the same study, the benefit of short-term outcomes could not be demonstrated. Another larger RCT of 244 patients reported superior outcomes and cost-effectiveness with US guided injection *vs.* the conventional blind/palpation technique, with an 81% reduction in injection pain, 35% reduction in pain scores and 38% increase in responder rate (63). In contrast, a large randomized trial examining the benefit of US in a clinical tight control regimen in RA (ARCTIC) did not find any significant difference in treatment efficacy between US guided and blind/palpation guided joint injections (64). There is a clear advantage of targeting pathologically active disease through US assessment prior to US guided injection given that treatment efficacy was observed when moderate PD synovitis was present, independent of whether the joint was clinically swollen (64). Given the multiple pathologies in PsA, it would seem reasonable to study targeted US injections based on region and type of pathology. Further research may clarify whether US guided joint injection for routine intra-articular joint injections can produce superior outcomes over routine blind approach, but the most recent data is limited (6).

CONCLUSIONS

Ultrasound is complementary to clinical examination by adding sensitivity and specificity to sites of disease in PsA enhancing the qualitative assessment. Several recent studies have shown added value of US in research by improving the understanding of disease. The clinical role of US for diagnosis is ever more assuring, yet there is discordance between clinical and US assessment that needs further research. Composite scoring measures remain research driven tools and are unlikely to be implemented in busy routine clinics in the near future. As US

becomes more widely used, its function as a disease monitoring tool is promising, but further research is required to clarify its specific role in the clinic.

AUTHOR CONTRIBUTIONS

All authors listed have made a substantial, direct and intellectual contribution to the work, and approved it for publication.

FUNDING

The authors were supported by the National Institute for Health Research (NIHR) Leeds Biomedical Research Centre (LBRC). The views expressed are those of the authors and not necessarily those of the (UK) National Health Service (NHS), the NIHR, or the (UK) Department of Health.

REFERENCES

1. Gladman DD, Antoni C, Mease P, Clegg DO, Nash P. Psoriatic arthritis: epidemiology, clinical features, course, and outcome. *Ann Rheum Dis.* (2005) 64(Suppl. 2):ii14–7. doi: 10.1136/ard.2004.032482
2. Tan AL, McGonagle D. The need for biological outcomes for biological drugs in psoriatic arthritis. *J Rheumatol.* (2016) 43:3–6. doi: 10.3899/jrheum.151296
3. Bogliolo L, Crepaldi G, Caporali R. Biomarkers and prognostic stratification in psoriatic arthritis. *Reumatismo.* (2012) 64:88–98. doi: 10.4081/reumatismo.2012.88
4. Takase-Minegishi K, Horita N, Kobayashi K, Yoshimi R, Kirino Y, Ohno S, et al. Diagnostic test accuracy of ultrasound for synovitis in rheumatoid arthritis: systematic review and meta-analysis. *Rheumatology.* (2018) 57:49–58. doi: 10.1093/rheumatology/kex036
5. Wiell C, Szkudlarek M, Hasselquist M, Møller JM, Vestergaard A, Nørregaard J, et al. Ultrasonography, magnetic resonance imaging, radiography, and clinical assessment of inflammatory and destructive changes in fingers and toes of patients with psoriatic arthritis. *Arthritis Res Ther.* (2007) 9:1–13. doi: 10.1186/ar2327
6. Zabotti A, Bandinelli F, Batticciotto A, Scirè CA, Iagnocco A, Sakellariou G. Musculoskeletal ultrasonography for psoriatic arthritis and psoriasis patients: a systematic literature review. *Rheumatology.* (2017) 56:1518–32. doi: 10.1093/rheumatology/kex179
7. Vreju AF, Chisalau BA, Parvanescu CD, Barbulescu A, Rogoveanu O, Firulescu S, et al. High frequency ultrasonography of the hand in rheumatoid arthritis, psoriatic arthritis, gout and osteoarthritis patients. *Curr Heal Sci J.* (2016) 42:35–9. doi: 10.12865/CHSJ.42.01.05
8. Fournié B, Margarit-Coll N, Champetier de Ribes TL, Zabraniecki L, Jouan A, Vincent V, et al. Extrasynovial ultrasound abnormalities in the psoriatic finger. Prospective comparative power-doppler study versus rheumatoid arthritis. *Jt Bone Spine.* (2006) 73:527–31. doi: 10.1016/j.jbspin.2006.01.019
9. Zabotti A, Salvin S, Quartuccio L, De Vita S. Differentiation between early rheumatoid and early psoriatic arthritis by the ultrasonographic study of the synovio-entheseal complex of the small joints of the hands. *Clin Exp Rheumatol.* (2016) 34:459–65.
10. Gutierrez M, Filippucci E, Salaffi F, Di Geso L, Grassi W. Differential diagnosis between rheumatoid arthritis and psoriatic arthritis: the value of ultrasound findings at metacarpophalangeal joints level. *Ann Rheum Dis.* (2011) 70:1111–4. doi: 10.1136/ard.2010.147272
11. Tang Y, Yang Y, Xiang X, Wang L, Zhang L, Qiu L. Power doppler ultrasound evaluation of peripheral joint, entheses, tendon, and bursa abnormalities in psoriatic patients: a clinical study. *J Rheumatol.* (2018) 45:811–7. doi: 10.3899/jrheum.170765
12. Zuliani F, Zabotti A, Errichetti E, Tinazzi I, Zanetti A, Carrara G, et al. Ultrasonographic detection of subclinical enthesitis and synovitis: a possible stratification of psoriatic patients without clinical musculoskeletal involvement. *Clin Exp Rheumatol.* (2019) 37:593–9.
13. Elnady B, El Shaarawy NK, Dawoud NM, Elkhouly T, Desouky DES, ElShafey EN, et al. Subclinical synovitis and enthesitis in psoriasis patients and controls by ultrasonography in Saudi Arabia; incidence of psoriatic arthritis during two years. *Clin Rheumatol.* (2019) 38:1627–35. doi: 10.1007/s10067-019-04445-0
14. Ruta S, Marin J, Felquer MLA, Ferreyra-Garrot L, Rosa J, García-Monaco R, et al. Utility of power doppler ultrasound-detected synovitis for the prediction of short-term flare in psoriatic patients with arthritis in clinical remission. *J Rheumatol.* (2017) 44:1018–23. doi: 10.3899/jrheum.161347
15. Benjamin M, McGonagle D. The enthesis organ concept and its relevance to the spondyloarthropathies. *Adv Exp Med Biol.* (2009) 649:57–70. doi: 10.1007/978-1-4419-0298-6_4
16. Zabotti A, Errichetti E, Zuliani F, Quartuccio L, Sacco S, Stinco G, et al. Early psoriatic arthritis versus early seronegative rheumatoid arthritis: role of dermoscopy combined with ultrasonography for differential diagnosis. *J Rheumatol.* (2018) 45:648–54. doi: 10.3899/jrheum.170962
17. Tinazzi I, McGonagle D, Zabotti A, Chessa D, Marchetta A, Macchioni P. Comprehensive evaluation of finger flexor tendon entheseal soft tissue and bone changes by ultrasound can differentiate psoriatic arthritis and rheumatoid arthritis. *Clin Exp Rheumatol.* (2018) 36:785–90.
18. Tinazzi I, McGonagle D, Aydin SZ, Chessa D, Marchetta A, Macchioni P. "Deep Koebner" phenomenon of the flexor tendon-associated accessory pulleys as a novel factor in tenosynovitis and dactylitis in psoriatic arthritis. *Ann Rheum Dis.* (2018) 77:922–5. doi: 10.1136/annrheumdis-2017-212681
19. Zabotti A, Piga M, Canzoni M, Sakellariou G, Iagnocco A, Scirè CA, et al. Ultrasonography in psoriatic arthritis: which sites should we scan? *Ann Rheum Dis.* (2018) 77:1537–8. doi: 10.1136/annrheumdis-2018-213025
20. Tang Y, Cheng S, Yang Y, Xiang X, Wang L, Zhang L, et al. Ultrasound assessment in psoriatic arthritis (PsA) and psoriasis vulgaris (non-PsA): which sites are most commonly involved and what features are more important in PsA? *Quant Imaging Med Surg.* (2020) 10:86–95. doi: 10.21037/qims.2019.08.09
21. Macía-Villa C, Falcao S, Gutierrez M, Medina J, Hammer HB, De Miguel E. What is metacarpophalangeal joint swelling in psoriatic arthritis? Ultrasound findings and reliability assessment. *Clin Exp Rheumatol.* (2018) 36:896–9. doi: 10.1136/annrheumdis-2017-eular.1437
22. McGonagle D, Gibbon W, Emery P. Classification of inflammatory arthritis by enthesitis. *Lancet.* (1998) 352:1137–40. doi: 10.1016/S0140-6736(97)12004-9
23. Kaeley GS, Eder L, Aydin SZ, Gutierrez M, Bakewell C. Enthesitis: a hallmark of psoriatic arthritis. *Semin Arthritis Rheum.* (2018) 48:35–43. doi: 10.1016/j.semarthrit.2017.12.008
24. Macchioni P, Salvarani C, Possemato N, Gutierrez M, Grassi W, Gasparini S, et al. Ultrasonographic and clinical assessment of peripheral enthesitis in patients with psoriatic arthritis, psoriasis, and fibromyalgia syndrome: the ULISSE study. *J Rheumatol.* (2019) 46:904–11. doi: 10.3899/jrheum.171411
25. Florescu A, Vere CC, Florescu LM, Mușetescu AE, Bondari A, Ciurea PL. Clinical and ultrasound assessment of enthesis in psoriatic arthritis in a romanian cohort. *Curr Heal Sci J.* (2018) 44:347–51. doi: 10.12865/CHSJ.44.04.04
26. Yamada Y, Inui K, Okano T, Mandai K, Mamoto K, Koike T, et al. Ultrasound assessment, unlike clinical assessment, reflects enthesitis in patients with psoriatic arthritis. *Clin Exp Rheumatol.* (2020). [Epub ahead of print].
27. Michelsen B, Diamantopoulos AP, Soldal DM, Hammer HB, Kavanaugh A, Haugeberg G. Achilles enthesitis defined by ultrasound is not associated with clinical enthesitis in patients with psoriatic arthritis. *RMD Open.* (2017) 3:1–5. doi: 10.1136/rmdopen-2017-000486
28. Balint P, Terslev L, Aegerter P, Bruyn G, Chary-Valckenaere I, Gandjbakhch F, et al. Reliability of a consensus-based ultrasound definition and scoring for enthesitis in spondyloarthritis and psoriatic arthritis: an OMERACT US initiative. *Ann Rheum Dis.* (2018) 77:1730–5. doi: 10.1136/annrheumdis-2018-213609
29. Wervers K, Luime JJ, Tchetverikov I, Gerards AH, Kok MR, Appels CWY, et al. Comparison of disease activity measures in early psoriatic arthritis in usual care. *Rheumatology.* (2019) 58:2251–9. doi: 10.1093/rheumatology/kez215

30. Arslan Alhussain F, Kasapoglu Gunal E, Kurum E, Bakirci S, Ozturk AB, McGonagle D, et al. Greater magnitude of entheseal microdamage and repair in psoriatic arthritis compared with ankylosing spondylitis on ultrasound. *Rheumatology*. (2019) 58:299–303. doi: 10.1093/rheumatology/key238
31. Yumusakhuylu Y, Kasapoglu-Gunal E, Murat S, Kurum E, Keskin H, Icagasioglu A, et al. A preliminary study showing that ultrasonography cannot differentiate between psoriatic arthritis and nodal osteoarthritis based on enthesopathy scores. *Rheumatology*. (2016) 55:1703–4. doi: 10.1093/rheumatology/kew218
32. Zabotti A, Mcgonagle DG, Giovannini I, Errichetti E, Zuliani F, Zanetti A, et al. Transition phase towards psoriatic arthritis: clinical and ultrasonographic characterisation of psoriatic arthralgia. *RMD Open*. (2019) 5:1067. doi: 10.1136/rmdopen-2019-001067
33. Wervers K, Herrings I, Luime JJ, Tchetverikov I, Gerards AH, Hazes JMW, et al. Association of physical activity and medication with enthesitis on ultrasound in psoriatic arthritis. *J Rheumatol.* (2019) 46:1290–4. doi: 10.3899/jrheum.180782
34. Girolimetto N, Macchioni P, Tinazzi I, Costa L, Peluso R, Tasso M, et al. Predominant ultrasonographic extracapsular changes in symptomatic psoriatic dactylitis: results from a multicenter cross-sectional study comparing symptomatic and asymptomatic hand dactylitis. *Clin Rheumatol.* (2019) 39:1157–65. doi: 10.1007/s10067-019-04683-2
35. Tinazzi I, McGonagle D, Macchioni P, Aydin SZ. Power Doppler enhancement of accessory pulleys confirming disease localization in psoriatic dactylitis. *Rheumatology*. (2019) 59:1–5. doi: 10.1093/rheumatology/kez549
36. McGonagle D, Tan AL, Watad A, Helliwell P. Pathophysiology, assessment and treatment of psoriatic dactylitis. *Nat Rev Rheumatol.* (2019) 15:113–22. doi: 10.1038/s41584-018-0147-9
37. Zabotti A, Sakellariou G, Tinazzi I, Batticciotto A, Canzoni M, Carrara G, et al. Clinical science novel and reliable DACTylitis global sonographic (DACTOS) score in psoriatic arthritis. *Ann Rheum Dis.* (2020) 1–7. doi: 10.1136/annrheumdis-2020-217191
38. Kaeley GS, Eder L, Aydin SZ, Gutierrez M, Bakewell C. Dactylitis: a hallmark of psoriatic arthritis. *Semin Arthritis Rheum.* (2018) 48:263–73. doi: 10.1016/j.semarthrit.2018.02.002
39. Rizzo G, Raffeiner B, Coran A, Ciprian L, Fiocco U, Botsios C, et al. Pixel-based approach to assess contrast-enhanced ultrasound kinetics parameters for differential diagnosis of rheumatoid arthritis. *J Med Imaging.* (2015) 2:034503. doi: 10.1117/1.JMI.2.3.034503
40. Sapundzhieva T, Karalilova R, Batalov A. Hand ultrasound patterns in rheumatoid and psoriatic arthritis: the role of ultrasound in the differential diagnosis. *Rheumatol Int.* (2020) 40:837–48. doi: 10.1007/s00296-020-04559-8
41. Sakellariou G, Scirè CA, Adinolfi A, Batticciotto A, Bortoluzzi A, Sedie AD, et al. Differential diagnosis of inflammatory arthropathies by musculoskeletal ultrasonography : a systematic literature review. *Front Med.* (2020) 7:141. doi: 10.3389/fmed.2020.00141
42. Aydin SZ, Bakirci S, Kasapoglu E, Castillo-Gallego C, Arslan Alhussain F, Ash ZR, et al. The relationship between physical examination and ultrasonography of large entheses of the achilles tendon and patellar tendon origin. *J Rheumatol.* (2019) 47:1026–30. doi: 10.3899/jrheum.190169
43. Husic R, Gretler J, Felber A, Graninger WB, Duftner C, Hermann J, et al. Disparity between ultrasound and clinical findings in psoriatic arthritis. *Ann Rheum Dis.* (2014) 73:1529–36. doi: 10.1136/annrheumdis-2012-203073
44. Pukšić S, Bolton-King P, Sexton J, Michelsen B, Kvien TK, Berner Hammer H. DAPSA and ultrasound show different perspectives of psoriatic arthritis disease activity: results from a 12-month longitudinal observational study in patients starting treatment with biological disease-modifying antirheumatic drugs. *RMD Open.* (2018) 4:e000765. doi: 10.1136/rmdopen-2018-000765
45. Bosch P, Husic R, Ficjan A, Gretler J, Lackner A, Graninger WB, et al. Evaluating current definitions of low disease activity in psoriatic arthritis using ultrasound. *Rheumatology*. (2019) 58:2212–20. doi: 10.1093/rheumatology/kez237
46. Mandl P, Navarro-Compán V, Terslev L, Aegerter P, Van Der Heijde D, D'Agostino MA, et al. EULAR recommendations for the use of imaging in the diagnosis and management of spondyloarthritis in clinical practice. *Ann Rheum Dis*. (2015) 74:1327–39. doi: 10.1136/annrheumdis-2014-206971
47. Hammer HB, Michelsen B, Sexton J, Haugen IK, Provan SA, Haavardsholm EA, et al. Swollen, but not tender joints, are independently associated with ultrasound synovitis: results from a longitudinal observational study of patients with established rheumatoid arthritis. *Ann Rheum Dis.* (2019) 78:1179–85. doi: 10.1136/annrheumdis-2019-215321
48. Højgaard P, Ellegaard K, Nielsen SM, Christensen R, Guldberg-Møller J, Ballegaard C, et al. Pain mechanisms and ultrasonic inflammatory activity as prognostic factors in patients with psoriatic arthritis: a prospective cohort study. *Arthritis Care Res.* (2019) 71:798–810. doi: 10.1002/acr.23693
49. Helliwell PS, Coates LC, Chew NS, Lettieri G, Moverley AR, Freeston JE, et al. Comparing psoriatic arthritis low-field magnetic resonance imaging, ultrasound and clinical outcomes: data from the TICOPA trial. *J Rheumatol.* (2019). doi: 10.3899/jrheum.181385. [Epub ahead of print].
50. Michelsen B, Diamantopoulos AP, Hammer HB, Soldal DM, Kavanaugh A, Haugeberg G. Ultrasonographic evaluation in psoriatic arthritis is of major importance in evaluating disease activity. *Ann Rheum Dis.* (2016) 75:2108–13. doi: 10.1136/annrheumdis-2015-208806
51. Østergaard M, Eder L, Christiansen SN, Kaeley GS. Imaging in the diagnosis and management of peripheral psoriatic arthritis—The clinical utility of magnetic resonance imaging and ultrasonography. *Best Pract Res Clin Rheumatol.* (2016) 30:624–37. doi: 10.1016/j.berh.2016.08.012
52. El Miedany Y, El Gaafary M, Youssef S, Ahmed I, Nasr A. Tailored approach to early psoriatic arthritis patients: clinical and ultrasonographic predictors for structural joint damage. *Clin Rheumatol.* (2015) 34:307–13. doi: 10.1007/s10067-014-2630-2
53. Araujo EG, Finzel S, Englbrecht M, Schreiber DA, Faustini F, Hueber A, et al. High incidence of disease recurrence after discontinuation of disease-modifying antirheumatic drug treatment in patients with psoriatic arthritis in remission. *Ann Rheum Dis.* (2015) 74:655–60. doi: 10.1136/annrheumdis-2013-204229
54. Ficjan A, Husic R, Gretler J, Lackner A, Graninger WB, Gutierrez M, et al. Ultrasound composite scores for the assessment of inflammatory and structural pathologies in psoriatic arthritis (PsASon-Score). *Arthritis Res Ther.* (2014) 16:476. doi: 10.1186/s13075-014-0476-2
55. Gutierrez M, Di geso L, Salaffi F, Bertolazzi C, Tardella M, Filosa G, et al. Development of a preliminary US power Doppler composite score for monitoring treatment in PsA. *Rheumatology*. (2012) 51:1261–8. doi: 10.1093/rheumatology/kes014
56. Schäfer VS, Fleck M, Kellner H, Strunk J, Sattler H, Schmidt WA, et al. Evaluation of the novel ultrasound score for large joints in psoriatic arthritis and ankylosing spondylitis: six month experience in daily clinical practice. *BMC Musculoskelet Disord*. (2013) 14:2–6. doi: 10.1186/1471-2474-14-358
57. Wervers K, Vis M, Rasappu N, van der Ven M, Tchetverikov I, Kok MR, et al. Modification of a sonographic enthesitis score to differentiate between psoriatic arthritis and young healthy volunteers. *Scand J Rheumatol.* (2018) 47:291–4. doi: 10.1080/03009742.2017.1393695
58. Macía-Villa C, De Miguel E. Updating the use of the madrid sonographic enthesis index (MASEI): a systematic review of the literature. *Rheumatology*. (2020) 59: 1031–40. doi: 10.1093/rheumatology/kez356
59. Fiorenza A, Bonitta G, Gerratana E, Marino F, Sarzi-Puttini P, Salaffi F, et al. Assessment of enthesis in patients with psoriatic arthritis and fibromyalgia using clinical examination and ultrasound. *Clin Exp Rheumatol.* (2020) 38:31–9.
60. Tom S, Zhong Y, Cook R, Aydin SZ, Kaeley G, Eder L. Development of a preliminary ultrasonographic enthesitis score in psoriatic arthritis - GRAPPA ultrasound working group. *J Rheumatol.* (2019) 46:384–90. doi: 10.3899/jrheum.171465
61. D'Agostino MA, Coates LC. The role of ultrasound in psoriatic arthritis - do we need a score? *J Rheumatol.* (2019) 46:337–9. doi: 10.3899/jrheum.181044
62. Cunnington J, Marshall N, Hide G, Bracewell C, Isaacs J, Platt P, et al. A randomized, double-blind, controlled study of ultrasound-guided

corticosteroid injection into the joint of patients with inflammatory arthritis. *Arthritis Rheum.* (2010) 62:1862–9. doi: 10.1002/art.27448

63. Sibbitt WL, Band PA, Chavez-Chiang NR, DeLea SL, Norton HE, Bankhurst AD. A randomized controlled trial of the cost-effectiveness of ultrasound-guided intraarticular injection of inflammatory arthritis. *J Rheumatol.* (2011) 38:252–63. doi: 10.3899/jrheum.100866
64. Nordberg LB, Lillegraven S, Aga AB, Sexton J, Lie E, Hammer HB, et al. The impact of ultrasound on the use and efficacy of intraarticular glucocorticoid injections in early rheumatoid arthritis: secondary analyses from a randomized trial examining the benefit of ultrasound in a clinical tight control regimen. *Arthritis Rheumatol.* (2018) 70:1192–9. doi: 10.1002/art.40494

Conflict of Interest: The authors declare that the research was conducted in the absence of any commercial or financial relationships that could be construed as a potential conflict of interest.

frontiers in Medicine

REVIEW
published: 02 September 2020
doi: 10.3389/fmed.2020.00468

Innovative Imaging Technique for Visualization of Vascularization and Established Methods for Detection of Musculoskeletal Inflammation in Psoriasis Patients

Michaela Köhm[1,2,3]*, *Lukas Zerweck*[3,4], *Phuong-Ha Ngyuen*[3,4], *Harald Burkhardt*[1,2,3,5] and *Frank Behrens*[1,2,3,5]

[1] Division of Rheumatology, Goethe-University Frankfurt, Frankfurt, Germany, [2] Clinical Research, Fraunhofer Institute for Molecular Biology and Applied Ecology IME, Branch for Translational Medicine and Pharmacology TMP, Frankfurt, Germany, [3] Fraunhofer Cluster of Excellence Immune-Mediated Diseases CIMD, Frankfurt, Germany, [4] Fraunhofer Institute for Applied Information Technology FIT, St. Augustin, Germany, [5] Centre of Innovative Diagnostics and Therapeutics Rheumatology/Immunology CIRI, Frankfurt, Germany

OPEN ACCESS

Edited by:
Raj Sengupta,
Royal National Hospital for Rheumatic Diseases, United Kingdom

Reviewed by:
Konstantinos Triantafyllias,
ACURA Karl Aschoff Rehabilitation Clinic, Germany
André Cavalcanti,
Federal Rural University of Pernambuco, Brazil

***Correspondence:**
Michaela Köhm
michaela.koehm@ime.fraunhofer.de

Specialty section:
This article was submitted to Rheumatology, a section of the journal Frontiers in Medicine

Received: 22 May 2020
Accepted: 13 July 2020
Published: 02 September 2020

Citation:
Köhm M, Zerweck L, Ngyuen P-H, Burkhardt H and Behrens F (2020) Innovative Imaging Technique for Visualization of Vascularization and Established Methods for Detection of Musculoskeletal Inflammation in Psoriasis Patients. Front. Med. 7:468. doi: 10.3389/fmed.2020.00468

Psoriasis (PsO) is one of the common chronic inflammatory skin diseases. Approximately 3% of the European Caucasian population is affected. Psoriatic arthritis (PsA) is a chronic immune-mediated disease associated with PsO characterized by distinct musculoskeletal inflammation. Due to its heterogeneous clinical manifestations (e.g., oligo- or polyarthritis, enthesitis, dactylitis, and axial inflammation), early diagnosis of PsA is often difficult and delayed. Approximately 30% of PsO patients will develop PsA. The responsible triggers for the transition from PsO only to PsA are currently unclear, and the impacts of different factors (e.g., genetic, environmental) on disease development are currently discussed. There is a high medical need, recently unmet, to specifically detect those patients with an increased risk for the development of clinically evident PsA early to initiate sufficient treatment to inhibit disease progression and avoid structural damage and loss of function or even intercept disease development. Increased neoangiogenesis and enthesial inflammation are hypothesized to be early pathological findings in PsO patients with PsA development. Different disease states describe the transition from PsO to PsA. Two of those phases are of value for early detection of PsA at-risk patients to prevent later development of PsA as changes in biomarker profiles are detectable: the subclinical phase (soluble and imaging biomarkers detectable, no clinical symptoms) and the prodromal phase (imaging biomarkers detectable, unspecific musculoskeletal symptoms such as arthralgia and fatigue). To target the unmet need for early detection of this at-risk population and to identify the subgroup of patients who will transition from PsO to PsA, imaging plays an important role in characterizing patients precisely. Imaging techniques such as ultrasound (US), magnetic resonance imaging (MRI), and computerized tomography (CT) are advanced techniques to detect sensitively inflammatory changes or changes in bone structure. With the use of these techniques, anatomic structures involved in inflammatory processes can be

identified. These techniques are complemented by fluorescence optical imaging as a sensitive method for detection of changes in vascularization, especially in longitudinal measures. Moreover, high-resolution peripheral quantitative CT (HR-pQCT) and dynamic contrast-enhanced MRI (DCE-MRI) may give the advantage to identify PsA-related early characteristics in PsO patients reflecting transition phases of the disease.

Keywords: psoriasis, psoriatic arthritis, early detection, imaging, musculoskeletal inflammation

INTRODUCTION

Psoriasis (PsO) is one of the common chronic inflammatory skin diseases. Approximately 3% of the European Caucasian population is affected. Psoriatic arthritis (PsA) is a chronic immune-mediated disease associated with PsO characterized by distinct musculoskeletal inflammation. Due to its heterogeneous clinical manifestations (e.g., oligo- or polyarthritis, enthesitis, dactylitis, and axial inflammation), and the fact that only classification criteria are available [ClASsification for Psoriatic ARthritis (CASPAR) criteria], early diagnosis of PsA is often difficult to set and frequently delayed. Approximately 30% of PsO patients will develop PsA in their lifetime. Moreover, many patients develop a destructive form of arthritis with substantial morbidity and disability (1). Reasons for the transition from PsO to PsA are currently unclear as well as their impact on disease development. It is currently discussed that different factors such as genetic and/or clinical–demographic risk factors (e.g., nail PsO, PsO severity and type) may promote PsA development and its progression. Risk factors are observed in different epidemiologic studies, but there seems to be as well a heterogeneous profile for different factors identified (2).

The underlying molecular mechanisms for the transition from PsO to PsA are still poorly defined but better understood due to the use of biologic treatments addressing different target molecules for both PsO and PsA. Similar to the predictive value of anti-citrullinated peptide antibodies (ACPAs) for the development of rheumatoid arthritis (RA) in patients with arthralgia, the medical condition of PsO as an underlying disease describes an at-risk population to develop PsA. There is a high medical need, recently unmet, to identify early those patients with an increased risk for PsA development and first signs of musculoskeletal inflammatory changes for clinically evident PsA development. Only by early detection, sufficient treatments to inhibit disease progression and avoid structural damage and loss of function can be initiated. Moreover, here, the interception of PsA may be targeted with sufficient treatment when initiated in a very early stage of the PsO patients at risk for PsA development (principle of disease interception). However, ∼50% of patients with PsO present with subclinical imaging enthesopathy, and only a subgroup of them will develop PsA (3). So, even as the evidence of signs for musculoskeletal inflammation being found by use of sensitive imaging technique may be of high value to identify the at-risk collective, the technique must also be appropriate to differentiate between disease-related changes of PsA to predict progression from PsO to clinically manifested PsA. Therefore, there is a need for a specific biomarker panel including either soluble molecular markers and/or sensitive imaging markers to solve this challenge. Different imaging techniques are available with various modes to identify inflammation or inflammatory changes and heterogeneous impact for sensitive detection of signs for very early musculoskeletal inflammatory changes.

THE TRANSITION FROM PSORIASIS TO PSORIATIC ARTHRITIS

PsA mostly develops in patients with established PsO; only in 15% of patients PsO occurs in parallel or after PsA development (4). The incidence of PsA with PsO onset increases with time, reaching ∼20% after 30 years (5). Nail, scalp, and inverse PsO and its severity are identified as potential clinical factors for increased risk for PsA development (4). In focusing on comorbidities, obesity is identified as a strong risk factor for PsA development (6), with an additional link of the magnitude of body mass index (BMI) and PsA risk (7). For genetic background, a first-degree relative with arthritis contributes to the risk (8). Moreover, arthralgia mainly in female PsO patients is a strong predictor for PsA development (9). This finding was confirmed by Zabotti et al. (10) in 2019 in a longitudinal study.

Scher et al. (2) recently proposed three clinically inconspicuous stages after PsO onset and before the clinical presentation of PsA: (a) a preclinical phase characterized by aberrant activation of the immune system which may originate from the skin, intestinal mucosa, or the entheses; (b) the subclinical PsA phase with the detection of soluble biomarkers and imaging findings without clinical symptoms; (c) the prodromal phase of PsA in which patients report unspecific symptoms such as arthralgia and fatigue without objective detection of signs of musculoskeletal inflammation with synovitis and/or enthesitis in physical examination (**Figure 1**).

So, the subclinical and prodromal phases are linked by changes that might be detectable by established biomarkers or a specific biomarker profile including imaging techniques predicting later clinical development of PsA. In the clinical care setting, patients will mainly be presented to a specialist rheumatologist in the prodromal phase, when clinical symptoms

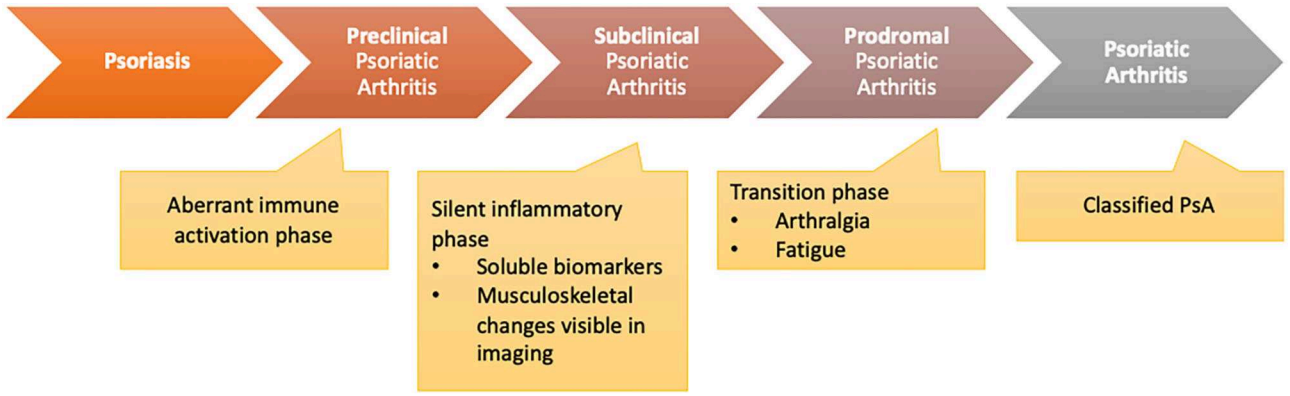

FIGURE 1 | Transition model from psoriasis to psoriatic arthritis [adapted from Scher et al. (2)].

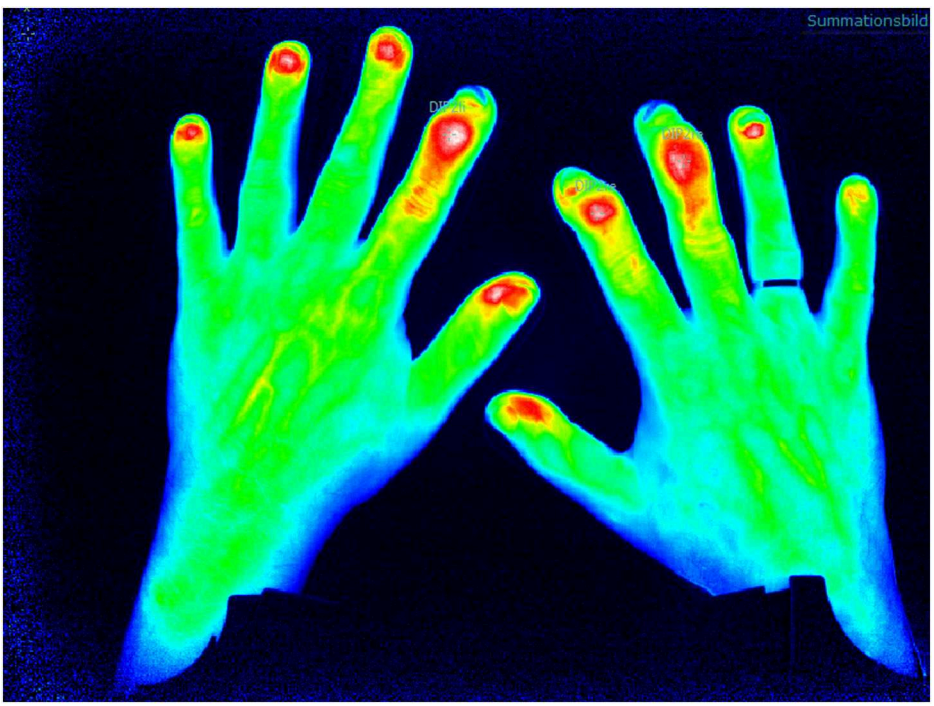

FIGURE 2 | Fluorescence optical imaging (FOI) assessment with detection of distal interphalangeal (DIP) arthritis.

such as arthralgia and fatigue occur. The subclinical identification of PsA will be necessary for dermatologists or general practitioners (GPs) to select the patients being presented to the rheumatologist or change treatment strategy.

In both scenarios, the biomarker to detect either patient in the subclinical or prodromal phase must be sensitive for detection of musculoskeletal inflammatory changes but also specific to identify those changes as PsA-related and highly predictive for later development of clinically evident PsA. Imaging studies of early PsA suggest that inflammatory enthesopathy is an early sign that is presented in PsA development (11). However, as shown in longitudinal studies, ∼50% of patients with PsO that present with subclinical imaging enthesopathy will develop clinically manifested PsA (3).

IMAGING TECHNIQUES FOR THE DETECTION OF EARLY CHANGES IN ANGIOGENESIS AND MUSCULOSKELETAL INFLAMMATION

Different imaging techniques are available in clinical routine care to determine inflammatory musculoskeletal changes and increase in angiogenesis (**Table 1**). Different vascular and

musculoskeletal compartments can be assessed and rated in focus on changes in vascularization, the severity of inflammation, disease manifestation, and disease state. Fluorescence optical imaging (FOI) is an indocyanine green (ICG)-tailored imaging technique that visualizes changes in micro-vascularization of the hands. FOI is a well-tolerated and fast method that seems sensitive for the detection of signs of inflammation and their changes over time. Nevertheless, it is limited by the rate of skin texture responsible for the penetration depth of the measurement system. Imaging of bone structure, entheses, and synovia is of high importance for classification of disease state and disease activity. By use of ultrasonography (US), changes in synovial and enthesial structure in early inflammation can be detected as it is commonly used but restricted by the experience of the observer and assessment algorithm. Moreover, by the use of US, changes of vascularization in the synovia and the enthesial structures can be easily evaluated using Doppler mode presenting as a sensitive marker for inflammation. Magnetic resonance imaging (MRI) is used to assess the presence of bone marrow edema, enthesitis, and changes in vascularization as early and disease activity indicators of inflammation of the joints, entheses, and spine. X-ray and computerized tomography (CT) can be used to assess structural damage in two and three dimensions. Innovative methods, such as high-resolution peripheral quantitative CT (HR-pQCT), can visualize pathophysiological processes and the morphological consequences at the bones even in the early stages of the disease. Moreover, techniques such as dual-energy CT (DECT) with iodine mapping may be helpful in discrimination of early arthritis.

TABLE 1 | Overview of imaging techniques available for diagnosis of psoriatic arthritis (PsA) in psoriasis (PsO) patients and their advantages and disadvantages.

Technique	Advantage	Disadvantage
X-Ray	• Bone structure can be assessed (late changes)	• (Availability) • Radiation • Sensitivity for early changes: only structural changes to be detected • Only one structure per examination
Computerized tomography (CT)	• Bone structure can be assessed in 3 dimensions and related to anatomically structures (late changes)	• Availability • Sensitivity for early changes: only structural changes to be detected • Radiation • Only one structure per examination
High-resolution peripheral quantitative CT (HR-pQCT)	• Sensitivity: early structural changes can be detected	• Availability • Radiation • Only one structure per examination
Scintigraphy	• Availability • Whole body scan for increased metabolism (related to inflammation)	• Application of radioactive tracer • Poor specificity
^{18}F-FDG PET	• Whole body scan for increased metabolism (related to inflammation)	• Availability • Tolerability • Poor specificity
Ultrasound (US)	• Availability • Tolerability • Scan of all anatomically related structures possible • Doppler function: increase in vascularisation	• Time consuming when used in all joints and msk structures • Rater dependent (experience)
Magnetic Resonance Imaging (MRI)	• Scan of all anatomically related structures possible • Bone structure and metabolism	• Availability • Tolerability (contrast agent) • Only one structure per examination
Whole Body MRI (WB-MRI)	• Scan of whole body in one examination • Bone structure and metabolism	• Availability • Tolerability (contrast agent)
Dynamic contrast enhanced MRI (DCE-MRI)	• Scan of all anatomically related structures possible • Bone structure and metabolism • Quantification of inflammation	• Availability • Tolerability (contrast agent) • Only one structure per examination
Fluorescence-optical imaging (FOI)	• Availability • Tolerability • displays changes in micro vascularisation of the hands	• Only hands • Depth of measure limited • Rater dependent for (maunal) assessment

Fluorescence Optical Imaging

Increase in micro-vascularization is identified as an early marker for PsA and of higher value than in other inflammatory joint diseases such as RA and may be a parameter to distinguish PsO from PsA in the subclinical phase of transition (12). FOI is an innovative imaging technique which detects changes in micro-vascularization of the hands as the camera system is only available for the hands by now. The method is tailored to indocyanine green injection which is a tolerable color agent used in different medical indication fields. The assessment lasts 360 s (one picture per second), and after measurement, the ICG kinetic profile is used for the (manual) assessment (**Figure 2**).

First studies to validate FOI were performed by assessment of its ability to detect synovitis/arthritis compared to the US and MRI examination (sensitivity 76%, specificity 94%) (13). Thuermel et al. (14) compared different disease states of synovitis between FOI and MRI findings. It was shown that mild synovitis was discriminated poorly by both FOI and MRI (81.6 vs. 86.8%), but with worsening of severity of synovitis, the potential for the discriminative ability increased in both methods with high correlation (moderate synovitis false positive in 12.5 vs. 16% for FOI and severe synovitis false positive in 0.7 vs. 2.4% for FOI). Additionally, Hirano et al. (15) confirmed the correlation of FOI measurement in the assessment of synovitis compared to US examination.

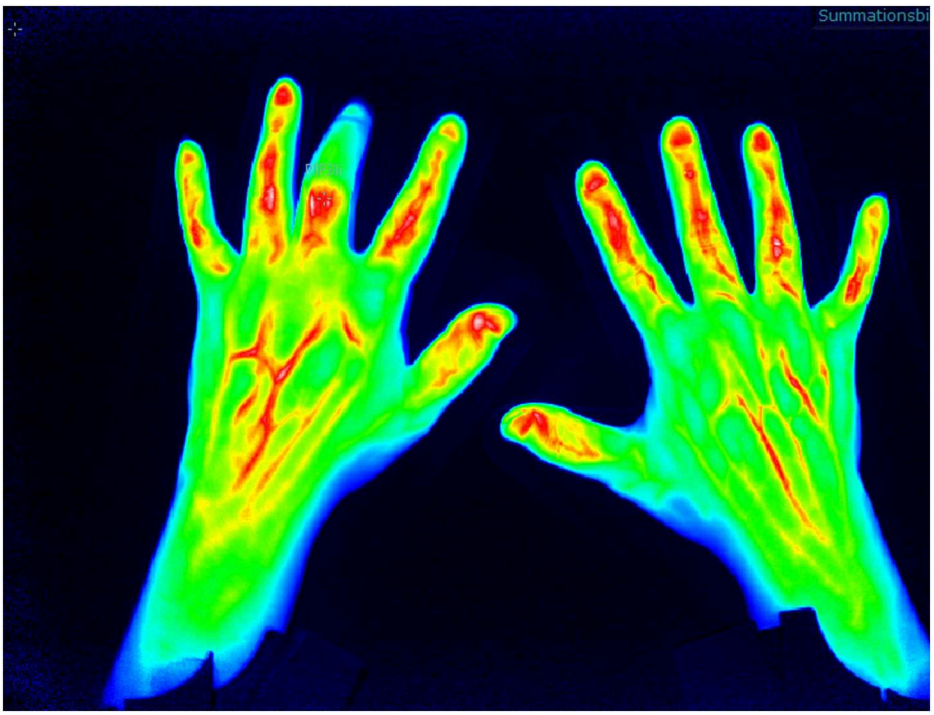

FIGURE 3 | Fluorescence optical imaging (FOI) assessment of arthritis/tendinitis in the hands.

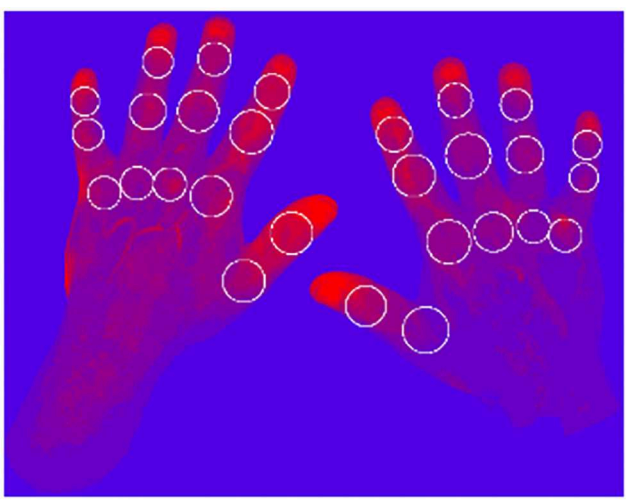

FIGURE 4 | Example: Nine clusters, maximum slope.

The different morphologic patterns can be identified in PsA patients that might be specific for the disease (**Figure 3**): in 94% of patients with clinically manifested PsA, a triangular increase of the color agent is detected at distal interphalangeal (DIP) joints (compared to 21% of RA patients), in 21% of PsA patients, a "green nail" sign was detectable (compared to 3% in RA patients), with a specificity of 87% and a sensitivity of 28% (16).

In the XCITING study, FOI was performed in patients with PsO and at risk for PsA development (nail PsO, musculoskeletal complaints within the last 6 months). In ∼46% of the patients, FOI showed an increase of micro-vascularization defined as related to subclinical PsA (with the determination of inflammatory changes in MRI in 37%). Here, longitudinal data will show how many of those patients develop PsA in a 24-month follow-up period (17) to indicate its potential to select the at-risk population of PsO patients with later overt PsA. Therefore, FOI might be a promising imaging technique with little limitations (injection of the tolerable color agent, manual reading with the need of an experienced reader) and high advantages (fast performance, high sensitivity) to be of value in early detection in the transition from PsO to PsA.

Objective Joint Evaluation Based on Fluorescence Optical Imaging

FOI is assessed with the use of a manual assessment algorithm published by Werner et al. (13). To use FOI for the screening of PsO patients for changes in vascularization suspect for PsA, an objective assessment method is needed to allow fast assessment of the images with an automated algorithm. Therefore, methods to automate the assessment of the fluorescence intensities are in development.

To visualize the micro-vascularization of the hands with the FOI technique, a time-dependent data set of 360 images is

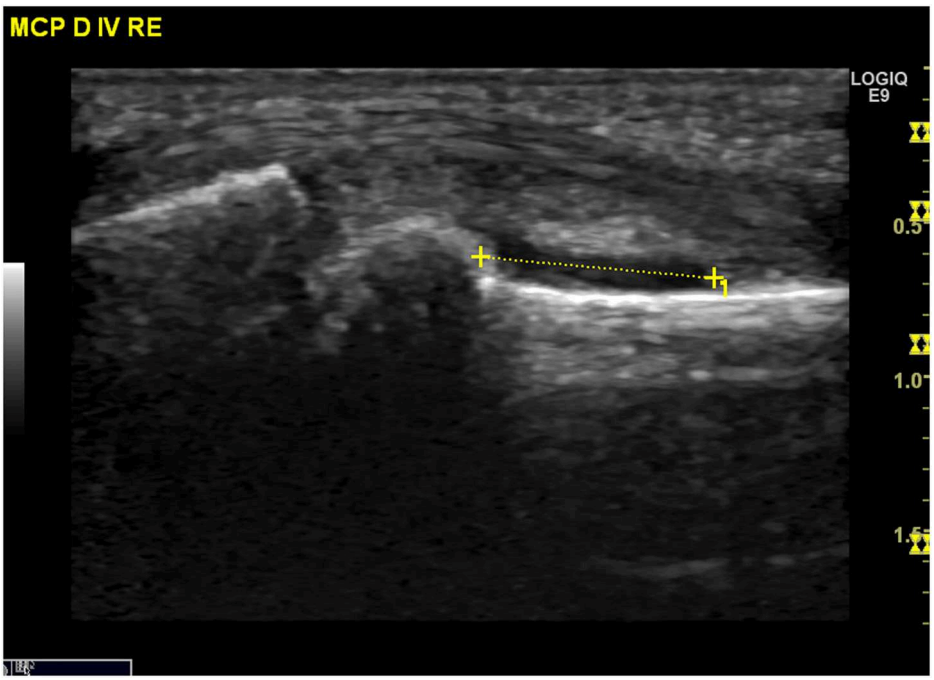

FIGURE 5 | Ultrasound assessment of synovitis metacarpophalangeal joint digit IV (MCP D IV).

acquired. Each image shows the current state of the proceeding distribution of the contrast agent ICG. To objectively evaluate the status of the subject's joints individually, the micro-vascularization at each joint position is evaluated.

To represent the status of each joint, several scores are calculated, representing different characteristics of the micro-vascularization. In the first step, each pixel (680 512) is represented by a time series containing 360 values. For each time series, three different features are extracted: the amplitude, the mean value during the signal increasing time, and the maximal gradient. Then, each of the three sets is clustered by k-means clustering, with $k \in \{3, 5, 7, 9\}$. Furthermore, each pixel is assigned a shade of red–blue, where the brightest (red) corresponds to the highest cluster indicating highest dynamics and the darkest to the lowest indicating the smallest dynamics (**Figure 4**).

Therefore, 12 heatmaps (three features 4 *k*s) are generated. Finally, scores for the defined joint areas are calculated based on the assigned cluster values, number of pixels in the joint area and the number of clusters *k*.

Applying this newly developed method to 271 clinical examination (CE) labeled patients with 6,426 healthy joints and 1,162 affected joints (tender, swollen, or both) results in a clear distinction between the scores for healthy and affected labeled joints. The summarized results for $k = 9$ are visualized in **Table 2**.

TABLE 2 | Resulting scores for $k = 9$ for all 271 patients.

Feature / Statistic value	Amplitude		Mean		Slope	
	Healthy	Affected	Healthy	Affected	Healthy	Affected
Average	0.503	0.528	0.486	0.509	0.395	0.414
Median	0.496	0.532	0.482	0.505	0.389	0.415

Ultrasound

Ultrasound (US) is used to identify structural and inflammatory changes in the joints and the musculoskeletal system (**Figures 5–7**). In different clinical studies, it has been demonstrated that US examination is more sensitive than radiography (18). The US is more sensitive than clinical examination for the assessment of inflammatory and structural changes in inflammatory arthritis, including PsA, and particularly synovitis, enthesitis, tenosynovitis, and bursitis (19, 20). Besides, US results are comparable to those of MRI, except for the detection of bone marrow edema. The reproducibility and low cost of US examination provide advantages compared to MRI for early PsA detection (21). However, a complete US examination of all joints, entheses, tendons, and bursae is extremely time-consuming and infeasible. Moreover, US examination is assessor related and depends on the experience of the rater.

As it was shown that inflammatory enthesopathy is a subclinical sign in the transition from PsO to PsA, the US may be a sensitive and feasible method to detect early inflammatory changes at entheses. Savage et al. (22) showed that subclinical enthesopathy and associated osteitis are present in patients with PsO but without arthritis, for which clinical examination is ineffective. And 49.3% of the PsO patients included had

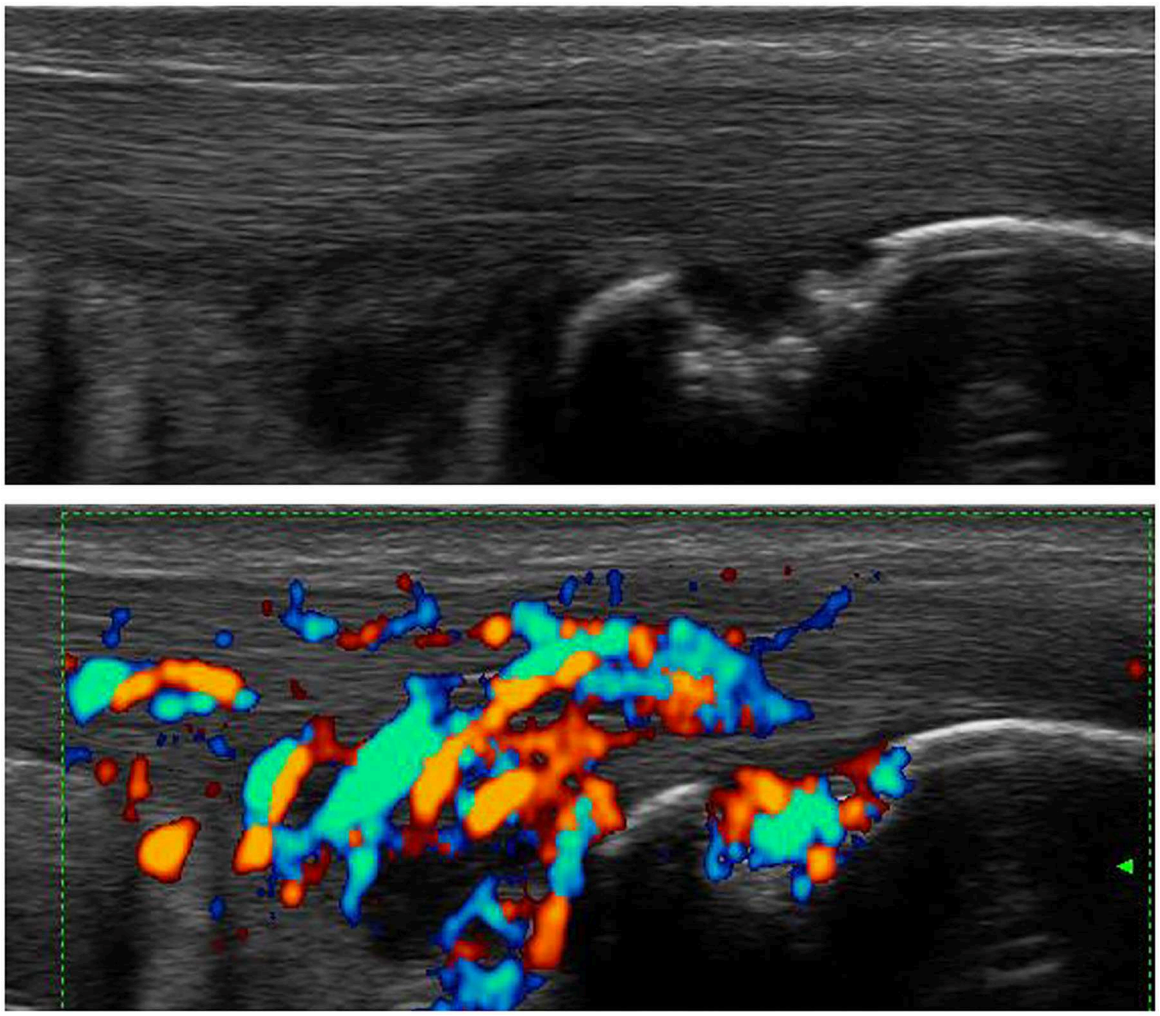

FIGURE 6 | Ultrasound assessment. Tendinitis of the Achilles tendon with the formation of osteophytes and power Doppler activity.

no evidence of clinically manifested PsA but showed at least one sonographic inflammatory abnormality that fulfilled the OMERACT definition of enthesopathy. These findings support the assumption that even in PsO, changes at the enthesial sites are detectable. It is necessary to assess in longitudinal how many of those patients developed overt PsA to specify these findings for risk stratification.

Magnetic Resonance Imaging

MRI is a very sensitive method for visualization of musculoskeletal structures that are involved in inflammatory processes. There are only little data on the detection of early PsA as the main studies on the detection of early arthritis were performed for the indication field of RA (23). With the use of MRI, arthritis, synovitis, tenosynovitis, periarticular inflammation, bone marrow edema, erosions, and bone proliferation can be sensitively visualized and anatomically classified. Limitations of MRI examination are the need of long examination times with illustration of only a single anatomic structure per examination and the need of contrast agent (tolerability). Definitions of disease-specific abnormalities are provided by the OMERACT working group, whereas enthesial disease criteria are only recently published (24). For inflammation and structural changes, T1-weighted sequences in two planes are performed (signal mainly reflecting fat content and a contrast agent), supplemented with a T2-weighted, fat-suppressed sequence or short tau inversion recovery (STIR) sequence (signal mainly reflecting water content). Performance of additional T1-weighted sequences (after intravenous gadolinium-containing contrast agent; **Figure 8**) with or without fat suppression assists in the assessment of tissue inflammation in peripheral joints. Use of contrast agent is needed for illustration of synovitis and tenosynovitis but not for detection of erosions, bony proliferation, and bone marrow edema (24).

Differences between PsA and other inflammatory diseases classified by MRI are reported. In PsA, enthesitis is not related to a focal inflammation but to a wider "synovio-enthesal complex"

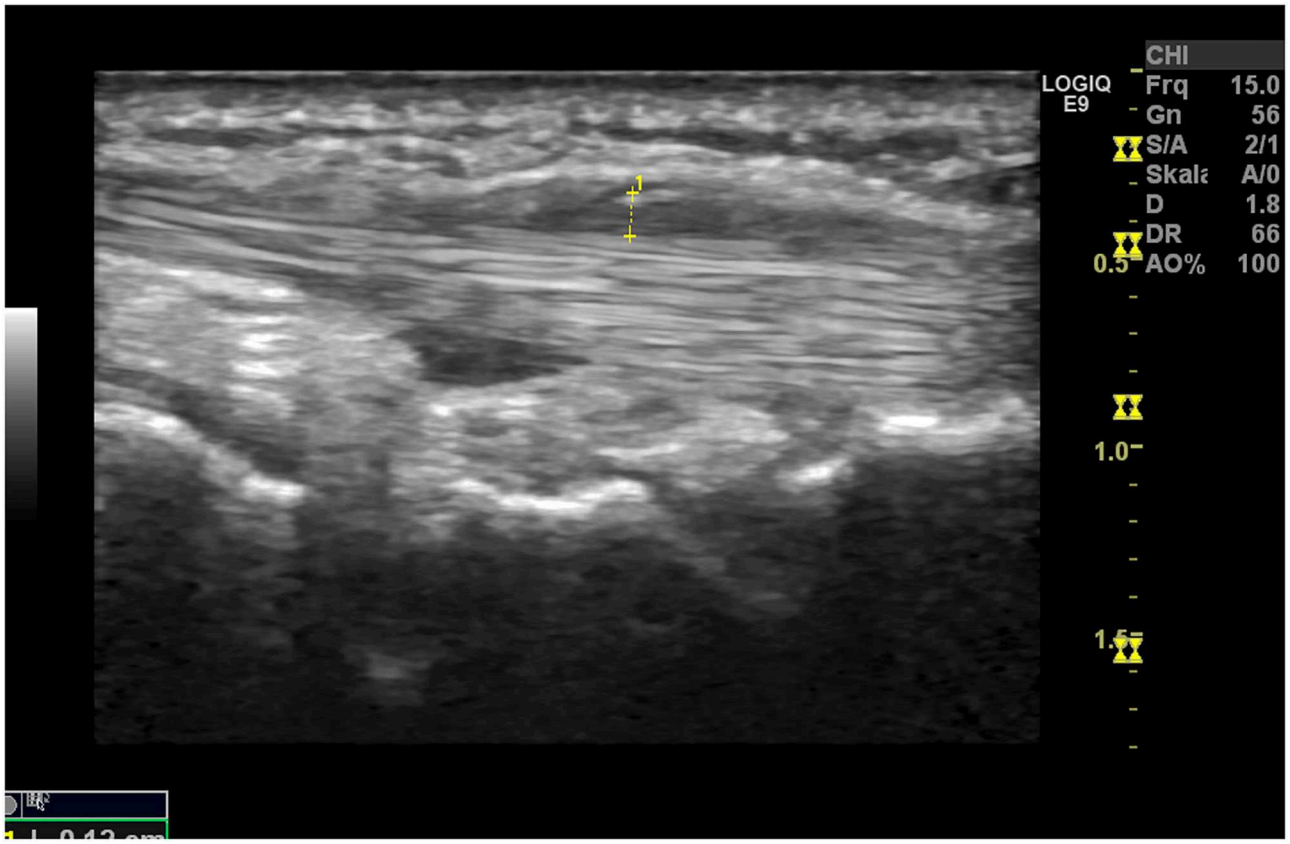

FIGURE 7 | Ultrasound assessment of flexor tendinitis.

(25), including adjacent tendons, periosteum, fibrocartilage, synovium, and bone at the attachment sites. Whereas, MRI findings such as synovitis, enthesitis, tenosynovitis, and bone marrow edema that appear frequently in PsA are not disease-specific and appear in any other inflammatory joint disease, PsA is characterized by more prevalent diaphyseal bone marrow and/or enthesitis, soft tissue inflammation, extracapsular inflammation, and involvement of primarily flexor tendons in contrast to extensor tendons in RA (26). Erosions are often located close to the collateral ligaments in contrast to osteoarthritis where they are frequently found centrally (27). In comparison to RA, in PsA, periostitis is found more frequent than erosions (28).

Assessments in PsO patients without evident arthritis revealed subclinical inflammation in both joints and entheses. Moreover, it was found that PsO patients with subclinical inflammation in MRI and arthralgia had a high risk (55.5%) for the later development of PsA, whereas patients without arthralgia had a low risk (15.3%) for PsA development (29). The specific pattern is recently not defined to detect PsO patients in subclinical development of PsA.

New methods of MRI such as whole-body MRI (WB-MRI) and dynamic contrast-enhanced MRI (DCE-MRI) are used in the research of PsO and PsA discrimination and prediction of PsA development. DCE-MRI allows semiautomated quantification of inflammation based on the measurement of contrast enhancement pattern over time in the selected region of interest. A recent report reports differences in RA and PsA in the pattern of enhancement of the synovial membrane with higher inflamed tissue in RA but a higher degree of inflammation in PsA (30). WB-MRI assessment indicated agreement between enthesitis on clinical scores and MRI results in PsA patients, suggesting value in detecting subclinical inflammation and the total burden of inflammation (31, 32).

Conventional X-Ray and Computerized Tomography

Conventional radiographic imaging methods such as x-ray (**Figure 9**) or conventional CT are often used to detect changes in bone structure in progressive PsA after clinical detection of inflammation by assessment of swollen or tender joints (33). The sensitivity for the detection of early changes in PsO patients at risk for PsA development is poor as only pronounced changes in bone structure are detectable being evident and often found only in a late stage of the disease.

FIGURE 8 | MRI of the left hand without signs of inflammation (T1 sequence).

Innovative Techniques Using Computerized Tomography Methods

Innovative methods, such as high-resolution peripheral quantitative CT (HR-pQCT) are available to sensitively detect early changes in bone metabolism in PsO patients compared to PsA and other joint diseases. Bone erosions can be detected early in the disease state of PsA (34), and the severity of erosions depends on its articular type and its activity (inflammation) status (35). Bone erosions in PsA pathophysiology result from an accumulation of osteoclasts in the joints, which is promoted by pro-inflammatory cytokines (36). Anabolic bone changes in PsA are mainly based on new bone formation. These changes typically occur at insertion sites of tendons to bone. Enthesial inflammation is a key process in PsA and most likely triggered by mechanical stress (37). Bone structure responses at the inflamed enthesial sites result in the formation of enthesophytes. An HR-pQCT-based study showed that the formation of enthesophytes are pronounced in PsA but are not found in rheumatoid arthritis (38). Furthermore, a more recent study revealed that enthesophytes occur early in patients with PsO without joint involvement, suggesting that their formation reflects a common process in PsO and PsA (39). In another study from Simon et al. (40), bone structure, number erosions, and enthesophytes were compared between different patient cohorts (PsO, PsA, and healthy controls) to measure a discriminative potential. Data on the extent of bone erosions and enthesophytes were collected and correlated to different categories of age, duration of PsO, and duration of PsA. Additionally, demographic and disease-specific data, including physical function [Health Assessment Questionnaire (HAQ)], were collected. A total of 203 patients were analyzed (101 with PsA, 55 with PsO, and 47 as healthy controls). Patients with PsA had a significantly higher number with a higher extent of erosions and enthesophytes compared to patients with PsO and healthy controls. Patients with PsO and healthy controls did not differ in number and extent of erosions, while enthesophytes were more frequent in patients with PsO

FIGURE 9 | Plain x-ray of the right hand with arthritis mutilans.

than in healthy controls. Bone erosions, but not enthesophytes, showed strong age dependency in all three groups. In contrast, enthesophytes were mostly influenced by the duration of PsO and PsA and, in contrast to bone erosions, were associated with poorer physical function, as measured by HAQ. Unfortunately, data on the association between the risk collective of PsO patients who develop PsA are currently missing but under examination. The longitudinal change will give more insights into the potential of HR-pQCT as an imaging method predicting PsA development in PsO patients.

Besides HR-pQCT, dual-energy CT (DECT) with iodine mapping to improve iodine contrast resolution may be a sensitive method to discriminate early inflammatory arthritis (41) but restricted in longitudinal measurement by radiation rate. Only a few studies were performed by now showing potential for early discrimination, but further studies are needed to confirm the findings in larger cohorts and over time.

Scintigraphy

Bone scintigraphy is an established method displaying an increase of metabolism of the tracer as a sign for abnormal metabolism rates, e.g., in the inflammatory state. It is used to detect inflammatory changes in the whole body, especially if other imaging techniques are not available. It has poor specificity and is limited by the use of the radioactive isotopes (tracers). In PsA, it was used in different cohorts to detect subclinical signs of inflammation in PsO patients without evident clinical PsA. The results were compared to the findings in US examination and clinical examination (42). It was revealed that a significantly higher number of joints were verified by the US to have increased uptake of tracer compared to clinical examination (34).

Fluorine-18-Labeled Fluorodeoxyglucose Positron Emission Tomography

Fluorine-18-labeled fluorodeoxyglucose positron emission tomography (^{18}F-FDG-PET) is a very sensitive imaging method for detection of changes in metabolism, e.g., inflammation-dependent early musculoskeletal changes indicating PsA-related changes. Takata et al. (43) performed a clinical study in PsO patients without clinically manifested PsA compared to PsA patients with long-lasting clinical overt PsA. Eighteen PsO and 28 PsA patients were enrolled for examination by positron emission tomography/computerized tomography (PET/CT) using ^{18}F-FDG. In the PsA cohort, ^{18}F-FDG accumulation was identified in all affected joints, illustrating its reliability in correlation to clinical examination sensitivity. In the PsO cohort, asymptomatic enthesitis was detected in six out of 18 PsO patients (33%), demonstrating its high sensitivity in the detection of inflammation at the entheses.

IMAGING TECHNIQUES FOR SENSITIVE AND SPECIFIC DETECTION OF EARLY PSORIATIC ARTHRITIS IN DIFFERENT TRANSITION PHASES

The transition from PsO to PsA contains different phases (preclinical, subclinical, and prodromal). In only two of those phases, early changes in soluble biomarkers/imaging can be detected (subclinical phase) or first unspecific clinical symptoms (e.g., arthralgia and fatigue) occur (prodromal phase). These two phases may be useful in early discrimination of the PsO patients at risk to develop overt PsA to prevent its occurrence (**Figure 10**).

In the transition model, the subclinical phase includes early musculoskeletal inflammatory changes in PsO patients without musculoskeletal complaints. In this phase of the disease, MRI, HR-pQCT, and high-frequency ultrasonography might have the highest potential to distinguish inflammatory changes in the defined at-risk-population with the limitation of the specificity to be PsA-related. By a combination of these techniques, patients are deeply characterized in focus on first musculoskeletal inflammatory changes and early changes in bone structure/bone metabolism. This characterization is completed by the use of FOI to generate additional information on early changes in vascularization as signs of increased angiogenesis, reported as an early marker in PsA progress (12). In different clinical studies within this special patient population, it was shown that in a high proportion of asymptomatic PsO patients, enthesial inflammation was detectable (44). Moreover, Simon

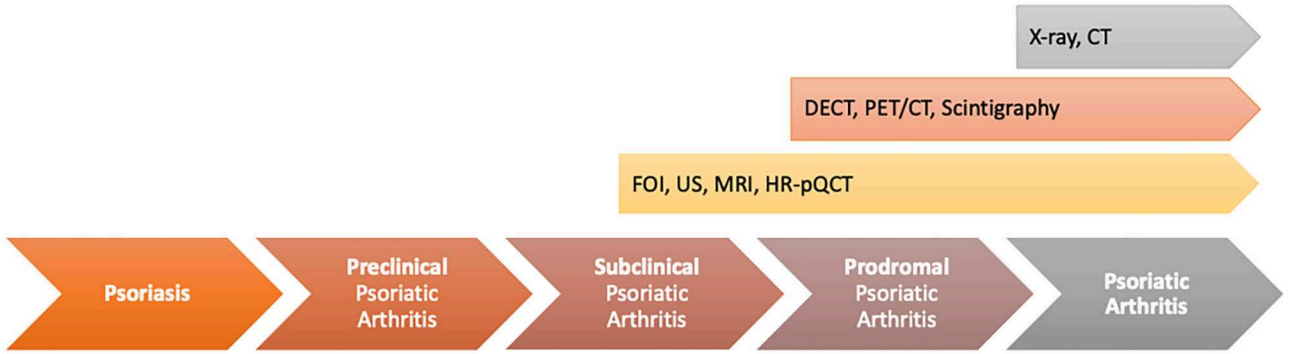

FIGURE 10 | Value of different imaging techniques to find unspecific musculoskeletal changes in psoriasis (PsO) patients with the transition phases from PsO to psoriatic arthritis (PsA).

et al. (40) showed that by the use of HR-pQCT, the number of enthesophytes was significantly higher in asymptomatic PsO patients than in healthy controls. Moreover, the duration of skin disease influenced the number of enthesophytes (45). Nevertheless, only a part of those patients will develop clinical overt PsA afterwards. The potential of imaging biomarker to detect the specific at-risk population is poor. Additionally, clinical definitions adapted from other inflammatory diseases such as the criteria for subclinical inflammation in RA are not usable in PsA as by its use, half of the asymptomatic PsO patients are classified as subclinical PsA, but only part of them will develop PsA later. So, within this phase is a high need of clear classification and characterization of patients to define the correct at-risk population for PsA development, maybe by a combination of different biomarkers (e.g., combination with soluble biomarkers, e.g., on miRNA base, biomarkers for comorbid conditions that were shown to occur early in the disease process or different imaging techniques). Beside the definition of the biomarker set, its usability must be high to be implemented into clinical routine care.

The prodromal phase of the disease is classified as unspecific clinical symptoms such as arthralgia and/or fatigue combined with the occurrence of inflammatory changes in imaging. A recent study showed that, in this phase, tenosynovitis was the most significant contributor to the reported musculoskeletal symptoms (PsO vs. PsO with arthralgia vs. PsA). In the US, in a high proportion of patients, tenosynovitis especially of the flexor tendon of the hands was detected (in 29.5% of the arthralgia patients compared to 5.3% in the PsO group) (10), whereas active enthesitis and synovitis did not reach a significant difference. In the longitudinal part of the study, in the US, determined enthesitis was the only US feature linked to the future evolution of PsA. Faustini et al. (29) confirmed this link between subclinical inflammation detected and PsA, highlighting that patients with synovitis detected by MRI and arthralgia had 55.5% likelihood to develop PsA within 1 year. In the IVEPSA (Interception in very early PsA) study, psoriatic patients with inflammatory arthralgia without joint swelling and with concomitant predictors of PsA [i.e., Psoriasis Area and Severity Index (PASI) >6 or scalp PsO or nail involvement] were treated with anti-interleukin (IL)-17 for a disease interception. Baseline MRI investigation of the dominant hand revealed at least one inflammatory lesion in 83% of patients, highlighting synovitis as the most prevalent (66.7%), followed by tenosynovitis (55.6%) (46).

DISCUSSION

PsO is one of the common chronic inflammatory skin diseases, affecting ∼3% of the European Caucasians. PsA is a chronic immune-mediated disease associated with PsO characterized by distinct musculoskeletal inflammation. Due to its heterogeneous clinical manifestations (e.g., oligo- and polyarthritis, enthesitis, dactylitis, and axial inflammation), early diagnosis of PsA is often difficult and delayed. PsO patients are of high risk for PsA development as ∼30% of PsO patients will be affected by (chronic) musculoskeletal inflammation.

The main events for the transition from PsO to PsA are currently unclear: the combination of genetic and clinical–demographic risk factors (e.g., nail PsO, PsO severity, and type) may promote PsA development and its progression. The underlying molecular mechanisms for the transition from PsO to PsA are still poorly defined. The increase of neoangiogenesis (12) and the development of enthesitis is hypothesized to be a primary manifestation in PsA, detectable early using imaging and clinical examination in patients developing later overt PsA (22).

Different phases were defined to describe the transition from PsO to PsA (2). Three phases are named between PsO and overt PsA of which two have high relevance to be detectable in the at-risk population with the use of sensitive biomarkers such as sensitive imaging techniques: the subclinical phase (detection of soluble biomarkers, e.g., on miRNA base and early musculoskeletal inflammation such as synovio-enthesitis detected in imaging but missing related clinical symptoms) and the prodromal phase (detection of musculoskeletal inflammation in imaging techniques and unspecific clinical symptoms such as fatigue and arthralgia).

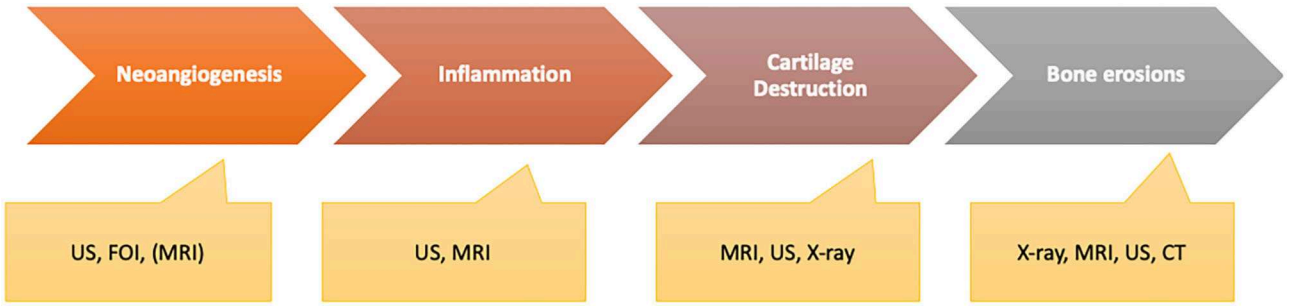

FIGURE 11 | Different disease activity characteristics with the ability of imaging methods to be measured adequately.

The potential of the available imaging techniques to detect patients in one of these two phases differs widely as all of these techniques characterize different pathophysiologic states of the inflammatory process that might have the highest value by being combined for deep characterization of the patients (**Figure 11**).

Besides sensitivity and specificity in the detection of anatomical and pathophysiological changes by use of advanced imaging techniques, standardized assessment tools are needed to bring innovative imaging methods in context to the suspected indications and process results to enable detection of coherence between saliences and the underlying disease. Technological advances should be integrated into assessment algorithms to use its full potential to be beneficial in the detection of at-risk patients especially in context to PsO and PsA patients.

FOI as an ICG-tailored imaging technique visualizes changes in micro-vascularization of the hands (13). It is a well-tolerated and fast method that seems sensitive for detection of early signs of inflammation related to changes in angiogenesis. Early changes of micro-vascularization may be indicators for early signs of inflammation of the joints and tendons as neoangiogenesis was identified as a symptom associated with musculoskeletal inflammation in PsA differently to other arthritides (47). Due to its mechanism, the detection of changes in micro-vascularization may be of value to define a very early disease state of PsA in the subclinical phase of transition when clinical signs such as arthralgia are missing. With its high sensitivity to detect changes, it is of value to be used in longitudinal observation. These aspects should be investigated in further studies as it gives an advantage to easily screen PsO patients without symptoms but defined risk profile early. Automated measurement of the fluorescence signals gives an objective assessment of the state and its changes over time when used in longitudinal assessments.

MRI and US are the recent widely used methods for sensitive detection of inflammation in the joints and musculoskeletal structures (entheses, bursa, tendons). Bone marrow edema, enthesitis, and changes in vascularization as early indicators of inflammation of the joints, entheses, and spine in the subclinical and prodromal phases can be visualized with high sensitivity by both (23). The US has the benefit of its availability as well as of its possibility to detect changes in synovial and enthesial structure in early inflammation. Changes of vascularization in the synovia and the enthesial structures can be easily evaluated using Doppler mode presenting as a sensitive marker for inflammation (subclinical and prodromal phase) (44). Structures of interest can be associated with anatomica structures, and due to their tolerability, longitudinal status can be measured easily.

HR-pQCT, developed from CT technique, might be of high value to detect early changes in bone metabolism and structure in PsO and PsA patients (compared to other inflammatory diseases), but the value for discrimination of PsO or PsO transient to PsA is recently not clear. Simon et al. (40) showed that in PsO and PsA patients, the formation of enthesophytes is pronounced compared to RA and healthy controls, but the differentiation of those findings between PsO in early PsA state is poor. Longitudinal data are missing to evaluate within this group. Dual-energy CT might be as well a very sensitive method to discriminate between PsO/PsA disease state, but its performance and repeatability are limited to radiation and validity.

Established methods such as x-ray or CT are not sensitive enough to detect early inflammatory changes of the musculoskeletal disease but changes in bone structure.

PET/CT and scintigraphy have established methods with a focus on metabolism and its changes in the inflammatory disease state. Both methods are limited by their poor specificity but sensitive to illustrate changes early and with focus on the whole body not restricted by use in one region of interest.

For US, MRI, and HR-pQCT, the relevance of the early findings of enthesophytes (HR-pQCT) or detection of enthesopathy (MRI, US) as signs for early musculoskeletal inflammation without clinical symptoms (subclinical phase) in PsO patients is still unclear. In a longitudinal study, it was found that although these findings were detectable in 50% of the PsO patients, only a part of them developed overt PsA later in their disease state (40, 45). So, these imaging findings are not specific for the definition of high risk for PsA development and must be completed by a multifactorial characterization of the patient profile, e.g., using data on the comorbid condition, clinical data, and data of soluble biomarker (in the investigation).

The potential of these imaging techniques increases in the prodromal phase when clinical symptoms appear, even if they are non-specific. Here, the at-risk population is enriched, and the combination of both imaging findings and arthralgia predicts the development of PsA significantly.

Overall, different imaging techniques are available with various methods to sensitively quantify vascularization and early signs of musculoskeletal inflammation in PsO and PsA patients. Advanced methods adapted from conventional techniques are of advantage to illustrate early changes in bone metabolism or quantify inflammation in the anatomical structure. With the use of these techniques, pathophysiological backgrounds of PsO and PsA are explored and can be characterized more precisely. New methods such as FOI might be able to complement other imaging techniques by quantification of changes in microvascularization as a very early sign of inflammation (subclinical PsA without clinical symptoms). Nevertheless, by now, it is not possible to specifically discriminate between PsO patients and those who will develop PsA by solely using imaging as a biomarker. So, further studies are needed to explore the impact of different characteristics/biomarkers (e.g., clinical data, comorbid condition, soluble/molecular biomarkers, different imaging techniques) and their impact in predicting PsA to characterize the at-risk patients precisely and explore their impact of PsO patient selection for a longitudinal follow-up to assess the development of PsA or its interception.

AUTHOR CONTRIBUTIONS

All authors listed have made a substantial, direct and intellectual contribution to the work, and approved it for publication.

FUNDING

The clinical research group Frankfurt was supported by the LOEWE-Center TMP of the state of Hesse (Germany) and the Fraunhofer Cluster of Excellence for Immune-Mediated Diseases CIMD.

ACKNOWLEDGMENTS

We would like to thank the participating patients and study center personnel.

REFERENCES

1. Ritchlin CT, Colbert RA, Gladman DD. Psoriatic Arthritis. *N Engl J Med*. (2017) 376:2095–6. doi: 10.1056/NEJMra1505557
2. Scher JU, Ogdie A, Merola JF, Ritchlin C. Preventing psoriatic arthritis: focusing on patients with psoriasis at increased risk of transition. *Nat Rev Rheumatol*. (2019) 15:153–66. doi: 10.1038/s41584-019-0175-0
3. Zabotti A, Tinazzi I, Aydin SZ, McGonagle D. From psoriasis to psoriatic arthritis: insights from imaging on the transition to psoriatic arthritis and implications for arthritis prevention. *Curr Rheumatol Rep*. (2020) 22:24. doi: 10.1007/s11926-020-00891-x
4. Gladman DD, Antoni C, Mease P, Clegg DO, Nash P. Psoriatic arthritis: epidemiology, clinical features, course, and outcome. *Ann Rheum Dis*. (2005) 64(Suppl. 2):ii14–7. doi: 10.1136/ard.2004.032482
5. Christophers E, Barker JN, Griffiths CE, Dauden E, Milligan G, Molta C, et al. The risk of psoriatic arthritis remains constant following initial diagnosis of psoriasis among patients seen in European dermatology clinics. *J Eur Acad Dermatol Venereol*. (2010) 24:548–54. doi: 10.1111/j.1468-3083.2009.03463.x
6. Eder L, Haddad A, Rosen CF, Lee KA, Chandran V, Cook R, et al. The incidence and risk factors for psoriatic arthritis in patients with psoriasis: a prospective cohort study. *Arthritis Rheumatol*. (2016) 68:915–23. doi: 10.1002/art.39494
7. Love TJ, Zhu Y, Zhang Y, Wall-Burns L, Ogdie A, Gelfand JM, et al. Obesity and the risk of psoriatic arthritis: a population-based study. *Ann Rheum Dis*. (2012) 71:1273–7. doi: 10.1136/annrheumdis-2012-201299
8. Myers A, Kay LJ, Lynch SA, Walker DJ. Recurrence risk for psoriasis and psoriatic arthritis within sibships. *Rheumatology*. (2005) 44:773–6. doi: 10.1093/rheumatology/keh589
9. Eder L, Polachek A, Rosen CF, Chandran V, Cook R, Gladman DD. The development of psoriatic arthritis in patients with psoriasis is preceded by a period of nonspecific musculoskeletal symptoms: a prospective cohort study. *Arthritis Rheumatol*. (2017) 69:622–9. doi: 10.1002/art.39973
10. Zabotti A, McGonagle DG, Giovannini I, Errichetti E, Zuliani F, Zanetti A, et al. Transition phase towards psoriatic arthritis: clinical and ultrasonographic characterisation of psoriatic arthralgia. *RMD Open*. (2019) 5:e001067. doi: 10.1136/rmdopen-2019-001067
11. McGonagle D, Gibbon W, Emery P. Classification of inflammatory arthritis by enthesitis. *Lancet*. (1998) 352:1137–40. doi: 10.1016/S0140-6736(97)12004-9
12. Veale DJ, Fearon U. What makes psoriatic and rheumatoid arthritis so different? *RMD Open*. (2015) 1:e000025. doi: 10.1136/rmdopen-2014-000025
13. Werner SG, Langer HE, Ohrndorf S, Bahner M, Schott P, Schwenke C, et al. Inflammation assessment in patients with arthritis using a novel *in vivo* fluorescence optical imaging technology. *Ann Rheum Dis*. (2012) 71:504–10. doi: 10.1136/annrheumdis-2010-148288
14. Thuermel K, Neumann J, Jungmann PM, Schaffeler C, Waldt S, Heinze A, et al. Fluorescence optical imaging and 3T-MRI for detection of synovitis in patients with rheumatoid arthritis in comparison to a composite standard of reference. *Eur J Radiol*. (2017) 90:6–13. doi: 10.1016/j.ejrad.2017.02.016
15. Hirano F, Yokoyama-Kokuryo W, Yamazaki H, Tsutsumino M, Sakai R, Satoh S, et al. Comparison of fluorescence optical imaging, ultrasonography and clinical examination with magnetic resonance imaging as a reference in active rheumatoid arthritis patients. *Immunol Med*. (2018) 41:75–81. doi: 10.1080/13497413.2018.1481578
16. Wiemann O, Werner SG, Langer HE, Backhaus M, Chatelain R. The "green nail" phenomenon in ICG-enhanced fluorescence optical imaging - a potential tool for the differential diagnosis of psoriatic arthritis. *J Dtsch Dermatol Ges*. (2019) 17:138–47. doi: 10.1111/ddg.13747
17. Koehm M, Rossmanith T, Langer HE, Backhaus M, Burmester GR, Wassenberg S, et al. Detection of clinical signs of arthritis and subclinical evidence of inflammation in psoriasis patients with risk for arthritis: value of clinical examination, ultrasound and fluorescence-optical imaging - results from the Prospective Multicentre Xciting Study [abstract]. *Arthritis Rheumatol*. (2017) 69 (Suppl. 10).
18. Wiell C, Szkudlarek M, Hasselquist M, Moller JM, Vestergaard A, Norregaard J, et al. Ultrasonography, magnetic resonance imaging, radiography, and clinical assessment of inflammatory and destructive changes in fingers and toes of patients with psoriatic arthritis. *Arthritis Res Ther*. (2007) 9:R119. doi: 10.1186/ar2327
19. Weiner SM, Jurenz S, Uhl M, Lange-Nolde A, Warnatz K, Peter HH, et al. Ultrasonography in the assessment of peripheral joint involvement in psoriatic arthritis : a comparison with radiography, MRI and scintigraphy. *Clin Rheumatol*. (2008) 27:983–9. doi: 10.1007/s10067-008-0835-y
20. Dougados M, Jousse-Joulin S, Mistretta F, d'Agostino MA, Backhaus M, Bentin J, et al. Evaluation of several ultrasonography scoring systems for synovitis and comparison to clinical examination: results from a prospective multicentre study of rheumatoid arthritis. *Ann Rheum Dis*. (2010) 69:828–33. doi: 10.1136/ard.2009.115493
21. Coates LC, Hodgson R, Conaghan PG, Freeston JE. MRI and ultrasonography for diagnosis and monitoring of psoriatic arthritis. *Best Pract Res Clin Rheumatol*. (2012) 26:805–22. doi: 10.1016/j.berh.2012.09.004
22. Savage L, Goodfield M, Horton L, Watad A, Hensor E, Emery P, et al. Regression of peripheral subclinical enthesopathy in therapy-naive patients treated with ustekinumab for moderate-to-severe chronic plaque psoriasis: a

fifty-two-week, prospective, open-label feasibility study. *Arthritis Rheumatol*. (2019) 71:626–31. doi: 10.1002/art.40778
23. McQueen F, Lassere M, Ostergaard M. Magnetic resonance imaging in psoriatic arthritis: a review of the literature. *Arthritis Res Ther*. (2006) 8:207. doi: 10.1186/ar1934
24. Ostergaard M, McQueen F, Wiell C, Bird P, Boyesen P, Ejbjerg B, et al. The OMERACT psoriatic arthritis magnetic resonance imaging scoring system (PsAMRIS): definitions of key pathologies, suggested MRI sequences, and preliminary scoring system for PsA Hands. *J Rheumatol*. (2009) 36:1816–24. doi: 10.3899/jrheum.090352
25. McGonagle D, Aydin SZ, Tan AL. The synovio-entheseal complex and its role in tendon and capsular associated inflammation. *J Rheumatol Suppl*. (2012) 89:11–4. doi: 10.3899/jrheum.120233
26. Narvaez J, Narvaez JA, de Albert M, Gomez-Vaquero C, Nolla JM. Can magnetic resonance imaging of the hand and wrist differentiate between rheumatoid arthritis and psoriatic arthritis in the early stages of the disease? *Semin Arthritis Rheum*. (2012) 42:234–45. doi: 10.1016/j.semarthrit.2012.03.016
27. Braum LS, McGonagle D, Bruns A, Philipp S, Hermann S, Aupperle K, et al. Characterisation of hand small joints arthropathy using high-resolution MRI–limited discrimination between osteoarthritis and psoriatic arthritis. *Eur Radiol*. (2013) 23:1686–93. doi: 10.1007/s00330-012-2739-0
28. Schoellnast H, Deutschmann HA, Hermann J, Schaffler GJ, Reittner P, Kammerhuber F, et al. Psoriatic arthritis and rheumatoid arthritis: findings in contrast-enhanced MRI. *AJR Am J Roentgenol*. (2006) 187:351–7. doi: 10.2214/AJR.04.1798
29. Faustini F, Simon D, Oliveira I, Kleyer A, Haschka J, Englbrecht M, et al. Subclinical joint inflammation in patients with psoriasis without concomitant psoriatic arthritis: a cross-sectional and longitudinal analysis. *Ann Rheum Dis*. (2016) 75:2068–74. doi: 10.1136/annrheumdis-2015-208821
30. Cimmino MA, Barbieri F, Boesen M, Paparo F, Parodi M, Kubassova O, et al. Dynamic contrast-enhanced magnetic resonance imaging of articular and extraarticular synovial structures of the hands in patients with psoriatic arthritis. *J Rheumatol Suppl*. (2012) 89:44–8. doi: 10.3899/jrheum.120242
31. Poggenborg RP, Eshed I, Ostergaard M, Sorensen IJ, Moller JM, Madsen OR, et al. Enthesitis in patients with psoriatic arthritis, axial spondyloarthritis and healthy subjects assessed by "head-to-toe" whole-body MRI and clinical examination. *Ann Rheum Dis*. (2015) 74:823–9. doi: 10.1136/annrheumdis-2013-204239
32. Poggenborg RP, Pedersen SJ, Eshed I, Sorensen IJ, Moller JM, Madsen OR, et al. Head-to-toe whole-body MRI in psoriatic arthritis, axial spondyloarthritis and healthy subjects: first steps towards global inflammation and damage scores of peripheral and axial joints. *Rheumatology*. (2015) 54:1039–49. doi: 10.1093/rheumatology/keu439
33. Siannis F, Farewell VT, Cook RJ, Schentag CT, Gladman DD. Clinical and radiological damage in psoriatic arthritis. *Ann Rheum Dis*. (2006) 65:478–81. doi: 10.1136/ard.2005.039826
34. Scarpa R, Cuocolo A, Peluso R, Atteno M, Gisonni P, Iervolino S, et al. Early psoriatic arthritis: the clinical spectrum. *J Rheumatol*. (2008) 35:137–41.
35. Queiro-Silva R, Torre-Alonso JC, Tinture-Eguren T, Lopez-Lagunas I. A polyarticular onset predicts erosive and deforming disease in psoriatic arthritis. *Ann Rheum Dis*. (2003) 62:68–70. doi: 10.1136/ard.62.1.68
36. Ritchlin CT, Haas-Smith SA, Li P, Hicks DG, Schwarz EM. Mechanisms of TNF-α- and RANKL-mediated osteoclastogenesis and bone resorption in psoriatic arthritis. *J Clin Invest*. (2003) 111:821–31. doi: 10.1172/JCI200316069
37. McGonagle D, Lories RJ, Tan AL, Benjamin M. The concept of a "synovio-entheseal complex" and its implications for understanding joint inflammation and damage in psoriatic arthritis and beyond. *Arthritis Rheum*. (2007) 56:2482–91. doi: 10.1002/art.22758
38. Finzel S, Englbrecht M, Engelke K, Stach C, Schett G. A comparative study of periarticular bone lesions in rheumatoid arthritis and psoriatic arthritis. *Ann Rheum Dis*. (2011) 70:122–7. doi: 10.1136/ard.2010.132423
39. Simon D, Faustini F, Kleyer A, Haschka J, Englbrecht M, Kraus S, et al. Analysis of periarticular bone changes in patients with cutaneous psoriasis without associated psoriatic arthritis. *Ann Rheum Dis*. (2016) 75:660–6. doi: 10.1136/annrheumdis-2014-206347
40. Simon D, Kleyer A, Faustini F, Englbrecht M, Haschka J, Berlin A, et al. Simultaneous quantification of bone erosions and enthesiophytes in the joints of patients with psoriasis or psoriatic arthritis - effects of age and disease duration. *Arthritis Res Ther*. (2018) 20:203. doi: 10.1186/s13075-018-1691-z
41. Fukuda T, Umezawa Y, Asahina A, Nakagawa H, Furuya K, Fukuda K. Dual energy CT iodine map for delineating inflammation of inflammatory arthritis. *Eur Radiol*. (2017) 27:5034–40. doi: 10.1007/s00330-017-4931-8
42. Raza N, Hameed A, Ali MK. Detection of subclinical joint involvement in psoriasis with bone scintigraphy and its response to oral methotrexate. *Clin Exp Dermatol*. (2008) 33:70–3. doi: 10.1111/j.1365-2230.2007.02581.x
43. Takata T, Taniguchi Y, Ohnishi T, Kohsaki S, Nogami M, Nakajima H, et al. (18)FDG PET/CT is a powerful tool for detecting subclinical arthritis in patients with psoriatic arthritis and/or psoriasis vulgaris. *J Dermatol Sci*. (2011) 64:144–7. doi: 10.1016/j.jdermsci.2011.08.002
44. Zabotti A, Bandinelli F, Batticciotto A, Scire CA, Iagnocco A, Sakellariou G. Musculoskeletal ultrasonography for psoriatic arthritis and psoriasis patients: a systematic literature review. *Rheumatology*. (2017) 56:1518–32. doi: 10.1093/rheumatology/kex179
45. Naredo E, Moller I, de Miguel E, Batlle-Gualda E, Acebes C, Brito E, et al. High prevalence of ultrasonographic synovitis and enthesopathy in patients with psoriasis without psoriatic arthritis: a prospective case-control study. *Rheumatology*. (2011) 50:1838–48. doi: 10.1093/rheumatology/ker078
46. Kampylafka E, Simon D, d'Oliveira I, Linz C, Lerchen V, Englbrecht M, et al. Disease interception with interleukin-17 inhibition in high-risk psoriasis patients with subclinical joint inflammation-data from the prospective IVEPSA study. *Arthritis Res Ther*. (2019) 21:178. doi: 10.1186/s13075-019-1957-0
47. Cantatore FP, Maruotti N, Corrado A, Ribatti D. Angiogenesis dysregulation in psoriatic arthritis: molecular mechanisms. *Biomed Res Int*. (2017) 2017:5312813. doi: 10.1155/2017/5312813

Conflict of Interest: The authors declare that the research was conducted in the absence of any commercial or financial relationships that could be construed as a potential conflict of interest.

frontiers in Medicine

PERSPECTIVE
published: 25 September 2020
doi: 10.3389/fmed.2020.545097

Multi-Modal Imaging to Assess the Interaction Between Inflammation and Bone Damage Progression in Inflammatory Arthritis

Justin J. Tse[1,2], *Scott C. Brunet*[1,2,3], *Peter Salat*[1,2], *Glen S. Hazlewood*[2,4], *Cheryl Barnabe*[2,4] *and Sarah L. Manske*[1,2,3]*

[1] Department of Radiology, Cumming School of Medicine, University of Calgary, Calgary, AB, Canada, [2] Cumming School of Medicine, McCaig Institute for Bone and Joint Health, University of Calgary, Calgary, AB, Canada, [3] Biomedical Engineering Graduate Program, Schulich School of Engineering, University of Calgary, Calgary, AB, Canada, [4] Division of Rheumatology, Department of Medicine, Cumming School of Medicine, University of Calgary, Calgary, AB, Canada

OPEN ACCESS

Edited by:
Raj Sengupta,
Royal National Hospital for Rheumatic Diseases, United Kingdom

Reviewed by:
Peter Mandl,
Medical University of Vienna, Austria
Naoki Iwamoto,
Nagasaki University Hospital, Japan
Ali Ghasem-Zadeh,
The University of Melbourne, Australia

***Correspondence:**
Sarah L. Manske
smanske@ucalgary.ca

Specialty section:
This article was submitted to Rheumatology, a section of the journal Frontiers in Medicine

Received: 24 March 2020
Accepted: 26 August 2020
Published: 25 September 2020

Citation:
Tse JJ, Brunet SC, Salat P, Hazlewood GS, Barnabe C and Manske SL (2020) Multi-Modal Imaging to Assess the Interaction Between Inflammation and Bone Damage Progression in Inflammatory Arthritis. Front. Med. 7:545097. doi: 10.3389/fmed.2020.545097

Combining results from multiple imaging techniques (i.e., multi-modal imaging) through image registration can result in the better characterization of joint tissue characteristics. In the context of inflammatory arthritis conditions, high-resolution peripheral quantitative computed tomography (HR-pQCT) provides excellent bone contrast while magnetic resonance imaging (MRI) provides superior contrast and resolution of soft tissue and inflammatory characteristics. Superimposing these imaging results upon each other provides a robust characterization of the joint. In a preliminary study of nine rheumatoid arthritis (RA) participants in clinical remission, we acquired HR-pQCT and MR images of their 2nd and 3rd metacarpophalangeal (MCP) joints at two timepoints 6 months apart. We present the benefits of a multi-modal imaging approach, in which we demonstrate the ability to localize regions of inflammation with subtle changes in bone erosion volume. Using HR-pQCT and MRI to visualize bone damage and inflammation, respectively, will improve our understanding of the impact that subclinical inflammation has on bone damage progression, and demonstrating if bone repair occurs where inflammation is resolved. The presented multi-modal imaging technique has the potential to study the progression of bone damage in relation to inflammation that otherwise would not be possible with either imaging technique alone. The multi-modal image registration technique will be helpful to understanding the development and pathogenesis of RA-associated bone erosions. Additionally, multi-modal imaging may provide a technique to probe the tissue-level changes that occur as a result of treatment regimes.

Keywords: high resolution peripheral quantitative computed tomography (HR-pQCT), magnetic resonance imaging, multi-modal imaging, image registration, rheumatoid arthritis, subclinical inflammation

MULTI-MODAL IMAGING: UTILIZING EACH INDIVIDUAL IMAGING MODALITY'S STRENGTHS

Inflammatory arthritis conditions are complex in pathophysiology and affect many joint tissues. Imaging plays an important role in the diagnosis, treatment evaluation and understanding of pathophysiological processes. Every imaging modality has its own strengths and weaknesses for tissue and disease assessment, due to their differing abilities to provide tissue contrast, spatial resolution, and access to joints of interest. In the context of inflammatory arthritis, conventional radiography provides 2-dimensional (2D) planar, projection images of structural damage (i.e., joint space narrowing, erosions, and osteophytes) of bony features. Computed tomography (CT) provides 3-dimensional (3D) views, resulting in greater contrast and spatial resolution to visualize the same bony features; however, this is at the expense of greater radiation exposure depending on the joints of interest and their proximity to radiation-sensitive tissues and organs. High-resolution peripheral quantitative computed tomography (HR-pQCT) is a CT modality adapted for imaging extremities and provides significantly enhanced contrast, superior spatial resolution of bony features, and reduced radiation dose when compared to conventional whole-body CT. While originally introduced to image the distal tibia and distal radius, applications of HR-pQCT have extended to include the hand, wrist and knee joints (1–3). HR-pQCT allows for the resolution of individual trabeculae (4), and the ability to quantitatively evaluate joint properties. Semi-automated techniques have been developed to assess periarticular bone mineral density and microarchitecture, joint space width as well as erosion volume (5–8). An overview of these techniques is provided in a review by Klose-Jensen et al. (9) in this special issue.

In contrast to HR-pQCT's excellent spatial resolution of bone, ultrasound and magnetic resonance imaging (MRI) have superior contrast and resolution of soft tissue and can detect features of inflammation. While ultrasound can acquire multiplanar images and facilitate the identification and grading of superficial bony features (10, 11), this imaging technique is limited in its application for analysis below the cortical surface and only provides images several centimeters below the probe (12). However, the presence of a power doppler signal identifies sites of active synovial inflammation without exogenous contrast enhancement. On the other hand, MRI facilitates the 3D visualization of internal features such as bone marrow edema but requires the administration of an intravenous gadolinium contrast agent for the accurate differentiation of inflammatory signals from fluid signals. An additional benefit of MRI is that a semi-quantitative assessment of inflammatory arthritis can be evaluated with MR images using validated scoring systems such as the RA MRI scoring system (RAMRIS) (13, 14) and the psoriatic arthritis MRI scoring system (15).

To date, most multi-modal imaging studies examine each imaging modality independently from one another. However, the 3D multiplanar image acquisition from CT and MRI can facilitate the superimposition of images after accurate image co-registration and transformation, providing complementary information (e.g., bone image from CT, synovitis and inflammation from MRI) to better characterize the entire joint.

IMAGE REGISTRATION

A strategy to visualize and understand bone damage in inflammatory arthritis within a patient is to align and superimpose images acquired from longitudinal time points or multiple imaging modalities using a computational tool known as image registration. We present a brief overview of image registration as a technique that can be used for joint-based imaging on HR-pQCT and MRI datasets.

Image registration is a computational process which iteratively searches for the best alignment based on common information within two or more images. The "best" alignment is defined by metrics such as mutual information or the cross-correlation coefficient (16, 17). The cross-correlation coefficient is typically used when measuring the similarity between image registration of images from the same modality, while mutual information is preferred for multi-modal images. The actual image registration can be performed in a *rigid* or *non-rigid* fashion. *Rigid* image registration aligns the anatomy within the images, without changing the shapes, by a series of rotations and translations. *Rigid* registration is particularly useful when aligning images from the same individual where differences in overall bone shape and size are not expected but the position may differ; acquired either at different times from the same modality, or from multiple modalities at the same time. In contrast, *non-rigid* or *deformable* image registration may allow for local image deformations to facilitate their registration. This technique is beneficial to align images from different individuals to either compare differences in shape or define a common region of interest across multiple individuals, or from the same individual when differences in anatomical shape or size exist between the images.

An initial guess of the translations and rotations is typically required to initialize the registration; this can be accomplished by identifying anatomical landmarks on each image, or by using physical properties of the image such as the center of mass. An optimization algorithm then iteratively searches for the most appropriate transformation (i.e., translations and rotations) to reorient and optimally fit one image onto another image (18), until no further improvement in the alignment metric is detected.

Assessing Longitudinal Changes and Bone Remodeling With HR-pQCT

As previously mentioned, *rigid* image registration is ideal to align baseline and follow-up images from the same participant on the same imaging modality—ensuring the same region-of-interest is evaluated at both timepoints and improve reproducibility (19, 20). In the context of erosion assessment, image registration allows for a careful comparison of bone changes at the site of the erosion that occur over time (20, 21). Specifically, recent developments have applied image-based bone remodeling

algorithms (22) to sensitively assess change in erosion volume over time by aligning, registering, and subtracting baseline from follow-up images (21, 23). *Rigid* image registration is particularly well-suited for follow-up imaging because the gross morphological features remain relatively constant over the time frames typically studied (e.g., 6 months to 2 years), and new structural damage is small relative to the overall size and shape of the bone. However, the main barriers to accurate measures of bone remodeling using this technique are patient motion during the scan time and slow bone remodeling rates, as thickness changes must exceed the true spatial resolution of the scanner at $\sim$100 μm (4). While we have demonstrated good performance of this algorithm in rheumatoid arthritis patients with relatively slow rates of bone changes, performance suffers if significant patient motion is present in the baseline or follow-up images (23).

Multi-Modal Image Registration

The main advantage of imaging the same individual with a different imaging modality is the ability to simultaneously study different tissue characteristics (i.e., CT for bone and MRI for synovitis and inflammation). As intensity values between imaging modalities represent different tissues, we use mutual information to align images from multiple modalities (24, 25). This technique identifies and matches common clusters of regions between the two images; for example, homogeneous regions of one image will be mapped to a homogeneous region in a second image (17).

USING HR-pQCT AND MRI TO INVESTIGATE THE ROLE OF INFLAMMATION IN BONE DAMAGE PROGRESSION

Rationale

Timely, target-driven therapeutic intervention with disease modifying medications is currently an effective mechanism to achieve clinical remission in rheumatoid arthritis (RA). Clinical remission is typically defined by a combination of low tender and swollen joint count, patient reported outcomes, and inflammatory biomarkers in RA patients. However, many patients classified as in clinical remission, with an absence of painful, tender or swollen joints on clinical exam, have evidence of "sub-clinical inflammation" present on MRI or ultrasound (26). Unfortunately, a subset of these patients continue to have worsening radiographic damage scores and progressive disability (27, 28). Cross-sectional evidence of patients in remission with inflammation, visualized on ultrasound, showed an altered trabecular bone mineral density as measured by HR-pQCT when compared with those with no subclinical inflammation (29). While acute inflammation plays an important role in bone repair (30), the significance of sustained subclinical inflammation on bone changes over time is unknown. Therefore, we present a pilot study in which we combined imaging modalities for soft tissue and inflammation (MRI) and bone (HR-pQCT) to determine whether we could provide important pathophysiological information on bone damage progression that is not possible with either imaging modality alone.

Methods

In a preliminary study of nine RA participants recruited based on physician-classified clinical remission, we acquired HR-pQCT (XtremeCTII, Scanco Medical, Brüttisellen, Switzerland) images of the 2nd and 3rd metacarpophalangeal (MCP) joints and MR images (1.5T Optima MR430s, GE Healthcare) of 2nd to 5th MCP joints of the same hand at baseline and 6-month follow-up. The combination of HR-pQCT and a 6-month follow-up was selected because previous research has demonstrated that bone changes may be detected with HR-pQCT as early as three- to 6-months (31); thus, HR-pQCT would provide the resolution necessary to image these changes. MR sequences included T1-weighted sequence with and without fat saturation using the Dixon method in the coronal and axial plane as well as a short tau inverted recovery (STIR) sequence in the coronal plane, and a repeat of T1-weighted sequences after administration of gadolinium contrast. Approval for all procedures was obtained from the Conjoint Health Research Ethics Board at the University of Calgary (REB17-0188).

Three-dimensional (3D) volumetric joint space width (JSW; volume, minimum, maximum, and mean) was quantified on HR-pQCT images (5). Erosion volume was quantified on HR-pQCT images at baseline and follow-up using the Medical Image Analysis Framework [MIAF, University of Erlangen; (6)]. A radiologist (PS) scored bone marrow edema, synovitis and erosions on MR images using the RAMRIS scoring system (13). A multi-modal image registration technique was adapted and employed to register and transform the MR image to be overlaid with the HR-pQCT image at each timepoint (32) (**Supplementary Figure 1**). On HR-pQCT images, a trained observer (SB) followed Study grouP for x-trEme Computed Tomography in Rheumatoid Arthritis (SPECTRA) guidelines for the definition of a bone erosion (33): a cortical break observed in two consecutive slices and two orthogonal planes. Bone marrow edema and erosion volume changes were confirmed by visual inspection after superimposition of HR-pQCT and MRI images.

Statistical analysis was completed using R (v3.4.3) in RStudio v1.1.423. To examine group-level time effects, the Wilcoxon rank sum test was used for clinical outcomes and RAMRIS scores, while a non-parametric marginal model for longitudinal designs [nparLD package in R (34)] was used for total erosion volume and JSW. Significance was observed if $p < 0.05$. Changes in erosion volume and JSW at the individual joint level were evaluated against the least significant change (LSC) (35), which was calculated based on previous scan-rescan reproducibility work (36). Using the LSC criteria, participants were classified in one of three groups for each outcome measure: a significant decrease, stable, or a significant increase (20). Results are presented as median and interquartile range (IQR) unless otherwise indicated.

Results

Clinical Outcomes

The nine participants (4 females and 5 males) in clinical remission [DAS28CRP 1.75 (1.63–2.6)], ESR 7 (3–11), CRP

3.4 (1.1–4.2), were 62 (59–63) years old, and had been diagnosed with RA for 7.8 (5.1–8.0) years. All participants were being treated with conventional disease-modifying anti-rheumatic drugs (DMARDs; methotrexate, sulfasalazine, and/or hydroxychloroquine), six with biologic DMARDs (3 with adalimumab, 1 golimumab, 1 abatacept, 1 rituximab), 1 with denosumab (a biologic non-DMARD) and 1 with 2.5 mg bi-daily prednisone.

Group level results are presented for those in clinical remission only. Over the 6-month follow-up, there was a significant improvement in patient global assessment (−1 improvement on a 1–10 scale, IQR −2 to 0, $p = 0.03$). There were trends toward further improvements in DAS28 (−0.42 IQR −0.82 to −0.03, $p = 0.07$), Jebsen Taylor Hand Function test z-score (−0.8 IQR −1.2 to −0.3, $p = 0.08$), HAQ score (−0.12, IQR −0.50 to −0.26, $p = 0.09$), the self-reported Disabilities of the Arm, Shoulder, and Hand questionnaire (DASH, −7.5, IQR −11.4 to 0, $p = 0.08$) and pain (−1 improvement on a 1–10 scale, IQR −2 to 0, $p = 0.06$).

HR-pQCT Outcomes

The analysis for JSW and erosions was performed on the acquired HR-pQCT of the 2nd and 3rd MCP joints; however, for both analyses, the same two participants were excluded due to motion (4 joints) and 2 additional joints from two separate participants could not be segmented accurately. Therefore, a total of 12 joints were analyzed across 7 participants. At the group level, there were no significant changes over time in any of the joint space outcomes ($p > 0.05$). When compared with the LSC, the joint space parameters remained stable except for one patient who showed a decrease in minimum joint space width (−0.42 mm) in one joint.

Across the 12 joints from 7 participants, 19 erosions were found to range in size from 0.19 mm^3 to 93.11 mm^3. Ten erosions were identified at the 2nd MCP, and 9 erosions identified at the 3rd MCP. At the group level, there were no significant changes in the total erosion volume per joint ($p = 0.11$). When compared against the LSC, 5 patients had erosion volumes that stayed stable in 10 joints, one patient had a decrease in total erosion volume (−2.3 mm^3) in one joint, and one participant had an increase in erosion volume (+2.1 mm^3) in one joint. These changes can be visualized with longitudinal image registration (**Figure 2**).

MRI Outcomes

The RAMRIS total score across MCP joints 2–5 for all 9 patients in clinical remission was 3.0 (1–6) for synovitis, 2.0 (1–2) for bone marrow edema, and 2 (2–4) for erosions at baseline. At follow-up the mean total scores were 5 (3–6) for synovitis, 2 (1–5) for bone marrow edema, and 3 (2–6) for erosions. There were no significant differences ($p > 0.05$) in RAMRIS scores between baseline and follow-up for synovitis, edema, or erosions.

When looking at the 2nd and 3rd MCPs only, at baseline, 1 joint had no evidence of synovitis while 9 joints had a synovitis score of 1 (mild), and 8 joints had a synovitis score of 2 (moderate). Over the 6-month period, 9 joints were scored as stable, 5 joints had an increase of 1, 1 joint had an increase of 2, and 3 joints had a decrease in synovitis.

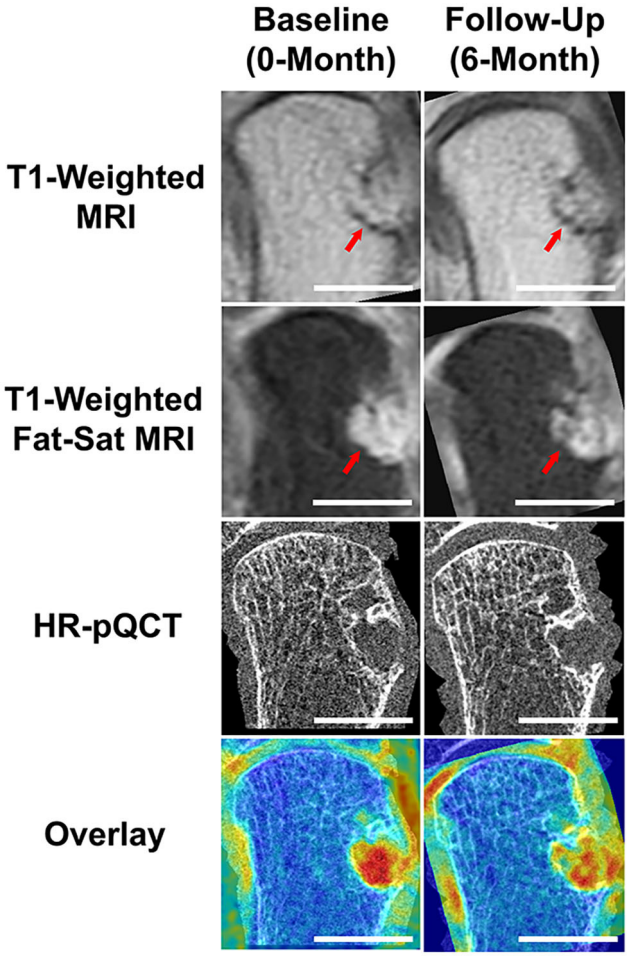

FIGURE 1 | Results demonstrating the benefits of multi-modal imaging. Using MRI and RAMRIS scoring, this RA participant was noted to have a dramatic increase in bone erosion score during their 6-month follow-up, when compared to their baseline score. The post-contrast (Gd) T1-weighted MRI visually displays a larger erosion in the follow-up image (note red arrows). Through accurate image co-registration and overlay, we can observe that the increase in bone erosion score may be due to the differences in positioning during acquisition. While the post-contrast, fat-saturated T1-weighted MRIs display a difference in intensities, the HR-pQCT demonstrates an almost identical erosion size. The Overlay demonstrates the addition of the T1-weighted MRI overlaid with the respective, co-registered HR-pQCT scans. Scalebars represent 1 cm.

For bone edema at baseline in the 2nd and 3rd MCPs, 10 joints had no edema at either the proximal phalange or distal metacarpal, and 8 joints had an edema score of 1 (which represents a volume of bone infiltration between 1 and 33% by the edema). Over the 6-month period, 11 joints had stable bone edema status, while 5 joints showed an increase in edema, and 2 joints showed a decrease in edema.

For the baseline erosions scored on MRI, 9 participants had evidence of erosions on the 2nd MCP. Eight of these had an erosion score of 1 (1–10% of bone covered by erosion) and one bone had an erosion score of 2 (11–20% bone covered

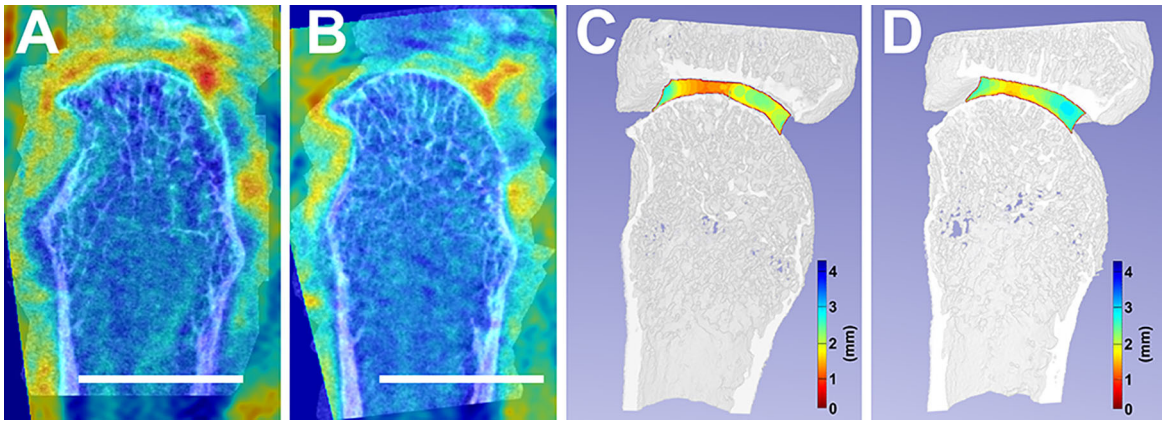

FIGURE 2 | Accurate image co-registration between a selected individual's baseline, 0-month **(A)**, and follow-up, 6-month **(B)** facilitated the overlay between their MRI and HR-pQCT. This image co-registration allows for the consistent analysis of the same areas-of-interest between timepoints. Additionally, joint space width changes from baseline **(C)** to follow-up **(D)** are compared. White scalebars represent 1 cm.

by erosion). For the 3rd MCP, 4 participants had evidence of erosions with 3 having a score of 1, and 1 participant having a score of 2. Over the 6-month period, 12 joints had stable erosion scores on MRI while 2 joints showed decreases and 4 joints showed increases.

Relationship Between MRI and HR-pQCT Outcomes

One participant with no evidence of bone marrow edema or synovitis near the site of the erosion underwent a significant decrease in erosion volume, assessed by HR-pQCT, over the 6-month follow-up. This was also consistent with a decrease in MRI erosion score. In contrast, all participants who presented with MRI-evidence of inflammation within the joints maintained no change in erosion volume over the 6-month follow-up, similarly to those in clinical remission.

At the group level, baseline bone marrow edema was not associated with increased erosion volume, however the participant with the largest increase in erosion volume also demonstrated progression in the bone marrow edema score. In addition, more participants had changes in erosion severity when evaluated by MRI than by HR-pQCT (**Figure 1**).

One participant had a significant decrease in minimum JSW (**Figure 2**). This participant had a synovitis score of 2 at baseline which decreased over 6-months, but also demonstrated a decrease in ESR, a moderate EULAR DAS28 response, and a large decrease in HAQ and pain.

DISCUSSION

We have presented the benefits of a multi-modal imaging approach through our ability to now localize how synovitis and bone marrow edema affect bone damage in RA patients. This was achieved by using accurate image registration, to facilitate improved reproducibility by adjusting for differences in positioning between scans and accurately mapping soft tissues and inflammation onto bone. In addition, we observed discordances in erosion changes assessed by HR-pQCT and MRI. The higher spatial resolution of the HR-pQCT images, combined with longitudinal registration allowed us to detect bone changes with greater sensitivity and reproducibility (19, 37, 38)—emphasizing the utility of multi-modal imaging approaches to fully understand all the tissue types involved in the progression of a disease.

While we have shown the utility of HR-pQCT for research purposes, its applicability as routine imaging in clinical studies remains unknown. Motion artifact due to patient motion during acquisitions can result in missing data. While we implemented an overlapping stacking process, which significantly reduced the need to discard scans due to motion artifact, rather than eliminating the artifact, this process simply smoothed the data (36). Currently, we have begun exploring implementing established motion correction algorithms that will increase the usability of acquired data (39, 40). Additionally, recent research has shown that the current SPECTRA defined bone erosion definition may result in the under-estimation of the number of bone erosions, when compared to histological evaluation (41). It should be noted that while we propose the implementation of HR-pQCT to measure disease progress in the research setting, the extra scanning will unavoidably increase radiation dose to the patient; however, a single HR-pQCT scan is < 20 μSv, which equates to a third of the radiation dose one would receive on a transcontinental flight. Regardless, the impact of the multi-modal imaging and in-depth erosion evaluation measures on clinical outcomes needs to be determined. Thus, a larger sample size, further in-depth analysis, and multiple reader assessments will be required to better understand how individual erosions changed over the time points.

Despite these limitations, the finding of more erosion changes in RAMRIS scores than HR-pQCT was surprising. Two of the joints with erosion progression on MRI had an erosion that

was identified at follow-up but not baseline on MRI; the same erosions were identified but at both times on HR-pQCT. This discrepancy may be the result of differences in positioning on the MRI at baseline and follow-up resulting in the inability to see the small erosion at baseline or the improved sensitivity of HR-pQCT as a tool for erosion identification. Also, there were scans that met our motion scoring criteria, but within the volume of the erosion on HR-pQCT there was motion that appeared to hinder the erosion volume segmentation on HR-pQCT. Finally, an increase of 1 for the RAMRIS erosion equates to only a 10% increase in erosion volume. Despite the increased sensitivity of HR-pQCT, a change of only 10% in the erosion volume would generally not result in a change that exceeds the LSC.

Despite the minimal bone changes observed across the participants over multiple time-points, likely explained by the patients' low disease activity, short follow-up period and sample size, we have presented the benefits of a multi-modal imaging approach that can be utilized to simultaneously visualize, localize, and characterize how synovitis and bone marrow edema may affect bone damage in RA patients. The combination of HR-pQCT and MRI to visualize bone damage and inflammation, respectively, provides the ability to probe mechanistic questions about whether bone loss occurs via an inside-out or outside-in approach (38, 42, 43), as well as how local inflammatory signals lead to bone erosion progression. This multi-modal imaging approach will improve our understanding of the role of both clinical levels of inflammation in arresting bone repair in inflammatory arthritis and the impact that subclinical inflammation has on bone damage progression. In addition, it will allow us to probe the pathophysiological processes that occur at the tissue level in the development and progression of bone damage, and the mechanisms by which treatments halt or repair bone damage, further increasing our understanding of the etiology and pathophysiology of diseases.

Overall, multi-modal imaging can be combined synergistically with functional and biochemical imaging. Examples of other applications include combining CT with positron emission tomography (PET). PET/CT using 2-deoxy-2[18F]fluoro-d-glucose (FDG) to visualize glucose metabolism has been has recently been used to investigate increased glycolysis due to inflammation in inflammatory arthritis, demonstrating correlations between metabolic markers identified with PET and clinical diseases activity in rheumatoid arthritis (44), and between PET activity score and inflammation score on MRI in patients with sacroiliitis in spondylarthropathy (45). Further, PET uptake predicts radiographic progression in RA (46). PET-MRI techniques are also emerging to investigate musculoskeletal disease, which allow linkage of bone metabolic activity with high levels of soft tissue contrast (47, 48), demonstrating that sites of synovitis and tenosynovitis identified on MRI are linked to increased FDG uptake.

Multi-modal imaging enables investigation of underlying tissue pathology using non-invasive techniques. Advances in hardware and software have enabled unprecedented spatial and contrast resolution. Combined with image registration and other image processing techniques, multi-modal imaging provides the great potential to study the mechanisms underlying tissue changes in inflammatory arthritis that otherwise would not be possible with any single imaging technique alone.

DATA AVAILABILITY STATEMENT

The raw data supporting the conclusions of this article will be made available by the authors, without undue reservation.

ETHICS STATEMENT

The studies involving human participants were reviewed and approved by Conjoint Health Research Ethics Board at the University of Calgary. The patients/participants provided their written informed consent to participate in this study.

AUTHOR CONTRIBUTIONS

PS, GH, CB, and SM contributed conception and design of the study. SB, CB, and SM acquired the data. SB and JT performed data analysis. JT and SM drafted the manuscript. All authors contributed to manuscript revision, read, and approved the submitted version.

FUNDING

This study was supported by the McCaig Institute for Bone and Joint Health Encore Catalyst Grant. JT received salary support from the T. Chen Fong Post-doctoral Fellowship. SB received salary support from the Natural Sciences and Engineering Research Council of Canada. SM received support from the Arthritis Society Stars Early Career Investigator Award (STAR-18-0189). GH was supported by a Canadian Institute for Health Research (CIHR) New Investigator Salary Award.

ACKNOWLEDGMENTS

We would like to thank the Rheum4U Investigators and Team for assistance with recruitment, our imaging technicians Anne Cooke, Stephanie Kwong and Irene Pauchard for image acquisition, and Shaheer Chishti for assistance with image processing.

SUPPLEMENTARY MATERIAL

The Supplementary Material for this article can be found online at: https://www.frontiersin.org/articles/10.3389/fmed.2020.545097/full#supplementary-material

Supplementary Figure 1 | Workflow for MRI-HR-pQCT image registration. **(A)** The T1-weighted MRI and HR-pQCT images are landmarked using common anatomy and the T1-weighted image is registered to the HR-pQCT image space. **(B)** The transformation is then applied to the contrast enhanced fat-saturated MRI image and **(C)** overlaid with the HR-pQCT image. A color map can be applied to visualize areas of inflammation (red) in relationship to the bone damage.

Supplementary Table 1 | Overall demographic parameters outlining our participants (top), and changes in their patient- and clinical-reported outcomes after 6-months (bottom). DAS, Disease Activity Score; ESR, Erythrocyte

Sedimentation Rate; CRP, C-Reactive Protein; JTHF, Jebsen-Taylor Hand Function Test; HAQ, Health Assessment Questionnaire; DASH, Disabilities of the Arm, Shoulder, and Hand. Values are reported as mean (range) unless reported otherwise [i.e., mean (IQR)].

Supplementary Table 2 | Reported outcomes from HR-pQCT and MRI displaying the changes in erosions and joint space width, as calculated from HR-pQCT, and RAMRIS score (i.e., synovitis, bone marrow edema, and erosions) as calculated from MRI. Values are reported as mean (IQR) unless noted otherwise.

REFERENCES

1. Boutroy S, Bouxsein ML, Munoz F, Delmas PD. *In vivo* assessment of trabecular bone microarchitecture by high-resolution peripheral quantitative computed tomography. *J Clin Endocrinol Metab.* (2005) 90:6508–15. doi: 10.1210/jc.2005-1258
2. Burghardt AJ, Lee CH, Kuo D, Majumdar S, Imboden JB, Lin TM, et al. Quantitative *in vivo* HR-pQCT imaging of 3D wrist and metacarpophalangeal joint space width in rheumatoid arthritis. *Ann Biomed Eng.* (2013) 41:2553–64. doi: 10.1007/s10439-013-0871-x
3. Kroker A, Zhu Y, Manske SL, Barber R, Mohtadi N, Boyd SK. Quantitative *in vivo* assessment of bone microarchitecture in the human knee using HR-pQCT. *Bone*. (2017) 97:43–8. doi: 10.1016/j.bone.2016.12.015
4. Manske SL, Zhu Y, Sandino C, Boyd SK. Human trabecular bone microarchitecture can be assessed independently of density with second generation HR-pQCT. *Bone.* (2015) 79:213–21. doi: 10.1016/j.bone.2015.06.006
5. Stok KS, Burghardt AJ, Boutroy S, Peters MPH, Manske SL, Stadelmann V, et al. Consensus approach for 3D joint space width of metacarpophalangeal joints of rheumatoid arthritis patients using high-resolution peripheral quantitative computed tomography. *Quanti Imaging Med Surg.* (2020) 10:314–25. doi: 10.21037/qims.2019.12.11
6. Topfer D, Finzel S, Museyko O, Schett G, Engelke K. Segmentation and quantification of bone erosions in high-resolution peripheral quantitative computed tomography datasets of the metacarpophalangeal joints of patients with rheumatoid arthritis. *Rheumatology.* (2014) 53:65–71. doi: 10.1093/rheumatology/ket259
7. Peters M, de Jong J, Scharmga A, van Tubergen A, Geusens P, Loeffen D, et al. An automated algorithm for the detection of cortical interruptions and its underlying loss of trabecular bone; a reproducibility study. *BMC Med imaging.* (2018) 18:13. doi: 10.1186/s12880-018-0255-7
8. Kocijan R, Finzel S, Englbrecht M, Engelke K, Rech J, Schett G. Decreased quantity and quality of the periarticular and nonperiarticular bone in patients with rheumatoid arthritis: a cross-sectional HR-pQCT study. *J Bone Mineral Res.* (2014) 29:1005–14. doi: 10.1002/jbmr.2109
9. Klose-Jensen R, Tse JJ, Keller KK, Barnabe C, Burghardt AJ, Finzel S, et al. High-resolution peripheral quantitative computed tomography for bone evaluation in inflammatory rheumatic disease. *Front Med Rheumatol.* (2020) 7:337. doi: 10.3389/fmed.2020.00337
10. Ohrndorf S, Halbauer B, Martus P, Reiche B, Backhaus TM, Burmester GR, et al. detailed joint region analysis of the 7-joint ultrasound score: evaluation of an arthritis patient cohort over one year. *Int J Rheumatol.* (2013) 2013:493848. doi: 10.1155/2013/493848
11. Backhaus M, Ohrndorf S, Kellner H, Strunk J, Backhaus TM, Hartung W, et al. Evaluation of a novel 7-joint ultrasound score in daily rheumatologic practice: a pilot project. *Arthritis Rheum.* (2009) 61:1194–201. doi: 10.1002/art.24646
12. Ihnatsenka B, Boezaart AP. Ultrasound: basic understanding and learning the language. *Int J Shoulder Surg.* (2010) 4:55–62. doi: 10.4103/0973-6042.76960
13. Ostergaard M, Peterfy C, Conaghan P, McQueen F, Bird P, jbjerg B, et al. OMERACT rheumatoid arthritis magnetic resonance imaging studies. Core set of MRI acquisitions, joint pathology definitions, and the OMERACT RA-MRI scoring system. *J Rheumatol.* (2003) 30:1385–6.
14. Østergaard M, Peterfy CG, Bird P, Gandjbakhch F, Glinatsi D, Eshed I, et al. The OMERACT rheumatoid arthritis Magnetic Resonance Imaging (MRI) scoring system: updated recommendations by the OMERACT MRI in arthritis working group. *J Rheumatol.* (2017) 44:1706–12. doi: 10.3899/jrheum.161433
15. Ostergaard M, McQueen F, Wiell C, Bird P, Boyesen P, Ejbjerg B, et al. The OMERACT psoriatic arthritis magnetic resonance imaging scoring system (PsAMRIS): definitions of key pathologies, suggested MRI sequences, and preliminary scoring system for PsA hands. *J Rheumatol.* (2009) 36:1816–24. doi: 10.3899/jrheum.090352
16. Klein S, Staring M, Murphy K, Viergever MA, Pluim JP. elastix: a toolbox for intensity-based medical image registration. *IEEE Trans Med Imaging.* (2010) 29:196–205. doi: 10.1109/TMI.2009.2035616
17. Mattes D, Haynor D, Vesselle H, Lewellyn T, Eubank W. Nonrigid multimodality image registration. *Med Imaging.* (2001) 4322:1–12. doi: 10.1117/12.431046
18. Alam F, Rahman SU, Khusro S, Ullah S, Khalil A. Evaluation of medical image registration techniques based on nature and domain of the transformation. *J Med Imaging Rad Sci.* (2016) 47:178–93. doi: 10.1016/j.jmir.2015.12.081
19. Ellouz R, Chapurlat R, van Rietbergen B, Christen P, Pialat JB, Boutroy S. Challenges in longitudinal measurements with HR-pQCT: evaluation of a 3D registration method to improve bone microarchitecture and strength measurement reproducibility. *Bone.* (2014) 63:147–57. doi: 10.1016/j.bone.2014.03.001
20. Topfer D, Gerner B, Finzel S, Kraus S, Museyko O, Schett G, et al. Automated three-dimensional registration of high-resolution peripheral quantitative computed tomography data to quantify size and shape changes of arthritic bone erosions. *Rheumatology.* (2015) 54:2171–80. doi: 10.1093/rheumatology/kev256
21. Peters M, van den Bergh JP, Geusens P, Scharmga A, Loeffen D, Weijers R, et al. Prospective follow-up of cortical interruptions, bone density, and micro-structure detected on HR-pQCT: a study in patients with rheumatoid arthritis and healthy subjects. *Calcif. Tissue Int.* (2019) 104:571–81. doi: 10.1007/s00223-019-00523-2
22. Christen P, Muller R. *In vivo* visualisation and quantification of bone resorption and bone formation from time-lapse imaging. *Curr Osteoporos Rep.* (2017) 15:311–17. doi: 10.1007/s11914-017-0372-1
23. Brunet SC, Bhatla JL, Lemay S, Pauchard Y, Salat P, Barnabe C, et al. The utility of multi-stack alignment and 3D longitudinal image registration to assess bone remodeling in rheumatoid arthritis patients from second generation HR-pQCT scans. *BMC Med Imaging.* (2019) 20:1–20. doi: 10.21203/rs.2.14575/v3
24. Studholme C, Hill DLG, Hawkes DJ. An overlap invariant entropy measure of 3D medical image alignment. *Pattern Recognit.* (1999) 32:71–86. doi: 10.1016/S0031-3203(98)00091-0
25. Maes F, Collignon A, Vandermeulen D, Marchal G, Suetens P. Multimodality image registration by maximization of mutual information. *IEEE Trans Med Imaging.* (1997) 16:187–98. doi: 10.1109/42.563664
26. Brown AK, Quinn MA, Karim Z, Conaghan PG, Peterfy CG, Hensor E, et al. Presence of significant synovitis in rheumatoid arthritis patients with disease-modifying antirheumatic drug-induced clinical remission: evidence from an imaging study may explain structural progression. *Arthritis Rheumat.* (2006) 54:3761–73. doi: 10.1002/art.22190
27. Brown AK, Conaghan PG, Karim Z, Quinn MA, Ikeda K, Peterfy GC, et al. An explanation for the apparent dissociation between clinical remission and continued structural deterioration in rheumatoid arthritis. *Arthritis Rheumat.* (2008) 58:2958–67. doi: 10.1002/art.23945
28. Forslind K, Svensson B. MRI evidence of persistent joint inflammation and progressive joint damage despite clinical remission during treatment of early rheumatoid arthritis. *Scand J Rheumatol.* (2016) 45:99–102. doi: 10.3109/03009742.2015.1070902
29. Kong S, Locrelle H, Amouzougan A, Denarie D, Collet P, Pallot-Prades B, et al. Remaining local subclinical joint inflammation is associated with deteriorated metacarpeal head bone microarchitecture in rheumatoid arthritis patients low disease activity. *Joint Bone Spine.* (2018) 85:569–72. doi: 10.1016/j.jbspin.2017.11.010
30. Claes L, Recknagel S, Ignatius A. Fracture healing under healthy and inflammatory conditions. *Nat Rev Rheumatol.* (2012) 8:133–43. doi: 10.1038/nrrheum.2012.1

31. Shimizu T, Choi HJ, Heilmeier U, Tanaka M, Burghardt AJ, Gong J, et al. Assessment of 3-month changes in bone microstructure under anti-TNFα therapy in patients with rheumatoid arthritis using high-resolution peripheral quantitative computed tomography (HR-pQCT). *Arthritis Res Ther.* (2017) 19:222. doi: 10.1186/s13075-017-1430-x
32. Kroker A, Besler BA, Bhatla JL, Shtil M, Salat P, Mohtadi N, et al. Longitudinal effects of acute anterior cruciate ligament tears on peri-articular bone in human knees within the first year of injury. *J Orthop Res.* (2019) 37:2325–36. doi: 10.1002/jor.24410
33. Barnabe C, Toepfer D, Marotte H, Hauge EM, Scharmga A, Kocijan R, et al. Definition for rheumatoid arthritis erosions imaged with high resolution peripheral quantitative computed tomography and interreader reliability for detection and measurement. *J Rheumatol.* (2016) 43:1935–40. doi: 10.3899/jrheum.160648
34. Noguchi K, Gel Y, Brunner E, Konietschke F. nparLD: an R software package for the nonparametric analysis of longitudinal data in factorial experiments. *J Stat Softw.* (2012) 50:1–23. doi: 10.18637/jss.v050.i12
35. Shepherd JA, Lu Y. Ageneralized least significant change for individuals measured on different DXA systems. *J Clin Densitom.* (2007) 10:249–58. doi: 10.1016/j.jocd.2007.05.002
36. Brunet SC, Finzel S, Engelke K, Boyd SK, Barnabe C, Manske SL. Bone changes assessed with High-Resolution peripheral Quantitative Computed Tomography (HR-pQCT) in early inflammatory arthritis: a 12-month cohort study. *Joint Bone Spine.* (in press). doi: 10.1016/j.jbspin.2020.07.014
37. Nishiyama KK, Pauchard Y, Nikkel LE, Iyer S, Zhang C, McMahon DJ, et al. Longitudinal HR-pQCT and image registration detects endocortical bone loss in kidney transplantation patients. *J Bone Mineral Res.* (2015) 30:554–61. doi: 10.1002/jbmr.2358
38. Schett G, Gravallese E. Bone erosion in rheumatoid arthritis: mechanisms, diagnosis and treatment. *Nat Rev Rheumatol.* (2012) 8:656–64. doi: 10.1038/nrrheum.2012.153
39. Sisniega A, Thawait GK, Shakoor D, Siewerdsen JH, Demehri S, Zbijewski W. Motion compensation in extremity cone-beam computed tomography. *Skelet Radiol.* (2019) 48:1999–2007. doi: 10.1007/s00256-019-03241-w
40. Sisniega A, Stayman JW, Yorkston J, Siewerdsen JH, Zbijewski W. Motion compensation in extremity cone-beam CT using a penalized image sharpness criterion. *Phys Med Biol.* (2017) 62:3712–34. doi: 10.1088/1361-6560/aa6869
41. Scharmga A, Keller KK, Peters M, van Tubergen A, van den Bergh JP, van Rietbergen B, et al. Vascular channels in metacarpophalangeal joints: a comparative histologic and high-resolution imaging study. *Sci Rep.* (2017) 7:8966. doi: 10.1038/s41598-017-09363-2
42. Jimenez-Boj E, Nobauer-Huhmann I, Hanslik-Schnabel B, Dorotka R, Wanivenhaus AH, Kainberger J, et al. Bone erosions and bone marrow edema as defined by magnetic resonance imaging reflect true bone marrow inflammation in rheumatoid arthritis. *Arthritis Rheumat.* (2007) 56:1118–24. doi: 10.1002/art.22496
43. van den Bergh J, Geusens P. Bone erosions in rheumatoid arthritis. *Rheumatology*. (2013) 53:4–5. doi: 10.1093/rheumatology/ket358
44. Raynor WY, Jonnakuti VS, Zirakchian Zadeh M, Werner TJ, Cheng G, Zhuang H, et al. Comparison of methods of quantifying global synovial metabolic activity with FDG-PET/CT in rheumatoid arthritis. *Int J Rheum Dis.* (2019) 22:2191–8. doi: 10.1111/1756-185X.13730
45. Raynal M, Bouderraoui F, Ouichka R, Melchior J, Morel O, Blum A, et al. Performance of (18)F-sodium fluoride positron emission tomography with computed tomography to assess inflammatory and structural sacroiliitis on magnetic resonance imaging and computed tomography, respectively, in axial spondyloarthritis. *Arthritis Res Ther.* (2019) 21:119. doi: 10.1186/s13075-019-1903-1
46. Suto T, Yonemoto Y, Okamura K, Okura C, Kaneko T, Kobayashi T, et al. Predictive factors associated with the progression of large-joint destruction in patients with rheumatoid arthritis after biologic therapy: a *post-hoc* analysis using FDG-PET/CT and the ARASHI (assessment of rheumatoid arthritis by scoring of large-joint destruction and healing in radiographic imaging) scoring method. *Mod Rheumatol.* (2017) 27:820–7. doi: 10.1080/14397595.2016.1266132
47. Kogan F, Broski SM, Yoon D, Gold GE. Applications of PET-MRI in musculoskeletal disease. *J Magn Reson Imaging.* (2018) 48:27–47. doi: 10.1002/jmri.26183
48. Miese F, Scherer A, Ostendorf B, Heinzel A, Lanzman RS, Kropil P, et al. Hybrid 18F-FDG PET-MRI of the hand in rheumatoid arthritis: initial results. *Clin Rheumatol.* (2011) 30:1247–50. doi: 10.1007/s10067-011-1777-3

Conflict of Interest: The authors declare that the research was conducted in the absence of any commercial or financial relationships that could be construed as a potential conflict of interest.

frontiers in Medicine

ORIGINAL RESEARCH
published: 25 September 2020
doi: 10.3389/fmed.2020.539870

Cartilage Degradation in Psoriatic Arthritis Is Associated With Increased Synovial Perfusion as Detected by Magnetic Resonance Imaging

Daniel B. Abrar[1†], Christoph Schleich[1†], Anja Müller-Lutz[1], Miriam Frenken[1], K. Ludger Radke[1], Stefan Vordenbäumen[2], Matthias Schneider[2], Benedikt Ostendorf[2] and Philipp Sewerin[2]*

[1] Department of Diagnostic and Interventional Radiology, Medical Faculty, University Dusseldorf, Düsseldorf, Germany,
[2] Department and Hiller Research Unit for Rheumatology, UKD, Heinrich Heine University Düsseldorf, Düsseldorf, Germany

OPEN ACCESS

Edited by:
Raj Sengupta,
Royal National Hospital for Rheumatic Diseases, United Kingdom

Reviewed by:
Cheng-De Yang,
Shanghai Jiao Tong University, China
Raul Antonio Castellanos-Moreira,
Hospital Clínic de Barcelona, Spain

***Correspondence:**
Philipp Sewerin
philipp.sewerin@med.uni-duesseldorf.de

[†]These authors have contributed equally to this work

Specialty section:
This article was submitted to Rheumatology, a section of the journal Frontiers in Medicine

Received: *02 March 2020*
Accepted: *21 August 2020*
Published: *25 September 2020*

Citation:
Abrar DB, Schleich C, Müller-Lutz A, Frenken M, Radke KL, Vordenbäumen S, Schneider M, Ostendorf B and Sewerin P (2020) Cartilage Degradation in Psoriatic Arthritis Is Associated With Increased Synovial Perfusion as Detected by Magnetic Resonance Imaging. Front. Med. 7:539870. doi: 10.3389/fmed.2020.539870

Objective: Even though cartilage loss is a known feature of psoriatic arthritis (PsA), research is sparse on its role in the pathogenesis of PsA and its potential use for disease detection and monitoring. Using delayed gadolinium-enhanced magnetic resonance imaging of cartilage (dGEMRIC) and dynamic contrast-enhanced MRI (DCE MRI), research has shown that early cartilage loss is strongly associated with synovial inflammation in rheumatoid arthritis (RA). The aim of this study was to determine if acute inflammation is associated with early cartilage loss in small finger joints of patients with PsA.

Methods: Metacarpophalangeal (MCP), proximal interphalangeal (PIP), and distal interphalangeal (DIP) joints of 17 patients with active PsA were evaluated by high-resolution 3 Tesla dGEMRIC and DCE MRI using a dedicated 16-channel hand coil. Semi-quantitative and quantitative perfusion parameters were calculated. Images were analyzed by two independent raters for dGEMRIC indices, PsA MRI scores (PsAMRIS), total cartilage thickness (TCT), and joint space width (JSW).

Results: We found significant negative correlations between perfusion parameters (except K_{ep}) and dGEMRIC indices, with the highest value at the MCP joints (K_{Trans}: $\tau = -0.54$, $p = 0.01$; K_{ep}: $\tau = -0.02$, $p = 0.90$; IAUC: $\tau = -0.51$, $p = 0.015$; Initial Slope: $\tau = -0.54$, $p = 0.01$; Peak: $\tau = -0.67$, $p = 0.002$). Heterogeneous correlations were detected between perfusion parameters and both, total PsAMRIS and PsAMRIS synovitis sub-scores. No significant correlation was seen between any perfusion parameter and JSW and/or TCT.

Conclusion: As examined by DCE MRI and dGEMRIC, there is a potential association between early cartilage loss and acute synovial inflammation in small finger joints of PsA patients.

Keywords: psoriatic arthritis, magnetic resonance imaging, dGEMRIC, cartilage, compositional imaging

INTRODUCTION

Psoriatic arthritis (PsA) is a chronic autoimmune disease that ultimately leads to joint destruction and functional disability (1). As in rheumatoid arthritis (RA), early diagnosis and treatment are pivotal for a better clinical outcome (2, 3). Therefore, treat-to-target (T2T) strategies have been introduced for the treatment of PsA (4, 5). Even though magnetic resonance imaging is not yet included in the classification criteria for PsA (CASPAR), it becomes increasingly important for the early detection and monitoring of disease-related joint changes (6–8). In 2009, the Outcome Measures in Rheumatology Clinical Trials (OMERACT) working group introduced a semi-quantitative PsA MRI score (PsAMRIS) that evaluates metacarpophalangeal (MCP), proximal (PIP), and distal interphalangeal joints concerning the osteodestructive (bone erosion), osteoproliferative (bone proliferation), and acute inflammatory (synovitis, flexor tenosynovitis, periarticular inflammation) features of PsA (9). Several studies have shown that the degree of synovial contrast enhancement in arthritic joints can be quantified by dynamic contrast-enhanced MRI (DCE MRI), and hence, have found a strong correlation between the synovitis sub-score of PsAMRIS and RA MRI score (RAMRIS) and DCE MRI parameters (10–12). Furthermore, elevated synovial perfusion assessed by DCE MRI reflects histological findings of acute synovitis (13). Even though cartilage damage is a known feature of PsA, research is sparse on its value in the pathogenesis and the disease course (14). That is why it is not included in the PsAMRIS as opposed to its RA equivalent (15). Several studies using delayed gadolinium-enhanced MRI of cartilage (dGEMRIC) have shown that early cartilage loss in RA is associated with the severity of synovitis (10, 16). dGEMRIC is a histologically validated and robust method that depicts proteoglycan loss in cartilage by measurement of fixed-charge density (17, 18). Proteoglycans have negatively charged side chains that allow for the inversely proportional penetration of similarly negatively charged contrast agent molecules (e.g., gadolinium) following intravenous administration. Consequently, proteoglycan depletion leads to an accumulation of gadolinium ions in degenerated cartilage.

However, the placement of region of interests in small joints is difficult using conventional MRI or with high-resolution MRI surface coils. We, therefore, used a 16-channel high-resolution hand coil to allow for an improved evaluation of smaller joints.

Herein, we set out to evaluate if there was any association between acute inflammation and early cartilage loss in small finger joints of patients with PsA.

METHODS

Study Population

Seventeen patients with PsA (mean age 53.7 ± 11.6; minimum/maximum 26/72 years, male/female 9/8) fulfilling the CASPAR criteria, mean disease duration 4 ± 3.6 years, and suffering from peripheral joint involvement of at least two MCP joints and dactylitis of at least one finger were prospectively recruited for the "Analysis of the DActylic Melange" (ADAM) research initiative. All patients had failed methotrexate (MTX) monotherapy and were escalated to etanercept therapy after a baseline MRI scan. Patient recruitment took place in the Department of Rheumatology from 06/ 2015 to 01/ 2017. The same study population has been included in a different study. However, this study has been published as a pre-print only (19).

The study was approved by the local ethics committee (study number: 4962R, "Analysis of the Dactylitic Melange (ADAM): Defining the morphological components of dactylitis in psoriatic arthritis and their responsiveness to etanercept therapy). Written and informed consent was obtained from all patients before initiation of the study. The Disease Activity Score 28 (DAS 28) was 2.42 ± 0.72 (range 1.8–4.3, median 2.2). C-reactive protein (CRP) levels were 0.87 ± 1.35 mg/dl (range 0.1–5.8 mg/dl, median 0.3 mg/dl).

MR Imaging

A 3T MRI scanner (Magentom Skyra, Siemens Healthineers, Erlangen, Germany) and a dedicated 16-channel hand coil (3T Tim Coil [receive only], Siemens Healthineers, Erlangen, Germany) was used for all patients. Patients were imaged in the prone position with their arm extended overhead ("superman position" with palm facing down).

The imaging protocol included coronal T1-weighted turbo spin echo (TSE) sequences before and after intravenous injection of an ionic gadolinium-based contrast agent (Gd-DOTA^{-} [Dotarem, Guerbet Villepinte, France] in double dose, 0.4 mmol/kg bodyweight). The intravenous injection was carried out by an injection pump followed by a saline chaser. Also, non-contrast enhanced, fat-saturated T2-weighted/short tau inversion recovery (STIR) as well as post-contrast fat-saturated T1-weighted sequences in at least two different orthogonal planes were obtained.

Compositional MRI using the dGEMRIC technique of the MCP, PIP, and DIP joints 2–5 was performed 40 min after intravenous contrast-agent administration. To this end, we used a flip-angle three-dimensional gradient-echo (GE) imaging (FLASH) sequence with two excitation flip angles (5° and 26°) as in previously published studies of our institute (17, 20, 21). 40 sagittal slices were acquired perpendicular to the joint surface. Total acquisition time was 2.25 min.

For perfusion imaging, a dynamic T1-weighted GE turbo FLASH sequence and two T1-weighted GE 3D-FLASH sequences with two different flipangles were acquired; the contrast agent was injected 20 s after sequence initiation. Total acquisition time was 7.20 min. B_1 shimming was applied to maximize image quality.

The detailed sequence parameters were as follows:

Coronal T1 turbo spin echo (TSE) (TR/TE 862/27 ms; flip angle 150°; slice thickness 2.5 mm; field of view 140 × 140 mm; imaging matrix: 512 × 512; pixel size 0.3 × 0.3 mm), coronal STIR (TR/TE, 5560/31 ms; flip angle 120°; slice thickness 2.5 mm; 8.0; slice thickness 3.0 mm; field of view 140 × 140 mm; imaging matrix: 448 × 312; pixel size 0.3 × 0.3 mm), sagittal proton density (PD) TSE fat-saturated (TR/TE 3150/47 ms, flip angle 150°, slice thickness 2.5 mm,

field of view 60 × 150 mm; imaging matrix: 448 × 182; pixel size 0.3 × 0.3 mm), transversal T2 TSE fat-saturated (TR/TE 5693.8/89 ms, flip angle 180°, slice thickness 3.0 mm, field of view 160 × 160 mm; imaging matrix: 512 × 358; pixel size 0.3 × 0.3 mm), transversal T1 SE fat-saturated after intravenous (iv) contrast administration (TR/TE 807/16 ms; flip angle 90°; slice thickness 3.0 mm; field of view 130 × 130 mm; imaging matrix: 384 × 288; pixel size 0.3 × 0.3 mm), coronal T1 TSE after iv contrast (TR/TE 862/27 ms; flip angle 150°; slice thickness 2.5 mm; field of view 140 × 140 mm; imaging matrix: 512 × 512; pixel size 0.3 × 0.3 mm), 3D FLASH GE (TR/TE 5.8/1.9 ms; flip angle 5/26°; slice thickness 3.0 mm; field of view 65 × 110 mm; imaging matrix: 384 × 228; pixel size 0.3 × 0.3 mm) and T1 GE Turbo FLASH (TR/TE 5.8 / 1.9 ms; flip angle 5°; slice thickness 3.0 mm; field of view 140 × 140 mm; imaging matrix: 128 × 96; pixel size 1.1 × 1.1 mm).

Image Analysis

MR images were independently read and analyzed by two radiologists (DBA and CS, trained in musculoskeletal imaging with 3 and 8 years experience) and one rheumatologist (PS, trained in musculoskeletal imaging with 8 years of experience) according to the OMCERACT PsAMRIS guidelines (9). In addition, joint space width (JSW; minimal distance in mm between the proximal and distal bone surface) and total cartilage thickness (TCT; sum of the proximal and distal cartilage layer) were measured for each MCP, PIP and DIP joint of finger 2–5. Measurements were performed perpendicular to the subchondral bone in the medial part of the joint using the inbuilt digital caliper tool of the picture archiving and communication system (PACS, Sectra Workstation IDS7, Sectra AB, Linköping, Sweden) on sagittal PDw images.

Perfusion in the MCP, PIP, and DIP joints of finger 2-5 was evaluated with quantitative and semi-quantitative analysis using The DCE Tool (The DCE Tool for ClearCanvas 2.0 SP1, http://thedcetool.com) as described in previously published studies of our institute (10). The quantitative analysis of this tool is based upon the Tofts model (22). Perfusion analysis requires the knowledge of T1 relaxation times. Therefore, the T1w GE 3D FLASH sequence with variable flip angles was used for a pixel-based calculation of the T1 time. For this calculation we applied the following formula:

$$T1\left(x,\ y,\ z\right) = \frac{\mathrm{TR}}{\ln\left[\frac{\sin\left(\alpha 1\right)\cos(\alpha 2) - Q(x,\ y,\ z)\sin(\alpha 2)\cos(\alpha 1)}{\sin\left(\alpha 1\right) - Q\ (x,\ y,\ z)\sin(\alpha 2)}\right)}$$

where

$$Q\ \left(x,\ y,\ z\right) = \frac{S\alpha 1\ \left(x,\ y, z\right)}{S\alpha 2\ \left(x,\ y, z\right)}$$

And $S_{\alpha 1}$ (x, y, z) and $S_{\alpha 2}$ (x, y, z) are the corresponding pixel intensities to flip angles α_1 and α_2. Then, the T1 relaxation was used for the perfusion analysis.

A region of interest (ROI) was placed on the radial and ulnar side of each joint by one reader (DBA). After ROI placement a second reader (CS) confirmed the optimal placement before each measured signal intensity was used to determine a corresponding concentration time curve using the following formula:

$$C_{GD}\ (t) = \frac{\mathrm{S}\ (t) - S_0}{S_0 T_{10} R}$$

where T_{10} is the native T1 time, $R = 4.5\ s^{-1}\ mM^{-1}$ is the relaxivity of the contrast agent, S is the average signal intensity in the ROI and S_0 is the average signal intensity in the ROI in absence of the contrast agent. This Tofts model requires the knowledge of the arterial input function (AIF). AIF can be calculated individually from the blood signal or, alternatively, a population average can be used (22). In this study, we used an analytically described AIF population average that can be used at any temporal resolution (22).

The following perfusions parameters were calculated:

Perfusion parameters are displayed and explained in **Table 1**: K_{Trans}, k_{ep} (quantitative parameters) and IAUC (integral of the signal curve over time), initial slope and peak (semiquantitative parameters).

For compositional analyses of cartilage quality with dGEMRIC, motion correction was applied using STROKETOOL (Digital Image Solutions, Frechen, Germany, http://www.digitalimagesolutions.de) for all images to reduce movement artifacts. This tool has been validated for dGEMRIC analyses of the finger joints and corrects for patient motion between the measurements using a dedicated image registration method (23).

Readers were allowed to adjust the window settings as required to guarantee optimal visualization of the intra- and periarticular structures for ROI placement. T1 maps were analyzed by first defining regions-of-interest (ROIs) on the central sagittal slice. ROI outlines comprising the full thickness of the proximal and distal portion of the articular cartilage of MPC, PIP and DIP joints of finger 2-5 were manually defined on the morphological images of the 3D T1-weighted FLASH sequence with the flip angle of 5° for dGEMRIC. Particular care was taken to exclude artifacts and surrounding structures such as synovial fluid and cortical bone. Consequently, four ROIs were set per digit (i.e., metacarpal, base of proximal phalanx, apex of proximal phalanx, and base of intermediate phalanx) and 16 ROIs per patient (i.e., four ROIs of four digits) and visually checked by the second and third reader to confirm that only cartilage was included. Next, ROIs were copied to the corresponding slices of the color-coded T1 parameter maps. Further analyses involved the pixel-wise calculation post-contrast T1 values as before (17, 24, 25). More specifically, the T1 maps representing the spatially resolved dGEMRIC indices were analyzed in terms of the ROIs as defined above the mean dGEMRIC indices [ms] were recorded. All images were analyzed by two readers (DBA and CS, radiologists) who were blinded for patients' data.

Statistical Analysis

All statistical analyses were performed using SPSS software (IBM, version 22, Armonk, NY, USA). For descriptive analysis mean,

TABLE 1 | Description of quantitative and semi-quantitative perfusion parameters. IAUC: initial area under the curve.

Quantitative parameters		Semi-quantitative parameters		
K_{Trans}	k_{ep}	IAUC	Initial slope	Peak
Transfer constant between EES and blood plasma	KTrans/Ve, V_e: relative volume of EES	Integral of the signal curve over time starting at the onset time (t_{onset}) of the bolus	Slope of the signal curve determined by linear regression within the initial seconds after onset	Maximal signal enhancement

EES, extravascular extracellular space.

standard deviation, minimum, and maximum were calculated. Due to the small sample size and the heterogeneity of our data, non-normal distribution was assumed. For comparison of means, Kruskal-Wallis test and a *post-hoc* Bonferroni test were performed. Correlation analysis was performed between each dGEMRIC indices, total PsAMRIS and all its sub-scores and TCT using the Kendall–Tau correlation coefficient. p-values < 0.05 were considered to be significant.

RESULTS

Descriptive Analysis of dGEMRIC Indices, Perfusion Parameters, JSW, and TCT at MCP and PIP Joints

The descriptive analysis (mean, standard deviation, and range) of dGEMRIC values, quantitative (K_{Trans}, K_{ep}) and semi-quantitative (IAUC, initial slope, peak) perfusion parameters, JSW, and TCT of MCP, PIP, and DIP joints and overall are displayed in **Table 2**.

Perfusion and dGEMRIC maps are shown in **Figure 1**.

Correlation Between Perfusion Parameters and JSW, TCT, Total PsAMRIS, Synovitis Sub-score, dGEMRIC Indices, CRP-Levels, and DAS 28

The correlation between perfusion parameters and JSW, TCT, total PsAMRIS, synovitis sub-score, DAS 28, and dGEMRIC indices is illustrated in **Table 3**.

There was no significant correlation between any perfusion parameter and JSW or TCT, neither overall nor at any joint level (MCP, PIP, DIP).

Overall, there was a significant negative correlation between dGEMRIC indices and all perfusion parameters except k_{ep}. The strongest correlation was found at the MCP joint level.

No significant correlation was seen between any perfusion parameter and overall PsAMRIS and/or synovitis sub-score at the MCP joints and overall. For PIP joints, we found a significant correlation for the parameter peak and total PsAMRIS ($\tau = 0.44$, $p = 0.032$) and for the parameters IAUC and peak and the synovitis sub-score ($\tau = 0.41$, $p = 0.042$; $\tau = 0.451$, $p = 0.032$). At the DIP level, there was a significant correlation between the perfusions parameters K_{Trans}, IAUC, initial slope, and peak and the total PsAMRIS ($\tau = 0.54$, $p = 0.07$; $\tau = 0.48$, $p = 0.018$; $\tau = 0.46$, $p = 0.024$; $\tau = 0.43$, $p = 0.032$). Further, no significant correlations were found between perfusion parameters and DAS 28 as well as serum CRP levels.

The negative correlations between dGEMRIC values and the quantitative parameter K_{Trans} and the semi-quantitative parameter peak at the MCP joint level are depicted in **Figure 2**.

DISCUSSION

Cartilage degradation is a known feature of PsA that can reliably be assessed by dGEMRIC (26). However, as opposed to RA, research is sparse on the role of cartilage in the pathogenesis of PsA. DCE MRI is a valid tool for the evaluation of inflammation in a given joint that has been validated for many types of arthritis (11, 12). In this study, we set out to investigate the relationship between joint inflammation and cartilage loss measured by DCE MRI and dGEMRIC.

We found a significant negative correlation of dGEMRIC indices and quantitative and semi-quantitative perfusion parameters, wherein MCP and PIP joints showed the highest values. The exact reason for the missing correlations at the DIP joints remain unclear, but might be due to a constitutively different proteoglycan content of cartilage along the finger joints or a higher loss of proteoglycans at MCP and PIP than at DIP joints in this specific population of PsA patients. This indicates that molecular cartilage loss is associated with inflammatory joint changes in patients with established PsA, and hence, high inflammation of joints leads to cartilage damage. These findings concur with previous research on cartilage loss, synovial inflammation and perfusion parameters in patients with early RA (10, 16, 20). Since biochemical MRI detects molecular cartilage degradation preceding structural damage, it might be applicable as a monitoring tool for very early disease-related joint changes in PsA.

The association of perfusion parameters and PsAMRIS (sub-scores) has not yet been evaluated. Previous studies on RA showed that perfusion parameters highly correlated with RAMRIS and histological synovitis in affected patients (10, 13, 27–29). As opposed to these findings, we found heterogeneous correlations of perfusion parameters and total PsAMRIS, as well as the synovitis sub-score in PsA patients. DCE MRI is known to indicate the severity of inflammation at a given joint; that is why one could have expected a strong association between perfusion parameters and PsAMRIS. However, previous research using DCE MRI has partially shown that PsA and RA can differ regarding the degree of their synovial enhancement, despite indistinguishable appearances on non-dynamic MRI (30, 31).

TABLE 2 | Descriptive analysis (mean, standard deviation (SD) and range (maximum, minimum) of quantitative and semi-quantitative perfusion parameters, delayed Gadolinium Enhanced Magnetic Resonance Imaging of Cartilage (dGEMRIC) indices, joint space width (JSW), and total cartilage thickness (TCT) of finger 2–5 at the metacarpophalangeal (MCP), proximal interphalangeal (PIP), and distal interphalangeal (DIP) joint region and overall.

		K trans ml/g per min	K ep 1/min	IAUC mM/l per s	Initial slope mM/l per s	Peak mM/l per s	dGEMRIC in ms	TCT in mm	JSW in mm
MCP	Mean	0.06	0.18	3.08	0.0023	0.15	542.65	1.15	1.5
	SD	0.04	0.13	2.46	0.002	0.10	130.34	0.26	0.17
	Max	0.14	0.53	8.45	0.007	0.36	828.03	1.59	1.83
	Min	0.02	0.03	0.81	0.0004	0.05	340.4	0.73	1.27
PIP	Mean	0.05	0.17	2.90	0.002	0.15	411.92	0.71	1.02
	SD	0.03	0.13	2.01	0.002	0.08	104.46	0.18	0.24
	Max	0.12	0.65	7.59	0.006	0.31	639.6	1.11	1.49
	Min	0.008	0.04	0.58	0.0004	0.04	237.18	0.38	0.69
DIP	Mean	0.06	0.21	3.72	0.003	0.16	352.86	0.57	0.8
	SD	0.04	0.15	2.72	0.002	0.08	98.75	0.2	0.18
	Max	0.17	0.68	9.96	0.009	0.29	585.03	0.79	1.19
	Min	0.01	0.06	0.43	0.0003	0.04	184.35	0	0.55
Overall	Mean	0.06	277.32	3.11	0.003	0.15	436.30	0.77	1.07
	SD	0.03	802.71	1.88	0.002	0.07	110.09	0.2	0.18
	Max	0.12	3141.11	7.67	0.006	0.30	670.98	1.13	1.44
	Min	0.01	0.04	0.57	0.0004	0.05	253.98	0.40	0.75
	MCP vs PIP	0.359	0.591	0.864	0.531	1.00	**0.019**	**0.029**	**<0.001**
p-value	MCP vs DIP	0.724	0.803	0.558	0.818	0.848	**0.001**	**0.02**	**0.007**
	PIP vs DIP	0.079	0.918	0.874	0.896	0.848	0.491	0.566	0.116

Mean values of each parameter were compared with a Kruskal-Wallis test and a post-hoc Bonferroni test. P-values <0.05 were considered significant and are given in bold type.

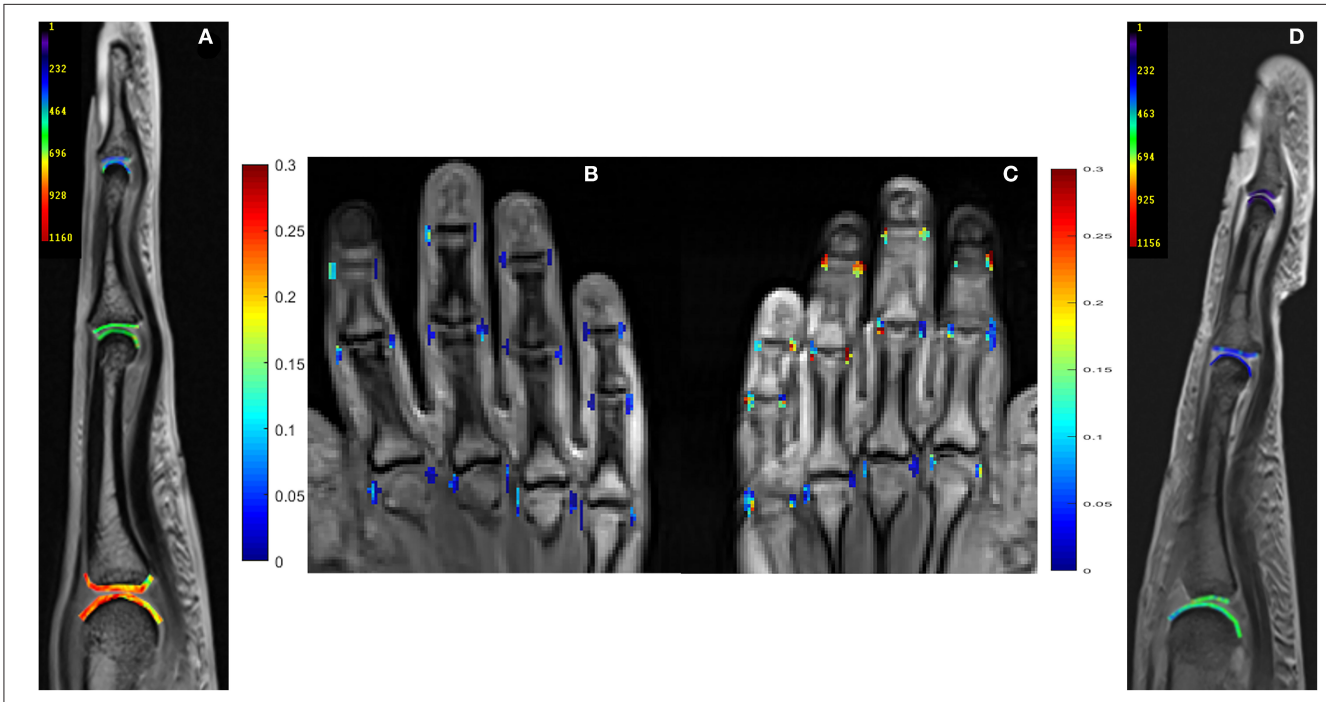

FIGURE 1 | Delayed Gadolinium Enhanced Magnetic Resonance Imaging of Cartilage (dGEMRIC) maps (ms, third digit) and perfusion maps (peak parameter) of metacarpophalangeal (MCP), proximal interphalangeal (PIP), and distal interphalangeal (DIP) joints in 26-year-old male **(A,B)** and a 59-year-old female **(C,D)** with PsA. Lower dGEMRIC values are illustrated in **(D)**, indicating more proteoglycan loss than in **(A)**. Higher peak values are depicted in **(C)**, indicating a higher severity of synovitis than in **(B)**. Peak parameter is illustrated in mM/l per second, dGEMRIC indices in ms.

TABLE 3 | Kendall Tau correlation τ between quantitative and semi-quantitative perfusion parameters and dGEMRIC indices, total Psoriatic arthritis magnetic resonance imaging score (PsAMRIS), PsAMRIS sub-score "synovitis."

		K_{Trans}		K_{ep}		IAUC		Initial slope		Peak	
		τ	*p*	τ	*p*	τ	*p*	τ	*p*	τ	*p*
Overall	JSW	0.1	0.35	−0.1	0.33	0.05	0.64	0.02	0.84	0.04	0.69
	TCT	0.03	0.8	−0.12	0.26	0	0.97	−0.12	0.91	−0.12	0.91
	dGEMRIC	−0.27	**0.014**	−0.29	**0.008**	−0.29	**0.008**	0.32	**0.004**	−0.26	**0.02**
	PsAMRIS	−0.44	0.826	−0.27	0.188	0.09	0.661	0.13	0.51	0.18	0.38
	Synovitis	0.17	0.409	−0.12	0.545	0.26	0.205	0.26	0.205	0.35	0.088
	DAS 28	0.19	0.335	−0.04	0.854	0.27	0.169	0.014	0.952	0.32	0.108
MCP	JSW	0.2	0.3	−0.01	0.96	0.03	0.87	0.03	0.87	0.12	0.55
	TCT	−0.21	0.3	−0.17	0.41	−0.25	0.2	−0.25	0.2	−0.25	0.2
	dGEMRIC	−0.54	**0.01**	−0.02	0.90	−0.51	**0.015**	−0.54	**0.01**	−0.67	**0.002**
	PsAMRIS	0.02	0.912	−0.16	0.44	0.09	0.657	0.14	0.375	0.23	0.268
	Synovitis	0.11	0.612	−0.04	0.866	0.16	0.463	0.23	0.284	0.3	0.159
	DAS28	0.24	0.459	−0.03	0.939	0.22	0.5	0.28	0.385	0.22	0.489
PIP	JSW	0.07	0.73	−0.03	0.88	0.11	0.59	0.17	0.41	0.17	0.41
	TCT	0.12	0.55	−0.06	0.77	0.15	0.43	0.22	0.27	0.22	0.27
	dGEMRIC	−0.43	**0.03**	0.07	0.7	−0.39	0.055	−0.51	**0.015**	−0.51	**0.015**
	PsAMRIS	0.34	0.089	0.02	0.920	0.34	0.089	0.26	0.205	0.44	**0.032**
	Synovitis	0.39	0.053	0.14	0.476	0.41	**0.042**	0.31	0.142	0.45	**0.032**
	DAS28	0.18	0.568	0.05	0.886	0.2	0.536	0.12	0.708	0.22	0.489
DIP	JSW	−0.1	0.62	−0.1	0.62	−0.03	0.87	−0.01	0.96	−0.25	0.21
	TC	−0.05	0.78	−0.1	0.62	0.01	0.96	0.03	0.87	−0.17	0.41
	dGEMRIC	−0.26	0.22	0.1	0.63	−0.18	0.39	−0.15	0.46	−0.08	0.71
	PsAMRIS	0.54	**0.007**	0.10	0.621	0.48	**0.018**	0.46	**0.024**	0.43	**0.032**
	Synovitis	0.22	0.294	−0.01	0.956	0.17	0.407	0.15	0.473	0.21	0.294
	DAS28	−0.06	0.848	0.01	0.901	−0.04	0.901	−0.12	0.722	0.07	0.829

Disease Activity Score 28 (DAS 28), JSW and TCT of finger 2–5 at the MCP, PIP, and DIP joint level and overall. p-values < 0.05 were considered significant and are written in bold type.

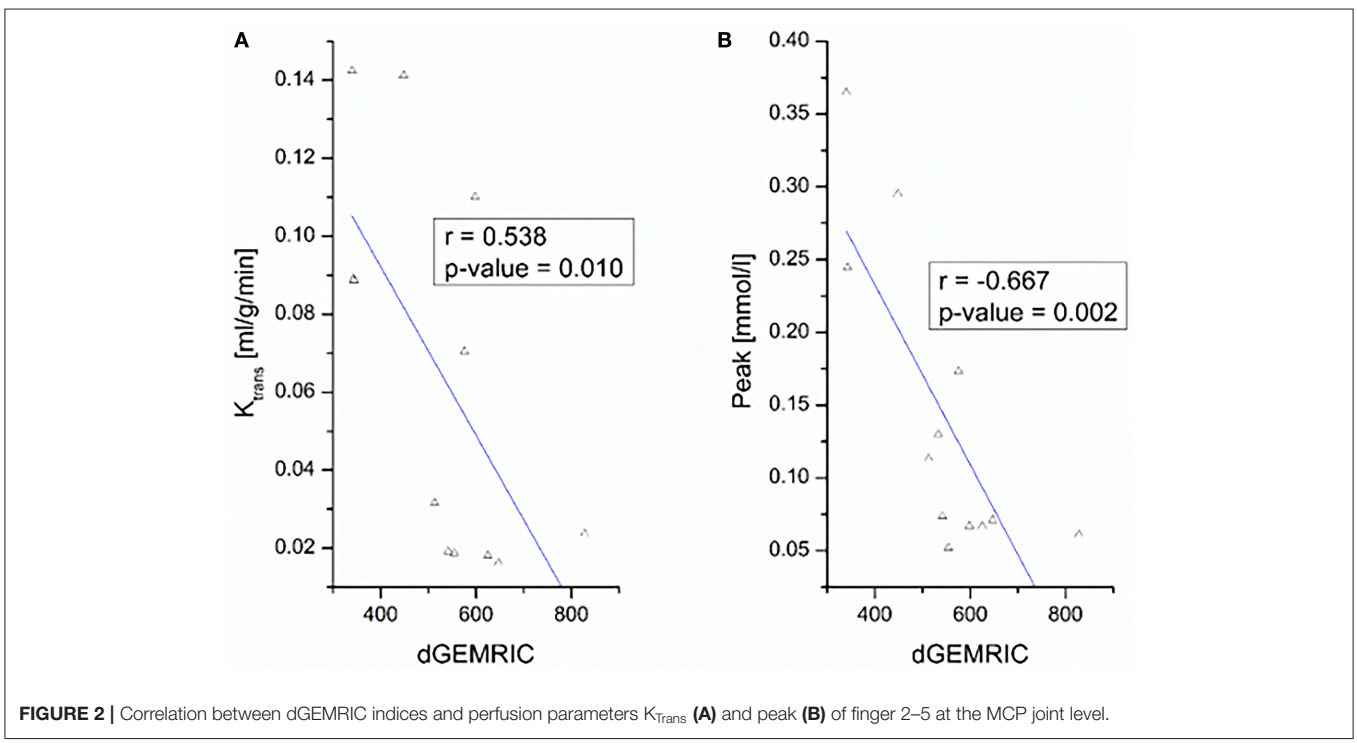

FIGURE 2 | Correlation between dGEMRIC indices and perfusion parameters K_{Trans} **(A)** and peak **(B)** of finger 2–5 at the MCP joint level.

Also, the synovial involvement of PsA histologically differs from RA regarding the extent of inflammation, synovial thickness, and blood supply (31–33). These differences of synovial changes are potentially due to the different pathogenesis of both entities, with RA being primarily a synovial and PsA being an entheseal-driven disease (34, 35). Therefore, the visual degree of synovitis using PsAMRIS could be over- or underrepresenting synovitis measured by DCE MRI, possibly due to a disease-specific type of synovial involvement. Further, for PsAMRIS scoring, we used coronal and transversal planes, wherein for DCE MRI, we only considered radial and ulnar ROI in coronal slices, which could also contribute to heterogeneous correlations of perfusion parameters and synovitis sub-scores. Additionally, the heterogeneity between MCP, PIP, and DIP joints could be explained by the known circumstances that the state of diffusion equilibrium is reached faster in smaller compared to larger joints (36).

Further, no significant correlations were found between perfusion parameters and clinical disease activity as measured by DAS 28. Previous studies have shown that MRI is more sensitive than clinical scores at the detection of joint inflammation (37, 38). Some studies even demonstrated an radiological progression despite clinical remission and postulated a "silent progression" (39–41). That is why, the lacking correlation of imaging features and clinical data could be due to the superior sensitivity of MRI, especially since a high-field MRI scanner and a dedicated hand-coil have been used resulting in high-resolution imaging.

Our Study Has Limitations

Firstly, our study population of PsA patients had a small sample size. That is why our results should only be considered exploratory and need confirmation by further research with larger populations.

Secondly, we did not use a synovial and cartilage biopsy as a means of validation regarding the extent of synovitis and the cartilage composition. However, previous studies have already histologically validated both DCE MRI and dGEMRIC data (13, 42).

In conclusion, there is a potential association between early cartilage loss and acute synovial inflammation in small finger joints of PsA patients.

DATA AVAILABILITY STATEMENT

The datasets generated for this study are available on request to the corresponding author.

ETHICS STATEMENT

The studies involving human participants were reviewed and approved by Ethics committee of the Heinrich-Heine University. The patients/participants provided their written informed consent to participate in this study.

AUTHOR CONTRIBUTIONS

DA: acquisition and analysis and interpretation of data. Draft and design of the work. PS: design and conception of the study. Analysis and interpretation of data. Draft and design of the work. Revision of the work. BO, MS, SV, and KR: analysis and interpretation of data. Draft and design of the work. Revision of the work. MF and AM-L: interpretation and analysis of data. Draft and design of the work. Revision of the work. CS: conception and design of the study. Interpretation and analysis of data. Draft and design of the work. Revision of the work. All authors read and approved the final manuscript. All authors contributed to the article and approved the submitted version.

FUNDING

DA was supported by the local research committee of the medical faculty. PS and SV received funding from Pfizer Germany with the Pfizer GIP Inflammation Germany Research Initiative 2014. PS and BO received funding from AbbVie Deutschland GmbH & Co. KG for the Delayed Gadolinium-enhanced MR Imaging of Cartilage—A pilot study to measure the effect of Adalimumab plus MTX vs. Placebo plus MTX on cartilage in early RA patients (CAR-ERA) Study. PS received a grant from the German Bundesministerium für Bildung und Forschung (BMBF), ArthroMark (01EC1009).

ACKNOWLEDGMENTS

We thank Mrs. Erika Rädisch for conducting all MRI studies.

REFERENCES

1. Sewerin P, Brinks R, Schneider M, Haase I, Vordenbäumen S. Prevalence and incidence of psoriasis and psoriatic arthritis. *Ann Rheum Dis.* (2019) 78:286–7. doi: 10.1136/annrheumdis-2018-214065
2. Coates LC, Navarro-Coy N, Brown SR, Brown S, McParland L, Collier H, et al. The TICOPA protocol (TIght COntrol of Psoriatic Arthritis): a randomised controlled trial to compare intensive management versus standard care in early psoriatic arthritis. *BMC Musculoskelet Disord.* (2013) 14:101. doi: 10.1186/1471-2474-14-101
3. Singh JA, Guyatt G, Ogdie A, Gladman DD, Deal C, Deodhar A, et al. Special article: 2018 American College of Rheumatology/National psoriasis foundation guideline for the treatment of psoriatic arthritis. *Arthritis Care Res.* (2019) 71:2–29. doi: 10.1002/art.40726
4. Coates LC. Treating to target in psoriatic arthritis. *Curr Opin Rheumatol.* (2015) 27:107. doi: 10.1097/BOR.0000000000000140
5. Coates LC, Lubrano E, Perrotta FM, Emery P, Conaghan PG, Helliwell PS. What should be the primary target of "treat to target" in psoriatic arthritis? *J Rheumatol.* (2019) 46:38–42. doi: 10.3899/jrheum.180267
6. Tillett W, Costa L, Jadon D, Wallis D, Cavill C, McHugh J, et al. The ClASsification for Psoriatic ARthritis (CASPAR) criteria–a retrospective feasibility, sensitivity, and specificity study. *J Rheumatol.* (2012) 39:154–6. doi: 10.3899/jrheum.110845
7. Coates LC, Conaghan PG, D'Agostino MA, Wit M de, FitzGerald O, Kvien TK, et al. Remission in psoriatic arthritis-where are we now? *Rheumatology.* (2018) 57:1321–31. doi: 10.1093/rheumatology/kex344
8. Yue J, Wu D, Tam L-S. The role of imaging in early diagnosis and prevention of joint damage in inflammatory arthritis. *Expert Rev Clin Immunol.* (2018) 14:499–511. doi: 10.1080/1744666X.2018.1476849

9. Ostergaard M, McQueen F, Wiell C, Bird P, Bøyesen P, Ejbjerg B, et al. The OMERACT psoriatic arthritis magnetic resonance imaging scoring system (PsAMRIS): definitions of key pathologies, suggested MRI sequences, and preliminary scoring system for PsA Hands. *J Rheumatol.* (2009) 36:1816–24. doi: 10.3899/jrheum.090352
10. Müller-Lutz A, Schleich C, Sewerin P, Gross J, Pentang G, Wittsack H-J, et al. Comparison of quantitative and semiquantitative dynamic contrast-enhanced MRI with respect to their correlation to delayed gadolinium-enhanced MRI of the cartilage in patients with early rheumatoid arthritis. *J Comput Assist Tomogr.* (2015) 39:64–9. doi: 10.1097/RCT.0000000000000164
11. Schwenzer NF, Kötter I, Henes JC, Schraml C, Fritz J, Claussen CD, et al. The role of dynamic contrast-enhanced MRI in the differential diagnosis of psoriatic and rheumatoid arthritis. *AJR Am J Roentgenol.* (2010) 194:715–20. doi: 10.2214/AJR.09.2671
12. Cimmino MA, Barbieri F, Boesen M, Paparo F, Parodi M, Kubassova O, et al. Dynamic contrast-enhanced magnetic resonance imaging of articular and extraarticular synovial structures of the hands in patients with psoriatic arthritis. *J Rheumatol Suppl.* (2012) 89:44–8. doi: 10.3899/jrheum.120242
13. Vordenbäumen S, Schleich C, Lögters T, Sewerin P, Bleck E, Pauly T, et al. Dynamic contrast-enhanced magnetic resonance imaging of metacarpophalangeal joints reflects histological signs of synovitis in rheumatoid arthritis. *Arthritis Res Ther.* (2014) 16:452. doi: 10.1186/s13075-014-0452-x
14. Bhattaram P, Chandrasekharan U. The joint synovium: A critical determinant of articular cartilage fate in inflammatory joint diseases. *Semin Cell Dev Biol.* (2017) 62:86–93. doi: 10.1016/j.semcdb.2016.05.009
15. Østergaard M, Peterfy CG, Bird P, Gandjbakhch F, Glinatsi D, Eshed I, et al. The OMERACT rheumatoid arthritis magnetic resonance imaging (MRI) scoring system: updated recommendations by the OMERACT MRI in arthritis working group. *J Rheumatol.* (2017) 44:1706–12. doi: 10.3899/jrheum.161433
16. Herz B, Albrecht A, Englbrecht M, Welsch GH, Uder M, Renner N, et al. Osteitis and synovitis, but not bone erosion, is associated with proteoglycan loss and microstructure damage in the cartilage of patients with rheumatoid arthritis. *Ann Rheum Dis.* (2014) 73:1101–6. doi: 10.1136/annrheumdis-2012-202850
17. Miese F, Buchbender C, Scherer A, Wittsack H-J, Specker C, Schneider M, et al. Molecular imaging of cartilage damage of finger joints in early rheumatoid arthritis with delayed gadolinium-enhanced magnetic resonance imaging. *Arthritis Rheum.* (2012) 64:394–9. doi: 10.1002/art.33352
18. van Tiel J, Kotek G, Reijman M, Bos PK, Bron EE, Klein S, et al. Is T1ρ mapping an alternative to delayed gadolinium-enhanced MR imaging of cartilage in the assessment of sulphated glycosaminoglycan content in human osteoarthritic knees? An *in vivo* validation study. *Radiology.* (2016) 279:523–31. doi: 10.1148/radiol.2015150693
19. Abrar DB, Schleich C, Brinks R, Vordenbäumen S, Frenken M, Goertz C, et al. Is a simplified version of PsAMRIS (sPsAMRIS) a potential tool for therapy monitoring in established psoriatic arthritis? *Res Square [Preprint].* (2019). doi: 10.21203/rs.2.14892/v1
20. Sewerin P, Schleich C, Brinks R, Müller-Lutz A, Fichter F, Eichner M, et al. Assessing associations of synovial perfusion, cartilage quality, and outcome in rheumatoid arthritis using dynamic contrast-enhanced magnetic resonance imaging. *J Rheumatol.* (2020) 47:15–9. doi: 10.3899/jrheum.180832
21. Sewerin P, Schleich C, Brinks R, Müller-Lutz A, Fichter F, Eichner M, et al. Synovial perfusion assessed by dynamic contrast-enhanced MRI is associated to treatment response, remission, and cartilage quality in rheumatoid arthritis. *J Rheumatol.* (2019). doi: 10.3899/jrheum.180832. [Epub ahead of print].
22. Tofts PS. T1-weighted DCE imaging concepts: modelling, acquisition and analysis. *MAGNETOM Flash.* (2010) 2010:30–9.
23. Miese F, Kröpil P, Ostendorf B, Scherer A, Buchbender C, Quentin M, et al. Motion correction improves image quality of dGEMRIC in finger joints. *Eur J Radiol.* (2011) 80:e427–31. doi: 10.1016/j.ejrad.2011.01.006
24. Miese FR, Ostendorf B, Wittsack H-J, Reichelt DC, Mamisch TC, Zilkens C, et al. Metacarpophalangeal joints in rheumatoid arthritis: delayed gadolinium-enhanced MR imaging of cartilage–a feasibility study. *Radiology.* (2010) 257:441–7. doi: 10.1148/radiol.10100459
25. Sewerin P, Müller-Lutz A, Abrar DB, Odendahl S, Eichner M, Schneider M, et al. Prevention of the progressive biochemical cartilage destruction under methotrexate therapy in early rheumatoid arthritis. *Clin Exp Rheumatol.* (2019) 37:179–85.
26. Sewerin P, Schleich C, Vordenbäumen S, Ostendorf B. Update on imaging in rheumatic diseases: cartilage. *Clin Exp Rheumatol.* (2018) 36 Suppl 114:139–44.
27. Hodgson R, Grainger A, O'Connor P, Barnes T, Connolly S, Moots R. Dynamic contrast enhanced MRI of bone marrow oedema in rheumatoid arthritis. *Ann Rheum Dis.* (2008) 67:270–2. doi: 10.1136/ard.2007.077271
28. Boesen M, Kubassova O, Bouert R, Axelsen MB, Ostergaard M, Cimmino MA, et al. Correlation between computer-aided dynamic gadolinium-enhanced MRI assessment of inflammation and semi-quantitative synovitis and bone marrow oedema scores of the wrist in patients with rheumatoid arthritis–a cohort study. *Rheumatology.* (2012) 51:134–43. doi: 10.1093/rheumatology/ker220
29. Wojciechowski W, Tabor Z, Urbanik A. Assessing synovitis based on dynamic gadolinium-enhanced MRI and EULAR-OMERACT scores of the wrist in patients with rheumatoid arthritis. *Clin Exp Rheumatol.* (2013) 31:850–6.
30. Sudoł-Szopińska I, Pracoń G. Diagnostic imaging of psoriatic arthritis. Part II: magnetic resonance imaging and ultrasonography. *J Ultrason.* (2016) 16:163–74. doi: 10.15557/JoU.2016.0018
31. Narváez J, Narváez JA, Albert M de, Gómez-Vaquero C, Nolla JM. Can magnetic resonance imaging of the hand and wrist differentiate between rheumatoid arthritis and psoriatic arthritis in the early stages of the disease? *Semin Arthritis Rheum.* (2012) 42:234–45. doi: 10.1016/j.semarthrit.2012.03.016
32. Sankowski AJ, Lebkowska UM, Cwikła J, Walecka I, Walecki J. Psoriatic arthritis. *Pol J Radiol.* (2013) 78:7–17. doi: 10.12659/PJR.883763
33. Sudoł-Szopińska I, Płaza M, Pracoń G. Selected issues in diagnostic imaging of spondyloarthritides: psoriatic arthritis and juvenile spondyloarthritis. *Reumatologia.* (2016) 54:310–7. doi: 10.5114/reum.2016.64908
34. McGonagle D, Hermann K-GA, Tan AL. Differentiation between osteoarthritis and psoriatic arthritis: implications for pathogenesis and treatment in the biologic therapy era. *Rheumatology.* (2015) 54:29–38. doi: 10.1093/rheumatology/keu328
35. Schett G, Coates LC, Ash ZR, Finzel S, Conaghan PG. Structural damage in rheumatoid arthritis, psoriatic arthritis, and ankylosing spondylitis: traditional views, novel insights gained from TNF blockade, and concepts for the future. *Arthritis Res Ther.* (2011) 2011:S4. doi: 10.1186/1478-6354-13-S1-S4
36. Peterfy CG. MR imaging. *Baillieres Clin Rheumatol.* (1996) 10:635–78. doi: 10.1016/S0950-3579(96)80055-0
37. Østergaard M, Hansen M, Stoltenberg M, Jensen KE, Szkudlarek M, Pedersen-Zbinden B, et al. New radiographic bone erosions in the wrists of patients with rheumatoid arthritis are detectable with magnetic resonance imaging a median of two years earlier. *Arthritis Rheum.* (2003) 48:2128–31. doi: 10.1002/art.11076
38. Ejbjerg BJ, Vestergaard A, Jacobsen S, Thomsen HS, Østergaard M. The smallest detectable difference and sensitivity to change of magnetic resonance imaging and radiographic scoring of structural joint damage in rheumatoid arthritis finger, wrist, and toe joints: a comparison of the OMERACT rheumatoid arthritis magnetic resonance imaging score applied to different joint combinations and the Sharp/van der Heijde radiographic score. *Arthritis Rheum.* (2005) 52:2300–6. doi: 10.1002/art.21207
39. Møller-Bisgaard S, Hørslev-Petersen K, Ejbjerg BJ, Boesen M, Hetland ML, Christensen R, et al. Impact of a magnetic resonance imaging-guided treat-to-target strategy on disease activity and progression in patients with rheumatoid arthritis (the IMAGINE-RA trial): study protocol for a randomized controlled trial. *Trials.* (2015) 16:178. doi: 10.1186/s13063-015-0693-2
40. Sewerin P, Vordenbaeumen S, Hoyer A, Brinks R, Buchbender C, Miese F, et al. Silent progression in patients with rheumatoid arthritis: is DAS28 remission an insufficient goal in RA? Results from the German Remission-plus cohort. *BMC Musculoskelet Disord.* (2017) 18:163. doi: 10.1186/s12891-017-1528-y

41. Hetland ML, Stengaard-Pedersen K, Junker P, Østergaard M, Ejbjerg BJ, Jacobsen S, et al. Radiographic progression and remission rates in early rheumatoid arthritis - MRI bone oedema and anti-CCP predicted radiographic progression in the 5-year extension of the double-blind randomised CIMESTRA trial. *Ann Rheum Dis.* (2010) 69:1789–95. doi: 10.1136/ard.2009.125534
42. Schmaranzer F, Arendt L, Liechti EF, Nuss K, Rechenberg B von, Kircher PR, et al. Do dGEMRIC and T2 imaging correlate with histologic cartilage degeneration in an experimental ovine FAI model? *Clin Orthop Relat Res.* (2019) 477:990–1003. doi: 10.1097/CORR.0000000000000593

Conflict of Interest: The authors declare that the research was conducted in the absence of any commercial or financial relationships that could be construed as a potential conflict of interest.

frontiers in Medicine

ORIGINAL RESEARCH
published: 25 September 2020
doi: 10.3389/fmed.2020.577739

Automatic Quantification of Interstitial Lung Disease From Chest Computed Tomography in Systemic Sclerosis

Alysson Roncally S. Carvalho[1,2,3]*, *Alan R. Guimarães*[2], *Flávio R. Sztajnbok*[4], *Rosana Souza Rodrigues*[5,6], *Bruno Rangel Antunes Silva*[7], *Agnaldo José Lopes*[7], *Walter Araujo Zin*[3], *Isabel Almeida*[8] *and Manuela Maria França*[9]

[1] Department of Radiology, Medical School, Centro Hospitalar Universitário do Porto (CHUP), Instituto de Ciências Biomédicas Abel Salazar (ICBAS), Porto University, Porto, Portugal, [2] Laboratory of Pulmonary Engineering, Biomedical Engineering Program, Alberto Luiz Coimbra Institute of Post-Graduation and Research in Engineering, Universidade Federal do Rio de Janeiro, Rio de Janeiro, Brazil, [3] Laboratory of Respiration Physiology, Carlos Chagas Filho Institute of Biophysics, Universidade Federal do Rio de Janeiro, Rio de Janeiro, Brazil, [4] Division of Pediatric Rheumatology, State University of Rio de Janeiro, Rio de Janeiro, Brazil, [5] Department of Radiology, Universidade Federal do Rio de Janeiro, Rio de Janeiro, Brazil, [6] IDOR - D'Or Institute for Research and Education, Rio de Janeiro, Brazil, [7] Graduate Program in Medical Sciences, School of Medical Sciences, State University of Rio de Janeiro, Rio de Janeiro, Brazil, [8] Clinical Immunology Unit, Deptartment of Medicine, Centro Hospitalar Universitário do Porto (CHUP), Instituto de Ciências Biomédicas Abel Salazar (ICBAS), Porto University, Porto, Portugal, [9] Radiology Department, Centro Hospitalar Universitário do Porto (CHUP), Instituto de Ciências Biomédicas Abel Salazar (ICBAS), Porto University, Porto, Portugal

OPEN ACCESS

Edited by:
Christian Dejaco,
Medical University of Graz, Austria

Reviewed by:
Gonçalo Boleto,
Hôpitaux Universitaires Pitié Salpêtrière, France
Sule Yavuz,
Istanbul Bilim University, Turkey

***Correspondence:**
Alysson Roncally S. Carvalho
roncally.carvalho@gmail.com

Specialty section:
This article was submitted to Rheumatology, a section of the journal Frontiers in Medicine

Received: *29 June 2020*
Accepted: *18 August 2020*
Published: *25 September 2020*

Citation:
Carvalho ARS, Guimarães AR, Sztajnbok FR, Rodrigues RS, Silva BRA, Lopes AJ, Zin WA, Almeida I and França MM (2020) Automatic Quantification of Interstitial Lung Disease From Chest Computed Tomography in Systemic Sclerosis. Front. Med. 7:577739. doi: 10.3389/fmed.2020.577739

Background: Interstitial lung disease (ILD) is a common complication in patients with systemic sclerosis (SSc), and its diagnosis contributes to early treatment decisions.

Purposes: To quantify ILD associated with SSc (SSc-ILD) from chest CT images using an automatic quantification method based on the computation of the weight of interstitial lung opacities.

Methods: Ninety-four patients with SSc underwent CT, forced vital capacity (FVC), and carbon monoxide diffusion capacity (DL_{CO}) tests. Seventy-three healthy individuals without radiological evidence of lung disease served as controls. After lung and airway segmentation, the ratio between the weight of interstitial opacities [densities between −500 and +50 Hounsfield units (HU)] and the total lung weight (densities between −1,000 and +50 HU) was used as an ILD indicator ($ILD[\%] = 100 \times [LW_{(-500\ to\ +50HU)}/LW_{(-1,000\ to\ +50HU)}]$). The cutoff of normality between controls and SSc was determined with a receiver operator characteristic curve. The severity of pulmonary involvement in SSc patients was also assessed by calculating Z scores of ILD relative to the average interstitial opacities in controls. Accordingly, SSc-ILD was classified as SSc Limited-ILD (Z score < 3) and SSc Extensive-ILD (Z score ≥ 3 or FVC $< 70\%$).

Results: Seventy-eight (83%) SSc patients were classified as presenting SSc-ILD (optimal ILD threshold of 23.4%, 0.83 sensitivity, 0.92 specificity, and 0.94 area under the receiver operator characteristic curve, 95% CI from 0.89 to 0.96, 0.93 positive predictive value, and 0.81 negative predictive value, $p < 0.001$) and exhibited radiological attenuations compatible with interstitial pneumonia dispersed in the lung parenchyma.

Thirty-six (38%) patients were classified as SSc Extensive-ILD (ILD threshold $\geq$ 29.6% equivalent to a Z score $\geq$ 3) and 42 (45%) as SSc Limited-ILD. Eighteen (50%) patients with SSc Extensive-ILD presented FVC $<$ 70%, being only five patients classified exclusively based on FVC. SSc Extensive-ILD also presented lower DL_{CO} (57.9 $\pm$ 17.9% vs. 73.7 $\pm$ 19.8%; $p < 0.001$) and total lung volume (2,916 $\pm$ 674 vs. 4,286 $\pm$ 1,136, $p < 0.001$) compared with SSc Limited-ILD.

Conclusion: The proposed method seems to provide an alternative to identify and quantify the extension of ILD in patients with SSc, mitigating the subjectivity of semiquantitative analyzes based on visual scores.

Keywords: systemic sclerosis, interstitial lung disease, chest computed tomography, quantitative chest CT-analysis, densitometry

KEY RESULTS

- Quantitative analysis of chest CT scans by densitometry was able to quantify the extent of interstitial lung disease associated with systemic sclerosis (SSc).
- Extensive pulmonary involvement in SSc subjects was associated with pulmonary function impairment.
- Interstitial lung disease almost completely involves lung parenchyma in patients classified as with SSc extensive—interstitial lung disease.

INTRODUCTION

Systemic sclerosis (SSc) is a rare multisystemic disease with heterogeneous clinical presentation characterized by extensive fibrosis and autoimmune and vascular dysfunction that may progress to multiple organ dysfunction including skin, lung, heart, and kidney involvement (1).

SSc clinical evolution is commonly insidious, progressive, and irreversible with considerable morbidity and mortality (2). The most common imaging and histopathologic pattern observed on computed tomography (CT) and surgical lung biopsy is nonspecific interstitial pneumonia (NSIP) (3, 4). On histopathology, this pattern is characterized by a relatively homogeneous thickening of the alveolar walls caused by inflammation (cellular-NSIP) and/or fibrosis (fibrotic-NSIP). In cellular-NSIP, alveolar septa are thickened by infiltration of lymphocytes and plasma cells, whereas in fibrotic-NSIP, the thickening is more related to collagen deposition (5). Chest CT findings usually reflect the histological pattern and are mainly characterized by ground-glass opacities, especially in cellular-NSIP. Interstitial reticular thickening with traction bronchiectasis and some focal consolidation are more frequently observed in fibrotic-NSIP (2).

As ILD associated with SSc (SSc-ILD) occurs in more than half of SSc patients (6) and as the extent of pulmonary involvement is quite variable, the severity of symptoms ranges from subclinical symptoms up to respiratory failure and death (7). Assuming that SSc-ILD considerably impacts morbidity and mortality, the early identification of patients with pulmonary involvement might help to mitigate both disease progression and severity of respiratory symptoms (2, 6).

CT is the gold standard for SSc-ILD detection (8). However, the visual quantification of ILD extension by CT generally results in low agreement even among experienced radiologists (9, 10). On the other hand, the quantitative assessment of chest CT, using dedicated software and methods, might overcome the observational limitation by quantifying the lung volume and tissue fraction in a voxel-by-voxel basis, allowing a more accurate calculation of the degree of pulmonary involvement (11, 12).

The main objective of this study was to assess whether the ratio between the weight of the interstitial opacities [densities between −500 and +50 Hounsfield units (HU)] and the total lung weight (LW) (densities between −1,000 and +50 HU) expressed in percentage values can be used as an ILD indicator. It is also intended to investigate the association between ILD severity and lung function impairment based on the assessment of forced vital capacity (FVC) and carbon monoxide diffusion capacity (DL_{CO}).

MATERIALS AND METHODS

Patients

This study reviewed CT and pulmonary function tests from 94 patients with SSc followed up at the Policlínica Piquet Carneiro da Universidade do Estado do Rio de Janeiro, Rio de Janeiro, Brazil, and at Centro Hospitalar Universitário do Porto, Porto, Portugal.

Patients had been diagnosed in accordance with ACR/EULAR criteria (13). Patients with clinical instability, history of respiratory infection 3 weeks before CT, who were previously or are currently smoking, with evidence of overlapping of scleroderma with other connective tissue diseases, and with a report of previous tracheal or pleuropulmonary disease not related to scleroderma were not included.

Cutaneous involvement was classified as limited (lc-SSc; thickening of the skin distal to the elbows and knees and proximal to the clavicles, including the face) or diffuse (dc-SSc; thickening of the proximal skin as well as of the skin distal to the elbows and knees and including the trunk and face) (14).

Anti-topoisomerase I (Scl-70) and anti-centromere (ACA) antibodies were determined by indirect immunofluorescence

using Hep-2 cells as substrates, and autoantibody specificities were further assessed by ELISA (Shield, Dundee, UK).

Seventy-three none smoking healthy individuals with no chronic tracheal or pleuropulmonary diseases, chest CT scans without radiological abnormalities, and matched anthropometrically with SSc patients served as controls.

The protocol was approved at the Research Ethics Committee from the Universidade do Estado do Rio de Janeiro (CAAE-50752615.9.0000.5259) and Centro Hospitalar Universitário do Porto (reference number 2019.353, 288-DEFI/307-CE), and it complied with the current national and international standards.

Pulmonary Function Tests

FVC, DL_{CO}, and DL_{CO} adjusted to alveolar volume (DL_{CO}/VA) were reviewed and expressed as percentages of the predicted values (15–18). Additionally, FVC(%)/DL_{CO}(%) ratio was calculated in subjects with severe reduced DL_{CO} (<55% predicted) to assess isolated pulmonary hypertension (19). The maximal accepted interval between pulmonary function and CT acquisition was 3 months in SSc patients.

Chest Computed Tomography Acquisition

CT scans were performed on a 64-channel multi-slice (Brilliance 40 scanner, Philips Medical Systems, Cleveland, OH, USA, and General Electrics Lightspeed VCT, Chicago Illinois, USA). The acquisitions were gathered in the axial plane with patients in the supine position with 120 kV and 120–300 mA (these parameters varied according to the biotype of the patient), slice thickness of 2 mm with 50% superposition. After the acquisition, all images were reconstructed with a matrix of 512 × 512/728 × 728 voxels using standard reconstruction algorithms.

Imaging Processing

Lung segmentation and airway segmentation were performed (20), and images were then exported to an in-house developed software (QUALI) written in MATLAB® (MathWorks®, Natick, MA, USA).

Before densitometry calculation, the average densities expressed in HU of air inside the trachea (HU_{Air}) and blood in the descending aorta (HU_{Tissue}) were measured (QUALI software). The intensity values of all voxels in lung parenchyma were then linearly rescaled, considering that HU_{Air} and HU_{Tissue} should be equal to −1,000 and +50 HU, respectively (21, 22).

Total lung volume (TLV) was calculated as previously described (23). LW, in grams, was calculated as:

$$\text{LW (g)} = [(\text{HU} - \text{HU}_{\text{Air}})/(\text{HU}_{\text{Aorta}} - \text{HU}_{\text{Air}})] \times \text{voxel volume} \times 1.04\ \text{g/ml} \quad (1)$$

where 1.04 mg/ml means lung tissue density, and HU is voxel density in an HU (21).

Additionally, LW related to hyperinflated (−1,000 to −901 HU), normally aerated (−900 to −501 HU), and to interstitial opacities (−500 to +50 HU) areas were also calculated and normalized to the whole LW (23).

Regional Densitometry Assessment

LW was calculated in three sub-volumes equally divided considering the number of slices, from the basal to the apical (basal, middle, and apical lung thirds), and was used for regional densitometry assessment. LW at regions of interest generated by an erosion process performed from the outermost layer of the 10-mm-thick pulmonary parenchyma, progressing to the hilar

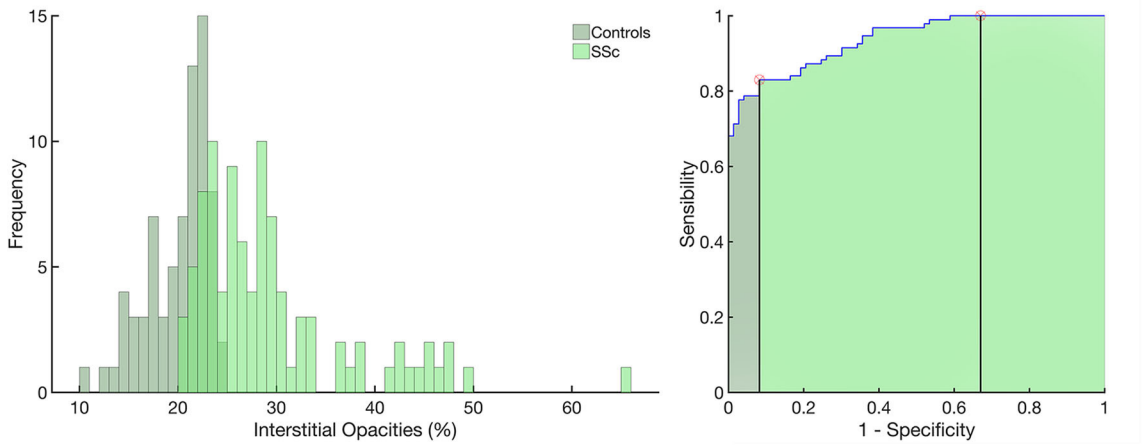

FIGURE 1 | Left panel: histograms of the frequency of occurrence of interstitial opacities in the control group (light green) and in patients with systemic sclerosis (SSc, in dark green). Right panel: receiver operator characteristic curve with the area under the curve (AUC) hatched in light green. Vertical lines mark the normality cutoff (equivalent to 23.4% of total lung weight represented by interstitial opacites) and the *Z* score = 3 (equivalent to 29.6% of the total lung weight and used to classify SSc patients as with extensive interstitial lung disease, SSc-Extensive ILD). Between the normality cutoff up to *Z* score < 3, SSc patients were classified as with limited interstitial lung disease. Use of interstitial opacities as an indicator of ILD presented 0.83 sensitivity, 0.92 specificity, with an receiver operator characteristic curve with the area under the curve of 0.94; 95% from CI 0.89–0.96 ($p < 0.001$) and 0.93 positive predictive value and 0.81 negative predictive value.

regions in 10-mm steps, until the entire pulmonary parenchyma was also calculated.

Identification of Systemic Sclerosis Patients With Interstitial Lung Disease

After lung and airway segmentation, the ratio between the weight of voxels with densities between −500 and +50 HU and the total LW ($100 \times [LW_{(-500\ to\ +50HU)}/LW_{(-1,000\ to\ +50HU)}]$) was defined as an indicator of ILD. The cutoff of normality between controls and SSc was determined with a receiver operator characteristic (ROC) curve (**Figure 1**). The severity of pulmonary involvement in SSc patients was also assessed by calculating *Z* scores of ILD relative to the average interstitial opacities in controls. Accordingly, SSc-ILD patients were classified as SSc Limited-ILD (*Z* score < 3) and SSc Extensive-ILD (*Z* score ≥ 3). To increase sensitivity, all SSc patients with FVC $< 70\%$ were reclassified as SSc Extensive-ILD (24).

Statistical Analysis

The normality of the data (Kolmogorov–Smirnov test with Lilliefors' correction) and the homogeneity of variances (Levene median test) were tested. As both conditions were always satisfied, all data are presented as mean and standard deviation.

From the ROC curve, the threshold limit, sensitivity, specificity, the area under the ROC curve, and bootstrapped 95% confidence intervals (CIs) (bias-corrected and accelerated), as well as positive and negative predictive values were assessed.

SSc-ILD and SSc without (SSc No-ILD) ILD were compared with a Student's *t*-test for independent samples. An ANOVA test followed by Bonferroni *post hoc* test assessed statistical differences among SSc Extensive-ILD, SSc Limited-ILD, and SSc No-ILD. Spearman correlation coefficient (r) was calculated to evaluate the associations between FVC, DL_{CO}, and DL_{CO}/VA with ILD-Extent in SSc patients. The criterion for determining significance was 5%. Statistical analysis was performed using Matlab® software (MathWorks®, Natick, MA, USA).

RESULTS

In SSc patients, the mean age at CT review was 54.5 ± 13.5 years, and 87 (92.5%) were women ($p = 0.19$ vs. controls). The disease durations were 4.21 ± 2.50 years from the onset of the non-Raynaud phenomenon and 9.65 ± 5.13 years from the onset of the Raynaud phenomenon. Sixty-four patients (68.1%) had lc-SSc, and 30 (31.9%) presented dc-SSc. Anti-topoisomerase I (Scl-70) antibody, anti-centromere antibody (ACA), and anti-RNA polymerase III were positive in 13 (13.8%), 50 (53.2%), and 3 (3.2%) patients, respectively. Twenty-eight patients (29.8%) did not present autoantibodies (**Table 1**).

SSc presented a significant reduction in TLV, whereas total LW and LW related to hyperinflated and interstitial opacities were significantly higher in SSc compared with those in controls (**Table 1**).

Seventy-eight (83%) SSc patients were classified as presenting SSc-ILD based on the ROC curve with an optimal ILD threshold of 23.4%, 0.83 sensitivity, 0.92 specificity, and 0.94 area under the ROC curve; 95% from CI 0.89–0.96 ($p < 0.001$), 0.93 positive predictive value, and 0.81 negative predictive value (**Figure 1**).

Thirty-six (38%) patients were classified as SSc Extensive-ILD (ILD threshold of 29.6%, 0.32 sensitivity, and 1.00 specificity) and exhibited radiological attenuations compatible with interstitial pneumonia diffusely distributed in the lung parenchyma (**Figure 2**, uppermost row). Forty-two (45%) patients were classified as SSc Limited-ILD, and radiological attenuations were mainly distributed in basal and middle lung thirds (**Figure 2**, second row). In SSc patients, SSc-ILDs, color-coded in green, were therefore interpreted, in addition to the peribronchial vessels, as ground-glass opacities, reticular consolidations, and possible compressed tissues broadly spread over the lung parenchyma (**Figure 2**, rightmost column). Note that the pattern of involvement of lung parenchyma differed between Extensive- and Limited-ILDs.

TABLE 1 | Demographic characteristics, clinical features, pulmonary function tests, and densitometry of the control group and scleroderma patients.

	SSc (94)	Control group (73)	*p*-value
Demographic data			
Females	87 (92.5%)	64 (87.7%)	
Age (years)	54.5 ± 13.5	57.9 ± 20.0	0.19
BMI (kg/m^2)	25.4 ± 5.5	26.2 ± 4.3	0.27
SSc cutaneous involvement			
lc-SSc	64 (68.1%)	–	–
dc-SSc	30 (31.9%)	–	–
Type of antibody			
Anti-topoisomerase I antibody	13 (13.8%)	–	–
Anti-centromere antibody	50 (53.2%)	–	–
Anti-RNA polymerase III	3 (3.2%)	–	–
Autoantibody not identified	28 (29.8%)	–	–
Lung function			
FVC (% predicted)	98.0 ± 26.9	–	–
DL_{CO}/VA (% predicted)	81.3 ± 18.6	–	–
DL_{CO} (% predicted)	69.9 ± 20.8	–	–
Densitometry			
TLV (ml)	**3,804.8 ± 1,160.9**	**4,170.7 ± 755.3**	**0.021**
Total $LT_{Fraction}$ (g)	**738.8 ± 156.1**	**611.4 ± 144.9**	**<0.001**
Hyperinflated (%)	**7.9 ± 4.7**	**18.0 ± 8.6**	**<0.001**
Normally aerated (%)	62.6 ± 7.1	62.0 ± 10.2	0.651
Interstitial opacities (%)	**29.5 ± 8.1**	**20.0 ± 3.2**	**<0.011**

Values are presented as mean ± standard deviation or number (percentage value). Bold characters indicate statistically significant differences. BMI, body mass index; lc-SSc, limited skin form; dc-SSc, diffuse skin form; FVC (%), forced vital capacity expressed as predicted values; DL_{CO}/VA, carbon monoxide diffusion capacity adjusted for alveolar volume expressed as predicted values; DL_{CO} (%), carbon monoxide diffusion capacity expressed as predicted values; TLV, total lung volume; Total $LT_{Fraction}$, lung tissue fraction related to densities from −1,000 to +50 Hounsfield units (HU); Hyperinflated, tissue fraction related to densities from −1,000 to −901 HU; Normally Aerated, tissue fraction related to densities from −900 to −501 HU; Interstitial Opacities, lung weight related to densities from −500 to +50 HU.

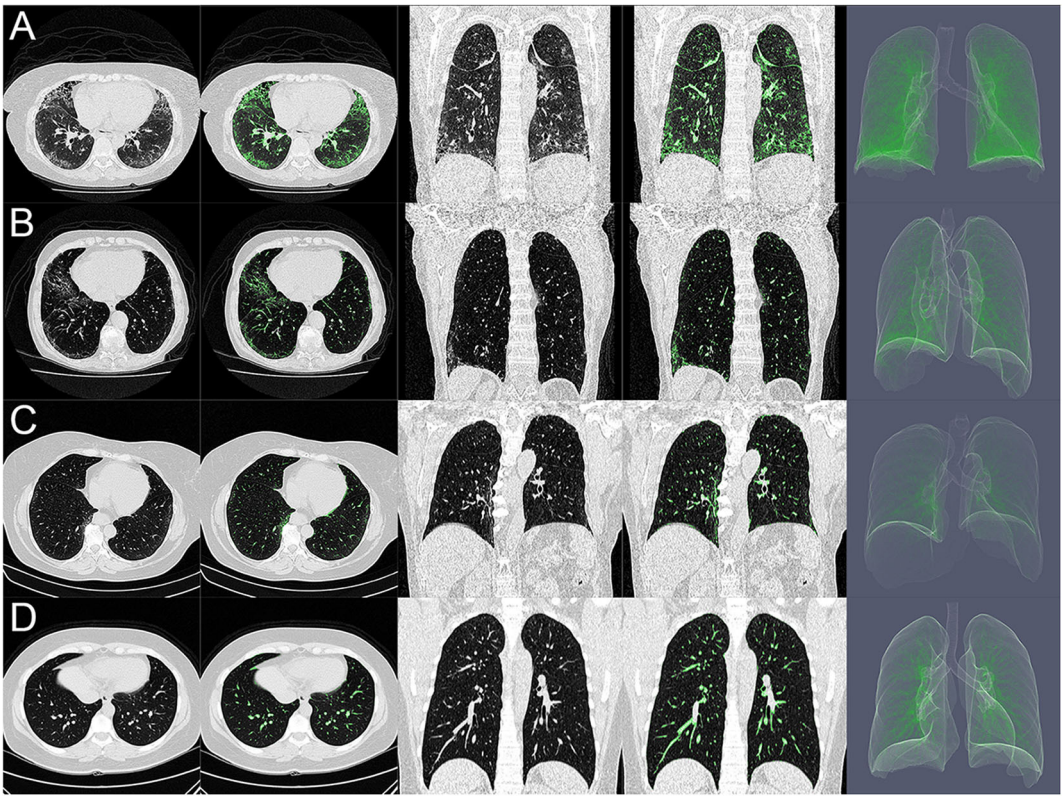

FIGURE 2 | (A–D) Show axial (columns 1 and 2) and coronal (columns 3 and 4) CT scans and three-dimensional rendering (column 5) of the lung of systemic sclerosis classified as with extensive interstitial lung disease (SSc Extensive-ILD, **A**), as with limited interstitial lung disease (SSc Limited-ILD, **B**), as with no interstitial lung disease (SSc No-ILD, **C**), and controls **(D)**. Note, in **(A)**, predominance of ground glass/reticular consolidation and compressed tissue likely related to cellular/fibrotic nonspecific interstitial pneumonia at basal lung third. Those in green are represented interstitial opacities with densities ranging from −500 and +50 HU that would represent the extent of pulmonary involvement.

In controls, interstitial opacities mainly represented peribronchial vessels and some ground glass (**Figure 2**, lowermost row), especially in dorsal–basal-dependent regions in older subjects (age $\geq$ 60 years) being quite comparable with SSc No-ILD patients (**Figure 2**, third row).

Eighteen (50%) patients with SSc Extensive-ILD presented FVC < 70%, being five patients initially classified as SSc Limited-ILD, and in only three SSc (8%) Extensive-ILD, a severe restrictive pattern (FVC < 50%) was observed. Moreover, SSc Extensive-ILD presented lower DL_{CO} (57.9 ± 17.9% vs. 73.7 ± 19.8%; $p < 0.001$) and TLV (2,916 ± 674 vs. 4,286 ± 1,136, $p < 0.001$), hyperinflated, and normally aerated tissue fraction, but not lower DL_{CO}/VA and total LW compared with those in SSc Limited-ILD (**Table 2**).

Moreover, the proportion of FVC/DL_{CO} ratio higher than 1.4 in subjects with severe DL_{CO} reduction (DL_{CO} < 55%) was very similar to that in patients with Extensive- and Limited-ILDs (22 and 21%, respectively).

Noteworthy, in five (31%) SSc No-ILD patients, a moderate reduction in DL_{CO} (55% < DL_{CO} < 80%) was observed with DL_{CO} ranging from 62 to 76% despite presenting no evidence of a restrictive pattern in spirometry. Additionally, the frequencies of occurrence of positive anti-topoisomerase I (ATA-1) and anti-centromere antibodies (ACA) were quite similar among SSc patients with no apparent relationship with ILD extent (**Table 2**).

In **Figure 3**, volume and tissue fractions are plotted against densities in HU. A reduction in the peak of volume and tissue fractions at densities related to normally aerated areas and a right-shift toward densities related to ground-glass opacities and consolidation were observed. In the **Supplementary Material**, videos of representative cases of SSc Extensive-ILD, Limited-ILD, and No-ILD are presented in axial and coronal slices (**Supplementary Videos 1**–**6**). Thus, it is possible to compare how tissue fractions vs. density relationships of patients with SSc differ from the control group, as the lung is visualized in axial and coronal sections.

Figure 4 presents the correlations between ILD extent, FVC (left panel), DL_{CO} (middle panel), and DL_{CO}/VA (right panel). A significant inverse and moderate to poor correlation were observed between ILD Extent and FVC ($r = -0.57$, $p < 0.001$) and between ILD extent and DL_{CO} ($r = -0.49$, $p < 0.001$) but not with DL_{CO}/VA ($r = 0.009$, $p = 0.99$).

Figure 5, upper panels, depicts ILD extent in the whole lung and the basal, middle, and apical thirds. Additionally, the extent of the pulmonary involvement from the subpleural layers to hilar

TABLE 2 | Demographic variables, pulmonary function tests, and densitometry considering scleroderma patients with less or greater pulmonary involvement.

	SSc-ILD (78)	SSc No-ILD (16)	*p*-value	
	SSc extensive- ILD (36)	SSc limited-ILD (42)		
Demographic data				
Females	34 (94%)	38 (90%)	15 (94%)	
Age (years)	51.7 ± 14.6	58.9 ± 12.3	49.5 ± 11.0	
BMI (kg/m^2)	25.8 ± 5.9	25.0 ± 5.7	25.4 ± 4.4	
SSc cutaneous involvement				
lc-SSc	22 (23%)	30 (32%)	12 (13%)	
dc-SSc	14 (15%)	12 (13%)	4 (4%)	
Type of antibody				
Anti-topoisomerase I antibody	4 (4%)	5 (5%)	4 (4%)	
Anti-centromere antibody	23 (24%)	25 (27%)	2 (2%)	
Anti-RNA polymerase III	–	2 (2%)	1 (1%)	
Autoantibody not identified	9 (9%)	10 (11%)	9 (9%)	
Pulmonary function tests				
FVC (% predicted)	**74.6 ± 22.0[a,b]**	**112.1 ± 18.5**	**113.5 ± 17.0**	**<0.001[a,b]**
50% < FVC < 70%	18 (50%)	0 (0%)	0 (0%)	
FVC < 50%	3 (8%)	0 (0%)	0 (0%)	
DL_{CO}/VA (% predicted)	84.1 ± 20.2	76.2 ± 18.5	88.3 ± 11.4	
DL_{CO} (% predicted)	**57.9 ± 17.9[a,b]**	**73.7 ± 19.8[c]**	**87.0 ± 13.3**	**<0.001[a,b] 0.04[c]**
DL_{CO} < 55%	17 (47%)	10 (24%)	0 (0%)	
55% < DL_{CO} < 80%	14 (39%)	12 (29%)	5 (31%)	
FVC(%)/DL_{CO}(%)	1.35 ± 0.38	1.62 ± 0.49	1.33 ± 0.25	**0.02[a]**
FVC(%)/DL_{CO}(%) > 1.4 and DL_{CO}(%) < 55%	8 (22%) **1.86 ± 0.28[a]**	9 (21%) **2.35 ± 0.48**	0 (0%)	**0.022**
CT densitometry				
TLV (mL)	**2,915.7 ± 673.9[a,b]**	**4,286.3 ± 1,136.5**	**4,541.0 ± 800.4**	**<0.001[a,b]**
Total lung weight (g)	723.3 ± 142.1	736.1 ± 158.7	780.7 ± 180.9	
Hyperinflated (%)	**4.6 ± 3.1[a,b]**	**9.8 ± 4.3**	**10.2 ± 4.5**	**<0.001[a,b]**
Normally aerated (%)	**58.7 ± 8.4[a,b]**	**63.9 ± 4.5**	**67.8 ± 4.9**	**0.002[a] <0.001[b]**
ILD Extent (%)	**36.7 ± 8.7[a,b]**	**26.3 ± 2.1[c]**	**22.0 ± 0.8**	**<0.001[a,b] 0.03[c]**

Values are presented as mean ± standard deviation. Bold characters indicate statistically significant differences.

[a] *Statistically significant difference between SSc Extensive-ILD and SSc Limited-ILD.*

[b] *Statistically significant difference between SSc Extensive-ILD and SSc No-ILD.*

[c] *Statistically significant difference between SSc Limited-ILD and SSc No-ILD.*

SSc No-ILD, scleroderma with no interstitial lung disease (ILD ≤ 25%); SSc-ILD, scleroderma with interstitial lung disease; SSc Limited-ILD, scleroderma with interstitial lung disease between 25 and 35%; SSc Extensive-ILD, scleroderma with interstitial lung disease higher than 35%; BMI, body mass index; FVC (%), forced vital capacity expressed as predicted values; DL_{CO}/VA, carbon monoxide diffusion capacity adjusted for alveolar volume expressed as predicted values; DL_{CO} (%), carbon monoxide diffusion capacity expressed as predicted values; TLV, total lung volume; Total lung weight, lung tissue fraction related to densities from −1,000 to +50 Hounsfield units (HU); Hyperinflated, tissue fraction related to densities from −1,000 to −901 HU; Normally Aerated, tissue fraction related to densities from −900 to −501 HU; ILD Extent, extent of interstitial lung disease defined as lung weight related to interstitial opacities normalized by total lung weight.

regions could be observed in SSc No-ILD and SSc Limited- and Extensive-ILDs (**Figure 5**, lower panels).

DISCUSSION

The main findings of the present study were (1) an optimal threshold of 23.4% of LW assigned as interstitial opacities was determined by ROC curve and used to classify 78 SSc patients as presenting ILD; (2) 36 (38%) SSc patients were classified as SSc Extensive-ILD and 42 (45%) as SSc Limited-ILD based on the *Z* score for interstitial opacities in patients with SSc relative to controls; (3) ILD extent negatively and moderately to poorly correlated with FVC and DL_{CO}, but not with DL_{CO}/VA; and (4) in patients with SSc Extensive-ILD, pulmonary involvement dispersed in all lung parenchyma from apical to basal thirds and from the periphery to hilar regions.

In healthy subjects, CT interstitial opacities are mainly related to vascular peribronchial network and, especially in older

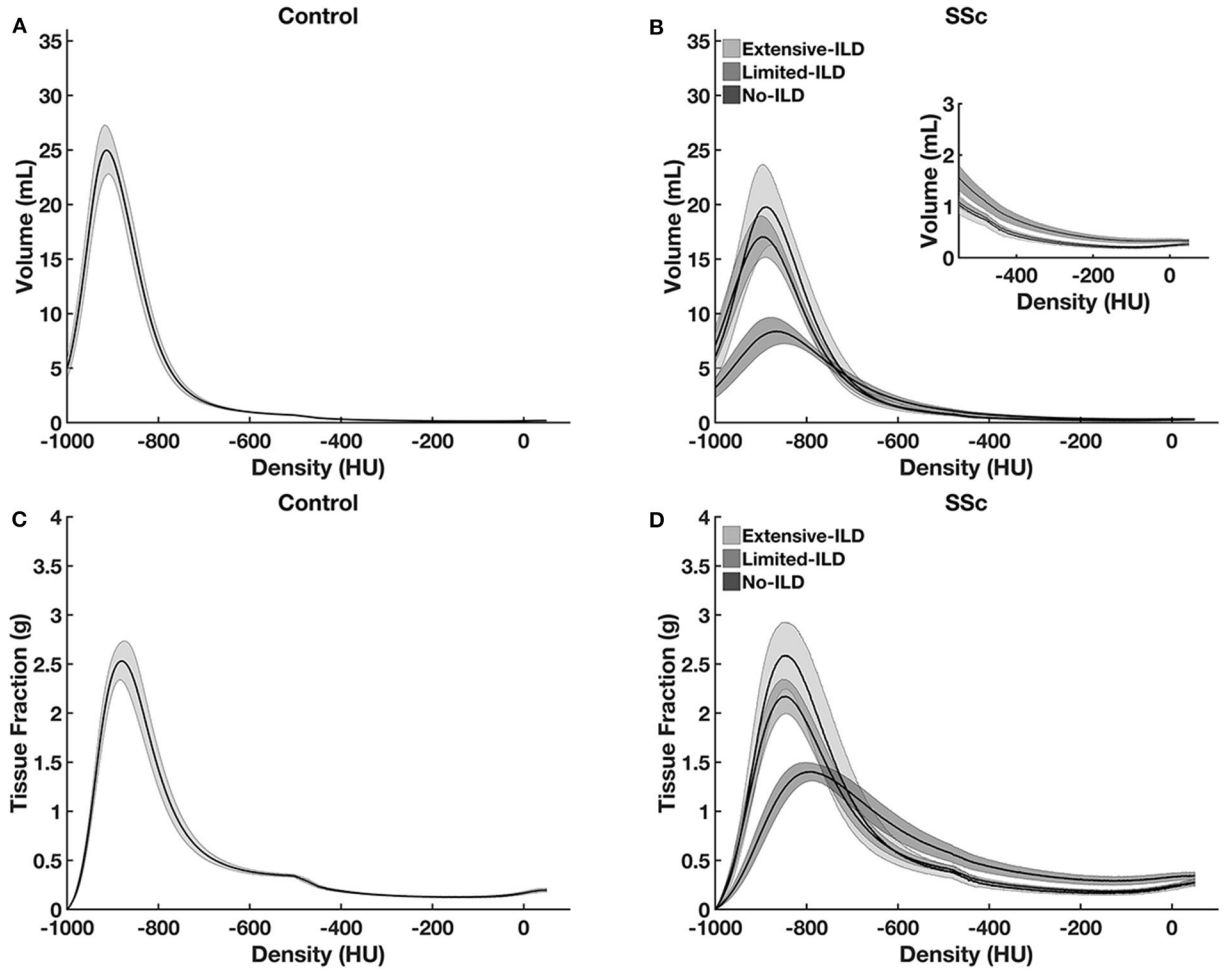

FIGURE 3 | Lung tissue volume **(A,C)** and lung tissue fraction **(B,D)** plotted against density in controls **(A,B)** and SSc-patients **(C,D)**. Note the peak volume and tissue fraction reduction and the right-shift of the histogram to higher densities from SSc No-ILD to SSc Extensive-ILD. Such aspect reflects lung volume reduction as well as tissue increase at higher densities, as ILD spreads through lung parenchyma. Graphs are presented with average, and the hatched areas correspond to the 95% coefficient interval.

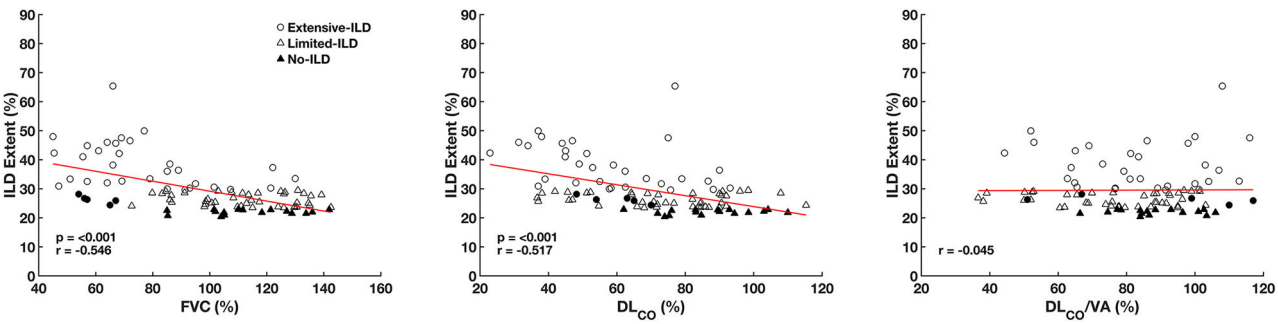

FIGURE 4 | Correlation between interstitial lung disease extent (ILD Extent), forced vital capacity (FVC), carbon monoxide diffusion capacity (DL_{CO}), and carbon monoxide diffusion capacity adjusted to alveolar volume (DL_{CO}/VA) expressed as predicted values considering all SSc patients. Circle symbols represent SSc Extensive-ILD, SSc Limited-ILD triangles, and SSc No-ILD patient filled triangles. Filled circles represent patients initially classified as SSc Limited-ILD but with an FVC < 70% being reclassified as SSc Extensive-ILD.

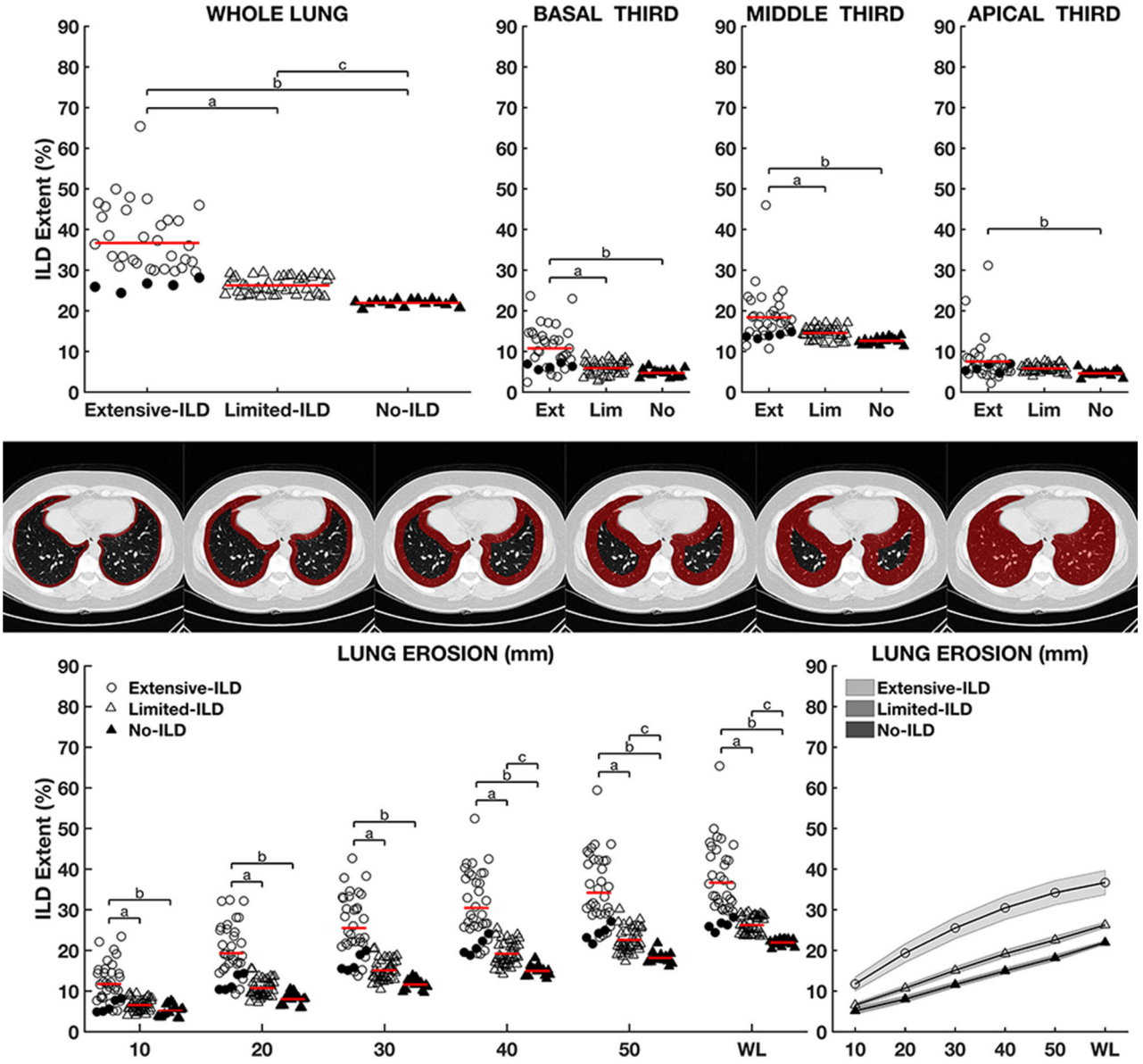

FIGURE 5 | Upper panels: Interstitial lung disease extent (ILD Extent) expressed as a percentage of total lung weight among groups considering the whole lung, basal, middle, and apical thirds. Lower panels: comparison between groups at different erosion depths from the outermost layer of the parenchyma hilar regions, outlined in the middle panels. Left panel shows ILD Extent in 10-mm steps, and right panel shows the continuous graphs with mean and 95% coefficient interval. Letters a, b, and c represent statistically significant differences between SSc Limited-ILD vs. No-ILD, SSc Diffuse-ILD vs. No-ILD, and SSc Diffuse-ILD vs. SSc Limited-ILD, respectively. Circle symbols represent SSc Extensive-ILD, SSc Limited-ILD and SSc No-ILD triangles, and patient filled triangles. Filled circles represent patients initially classified as SSc Limited-ILD but with an FVC < 70% being reclassified as SSc Extensive-ILD. Noteworthy, ILD Extent in SSc Extensive-ILD group was always significantly higher than in SSc Limited- and SSc No-ILD even in the subpleural surface (**Figure 4**, lower panels).

subjects and at dorsal-dependent regions, to areas with low ventilation/perfusion ratio (25–28). Thus, we speculate that tissue weight related to such opacities could be used as a potential indicator of ILD in SSc patients. Hence, the laborious exclusion of peribronchial vessels would not be necessary, and values above a certain normality threshold could be interpreted as ILD in patients with SSc.

The ROC curve from the weight of interstitial opacities in controls and SSc patients determined the optimal limit of normality of 23.4% of tissue weight related to interstitial opacities (**Figure 1**). The visual inspection of CT matched with computed interstitial opacities indicated that, in addition to peribronchial vessels, ground-glass opacities and reticular/focal consolidations were also identified (**Figure 2**) and could represent more than

40% of the total LW in one-third of patients classified as SSc Extensive-ILD (**Figures 1**, **5**).

The prevalence of ILD based on our proposed criteria was around 83% and is just slightly larger than previously reported data (prevalence of SSc-ILD up to 80%) (29). A spread distribution of ILD was observed in patients classified as SSc Extensive-ILD involving basal, middle, and apical lung thirds as well as lung periphery and central regions. On the other hand, SSc Limited-ILD pulmonary involvement concerned basal and middle thirds more extensively than SSc No-ILD (**Figure 4**).

An impaired pulmonary function was observed in patients classified as SSc Extensive-ILD with 58% presenting moderate/severe restrictive pattern in spirometry without airway obstruction and 86% presenting moderate/severe reduction in lung diffusion capacity. FVC is the main marker of restrictive ventilatory pattern, which is likely to be associated with fibrosis, whereas DL_{CO} is an indicator of alveolitis, ventilation–perfusion mismatch, vascular involvement, and fibrosis (27).

DL_{CO} seems to be more sensitive in detecting lung involvement than FVC, although it is less specific regarding ILD, as pulmonary vascular disease and coexisting fibrosis may also lead to decreased DL_{CO} (27, 28). Thus, a moderate and isolated reduction in DL_{CO} may also indicate just subclinical alveolitis (19), which might have occurred in 5 (31%) of our patients classified as SSc No-ILD.

Interestingly, no significant differences among SSc-ILD subjects were observed in terms of DL_{CO}/VA (**Table 2**). DL_{CO}/VA more specifically represents diffusion, as the transfer factor is clearly related to available lung surface estimated by VA (27). Thus, one could speculate that the observed DL_{CO} reduction in SSc Extensive-ILD was mainly associated with isolated pulmonary hypertension and not to a reduction of lung surface available for gas exchange.

However, the same proportion of SSc Extensive- (22%) and Limited-ILD patients (21%) had both DL_{CO} and FVC severely reduced, thus presenting an FVC/DL_{CO} ratio higher than 1.4, stressing that isolated pulmonary hypertension could not exclusively explain the reduction in DL_{CO} (19) both in Extensive- and Limited-ILDs.

The main limitation of this study is the small number of SSc patients. This aspect could have an impact on the power of our study. However, patients included herein were well characterized clinically, radiographically, and functionally. Another important limitation is the need for a threshold of normality for ILD determination in SSc patients as well as a severity classification, with Z score mainly related to the average weight of interstitial opacities in controls. Although an impaired pulmonary function was observed in SSc Extensive-ILD, it is not yet possible to assess whether those classified as SSc Limited-ILD would benefit from any specific antifibrotic therapy (30).

Finally, the application of densitometry is not the only method for quantitative evaluation in chest CT images. Other methods based on deep-learning or even texture analysis (31, 32) have been successfully applied to similar subjects. However, densitometric assessment methods are computationally very simple and do not require prior preparation of libraries or image banks with their respective radiological pattern classification.

In conclusion, SSc-ILD could be automatically quantified by computing LW related to interstitial opacities in densities ranging from −500 to +50 HU. Patients with SSc, who had an ILD extent greater than about 30% of total LW, exhibited moderate to severe restrictive pattern and reduced diffusion capacity with ILD spread throughout the entire lung parenchyma. The proposed method seems to provide an alternative to estimate ILD in patients with SSc, mitigating the subjectivity of semiquantitative analyzes based on visual scores. Further follow-up studies of SSc patients using the presently described method could clarify the extent of pulmonary involvement and suggest the therapeutic window for pulmonary fibrosis-inhibiting drugs.

DATA AVAILABILITY STATEMENT

All datasets presented in this study are included in the article/**Supplementary Material**.

ETHICS STATEMENT

The protocol was approved at the Research Ethics Committee from the UERJ (CAAE-50752615.9.0000.5259) and from CHUP (reference number 2019.353, 288-DEFI/307-CE), and it complied with the current national and international standards. The ethics committee waived the requirement of written informed consent for participation. Written informed consent was obtained from the individual(s) for the publication of any potentially identifiable images or data included in this article.

AUTHOR CONTRIBUTIONS

AC: image processing and analysis of results, statistical evaluation, theoretical development of software, the computation method of voxel-to-voxel analysis, and writing of the text and submission of the article. AG: image processing and segmentation and statistical evaluation. FS and MF: capture and organization of clinical data and draft review. RR: capture and organization of clinical data, discussion of results, and draft review. BS, AL, and IA: capture and organization of clinical data. WZ: draft review. All authors contributed to the article and approved the submitted version.

FUNDING

This research was supported by the Brazilian Council for Scientific and Technological Development (Conselho Nacional de Desenvolvimento Científico e Tecnológico-CNPq) and the Rio de Janeiro State Research Supporting Foundation (Fundação de Amparo à Pesquisa do Estado do Rio de Janeiro-FAPERJ).

SUPPLEMENTARY MATERIAL

The Supplementary Material for this article can be found online at: https://www.frontiersin.org/articles/10.3389/fmed.2020.577739/full#supplementary-material

Supplementary Videos | Axial (Videos 1–3) and coronal (Videos 4–6) chest CT scans of representative patient with systemic sclerosis classified as with extensive (SSc Extensive-ILD, Video 1), limited (SSc Limited-ILD, Video 2) and with no interstitial lung disease (SSc No-ILD, Video 3). Lung tissue fraction is plotted against density in controls, as mean (white line) and one standard deviation (hatched area). In each slice the plot of cumulative lung tissue fraction against density is presented in each SSc subgroups (green line). Note the progressive separation from the control group. For comparison purposes, the average values of hyperinflated areas, normally aerated and the tissue weight related to interstitial opacities are presented (outermost right panels) in the control group (gray) and in each group of patients with systemic sclerosis (red bars).

REFERENCES

1. Doyle TJ, Dellaripa PF. Lung manifestations in the rheumatic diseases. *Chest*. (2017) 152:1283–95. doi: 10.1016/j.chest.2017.05.015
2. Saketkoo LA, Magnus JH, Doyle MK. The primary care physician in the early diagnosis of systemic sclerosis: the cornerstone of recognition and hope. *Am J Med Sci*. (2014) 347:54–63. doi: 10.1097/MAJ.0b013e3182a55d24
3. Desai SR, Veeraraghavan S, Hansell DM, Nikolakopolou A, Goh NSL, Nicholson AG, et al. CT features of lung disease in patients with systemic sclerosis: comparison with idiopathic pulmonary fibrosis and nonspecific interstitial pneumonia. *Radiology*. (2004) 232:560–7. doi: 10.1148/radiol.2322031223
4. Wells AU, Margaritopoulos GA, Antoniou KM, Denton C. Interstitial lung disease in systemic sclerosis. *Semin Respir Crit Care Med*. (2014) 35:213–21. doi: 10.1055/s-0034-1371541
5. Bouros D, Wells AU, Nicholson AG, Colby TV, Polychronopoulos V, Pantelidis P, et al. Histopathologic subsets of fibrosing alveolitis in patients with systemic sclerosis and their relationship to outcome. *Am J Respir Crit Care Med*. (2002) 165:1581–6. doi: 10.1164/rccm.2106012
6. Cappelli S, Bellando Randone S, Camiciottoli G, De Paulis A, Guiducci S, Matucci-Cerinic M. Interstitial lung disease in systemic sclerosis: where do we stand? *Eur Respir Rev*. (2015) 24:411–9. doi: 10.1183/16000617.00002915
7. Hoffmann-Vold A-M, Aaløkken TM, Lund MB, Garen T, Midtvedt Ø, Brunborg C, et al. Predictive value of serial high-resolution computed tomography analyses and concurrent lung function tests in systemic sclerosis. *Arthritis Rheumatol*. (2015) 67:2205–12. doi: 10.1002/art.39166
8. Hansell DM, Goldin JG, King TE, Lynch DA, Richeldi L, Wells AU. CT staging and monitoring of fibrotic interstitial lung diseases in clinical practice and treatment trials: a position paper from the Fleischner Society. *Lancet Respir Med*. (2015) 3:483–96. doi: 10.1016/S2213-2600(15)00096-X
9. Walsh SLF, Calandriello L, Sverzellati N, Wells AU, Hansell DM, Observer Consort UIP. Interobserver agreement for the ATS/ERS/JRS/ALAT criteria for a UIP pattern on CT. *Thorax*. (2016) 71:45–51. doi: 10.1136/thoraxjnl-2015-207252
10. Watadani T, Sakai F, Johkoh T, Noma S, Akira M, Fujimoto K, et al. Interobserver variability in the CT assessment of honeycombing in the lungs. *Radiology*. (2013) 266:936–44. doi: 10.1148/radiol.12112516
11. Ariani A, Silva M, Bravi E, Saracco M, Parisi S, De Gennaro F, et al. Operator-independent quantitative chest computed tomography versus standard assessment of interstitial lung disease related to systemic sclerosis: a multi-centric study. *Modern Rheumatol*. (2015) 25:724–30. doi: 10.3109/14397595.2015.1016200
12. Tashkin DP, Volkmann ER, Tseng C-H, Kim HJ, Goldin J, Clements P, et al. Relationship between quantitative radiographic assessments of interstitial lung disease and physiological and clinical features of systemic sclerosis. *Ann Rheum Dis*. (2016) 75:374–81. doi: 10.1136/annrheumdis-2014-206076
13. van den Hoogen F, Khanna D, Fransen J, Johnson SR, Baron M, Tyndall A, et al. 2013 classification criteria for systemic sclerosis: an American College of Rheumatology/European League against Rheumatism collaborative initiative. *Ann Rheum Dis*. (2013) 72:2737–47. doi: 10.1136/annrheumdis-2013-204424
14. LeRoy EC, Black C, Fleischmajer R, Jablonska S, Krieg T, Medsger TA, et al. Scleroderma. (systemic sclerosis): classification, subsets and pathogenesis. *J Rheumatol*. (1988) 15:202–5.
15. Miller MR. General considerations for lung function testing. *Eur Respir J*. (2005) 26:153–61. doi: 10.1183/09031936.05.00034505
16. Neder JA, Andreoni S, Castelo-Filho A, Nery LE. Reference values for lung function tests. I Static volumes. *Braz J Med Biol Res*. (1999) 32:703–17. doi: 10.1590/S0100-879X1999000600006
17. Neder JA, Andreoni S, Peres C, Nery LE. Reference values for lung function tests. III Carbon monoxide diffusing capacity (transfer factor). *Braz J Med Biol Res*. (1999) 32:729–37. doi: 10.1590/S0100-879X1999000600008
18. de Pereira CA, Sato T, Rodrigues SC. New reference values for forced spirometry in white adults in Brazil. *J Bras Pneumol*. (2007) 33:397–406. doi: 10.1590/S1806-37132007000400008
19. Steen VD, Graham G, Conte C, Owens G, Medsger TA. Isolated diffusing capacity reduction in systemic sclerosis. *Arthritis Rheum*. (1992) 35:765–70. doi: 10.1002/art.1780350709
20. Fedorov A, Beichel R, Kalpathy-Cramer J, Finet J, Fillion-Robin J-C, Pujol S, et al. 3D Slicer as an image computing platform for the Quantitative Imaging Network. *Magn Reson Imaging*. (2012) 30:1323–41. doi: 10.1016/j.mri.2012.05.001
21. Staring M, Bakker ME, Stolk J, Shamonin DP, Reiber JHC, Stoel BC. Towards local progression estimation of pulmonary emphysema using CT. *Med Phys*. (2014) 41:021905. doi: 10.1118/1.4851535
22. Stoel BC, Vrooman H, Stolk J, Reiber J. Sources of error in lung densitometry with CT. *Invest Radiol*. (1999) 303–9. doi: 10.1097/00004424-199904000-00008
23. Camilo GB, Carvalho ARS, Machado DC, Mogami R, Melo PL, Lopes AJ. CT pulmonary densitovolumetry in patients with acromegaly: a comparison between active disease and controlled disease. *Br J Radiol*. (2015) 88:20150315. doi: 10.1259/bjr.20150315
24. Goh NSL, Desai SR, Veeraraghavan S, Hansell DM, Copley SJ, Maher TM, et al. Interstitial lung disease in systemic sclerosis: a simple staging system. *Am J Respir Crit Care Med*. (2008) 177:1248–54. doi: 10.1164/rccm.200706-877OC
25. Millar AB, Denison DM. Vertical gradients of lung density in supine subjects with fibrosing alveolitis or pulmonary emphysema. *Thorax*. (1990) 45:602–5. doi: 10.1136/thx.45.8.602
26. Sa RC, Cronin MV, Cortney Henderson A, Holverda S, Theilmann RJ, Arai TJ, et al. Vertical distribution of specific ventilation in normal supine humans measured by oxygen-enhanced proton MRI. *J Appl Physiol*. (2010) 109:1950–9. doi: 10.1152/japplphysiol.00220.2010
27. Behr J, Furst DE. Pulmonary function tests. *Rheumatology*. (2008) 47:v65–7. doi: 10.1093/rheumatology/ken313
28. Guttadauria M, Ellman H, Emmanuel G, Kaplan D, Diamond H. Pulmonary function in scleroderma. *Arthritis Rheum*. (1977) 20:1071–9. doi: 10.1002/art.1780200506
29. Taormina VJ, Miller WT, Gefter WB, Epstein DM. Progressive systemic sclerosis subgroups: variable pulmonary features. *AJR Am J Roentgenol*. (1981) 137:277–85. doi: 10.2214/ajr.137.2.277
30. Distler O, Highland KB, Gahlemann M, Azuma A, Fischer A, Mayes MD, et al. Nintedanib for systemic sclerosis-associated interstitial lung disease. *N Engl J Med*. (2019) 380:2518–28. doi: 10.1056/NEJMoa1903076
31. Occhipinti M, Bosello S, Sisti LG, Cicchetti G, de Waure C, Pirronti T, et al. Quantitative and semi-quantitative computed tomography analysis of interstitial lung disease associated with systemic sclerosis: a longitudinal evaluation of pulmonary parenchyma and vessels. *PLoS ONE*. (2019) 14:e0213444. doi: 10.1371/journal.pone.0213444
32. Yabuuchi H, Matsuo Y, Tsukamoto H, Horiuchi T, Sunami S, Kamitani T, et al. Evaluation of the extent of ground-glass opacity on high-resolution

CT in patients with interstitial pneumonia associated with systemic sclerosis: comparison between quantitative and qualitative analysis. *Clin Radiol*. (2014) 69:758–64. doi: 10.1016/j.crad.2014.03.008

Conflict of Interest: The authors declare that the research was conducted in the absence of any commercial or financial relationships that could be construed as a potential conflict of interest.

frontiers in Medicine

REVIEW
published: 30 October 2020
doi: 10.3389/fmed.2020.587827

The Role of Ultrasound Across the Inflammatory Arthritis Continuum: Focus on "At-Risk" Individuals

Laurence Duquenne[1,2*†], *Rahaymin Chowdhury*[3†], *Kulveer Mankia*[1,2] *and Paul Emery*[1,2]

[1] Leeds Biomedical Research Centre—NIHR, Leeds, United Kingdom, [2] Leeds Institute of Rheumatic and Musculoskeletal Medicine, University of Leeds, Leeds, United Kingdom, [3] Leeds Teaching Hospital Trust, Leeds, United Kingdom

In individuals at-risk of developing inflammatory arthritis, the value of an ultrasound (US) scan assessment to predict progression has been demonstrated repeatedly. However, depending on recruitment criteria, these individuals may be at different stages in the arthritis development continuum, therefore representing a heterogeneous population. As a consequence, the predictive value of ultrasound results may differ between cohorts. As other reviews have focused on the challenges in population recruitment or have combined biomarkers predicting value according to one recruitment pathway, we wanted to focus on the sole use of ultrasound assessment and its variation according to population recruitment criteria. In this review, we discuss the use of ultrasound in the different at-risk populations across the inflammatory arthritis disease continuum. This review demonstrates that although some sub-population data is scarce, ultrasound is best predictive in three at-risk populations: those with a positive ACPA test in the context of non-specific MSK symptoms, those with clinically suspect arthralgia and those with palindromic rheumatism. We consider that ultrasound assessment will be a cornerstone in prediction risk modeling and prevention studies of the preclinical phases of IA in the future.

Keywords: arthritis (including rheumatoid arthritis), ultrasound, at risk, prediction, ACPA, anti-cyclic citrullinated peptide antibodies

OPEN ACCESS

Edited by:
Raj Sengupta,
Royal National Hospital for Rheumatic Diseases, United Kingdom

Reviewed by:
Jose Inciarte-Mundo,
Hospital Clínic de Barcelona, Spain
Arti Mahto,
King's College Hospital NHS Foundation Trust, United Kingdom

***Correspondence:**
Laurence Duquenne
l.duquenne@leeds.ac.uk

†These authors share first authorship

Specialty section:
This article was submitted to Rheumatology, a section of the journal Frontiers in Medicine

Received: *27 July 2020*
Accepted: *12 October 2020*
Published: *30 October 2020*

Citation:
Duquenne L, Chowdhury R, Mankia K and Emery P (2020) The Role of Ultrasound Across the Inflammatory Arthritis Continuum: Focus on "At-Risk" Individuals. Front. Med. 7:587827. doi: 10.3389/fmed.2020.587827

INTRODUCTION

Since the availability of biologic therapies, rheumatology practice has entered a new era where achieving damage free remission in rheumatoid arthritis (RA) is not only feasible, but common. As early treatment decreases long term joint damage and impaired quality of life, much effort has been made to refer, diagnose and treat patients early (1). We are now evolving toward the next stage of inflammatory arthritis management: prevention. The new priority is to identify individuals that might eventually develop inflammatory arthritis (IA): the "At-risk" individuals and treat them before arthritis occurs thereby preventing progression to RA. At-risk individuals with subclinical inflammation are at increased risk of arthritis development. It is therefore logical to suggest that this population should be considered for treatment, therefore should be included in the "window of opportunity" (2).

One of the many challenges is that arthritis development is a late step in a long process sometimes called "the inflammatory arthritis disease continuum" (3), where the preclinical phase

includes, genetic, environmental, and systemic factors which may arise years before arthritis occurs (4, 5). When recruited into research cohorts, at-risk individuals might be at different stages of the continuum therefore representing heterogeneous populations, with differing risks of progression to IA.

In this review, we discuss the use of ultrasound (US) in the different at-risk populations across the arthritis disease continuum (see **Figure 1**). The populations in which US may be most informative will be discussed. We included peer-reviewed, published research including, retrospective and prospective analyses, observational, and interventional studies that were relevant for research and clinical practice. Only articles in English language were included.

US Findings in Healthy Subjects

As the aim of this review is to describe the evidence of US abnormalities in the preclinical phase of IA, it seems important to first consider their prevalence in healthy subjects. A first analysis found a power Doppler (PD) signal in 11% of hands and wrists of 27 healthy volunteers, especially in the wrists (6). Using the OMERACT consensus, analysis of 127 healthy controls (HC) matched with another 127 patients with early arthritis from the ESPOIR cohort found that 11% of the MCP joints 2–4 and fifth MTP joints analyzed had bone erosions (BE), 22% had synovial hypertrophy (SH) $\geq$ grade 1 and 9% $\geq$ grade 2 (7). Another study showed high prevalence of SH grade 1 in healthy subjects (15%) as well as in RA patients (56%), and no association with PD, tenderness or swelling, suggesting that only Grade $\geq$ 2 should be considered pathological (8). This is also suggested by a analysis on 46 young healthy subject who showed SE in almost 20% of them (9).

The most comprehensive analysis included 32 joints of 207 HC subjects (6,621 joints in total) (10), showing that the prevalence of US abnormalities was low at joint level but high at individual level 9 vs. 88%), and most commonly synovial effusion (SE) (69% of joints with an abnormality). BE were found only in first metatarso-phalangeal (MTP1) joints ($n = 4$) and always with PD. The most prevalent joints with US findings were the MTP1 joints followed by MTP joints 2 to 5, then wrists, metacarpo-phalangeal (MCP) joints (especially the third), and finally proximal inter-phalangeal (PIP) joints which were almost never involved. Grade 1 was the most commonly score found, higher grades were only found in feet (10). Grade 1 SE and SH were highly prevalent in healthy subjects, the authors suggested excluding these parameters from the OMERACT ultrasound protocols (7, 10). None of the analyses showed differences between men and women. Only one study showed significant effect of age, especially in the feet (10). While all of the above studies used semi-quantitative measurement, another analysis of 78 individuals determined quantitative measurement of the radio-carpal abnormalities with a greater chance to indicate RA (11).

Taken together the above studies suggest that the presence of low grade US abnormalities (especially grade 1 SE and SH and feet localization) are often present and therefore should not be considered pathognomonic for inflammatory arthritis. It is interesting to notice differences between each MTP, the first and fifth showing the most abnormalities and that larger joints such as elbows, ankles and shoulders have not been analyzed. Also, midfoot joints are not considered in any of the studies. The EULAR-OMERACT combined score defined synovitis as both PD and GS$\geq$1 (GS including SH and SE), including only small joints, with no difference of scoring between joints (12).

The Use of US in First Degree Relatives of Patients With RA

Because a family history of RA has been shown to increase the risk of developing this disease, the use of

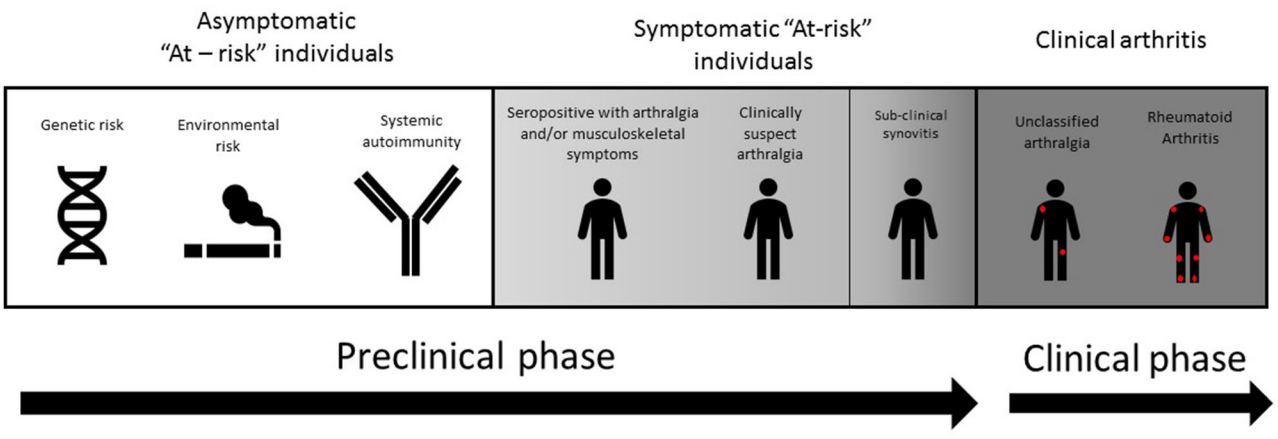

FIGURE 1 | Evolution toward rheumatoid arthritis (RA) can be considered as a disease continuum encompassing pathogenic phases which conclude in the development of arthritis. Preclinical phases can comprise of a symptomatic at-risk individuals with genetic risk (e.g. an affected first degree relative), environmental risk (including smoking and mucosal inflammation), and RA-related systematic autoimmunity (e.g. ACPA antibodies). Subclinical synovitis is more often found in symptomatic at-risk individuals, either in the presence of RA associated autoantibodies, or clinically suspect arthralgia (CSA).

US as a prediction tool for the development of arthritis in first degree relatives (FDRs) of RA probands has been investigated.

A small study of 20 patients with RA and 25 of their FDRs was undertaken to explore the presence of abnormal US findings in FDRs without clinical arthritis (13, 14). Eight FDRs had arthralgia symptoms, but all were negative for RF and ACPA. The study confirmed the presence on US of inflammatory activity in FDRs (10/25 patients, 40%) and offers support for the use of US as a screening tool in this at-risk population. This study was limited by the small number of participants and did not present the US findings in detail.

A large prospective study investigated a cohort of 237 FDRs of RA patients (15). The population included a spread across the spectrum of RA development and was classified into four groups (three preclinical and one clinical). The first group were those "without risk factors," meaning those negative for the shared epitope, anti-citrullinated protein antibody (ACPA) or rheumatoid factor (RF) and had no symptoms of possible RA ($n = 45$). The second group had risk factors, with either presence of one or two copies of the shared epitope or an ACPA positive test but no symptoms associated with possible RA ($n = 38$). The third group included subjects with inflammatory arthralgia, or self-reported symptoms associated with possible RA ($n = 132$) and the fourth group had features of unclassified arthritis (UA) ($n = 58$). The authors found that active US findings were associated with the presence of UA on examination but not with the earlier preclinical phases of RA development, including those who had genetic risk factors but were asymptomatic. There was no statistical significance between the US results of ACPA positive and negative FDRs, however it is worth noting that the US scores for these groups were quite low, [mean B-mode score (SD): 6.7 (3.6) vs 6.8 (3.6)], OR: 1.0 (95% CI: 0.9 to 1.1); mean Doppler score (SD): 0.8 (1.3) vs. 1.2 (1.9), OR: 1.2 [95% CI: (0.9 to 1.6]). In addition, there were no demographic or clinical risk factors significantly associated with active US findings except for older age.

These results do not support a role for US in FDRs without symptoms, as part of a screening strategy for preclinical RA detection in FDRs, with the possible exception of those with UA features. Further analysis on the individuals who are positive with the shared epitope and/or an ACPA tests would improve categorizing risk populations.

The Use of US in Individuals With Clinically Suspect Arthralgia

Other studies have explored the use of ultrasound in predicting IA in patients with clinically suspect arthralgia (CSA). CSA was defined by EULAR as a set of characteristics to be used in patients with arthralgia without clinical arthritis and without other diagnosis or explanation for the arthralgia (16).

Although many of the following studies were performed prior to this definition, they do follow the same theme of including patients who had inflammatory arthralgia but had no clinical synovitis (CS). An example of this is a large multicentre study which included patients who presented with at least two painful joints but no CS, with symptoms that lasted less than a year (17). Of the 196 patients who were included, 159 patients completed follow up over a 1 year period, only 15% were ACPA positive. The authors defined US synovitis as GS ≥ 2 and PD ≥ 1 and reported a statistically significant association between US synovitis and prediction of IA (OR 3.03, 95% [CI: 1.69–5.41]). They concluded that the lack of US synovitis was a strong negative predictor for IA. These findings were further supported by a retrospective analysis of 80 consecutive patients using SONAR B-mode criteria to determine significant synovitis (18, 19). They found that significant US GS synovitis appeared to be the only independent predictor of RA on multivariate analysis (OR 7.4 [95%CI: 1.19–42.8]) in ACPA negative patients who presented with poly-arthralgia and no CS.

A recent study compared the US and MRI results of 70 individuals with CSA ($n = 40$) and early IA ($n = 30$). They showed an overall significant correlation between both imaging techniques regarding synovitis and tenosynovitis, especially in the MCP and wrists joints, although MRI was more sensitive. Although less frequently present in the CSA subgroup, similar results of concordance were found, but with a lower sensitivity (20).

Thus, the literature would suggest that US does add additional value to clinical and laboratory investigations in predicting IA in those with CSA. However, there are a paucity of data on US as MRI has been preferred and further US investigation is recommended.

The Use of US in ACPA (and/or RF) Positive Individuals With Musculoskeletal Symptoms

There have been various studies on the use of US to predict RA in at-risk populations who have been selected on the base of an ACPA and/or RF positive, with MSK symptoms (including arthralgia), but no CS.

An important observational cohort study investigating US as a predictor for IA in ACPA positive at-risk individuals was conducted by a group in Leeds (21). The 100 consecutive participants included were ACPA positive, had a new non-specific musculoskeletal (MSK) symptom, but no CS. They demonstrated in multivariable analysis a significant association between PD at the patient level and the development of IA (HR 1.88 [95% CI 1.07–3.29]) and incorporated it in a prediction model including serological and clinical measures. In Amsterdam, a prospective cohort study of 192 participants who were ACPA and/or RF positive, found that Gray Scale (GS) and PD were predictive for IA at the joint level, but this did not reach statistical significance at the patient level, meaning that there was a significance in US findings predicting which joint would progress to clinical arthritis, but not which patients would progress to IA (22). It is useful to note that US protocols varied between both studies; while Amsterdam's US protocol included only painful, adjacent, and contralateral joints if hands were involved, the Leeds study included all MCP joints, PIP joints and both wrists. A follow up study in Leeds included 136 individuals and added MTP joints to the analysis (23), they concluded that all US findings (BE grade ≥ 1, GS grade ≥ 2 and PD grade ≥ 1)

could predict progression to IA and its timing, with the risk being greatest in those patients with at least one joint with PD signal on US. Unlike the Amsterdam cohort, the predictive value of PD was significant at both the joint and patient level. The discrepancy in findings may have been due to the differing inclusion criteria in the studies. While the Amsterdam cohort included about a third of RF positive—ACPA negative individuals, Leeds group included only ACPA positivity, suggesting that individuals in the two cohorts could have been at different level of progression risk. Additionally, the US protocols in both studies were different, Leeds scanned 32 joints including bilateral wrists, MCPs, PIPs and MTPs. Both studies were amongst the first to include only patients without CS.

A follow up prospective cohort study from Amsterdam (24) included a cohort of 163 seropositive (RF and/or ACPA) patients who had arthralgia but no CS in a prospective cohort. After excluding metatarsophalangeal joints (MTPs), they showed that GS had a significant predictive value to progression to IA (OR 6.6 [95%CI 1.9–22]). Unlike the other above studies, PD was not found to be predictive in this study. The authors attributed this main difference to the alternative scanning protocol and technical differences in US machines. Differences can also be ascribed to the inclusion criteria, as Nam et al. included ACPA positive patients only (18).

In two further analyses, the first (25) analyzed US images from 319 patients and found that the number of joints with PD or tenosynovitis (TSV) was predictive of progression to IA with high specificity and moderate sensitivity with respective hazard ratios of 1.2 ($p = 0.026$) and 1.13 ($p = 0.025$), the addition of ACPA titer improved the predictive value of the number of joints with PD with a specificity/sensitivity of 0.92/0.34 (AUC 0.964). The authors also suggested that a selection of joints—mainly in the hands and feet—with better predictive power could improve US sensitivity. Another multivariable analysis on the same population ($n = 488$) showed that individuals with 1–3 joints with a PD signal or 1–2 with BE were twice as likely to develop IA, those with ≥ 4 joints with a PD signal were more than six times more likely (26). A more recent study (27) analyzed baseline US scans of a further 419 CCP positive at-risk individuals from the Leeds CCP cohort. In this analysis, the most predictive features for the development of clinical arthritis on US were BE in >1 joint or BE combined with synovitis in the MTP5 joint (OR 10.6 [95% CI 1.9 to 60.4] $p < 0.01$) and 5.1 [95% CI 1.4 to 18.9] $p = 0.02$] respectively. While presence of BE in any joint was previously described predictive of progression to IA (23), this study suggests that some joints might be more specific for progression.

Overall, the discrepancies in some of the findings are likely due to population variability: whether selected individuals are tested positive for RF and/or ACPA, associated symptoms and set of joints analyzed, but also the factors around how to perform the US itself, defining US synovitis, the optimum number and specific joints to be incorporated in the US protocol and the use of different scoring systems.

The above studies demonstrate that there is strong evidence that all US features including GS, BE, TSV, and especially PD presence, have an important part to play in predicting IA in seropositive at-risk individuals with MSK symptoms. They also discussed scanning protocols, while a limited, focused joint set can be used to identify erosions and predict arthritis; pragmatic scanning protocol could be easily incorporated into clinical practice. Ideally future studies should use standardized US protocols and scoring systems.

The Use of US in Individuals With Palindromic Rheumatism

Some individuals—ACPA positive or not—present with intermittent inflammatory flares, alternating between short attacks of pain and swelling and asymptomatic periods. Specific clinical and US features found in these individuals suggest that palindromic rheumatism (PR) could be a discrete pathological entity (28). However, shared risk factors with RA suggest PR could also be considered a phase of the RA continuum (3). Different studies have focused on this population, whether it be during or in-between flares of joint symptoms. In all these analyses, the proportion of ACPA positive patients ranges between 13 and 66.7%.

In 2014, a group analyzed 11 joints in the hands of 54 patients outside of a flare (29). The joints reported to be involved in the first flare varied according to ACPA status, with an increased ratio of small joints involvement in ACPA positive participants. This antibody based discrepancy was confirmed on US performed between flares. At the joint level, they found that only 2.8% of the 1,188 joints analyzed had SH$\geq$2, with PD$\geq$1 in 1.4% of these, mostly wrists and MCP. At the patient level, 25.9% of them presented US synovitis in at least one joint (SH$\geq$2, or PD$\geq$1). Patients in this cohort had long disease duration (mean duration of 11.6 years) and 61.1% were on DMARDs (mainly hydroxychloroquine). Ten patients of this study were also assessed during a flare, none of them showed periarticular US abnormalities, seven showed an intra-articular PD signal.

In a small cohort ($n = 15$), analysis of US scans taken during flares in the hands and wrists showed US synovitis in 60% of individuals ($n = 9/15$), with PD in 6 of them (30). The largest analysis to date was based on 84 PR patients during a flare (31). While 78% of the participants had signs of PD presence, only 31% of these were intra-articular PD, the rest were features of TSV and/or periarticular soft tissue inflammation. Moreover, Intra-articular PD presence and ACPA positivity were both recognized as predictors of progression to RA (respectively: OR = 2.28 [95%CI: 0.67–7.68] and OR = 6.18 [95% CI: 1.50–25.52]).

The most recent imaging analysis in PR was performed on 79 individuals comparing US and MRI (32). This analysis was the first to include treatment-naïve individuals, with a short duration of symptoms. The authors compared US examinations taken during and between flares, and showed US of the flaring area showed significantly more TSV (23 vs. 4%), more signs of extra-capsular inflammation (61 vs. 15%), particularly periarticular inflammation (39 vs. 4%), (and non-significantly different PD synovitis [23 vs. 7%]) than in-between flares. Interestingly, there was no influence of the antibody status on the US features. These results suggest that palindromic rheumatism has a discrete imaging phenotype and that some features such as ACPA positivity and intra-articular inflammation during a flare may increase the risk of developing RA.

These studies all included individuals with PR, which US has revealed some specific features such as higher proportion of extra-capsular abnormalities compared to at-risk and RA individuals. Discrepancies can be explained by recruitment criteria differences such as the use of previous medication, proportion of ACPA positive individuals and symptoms duration. Two analyses showed predominance of US extra-articular inflammation while all showed presence of sub-clinical inflammation.

Ultrasound in Undifferentiated Arthritis

Early diagnosis is a priority, it is therefore essential to improve diagnostic success rates at first referral. Because of its power and accessibility, US is now recognized as an essential tool for IA diagnosis and management. We have discussed US findings and implication in individuals with no CS (the at-risk populations), individuals with intermittent CS (palindromic rheumatism). Here we discuss how US use has been a major tool in assessing patients at CS onset. This chapter will not focus on RA patients but those with undifferentiated arthritis (UA) who are presenting with early CS but do not meet classification criteria for a specific rheumatic disease."

Many studies have shown US superiority to clinical examination in detecting synovitis (33–35). In a cohort of 50 ACPA and RF negative patients with UA from early arthritis clinics, they showed that IA probability increased from 6 to 8–85% depending on which two US features were present (GS = 3, PD $\geq$ 1 or BE presence) (36). This was confirmed in a large study ($n = 831$) where 31% of patients progressed to persistent IA, baseline serological and clinical biomarkers were already predictive of progression, but US improved all predictive values, particularly in the seronegative patients (AUC increase of 9%, $p < 0.001$) (37). Another study focused on EULAR classification criteria for RA, with the same recruitment criteria ($n = 109$), 61% of participants presented with a swollen joint, 30% were ACPA+ (compared to 15.4% in the previous study). They showed that GS$\geq$1 improved the sensitivity of the 2010 criteria from 58 up to 78% without decreasing specificity (AUC 0.868), which was 93.7% if GS $\geq$ 2 or PD $\geq$ 1 were present, but at the price of decreased specificity which went down to 56.1% (AUC 0.844) (38). US was also shown to be especially useful in RA diagnosis in CCP negative very early UA. Indeed, in a study recruiting only CCP negative individuals with suspected UA, US synovitis significantly improved the sensitivity of the 2010 classification criteria up to 86.2% (39), meaning that US could counterbalance the absence of specific serology findings. While using a probabilistic approach depending on the practitioner's impression, another group showed that the addition of US to routine investigations increased the diagnostic certainty of UA from 31.1 to 61.2% ($p < 0.001$) (40). It is interesting that in these studies, more than half of patients presented abnormalities on first US but not all developed a persistent disease, suggesting that, focusing on the most specific US features such as PD presence and/or GS $\geq$ 2 might improve US accuracy. Another study showed that GS was more effective at showing synovitis than clinical examination, laboratory investigation ($p = 0.00015$), and plain film radiography ($p = 0.0002$) (41). In a study recruiting individuals with at least one swollen joint, the same improvement of the AUC for RA diagnosis was found, they also showed that MCP joints were highly specific for IA (42). Others found that selecting PD grade 2 increased discriminative ability (43).

Interestingly, in a large ($n = 379$) retrospective analysis on a cohort of patients referred to early arthritis clinic and followed for minimum 12 months, US parameters did not show significant predictive value for persistent IA in comparison to clinical parameters alone, (AUC curve both metrics: 0.91; [95% CI 0.89–0.94] [95% CI 0.88 to 0.94] respectively) (44). This same group did a further study with different scanning protocol and comparison methodology between clinical and US variables, which did show improvement of predictive values when comparing to clinical parameters alone (37).

The same team developed two "risk metrics" computerized tools using logistic regression to predict the development of persistent IA whereas the first models used multivariate and ROC curve analysis to identify discriminators of IA and the added value of US parameters (44). Another diagnostic model for progression from UA to RA was designed combining symptoms and morning stiffness durations, raised inflammatory markers, CCP and or RF positivity and PDUS presence in 1, 2 or $\geq$3 joints, which provided an impressive AUC of 0.919 ($n = 149$) (45).

After a RA diagnosis has been made, US has also shown a good correlation with composite scores of disease activity at all points of disease evolution, as well as with radiological damage (33, 46–48). It is suggested for use in the assessment of remission, prediction of flares, and to assess risk of relapse when tapering treatment as well as to inform the need to intensify treatment (49–55). PROMPT trial randomized 110 UA individuals to receive methotrexate (MTX) vs. placebo for 1 year depending on US results. At 5 years, they showed no difference in progression rates to RA, only a delay in progression in the treated ACPA positive participants (56).

Overall, US has proved its place in diagnosis, disease activity and remission assessment while, for now, US driven trials have shown variable results.

DISCUSSION

The main challenge in populations at-risk of RA is to categorize biomarkers that are specific, sensitive, and reproducible in predicting disease progression. Some of them may be present years before progression and remain stable—such as specific antibodies or genetic predisposition—whilst others may vary with time or only appear closer to the clinical phase of the disease such as abnormalities on high-resolution imaging, for example, US. Defining the phase where sub-clinical inflammation on imaging appears is particularly important, as it represents the initial onset of articular inflammation and as such, the phase where clinical arthritis is imminent. Indeed, as one RCT has shown to delay the onset of RA (57), the preclinical phase of RA could be the optimal time point to initiate treatment as damages have not occurred yet, thus re-defining the window of opportunity. Delaying or even preventing the onset of RA will have major social, financial, and personal impact on patients and society.

Retrospective studies on RA patients were highly useful initially to find out biomarkers that were present before

symptoms, but these are limited in the quantity and quality of the data. For example, not all analysis was possible on frozen blood samples, no imaging was performed, and clinical data were absent. Therefore, observational studies on RA prediction should now be all prospective. Another important challenge in at-risk population studies are the discrepancies between and within cohorts depending on the recruitment criteria. This implies that results are difficult to replicate and/or compare between populations. We discussed above the various pathways of prospective recruitment, for example, CSA and ACPA+ individuals, with a usual progression to IA rate of around one third of participants. This low progression rate increases duration of follow-up needed, tests and visits to be repeated, and the need for large cohorts to get significant results. Only a few centers are able to support this.

Identifying individuals who would benefit the most from an US assessment is of major importance. Indeed, although US sub-clinical inflammation can be found throughout the whole disease continuum toward RA, US abnormalities have shown—at present—only of predictive value for disease development in specific populations. The most representative are symptomatic at-risk individuals who have been identified by antibody positivity while in some populations, for example, in FDRs and CSA individuals, data are sparse and would benefit from further study. Another limitation is that not all analysis used the same US protocols. Even if we nowadays tend to follow EULAR/OMERACT recommendation, this has not always been the case. Although some US protocols focusing on specific joint sets are suggested in RA to improve US pragmatic use in clinic (58, 59), no joint based analysis have been performed on at-risk individuals yet. Nevertheless, focus is often on the small joints such as MCP, PIP, MTP, and wrists.

The studies investigating the role of US in FDRs do not support its use in those without symptoms. There is however a paucity of data in this area and further exploration is needed. On the other hand, the predictive value of US for IA development was greater in the individuals with MSK symptoms identified by a positive ACPA test. In this group particularly, depending on the US scan protocols and the recruitment criteria, US features have shown significant predictive value at the joint and patient level, for GS, BE, TSV, and especially for PD presence. This is more consistent if we consider the studies of individuals with more stringent inclusion criteria, with cohorts more likely to be at imminent risk of progression. In individuals with CSA, MRI-US comparison has shown good correlation, mainly for specificity. At diagnosis of early UA, some studies showed US superiority to clinical examination, efficacy in RA diagnosis, disease activity assessment, and treatment efficacy. In this population, efficacy is not dependent on the serological results and might be of more value in the seronegative individuals. It has good discriminative value, improving the classification criteria's sensitivity. In established RA, although it has been shown to be a good predictor in treatment response, remission assessment, and flare prediction, two trials comparing conventional T2T approach with US lead approach did not show significant differences in DAS28 remission, and lead to an increased treatment regimen is the US groups (60, 61). Nevertheless, secondary analysis showed that Boolean remission was more often reached in the US arm (61).

At present without guidance, rheumatologists have different approaches to managing at-risk individuals. A survey conducted in 2019 across the UK showed that 73% of practitioners would treat ACPA positive individuals if at least one joint showed PD presence on US (62). This reflects the pragmatic approach used due to the lack evidence on which treatment is the most appropriate, which population would respond well and what is the most appropriate timing to start treatment. This lack of global consensus emphasizes the need for research studies to assess these questions (63). Although individuals followed in preventive observational cohorts showed milder disease activity at progression (64), long term impact of prevention clinics have not been assessed yet. A few randomized controlled trials have been designed on individuals without CS. While one used the presence of US inflammation as part of the recruitment criteria (57), another one collected US data along the study for secondary analysis, results are not published yet (65), none of the others included US as an outcome or collected longitudinal data (66–68). Some RA treatments have been tested on individuals with UA (56) or even before CS occurs (65), the complexity here is to define the optimal high risk individuals who may benefit from treatment as well as the participant acceptance for a medication without confirmed disease (69, 70). At present, no formal economic analyses for use of US or treatment in at-risk individuals have been conducted, it therefore represents an important area for future work.

All aspects of US findings throughout the RA continuum have shown its high predictive value for progression to clinical synovitis, perhaps with PD standing out to be most predictive. However, it is difficult to compare these aspects due to the different definitions of US synovitis and scanning protocols through the studies. Overall, US does offer clear assistance in identifying sub-clinical inflammation in individuals at-risk of IA. However, we have to consider the time and resources needed for systemic prevention to be put in place. All populations considered, it appears that the greatest impact on IA prediction of US examination can be found in three at-risk populations: those with a positive ACPA test in the context of non-specific MSK symptom, those with CSA, and those with palindromic rheumatism. Since it has shown such good predictive value in IA and in the preclinical phases of IA, it is expected that US will be a cornerstone in prediction risk modeling and prevention studies. Nonetheless, further studies with unified selection criteria, specific joints and/or feature selections are still needed to improve US impact relevance.

AUTHOR CONTRIBUTIONS

LD and RC have participated with equal contribution and would like to share first authorship. KM: important part in topic choices, discussion, proof reading, and time input. PE: topic choices, discussion, and final approval for submission. All authors contributed to the article and approved the submitted version.

REFERENCES

1. Nell VP, Machold KP, Eberl G, Stamm TA, Uffmann M, Smolen JS. Benefit of very early referral and very early therapy with disease-modifying anti-rheumatic drugs in patients with early rheumatoid arthritis. *Rheumatology.* (2004) 43:906–14. doi: 10.1093/rheumatology/keh199
2. Burgers LE, Raza K, van der Helm-van Mil AH. Window of opportunity in rheumatoid arthritis—definitions and supporting evidence: from old to new perspectives. *RMD Open.* (2019) 5:e000870. doi: 10.1136/rmdopen-2018-000870
3. Mankia K, Emery P. Palindromic rheumatism as part of the rheumatoid arthritis continuum. *Nat Rev Rheumatol.* (2019) 15:687–95. doi: 10.1038/s41584-019-0308-5
4. Nielen MM, van Schaardenburg D, Reesink HW, van de Stadt RJ, van der Horst-Bruinsma IE, de Koning MH, et al. Specific autoantibodies precede the symptoms of rheumatoid arthritis: a study of serial measurements in blood donors. *Arthritis Rheum.* (2004) 50:380–6. doi: 10.1002/art.20018
5. Silman AJ, Hennessy E, Ollier B. Incidence of rheumatoid arthritis in a genetically predisposed population. *Brit J Rheumatol.* (1992) 31:365–8. doi: 10.1093/rheumatology/31.6.365
6. Terslev L, Torp-Pedersen S, Qvistgaard E, von der Recke P, Bliddal H. Doppler ultrasound findings in healthy wrists and finger joints. *Ann Rheum Dis.* (2004) 63:644–8. doi: 10.1136/ard.2003.009548
7. Millot F, Clavel G, Etchepare F, Gandjbakhch F, Grados F, Saraux A, et al. Musculoskeletal ultrasonography in healthy subjects and ultrasound criteria for early arthritis (the ESPOIR cohort). *J Rheumatol.* (2011) 38:613–20. doi: 10.3899/jrheum.100379
8. Witt M, Mueller F, Nigg A, Reindl C, Leipe J, Proft F, et al. Relevance of grade 1 gray-scale ultrasound findings in wrists and small joints to the assessment of subclinical synovitis in rheumatoid arthritis. *Arthritis Rheum.* (2013) 65:1694–701. doi: 10.1002/art.37954
9. Rosenberg C, Arrestier S, Etchepare F, Fautrel B, Rozenberg S, Bourgeois P. High frequency of ultrasonographic effusion in interphalangeal joints of healthy subjects: a descriptive study. *Joint Bone Spine.* (2009) 76:265–7. doi: 10.1016/j.jbspin.2008.06.017
10. Padovano I, Costantino F, Breban M, D'Agostino MA. Prevalence of ultrasound synovial inflammatory findings in healthy subjects. *Ann Rheum Dis.* (2016) 75:1819–23. doi: 10.1136/annrheumdis-2015-208103
11. Machado FS, Furtado RN, Takahashi RD, de Buosi AL, Natour J. Sonographic cutoff values for detection of abnormalities in small, medium and large joints: a comparative study between patients with rheumatoid arthritis and healthy volunteers. *Ultrasound Med Biol.* (2015) 41:989–98. doi: 10.1016/j.ultrasmedbio.2014.12.004
12. D'Agostino MA, Terslev L, Aegerter P, Backhaus M, Balint P, Bruyn GA, et al. Scoring ultrasound synovitis in rheumatoid arthritis: a EULAR-OMERACT ultrasound taskforce-Part 1: definition and development of a standardised, consensus-based scoring system. *RMD Open.* (2017) 3:e000428. doi: 10.1136/rmdopen-2016-000428
13. Soliman E. SAT0650 Musculoskeletal ultrasound in first degree relatives of rheumatoid arthritis patients. *Ann Rheum Dis.* (2018) 77(Suppl. 2):1175. doi: 10.1136/annrheumdis-2018-eular.2349
14. Soliman E, Ohrndorf S, Zehairy M, Matrawy K, Alhadidy A, Abdelati A. Osteopontin, osteoprotegerin and musculoskeletal ultrasound findings in first-degree relatives of rheumatoid arthritis: potential markers of preclinical disease. *Preprint*. (2020). doi: 10.21203/rs.3.rs-20512/v1
15. Brulhart L, Alpízar-Rodríguez D, Nissen MS, Zufferey P, Ciubotariu I, Fleury G, et al. Ultrasound is not associated with the presence of systemic autoimmunity or symptoms in individuals at-risk for rheumatoid arthritis. *RMD Open.* (2019) 5:e000922. doi: 10.1136/rmdopen-2019-000922
16. van Steenbergen HW, Aletaha D, Beaart-van de Voorde LJ, Brouwer E, Codreanu C, Combe B, et al. Eular definition of arthralgia suspicious for progression to rheumatoid arthritis. *Ann Rheum Dis.* (2017) 76:491–6. doi: 10.1136/annrheumdis-2016-209846
17. van der Ven M, van der Veer-Meerkerk M, Ten Cate DF, Rasappu N, Kok MR, Csakvari D, et al. Absence of ultrasound inflammation in patients presenting with arthralgia rules out the development of arthritis. *Arthritis Res Ther.* (2017) 19:202. doi: 10.1186/s13075-017-1405-y
18. Zufferey P, Rebell C, Benaim C, Ziswiler HR, Dumusc A, So A. Ultrasound can be useful to predict an evolution towards rheumatoid arthritis in patients with inflammatory polyarthralgia without anticitrullinated antibodies. *Joint, Bone, Spine.* (2017) 84:299–303. doi: 10.1016/j.jbspin.2016.05.011
19. Zufferey P, Brulhart L, Tamborrini G, Finckh A, Scherer A, Moller B, et al. Ultrasound evaluation of synovitis in RA: correlation with clinical disease activity and sensitivity to change in an observational cohort study. *Joint Bone Spine.* (2014) 81:222–7. doi: 10.1016/j.jbspin.2013.08.006
20. Ohrndorf S, Boer AC, Boeters DM, Ten Brinck RM, Burmester GR, Kortekaas MC, et al. Do musculoskeletal ultrasound and magnetic resonance imaging identify synovitis and tenosynovitis at the same joints and tendons? A comparative study in early inflammatory arthritis and clinically suspect arthralgia. *Arthritis Res Ther.* (2019) 21:59. doi: 10.1186/s13075-019-1824-z
21. Rakieh C, Nam JL, Hunt L, Hensor EM, Das S, Bissell LA, et al. Predicting the development of clinical arthritis in anti-CCP positive individuals with non-specific musculoskeletal symptoms: a prospective observational cohort study. *Ann Rheum Dis.* (2015) 74:1659–66. doi: 10.1136/annrheumdis-2014-205227
22. van de Stadt LA, Bos WH, Meursinge Reynders M, Wieringa H, Turkstra F, van der Laken CJ, et al. The value of ultrasonography in predicting arthritis in auto-antibody positive arthralgia patients: a prospective cohort study. *Arthritis Res Ther.* (2010) 12:R98. doi: 10.1186/ar3028
23. Nam JL, Hensor EM, Hunt L, Conaghan PG, Wakefield RJ, Emery P. Ultrasound findings predict progression to inflammatory arthritis in anti-CCP antibody-positive patients without clinical synovitis. *Ann Rheum Dis.* (2016) 75:2060–7. doi: 10.1136/annrheumdis-2015-208235
24. van Beers-Tas MH, Blanken AB, Nielen MMJ, Turkstra F, van der Laken CJ, Meursinge Reynders M, et al. The value of joint ultrasonography in predicting arthritis in seropositive patients with arthralgia: a prospective cohort study. *Arthritis Res Ther.* (2018) 20:279. doi: 10.1186/s13075-018-1767-9
25. Duquenne L, Mankia K, Montoya L, Di Matteo A, Nam J, Emery P. P240 Can ultrasound alone predict the need to treat ACPA positive individuals without synovitis? *Rheumatology.* (2020) 59. doi: 10.1093/rheumatology/keaa111.234
26. Duquenne L. MK, Di Matteo A, Garcia-Montoya L, Nam J, Emery P. ACPA positive At-risk individuals without clinical arthritis, is ultrasound sufficiently accurate to predict progression to inflammatory arthritis? *Ann Rheum Dis.* (2020) 79:260.
27. Di Matteo A, Mankia K, Duquenne L, Cipolletta E, Wakefield RJ, Garcia-Montoya L, et al. Ultrasound erosions in the feet best predict progression to inflammatory arthritis in anti-CCP positive at-risk individuals without clinical synovitis. *Ann Rheum Dis.* (2020) 79:901–7. doi: 10.1136/annrheumdis-2020-217215
28. Mankia K, Emery P. What can palindromic rheumatism tell us? *Best Pract Res Clin Rheumatol.* (2017) 31:90–8. doi: 10.1016/j.berh.2017.09.014
29. Cabrera-Villalba S, Ramirez J, Salvador G, Ruiz-Esquide V, Hernández MV, Inciarte-Mundo J, et al. Is there subclinical synovitis in patients with palindromic rheumatism in the intercritical period? a clinical and ultrasonographic study according to anticitrullinated protein antibody status. *J Rheumatol.* (2014) 41:1650–5. doi: 10.3899/jrheum.131545
30. Bugatti S, Caporali R, Manzo A, Sakellariou G, Rossi S, Montecucco C. Ultrasonographic and MRI characterisation of the palindromic phase of rheumatoid arthritis. *Ann Rheum Dis.* (2012) 71:625–6. doi: 10.1136/annrheumdis-2011-200077
31. Chen HH, Lan JL, Hung GD, Chen YM, Lan HH, Chen DY. Association of ultrasonographic findings of synovitis with anti-cyclic citrullinated peptide antibodies and rheumatoid factor in patients with palindromic rheumatism during active episodes. *J Ultrasound Med.* (2009) 28:1193–9. doi: 10.7863/jum.2009.28.9.1193
32. Mankia K, D'Agostino MA, Wakefield RJ, Nam JL, Mahmood W, Grainger AJ, et al. Identification of a distinct imaging phenotype may improve the management of palindromic rheumatism. *Ann Rheum Dis.* (2019) 78:43–50. doi: 10.1136/annrheumdis-2018-214175
33. Terslev L, von der Recke P, Torp-Pedersen S, Koenig MJ, Bliddal H. Diagnostic sensitivity and specificity of doppler ultrasound in rheumatoid arthritis. *J Rheumatol.* (2008) 35:49–53.
34. Szkudlarek M, Court-Payen M, Strandberg C, Klarlund M, Klausen T, Ostergaard M. Power Doppler ultrasonography for assessment of synovitis in the metacarpophalangeal joints of patients with rheumatoid arthritis: a comparison with dynamic

magnetic resonance imaging. *Arthritis Rheum.* (2001) 44:2018–23. doi: 10.1002/1529-0131(200109)44:9<2018::AID-ART350>3.0.CO;2-C
35. Wakefield RJ, Freeston JE, O'Connor P, Reay N, Budgen A, Hensor EM, et al. The optimal assessment of the rheumatoid arthritis hindfoot: a comparative study of clinical examination, ultrasound and high field MRI. *Ann Rheum Dis.* (2008) 67:1678–82. doi: 10.1136/ard.2007.079947
36. Freeston JE, Wakefield RJ, Conaghan PG, Hensor EM, Stewart SP, Emery P. A diagnostic algorithm for persistence of very early inflammatory arthritis: the utility of power Doppler ultrasound when added to conventional assessment tools. *Ann Rheum Dis.* (2010) 69:417–9. doi: 10.1136/ard.2008.106658
37. Iqbal K, Lendrem DW, Hargreaves B, Isaacs JD, Thompson B, Pratt AG. Routine musculoskeletal ultrasound findings impact diagnostic decisions maximally in autoantibody-seronegative early arthritis patients. *Rheumatology.* (2019) 58:1268–73. doi: 10.1093/rheumatology/kez008
38. Nakagomi D, Ikeda K, Okubo A, Iwamoto T, Sanayama Y, Takahashi K, et al. Ultrasound can improve the accuracy of the (2010). American College of Rheumatology/European League against rheumatism classification criteria for rheumatoid arthritis to predict the requirement for methotrexate treatment. *Arthritis Rheum.* (2013) 65:890–8. doi: 10.1002/art.37848
39. Ji L, Deng X, Geng Y, Song Z, Zhang Z. The additional benefit of ultrasonography to 2010 ACR/EULAR classification criteria when diagnosing rheumatoid arthritis in the absence of anti-cyclic citrullinated peptide antibodies. *Clin Rheumatol.* (2017) 36:261–7. doi: 10.1007/s10067-016-3465-9
40. Rezaei H, Torp-Pedersen S, af Klint E, Backheden M, Kisten Y, Gyori N, et al. Diagnostic utility of musculoskeletal ultrasound in patients with suspected arthritis–a probabilistic approach. *Arthritis Res Ther.* (2014) 16:448. doi: 10.1186/s13075-014-0448-6
41. Zhang YH, Li K, Xiao J, Zhang HD, Zhang XY. Comparison of ultrasound, radiography, and clinical investigations in the diagnosis of early rheumatoid synovitis in patients with nonspecific musculoskeletal symptoms: a multicenter cross-sectional study. *Med Sci Monit.* (2018) 24:4372–8. doi: 10.12659/MSM.908755
42. Filer A, de Pablo P, Allen G, Nightingale P, Jordan A, Jobanputra P, et al. Utility of ultrasound joint counts in the prediction of rheumatoid arthritis in patients with very early synovitis. *Ann Rheum Dis.* (2011) 70:500–7. doi: 10.1136/ard.2010.131573
43. Kawashiri SY, Fujikawa K, Nishino A, Okada A, Aramaki T, Shimizu T, et al. Ultrasound-detected bone erosion is a relapse risk factor after discontinuation of biologic disease-modifying antirheumatic drugs in patients with rheumatoid arthritis whose ultrasound power Doppler synovitis activity and clinical disease activity are well controlled. *Arthritis Res Ther.* (2017) 19:108. doi: 10.1186/s13075-017-1320-2
44. Pratt AG, Lorenzi AR, Wilson G, Platt PN, Isaacs JD. Predicting persistent inflammatory arthritis amongst early arthritis clinic patients in the UK: is musculoskeletal ultrasound required? *Arthritis Res Ther.* (2013) 15:R118. doi: 10.1186/ar4298
45. Salaffi F, Ciapetti A, Gasparini S, Carotti M, Filippucci E, Grassi W. A clinical prediction rule combining routine assessment and power Doppler ultrasonography for predicting progression to rheumatoid arthritis from early-onset undifferentiated arthritis. *Clin Exp Rheumatol.* (2010) 28:686–94.
46. Damjanov N, Radunovic G, Prodanovic S, Vukovic V, Milic V, Simic Pasalic K, et al. Construct validity and reliability of ultrasound disease activity score in assessing joint inflammation in RA: comparison with DAS-28. *Rheumatology.* (2012) 51:120–8. doi: 10.1093/rheumatology/ker255
47. Naredo E, Möller I, Cruz A, Carmona L, Garrido J. Power Doppler ultrasonographic monitoring of response to anti-tumor necrosis factor therapy in patients with rheumatoid arthritis. *Arthritis Rheum.* (2008) 58:2248–56. doi: 10.1002/art.23682
48. Ribbens C, Andre B, Marcelis S, Kaye O, Mathy L, Bonnet V, et al. Rheumatoid hand joint synovitis: gray-scale and power Doppler US quantifications following anti-tumor necrosis factor-alpha treatment: pilot study. *Radiology.* (2003) 229:562–9. doi: 10.1148/radiol.2292020206
49. Gul HL, Eugenio G, Rabin T, Burska A, Parmar R, Wu J, et al. Defining remission in rheumatoid arthritis: does it matter to the patient? A comparison of multi-dimensional remission criteria and patient reported outcomes. *Rheumatology.* (2019) 59:613–21. doi: 10.1093/rheumatology/kez330
50. Paulshus Sundlisæter N, Aga AB, Olsen IC, Hammer HB, Uhlig T, van der Heijde D, et al. Clinical and ultrasound remission after 6 months of treat-to-target therapy in early rheumatoid arthritis: associations to future good radiographic and physical outcomes. *Ann Rheum Dis.* (2018) 77:1421–5. doi: 10.1136/annrheumdis-2017-212830
51. Wang L, Geng Y, Han J, Sun X, Zhang Z. A combination model to predict relapse and successful conventional DMARDs de-escalation in rheumatoid arthritis patients with sustained clinical remission. *Clin Exp Rheumatol.* (2019) 37:120–6.
52. Han J, Geng Y, Deng X, Zhang Z. Subclinical synovitis assessed by ultrasound predicts flare and progressive bone erosion in rheumatoid arthritis patients with clinical remission: a systematic review and metaanalysis. *J Rheumatol.* (2016) 43:2010–8. doi: 10.3899/jrheum.160193
53. Geng Y, Han J, Deng X, Zhang Z. Deep clinical remission: an optimised target in the management of rheumatoid arthritis? Experience from an ultrasonography study. *Clin Exp Rheumatol.* (2016) 34:581–6.
54. Janta I, Valor L, De la Torre I, Martínez-Estupiñán L, Nieto JC, Ovalles-Bonilla JG, et al. Ultrasound-detected activity in rheumatoid arthritis on methotrexate therapy: which joints and tendons should be assessed to predict unstable remission? *Rheumatol Int.* (2016) 36:387–96. doi: 10.1007/s00296-015-3409-8
55. Han J, Geng Y, Deng X, Zhang Z. Risk factors of flare in rheumatoid arthritis patients with both clinical and ultrasonographic remission: a retrospective study from China. *Clin Rheumatol.* (2017) 36:1721–7. doi: 10.1007/s10067-017-3736-0
56. van Aken J, Heimans L, Gillet-van Dongen H, Visser K, Ronday HK, Speyer I, et al. Five-year outcomes of probable rheumatoid arthritis treated with methotrexate or placebo during the first year (the PROMPT study). *Ann Rheum Dis.* (2014) 73:396–400. doi: 10.1136/annrheumdis-2012-202967
57. Gerlag DM, Safy M, Maijer KI, Tang MW, Tas SW, Starmans-Kool MJF, et al. Effects of B-cell directed therapy on the preclinical stage of rheumatoid arthritis: the PRAIRI study. *Ann Rheum Dis.* (2019) 78:179–85. doi: 10.1136/annrheumdis-2017-212763
58. Backhaus M, Ohrndorf S, Kellner H, Strunk J, Backhaus TM, Hartung W, et al. Evaluation of a novel 7-joint ultrasound score in daily rheumatologic practice: a pilot project. *Arthritis Rheum.* (2009) 61:1194–201. doi: 10.1002/art.24646
59. Naredo E, Rodríguez M, Campos C, Rodríguez-Heredia JM, Medina JA, Giner E, et al. Validity, reproducibility, and responsiveness of a twelve-joint simplified power doppler ultrasonographic assessment of joint inflammation in rheumatoid arthritis. *Arthritis Rheum.* (2008) 59:515–22. doi: 10.1002/art.23529
60. Dale J, Stirling A, Zhang R, Purves D, Foley J, Sambrook M, et al. Targeting ultrasound remission in early rheumatoid arthritis: the results of the TaSER study, a randomised clinical trial. *Ann Rheum Dis.* (2016) 75:1043–50. doi: 10.1136/annrheumdis-2015-208941
61. Norvang V, Brinkmann GH, Yoshida K, Lillegraven S, Aga AB, Sexton J, et al. Achievement of remission in two early rheumatoid arthritis cohorts implementing different treat-to-target strategies. *Arthritis Rheumatol.* (2020) 72:1072–81. doi: 10.1002/art.41232
62. Mankia K, Briggs C, Emery P. How are rheumatologists managing anticyclic citrullinated peptide antibodies-positive patients who do not have arthritis? *J Rheumatol.* (2020) 47:305–6. doi: 10.3899/jrheum.190211
63. Mankia K, Emery P. Preclinical rheumatoid arthritis: progress toward prevention. *Arthritis Rheumatol.* (2016) 68:779–88. doi: 10.1002/art.39603
64. Duquenne LPP, Mankia K, Nam J, Hunt L, Tan AL, Garcia-Montoya L, Emery P. At diagnosis of rheumatoid arthritis, at-risk patients followed in ccp+ clinic showed milder disease activity than conventionally referred patients. *Ann Rheum Dis.* (2018) 77:A935. doi: 10.1136/annrheumdis-2018-eular.5704
65. Al-Laith M, Jasenecova M, Abraham S, Bosworth A, Bruce IN, Buckley CD, et al. Arthritis prevention in the pre-clinical phase of RA with abatacept (the APIPPRA study): a multi-centre, randomised, double-blind, parallel-group, placebo-controlled clinical trial protocol. *Trials.* (2019) 20:429. doi: 10.1186/s13063-019-3403-7
66. Bos WH, Dijkmans BA, Boers M, van de Stadt RJ, van Schaardenburg D. Effect of dexamethasone on autoantibody levels and arthritis development in

patients with arthralgia: a randomised trial. *Ann Rheum Dis.* (2010) 69:571–4. doi: 10.1136/ard.2008.105767

67. *Strategy to Prevent the Onset of Clinically-Apparent Rheumatoid Arthritis (StopRA).* (2020). Available online at: https://www.clinicaltrials.gov/ct2/show/NCT02603146 (accessed April 1, 2020).
68. Van Boheemen SAT, Van Beers - Tas MH, Bos WH, Marsman D, Griep EN, Starman M, et al. Statins to prevent rheumatoid arthritis: inconclusive results of the STAPRA trial. *Ann Rheum Dis.* (2020) 79(Suppl. 1):1415–6. doi: 10.1136/annrheumdis-2020-eular.2805
69. Burgers LE, Allaart CF, Huizinga TWJ, van der Helm-van Mil AHM. Brief report: clinical trials aiming to prevent rheumatoid arthritis cannot detect prevention without adequate risk stratification: a trial of methotrexate versus placebo in undifferentiated arthritis as an example. *Arthritis Rheumatol.* (2017) 69:926–31. doi: 10.1002/art.40062
70. Falahee M, Finckh A, Raza K, Harrison M. Preferences of patients and at-risk individuals for preventive approaches to rheumatoid arthritis. *Clin Ther.* (2019) 41:1346–54. doi: 10.1016/j.clinthera.2019.04.015

Conflict of Interest: KM reports personal fees from Abbvie, UCB, and Eli Lilly, outside the submitted work and research grants from BMS, Eli Lilly. PE reports consultant fees from BMS, AbbVie, Gilead, Galapagos, Lilly, MSD, Pfizer, Novartis, Roche, Samsung outside the submitted work and research grants from UCB, AbbVie, Lilly, Novartis, BMS, Pfizer, MSD, and Roche, outside the submitted work.

The remaining authors declare that the research was conducted in the absence of any commercial or financial relationships that could be construed as a potential conflict of interest.

frontiers in Medicine

BRIEF RESEARCH REPORT
published: 12 February 2021
doi: 10.3389/fmed.2021.637459

High Prevalence of Ultrasound Verified Enthesitis in Patients With Inflammatory Bowel Disease With or Without Spondylarthritis

*Rusmir Husic[1], Angelika Lackner[1], Patrizia Katharina Kump[2], Christoph Högenauer[2], Winfried Graninger[1] and Christian Dejaco[1,3]**

[1] Department of Rheumatology and Immunology, Medical University Graz, Graz, Austria, [2] Department of Gastroenterology and Hepatology, Medical University Graz, Graz, Austria, [3] Department of Rheumatology, Hospital of Brunico (Südtiroler Sanitätsbetrieb-Azienda Sanitaria dell'Alto Adige), Brunico, Italy

OPEN ACCESS

Edited by:
Francesco Ciccia, University of Campania Luigi Vanvitelli, Italy

Reviewed by:
Sandra Salvador Falcao, New University of Lisbon, Portugal
Carlo Selmi, University of Milan, Italy

***Correspondence:**
Christian Dejaco
christian.dejaco@gmx.net

Specialty section:
This article was submitted to Rheumatology, a section of the journal Frontiers in Medicine

Received: *03 December 2020*
Accepted: *18 January 2021*
Published: *12 February 2021*

Citation:
Husic R, Lackner A, Kump PK, Högenauer C, Graninger W and Dejaco C (2021) High Prevalence of Ultrasound Verified Enthesitis in Patients With Inflammatory Bowel Disease With or Without Spondylarthritis. Front. Med. 8:637459. doi: 10.3389/fmed.2021.637459

Background: Inflammatory bowel disease (IBD) is closely associated with spondylarthritis (SpA) and enthesitis, as an important feature of SpA, is a common extraintestinal manifestation of IBD. Enthesitis may be clinically silent in a high proportion of patients with IBD without clinical signs or a diagnosis of SpA.

Objectives: The aim of this study was to compare the prevalence of ultrasound (US) verified enthesitis in IBD patients with and without SpA, with patients with irritable bowel syndrome (IBS) and healthy subjects (HC) serving as controls.

Methods: IBD patients with or without SpA, patients with IBS and HC were prospectively recruited and clinically assessed. Ultrasound examination was performed at 14 entheses. The ultrasound abnormalities were scored according to the Madrid Ankylosing Spondylitis Enthesitis Index (MASEI).

Results: We included 33 IBD patients without SpA, 14 IBD patients with SpA, 26 IBS patients and 18 HC. Higher MASEI scores were found in patients with IBD without SpA [median 21.0 range (8.0–53.0)] and IBD associated SpA [33.0 (8–50)] than in IBS patients [10.5 (0–42.0)-$p < 0.001$ for both comparison] and HC [12.0 (2.0–38.0)-$p < 0.01$]. PD, enthesophytes and erosions were more common in patients with IBD with or without SpA as compared to IBS patients and HC. IBD patients with SpA compared to IBD without SpA demonstrated significant higher prevalence of erosion and structural irregularity and consequently significant higher MASEI ($p < 0.05$ for all comparison).

Conclusions: Ultrasound verified enthesitis is more common in patients with IBD with or without SpA as compared to patients with IBS or HC.

Keywords: enthesitis, spondyloarthropathies, inflammatory bowel diseases, ultrasound, power Doppler ultrasonography

INTRODUCTION

Enthesitis is defined as inflammation of the insertion of tendons, ligaments, and capsules into bone (1). There are some observations suggesting that repeated mechanical overload or excessive irritation of entheses may lead to enthesal inflammation and given that lower limbs are exposed to higher mechanical load, this might explain why enthesitis primarily involves the lower limbs in patients with spondylarthritis (SpA).

Enthesitis is considered to be the initial lesion in SpA that only secondarily involves bone and synovial tissue leading to spondylitis and arthritis (2). The detection of enthesitis at early stages of SpA might be an interesting window of opportunity to treat patients with this disease.

There is a close link between intestinal disease and SpA. We know that 15% of inflammatory bowel disease (IBD) patients develop peripheral SpA and 36% suffer from sacroilitis (3). Besides, subclinical intestinal inflammation has been identified in up to 60–70% of patients with axial SpA (4, 5). Other patients with IBD might present subclinical or abortive forms of SpA which might only later evolve in clinically manifest SpA.

The prevalence of sub-clinical entheseal involvement in IBD patients, detected with ultrasound, seems to be more common in IBD patients compared to the healthy controls and in sum there is no difference between IBD and SpA (6, 7).

Ultrasound has been used to detect subclinical enthesitis, mainly in lower limbs of patients with SpA (8–10). In patients with psoriasis, another disease that is closely related to SpA and where a proportion of patients develop clinical manifestations of SpA, a high prevalence of subclinical enthesitis was detected by imaging. In psoriasis, it has even been observed that ultrasound verified enthesitis predicted the later development of psoriatic arthritis (11, 12). In patients with IBD, reports about the prevalence and the possible predictive value of subclinical enthesitis are scarce despite the known link between axial, articular, and intestinal inflammation.

The aim of the present study was to investigate the prevalence of enthesitis using sonography in patients with IBD without associated SpA and to compare them to patients with IBD associated SpA, irritable bowel syndrome (IBS) and healthy subjects (HC).

METHODS

We prospectively recruited 47 IBD patients: 33 patients had no clinical symptoms or history of SpA [i.e., no axial, articular, or enthesal pain and 14 patients with confirmed SpA fulfilling the ASAS classification criteria (13)]. All patients fulfilled the diagnostic criteria for IBD (14, 15). As controls, we recruited 26 consecutive IBS patients who all fulfilled the Rome criteria for IBS (16) and 18 HC. All patients and controls gave written informed consent to participate in the study, and the study was approved by the institutional ethics committee (Prot. Number: 23-432 ex 10/11).

Clinical Assessment

Demographics, level of regular sport activity (defined as sport or physical activity at least once a week) and body mass index (BMI) were determined in all participants. All patients with IBD underwent routine clinical and laboratory examinations and assessment of IBD activity using the Crohn's disease activity index (CDAI) for patients with Crohn's disease and the partial Mayo score for ulcerative colitis (17, 18). The Bath Ankylosing Spondylitis Disease Activity Index (BASDAI) was determined in all IBD patients (19). Clinical examination of entheses was conducted in all study participants by a rheumatologist blinded to ultrasound results. Enthesitis was defined as tenderness or swelling at clinical examination at the following sites: entheses of the common extensor tendon at lateral epicondyle, distal insertion of the triceps into the olecranon, quadriceps insertion into the upper pole of the patella, patellar tendon insertion into the lower pole of the patella and into the tibial anterior tuberosity, insertion of the Achilles tendon as well as the insertion of plantar aponeurosis into calcaneal bone.

Ultrasound Protocol

Ultrasound examination was performed by one of two investigators blinded to clinical results (CD or RH). In total 14 entheses were examined in every subject: bilateral triceps, lateral epicondyles, distal insertion of quadriceps, proximal and distal insertion of patellar tendon, distal insertion of Achilles tendon and plantar fascia using an Esaote MyLab Twice ultrasound device with 18-MHz linear array transducer (20). B-mode and Power Doppler (PD) sonography was performed in a darkened room in which the temperature was held constant at 20°C. PD-settings were standardized accordingly: frequency 9.1 MHz, pulse repetition frequency 750 Hz and medium persistence. The PD-gain was optimized by increasing gain until noise appeared and then reduced just enough to suppress the noise.

The following abnormalities were scored according to the Madrid Ankylosing Spondylitis Enthesitis Index (MASEI) as appropriate: Power Doppler (PD) changes, enthesophytes, erosions, enthesal thickening, bursitis, and structural abnormalities (21, 22). According to (MASEI): Structure was considered pathological (score = 1) if there was a loss of fibrillar pattern, hypoechoic aspect, or fusiform thickening of the entheses. Erosions were defined as a cortical breakage with a step-down contour defect at the attachment of entheses at bone and graded with 0 = absent or 3 = present. Fascia and tendon thickness were measured at the point of maximum thickness on the bony insertion and graded with 0 = normal or 1 = thickened according to the reference values published previously. Enthesophytes were defined as calcifications at the entheses insertion into bone and graded with 0 = absent, 1 = small calcification, 2 = clear presence of enthesophyte/calcification, 3 = large calcifications or ossifications (see **Figure 1**). PD-signals within entheses were scored with 0 = absent or 3 = present. Bursitis was investigated at the level of distal patellar tendon (infrapatellar bursitis) and at the level of Achilles tendon. Bursitis was defined as a well-circumscribed anechoic or hypoechoic area at the site of an anatomical bursa and which was compressible by the transducer. The total (MASEI) score ranges from 0 to 136 for

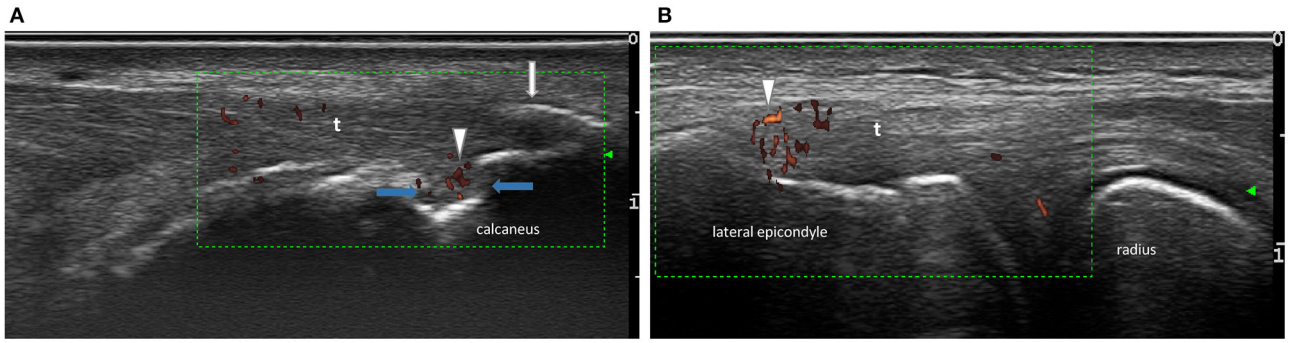

FIGURE 1 | Examples of ultrasound findings. **(A)** Longitudinal scan of a achilles tendon revealing active PD signal (arrows heads), enthesophyt (white arrow), erosion on insertion (blue arrow), **(B)** longitudinal scan of tendon insertion on lateral epicondyl with PD signal (arrow heads), t-tendon.

both sides of 12 entheses. In order to calculate the difference of separate ultrasound findings between the groups we calculated a modified MASEI. The MASEI was modified toward the inclusion of the lateral epicondyle given that this site is incorporated in clinical enthesitis scores such as the Leeds Enthesitis Index (LEI) and because previous studies demonstrated a high prevalence of enthesitis at this site in SpA patients (23–26). For this modified score, only the presence =1 or absence = 0 of each abnormality was counted in order to avoid the higher weighting of PD and erosions (presence of any lesions adds three points to the total score) er of enthesophytes (semiquantitative scale of 0–3) as compared to other lesions.

Statistical Analysis

Statistical analysis was performed using SPSS v22. Descriptive statistics were used to summarize the data. Independent groups of quantitative data were compared with the Student's *T*-Test (parametric) or the Mann-Whitney *U*-test (non-parametric distribution), as appropriate. Correlations analysis was conducted using Pearson *r* (parametric) or Spearman-Rho test (non-parametric data), as appropriate. All statistical analyses were performed using IBM SPSS Statistics (v23.0). Inter-reader agreement between ultrasound examiners was tested in seven patients, in which entheses were scanned by both investigators, and by using the Intra-class correlation coefficient (ICC).

RESULTS

Patients' characteristics are depicted in **Table 1**. A greater proportion of the recruited IBD patients ($n = 47$) were male, however we did not observe any gender-based difference of clinical activity of IBD or the MASEI score within the IBD group. The disease duration of IBD showed no significant correlation with IBD activity or with MASEI score. Crohn disease (CD) and Ulcerative colitis (UC) patients yielded the same frequency of therapy with TNFi, Azathioprine or Masalazine. One (7.1%) patient with CD associated SpA and 6 (18.2%) CD patients showed a CDAI score above 150.

In all examined entheses ($n = 1,274$, all groups), the most common ultrasound abnormalities were enthesophyte/calcification [$n = 397$ (31%)], structural irregularity [$n = 372$ (29%)], increased thickness [$n = 303$ (24%)], bursitis [$n = 101$ (8%)], erosions [$n = 95$ (7%)], and positive PD [$n = 58$ (5%)].

At least one positive PD-signal was observed in nine (64%) patients with IBD and SpA, in 22 (67%) patients with IBD without SpA, in five (19%) patients with IBS and in four (22%) HC. A highest prevalence of PD was observed at lateral epicondyle [39 entheses (67% of all PD positive enthesis)] followed by distal insertion of patellar tendon [$n = 7$ (12%)]. A presence of positive PD at lateral epicondyle did not yield significant difference in group IBD with or without SpA but it was significantly higher compared to IBS and HC ($p < 0.01$). The distribution of PD positive enthesitis among the sites investigated was similar in healthy controls. In patients with IBS, however, lateral epicondyle was more commonly involved than the other enthesis ($p < 0.05$). Comparing prevalence of PD signs at other entheses yielded no difference between groups. There was no difference between involvements of left or right sites.

At least one erosion was observed in 11 (79%, group IBD and SpA), 18 (55 %, group IBD without SpA), 10 (39%, group IBS) patients and 2 (11%) HC. The erosions were found more frequently with comparable distribution in the following enthesis: distal insertion of patellar tendon [22 erosions (23% of all erosions)], triceps tendon [$n = 19$ (20%)] and Achilles tendon [$n = 18$ (19%)]. Bursitis was most frequently observed in distal insertion of patellar tendon 65 (36% out examined enthesis) and in achileon 29 (16% out examined enthesis). Enthesophytes were most commonly observed in the achilleon, followed by lateral epicondyle, triceps tendon, and distal insertion of patellar tendon.

Higher MASEI scores were found in patients with IBD without SpA [median 21.0 range (8.0–53.0)] and IBD associated SpA [33.0 (8–50)] than in IBS patients [10.5 (0–42.0)-$p < 0.001$ for both comparison] and HC [12.0 (2.0–38.0)-$p < 0.01$ for both comparisons]. The MASEI score was significantly higher in IBD with SpA compared to IBD without SpA ($p < 0.05$). Only one patient with IBS did not reveal any US abnormalities according to the MASEI score.

As shown in the **Table 2**, all separate ultrasound findings were significantly higher in IBD patients with or without SpA than IBS and HC. The modified MASEI score in IBD

TABLE 1 | Clinical characteristics of IBD patients and controls.

	IBD without SpA $n = 33$	IBD with SpA $n = 14$	IBS $n = 26$	HC $n = 18$
Male, *n* (%)	22 (66.7%)	10 (71.4%)	7 (26.9%) $p < 0.05$*	5 (27.8%) $p < 0.05$*
IBD type	CD $n = 27$ UC $n = 6$	CD $n = 8$ UC $n = 6$		
Age years‡	44 (19–62)	45 (21–56)	41 (18–65)	43 (21–58)
Disease duration of IBD in years‡	10 (1–30)	7.5 (1–21)		
ESR‡	9 (1–45)	10 (3–25)	_	_
CRP‡	3.5 (0.6–39.2)	3 (0.1–41.0)	_	_
Anti-TNF therapy, *n* (%)	15 (45)	10 (71.4)	_	_
Azathioprin / Mesalazin, *n* (%)	9 (27) / 7 (21)	1 (7) / 2 (14)		
BASDAI‡	2.99 (0.3–7.1)	3.5(1.4–5.9)	_	_
CDAI†	87.3 (55.5)	84.9 (50.2)		
Partial Mayo score†	4 (1–7)	3.1 (0–5)		
BMI‡	24.9 (17.3–34.1)	24.3 (18.8–38.1)	23.6 (16.3–33.2)	22.5 (19.1–31.2)
Sport activity, *n* (%)	13 (39)	6 (43)	19 (73.1)	10 (56)
HLA B 27 positive	-	10 (71%)		

‡*Median (range);* †*mean (standard deviation); BASDAI, Bath Ankylosing Spondylitis Disease Activity Index; BMI, Body Mass Index; CDAI, Crohn's Disease Activity Index; CD, Crohn disease; UC, Ulcerative colitis; CRP, C-reactive protein (normal values 0–5 mg/L); ESR, erythrocyte sedimentation rate (normal values 1–10 mm/1st h); MASEI, Madrid Ankylosing Spondylitis Enthesitis Index; Sport activity defined as sport or physical activity at least once a week; IBD with/without SpA inflammatory bowel disease with or without Spondylarthritis; IBS, irritable bowel syndrome; HC, healthy subjects.*
**p < 0.05 compared to IBD patients without and with SpA.*

with SpA [median 29.5 range (9–51)] und IBD without SpA [median 22.0 range (9–39)] did not show significant difference between each other but it was significantly higher compared to IBS [median 10.5 range (2–32)] and HC [median 11.5 (5–33)]. Patients with IBD and SpA demonstrated significantly more erosions ($p < 0.001$) and structural abnormalities ($p < 0.05$) compared to patients with IBD.

No association was found between clinical IBD activity (CDAI and partial Mayo score) and MASEI, nor between clinical IBD activity and erosion-, PD- and enthesophyte subscores. We found no influence on the enthesitis scores by any current therapy or regular sport activities. Out of 25 patients with ongoing TNFi therapy 16 (64%) received Infliximab, eight (32%) Adalimumab and one (4%) Etanercept. We observed no significant difference in the MASEI score between patients receiving the different TNF inhibitors ($p = 0.75$). Besides, we found significant, moderate correlation of BMI with MASEI in the IBS group ($r = 0.453$, $p < 0.05$) and HC ($r = 0.538$, $p < 0.05$).

TABLE 2 | Distribution of ultrasound findings in IBD patients and control population (IBS and HC).

	Enthesophyte	Structure	Thickness	Bursitis	Erosion	PD
IBD with SpA	7 (0–13)	9 (3–14)	6 (0–9)	1.5 (1.6)	3 (0–4)	1 (0–3)
IBD without SpA	6 (2–14)	6 (0–13)**	4 (0–8)	2 (0–3)	1 (0–4)**	1 (0–2)
IBS	3 (0–12)*	0 (0–9)*	1 (0–12)*	0 (0–3)*	0.5 (0–2)*	0 (0–2)*
HC	4 (0–12)*	1.5 (0–7)*	1.8 (1.9)*	1 (0–4)*	0 (0–2)*	0 (0–3)*

PD, Power Doppler; Structure, pathological structure of the enthesis; IBD with/without SpA, inflammatory bowel disease with or without spondylarthritis; IBS, irritable bowel syndrome; HC, healthy subjects.
Data indicate the median (range) ultrasound score for each abnormalities IBD /IBS per patient or control subjects. Statistical differences were tested with the Wilcoxon test.
**p < 0.05 compared to IBD patients without or with SpA.*
***p < 0.05 compared to IBD patient with SpA.*

Reliability Exercise

The inter-reader agreement for the MASEI was good, revealing an ICC of 0.89 (0.52–0.98).

DISCUSSION

In the present study we demonstrated that ultrasound verified enthesitis is higher in patients with IBD with or without SpA in comparison to IBS patients and HC. All components of enthesitis were more common in both IBD subgroups.

The most interesting finding of our study is that PD, a sign of active inflammation of entheses, was equally present in patients with IBD with or without associated SpA. Structural changes of entheses including erosions, tended to be higher in IBD with SpA. This also accounted for the higher MASEI score in the latter group. All changes were more common in IBD than in IBS and HC. This indicates that active inflammation of entheses is a common extra-intestinal manifestation in IBD, independent of clinical symptoms of enthesitis (and SpA) as well as IBD activity. Subclinical enthesitis might precede or even predict the development of clinical manifest SpA, as has been the case in psoriasis, but future follow-up studies are required to clarify this issue (11). Structural changes might be the consequence of previous active enthesitis and seem to be linked more closely to clinical features of SpA than PD, but are also independent of current IBD activity.

In our study the prevalence of PD positive enthesis in IBD patients (64%) was higher than reported by Bandinelli at al. who found a positive PD only in 16% IBD patients (6). Possible explanations for the difference are the use of a highly-sensitive 18-MHz linear array transducer in our study compared to a 10-MHz used by Bandinelli. Furthermore, the extensor tendon at lateral epicondyle was frequently a PD positive enthesis in our study and this site was not examined in the Bandinelli study. After the exclusion of lateral epicondyle from the calculation, the distribution of vascularity in IBD patient was in line with other studies like from Rovicso et al. (7). The prevalence of PD and entheseal thickening in IBS and HC in our study was comparable

with the data of prevalence of such abnormalities in healthy subjects (27).

The occurrence of a new PsA in a group of patients with asymptomatic enthesitis and in psoriasis was 4.3% during a 2-year observation (12). In CED, 17–39% of patients develop clinically manifest SpA during the course of the disease, however, how many of these cases have asymptomatic enthesitis or other subclinical musculoskeletal manifestation preceding the clinical onset of SpA is unknown and can only be clarified by prospective follow-up studies (28). Our data, however, suggest that the presence of erosion might help in distinguishing between subclinical and definitive SpA in patients with IBD.

Another unresolved issue is the interpretation of clinical and imaging signs of enthesitis in patients with SpA and SpA-related diseases. We know from the present and previous studies that clinical and ultrasound examination of enthesitis only partially overlap. While pain (spontaneous and by palpation) is the most frequent symptom of enthesitis and is also part of the ASAS classification criteria for SpA, it is neither sensitive nor specific for enthesitis, particularly when deep tendon insertions like the plantar facia are affected (29). Nevertheless, little is known about the clinical impact of imaging verified subclinical enthesitis: data is limited on whether patients will develop clinical manifestations of enthesitis later, or if subclinical enthesitis provokes structural damage, or whether it has an impact on the future functionality or quality of life. Further, the response of subclinical, imaging verified enthesitis on anti-inflammatory therapy is unknown. Currently, it is not necessary to treat subclinical enthesitis in IBD patients. Follow-up studies are needed to address these open issues.

While the MASEI included retrocalcaneal and infrapatellar bursitis in the score, bursitis is not considered an elementary lesion of enthesitis according to OMERACT. The OMERACT experts were of the opinion, that bursae are not part of the enthesitis complex and that inflammation affects them only at a later stage of enthesitis when it extends toward the tendon and peri-tendinous structures (30).

While in Rheumatoid arthritis, MSK ultrasound is mainly used to investigate the presence of synovial inflammation, in PsA and SpA it is also applied to investigate enthesitis. Ultrasound verified synovitis in RA predicted the progression of bone erosions and occurrence of a clinical relapse even in the absence of clinical inflammation (31). Whether ultrasound verified synovitis has a similar predictive value in PsA and SpA is unclear. Earlier studies in SpA and PsA demonstrated that ultrasound verified enthesitis does not correlate with clinical signs of enthesitis (20). We previously observed that enthesophytes but neither PD nor clinical tenderness at entheses were linked with radiographic enthesal progression (32). Whether similar result could be found in SpA and whether clinically quiescent but sonographically active enthesitis would predict future clinical worsening are questions that only future research can clarify.

The main strength of our study is the inclusion of IBD patients with and without SpA as well as IBS patients as a relevant control group. While low-grade intestinal inflammation and other factors contribute to the pathophysiology of IBS, there is a clear difference in terms of extra-intestinal enthesal inflammation in comparison to IBD patients, as our data clearly demonstrates. Whether the presence of subclinical enthesitis might also be used for diagnostic purposes (i.e., to differentiate between IBD and IBS patients, needs to be evaluated further). We also took into account the possible influence of external factors such as sport and BMI on the level of enthesitis, however no relevant association was observed in our IBD group.

The main limitations of our study are the limited sample size and the absence of follow-up data which would have been important to analyse the relevance of subclinical enthesitis for future outcomes as stated above. Other limitations are the relatively low level of clinical activity (concerning the intestine) of IBD patients, as well as the heterogeneity of them in regard to disease duration and treatment. All these factors, however, had no influence on the level of ultrasound verified enthesitis in our analyses.

In conclusion, ultrasound verified enthesitis components are more common in patients with IBD with or without SpA as compared to patients with IBS or HC.

DATA AVAILABILITY STATEMENT

The raw data supporting the conclusions of this article will be made available by the authors, without undue reservation.

ETHICS STATEMENT

The studies involving human participants were reviewed and approved by Ethikkommission der Medizinischen Universität Graz. The patients/participants provided their written informed consent to participate in this study.

AUTHOR CONTRIBUTIONS

RH, CD, PK, and CH substantially contributed to study conception and design, acquisition of data, and analysis and interpretation of data. AL was involved in planning, acquisition of data, and supervised the work. RH and CD wrote the paper. All the authors revised the paper and approved the final version of the article to be published.

ACKNOWLEDGMENTS

The content of this manuscript has been presented in part at the EULAR 2015, SAT0628 High Prevalence of Ultrasound Verified Enthesitis in Patients with Inflammatory Bowel Disease with or without Spondylarthritis, Annals of the Rheumatic Diseases 2015;74:888–889.

REFERENCES

1. McGonagle D, Khan MA, Marzo-Ortega H, O'Connor P, Gibbon W, Emery P. Enthesitis in spondyloarthropathy. *Curr Opin Rheumatol.* (1999) 11:244–50. doi: 10.1097/00002281-199907000-00004
2. McGonagle D, Gibbon W, Emery P. Classification of inflammatory arthritis by enthesitis. *Lancet.* (1998) 352:1137–40. doi: 10.1016/S0140-6736(97)12004-9
3. Turkcapar N, Toruner M, Soykan I, Aydintug OT, Cetinkaya H, Duzgun N, et al. The prevalence of extraintestinal manifestations and HLA association in patients with inflammatory bowel disease. *Rheumatol Int.* (2006) 26:663–8. doi: 10.1007/s00296-005-0044-9
4. Harbord M, Annese V, Vavricka SR, Allez M, Acosta MB de, Boberg KM, et al. The first european evidence-based consensus on extra-intestinal manifestations in inflammatory bowel disease. *J Crohn's Colitis.* (2016) 10:239–54. doi: 10.1093/ecco-jcc/jjv213
5. Mielants H, Veys EM, Cuvelier C, De Vos M, Goemaere S, De Clercq L, et al. The evolution of spondyloarthropathies in relation to gut histology. III. Relation between gut and joint. *J Rheumatol.* (1995) 22:2279–84.
6. Bandinelli F, Milla M, Genise S, Giovannini L, Bagnoli S, Candelieri A, et al. Ultrasound discloses entheseal involvement in inactive and low active inflammatory bowel disease without clinical signs and symptoms of spondyloarthropathy. *Rheumatology.* (2011) 50:1275–9. doi: 10.1093/rheumatology/keq447
7. Rovisco J, Duarte C, Batticcioto A, Sarzi-Puttini P, Dragresshi A, Portela F, et al. Hidden musculoskeletal involvement in inflammatory bowel disease: a multicenter ultrasound study. *BMC Musculoskelet Disord.* (2016) 17:1–7. doi: 10.1186/s12891-016-0932-z
8. Lehtinen A, Taavitsainen M, Leirisalo-Repo M. Sonographic analysis of enthesopathy in the lower extremities of patients with spondylarthropathy. *Clin Exp Rheumatol.* (1994) 12:143–8.
9. Kiris A, Kaya A, Ozgocmen S, Kocakoc E. Assessment of enthesitis in ankylosing spondylitis by power Doppler ultrasonography. *Skeletal Radiol.* (2006) 35:522–8. doi: 10.1007/s00256-005-0071-3
10. Gisondi P, Tinazzi I, El-Dalati G, Gallo M, Biasi D, Barbara LM, et al. Lower limb enthesopathy in patients with psoriasis without clinical signs of arthropathy: a hospital-based case-control study. *Ann Rheum Dis.* (2008) 67:26–30. doi: 10.1136/ard.2007.075101
11. El Miedany Y, El Gaafary M, Youssef S, Ahmed I, Nasr A. Tailored approach to early psoriatic arthritis patients: clinical and ultrasonographic predictors for structural joint damage. *Clin Rheumatol.* (2015) 34:307–13. doi: 10.1007/s10067-014-2630-2
12. Elnady B, El Shaarawy NK, Dawoud NM, Elkhouly T, Desouky DES, ElShafey EN, et al. Subclinical synovitis and enthesitis in psoriasis patients and controls by ultrasonography in Saudi Arabia; incidence of psoriatic arthritis during 2 years. *Clin Rheumatol.* (2019) 38:1627–35. doi: 10.1007/s10067-019-04445-0
13. Rudwaleit M, van der Heijde D, Landewé R, Akkoc N, Brandt J, Chou CT, et al. The Assessment of SpondyloArthritis International Society classification criteria for peripheral spondyloarthritis and for spondyloarthritis in general. *Ann Rheum Dis.* (2011) 70:25–31. doi: 10.1136/ard.2010.133645
14. Gomollón F, Dignass A, Annese V, Tilg H, Van Assche G, Lindsay JO, et al. 3rd European evidence-based consensus on the diagnosis and management of crohn's disease 2016: part 1: diagnosis and medical management. *J Crohns Colitis.* (2017) 11:3–25. doi: 10.1093/ecco-jcc/jjw168
15. Magro F, Gionchetti P, Eliakim R, Ardizzone S, Armuzzi A, Barreiro-de Acosta M, et al. Third European evidence-based consensus on diagnosis and management of ulcerative colitis. Part 1: definitions, diagnosis, extra-intestinal manifestations, pregnancy, cancer surveillance, surgery, and ileo-anal pouch disorders. *J Crohns Colitis.* (2017) 11:649–70. doi: 10.1093/ecco-jcc/jjx008
16. Longstreth GF, Thompson WG, Chey WD, Houghton La, Mearin F, Spiller RC. Functional bowel disorders. *Gastroenterology.* (2006) 130:1480–91. doi: 10.1053/j.gastro.2005.11.061
17. Best WR, Becktel JM, Singleton JW, Kern FJ. Development of a Crohn's disease activity index. National Cooperative Crohn's Disease Study. *Gastroenterology.* (1976) 70:439–44. doi: 10.1016/S0016-5085(76)80163-1
18. Moss AC, Farrell RJ. Infliximab for induction and maintenance therapy for ulcerative colitis. *Gastroenterology.* (2006) 131:1649–51. doi: 10.1053/j.gastro.2006.09.039
19. Garrett S, Jenkinson T, Kennedy LG, Whitelock H, Gaisford P, Calin A. A new approach to defining disease status in ankylosing spondylitis: the Bath Ankylosing Spondylitis Disease Activity Index. *J Rheumatol.* (1994) 21:2286–91.
20. Husic R, Gretler J, Felber A, Graninger WB, Duftner C, Hermann J, et al. Disparity between ultrasound and clinical findings in psoriatic arthritis. *Ann Rheum Dis.* (2014) 73:1529–36. doi: 10.1136/annrheumdis-2012-203073
21. Balint PV, Kane D, Wilson H, McInnes IB, Sturrock RD. Ultrasonography of entheseal insertions in the lower limb in spondyloarthropathy. *Ann Rheum Dis.* (2002) 61:905–10. doi: 10.1136/ard.61.10.905
22. Miguel E de, Cobo T, Mun S, Naredo E, Uso J, Acebes JC. Validity of enthesis ultrasound assessment in spondyloarthropathy. *Ann Rheum Dis.* (2009) 68:169–74. doi: 10.1136/ard.2007.084251
23. Healy PJ, Helliwell PS. Measuring clinical enthesitis in psoriatic arthritis: assessment of existing measures and development of an instrument specific to psoriatic arthritis. *Arthritis Rheum.* (2008) 59:686–91. doi: 10.1002/art.23568
24. Ficjan A, Husic R, Gretler J, Lackner A, Graninger WB, Gutierrez M, et al. Ultrasound composite scores for the assessment of inflammatory and structural pathologies in Psoriatic Arthritis (PsASon-Score). *Arthritis Res Ther.* (2014) 16:1–13. doi: 10.1186/s13075-014-0476-2
25. Mouterde G, Aegerter P, Correas J-M, Breban M, D'Agostino M-A. Value of contrast-enhanced ultrasonography for the detection and quantification of enthesitis vascularization in patients with spondyloarthritis. *Arthritis Care Res.* (2014) 66:131–8. doi: 10.1002/acr.22195
26. Tom S, Zhong Y, Cook R, Aydin SZ, Kaeley G, Eder L. Development of a preliminary ultrasonographic enthesitis score in psoriatic arthritis—GRAPPA ultrasound working group. *J Rheumatol.* (2019) 46:384–90. doi: 10.3899/jrheum.171465
27. Di Matteo A, Filippucci E, Cipolletta E, Martire V, Jesus D, Musca A, et al. How normal is the enthesis by ultrasound in healthy subjects? *Clin Exp Rheumatol.* (2020) 38:472–8.
28. Peluso R, Di Minno MND, Iervolino S, Manguso F, Tramontano G, Ambrosino P, et al. Enteropathic spondyloarthritis: from diagnosis to treatment. *Clin Dev Immunol.* (2013) 2013:631408. doi: 10.1155/2013/631408
29. Klauser AS, Wipfler E, Dejaco C, Moriggl B, Duftner C, Schirmer M. Diagnostic values of history and clinical examination to predict ultrasound signs of chronic and acute enthesitis. *Clin Exp Rheumatol.* (2008) 26:548–53.
30. Balint PV, Terslev L, Aegerter P, Bruyn GAW, Chary-Valckenaere I, Gandjbakhch F, et al. Reliability of a consensus-based ultrasound definition and scoring for enthesitis in spondyloarthritis and psoriatic arthritis: an OMERACT US initiative. *Ann Rheum Dis.* (2018) 77:1730–5. doi: 10.1136/annrheumdis-2018-213609
31. Brown AK, Quinn MA, Karim Z, Conaghan PG, Peterfy CG, Hensor E, et al. Presence of significant synovitis in rheumatoid arthritis patients with disease-modifying antirheumatic drug-induced clinical remission: evidence from an imaging study may explain structural progression. *Arthritis Rheum.* (2006) 54:3761–73. doi: 10.1002/art.22190
32. Lackner A, Heber D, Bosch P, Adelsmayr G, Duftner C, Ficjan A, et al. Ultrasound verified enthesophytes are associated with radiographic progression at entheses in psoriatic arthritis. *Rheumatology.* (2020) 28:1–5. doi: 10.1093/rheumatology/keaa028

Conflict of Interest: The authors declare that the research was conducted in the absence of any commercial or financial relationships that could be construed as a potential conflict of interest.

frontiers in Medicine

ORIGINAL RESEARCH
published: 23 March 2021
doi: 10.3389/fmed.2021.653994

Bone Erosions Detected by Ultrasound Are Prognostic for Clinical Arthritis Development in Patients With ACPA and Musculoskeletal Pain

Michael Ziegelasch[1], Emma Eloff[1], Hilde B. Hammer[2], Jan Cedergren[1], Klara Martinsson[1], Åsa Reckner[1], Thomas Skogh[1], Mattias Magnusson[1] and Alf Kastbom[1]*

[1] Department of Rheumatology, Department of Clinical and Experimental Medicine, Linköping University, Linköping, Sweden, [2] Department of Rheumatology, Diakonhjemmet Hospital, Oslo, Norway

OPEN ACCESS

Edited by:
Christian Dejaco, Medical University of Graz, Austria

Reviewed by:
Garifallia Sakellariou, University of Pavia, Italy
Stephanie Finzel, University of Freiburg, Germany

***Correspondence:**
Michael Ziegelasch
michael.ziegelasch@liu.se

Specialty section:
This article was submitted to Rheumatology, a section of the journal Frontiers in Medicine

Received: *15 January 2021*
Accepted: *01 March 2021*
Published: *23 March 2021*

Citation:
Ziegelasch M, Eloff E, Hammer HB, Cedergren J, Martinsson K, Reckner Å, Skogh T, Magnusson M and Kastbom A (2021) Bone Erosions Detected by Ultrasound Are Prognostic for Clinical Arthritis Development in Patients With ACPA and Musculoskeletal Pain. Front. Med. 8:653994. doi: 10.3389/fmed.2021.653994

Anti-citrullinated protein antibodies (ACPA) often precede onset of rheumatoid arthritis (RA) by years, and there is an urgent clinical need for predictors of arthritis development among such at-risk patients. This study assesses the prognostic value of ultrasound for arthritis development among ACPA-positive patients with musculoskeletal pain. We prospectively followed 82 ACPA-positive patients without clinical signs of arthritis at baseline. Ultrasound at baseline assessed synovial hypertrophy, inflammatory activity by power Doppler, and erosions in small joints of hands and feet. We applied Cox regression analyses to examine associations with clinical arthritis development during follow-up (median, 69 months; range, 24–90 months). We also compared the ultrasound findings among the patients to a control group of 100 blood donors without musculoskeletal pain. Clinical arthritis developed in 39/82 patients (48%) after a median of 6 months (range, 1–71 months). One or more ultrasound erosions occurred in 13/82 patients (16%), with none in control subjects ($p < 0.001$). Clinical arthritis development was more common among patients with baseline ultrasound erosions than those without (77 vs. 42%, $p = 0.032$), and remained significant in a multivariable Cox regression analysis that included previously described prognostic factors (HR 3.9, 95% CI 1.6–9.4, $p = 0.003$). Ultrasound-detected tenosynovitis was more frequent among the patients and associated with clinical arthritis development in a univariable analysis (HR 2.5, 95% CI 1.1–5.7, $p = 0.031$), but did not remain statistically significant in multivariable analysis. Thus, bone erosions detected by ultrasound are independent predictors of clinical arthritis development in an ACPA-positive at-risk population.

Trial Registration: Regional Ethics Committee in Linköping, Sweden, Dnr M220-09. Registered 16 December 2009, https://etikprovningsmyndigheten.se/.

Keywords: anti-citrullinated protein antibodies, rheumatoid arthritis, ultrasound, musculoskeletal pain, erosions, clinical arthritis

BACKGROUND

Autoimmune features, such as the presence of circulating rheumatoid factor (RF) and/or anti-citrullinated protein antibodies (ACPA), typically precede the onset of clinically manifest rheumatoid arthritis (RA) (1, 2), as defined by the 1987 American College of Rheumatology (ACR87) or the 2010 ACR/EULAR classification criteria (3, 4). Neither of these RA classification criteria is applicable to patients who are suffering from musculoskeletal (MSK) pain in the absence of clinical synovitis. However, given the benefits of modern early immunomodulatory therapies for RA (5) and the high diagnostic specificity of ACPA (6), patients within this category may benefit from anti-rheumatic drug therapy prior to fulfilling the classification criteria for RA. Nonetheless, considering the substantial risk of over-treatment with potent agents of immunomodulation in this clinical setting, there is a pressing need for predictors of disease development and progression. Ultrasound, which is an imaging modality that allows the detection of subclinical inflammation in musculoskeletal structures (7), could be valuable in identifying patients who could benefit from very early treatment.

Gray scale (GS) ultrasound visualizes thickening of the synovial membranes (synovial hypertrophy; SH) in joints and tendons, effusions, and structural bone changes, such as erosions (8). The addition of power Doppler (PD) to GS ultrasound findings allows for the detection of hyperemia, which is a sign of active inflammation (9). The use of MSK ultrasound to detect ongoing inflammation and, thereby, predict clinical arthritis development has shown potential in different at-risk populations (10–13), in particular regarding PD (14). However, there are divergent results regarding both the value of each ultrasound feature and whether or not they are predictive at the patient level (14, 15). Also, ultrasound findings of arthritis may occur among non-arthritic controls, although the frequency and magnitude need to be further elucidated. Previous smaller studies have suggested that SH, particularly in the toes, may occur frequently in control populations without clinical arthritis (12, 14, 16).

In experienced hands, ultrasound appears to be more sensitive than conventional radiography for the detection of minimal structural changes located at bone surfaces, at least in certain anatomic sites such as the MCP II and the MCP V (17, 18). However, the prognostic value of ultrasound-detected erosions has been much less studied than SH and PD. One previous study reported a significant association between baseline ultrasound-detected erosions and subsequent development of arthritis, albeit without adjusting for possible confounders (14).

Ultrasound is increasingly used in clinical practice. In patients with RA-related autoantibodies and arthralgia, but no clinical arthritis, it is used for risk stratification and occasionally used for deciding on the initiation of disease-modifying anti-rheumatic drugs (DMARDs). However, a recent literature review concluded that the available evidence remains limited to moderate regarding the prognostic value of SH and PD, and insufficient concerning tenosynovitis and erosions (13).

Therefore, to fill these knowledge gaps, we compared the ultrasound findings of ACPA-positive patients with MSK pain but no clinical arthritis to the findings of healthy controls and investigated the prognostic value of ultrasound findings for subsequent clinical arthritis development.

METHODS

Patients and Control Subjects

We set up a prospective observational study, designated "TIRx" (Swedish acronym for "X-tra early rheumatology follow-up"), which enrolled 116 patients in the period of 2010–2013 at the University Hospital in Linköping, Sweden. The patients were referred from primary care centers within the Östergötland County in southeast Sweden to the rheumatology clinic, based on ACPA-positivity and any kind and duration of MSK symptom. Screening, enrolment, and follow-up were performed by four experienced rheumatologists (AK, JC, TS, and ÅR). In this study we included patients with MSK pain of any sort and duration and a positive anti-cyclic citrullinated peptide (anti-CCP) antibody test in clinical routine practice. The exclusion criteria were: fulfillment of the ACR1987 criteria (3); oral or intraarticular corticosteroid therapy within 6 weeks prior to screening; previous diagnosis of inflammatory rheumatic disease; and age <18 years. Twelve patients (10%) discontinued and 22 (19%) had clinical arthritis at baseline. Thus, 82 ACPA-positive at-risk patients were available for further analysis (**Figure 1**). The baseline characteristics of the study subjects are shown in **Table 1**. Follow-up visits were scheduled at months 3, 12, 24, and 36, and thereafter every other year. Patients were instructed to contact the clinic without delay in case of increased symptoms between scheduled visits. At each visit, we obtained a 28-joint disease activity score (DAS28) (19) and conducted a clinical examination of symptomatic joint(s) not included in the 28-joint status. Pharmacotherapy and non-pharmacologic interventions were instituted as suggested by the physician and with the patient's acceptance. Development of arthritis was defined by clinical examination conducted by

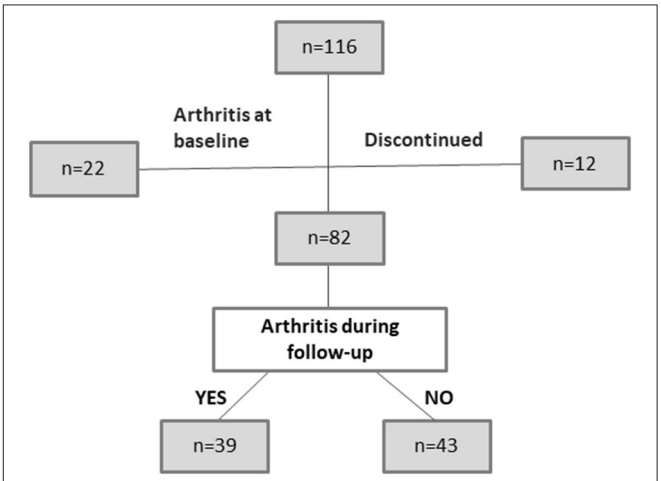

FIGURE 1 | Distribution of patients during the study.

TABLE 1 | Baseline characteristics of study participants.

Characteristic		Patients ($N = 82$)	Controls ($n = 100$)
Age, years		52 (14)	52 (14)
Gender, females		66 (81%)	50 (50%)
Symptom duration	0–6 months	15 (18%)	
	6–12 months	37 (45%)	
	>18 months	30 (37%)	
ACPA-level	Low (<3 × cutoff)	32 (39%)	
	High (≥3 × cutoff)	50 (61%)	
RF	Negative	58 (71%)	
	Positive	24 (29%)	
CRP, mg/L		6 (6.0)	
ESR, mm/h		12 (9.5)	
DAS28		2.5 (1.1)	
Smoking	Non-smoker	43 (52%)	
	Ex-smoker	26 (32%)	
	Current smoker	13 (16%)	

ACPA, Anti-citrullinated protein antibodies; CRP, C-reactive protein; DAS, disease activity score; ESR, erythrocyte sedimentation rate; HAQ, health assessment questionnaire; RF, rheumatoid factor; SD Standard deviation. Values are mean (SD) unless otherwise indicated.

an experienced rheumatologist. Follow-up was until September 1st 2017, resulting in a median follow-up time of 69 months [range, 24–90 months, interquartile range (IQR) 57–77] for those patients who did not develop arthritis.

As controls, we recruited 100 blood donors without MSK pain (**Table 1**) from the Department of Transfusion Medicine at Linköping University Hospital. This control group did not have arthralgia and was selected so as to have a similar mean age as the TIRx patient group, and underwent ultrasound examination once according to the procedure described below. One out of the 100 healthy controls tested positive for ACPA, which is an expected number given the specificity of the test.

Ethics Approval and Consent to Participate

The study was conducted in accordance with the principles of the Helsinki Declaration. The study protocol was approved by the Regional Ethics Committee in Linköping, Sweden (DnR 220-09 and 2015/236-32), and all participants gave written informed consent to participate.

Ultrasound Examinations

All ultrasound examinations were performed by an experienced rheumatologist (MZ). The ProFocus system from BK Medical (BK Global Headquarters, Peabody, MA) with a linear scanner at 6–15 MHz was used. Synovial hypertrophy and bone erosions were assessed with identical GS settings for all participants (B-mode frequency, 12 MHz; B-mode gain, 25 dB), while inflammatory activity was assessed by power Doppler (frequency, 7.5 MHz; Doppler gain 44dB; pulse repetition frequency, 0.8 kHz; and the lowest possible wall filter to avoid artifacts). The protocol included dorsal assessments of the following 36 joints: bilateral radiocarpal, intercarpal, distal radioulnar, metacarpophalangeal (MCP) joints 1–5, interphalangeal (IP) thumb joints, proximal interphalangeal (PIP) joints 2–5, and metatarsophalangeal (MTP) joints 1–5. To grade synovitis, we used the semi-quantitative scoring system introduced by Szkudlarek et al. (20) in which gray-scale synovial SH and hyperemia (PD) were graded on a scale of 0–3. We used the commonly applied definition of ultrasound arthritis of SH ≥2 and/or PD grade ≥1 as the cutoff for a pathologic ultrasound finding (8, 16, 21–24). PD signals were assessed only in joints with SH ≥1. Sum scores from the 36 investigated joints were calculated for SH and PD, respectively, resulting in a maximum score of 108 for both SH and PD.

In addition, three of the most commonly involved tendons in RA were examined bilaterally (extensor carpi ulnaris (ECU), tibialis posterior tendon (TPT), and common flexor digitorum longus (CFDL) in the feet) (25). Tenosynovitis was scored by GS according to OMERACT (8), and PD signals were scored as: 0 = none; 1 = minor; 2 = moderate; and 3 = major presence (25).

Regarding erosions, easily assessable and typical sites (MCP 2 and 5, ulnar head, PIP 2–5, and MTP 1 and 5) were dynamically examined on dorsal and lateral aspects, and erosions were reported as present (≥1) or not present. Erosion was defined as an interruption of the bone surface observed in two perpendicular planes with a diameter of ≥1 mm (8).

MTP I can be affected by concomitant conditions such as osteoarthritis. However, we chosen to report changes in this joint, since it is possible to distinguish typical erosive changes that do not rise above the bone surface from those degenerative changes with bone-proliferative features.

The ultrasound investigator did not participate in the clinical management of the patients, and the ultrasound results were blinded to both the patients and their respective physicians during the first 3 years of the study. Thereafter, they were available upon request. To determine the intra-reader reliability, baseline ultrasound images of 36 joints from 10 randomly chosen patients (in total 360 joints) were saved and re-assessed at least 2 weeks later, resulting in a kappa value of 0.948 for the presence of ultrasound synovitis (categorically as defined above), and 1.0 for the presence of erosions.

Laboratory Analyses

Erythrocyte sedimentation rate (ESR) and C-reactive protein (CRP) were analyzed according to clinical routine practice at the Clinical Chemistry Laboratory, Linköping University Hospital. Agglutinating RF was analyzed by nephelometry at the accredited Clinical Immunology Laboratory, Linköping University Hospital (cutoff, 30 U/ml). In serum samples collected at baseline and stored at −80°C, anti-CCP antibodies were analyzed using the 2nd generation enzyme immunoassay (Immunoscan CCPlus; EuroDiagnostica AB, Malmö, Sweden). The cutoff was set at 25 AU/ml according to the manufacturer.

Statistical Analyses

Statistical analyses were performed using the IBM SPSS Statistics 23 software. Continuous data were summarized with mean values and standard deviation, and non-normally distributed data with median values and IQR. Differences between groups were tested

using the Student's *t*-test regarding continuous variables, and proportions were compared using the Chi-squared test. To assess the prognostic value of ultrasound features for clinical arthritis development, we performed univariable Cox regression analysis. Significant findings were further tested in a multivariable analysis that included baseline variables of potential importance for arthritis development (age, sex, symptom duration, RF status, ACPA levels, smoking habits, ESR, and CRP levels). Positive predictive values (PPV) and negative predictive values (NPV) for the ultrasound findings were calculated for significant associations in the multivariable model. Statistical significance was adjudged for two-sided *p*-values <0.05.

RESULTS

Ultrasound Findings in Patients and Controls

At the joint level, significantly more MCP and PIP joints had SH ≥ 2 among the patients, as compared to the controls (**Table 2**). In contrast, SH ≥ 2 was more prevalent in MTP 1–5 among controls than among patients (30.2 vs. 18.7%, $p < 0.001$). Among the controls, SH was more frequent in MTP 1–4 than in any other location and was significantly over-represented compared to the patients (**Table 2**). Therefore, we decided to present MTP 1–4 separately from MTP 5, and to exclude MTP 1–4 from the analyses of SH vs. arthritis development in the patients.

PD signals (PD ≥ 1) were most commonly seen in wrists, i.e., radiocarpal, intercarpal, and/or radioulnar joints (7.9% of patient joints vs. 2.0% of control joints, $p < 0.001$), and were infrequent in other locations (≤3%; **Table 2**). A detectable PD signal (PD ≥ 1) at any location occurred in 37/82 (45%) of the patients, as compared to 5/100 (5%) of the controls ($p < 0.001$).

Tenosynovitis at baseline was found in 10/82 patients (ECU in 3 patients, TPT in 5, CFDL in 1, and both ECU and TPT in 1) and in 3/100 controls (ECU in 2, and CFDL in 1) ($p = 0.021$).

Ultrasound detected erosions in 13 patients (10 patients had 1, while 3 patients had 2 erosions), whereas, none of the controls had any erosions ($p < 0.001$, **Table 3**). Of the 16 erosions, 1 was localized in a PIP 2 joint radially, 4 in MCP 2 joints radially, 1 in MCP 5 joints ulnar, 4 in the head of ulna, 2 in MTP 1 medially, and 4 in MTP 5 joints laterally. At baseline, 6 of the

TABLE 3 | Baseline ultrasound findings in patients without clinical arthritis at baseline compared to controls.

		Patients (*N* = 82)	Controls (*N* = 100)	*p*-value
Hands	SH	4.0 (4.7)	2.1 (2.5)	**0.001**
	PD	1.0 (1.8)	0.04 (0.2)	**<0.001**
MTP1-4	SH	4.1 (4.1)	7.7 (4.3)	**<0.001**
	PD	0.2 (0.7)	0.04 (0.3)	**0.016**
MTP5	SH	0.3 (0.8)	0.2 (0.6)	0.462
	PD	0.04 (0.2)	0	0.181
Total (Hands + MTP1-5)	SH	8.4 (7.2)	9.9 (5.6)	0.102
Total (Hands + MTP1-5)	PD	1.3 (2.0)	0.1 (0.4)	**<0.001**
Tendons	SH	0.5 (1.1)	0.1 (0.4)	**0.005**
	PD	0.1 (0.6)	0 (0)	0.063
≥1 erosion present		13/82 (16%)	0 (0%)	**<0.001**

Values shown are mean (standard deviation) sum scores unless otherwise indicated. Hands include wrists, metacarpophalangeal joints 1–5, and proximal interphalangeal joints 2–5. SH, Synovial hypertrophy; MTP, metatarsophalangeal joint; PD, power Doppler. Significant p-values are shown in bold.

TABLE 2 | Comparison of ultrasound abnormalities at among anti-citrullinated protein antibody-positive at-risk patients vs. controls.

Joint(s)	Synovial hypertrophy ≥2			Power doppler ≥1		
	Patients (*n* = 82)	Controls (*n* = 100)	*p*-value	Patients (*n* = 82)	Controls (*n* = 100)	*p*-value
Wrist	8.9% (44/492)	7.0% (42/600)	0.259	7.9% (39/492)	2% (12/600)	**<0.001**
MCP 1-5	3.5% (29/820)	0.5% (5/1000)	**<0.001**	0.7% (6/820)	0% (0/1000)	**0.008**
PIP 2-5	5.0% (33/656)	0.6% (5/800)	**<0.001**	1.7% (11/656)	0% (0/800)	**<0.001**
MTP 1–4	22.1% (145/656)	37.4% (299/800)	**<0.001**	2.1% (14/656)	0.3% (2/800)	**0.001**
MTP 5	4.9% (8/164)	1.5% (3/200)	0.071	1.2% (2/164)	0% (0/200)	0.202
Total	9.3% (259/2788)	10.4% (354/3400)	0.146	2.6% (72/2788)	0.4% (14/3400)	**<0.001**
Total (excl. MTP 1–4)	5.3% 114/2132)	2.1% (55/2600)	**<0.001**	2.7% (58/2132)	0.5% (12/2600)	**<0.001**
Tendons	2.2% (11/492)	0.5% (3/600)	**0.014**	1.2% (6/492)	0% (0/600)	**0.008**

MCP, Metacarpophalangeal joint; MTP, metatarsophalangeal joint; PIP, proximal interphalangeal joint of the finger. Significant p-values are shown in bold.

16 joints with bone erosions (38%) had synovitis according to ultrasound (SH ≥ 2 and/or PD ≥ 1). Conventional radiographs from baseline detected 1 out of the 16 (6%) bone erosions detected by ultrasound.

Table 3 summarizes the ultrasound findings at the patient level. The PD sum scores were higher in patients than in controls. SH showed site-specific differences: in the hands, the SH sum scores were higher among the patients, whereas, the SH sum scores in MTP 1–4 were higher among the controls. When excluding the feet, ultrasound-detected synovitis (defined as either SH ≥ 2 and/or PD ≥ 1) was noted in 55 patients (67%) and 33 controls (33%) ($p < 0.001$).

Ultrasound Findings and Subsequent Arthritis Development

Ultrasound synovitis occurred in 55 patients (67%) when excluding the feet, and in 66 patients (81%) when including the feet. Neither the presence of ultrasound synovitis nor the SH or PD sum scores were significantly associated with the development of clinical arthritis (**Table 4**). However, 10 out of the 13 patients (77%) with ≥1 baseline erosion on ultrasound developed clinical arthritis during the follow-up period, as compared to 29/69 (42%) of those without erosions ($p = 0.032$). In the univariable Cox regression analysis, baseline erosions were associated with clinical arthritis development [Hazard Ratio (HR) 2.8, 95% CI 1.4–5.8, $p = 0.005$] (**Table 4**). We also tested whether erosions by ultrasound combined with inflammatory changes in joints and tendons increased the prognostic value concerning clinical arthritis development. Neither the HR for synovitis nor tenosynovitis in combination with bone erosions were higher than the HR for erosions alone (**Table 4**). After including potential confounders (sex, age, symptom duration, smoking habits, ESR, CRP levels, RF status, and ACPA levels) in the Cox regression model, the association between ultrasound-detected erosions and arthritis development remained statistically significant (HR 3.9, 95% CI 1.6–9.4, $p = 0.003$) (**Figure 2**). Since this model included a large number of variables ($n = 10$) in relation to events ($n = 39$), we also tested the prognostic value of erosions in a more strict multivariable model including CRP levels, RF status, and ACPA levels. Results remained very similar (**Supplementary Table 1**). The PPV for the development of arthritis in patients with baseline erosions was 77% and the NPV was 58%.

Seven patients started treatment with DMARDs or oral corticosteroids during the follow-up despite no confirmed arthritis upon clinical examination. When we performed a multivariable Cox regression analyses while excluding these patients, erosions remained significantly associated with arthritis development (HR 4.2; 95% CI 1.7–10.0, $p = 0.001$), while SH and PD were still not significantly associated with arthritis development. In another sensitivity analysis, we restricted the analysis to the initial 3 years when the ultrasound results were completely blinded. During this period, 32/82 patients (39%) developed clinical arthritis, and the association with baseline ultrasound-detected erosions remained significant in the multivariable analysis (HR 3.5, 95% CI 1.3–9.0, $p = 0.011$).

The presence of baseline tenosynovitis in patients was associated with the development of clinical arthritis in the

TABLE 4 | Univariable Cox regression analysis of ultrasound findings with development of clinical arthritis as outcome.

Ultrasound finding	Score/ presence	*N*	Hazard ratio	95% CI	*p*-value
Synovial hypertrophy sum score	0–1	28	Reference		
	2–3	18	1.53	0.65–3.60	0.33
	≥4	36	1.48	0.70–3.13	0.31
Power Doppler sum score	0	45	Reference		
	≥1	37	1.68	0.89–3.15	0.11
Ultrasound synovitis	No	27	Reference		
	Yes	55	1.70	0.83–3.50	0.15
Ultrasound tenosynovitis	No	72	Reference		
	Yes	10	2.48	1.09–5.66	**0.031**
Ultrasound erosions	0	69	Reference		
	≥1	13	2.82	1.37–5.82	**0.005**
Erosions + synovitis	No	70	Reference		
	Yes	12	2.69	1.27–5.68	**0.010**
Erosion + tenosynovitis	No	79	Reference		
	Yes	3	2.76	0.66–11.6	0.165
Synovitis + tenosynovitis	No	73	Reference		
	Yes	9	2.23	0.93–5.36	0.072
Erosion + synovitis + tenosynovitis	No	79	Reference		
	Yes	3	2.76	0.66–11.6	0.165

Ultrasound synovitis and ultrasound tenosynovitis are defined as SH ≥ 2 and/or PD ≥ 1. Significant p-values are shown in bold.

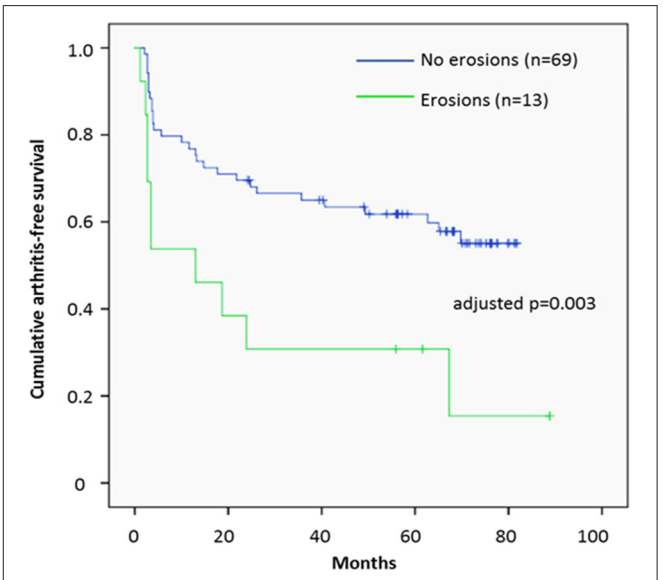

FIGURE 2 | Clinical arthritis development in relation to baseline ultrasound erosions. Survival plot illustrating the development of clinical arthritis during follow-up in relation to the presence of ultrasound erosions at baseline among patients who had anti-citrullinated protein antibodies and musculoskeletal pain.

univariable analysis (**Table 4**). However, it did not remain statistically significant in the multivariable analysis (HR 1.93, 95% CI 0.75–4.97, $p = 0.18$).

DISCUSSION

This prospective observational study identifies ultrasound-detected bone erosions as an independent prognostic factor for clinical arthritis development in ACPA-positive at-risk patients without signs of clinical arthritis at baseline. This association persisted when other known predictors were considered, suggesting that ultrasound scanning for erosions is a valuable tool to risk-stratify ACPA-positive patients with MSK pain, at least concerning the outcome of clinical arthritis. Whether or not ultrasound erosions also predict progression of structural joint damage should be addressed in future studies.

Gray-scale ultrasound findings of SH were not significantly associated with progression to clinical arthritis in the current study, and the existing literature concerning the prognostic value of SH is divergent. Van der Stadt et al. (12) did not find a predictive value for GS at the patient level, while two studies have reported significant associations with arthritis development, albeit only after excluding the feet (14, 26). A recent Dutch study has shown a predictive value for SH in combination with PD, although SH was not reported separately (22). From the healthy controls included in the current study, we conclude that SH is a common finding, also when looking outside the feet (27). Therefore, findings of SH must be interpreted with caution and not *per se* be regarded as "ultrasound synovitis."

While over-represented among the patients, the PD findings also failed to show a significant prognostic value. As for SH, the literature regarding PD includes both studies that demonstrate significant associations with arthritis development (22) and those that do not (12, 14), although all report numerically increased risk estimates. Differences in ultrasound equipment may influence PD performance across studies, and more recently introduced devices may have superior PD sensitivity than the device used in our study. Nevertheless, we conclude that PD is more specific than SH when comparing ACPA-positive MSK patients to similarly aged controls without MSK pain, but larger studies are warranted to characterize more precisely the possible prognostic value of PD signals in at-risk patients.

Recent data suggests that inflammatory tendon abnormalities are uncommon in healthy subjects (28), which is in line with our findings among healthy controls. Previous data on tenosynovitis in at-risk patients are scarce. We found an increased prevalence among ACPA-positive patients, and a significant association with progression to clinical arthritis. However, the multivariable analysis did not confirm an independent prognostic value.

Ultrasound erosions were very specific findings in our study, being detected in 16% of the ACPA-positive patients with MSK but not in any of the controls. Our results are in line with the study of Nam et al., in which none of the 48 controls had erosions in any of the examined joints in the hands or wrist, only two had a small erosion in one of their fifth MTP joints (14). Since bone-specific effects of ACPA have been discussed extensively in recent years (29, 30), it is intriguing that the ultrasound feature with the strongest prognostic value in our ACPA-positive study population reflects bone damage rather than inflammation. Fewer than half of the joints with ultrasound-detected erosions concurrently had ultrasound-detected synovitis (and none had clinical arthritis), which is compatible with the hypothesis of structural damage preceding arthritis in at least a subset of ACPA-positive individuals (31). The one previous study on ultrasound erosions in ACPA-positive at-risk patients found a HR very similar to ours (14). Taken together, the studies strongly support the use of ultrasound scanning for erosions in ACPA-positive patients with MSK symptoms to improve prognostic capability. Given the general benefit of early initiation of anti-rheumatic therapy in patients with RA, the issue as to whether patients with ultrasound erosions would benefit from very early pharmacotherapy needs to be addressed in future studies.

A strength of the current study is the long follow-up period, which increases the chances to identify those at risk of developing arthritis after several years. In addition, the large control population places the ultrasound data in perspective, for instance by demonstrating that SH in MTP 1–4 must be interpreted with caution. Furthermore, the ultrasound results were blinded to the patients and the treating physicians, thereby removing the risk of influencing clinical judgement and treatment decisions.

A limitation of the study is that treatment was not defined in the study protocol. Importantly, however, the analyses that excluded the seven patients who were subjected to corticosteroid and/or DMARD therapy without a confirmed clinical arthritis did not alter the results in any substantial way. A second limitation of this work is the relatively small sample size, resulting in rather wide CIs and difficulties to reliably look into subgroups of patients. Another potential limitation is the fact that there was only one ultrasound investigator, who was not blinded to participant status (patient vs. control). However, the ultrasound sonographer still graded controls with more SH in the MTP joints, and we therefore not believe that non-blinding resulted in overrated findings among patients compared to controls. Finally, due to practical reasons, arthritis development was not confirmed by a second investigator or compared with ultrasound findings in the same joint. However, the clinical investigators were experienced, and patients were seen by the same doctor at most of the visits.

CONCLUSIONS

We conclude that bone erosions detected by ultrasound are independent predictors for the development of clinical arthritis in ACPA-positive patients with MSK pain and without baseline arthritis. Thus, ultrasound examinations in this clinical setting should include assessments of bone erosions, in order to improve risk stratification.

DATA AVAILABILITY STATEMENT

The raw data supporting the conclusions of this article will be made available by the authors upon reasonable request.

ETHICS STATEMENT

The studies involving human participants were reviewed and approved by Regional Ethics Committee in Linköping, Sweden (DnR 220-09 and 2015/236-32). The patients/participants provided their written informed consent to participate in this study.

AUTHOR CONTRIBUTIONS

MZ, TS, and AK conceived the study. MZ performed the ultrasound examinations and was responsible for study coordination. EE, JC, ÅR, TS, and AK were involved in the recruitment and characterization of patients. HH and MZ developed the ultrasound protocols. MM and MZ performed statistical analyses. KM was responsible for the laboratory analyses. MZ, MM, and AK drafted the manuscript and received critical input from all the co-authors. All authors contributed to the article and approved the submitted version.

FUNDING

This work was supported by the Swedish Society of Medicine [Grant No. SLS-682741], King Gustaf V's 80-year foundation [FAI-2017-0420], the Swedish Rheumatism Association [R-754141], and the Östergötland County Council [LIO-700501].

ACKNOWLEDGMENTS

We thank the TIRx patients and control subjects for their participation in this study.

SUPPLEMENTARY MATERIAL

The Supplementary Material for this article can be found online at: https://www.frontiersin.org/articles/10.3389/fmed.2021.653994/full#supplementary-material

REFERENCES

1. Rantapaa-Dahlqvist S, de Jong BA, Berglin E, Hallmans G, Wadell G, Stenlund H, et al. Antibodies against cyclic citrullinated peptide and iga rheumatoid factor predict the development of rheumatoid arthritis. *Arthritis Rheum*. (2003) 48:2741–9. doi: 10.1002/art.11223
2. Verheul MK, Bohringer S, van Delft MAM, Jones JD, Rigby WFC, Gan RW, et al. Triple positivity for anti-citrullinated protein autoantibodies, rheumatoid factor, and anti-carbamylated protein antibodies conferring high specificity for rheumatoid arthritis: implications for very early identification of at-risk individuals. *Arthritis Rheumatol*. (2018) 70:1721–31. doi: 10.1002/art.40562
3. Arnett FC, Edworthy SM, Bloch DA, McShane DJ, Fries JF, Cooper NS, et al. The american rheumatism association 1987 revised criteria for the classification of rheumatoid arthritis. *Arthritis Rheum*. (1988) 31:315–24. doi: 10.1002/art.1780310302
4. Aletaha D, Neogi T, Silman AJ, Funovits J, Felson DT, Bingham CO III, et al. 2010 rheumatoid arthritis classification criteria: an American College of Rheumatology/European League against rheumatism collaborative initiative. *Arthritis Rheum*. (2010) 62:2569–81. doi: 10.1002/art.27584
5. Smolen JS, Landewe R, Bijlsma J, Burmester G, Chatzidionysiou K, Dougados M, et al. Eular recommendations for the management of rheumatoid arthritis with synthetic and biological disease-modifying antirheumatic drugs: 2016 update. *Ann Rheum Dis*. (2017) 76:960–77. doi: 10.1136/annrheumdis-2016-210715
6. Avouac J, Gossec L, Dougados M. Diagnostic and predictive value of anti-cyclic citrullinated protein antibodies in rheumatoid arthritis: a systematic literature review. *Ann Rheum Dis*. (2006) 65:845–51. doi: 10.1136/ard.2006.051391
7. Brown AK, Conaghan PG, Karim Z, Quinn MA, Ikeda K, Peterfy CG, et al. An explanation for the apparent dissociation between clinical remission and continued structural deterioration in rheumatoid arthritis. *Arthritis Rheum*. (2008) 58:2958–67. doi: 10.1002/art.23945
8. Wakefield RJ, Balint PV, Szkudlarek M, Filippucci E, Backhaus M, D'Agostino MA, et al. Musculoskeletal ultrasound including definitions for ultrasonographic pathology. *J Rheumatol*. (2005) 32:2485–7.
9. Porta F, Radunovic G, Vlad V, Micu MC, Nestorova R, Petranova T, et al. The role of doppler ultrasound in rheumatic diseases. *Rheumatology*. (2012) 51:976–82. doi: 10.1093/rheumatology/ker433
10. Backhaus M, Burmester GR, Sandrock D, Loreck D, Hess D, Scholz A, et al. Prospective two year follow up study comparing novel and conventional imaging procedures in patients with arthritic finger joints. *Ann Rheum Dis*. (2002) 61:895–904. doi: 10.1136/ard.61.10.895
11. Freeston JE, Wakefield RJ, Conaghan PG, Hensor EM, Stewart SP, Emery P. A diagnostic algorithm for persistence of very early inflammatory arthritis: the utility of power doppler ultrasound when added to conventional assessment tools. *Ann Rheum Dis*. (2010) 69:417–9. doi: 10.1136/ard.2008.106658
12. van de Stadt LA, Bos WH, Meursinge Reynders M, Wieringa H, Turkstra F, van der Laken CJ, et al. The value of ultrasonography in predicting arthritis in auto-antibody positive arthralgia patients: a prospective cohort study. *Arthritis Res Ther*. (2010) 12:R98. doi: 10.1186/ar3028
13. van den Berg R, Ohrndorf S, Kortekaas MC, van der Helm-van Mil AHM. What is the value of musculoskeletal ultrasound in patients presenting with arthralgia to predict inflammatory arthritis development? A systematic literature review. *Arthritis Res Ther*. (2018) 20:228. doi: 10.1186/s13075-018-1715-8
14. Nam JL, Hensor EM, Hunt L, Conaghan PG, Wakefield RJ, Emery P. Ultrasound findings predict progression to inflammatory arthritis in anti-ccp antibody-positive patients without clinical synovitis. *Ann Rheum Dis*. (2016) 75:2060–7. doi: 10.1136/annrheumdis-2015-208235
15. Pratt AG, Lorenzi AR, Wilson G, Platt PN, Isaacs JD. Predicting persistent inflammatory arthritis amongst early arthritis clinic patients in the uk: Is musculoskeletal ultrasound required? *Arthritis Res Ther*. (2013) 15:R118. doi: 10.1186/ar4298
16. Witt M, Mueller F, Nigg A, Reindl C, Leipe J, Proft F, et al. Relevance of grade 1 gray-scale ultrasound findings in wrists and small joints to the assessment of subclinical synovitis in rheumatoid arthritis. *Arthritis Rheum*. (2013) 65:1694–701. doi: 10.1002/art.37954
17. Camerer M, Ehrenstein B, Hoffstetter P, Fleck M, Hartung W. High-resolution ultrasound of the midfoot: sonography is more sensitive than conventional radiography in detection of osteophytes and erosions in inflammatory and non-inflammatory joint disease. *Clin Rheumatol*. (2017) 36:2145–9. doi: 10.1007/s10067-017-3658-x
18. Wakefield RJ, Gibbon WW, Conaghan PG, O'Connor P, McGonagle D, Pease C, et al. The value of sonography in the detection of bone erosions in patients with rheumatoid arthritis: a comparison with conventional radiography. *Arthritis Rheum*. (2000) 43:2762–70. doi: 10.1002/1529-0131(200012)43:12<2762::AID-ANR16>3.0.CO;2-#

19. Prevoo ML, van 't Hof MA, Kuper HH, van Leeuwen MA, van de Putte LB, van Riel PL. Modified disease activity scores that include twenty-eight-joint counts. Development and validation in a prospective longitudinal study of patients with rheumatoid arthritis. *Arthritis Rheum*. (1995) 38:44–8. doi: 10.1002/art.1780380107
20. Szkudlarek M, Court-Payen M, Jacobsen S, Klarlund M, Thomsen HS, Ostergaard M. Interobserver agreement in ultrasonography of the finger and toe joints in rheumatoid arthritis. *Arthritis Rheum*. (2003) 48:955–62. doi: 10.1002/art.10877
21. Horton SC, Tan AL, Wakefield RJ, Freeston JE, Buch MH, Emery P. Ultrasound-detectable grey scale synovitis predicts future fulfilment of the 2010 acr/eular ra classification criteria in patients with new-onset undifferentiated arthritis. *RMD Open*. (2017) 3:e000394. doi: 10.1136/rmdopen-2016-000394
22. van der Ven M, van der Veer-Meerkerk M, Ten Cate DF, Rasappu N, Kok MR, Csakvari D, et al. Absence of ultrasound inflammation in patients presenting with arthralgia rules out the development of arthritis. *Arthritis Res Ther*. (2017) 19:202. doi: 10.1186/s13075-017-1405-y
23. Terslev L, Naredo E, Aegerter P, Wakefield RJ, Backhaus M, Balint P, et al. Scoring ultrasound synovitis in rheumatoid arthritis: a eular-omeract ultrasound taskforce-part 2: reliability and application to multiple joints of a standardised consensus-based scoring system. *RMD Open*. (2017) 3:e000427. doi: 10.1136/rmdopen-2016-000427
24. Nakagomi D, Ikeda K, Okubo A, Iwamoto T, Sanayama Y, Takahashi K, et al. Ultrasound can improve the accuracy of the 2010 American College of Rheumatology/European league against rheumatism classification criteria for rheumatoid arthritis to predict the requirement for methotrexate treatment. *Arthritis Rheum*. (2013) 65:890–8. doi: 10.1002/art.37848
25. Hammer HB, Kvien TK. Ultrasonography shows significant improvement in wrist and ankle tenosynovitis in rheumatoid arthritis patients treated with adalimumab. *Scand J Rheumatol*. (2011) 40:178–82. doi: 10.3109/03009742.2010.517549
26. van Beers-Tas MH, Blanken AB, Nielen MMJ, Turkstra F, van der Laken CJ, Meursinge Reynders M, et al. The value of joint ultrasonography in predicting arthritis in seropositive patients with arthralgia: a prospective cohort study. *Arthritis Res Ther*. (2018) 20:279. doi: 10.1186/s13075-018-1767-9
27. Padovano I, Costantino F, Breban M, D'Agostino MA. Prevalence of ultrasound synovial inflammatory findings in healthy subjects. *Ann Rheum Dis*. (2016) 75:1819–23. doi: 10.1136/annrheumdis-2015-208103
28. Trickey JSI, Bortoluzzi A, Iagnocco A, Pineda C, Sifuentes-Cantú C, Ciurtin C, et al. Very low prevalence of ultrasound determined tendon abnormalities in healthy subjects throughout the age range: An outcome measures in rheumatology (omeract) ultrasound minimal disease study. *Arthritis Rheumatol*. (2019) 78:603. doi: 10.1136/annrheumdis-2019-eular.4746
29. Harre U, Georgess D, Bang H, Bozec A, Axmann R, Ossipova E, et al. Induction of osteoclastogenesis and bone loss by human autoantibodies against citrullinated vimentin. *J Clin Investigat*. (2012) 122:1791–802. doi: 10.1172/JCI60975
30. Harre U, Lang SC, Pfeifle R, Rombouts Y, Fruhbeisser S, Amara K, et al. Glycosylation of immunoglobulin g determines osteoclast differentiation and bone loss. *Nat Commun*. (2015) 6:6651. doi: 10.1038/ncomms7651
31. Kleyer A, Finzel S, Rech J, Manger B, Krieter M, Faustini F, et al. Bone loss before the clinical onset of rheumatoid arthritis in subjects with anticitrullinated protein antibodies. *Ann Rheum Dis*. (2014) 73:854–60. doi: 10.1136/annrheumdis-2012-202958

Conflict of Interest: The authors declare that the research was conducted in the absence of any commercial or financial relationships that could be construed as a potential conflict of interest.

frontiers in Medicine

REVIEW
published: 22 April 2021
doi: 10.3389/fmed.2021.658538

Axial Spondyloarthritis: Mimics and Pitfalls of Imaging Assessment

António Proença Caetano[1†], *Vasco V. Mascarenhas*[2,3†] *and Pedro M. Machado*[4,5,6*†]

[1] *Radiology Department, Hospital de Curry Cabral, Centro Hospitalar Universitário Lisboa Central, Lisbon, Portugal,* [2] *Musculoskeletal Imaging Unit, Grupo Luz Saúde, Radiology Department, Imaging Center, Hospital da Luz, Lisbon, Portugal,* [3] *EpiDoC Unit, Chronic Diseases Research Centre, NOVA Medical School, Lisbon, Portugal,* [4] *Centre for Rheumatology & Department of Neuromuscular Diseases, University College London, London, United Kingdom,* [5] *National Institute for Health Research (NIHR) Biomedical Research Centre, University College London Hospitals National Health Service Foundation Trust, London, United Kingdom,* [6] *Department of Rheumatology, London North West University Healthcare National Health Service Trust, London, United Kingdom*

Axial spondyloarthritis (axSpA) is a chronic inflammatory disorder that predominantly involves the axial skeleton. Imaging findings of axSpA can be divided into active changes, which include bone marrow edema, synovitis, enthesitis, capsulitis, and intra-articular effusion, and structural changes, which include erosions, sclerosis, bone fatty infiltration, fat deposition in an erosion cavity, and bone bridging or ankylosis. The ability to distinguish between imaging lesions suggestive of axSpA and artifacts or lesions suggestive of other disorders is critical for the accurate diagnosis of axSpA. Diagnosis may be challenging, particularly in early-stage disease and magnetic resonance imaging (MRI) plays a key role in the detection of subtle or inflammatory changes. MRI also allows the detection of structural changes in the subchondral bone marrow that are not visible on conventional radiography and is of prognostic and monitoring value. However, bone structural changes are more accurately depicted using computed tomography. Conventional radiography, on the other hand, has limitations, but it is easily accessible and may provide insight on gross changes as well as rule out other pathological features of the axial skeleton. This review outlines the imaging evaluation of axSpA with a focus on imaging mimics and potential pitfalls when assessing the axial skeleton.

Keywords: axial spondyloarthritis, magnetic resonance imaging, radiography, computed tomography, differential diagnosis, pitfall, normal variant, mimic

OPEN ACCESS

Edited by:
Xenofon Baraliakos, Rheumazentrum Ruhrgebiet, Germany

Reviewed by:
Juan Carlos Nieto González, Gregorio Marañón Hospital, Spain
Mauro Waldemar Keiserman, Hospital São Lucas da PUCRS, Brazil

***Correspondence:**
Pedro M. Machado
p.machado@ucl.ac.uk
orcid.org/0000-0002-8411-7972

[†]These authors have contributed equally to this work

Specialty section:
This article was submitted to Rheumatology, a section of the journal Frontiers in Medicine

Received: *26 January 2021*
Accepted: *11 March 2021*
Published: *22 April 2021*

Citation:
Caetano AP, Mascarenhas VV and Machado PM (2021) Axial Spondyloarthritis: Mimics and Pitfalls of Imaging Assessment. Front. Med. 8:658538. doi: 10.3389/fmed.2021.658538

INTRODUCTION

Axial spondyloarthritis (axSpA) is an umbrella term encompassing a group of chronic immune-mediated inflammatory diseases of the axial skeleton. This group includes patients with radiographic axSpA, with established sacroiliitis on radiographs, and a further subgroup called non-radiographic axSpA, who typically have evidence of sacroiliitis on magnetic resonance imaging (MRI) in the absence of definite radiographic changes.

Historically, the diagnosis of axSpA has often been delayed since radiographic abnormalities may take years to develop. Computed tomography (CT) allows for detection of smaller structural lesions in patients with chronic sacroiliitis that would otherwise be invisible on conventional radiography, thus aiding in the diagnostic work up of axSpA. In recent years, the introduction of MRI into clinical practice has facilitated earlier diagnosis of axSpA, and therefore earlier initiation of appropriate treatment. The Assessment of Spondyloarthritis International Society (ASAS) MRI working group has recently generated a consensus update on standardized definitions for MRI

lesions in the sacroiliac joint (SIJ) of patients with axSpA (1). Multi-reader validation performed by the working group demonstrated substantial reliability for the most frequently detected lesions and comparable reliability between active and structural lesions. A similar exercise has been conducted for spine lesions and recently published in abstract format (2). The new consensus definitions for MRI lesions in the spine will replace a previous consensus manuscript by the same group (3).

Importantly, the full range and combination of active and structural lesions of the SIJ and spine should be taken into account when deciding if the MRI scan is suggestive of axSpA or not (i.e., contextual interpretation of active and structural lesions is key to enhancing diagnostic utility of MRI in patients with suspected axSpA), as imaging cannot be viewed in isolation and needs to be interpreted in the light of clinical presentation and results of laboratory investigations (4, 5).

MRI evaluation of the SIJ can be quite challenging even for experienced radiologists, due to several pitfalls. Being familiar with the main imaging findings and terminology of axSpA (**Table 1**) as well as knowing the topographic distribution of common and uncommon conditions involving the SIJ is key to establishing a confident diagnosis (**Figures 1A,B**).

In this article, we will review common and uncommon pitfalls, congenital disorders, normal variants and pathological conditions that may mimic spondyloarthritis affecting the axial skeleton.

TABLE 1 | Imaging findings of active and chronic changes of the sacroiliac joint and spine in axial spondyloarthritis.

	Sacroiliac joint	Spine
Active changes	• Bone marrow edema/osteitis • Inflammation at the site of erosion • Synovitis and synovial proliferation • Intra-articular fluid collection • Capsulitis • Enthesitis	• Spondylitis (anterior or posterior corner inflammatory lesions) and enthesitis* • Asseptic spondylodiscitis (Andersson lesion) • Zygoaphophyseal/facet joint arthritis • Costovertebral and costo-transverse joint arthritis • Inflammation of other vertebral elements (e.g., pedicles and spinous processes) • Inflammation of spinal ligaments
Chronic changes	• Cortical bone erosions and pseudo-widening of joint space • Joint space narrowing • Subchondral sclerosis • Fat depositions/collections (including fat deposition in an erosion cavity, also known as "backfill") • Ankylosis/bone bridging • Juxta-articular osteoporosis	• Syndesmophytes • Ankylosis/bone bridging • Ligament calcifications • Erosions • Sclerotic changes • Fat deposition on vertebral corners and other previously inflamed bone marrow • Osteopenia

**The terms "Romanus spondylitis" and "shiny corners" have been used in the context of MRI assessment but should be avoided as they were initially described in plain radiographs: "Romanus spondylitis" appears as irregularity and erosion involving the anterior and posterior corners/edges of the vertebral endplates, while "shiny corners" represent reactive sclerosis secondary to inflammatory process.*

ANATOMY OF THE SACROILIAC JOINTS AND THE SPINE

The SIJ is the largest joint of the axial skeleton and consists of an amphiarthrosis, exhibits restricted mobility and is separated into a ligamentous (posterior) and synovial (anterior) component. The cartilage covering the synovial segment is thicker on the sacral side and, thus, less prone to lesions (6).

The SIJ is lined by a capsule. Several ligaments contribute to its stability and may be affected in axSpA, namely the anterior and posterior sacroiliac ligaments and interosseus ligament connecting the tuberosities of the sacrum and ilium deeply in the ligamentous portion. The intervertebral disc is also an amphiarthrosis and is comprised of an inner core—the *nucleus pulposus*—and an outer fibrous ring—the *annulus fibrosus*. There is also cartilage lining on the superior and inferior vertebral plates that protects the subchondral bone at this level. The inner core is generally spared in axSpA, but the *annulus fibrosus* attaches to the periphery of the vertebral plates where there is no cartilage protection, and interweaves with the anterior and posterior longitudinal ligaments of the spine, working as an enthesis.

Besides the *annulus fibrosus*, several ligaments stabilizing the spine are prone to inflammation at their insertion point, namely the anterior and posterior longitudinal, supraspinous, interspinous, intertransverse ligaments, and *ligamentum flavum*.

NORMAL VARIANTS AND PITFALLS

In this section we will describe potential anatomical variants and pitfalls of the SIJ and spine that may mimic axSpA findings (**Table 2**).

Coil Effect

Technical artifact responsible for artificial hyperintensity of structures near the receiver coils. These structures may be mistaken for bone marrow or soft tissue edema. Such findings, however, can be distinguished from true inflammatory changes due to their topographic distribution, which is predominantly peri-articular in the latter scenario.

Inadequate fat suppression is higher in patients with higher body mass index (BMI). Radial k-space sampling, an imaging reconstruction technique utilized in MRI data acquisition that is relatively insensitive to motion artifacts, seems to have a positive impact on image quality in such patients (7). Another solution might be to change saturation techniques, from a spectral pre-saturation of fat signal to a short tau inversion recovery (STIR) sequence, which homogeneously suppresses fat, with the caveat of reducing overall signal.

The type of coil also seems to have a significant impact on image quality, more so when combined with the correct sequence in reducing artifacts. This combination yields the best inter-observer agreement for bone marrow edema (BME) detection and lowest number of doubtful BME zones (8).

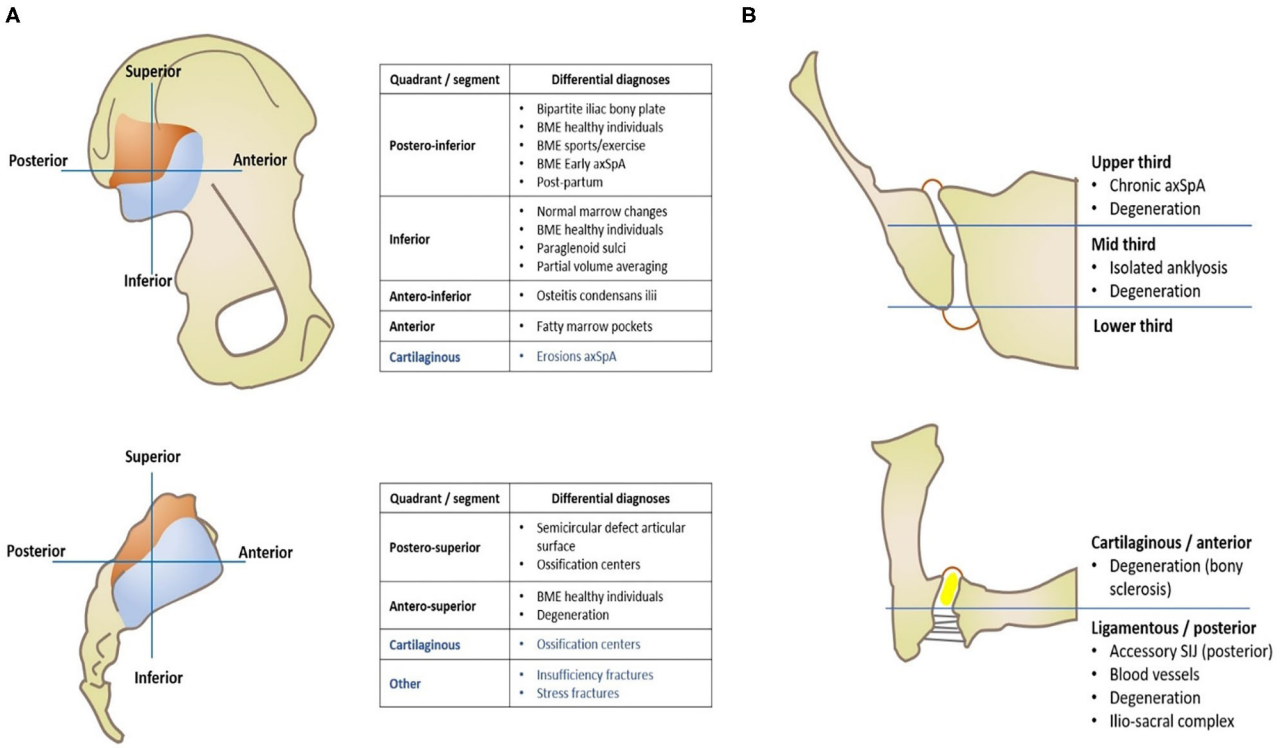

FIGURE 1 | Imaging of the sacroiliac joint—Topographic distribution of main anatomical variants and pathological conditions that mimic axSpA, separated by quadrants of each articular surface **(A)** and orthogonal planes **(B)**, namely coronal oblique (right upper image) and axial oblique (right lower image).

Phase-Encoded Motion Artifacts

Motion artifact may occur due to vessels, intestinal motion and patient motion. This artifact may cause blurring or a hyperintense image superimposed at or adjacent to the SIJ and mimic BME. Cross-reference between two perpendicular planes may allow avoidance of overcalling lesions (8, 9). Cerebrospinal fluid (CSF) and blood motion artifacts are also common in spine MR imaging (10).

Again, radial k-space sampling offers a higher signal-to-noise ratio and contributes to reduction in motion-related blurring. Application of motion-resistant sequences is also recommended (7). Other techniques may be employed, such as increasing the number of excitations, changing the phase-encoding axis (along the direction of CSF flow) or applying pre-saturation pulses outside the region of interest (11). Repetitive motion from breathing or cardiac motion may be reduced with gating techniques that perform data acquisition at specific intervals.

Blood Vessels

Blood vessels coursing close to the SIJ and spine along the acquisition plane may simulate bone marrow or soft tissue edema, synovitis or joint fluid on fluid-sensitive sequences. They present as linear hyperintensities along the acquisition plane and may ramify with other vessels on adjacent slices. CSF motion may also be an issue in spine imaging.

Intense vascularization may be seen at the transition between cartilaginous and ligamentous portion of the joint, at the ligamentous portion and adjacent to certain anatomical variants such as the iliosacral complex and the semi-circular sacral defect, which are described in more detail below (12). Vessels can also run along bones.

Normal Marrow Changes

Red marrow replacement occurs in a centrifugal fashion in individual bones and in a centripetal fashion in the skeleton. The extremities are primarily affected by this physiological aging phenomenon and, by the middle of the third decade (13), most of the bone marrow in long bones has an overall fatty marrow. Individually, conversion into fatty marrow starts in the diaphysis of long bones and progresses to the metaphysis, ultimately converting the distal epiphysis and, lastly, the proximal epiphysis. In the axial skeleton, the pattern of reconversion is less predictable and several patterns have been described in the spine (14). In the pelvis, small pockets of yellow marrow arise in the third decade in the acetabulum and anterior ilium. In the sacrum of male patients there is higher fat content in the lateral masses compared to females (15) and localized aggregates of fat marrow in the lumbar spines and lateral sacral ala are considered normal variants (16).

General Population and People With Chronic Non-specific Back Pain

Weber et al. showed that 25% of healthy individuals have signs suggestive of sacroiliitis on MRI (17). Similarly, Arnbak et al.

TABLE 2 | Congenital disorders and normal variants of the sacroiliac joints and spine that mimic axial spondyloarthritis.

Condition	Type	Characteristic features
Blood vessels	–	Location–ligamentous portion of the SIJ, adjacent, adjacent to anatomical variants, lower ilium (partial volume)
Normal marrow changes	–	Location–lower iliac bone Low SPARCC scores
Healthy individuals	–	Location–anterior upper sacrum, posterior lower ilium
Sports/exercise related	–	Topographic distribution overlaps with axSpA
Port-partum	–	Extent and distribution indistinguishable from axSpA Structural changes are rare
Schmorl nodes	–	Location–lower thoracic and upper lumbar vertebrae, along the *nucleus pulposus* axis
Block vertebra	Congenital	Location–cervical segments Other associated conditions
	Acquired	Other findings–post-surgical, degenerative disc disease, advanced axSpA
SIJ normal variants	Iliosacral complex	Location–Ilium opposite posterolateral sacrum, extra-articular, ligamentous portion Other–women
	Paraglenoid sulci	Location–inferior ilium Other–women
	Ossification centers sacral wings	Location–postero-superior border, cartilaginous portion Other–triangular shape
	Bipartite iliac bony plate	Location–postero-inferior segment Other–unilateral, women
	Accessory iliac joints	Location–between iliac and sacral surfaces at posterior joint
	Semicircular defect articular surface	Location–ligamentous portion, postero-superior, focal sacral depression Other–women, bilateral
	Isolated ankylosis	Location–mid-third of the SIJ
Transitional vertebrae/Bertolotti syndrome	–	Variable presentation (Castellvi classification) Types II and IV correlate with symptoms and disc herniation
Spina bifida occulta	–	Location–5th lumbar segment Other–correlation with spondylolysis
Intra-osseous pneumatocyst	–	Location–iliac bone adjacent to SIJ, lumbar or cervical spine
Tarlov cysts	–	Location–sacrum Other–bilateral, women, 40 years-old

found that, in 1,020 unselected individuals, 21% had sacroiliitis on MRI according to ASAS criteria.

Other authors (18) suggested that one fourth of asymptomatic individuals and more than half of women with post-partum back pain without axSpA had MRI positive sacroiliitis according to ASAS criteria. This study also showed that frequent runners have similar findings compared to asymptomatic individuals and that scoring high on a specific scoring system used for axSpA activity (Spondyloarthritis Research Consortium of Canada Scoring System for Sacroiliitis, SPARCC) is rare in healthy individuals and runners. Furthermore, deep lesions are specific for axSpA-related sacroiliitis and BME lesions in healthy individuals are preferentially located in the lower iliac bone.

Indeed, others studies have documented the presence of BME in healthy individuals without any symptoms of low back pain, which does not change in the setting of mechanical stresses or physical exercise (19) (**Figures 2A,B**). Recently, however, a large population study by Baraliakos et al. (20) confirmed a high prevalence of inflammatory and fatty changes in the SIJ and spine, which increases in frequency with age, suggesting a mechanical factor to their development.

Sports/Exercise Related BME

Evaluation of MRI lesions in athletes poses a significant challenge when attempting to discriminate healthy individuals from early axSpA. In fact, 30–35% of recreational runners and 41% of elite hockey skaters have shown ASAS criteria for axSpA when evaluated for sacroiliitis (17). Partial volume effect of vascular structures, mechanically triggered BME due to axial strain and normal anatomical variants are thought to be the main reasons for such findings. Applying a complementary semi-axial plane for evaluation seems to significantly reduce ASAS positivity to 20 and 18%, respectively for recreational runners and elite hockey skaters (8).

The two most common portions of the joint affected by BME are the anterior upper sacrum and the posterior lower ilium, the latter associated with partial volume effect of vessels and deep iliac ligament insertion. Unfortunately, it is well-recognized that the early incipient findings of inflammatory changes in axSpA patients show a topographic overlap with BME associated with constitutional features on the dorso-caudal portion of the SIJ, at the posterior lower ilium.

Low-grade BME lesions may indeed have several potential triggers such as mechanical overload or stress, anatomical

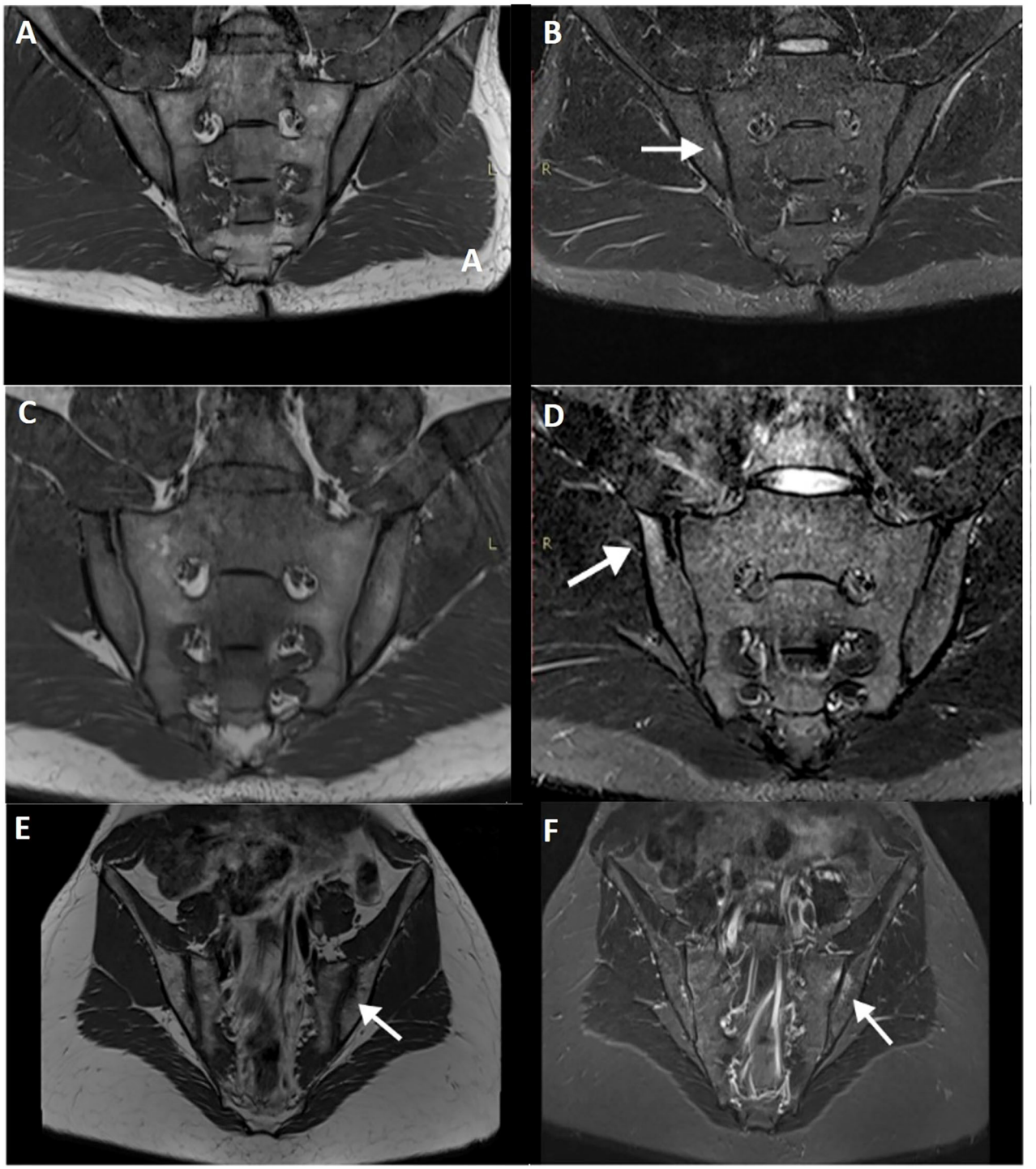

FIGURE 2 | T1WI **(A)** and STIR image **(B)** of a military subject showing a small, peri-articular, area of bone edema (arrow) on the iliac side of the right sacroiliac joint. T1WI **(C,E)** and STIR **(D,F)** images of a post-partum female with bilateral foci of bone edema (arrows) adjacent to the sacroiliac joint.

variations, heavy load work, overweight and post-partum. Discriminative factors that may indicate possible or probable axSpA have not been determined—BME extension alone has not proven to be a relevant criterion (9), but evaluation of extent and topographical pattern might be able to reduce false-positive assessments of ASAS MRI positive sacroiliitis. Assessment of other structural features and active lesions may improve specificity (21, 22).

Post-partum

Low back pain is common during pregnancy and shortly after birth, typically resolving 6 weeks post-partum. Some patients, however, experience long-standing low back pain more than 6 months after childbirth (23).

Causes for post-partum symptoms are multifactorial and involve mechanical stress and hormonal changes, child and birth characteristics (24). Post-partum SIJ infection is an important differential diagnosis as it accounts for 15% of septic sacroiliitis events; auto-inflammatory conditions may also manifest during pregnancy or after childbirth.

Agten et al. (25) compared the SIJ of post-partum women and women with known axSpA and found no distinguishable features based on extent and distribution, making it difficult to avoid overcalling axSpA in such patients (**Figures 2C–F**). Presence of structural changes, however, was more frequent in the axSpA group and only rarely found in the post-partum group. Furthermore, pain referral and pain intensity were not correlated with BME in the post-partum group. Importantly, puerperal diastasis of the pubic symphysis and SIJ is physiological to some degree and only in rare situations is associated with complications (26).

Nonetheless, Winter et al. showed positive findings on MRI of post-partum women with back pain, which was consistent with previous data that reported 60% of such patients having SIJ BME lesions on MRI (18, 27).

Schmorl Nodes

Schmorl nodes correspond to herniation of nucleus material through the endplate of the vertebral bodies into the subchondral bone (28).

Schmorl nodes are usually marginated by a well-defined sclerotic border which may be irregular and are more prevalent in the lower thoracic and upper lumbar segments. The etiology of Schmorl nodes is multifactorial, involving trauma and congenital causes. There is also an association with smoking habits, vertebral body length, and age (28). Patients with Schmorl nodes may be asymptomatic or present with low back pain, and an association with degenerative spine disease and disc degeneration has been established (29). If Schmorl nodes become symptomatic, MRI may demonstrate inflammation and edema in the bone marrow surrounding the Schmorl node. Vertebroplasty has been tried out and proven to be effective and safe when symptoms do not resolve with medical or physical therapy (30, 31).

Acute Schmorl nodes may mimic other inflammatory conditions affecting the spine. Imaging features are of a concentric ring-type edema and involvement of the adjacent end-plate to the herniated node, without diffuse signal abnormalities (32).

Block Vertebrae

Block vertebrae may be congenital or acquired. Congenital blocked vertebra is generally found in the cervical spine and associated with Klippel-Feil syndrome (short neck, low hair line, and neck movement restriction). Other abnormalities associated with congenital block vertebra include syringomyelia, diastematomyelia, or tethered cord (33).

Acquired vertebral fusion may be a desired surgical outcome in cases of advanced degenerative disc disease or cases of joint instability (34, 35). Also, late-onset ankylosing spondylitis with extensive calcification may lead to bamboo spine due to dystrophic and ligament calcifications so extensive that they merge both endplates of the disc joint. Interbody fusion requires disc removal through a posterior or anterior approach, insertion of a bone graft and/or fusion hardware. The purpose is to achieve an arthrodesis along the disc space. Complications include pseudarthrosis, when bone bridging does not develop or is insufficient. Studies to evaluate post-operative fusion include CT, MRI and bone scintigraphy.

SIJ Anatomical Variants

Synovial recesses, bony and cartilage clefts that may mimic bone erosion, intense vascularization on the ligamentous portion that enhances avidly and fat infiltration of the sacral bone marrow without pathological significance may be evident on SIJ imaging and are addressed in other sections of this article.

In this section we briefly describe the seven anatomical variants of the SIJ that have been documented to date. The morphology of the sacral and iliac surfaces is well-depicted on CT. The most frequent variants are accessory SIJ and iliosacral complex (**Figures 3A,B**). These variants are sometimes associated with edematous or structural changes suspected to be mechanical in nature. Positive association between anatomical variations and degenerative changes is somewhat controversial (36, 37). To the best of the authors' knowledge, only one study has analyzed MRI changes in morphological variants of the SIJ (38).

Accessory Sacroiliac Joints

The most common variant is an accessory sacroiliac joint (3.6–50%), which is more common in females and has a positive association with increased BMI (38, 39). Accessory SIJ is detected between the iliac and sacral articular surfaces in the posterior aspect of the joint.

It is however not certain if the accessory SIJ are congenital or acquired. In fact, degenerative ankylosis and overall structural changes may masquerade accessory SIJ.

This variation is best depicted on axial slices and is located at the level of the first or second sacral foramen. Signal intensity changes are depicted in a proportion of patients, mostly related to sclerotic or fatty changes, but rarely edematous.

Iliosacral Complex

The iliosacral complex corresponds to a marked prominence of the ilium opposite a concave depression of the posterolateral sacrum (40). An iliosacral complex is present in 4% (5.8–11.7%) of individuals and is the second most common anatomical variant and seen bilaterally with slightly increased frequency in women (38). The iliosacral complex is mostly found at the level of the S1 foramen and corresponds to a marked prominence of the ilium projecting to a concavity of the lateral sacrum, in an extra-articular portion of the SIJ (39). This variant is best depicted on coronal images and mainly located between the first and second sacral foramen. Half of cases show prominent vascular structures adjacent to the complex, which may mimic enthesitis.

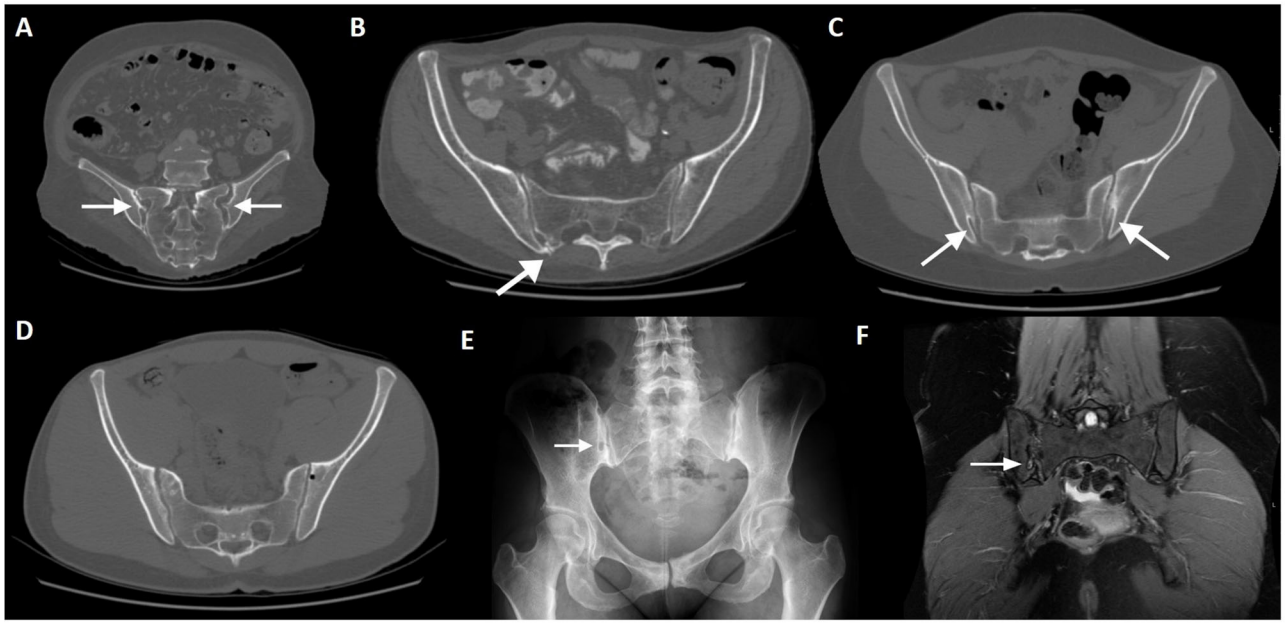

FIGURE 3 | Normal variants and incidental findings of the sacroiliac joint (arrows). CT reconstructions with oblique orientation depict bilateral iliosacral complexes **(A)**, the most common sacroiliac joint variant; right accessory sacroiliac joint **(B)**; bilateral bipartite iliac bony plate **(C)**; left iliac bone pneumatocyst **(D)**. A patient with an incidental finding on the right sacroiliac joint seen on pelvic radiography performed MRI, which revealed an iliac bone cleft filled with fluid **(E,F)**. Note the sclerosis of the symphysis pubis **(E)**, compatible with *osteitis pubis*.

The interpretation of the SIJ and, specifically, the joint space width, should take into account these variations and the presence of significant extra-articular portions of the ilium and sacrum at different levels. The sacroiliac ligaments insert in such depressions and cavities at the posterior-inferior ilium.

SIJ degeneration is more prevalent in patients with iliosacral complex compared to other morphological variations (36).

Other Anatomical Variants

The **ossification centers** of the sacral wings may be persistent in adulthood. They are located at the posterior-superior border of the SIJ, involve the cartilaginous portion of the joint and have a triangular shape.

Paraglenoid sulci are small bilateral grooves located in the inferior ilium lateral to the SIJ, more prevalent in women.

Visible at the level of the S2 foramen, **semicircular defects** in the articular surface are represented by an indentation of the ilium toward a mild depression of the sacrum (40). This variant has been described elsewhere as a round defect of the sacrum with or without an opposing iliac defect in the axial plane. It involves the posterior-superior aspect of the ligamentous portion of the joint, is more common in females and mostly bilateral (38).

Bipartite iliac bony plate is more frequently unilateral and seen in women, at the posterior-inferior portion of the joint. Crescent-like iliac bony plates have also been described and are seen in 2–5% of patients (36, 39) (**Figure 3C**).

An **isolated synostosis** has been rarely depicted in two previous studies, in the mid third of the SIJ at the level of the first sacral foramen (38, 41). Absence of structural or inflammatory changes in the remaining SIJ and contralateral side should raise suspicion for an anatomical variation.

Lumbosacral Transitional Vertebrae and Bertolotti Syndrome

Lumbosacral transitional vertebra (LSTV) refers to a spectrum of congenital anomalies of the last lumbar and first sacral vertebrae, where an elongated transverse process of the lumbar vertebra articulates or fuses with the first sacral segment (42) (**Figure 4**). The overall incidence ranges from 4 to 35.6% (43, 44).

Partial articulation and fusion between L5 and S1 lead to limited motion at the lumbosacral joint. This raises mechanical stress to the level above and results in accelerated degeneration of the L4–L5 joint.

The Castellvi classification of LSTV divides in four types (45): (Ia) unilateral, (Ib) dysplastic transverse process with a height >19 mm, (II) incomplete unilateral (a) or bilateral (b) lumbarization/sacralization with engorged transverse process articulating with the sacrum, (III) unilateral (a) or bilateral (b) complete osseous fusion of the engorged transverse processes to the sacrum, (IV) unilateral type II transition with contralateral type III. The most common types in patients with low back pain are IV, IIIb, and II (43). Another study also concluded that LSTV types II and IV positively correlate with prevalence and severity of low back pain (46).

Association between LSVT and low back pain has been termed Bertolotti syndrome, in honor of Dr. Bertolotti who first

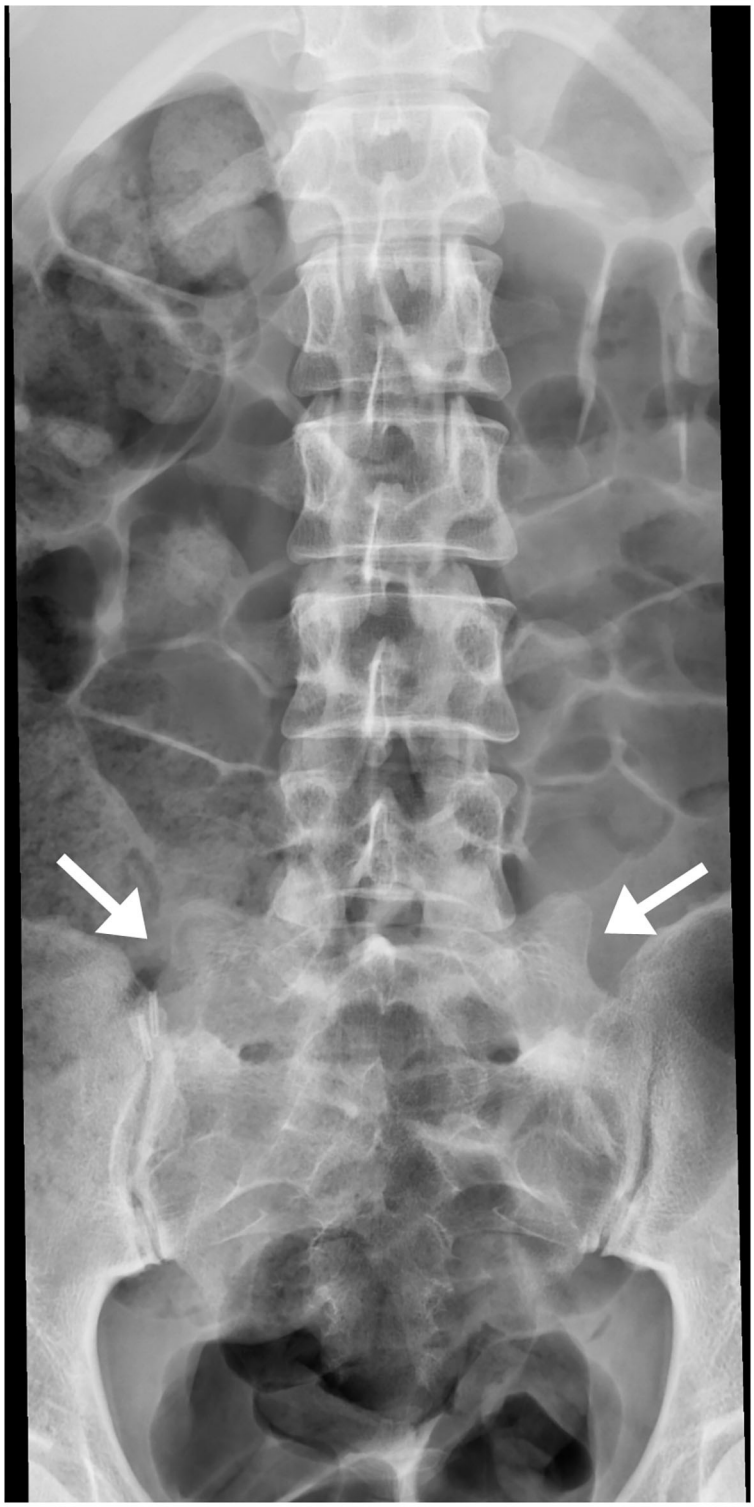

FIGURE 4 | Bilateral transitional vertebra (sacralization of L5), with neo-articulation of both hypertrophic transverse apophyses with the sacrum (arrows).

described the morphological abnormalities, and is an important etiology of low back pain in young patients. LSVT may cause radicular changes and MRI is the examination of choice to evaluate the intervertebral disc as well as the neural foramina (45, 47). An association between LSTV and disc herniation has also been found (48–51).

Spina bifida occulta

Spina bifida occulta (SBO) and LSVT are the most common congenital lumbosacral deformities and involve the 5th lumbar segment (52). SBO is a result of failed fusion of the posterior vertebral elements without affecting the spinal cord or meninges. Its prevalence is estimated between 0.6 and 25% (49).

While SBO occurring in the most frequent segment (L5) does not seem to have any correlation with disc herniation, a previous study has reported an association between SBO of the S1 segment and posterior disc herniation (49). In both pediatric and adult patients, there is a positive correlation of SBO with spondylolysis (53). SBO at other levels is rare (54).

Intra-Osseous Pneumatocyst and Synovial Cyst

Simple bone pneumatization cysts of the pelvic bones are a common, but poorly understood, innocuous findings on CT (**Figure 3D**). There have been occasional reports in the literature (55–57) and imaging features include well-circumscribed air-filled round defects of bone with a thin sclerotic rim, usually found adjacent to the SIJ on the iliac bone. They may be an unusual cause of pain that is indistinguishable from other causes of low back pain. In the spine, there are also scarce publications indicating the presence of vertebral pneumatocysts, especially in the lumbar or cervical spine (58).

Synovial cysts, on the other hand, are fluid-filled para-articular lesions that may, but not always, communicate with the joint. These lesions have been described in the SIJ and in the spine, although they are exceedingly rare near the SIJ joint (59, 60) (**Figures 3E,F**). In the spine, they are most commonly originated from the zygapophyseal joints, in association with degenerative disease.

Meningeal and Perineural (Tarlov) Cysts

Meningeal cysts may be apparent on pelvic or spinal MRI. These lesions are of unknown origin, and include perineural or Tarlov cysts and arachnoid cysts.

Tarlov cysts, also termed perineural cysts, are common incidental findings on pelvic CT or MRI. They correspond to meningeal dilations of the nerve sheath filled with liquor at the junction of the dorsal ganglion and spinal posterior nerve root at the level of the sacrum. They are typically bilateral, small and asymptomatic and are more common in females at an average age of 40 years (61). Tarlov cysts are visualized on 1–2% of sacral MRIs and 25% are believed to cause symptoms such as low back pain, perineal or lumbar pain, sciatica and rarely, *cauda equina* syndrome (62).

When large, Tarlov cysts may exhibit adjacent bone erosion or endopelvic extension. Enhancement of the cyst should prompt a different diagnosis, such as schwannoma or neurofibroma (63).

Tarlov cysts have originally been described in the sacrum, but they can be found anywhere in the spine (64). Cervical cysts have been increasingly described with MRI. Differential diagnosis includes facet joint cysts and nerve sheath tumors.

Arachnoid cysts arise from the arachnoid membrane through a congenital weakness toward the epidural space. Contrary to Tarlov cysts, the walls or cavities do not contain nerves. They may enlarge and widen the medullary canal or foramina, and cause localized or referred pain (65).

Meningoceles, while not truly cysts, may be confounded with the previous conditions. They constitute protrusions of membrane-lined spinal canal contents through a defect in the column (66). Depending on the herniated content, they may be named myeloceles, myelomeningoceles, or lipomyelomeningoceles. Posterior sacral meningoceles are associated with tethered cord syndrome.

PATHOLOGICAL CONDITIONS

In this section we will describe several pathological conditions that may mimic axSpA findings (**Table 3**).

Degenerative Changes

Sacroiliac Joint

Subchondral BME occurs in early phases of degenerative processes resulting from vascularization of fibrous tissue. It is important to notice the site of edema, since hyperintensity on synovial portions of the SIJ favors inflammatory disease, while ligamentous portion involvement favors degenerative disease.

Degenerative changes are more common in men than women and involve osteophyte formation and ankylosis (**Figure 5A**). A clear connection between CT findings of SIJ degeneration and symptoms has not been found.

SIJ degeneration is common in early decades of life and increases with age. There is a high prevalence of asymptomatic patients with degenerative changes, so caution is recommended when attributing low back pain to SIJ degenerative disease.

SIJ space narrowing is only present in about 25% of patients with degenerative changes. Bone sclerosis is the most common finding, usually at the anterior and middle thirds of the joint and commonly associated with pubic symphysis degeneration.

Spine

Degenerative disease of the spine may be confounded with acute or chronic inflammatory changes due to axSpA (67, 68). Progression of intervertebral disc degeneration follows an MRI classification (Modic) that compounds three stages analogous to the Andersson lesions seen in ankylosing spondylitis (AS) (69). Other structures of the spine are usually affected, such as the atlanto-occipital joints, atlanto-odontoid joint, facet joints and the *ligamentum flavum* (70).

The main differences of Modic lesions compared to inflammatory lesions is their topographic location (along the main weight-bearing axis), clinical context (old age and associated with other degenerative findings) and lab work (**Figures 5B,C**). A multidimensional approach usually suffices to establish the correct diagnosis.

Scheuermann Disease

Also termed juvenile kyphosis, Scheuermann disease (SD) is the most common cause of symptomatic structural thoraco-lumbar hyperkyphosis in adolescents (13–16 years-old) (71). Its etiology is unknown but several theories have been proposed, such as impaired collagen fibril formation due to changes

TABLE 3 | Pathological conditions that mimic axial spondyloarthritis.

Condition	Type	Characteristic features
Degenerative changes	Spine	Location–weight-bearing axis Other–old age, other degenerative findings, Modic classification
	Sacroiliac joint	Location–ligamentous portion, bone sclerosis of anterior and middle third Other–male, osteophytes, associated with pubic symphysis degeneration
Scheuermann disease	–	Location–thoracolumbar Other–adolescents, Schmorl nodes
Osteitis condensans illi	–	Location–iliac side at the ventro-caudal portion Other–bilateral, symmetric, women, middle-age, sclerotic area with triangular configuration, may demonstrate BME below arcuate line, no erosions
DISH and OPLL	DISH	Location–thoracic and lumbar segments, superior non-cartilaginous portion of the SIJ Other–old age, obesity, diabetes mellitus, occasional bridging, appendicular involvement
	OPLL	Location–cervical spine Associated with DISH
Fractures (sacrum/Ilium/vertebrae)	Acute Insufficiency Stress response Post-trauma inflammatory-like SIJ diastasis/incongruence	Insufficiency–more common at the sacral alae and bilateral, women Stress–clinical history, unilateral and sacral side, no involvement of the subchondral bone, involvement of the pars interarticularis in the spine Diastasis–clinical history of major pelvic trauma, may have backfill, asymmetry, posterior offset General–suggestive clinical history, absence of other findings to support axSpA
Septic arthritis	Familial mediterranean fever/brucellosis Staphylococcus aureus Pyogenic spondylodiscitis Fungal Tuberculosis	Pronounced edema and other inflammatory osseus and soft tissue changes
Metabolic diseases	Idiopathic hypoparathyrodism Hyperparathyroidism Alkaptonuria Hypophosphatemic osteomalacia Paget disease	– Other associated findings – – Bone expansion, cortical thickening, coarsened trabecula
Crystal deposition arthropathy	Gouty sacroiliitis	Location–lumbar spine > rest of the spine or SIJ Other–middle-aged men, perimenopausal women, monoarthritis (mostly lower extremities), SIJ gout is non-specific
	Spinal/Sacro-iliac CPPD	Location–cervical > lumbar segments, atlanto-odontoid joint Other–peripheral arthritis more common, inflammatory flares at the intervertebral endplates
SAPHO syndrome/CRMO	–	Location–clavicles and sternum Other–Extra-musculoskeletal findings, progression from lytic to sclerotic and hypertrophic lesions
Charcot spine	–	Location–thoracolumbar segments Other–spinal cord injury, heterotopic ossification at the elbows and hip, paravertebral masses, bridging osteophytes, degeneration, bone erosions, pseudarthrosis, atrophic to hypertrophic forms
Behçet disease	–	Extra–articular findings, peripheral skeleton most involved, sacroiliitis controversial, atlanto-axial subluxation (anedoctal)
Rheumatoid arthritis	–	SIJ–bilateral and symmetric Other–femoroacetabular joints affected, clinical presentation
Hemoglobinopathies	–	Bone infarctions, bone marrow expansion and hyperplasia, growth disturbance, H-shaped vertebra, red marrow reconversion, extra-musculoskeletal findings
Sarcoidosis	–	Location–throacolumbar segments Other–women, extra-musculoskeletal findings, spinal involvement associated with CNS lesions, lytic, and/or sclerotic lesions in lacework pattern
Early axSpA		Location–dorso-caudal portion of the SIJ (posterior lower ilium)

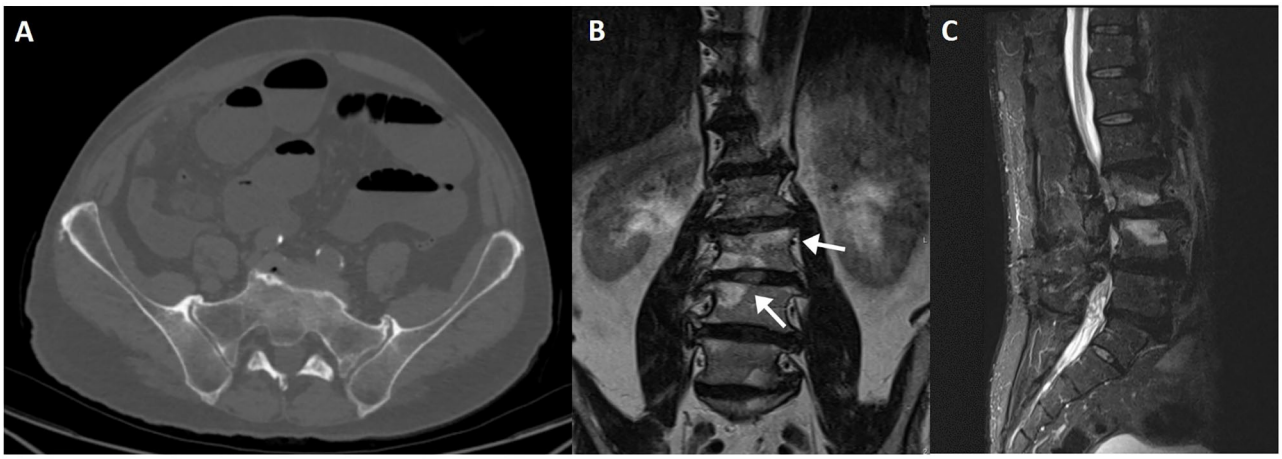

FIGURE 5 | CT axial slice showing degenerative changes of the sacroiliac joint **(A)**, with marginal osteophytes and bone sclerosis. Modic endplate changes at the weight bearing surfaces of the distal lumbar spine (arrows), seen on coronal T1 **(B)** and sagittal fluid-sensitive **(C)** sequences. Bone marrow signal changes are high on T1WI and fat-saturated T2WI, compatible with Modic type 2.

in growth hormone levels with consequent weakening of the vertebral endplates (72). A strong genetic background has also been reported in recent studies (72). Radiological criteria for establishing SD is not consistent in the literature—some authors describe anterior wedging >5° in at least three adjacent vertebral bodies; others include wedging in one or two vertebral bodies, changes in vertebral endplate, narrowed disc space and anterior Schmorl nodules. An atypical form has been described by Heithoff et al. (73) in the presence of three of the following findings–narrowed disc space, disc dehydration, endplate irregularity, anterior vertebral body edge wedging and Schmorl nodules.

Degenerative disease of the spine is typically present in young patients with SD, namely spondylosis, spondylolisthesis, endplate irregularity and narrowed disc space (with or without associated disc herniation).

Osteitis condensans ilii

Osteitis condensans ilii (OCI) is typically seen in middle-aged women in whom it manifests as sclerotic areas, mainly in the iliac bone, with relatively normal joint spaces, occurring symmetrically and bilaterally at the ventral-caudal portion of the SIJ (74). Its cause is largely unknown but the most accepted hypothesis is that of a mechanical stress, given that such condition is more commonly observed in patients who have given birth, albeit not exclusive.

Radiographs may demonstrate bilateral triangular sclerosis of the iliac wing surface at the SIJ, but osteitis can be unilateral. *Osteitis condensans ilii* is usually asymptomatic, but may present as non-inflammatory chronic back or hip pain.

Differential diagnosis with inflammatory conditions is possible due to lack of erosions, joint space narrowing, ligament calcifications or bone bridging. Sclerosis is present in both groups, but is more pominent in OCI patients. Nonetheless, it has been shown that this condition demonstrates BME on MRI in a significant portion of patients (75), which ranges from mild to as high as vessel signal intensity. BME from OCI is seen in a continuous distribution pattern centered in the ventral-cartilaginous joint part of the ilium and spreads beneath the arcuate line, while BME from axSpA may be scattered and preferentially located at the dorsal-cartilaginous part of the joint and rarely spreads to the marrow beneath the arcuate line (**Figures 6A–F**).

Some axSpA specific parameters are also present in OCI patients, such as HLA-B27 positivity, inflammatory back pain, and peripheral and extra-articular manifestations, albeit in a smaller proportion of patients (76, 77). Erosions are almost exclusively seen in axSpA patients, especially when multiple.

Diffuse Idiopathic Skeletal Hyperostosis and Posterior Longitudinal Ligament Calcification

Diffuse idiopathic skeletal hyperostosis (DISH) is characterized by undulating or flowing ossifications along the anterior column of the vertebrae, but also affecting ligaments, tendons, joint capsule, and periosteum, with relative preservation of the disc spaces and absence of radiographic changes associated with degenerative disease (78). It affects older, obese and diabetic patients with increased incidence and may involve any segment of the vertebral column, with affinity to the thoracic and lumbar segments (79) (**Figure 7A**). Preferential involvement of the superior non-cartilaginous portion of the SIJ is seen, with occasional bridging. There is no sacroiliitis or facet ankylosis. Bone mineral density of the affected segments is also maintained (80, 81).

Radiographs are generally sufficient to make the diagnosis. Other structures beside the axial skeleton might be involved and support the diagnosis, such as the iliac crest, ischial tuberosities, femoral trochanters and the non-articular portion of the patella, with decreasing order of frequency (82). In such places, extensive

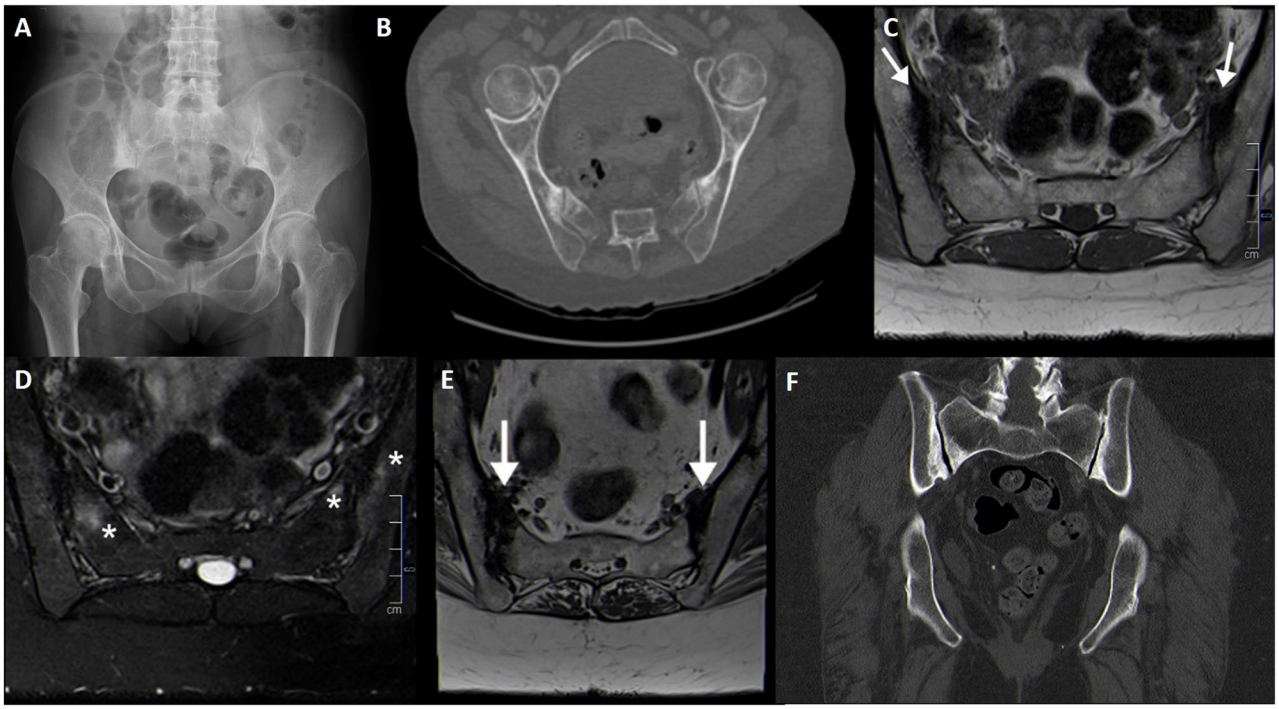

FIGURE 6 | Fifty seven-year-old female patient with bilateral *osteitis condensans ilii* evident on pelvis radiography **(A)** and CT **(B)**. Another patient, with post-partum bilateral bone marrow edema of the sacroiliac joint and sclerotic changes compatible with *osteitis condensans ilii* (arrows, asterisks), shown on MRI sequences **(C–E)** and CT **(F)**.

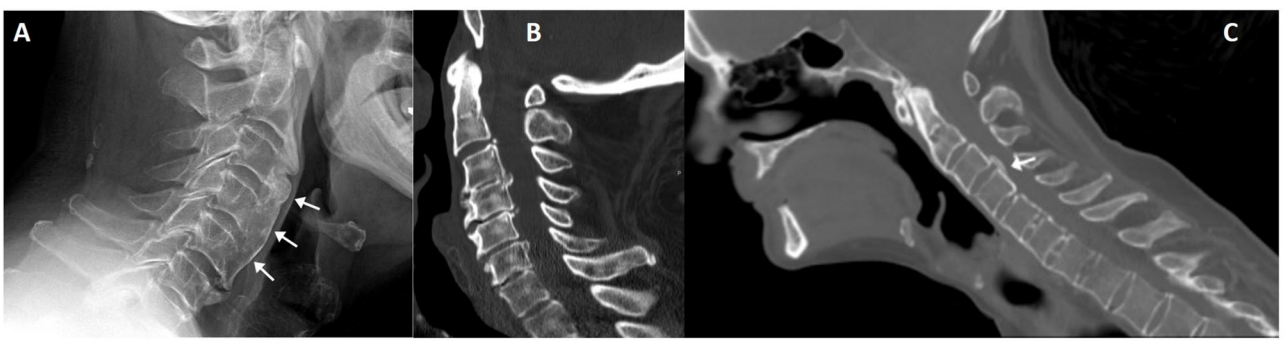

FIGURE 7 | Lateral cervical radiography of a patient with cervical undulating anterior longitudinal ligament ossification (arrows), compatible with DISH **(A)**. Another patient **(B)** with cervical DISH and ossification of the posterior longitudinal ligament; differential diagnosis with posterior syndesmophytes is not always straightforward, as seen in a CT sagittal reconstruction of a patient with ankylosing spondylitis [**(C)**, arrow].

wavy calcifications are found where ligaments, tendons and capsules attach to bone.

CT and MRI are reserved for whenever there is suspicion of complications, such as dysphagia, nerve compression or fracture (83). Special care should be taken to assess for fractures, which may occur with minor trauma and have a characteristic "carrot stick" appearance that can compress the spinal cord (84, 85).

DISH may be seen in association with posterior longitudinal ligament ossification (OPLL). In fact, both conditions are frequently seen together in nearly half of patients. OPLL predominantly affects the cervical spine and has a more sinister course as it is adjacent to the spinal canal (**Figure 7B**). It may, however, be difficult to differentiate from a posterior syndesmophyte, as shown in **Figure 7C** in a patient with ankylosing spondylitis.

Trauma

Insufficiency Fractures and Stress Reaction

There are mainly two types of sacral fractures—insufficiency and fatigue fractures. Insufficiency fractures are more common and occur with minimal trauma in an osteoporotic bone, are

frequently bilateral and have a higher incidence in women (86, 87) (**Figure 8**).

Sacral stress (or fatigue) fractures are seen in athletes and frequent runners. A stress reaction or fracture may be documented by MRI as a unilateral, sacral side BME without involvement of the subchondral bone. A vertical fracture line within the affected sacrum may be seen and raise suspicion for the diagnosis.

Sacral insufficiency fractures are common (1–1.8%, as high as 5% in some series) and underdiagnosed as a source of low back pain (88). Likewise, vertebral osteoporotic fractures constitute a significant cause of low back pain and disability.

Etiologies include a weakened bone (osteoporosis, steroid-induced osteopenia, infiltrative disease), SIJ pathology (e.g., rheumatoid arthritis) with energy transfer to the sacrum, post-menopause and pelvic radiation. Paget disease, hyperparathyroidism and post-partum sacral fractures have also been reported. Interestingly, 1.6% of regular runners have sacral injuries (89). Mean age of presentation is 70–75 years.

Radiographs are usually unremarkable (20–38% sensitivity, 12.5% with visible fracture line), but when present, fractures are more often seen in the sacral ala (88). Some articles report a sensitivity approaching 0% (90). MRI is the examination of choice given its higher sensitivity, and shows BME.

Fractures involving the spine are more common in the pedicles and *pars interarticularis*, the latter ultimately leading to spondylolysis. Spondylolysis is one of the most common causes of low back pain in young athletes and may be present in up to 47% of symptomatic patients from this group (91).

A radiographic sign of spondylolysis is lateral deviation of the spinous process of the affected level, due to rotation toward the shorter laminae. Radiographs are, nonetheless, limited in documenting this condition and are most useful at depicting spondylolisthesis, which may be another sign of accompanying spondylolysis. CT is the gold standard for detailing bone morphology and detecting pars defects. MRI has a good correlation with CT and SPECT imaging (87). An MRI grading for spondylolysis characterization has been developed (92).

Pedicle stress fractures are also commonly seen among athletes, but may arise as a complication of laminectomy, scoliosis interventions and spine fusion (93, 94). Prevalence in the population is unknown and pathophysiology is controversial. Radiographs may show sclerosis of the pedicles, but other imaging methods are more sensitive, such as MRI or SPECT (91).

Post-traumatic Inflammatory-Like Arthritis

Inflammatory-like structural changes of the SIJ have been described in patients after major pelvic trauma, namely fracture or diastasis (95). Clinical symptoms may be of inflammatory or mechanical nature. It is uncertain whether these findings support the theory that axSpA may be triggered through traumatic events or are short-term and self-limited events. Backfill (fat deposition in an erosion cavity), a specific sign of axSpA seen on MRI, has been documented in post-traumatic SIJ diastasis, but may represent a physiological event of bone remodeling in unstable SIJ (95).

SIJ trauma with intra-articular step-off has not been linked to inflammatory-like structural changes.

Sacroiliac Joint Laxity and Diastasis

The SIJ space shows important variations depending on the location where it is measured. A joint space under 2 mm is considered pathologically reduced (frequently due to degeneration) (96, 97). However, a detailed anatomy of the SIJ is relevant to avoid erroneous measurements. It is important to take into account that anatomical variants, which are not infrequent, have an impact on SIJ width measurements.

AxSpA affecting the SIJ may produce joint space widening (so-called pseudo-widening) due to cartilage or bone erosions, as well as joint-space narrowing, due to bone remodeling, bridging, and ankylosis. Other conditions described in this article may produce similar findings in the same manner (e.g., erosions in hyperparathyroidism) or in a different fashion

FIGURE 8 | CT (left), T1WI (middle), and fat-saturated PD (right) MRI of a patient with sacral insufficiency fractures (arrows). T1WI shows diffuse slightly hypointense signal of the left sacral wing and a linear hypointensity compatible with a sacral fracture; corresponding fat-saturated PD image documents marked bone marrow edema.

(e.g., cartilage wear in degenerative changes). Furthermore, knowledge of patient history is essential; history of trauma to the pelvic ring might cause SIJ diastasis, especially in open-book fractures where the anterior ligaments are torn (98). In these cases, asymmetric widening, evidence of a posterior offset and absence of other findings hint at the probable diagnosis (39, 97).

Sacroiliac joint laxity and hypermobility has been described and may lead to joint instability, disturbance of mechanical loading and development of symptoms.

Septic Arthritis and Spine Infections

SIJ infections arise most often from blood-borne pathogens; erosions of the SIJ may be seen associated with osteomyelitis or soft-tissue abscess (99) (**Figures 9A–D**). Bacterial forms of SIJ infection may occur through different routes, namely hematogenous, contiguous spread, direct inoculation, or post-surgical. Joint aspiration is often necessary for diagnosis, but clinical and laboratory investigations, aided by CT and MRI showing suggestive findings (see below) may suffice in the presence of a suggestive clinical context. Juxta-articular bone demineralization, considered the earliest finding of infectious sacroiliitis, can be seen on CT. Soft tissue involvement and unilaterality also help in diagnosis (100).

In specific subsets of patients, certain agents might be suspected. Drug addicts are susceptible to infection caused by rare organisms, such as *Klebisella*, *Enterobacter*, *Streptococcus*, *Candida albicans*, and *Pseudomonas spp*.

Facet joint infection is an increasingly recognized entity arising from non-hematogenous sources such as respiratory or genitourinary infections and interventional procedures. Clinical symptoms are similar to spondylodiscitis but generally unilateral erosive bone changes, thickening of the *ligamentum flavum* and obliteration of fat planes may be inconspicuous on CT and only detected on MRI.

Spine infection should be suspected in the clinical setting of new or worsening back pain and fever, intravenous access or hemodialysis, recent bacteremia, endocarditis, intravenous drug abuse or new neurologic deficits (100, 101). It starts as an endplate infection which progresses to discitis. Subtle endplate edema may be the very earliest signs of spondylodiscitis (102). Edema or fluid in the psoas musculature, termed MRI psoas sign, is another finding consistent with early spondylodiscitis (103).

Pyogenic Spondylodiscitis

Pyogenic spondylodiscitis is typically centered at the disc space, but may manifest in the bony spinal column and ligaments of the extradural spine. Hematogenous spread is the main route of infection, through arterial supply or paravertebral venous plexus (104). The most common causative agent is *Staphylococcus aureus* (105). Disease has a higher incidence in diabetic and male patients and has an anatomical predilection for the lumbar spine.

In adults, infection spreads from the anterior vertebral body to the remaining body, endplates and adjacent discs. Spread to the paraspinal soft-tissues is common. Documentation of spinal abscesses is particularly relevant as it constitutes an emergency (106). Pediatric patients still have a robust arterial anastomotic network which protects the bone, but the disc is more vulnerable and highly vascularized, thus making it the primary site of infection.

Pyogenic spondylodiscitis reduces disc height and shows hyperintensity on fluid-sensitive sequences that is distinct from the normal hydrated disc pattern. The disc also enhances after gadolinium administration. Bone surface irregularity, destruction and enhancement of the endplates and vertebral bodies is also typical. Extension to the epidural and paravertebral spaces with development of inflammatory swelling, phlegmon, or abscesses is possible (107).

Hyperparathyroidism, neuropathic arthropathy, acute Schmorl nodes, SAPHO syndrome, AS and tumors are non-infectious mimics that may resemble pyogenic spondylodiscitis. Of note, tumor lesions never cross the disc space and the disc height is generally preserved.

Familial Mediterranean Fever—Brucellosis

Brucellosis is the most common zoonotic infection worldwide (108). Gram negative bacteria have affinity for the SIJ and up to 35–37% of patients with brucellosis have SIJ involvement, usually unilateral.

The most common manifestations of brucella infection are musculoskeletal and include arthralgia, myalgia and low back pain. Although sacroiliitis is less common than spondylitis, it is still a diagnostic consideration in specific clinical settings.

Brucellosis can mimic axSpA and even fulfill ASAS classification criteria for axial or peripheral SpA (99, 108, 109), when assessing for clinical, laboratory and imaging findings. The most important MRI changes are BME and bone erosions in SIJ. Compared to axSpA patients, BME in brucellosis has higher T2-intensity and usually crosses anatomical borders to affect adjacent muscles. Backfill is also documented, but resolves with antibiotic treatment.

Fungal Spondylodiscitis

Fungal spondylodiscitis is a rare occurrence, but incidence has increased over the years due to increase in immunocompromised patients (110). The most common agent is *Candida albicans*, followed by *Aspergillus fumigatus*. Diagnosis is multidisciplinary but the gold standard is histological or culture confirmation from tissue samples. The most affected segments remain the lower thoracic and lumbar spine. Imaging is non-specific and mimics pyogenic or tuberculous infection.

Tuberculous Spondylodiscitis

Spinal tuberculosis (TbS) is a common form of extrapulmonary tuberculosis and accounts for 50% of musculoskeletal tuberculosis cases (111) (**Figures 9E–G**). Clinical presentation is non-specific long-standing back pain, which may be investigated only after onset of neurological deficits and bone deformities. Nevertheless, in countries with a high prevalence of tuberculosis clinicians should be alerted to this possibility and include it at an early stage in the differential diagnoses, thus avoiding misdiagnosis.

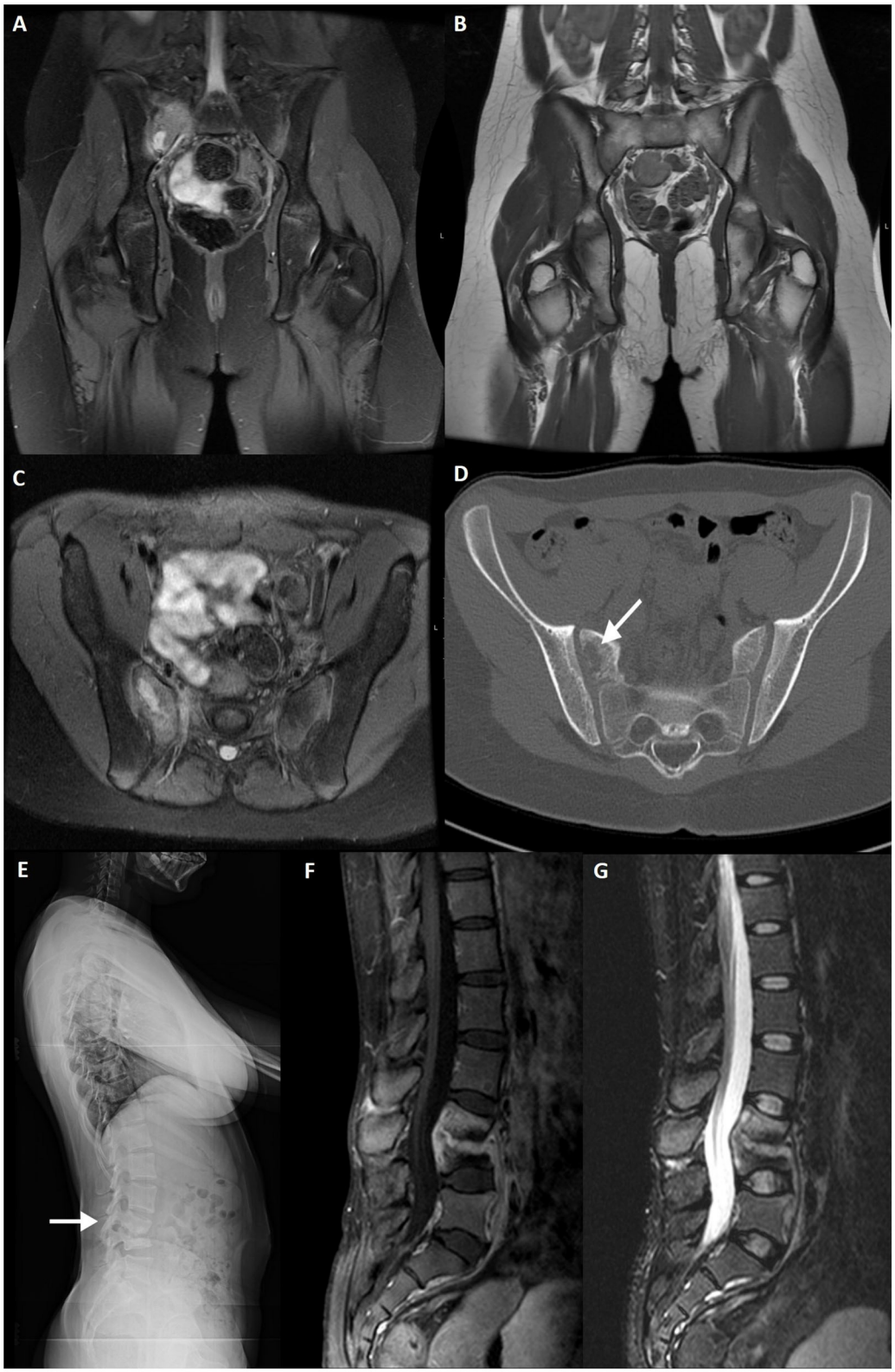

FIGURE 9 | Fat-saturated PD **(A)** and T1WI **(B)** coronal slices, fat-saturated PD **(C)** axial and CT axial slices **(D)** of a 12-year-old female patient with proven *Streptococcus* spp. osteomyelitis of the right sacrum (arrow). A lytic lesion is seen adjacent to the right sacroiliac joint. Lateral lumbar radiography **(E)**, post-contrast fat-saturated T1WI **(F)** and TIRM **(G)** sagittal slices of a 26-year-old female patient with confirmed tuberculous spondylodiscitis of L3–L4 segment (arrow).

Radiographs show loss of endplate margin definition, kyphotic changes, narrowing of the intervertebral disc space and calcified paravertebral masses.

TbS may resemble other pyogenic infections involving the disc. Some findings that favor TbS include: larger collections, cold abscesses adjacent to the affected spine, thoracolumbar junction, no/less involvement of the disc space, skip lesions involving multiple ligaments through subligamentous spread and whole vertebral body or posterior involvement (107, 112). Suggestion of a degenerative nature relates to the presence of vacuum phenomenon, preservation of the cortical boundaries, lack of soft-tissue involvement and stability of radiological findings.

Modic type 1 degeneration may mimic TbS, but contrast enhancement of active degenerative lesions is milder compared to TbS.

SAPHO Syndrome and CRMO

Synovitis, acne, pustulosis, hyperostosis and osteitis (SAPHO) syndrome is a rare auto-inflammatory condition that shares musculoskeletal and cutaneous manifestations (113). Chronic recurrent multifocal osteomyelitis (CRMO) is considered the pediatric counterpart of SAPHO syndrome, arising from sterile osteomyelitis (**Figures 10A–C**). In CRMO, cutaneous involvement is less common and long bones are more affected compared to the sternum and clavicles in SAPHO syndrome.

SAPHO syndrome has been considered an umbrella term including several idiopathic disorders sharing similar clinical and radiological features, namely CRMO in children and adolescents.

Radiographs are generally normal in early-stage CRMO but may eventually show small lytic lesions which become progressively more sclerotic (114). This condition may be self-limited and eventually resolve or lead to marked hyperostosis (115).

Whole-body MRI is the gold standard modality for evaluation of SAPHO and CRMO, due to its sensitivity and lack of radiation (116). The most frequent findings are:

- Lytic lesions in early-stage
- Sclerosis, bony expansion or mixed lytic and sclerotic changes in later-stage
- Pathological or compression fractures, with associated deformities in fluid-sensitive sequences
- Bone expansion / hyperostosis in late-stage

Spinal SAPHO syndrome may mimic infectious spondylodiscitis (117). However, absence of soft-tissue masses and epidural involvement as well as the presence of anterior vertebral corner erosions differentiate it from an infectious nature. Nonetheless, bone biopsy is necessary to exclude infection or malignancy.

Metabolic Diseases

Certain metabolic diseases may show imaging changes suggestive of axSpA.

Hypoparathyroidism occasionally courses with syndesmophytosis and para-spinal ligament calcifications that resembles psoriatic arthropathy (118, 119). Other radiographic findings include diffuse increased bone mass, osteosclerosis of the calvarium with narrowed diploic space (120).

Hyperparathyroidism may course with subchondral bone resorption anywhere in the axial skeleton (**Figures 11A–D**). Musculoskeletal changes in hyperparathyroidism are most common in the hands (95%) (121), with pathognomonic subperiosteal bone resorption on the radial side of the middle phalanges of the middle and index fingers (122). Acro-osteolysis may also be seen, due to bone resorption of the distal phalanges. Other forms of bone resorption have been described, such as subligamentous, intracortical, subchondral, endosteal, or subtendinous locations. Subperiosteal resorption may also affect the ribs, tooth sockets, humerus, femur, and tibia. Subchondral resorption in particular can occur in any joint, along the interphalangeal and metacarpophalangeal joints, acromioclavicular joint, SIJ, and sternoclavicular joint. Subtendinous resorption is more typically found in the calcaneus, clavicle, proximal humerus

FIGURE 10 | Fat-saturated T2WI sagittal MRI sequence **(A)** of the lumbar spine in a 16-year-old female patient with CRMO (arrows), mimicking corner inflammatory lesions. Fat-saturated PD axial slice **(B)** of the same patient depicting involvement of the right SIJ. Fat-saturated T2WI axial slice **(C)** of the neck shows involvement of the left mandibular ramus.

FIGURE 11 | CT sagittal reconstruction of the dorsal and lumbar spine **(A,B)** of a patient with renal osteodystrophy depicts abnormal bone turnover and mineralization, with diffuse osteosclerosis and multiple areas of subperiosteal resorption. Lateral lumbar spine radiography **(C)** shows the characteristic "rugger jersey" spine, with alternating bands of increased and normal bone density of the vertebral bodies. Note a large brown tumor of the left iliac bone on CT **(D)**.

and femur, ischial tuberosity, and anterior-inferior iliac spine. BME and other active and chronic features may be seen in the SIJ, but with the same frequency as that seen in healthy individuals and lower than in patients with axSpA (123).

Changes in hyperparathyroidism resemble those from AS but are distinguished due to abscence of joint space narrowing and less pronounced articular surface irregularities.

Hypophosphatasia is a rare genetic disorder that results in accumulation of pyrophosphate, an inhibitor of bone

mineralization, and development of hypophosphatemic osteomalacia. Radiological findings are similar to rickets and osteomalacia and vary according to age of presentation (121).

Paget Disease

Paget disease (PD) of bone, also known as *osteitis deformans* and described for the first time in 1877 by Sir James Paget, is a chronic skeletal disorder characterized by abnormal and excessive bone turnover (124) (**Figures 12A–C**).

PD is more prevalent among Anglo-Saxon descendants, males and patients over 50 years old. Prevalence increases with age but incidence has been declining over the last 20 years.

PD is a disease of largely unknown causes, but the role of environmental factors on a background of genetic susceptibility have been increasingly recognized and are proposed by some authors as the most likely etiology. Viruses seem to be the main causative agent, since patients present with intranuclear and intracytoplasmic inclusion bodies in osteoclasts and giant osteoclasts (classic features of virus infection).

The disease course can be divided in three main phases (lytic, mixed, and sclerotic), although some authors describe a fourth inactive phase. All phases can occur simultaneously in the same patient at different sites (125).

Most patients will be asymptomatic at the time of diagnosis, explaining why the disease is most often discovered incidentally. Symptoms, when present, vary depending on the distribution of the disease, with pain being the major complaint. Fractures are the most common complication (126).

Distribution is generally asymmetric, most commonly affecting the lower extremities with a slight tendency for the right-side. The most common affected sites are the lumbar spine (L4 and L5), pelvis, sacrum, femur, and calvarium (127).

PD typically begins with bone destruction translated into a lytic phase, which is characterized by intense osteoclastic activity

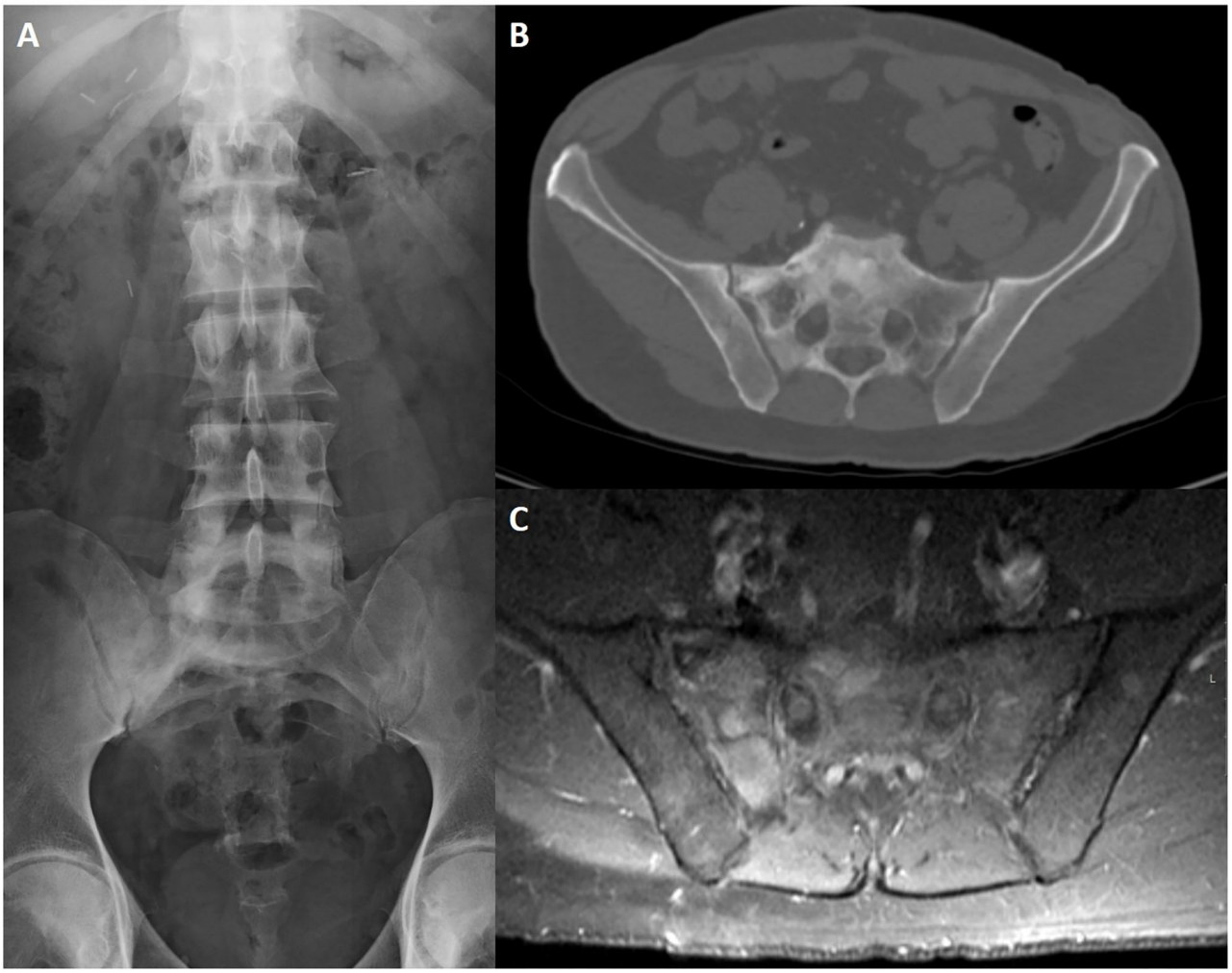

FIGURE 12 | Lumbosacral radiography **(A)**, CT axial slice **(B)** and post-contrast fat-saturated T1WI **(C)** of a 65-year-old male patient with Paget disease of the sacrum and right iliac bone. Typical findings include an expanded bone with coarsened trabecular pattern and sclerotic changes that are more evident on conventional radiography. There is increased uptake after intravenous contrast injection **(C)**.

displayed as osteolysis. Progression of the disease into a mixed lytic and sclerotic phase usually occurs with time. The four cardinal features of this stage include:

- Advancing edge of osteolysis
- Coarsening and thickening of bone trabeculae along the stress lines
- Cortical thickening
- Osseous widening/bone expansion (pathognomonic)

In long bones, early-stage PD will appear as an advancing edge of osteolysis which begins in the subchondral bone and extends to the metaphysis and diaphysis, giving the characteristic "flame" or "blade of grass" configuration.

In the spine, cortical thickening along the four margins of the vertebral body cortexes is usually seen, giving a "picture-frame appearance."

Osteosclerotic phase is characterized by increased bone density. Coarsening of the trabeculae and cortical thickening, associated with marked widening and enlargement of bones, will be apparent in long bones and pelvis. Diffuse sclerosis of the vertebral body is typical in this stage, giving the appearance of ivory vertebra. Involvement of the spine may affect one vertebral level, multiple levels, or even all vertebral segments. Posterior vertebral elements may also be affected.

PD can also invade the intervertebral disc and articular surfaces directly, extend to ligaments, and cause ligamentous ossification.

Crystal Deposition Arthropathies

Gouty Sacroiliitis

Gout is a common metabolic disease that frequently affects middle-aged men and postmenopausal women. The most frequent manifestation is monoarthritis secondary to tophi deposition, more common at the lower extremities but eventually involving any appendicular or axial joint (128). Initial involvement of the first metatarsal-phalangeal joint may be followed by tarsal, ankle, knee, finger, wrist and elbow involvement and, less frequently, shoulders, hips, spine, and SIJ. Both the spine and SIJ may be affected, but the most common location is the lumbar spine.

Sacroiliac gout has an incidence of 7–17% (129) and symptoms are non-specific, mimicking other inflammatory, or infectious conditions. In fact, this condition is frequently misdiagnosed as AS. A correct diagnosis may require biopsy or aspiration with polarized microscopy evaluation to reveal the monosodium urate crystals.

Imaging findings are non-specific and CT is the preferred method of choice for detection of subcutaneous tophi and structural changes suggesting gouty arthritis. Dual energy CT may directly visualize and quantify crystal deposition (130).

Spinal/Sacro-iliac CPPD

Calcium pyrophosphate dihydrate crystal deposition (CPPD) may be secondary to metabolic disorders such as hemochromatosis, hyperparathyroidism and hypomagnesemia, or less commonly, a monogenic familial disease. CPPD may occur in cartilage and fibrocartilaginous joints, a process termed chondrocalcinosis. Other structures may be affected by CPPD, such as ligaments and tendons, the *nucleus pulposus* and *annulus fibrosus* of the intervertebral disc. CPPD is predominantly a peripheral arthritis, but spinal involvement has been documented (131).

A destructive arthropathy affecting the cervical and, less commonly, lumbar segments is seen and, among these segments, the transverse ligament of the atlas and, thus, the atlanto-odontoid joint is the most frequent (132, 133). CPPD deposits in the peri-odontoid region may lead to a condition called crown dens syndrome when associated with acute symptoms (134, 135). Furthermore, severe retro-odontoid deposits may generate cervical myelopathy due to spinal cord compression.

Aseptic discitis is a well-known complication of CPPD arthropathy in the axial skeleton and causes recurrent inflammatory flares (136) (vertebral endplate erosions, intervertebral disc narrowing, and gadolinium enhancement of the disc and endplate lesions.) A percutaneous biopsy of the affected structures may be necessary to exclude infection or other etiologies.

The SIJ is rarely affected but may also be responsible for acute flares. Degenerative changes in asymptomatic individuals and, occasionally, destructive changes have been described. Again, such changes are non-specific and other diagnoses should be excluded.

MRI has poor sensitivity to detect CPPD deposits, but reveals inflammatory changes of the endplates and SIJ.

Bone Tumors

Diagnosis of primary or secondary bone tumors is usually straightforward, but they may appear like BME on MRI, especially when infiltrative in nature (Lodwick type IC, II and III) (137). Their typical location, however, is not near the SIJ and lesions are better demarcated after endovenous contrast injection. The sacrum is a common site for multiple myeloma, plasmacytoma and metastasis involvement. Vertebrae are also a frequent site of metastases (**Figures 13A–I**).

Benign Primary Tumors–Pelvis

Most benign tumors of the pelvis occur before the age of 40. In general, benign tumors have geographical well-defined borders (Lodwick type IA or IB) and may be expansile, unlike inflammatory conditions, but occasionally appear more aggressive and have blurred borders (Lodwick type IC) (137).

In an initial assessment, benign tumors involving the posterior sacrum may be confounded with other entities, especially when seen in a young patient.

Osteochondromas are among the most common benign tumors and have a characteristic appearance of a cartilage-covered bony projection, usually pointing away from the nearby joint (138).

Giant cell tumors (GCT) are more common in women than men and usually appear in the third and fourth decades of life, after physeal closure. They can have locally aggressive features and high vascularity. A small subset of GCT is malignant (5–10%) (138). The sacrum is the most common site of involvement in the axial skeleton and GCT is the second

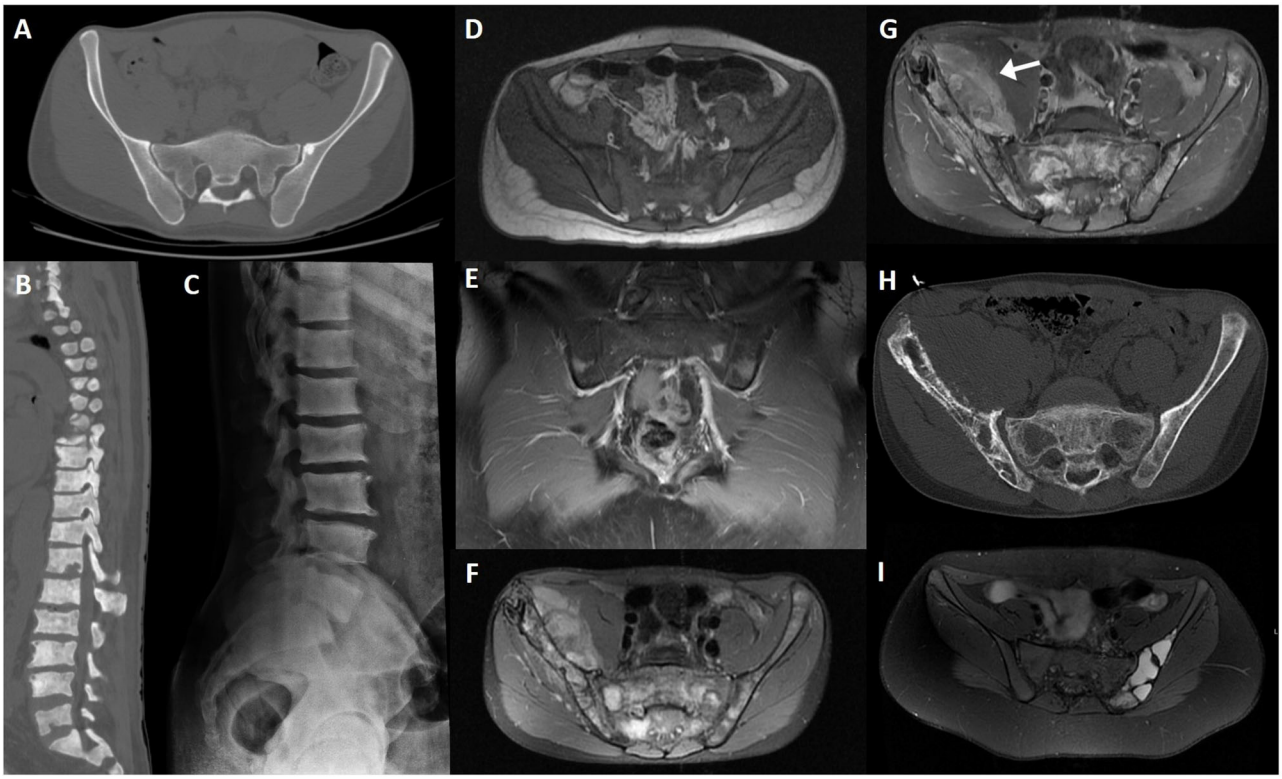

FIGURE 13 | CT axial slice **(A)** of an iliac bone enostosis mimicking peri-articular sclerosis; CT sagittal reconstruction **(B)** of the dorsal and lumbar spine in a patient with diffuse osteoblastic metastasis due to prostate cancer; lateral lumbar radiograph of the same patient **(C)**; T1WI axial slice **(D)**; and post-contrast fat-saturated T1WI coronal slice **(E)** of a patient with leukemic infiltration of the sacrum and iliac bones, showing diffuse bone marrow T1 hypointensity due to tumoral infiltration and multifocal patchy uptake, respectively; fat-saturated PD **(F)**, post-contrast fat-saturated T1WI **(G)** MRI and CT axial slice **(H)** of a 18-year-old male patient with Ewing sarcoma; fat-saturated PD **(I)** MRI sequence of an aneurysmatic bone cyst of the left iliac bone.

most common tumor involving this bone, following chordoma. Imaging findings include a lytic soft-tissue mass with increased vascularity, occasionally crossing the SIJ, with low signal intensity on T1 and heterogeneous on T2 (hypointensity of the solid component) weighted-imaging. There is no periostitis or bone matrix formation; GCT may have an associated aneurysmal bone cyst, with evidence of fluid-fluid levels.

Aneurysmal bone cysts are typically lytic and well-circumscribed, expansile with thinning of the cortex. Variable T1 and T2 weighted imaging signal intensity due to the presence of blood products with different ages is common; fluid-fluid levels are characteristic, but not specific.

Benign Primary Tumors–Spine

Vertebral hemangiomas are common spinal tumors and typically multiple (139). Hemangiomas may have distinct presentations, but the most common appearance on MRI is T1 and T2 weighted imaging hyperintensity owing to their hamartomatous nature with vascular and fatty components.

Other tumors involving the spine that are more frequently seen include eosinophilic granuloma, osteoblastoma, GCT, aneurysmatic bone cyst, and osteochondroma. A detailed description goes beyond the scope of this article and is expertly addressed elsewhere (139).

Bone Marrow Infiltrative Lesions—Lymphoma, Leukemia, Multiple Myeloma, Plasmacytoma, Ewing Sarcoma, Metastasis

A wide range of conditions affect marrow composition either through infiltration or component replacement. Neoplastic and myeloproliferative processes increase cellularity and have distinct imaging patterns.

In general, tumor cells have long T1 values (decreased signal) and variable T2 values. Imaging has a role not only in diagnosis, but also evaluation of remission or progression of disease. Infiltrative marrow has a decreased T1 signal intensity, with the exception of melanoma and some cases of myeloma (140). T2 signal is more variable.

Lymphoma, leukemia, plasma cell myeloma, primary bone neoplasms, and metastatic disease may have either a focal or diffuse distribution in the bone marrow. The spine and pelvis are among the most common bones involved in these conditions (141, 142).

Spinal metastases generally appear on the posterior-superior aspect of the vertebras, in the vertebral body, and destruction

of a pedicle is not an uncommon finding. Focal lytic metastases demonstrate decreased signal on T1 compared to muscle or disc, and increased signal on T2 compared to normal marrow. Blastic lesions have decreased signal on T1 and T2 weighted imaging (143). Post-contrast T1 weighted imaging sequences demonstrate mild to moderate enhancement.

MRI may document other signs of an infiltrative process, namely vertebral collapse, intra-spinal soft-tissue and cord compression, muscle infiltration or lymph node enlargement.

Both Hodgkin and non-Hodgkin lymphoma tend to affect the spine (144) in a focal nodular pattern. Signal intensity on conventional MRI sequences is similar to metastatic disease from solid neoplasms, with abnormal lymphomatous marrow enhancement. Vertebral collapse and soft-tissue mass may be found.

Ewing sarcoma affecting the axial skeleton is most common in the ribs and pelvis (138).

Multiple Myeloma and Solitary Plasmacytoma

Multiple myeloma (MM) is a plasma cell dyscrasia with proliferation and accumulation of monoclonal plasma cells (145).

Conventional radiography has a low sensitivity for detection of lytic lesions, and new advances in the last 2 decades have increased the role of MRI and PET CT to evaluate bone marrow infiltration in early and late stages.

The most frequently used conventional sequences are T1 and T2 weighted acquisitions with and without fat suppression for qualitative determination of bone marrow composition and mineralized matrix (146). Dynamic contrast-enhanced and diffusion-weighted imaging also play a role in diagnosis.

Lesions appear hypointense on T1 and relatively hyperintense on fat-suppressed T2 due to high cellularity and water amount. MM favorably affects the axial skeleton (lower thoracic and lumbar spine) and pelvis, but also the ribs, shoulders, skull, and proximal femurs. Patterns of infiltration may differ—no change, focal infiltration, diffuse disease, salt-and-pepper involvement or combined. Almost one third of patients exhibit normal appearing marrow signal on T1 and fat-suppressed T2 weighted imaging. MM lesions have high contrast-enhancement due to neo-angiogenesis, with washout. High signal on high *b*-value images correspond to bone marrow infiltration.

Red bone marrow, usually more pronounced in young individuals, tends to have the same signal intensity changes compared to MM infiltrated bone marrow. Contrast-enhancement curves may vary, and Dixon techniques may be applied to distinguish red bone marrow hyperplasia from an infiltrating lesion (147).

Mean age of patients with MM is over 50 years. Subchondral geodes, schwannomas, Schmorl nodules and scar tissue from bone marrow biopsy may simulate MM on conventional MRI.

Plasmacytoma lesions generally have hypointense signal on T1 and hyperintense signal on T2 weighted imaging. Post-contrast sequences demonstrate intense enhancement. These lesions are expansile and may show a "mini-brain" appearance on axial images. Distinction from other entities such as metastasis, lymphoma or leukemia may be challenging (148).

Other Malignant Primary Tumors

Chordoma is the most common primary sacral tumor (149). It is a low-grade malignant tumor arising from notochordal remnants. Imaging shows a heterogenous sacral mass causing bone destruction and expansion. Chondrosarcoma, Ewing sarcoma and osteosarcoma also favor the pelvis, but diagnosis is usually straightforward and a detailed description goes beyond the scope of this article.

Charcot Arthropathy

Charcot neuroarthropathy of the spine, also called Charcot spine, is progressive destruction of the spinal joint due to innervation abnormalities (98, 150). Charcot spine and heterotopic ossification are possible outcomes of spinal cord injury. Heterotopic ossification occurs most often around the hip or elbow joints (151). Insensitivity to pain with failure to activate muscle contraction is the proposed etiology to these conditions.

The spinal column is involved in 6–21% of patients with neuroarthropathy (152), more often in the lower thoracic (below T10) and lumbar segments (L4–L5) (153). Imaging findings include spinal instability, bridging osteophytes, paravertebral masses, cartilaginous destruction, intervertebral disc degeneration, bone erosion, early face destruction, and pseudarthrosis. CT plays an important role in depiction of most abnormalities, with MRI providing better resolution of the adjacent soft-tissue. Description of an atrophic form and progression to a hypertrophic form may explain differences in presentation.

Spinal fusion is recommended, with high rates of recurrence.

Sclerosing Dysplasias

Sclerosing bone dysplasias (SBD) are a group of skeletal abnormalities characterized by a wide variety of clinical and radiological presentations. Hereditary SBD include osteopetrosis, pyknodysostosis, osteopathia striata, osteopoikilosis, and progressive diaphyseal dysplasia. There are some non-hereditary forms, namely melorheostosis, intramedullary osteosclerosis and overlap syndromes.

Such conditions manifest with increased bone density that may be diffuse (e.g., osteopetrosis) or focal (e.g., melorheostosis), affecting the periosteum, endosteal cortical lining, or the medullary canal, with variable distribution.

Recognition of SBD may be difficult and such conditions may mimic bone metastasis, metabolic and hematological disorders as well as inflammatory conditions.

A more detailed depiction of the most common conditions goes beyond the scope of this text and is best described elsewhere (154, 155).

Behçet Disease

Behçet Disease is a multisystem inflammatory disorder mainly manifested by oral and genital aphthous ulcers, skin lesions, and uveitis. Other systems may be less frequently affected, such as the gastrointestinal, central nervous and musculoskeletal systems, as well as the lungs and kidneys. Arthritis and arthralgia are the commonest musculoskeletal findings, interestingly associated with enthesitis in some clusters of patients (156). The chronic and

vascular nature of Behçet disease, associated with drug targets that change bone metabolism might lead to reduction in bone mineral density and osteoporosis (157).

Joint manifestations are typically non-erosive, non-deforming and involve the peripheral skeleton in an oligoarticular fashion. The knee is the most frequently affected joint.

In the axial skeleton, prevalence of sacroiliitis in patients with Behçet disease is controversial–some authors report a higher prevalence while others found that there is no significant difference when compared to healthy controls (158, 159). Anecdotal reports have described other forms of axial skeleton involvement, such as atlanto-axial subluxation and instability (160).

Hemoglobinopathies

Hemoglobinopathies are genetic defects resulting in abnormal structure of the globin chain of hemoglobin molecules, and comprise sickle cell anemia and thalassemia. Sickle cell disease is an autosomal recessive disorder that results in an abnormal morphology of the red blood cell when certain stresses occur. This altered shape leads to vascular stasis, occlusion and infarction.

Musculoskeletal manifestations include bone infarction with or without superimposed infection, bone marrow expansion and hyperplasia (161) (**Figures 14A–C**). In an acute setting, bone infarcts may have a diffuse appearance, and eventually consolidate into a more sclerotic lesion. On MRI, a serpentine, well-demarcated appearance is seen. Growth disturbances can involve the vertebral bodies and cause decreased height, sclerosis due to bone infarcts and endplate depressions, with the classic H-shaped vertebra (162). Bone marrow hyperplasia on the anterior and posterior borders of the vertebral bodies, accompanied by central depression cause the typical "fish-like" appearance.

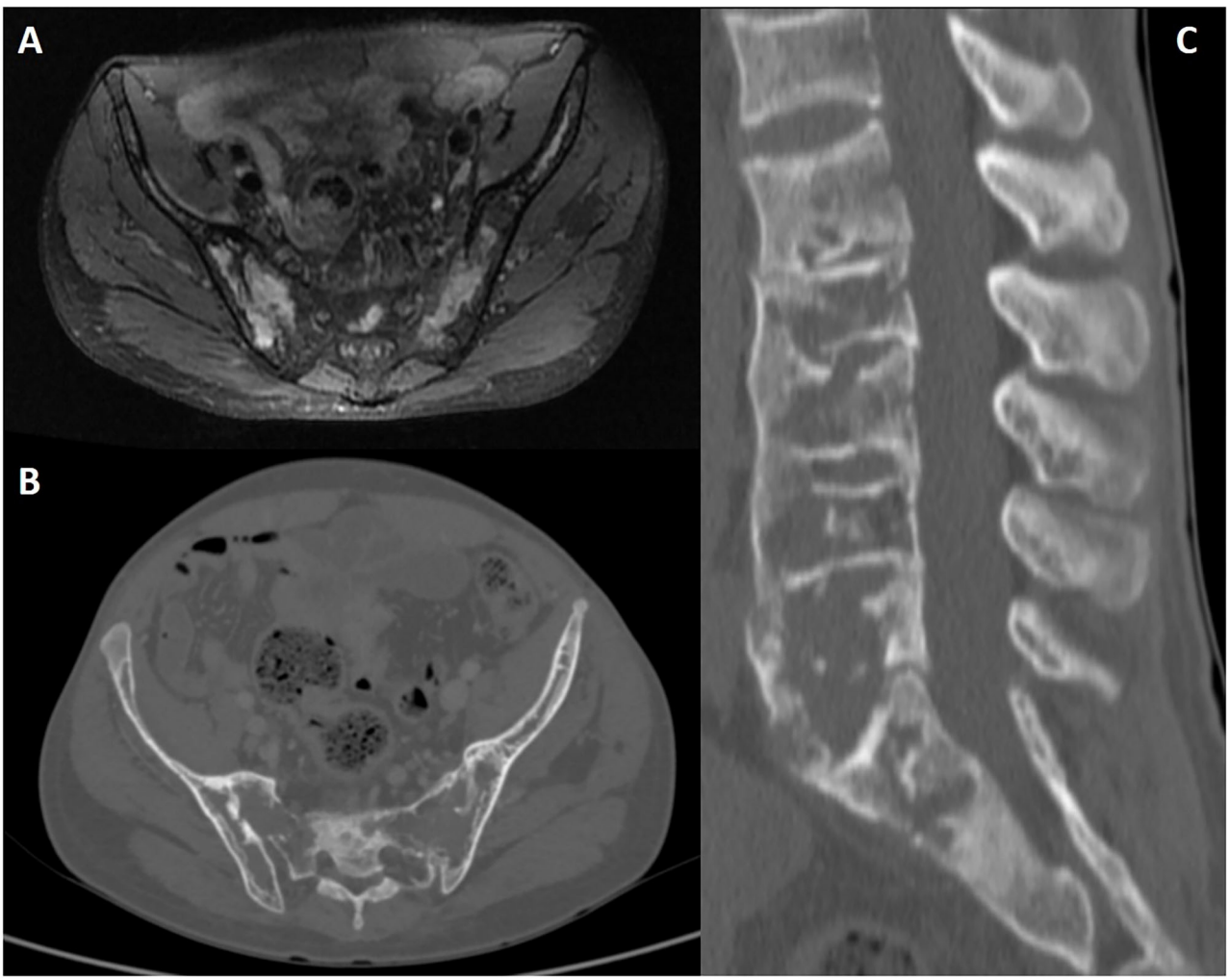

FIGURE 14 | Fat-saturated PD **(A)** MRI sequence, CT axial slice **(B)**, and sagittal lumbar spine reconstruction **(C)** of a 31-year-old male patient with Sickle cell disease and extensive bone marrow changes causing widening of the medullary spaces and thinning of cortical bone.

Red marrow reconversion in such patients lowers the high T1 signal intensity that is generally seen in fatty marrow of adult patients. Chemical shift imaging and the Dixon technique in particular may play a role in excluding malignant infiltration of affected bone marrow (physiologic red and fatty bone marrow will show a signal drop on out-of-phase images, but malignancy will not).

A detailed description of the musculoskeletal findings in sickle cell anemia and thalassemias goes beyond the scope of this text and has been expertly outlined elsewhere (163).

CONCLUSION

Low back pain (LBP) is one of the leading causes of morbidity and poses a significant economic burden in western countries with large numbers of work days lost. The SIJ and lower spine undoubtedly play a fundamental role in the pathogenesis of LBP, even in young and otherwise healthy patients. In fact, the sacrum has been coined the keystone of the pelvis, and deservedly so. Don't let the SIJ fool you—the apparent simplicity of its anatomical and biomechanical properties is only the tip of the iceberg.

AxSpA is an important inflammatory cause of chronic LBP. Clinical evaluation and identification of features suggestive of axial SpA, namely imaging features, is key to early diagnosis and to avoiding misdiagnosis. MRI is of major interest in the assessment of SIJ and the spine when an axSpA diagnosis is suspected. However, clinicians must be aware of imaging mimics and potential pitfalls. For example, although BME is an important imaging finding in axSpA, it is definitely not exclusive of this condition and mimicking changes can also be found in SIJ of healthy subjects, or SIJ presenting with morphological variants, changes related to mechanical stress, degenerative disorders, infection, and neoplastic conditions.

As a general rule of thumb, certain patterns of BME (deep involvement from articular surface, extensive lesions and close relation to other lesion types) as well as the presence of structural lesions, particularly bone erosion, ankylosis, or backfill (or fat deposition in an erosion cavity) increase the likelihood of axSpA. Contextual interpretation of the changes detected on MRI is critical. Ultimately, this information needs to be combined with clinical information, and clinical judgement remains the mainstay for the diagnosis of axSpA.

AUTHOR CONTRIBUTIONS

All authors listed have made a substantial, direct and intellectual contribution to the work, and approved it for publication.

FUNDING

PM is supported by the National Institute for Health Research (NIHR) University College London Hospitals (UCLH) Biomedical Research Center (BRC).

ACKNOWLEDGMENTS

We thank Drs Manouk de Hooge, Filip van den Bosch and Dirk Elewaut for providing **Figure 2** (images of a military subject and a postpartum female).

REFERENCES

1. Maksymowych WP, Lambert RG, Ostergaard M, Pedersen SJ, Machado PM, Weber U, et al. MRI lesions in the sacroiliac joints of patients with spondyloarthritis: an update of definitions and validation by the ASAS MRI working group. *Ann Rheum Dis.* (2019) 78:1550–8. doi: 10.1136/annrheumdis-2019-215589
2. Maksymowych WP, Eshed I, Machado PM, Pedersen SJ, Weber U, de Hooge M, et al. Consensus definitions for MRI lesions in the spine of patients with acial spondyloarthritis: first analysis from the assessments in spondyloarthritis international society classification cohort. *Ann Rheum Dis.* (2020) 79:749–50. doi: 10.1136/annrheumdis-2020-eular.6304
3. Hermann KG, Baraliakos X, van der Heijde DM, Jurik AG, Landewe R, Marzo-Ortega H, et al. Descriptions of spinal MRI lesions and definition of a positive MRI of the spine in axial spondyloarthritis: a consensual approach by the ASAS/OMERACT MRI study group. *Ann Rheum Dis.* (2012) 71:1278–88. doi: 10.1136/ard.2011.150680
4. Bray TJP, Jones A, Bennett AN, Conaghan PG, Grainger A, Hodgson R, et al. Recommendations for acquisition and interpretation of MRI of the spine and sacroiliac joints in the diagnosis of axial spondyloarthritis in the UK. *Rheumatology.* (2019) 58:1831–8. doi: 10.1093/rheumatology/kez173
5. Carvalho PD, Machado PM. How to investigate: early axial spondyloarthritis. *Best Pract Res Clin Rheumatol.* (2019) 33:101427. doi: 10.1016/j.berh.2019.07.001
6. Salsabili N, Valojerdy MR, Hogg DA. Variations in thickness of articular cartilage in the human sacroiliac joint. *Clin Anatomy.* (1995) 8:388–90. doi: 10.1002/ca.980080603
7. Gondim Teixeira PA, Bravetti M, Hossu G, Lecocq S, Petit D, Loeuille D, et al. Protocol optimization of sacroiliac joint MR Imaging at 3 Tesla: impact of coil design and motion resistant sequences on image quality. *Diagn Interv Imaging.* (2017) 98:865–71. doi: 10.1016/j.diii.2017.06.013
8. Weber U, Jurik AG, Zejden A, Larsen E, Jorgensen SH, Rufibach K, et al. MRI of the sacroiliac joints in athletes: recognition of non-specific bone marrow oedema by semi-axial added to standard semi-coronal scans. *Rheumatology.* (2020) 59:1381–90. doi: 10.1093/rheumatology/kez458
9. Lambert RG, Dhillon SS, Jaremko JL. Advanced imaging of the axial skeleton in spondyloarthropathy: techniques, interpretation, and utility. *Semin Musculoskelet Radiol.* (2012) 16:389–400. doi: 10.1055/s-0032-1329882
10. Taber KH, Herrick RC, Weathers SW, Kumar AJ, Schomer DF, Hayman LA. Pitfalls and artifacts encountered in clinical MR imaging of the spine. *Radiographics.* (1998) 18:1499–521. doi: 10.1148/radiographics.18.6.9821197
11. Krupa K, Bekiesinska-Figatowska M. Artifacts in magnetic resonance imaging. *Pol J Radiol.* (2015) 80:93–106. doi: 10.12659/PJR.892628
12. Vleeming A, Schuenke MD, Masi AT, Carreiro JE, Danneels L, Willard FH. The sacroiliac joint: an overview of its anatomy, function and potential clinical implications. *J Anat.* (2012) 221:537–67. doi: 10.1111/j.1469-7580.2012.01564.x
13. Wang D. Magnetic resonance imaging of bone marrow: a review – part I. *J Am Osteopath Coll Radiol.* (2012) 1:1–12. Available online at: https://www.jaocr.org/articles/magnetic-resonance-imaging-of-bone-marrow-a-review-part-i
14. Ricci C, Cova M, Kang YS, Yang A, Rahmouni A, Scott WW et al. Normal age-related patterns of cellular and fatty bone marrow distribution

in the axial skeleton: MR imaging study. *Radiology.* (1990) 177:83–8. doi: 10.1148/radiology.177.1.2399343
15. SH. D, Laniado M, Schick F, Strayle M, Claussen C. Normal sacrum bone marrow in the sacrum of young adults: differences between the sexes seen on chemical-shift MR imaging. *AJR.* (1994) 164:935–40. doi: 10.2214/ajr.164.4.7726052
16. Nouh MR, Eid AF. Magnetic resonance imaging of the spinal marrow: Basic understanding of the normal marrow pattern and its variant. *World J Radiol.* (2015) 7:448–58. doi: 10.4329/wjr.v7.i12.448
17. Weber U, Jurik AG, Zejden A, Larsen E, Jorgensen SH, Rufibach K, et al. Frequency and anatomic distribution of magnetic resonance imaging features in the sacroiliac joints of young athletes: exploring "background noise" toward a data-driven definition of sacroiliitis in early spondyloarthritis. *Arthritis Rheumatol.* (2018) 70:736–45. doi: 10.1002/art.40429
18. de Winter J, de Hooge M, van de Sande M, de Jong H, van Hoeven L, de Koning A, et al. Magnetic resonance imaging of the sacroiliac joints indicating sacroiliitis according to the assessment of spondyloarthritis international society definition in healthy individuals, runners, and women with postpartum back pain. *Arthritis Rheumatol.* (2018) 70:1042–8. doi: 10.1002/art.40475
19. Varkas G, de Hooge M, Renson T, De Mits S, Carron P, Jacques P, et al. Effect of mechanical stress on magnetic resonance imaging of the sacroiliac joints: assessment of military recruits by magnetic resonance imaging study. *Rheumatology.* (2018) 57:508–13. doi: 10.1093/rheumatology/kex491
20. Baraliakos X, Richter A, Feldmann D, Ott A, Buelow R, Schmidt CO, et al. Frequency of MRI changes suggestive of axial spondyloarthritis in the axial skeleton in a large population-based cohort of individuals aged <45 years. *Ann Rheum Dis.* (2020) 79:186–92. doi: 10.1136/annrheumdis-2019-215553
21. Weber U, Ostergaard M, Lambert RG, Pedersen SJ, Chan SM, Zubler V, et al. Candidate lesion-based criteria for defining a positive sacroiliac joint MRI in two cohorts of patients with axial spondyloarthritis. *Ann Rheum Dis.* (2015) 74:1976–82. doi: 10.1136/annrheumdis-2014-205408
22. Weber U, Lambert RG, Pedersen SJ, Hodler J, Ostergaard M, Maksymowych WP. Assessment of structural lesions in sacroiliac joints enhances diagnostic utility of magnetic resonance imaging in early spondylarthritis. *Arthritis Care Res.* (2010) 62:1763–71. doi: 10.1002/acr.20312
23. Larsen E, Wilken-Jensen C, Hansen A, Jensen D, Johansen S, Minck H, et al. Symptom-giving pelvic girdle relaxation in pregnancy - part I: prevalence and risk factors. *Acta Obstet Gynecol Scand.* (1999) 78:105–10. doi: 10.1034/j.1600-0412.1999.780206.x
24. Renson T, Depicker A, De Craemer AS, Deroo L, Varkas G, de Hooge M, et al. High prevalence of spondyloarthritis-like MRI lesions in postpartum women: a prospective analysis in relation to maternal, child and birth characteristics. *Ann Rheum Dis.* (2020) 79:929–34. doi: 10.1136/annrheumdis-2020-217095
25. Agten CA, Zubler V, Zanetti M, Binkert CA, Kolokythas O, Prentl E, et al. Postpartum bone marrow edema at the sacroiliac joints may mimic sacroiliitis of axial spondyloarthritis on MRI. *AJR Am J Roentgenol.* (2018) 211:1306–12. doi: 10.2214/AJR.17.19404
26. Cicek H, Keskin HL, Tuhanioglu U, Kilicarslan K, Ogur HU. Simultaneous disruption of the pubic symphysis and sacroiliac joint during vaginal birth. *Case Rep Orthop.* (2015) 2015:812132. doi: 10.1155/2015/812132
27. Lambert RG, Bakker PA, van der Heijde D, Weber U, Rudwaleit M, Hermann KG, et al. Defining active sacroiliitis on MRI for classification of axial spondyloarthritis: update by the ASAS MRI working group. *Ann Rheum Dis.* (2016) 75:1958–63. doi: 10.1136/annrheumdis-2015-208642
28. Moustarhfir M, Bresson B, Koch P, Perozziello A, Barreau G, Schouman-Claeys E, et al. MR imaging of Schmorl's nodes: Imaging characteristics and epidemio-clinical relationships. *Diagn Interv Imaging.* (2016) 97:411–7. doi: 10.1016/j.diii.2016.02.001
29. Abbas J, Hamoud K, Peled N, Hershkovitz I. Lumbar schmorl's nodes and their correlation with spine configuration and degeneration. *Biomed Res Int.* (2018) 2018:1574020. doi: 10.1155/2018/1574020
30. He S, Zhong B, Zhu H, Fang W, Chen L, Guo J, et al. Percutaneous vertebroplasty for symptomatic schmorl's nodes: 11 cases with long-term follow-up and a literature review. *Pain Physician.* (2017) 20:69–76. doi: 10.36076/ppj/2017/75
31. Masala S, Pipitone V, Tomassini M, Massari F, Romagnoli A, Simonetti G. Percutaneous vertebroplasty in painful schmorl nodes. *Cardiovasc Intervent Radiol.* (2006) 29:97–101. doi: 10.1007/s00270-005-0153-6
32. Diehn FE, Maus T, Morris J, Carr C, Kotsenas A, Luetmer P, et al. Uncommon manifestations of intervertebral disk pathologic conditions. *Radiographics.* (2016) 36:801–23. doi: 10.1148/rg.2016150223
33. Chaturvedi A, Klionsky NB, Nadarajah U, Chaturvedi A, Meyers SP. Malformed vertebrae: a clinical and imaging review. *Insights Imaging.* (2018) 9:343–55. doi: 10.1007/s13244-018-0598-1
34. Rutherford E, Tarplett L, Davies E, Harley J, King L. Lumbar spine fusion and stabilization: hardware, techniques, and imaging appearances. *Radiographics.* (2007) 27:1737–49. doi: 10.1148/rg.276065205
35. Ghodasara N, Yi PH, Clark K, Fishman EK, Farshad M, Fritz J. Postoperative spinal CT: what the radiologist needs to know. *Radiographics.* (2019) 39:1840–61. doi: 10.1148/rg.2019190050
36. Tok Umay S, Korkmaz M. Frequency of anatomical variation of the sacroiliac joint in asymptomatic young adults and its relationship with sacroiliac joint degeneration. *Clin Anat.* (2020) 33:839–43. doi: 10.1002/ca.23539
37. Cihan OF, Karabulut M, Kilincoglu V, Yavuz N. The variations and degenerative changes of sacroiliac joints in asymptomatic adults. *Folia Morphol.* (2020) doi: 10.5603/FM.a2020.0032
38. El Rafei M, Badr S, Lefebvre G, Machuron F, Capon B, Flipo RM, et al. Sacroiliac joints: anatomical variations on MR images. *Eur Radiol.* (2018) 28:5328–37. doi: 10.1007/s00330-018-5540-x
39. Demir M, Mavi A, Gumusburun E, Bayram M, Gursoy S, Nishio H. Anatomical variations with joint space measurements on CT. *Kobe J Med Sci.* (2007) 53:209–17.
40. Postacchini R, Trasimeni G, Ripani F, Sessa P, Perotti S, Postacchini F. Morphometric anatomical and CT study of the human adult sacroiliac region. *Surg Radiol Anat.* (2017) 39:85–94. doi: 10.1007/s00276-016-1703-0
41. Benz RM, Daikeler T, Mameghani AT, Tamborrini G, Studler U. Synostosis of the sacroiliac joint as a developmental variant, or ankylosis due to sacroiliitis? *Arthritis Rheumatol.* (2014) 66:2367. doi: 10.1002/art.38691
42. Jagannathan D, Indiran V, Hithaya F, Alamelu M, Padmanaban S. Role of anatomical landmarks in identifying normal and transitional vertebra in lumbar spine magnetic resonance imaging. *Asian Spine J.* (2017) 11:365–79. doi: 10.4184/asj.2017.11.3.365
43. Shaikh A, Khan SA, Hussain M, Soomro S, Adel H, Adil SO, et al. Prevalence of Lumbosacral Transitional Vertebra In Individuals With Low Back Pain: Evaluation Using Plain Radiography And Magnetic Resonance Imaging. *Asian Spine J.* (2017) 11:892–7. doi: 10.4184/asj.2017.11.6.892
44. Tins BJ, Balain B. Incidence of numerical variants and transitional lumbosacral vertebrae on whole-spine MRI. *Insights Imaging.* (2016) 7:199–203. doi: 10.1007/s13244-016-0468-7
45. Ravikanth R, Majumdar P. Bertolotti's syndrome in low-backache population: Classification and imaging findings. *Ci Ji Yi Xue Za Zhi.* (2019) 31:90–5. doi: 10.4103/tcmj.tcmj_209_17
46. Adams R, Herrera-Nicol S, Jenkins AL, 3rd. Surgical treatment of a rare presentation of bertolotti's syndrome from castellvi type IV lumbosacral transitional vertebra: case report and review of the literature. *J Neurol Surg Rep*. (2018) 79:e70–4. doi: 10.1055/s-0038-1667172
47. Alonzo F, Cobar A, Cahueque M, Prieto JA. Bertolotti's syndrome: an underdiagnosed cause for lower back pain. *J Surg Case Rep.* (2018) 2018:rjy276. doi: 10.1093/jscr/rjy276
48. Vergauwen S, Parizel P, Breusegem L, Goethem J, Nackaerts Y, Hauwe L, et al. Distribution and incidence of degenerative spine changes in patients with a lumbo-sacral transitional vertebra. *Eur Spine J.* (1997) 6:168–72. doi: 10.1007/BF01301431
49. Kurt EE, Turkyilmaz AK, Dadali Y, Erdem HR, Tuncay F. Are transitional vertebra and spina bifida occulta related with lumbar disc herniation and clinical parameters in young patients with chronic low back pain? *Eurasian J Med.* (2016) 48:177–80. doi: 10.5152/eurasianjmed.2016.0285
50. Castellvi AE, Goldstein LA, Chan DP. Lumbosacral transitional vertebrae and their relationship with lumbar extradural defects. *Spine.* (1984) 9:493–5. doi: 10.1097/00007632-198407000-00014
51. Milieie C, Krolo I, Anticevic D, Roic G, Zadravec D, Bojic D, et al. Causal connection of non-specific low back pain and disc degeneration in children

with transitional vertebra and/or spina bifida occulta: role of magnetic resonance – prospective study. *Coll Antropol.* (2012) 36:627–33.
52. Manenti G, Iundusi R, Picchi E, Marsico S, D'Onofrio A, Rossi G, et al. Anatomical variation: T1 spina bifida occulta. Radiological findings. *Radiol Case Rep.* (2017) 12:207–9. doi: 10.1016/j.radcr.2016.11.003
53. Urrutia J, Cuellar J, Zamora T. Spondylolysis and spina bifida occulta in pediatric patients: prevalence study using computed tomography as a screening method. *Eur Spine J.* (2016) 25:590–5. doi: 10.1007/s00586-014-3480-y
54. Byun WM, Kim JW, Lee JK. Differentiation between symptomatic and asymptomatic extraforaminal stenosis in lumbosacral transitional vertebra: role of three-dimensional magnetic resonance lumbosacral radiculography. *Korean J Radiol.* (2012) 13:403–11. doi: 10.3348/kjr.2012.13.4.403
55. Monu J, Crotty J, Pope T. Intraosseous pneumatocyst of the iliac bone. *Clin Orthop Relat Res.* (1996) 330:190–2. doi: 10.1097/00003086-199609000-00024
56. Catalano O. Intraosseous pneumatocyst of the ilium: CT findings in two cases and literature review. *Eur Radiol.* (1997) 7:1449–51 doi: 10.1007/s003300050315
57. Al-Tarawneh E, Al-Qudah M, Hadidi F, Jubouri S, Hadidy A. Incidental intraosseous pneumatocyst with gas-density-fluid level in an adolescent: a case report and review of the literature. *J Radiol Case Rep.* (2014) 8:16–22. doi: 10.3941/jrcr.v8i3.1540
58. Cosar M, Eser O, Aslan A, Kormaz S, Boyaci G, Degirmenchi B, et al. Vertebral body pneumatocyst in the cervical spine and review of the literature. *Turkish Neurosurgery.* (2008) 18:197– 9.
59. Bekmez S, Ayvaz M, Mermerkaya MU, Tokgozoglu M. Iliac bone cysts adjacent to the sacroiliac joint: an unusual cause of sacroiliac pain. *Acta Orthop Traumatol Turc.* (2014) 48:495–9. doi: 10.3944/AOTT.2014.14.0039
60. Hughes RJ, Harish S, Saifuddin A, O'Donnell P. On the AJR digital viewbox. Large synovial cyst arising from the sacroiliac joint. *AJR Am J Roentgenol.* (2006) 187:W137. doi: 10.2214/AJR.05.0842
61. Strully K. Lumbar and sacral cysts of meningeal origin. *Radiology.* (1994) 62:544–9. doi: 10.1148/62.4.544
62. Murphy K, Oaklander AL, Elias G, Kathuria S, Long DM. Treatment of 213 patients with symptomatic tarlov cysts by CT-guided percutaneous injection of fibrin sealant. *AJNR Am J Neuroradiol.* (2016) 37:373–9. doi: 10.3174/ajnr.A4517
63. Boukobza M, Roussel A, Fernandez-Rodriguez P, Laissy JP. Giant multiple and bilateral presacral tarlov cysts mimicking adnexal mass - imaging features. *Int Med Case Rep J.* (2018) 11:181–4. doi: 10.2147/IMCRJ.S147791
64. Gossner J. High prevalence of cervical perineural cysts on cervical spine MRI-case series. *Int J Anat Var.* (2018) 11:18–9. Available online at: https://www.pulsus.com/scholarly-articles/high-prevalence-of-cervical-perineural-cysts-on-cervical-spine-mricase-series-4271.html
65. Rafiq MK. A cyst in the sacrum. *BMJ Case Rep.* (2009) 2009. doi: 10.1136/bcr.11.2008.1285
66. Diel J, Ortiz O, Losada RA, Price DB, Hayt MW, Katz DS. The sacrum: pathologic spectrum, multimodality imaging, and subspecialty approach. *Radiographics.* (2001) 21:83–104. doi: 10.1148/radiographics.21.1.g01ja0883
67. Quattrocchi CC, Giona A, Di Martino A, Gaudino F, Mallio CA, Errante Y, et al. Lumbar subcutaneous edema and degenerative spinal disease in patients with low back pain: a retrospective MRI study. *Musculoskelet Surg.* (2015) 99:159–63. doi: 10.1007/s12306-015-0355-2
68. Baraliakos X, Hermann KG, Braun J. Imaging in axial spondyloarthritis: diagnostic problems and pitfalls. *Rheum Dis Clin North Am.* (2012) 38:513–22. doi: 10.1016/j.rdc.2012.08.011
69. Kushchayev SV, Glushko T, Jarraya M, Schuleri KH, Preul MC, Brooks ML, et al. ABCs of the degenerative spine. *Insights Imaging.* (2018) 9:253–74. doi: 10.1007/s13244-017-0584-z
70. Song Q, Liu X, Chen DJ, Lai Q, Tang B, Zhang B, et al. Evaluation of MRI and CT parameters to analyze the correlation between disc and facet joint degeneration in the lumbar three-joint complex. *Medicine.* (2019) 98:e17336. doi: 10.1097/MD.0000000000017336
71. Damborg F, Engell V, Nielsen J, Kyvik KO, Andersen MO, Thomsen K. Genetic epidemiology of Scheuermann's disease. *Acta Orthop.* (2011) 82:602–5. doi: 10.3109/17453674.2011.618919
72. Zaidman AM, Zaidman MN, Strokova EL, Korel AV, Kalashnikova EV, Rusova TV, et al. The mode of inheritance of Scheuermann's disease. *Biomed Res Int.* (2013) 2013:973716. doi: 10.1155/2013/973716
73. Heithoff KB, Gundry CR, Burton CV, Winter RB. Juvenile discogenic disease. *Spine.* (1994) 19:335–40. doi: 10.1097/00007632-199402000-00014
74. Cidem M, Capkin E, Karkucak M, Karaca A. *Osteitis condensans ilii* in differential diagnosis of patients with chronic low back pain: a review of the literature. *Mod Rheumatol.* (2012) 22:467–9. doi: 10.3109/s10165-011-0513-9
75. Ma L, Gao Z, Zhong Y, Meng Q. Osteitis condensans ilii may demonstrate bone marrow edema on sacroiliac joint magnetic resonance imaging. *Int J Rheum Dis.* (2018) 21:299–307. doi: 10.1111/1756-185X.13125
76. Poddubnyy D, Weineck H, Diekhoff T, Redeker I, Gobejishvili N, Llop M, et al. Clinical and imaging characteristics of *Osteitis condensans ilii* as compared with axial spondyloarthritis. *Rheumatology.* (2020) 59:3798–806. doi: 10.1093/rheumatology/keaa175
77. Slobodin G, Lidar M, Eshed I. Clinical and imaging mimickers of axial spondyloarthritis. *Semin Arthritis Rheum.* (2017) 47:361–8. doi: 10.1016/j.semarthrit.2017.05.009
78. Mader R, Verlaan JJ, Eshed I, Bruges-Armas J, Puttini PS, Atzeni F, et al. Diffuse idiopathic skeletal hyperostosis (DISH): where we are now and where to go next. *RMD Open.* (2017) 3:e000472. doi: 10.1136/rmdopen-2017-000472
79. Toyoda H, Terai H, Yamada K, Suzuki A, Dohzono S, Matsumoto T, et al. Prevalence of diffuse idiopathic skeletal hyperostosis in patients with spinal disorders. *Asian Spine J.* (2017) 11:63–70. doi: 10.4184/asj.2017.11.1.63
80. Olivieri I, D'Angelo S, Palazzi C, Padula A, Mader R, Khan M. Diffuse idiopathic skeletal hyperostosis: differentiation from ankylosing spondylitis. *Curr Rheumatol Rep.* (2009) 11:321–8. doi: 10.1007/s11926-009-0046-9
81. Diederichs G, Engelken F, Marshall LM, Peters K, Black DM, Issever AS, et al. Diffuse idiopathic skeletal hyperostosis (DISH): relation to vertebral fractures and bone density. *Osteoporos Int.* (2011) 22:1789–97. doi: 10.1007/s00198-010-1409-9
82. Panwar J, Mathew AJ, Jindal N, Danda D. Utility of plain radiographs in metabolic bone disease - a case-based pictorial review from a tertiary centre. *Pol J Radiol.* (2017) 82:333–44. doi: 10.12659/PJR.901601
83. Mader R, Baraliakos X, Eshed I, Novofastovski I, Bieber A, Verlaan JJ, et al. Imaging of diffuse idiopathic skeletal hyperostosis (DISH). *RMD Open.* (2020) 6:e001151. doi: 10.1136/rmdopen-2019-001151
84. Kim BS, Moon MS, Yoon MG, Kim ST, Kim SJ, Kim MS, et al. Prevalence of diffuse idiopathic skeletal hyperostosis diagnosed by whole spine computed tomography: a preliminary study. *Clin Orthop Surg.* (2018) 10:41–6. doi: 10.4055/cios.2018.10.1.41
85. Hiyama A, Katoh H, Sakai D, Sato M, Tanaka M, Watanabe M. Prevalence of diffuse idiopathic skeletal hyperostosis (DISH) assessed with whole-spine computed tomography in 1479 subjects. *BMC Musculoskelet Disord.* (2018) 19:178. doi: 10.1186/s12891-018-2108-5
86. Campbell SE, Fajardo RS. Imaging of stress injuries of the pelvis. *Semin Musculoskelet Radiol.* (2008) 12:62–71. doi: 10.1055/s-2008-1067938
87. Micheli LJ, Curtis C. Stress fractures in the spine and sacrum. *Clin Sports Med.* (2006) 25:75–88, ix. doi: 10.1016/j.csm.2005.08.001
88. Urits I, Orhurhu V, Callan J, Maganty NV, Pousti S, Simopoulos T, et al. Sacral insufficiency fractures: a review of risk factors, clinical presentation, and management. *Curr Pain Headache Rep.* (2020) 24:10. doi: 10.1007/s11916-020-0848-z
89. Kinoshita H, Miyakoshi N, Kobayashi T, Abe T, Kikuchi K, Shimada Y. Comparison of patients with diagnosed and suspected sacral insufficiency fractures. *J Orthop Sci.* (2019) 24:702–7. doi: 10.1016/j.jos.2018.12.004
90. Cho CH, Mathis JM, Ortiz O. Sacral fractures and sacroplasty. *Neuroimaging Clin N Am.* (2010) 20:179–86. doi: 10.1016/j.nic.2010.02.004
91. Murthy NS. Imaging of stress fractures of the spine. *Radiol Clin North Am.* (2012) 50:799–821. doi: 10.1016/j.rcl.2012.04.009
92. Hollenberg GM, Beattie PF, Meyers SP, Weinberg EP, Adams MJ. Stress reactions of the lumbar pars interarticularis. *Spine.* (2002) 27:181–6. doi: 10.1097/00007632-200201150-00012
93. Kiel J, Kaiser K. *Stress Reaction and Fractures*. Bethesda, MD: StatPearls Publishing (2020)

94. Nusselt T, Klinger H, Schultz W, Baums M. Fatigue stress fractures of the pelvis: a rare cause of low back pain in female athletes. *Acta Orthop Belg.* (2010) 76:838–43.
95. Rotem G, Herman A, Lidar M, Eshed I. Post-traumatic arthritis of the sacroiliac joints mimicking inflammatory sacroiliitis: analysis of consecutive computed tomography examinations. *Clin Radiol.* (2020) 75:433–40. doi: 10.1016/j.crad.2020.01.004
96. Habib N, Filardo G, Delcogliano M, Arigoni M, Candrian C. An algorithm to avoid missed open-book pelvic fractures. *Eur Rev Med Pharmacol Sci.* (2018) 22:2973–7. doi: 10.26355/eurrev_201805_15052
97. Tonne B, Kempton L, Lack W, Karunakar M. Posterior iliac offset: description of a new radiological measurement of sacroiliac joint instability. *Bone Joint J.* (2014) 96:1535–9. doi: 10.1302/0301-620X.96B11.33633
98. Yoo SJ, Lee S, Ryu JA. Differential imaging features of widening and pseudo-widening of the sacroiliac joints. *Arthritis Rheumatol.* (2018) 70:755. doi: 10.1002/art.40440
99. Wang Y, Gao D, Ji X, Zhang J, Wang X, Jin J, et al. When brucellosis met the assessment of spondyloarthritis international society classification criteria for spondyloarthritis: a comparative study. *Clin Rheumatol.* (2019) 38:1873–80. doi: 10.1007/s10067-019-04481-w
100. Hermet M, Minichiello E, Flipo R, Dubost J, Allanore Y, Ziza J, et al. Infectious sacroiliitis: a retrospective, multicentre study of 39 adults. *BMC Infect Dis.* (2012) 12:305. doi: 10.1186/1471-2334-12-305
101. Mavrogenis AF, Megaloikonomos PD, Igoumenou VG, Panagopoulos GN, Giannitsioti E, Papadopoulos A, et al. Spondylodiscitis revisited. *EFORT Open Rev.* (2017) 2:447–61. doi: 10.1302/2058-5241.2.160062
102. Dunbar JA, Sandoe JA, Rao AS, Crimmins DW, Baig W, Rankine JJ. The MRI appearances of early vertebral osteomyelitis and discitis. *Clin Radiol.* (2010) 65:974–81. doi: 10.1016/j.crad.2010.03.015
103. Laur O, Mandell JC, Titelbaum DS, Cho C, Smith SE, Khurana B. Acute nontraumatic back pain: infections and mimics. *Radiographics.* (2019) 39:287–8. doi: 10.1148/rg.2019180077
104. Raghavan M, Lazzeri E, Palestro CJ. Imaging of spondylodiscitis. *Semin Nucl Med.* (2018) 48:131–47. doi: 10.1053/j.semnuclmed.2017.11.001
105. Babic M, Simpfendorfer CS. Infections of the Spine. *Infect Dis Clin North Am.* (2017) 31:279–97. doi: 10.1016/j.idc.2017.01.003
106. Tali ET, Oner AY, Koc AM. Pyogenic spinal infections. *Neuroimaging Clin N Am.* (2015) 25:193–208. doi: 10.1016/j.nic.2015.01.003
107. Diehn FE. Imaging of spine infection. *Radiol Clin North Am.* (2012) 50:777–98. doi: 10.1016/j.rcl.2012.04.001
108. Ye C, Shen GF, Li SX, Dong LL, Yu YK, Tu W, et al. Human brucellosis mimicking axial spondyloarthritis: a challenge for rheumatologists when applying the 2009 ASAS criteria. *J Huazhong Univ Sci Technolog Med Sci.* (2016) 36:368–71. doi: 10.1007/s11596-016-1593-8
109. Garip Y, Eser F, Erten S, Yilmaz O, Yildirim P. Brucellosis in spondyloarthritis mimicking an exacerbation. *Acta Reumatol Port.* (2014) 39:351–2.
110. Caldera G, Cahueque Lemus MA. Fungal spondylodiscitis: review. *J Spine.* (2016) 5:1–6. doi: 10.4172/2165-7939.1000302
111. Ali A, Musbahi O, White VLC, Montgomery AS. Spinal tuberculosis: a literature review. *JBJS Rev.* (2019) 7:e9. doi: 10.2106/JBJS.RVW.18.00035
112. Afonso P, Almeida A. Espondilodiscite tuberculosa - aspectos imagiológicos. *Acta Med Port.* (2011) 24:349–54. Available online at: https://www.actamedicaportuguesa.com/revista/index.php/amp/article/viewFile/1611/1194
113. Figueiredo ASB, Oliveira AL, Caetano A, Moraes-Fontes MF. SAPHO: has the time come for tailored therapy? *Clin Rheumatol.* (2020) 39:177–87. doi: 10.1007/s10067-019-04675-2
114. Jurik AG, Klicman RF, Simoni P, Robinson P, Teh J. SAPHO and CRMO: the value of imaging. *Semin Musculoskelet Radiol.* (2018) 22:207–24. doi: 10.1055/s-0038-1639469
115. Zhao Y, Ferguson PJ. Chronic nonbacterial osteomyelitis and chronic recurrent multifocal osteomyelitis in children. *Pediatr Clin North Am.* (2018) 65:783–800. doi: 10.1016/j.pcl.2018.04.003
116. Andronikou S, Mendes da Costa T, Hussien M, Ramanan AV. Radiological diagnosis of chronic recurrent multifocal osteomyelitis using whole-body MRI-based lesion distribution patterns. *Clin Radiol.* (2019) 74:737.e3–15. doi: 10.1016/j.crad.2019.02.021
117. Sato TS, Watal P, Ferguson PJ. Imaging mimics of chronic recurrent multifocal osteomyelitis: avoiding pitfalls in a diagnosis of exclusion. *Pediatr Radiol.* (2020) 50:124–36. doi: 10.1007/s00247-019-04510-5
118. Kajitani TR, Silva RV, Bonfa E, Pereira RM. Hypoparathyroidism mimicking ankylosing spondylitis and myopathy: a case report. *Clinics.* (2011) 66:1287–90. doi: 10.1590/S1807-59322011000700028
119. Memetoglu O, Ozkan F, Taraktas A, Aktas I, Nazikoglu C. Idiopathic hypoparathyroidism mimicking ankylosing spondylitis: a case report. *Acta Reumatol Port.* (2016) 41:82–5.
120. Goswami R, Ray D, Sharma R, Tomar N, Gupta R, Gupta N, et al. Presence of spondyloarthropathy and its clinical profile in patients with hypoparathyroidism. *Clin Endocrinol.* (2008) 68:258–63. doi: 10.1111/j.1365-2265.2007.03032.x
121. Chang C, Rosenthal D, Mitchell D, Handa A, Kattapuram S, Huang A. Imaging findings of metabolic bone disease. *Radiographics.* (2016) 36:1871–87. doi: 10.1148/rg.2016160004
122. Patel CN, Scarsbrook AF. Multimodality imaging in hyperparathyroidism. *Postgrad Med J.* (2009) 85:597–605. doi: 10.1136/pgmj.2008.077842
123. Tezcan ME, Temizkan S, Ozal ST, Gul D, Aydin K, Ozderya A, et al. Evaluation of acute and chronic MRI features of sacroiliitis in asymptomatic primary hyperparathyroid patients. *Clin Rheumatol.* (2016) 35:2777–82. doi: 10.1007/s10067-016-3172-6
124. Lalam RK, Cassar-Pullicino VN, Winn N. Paget disease of bone. *Semin Musculoskelet Radiol.* (2016) 20:287–99. doi: 10.1055/s-0036-1592368
125. Smith S, Murphey MD, Motamedi K, Mulligan ME, Resnik CS, Gannon FH. From the archives of the AFIP - radiologic spectrum of paget disease of bone and its complications with pathologic correlation. *Radiographics.* (2002) 22:1191–216. doi: 10.1148/radiographics.22.5.g02se281191
126. Theodorou DJ, Theodorou SJ, Kakitsubata Y. Imaging of paget disease of bone and its musculoskeletal complications: self-assessment module. *AJR Am J Roentgenol.* (2011) 196 (6 Suppl):WS53–6. doi: 10.2214/AJR.10.7303
127. Cortis K, Micallef K, Mizzi A. Imaging paget's disease of bone–from head to toe. *Clin Radiol.* (2011) 66:662–72. doi: 10.1016/j.crad.2010.12.016
128. de Mello FM, Helito PV, Bordalo-Rodrigues M, Fuller R, Halpern AS. Axial gout is frequently associated with the presence of current tophi, although not with spinal symptoms. *Spine.* (2014) 39:E1531–6. doi: 10.1097/BRS.0000000000000633
129. Chen W, Wang Y, Li Y, Zhao Z, Feng L, Zhu J, et al. Gout mimicking spondyloarthritis: case report and literature review. *J Pain Res.* (2017) 10:1511–4. doi: 10.2147/JPR.S133572
130. Namas R, Hegazin SB, Memisoglu E, Joshi A. Lower back pain as a manifestation of acute gouty sacroiliitis: utilization of dual-energy computed tomography (DECT) in establishing a diagnosis. *Eur J Rheumatol.* (2019) 6:216–8. doi: 10.5152/eurjrheum.2019.18097
131. Moshrif A, Laredo JD, Bassiouni H, Abdelkareem M, Richette P, Rigon MR, et al. Spinal involvement with calcium pyrophosphate deposition disease in an academic rheumatology center: a series of 37 patients. *Semin Arthritis Rheum.* (2019) 48:1113–26. doi: 10.1016/j.semarthrit.2018.10.009
132. Kakitsubata Y, Boutin R, Theodorou D, Kerr R, Steinbach L, Chan K, et al. Calcium pyrophosphate dihydrate crystal deposition in and around the atlantoaxial joint: association with type 2 odontoid fractures in nine patients. *Radiology.* (2000) 216:213–9. doi: 10.1148/radiology.216.1.r00jl36213
133. Chang E, Lim W, Wolfson T, Gamst A, Chung C, Bae W, et al. Frequency of atlantoaxial calcium pyrophosphate dihydrate deposition at CT. *Radiology.* (2013) 269:519–24. doi: 10.1148/radiol.13130125
134. Oka A, Okazaki K, Takeno A, Kumanomido S, Kusunoki R, Sato S, et al. Crowned dens syndrome: report of three cases and a review of the literature. *J Emerg Med.* (2015) 49:e9–13. doi: 10.1016/j.jemermed.2015.02.005
135. Scutellari PN, Galeotti R, Leprotti S, Ridolfi M, Franciosi R, Antinolfi G. The crowned dens syndrome. Evaluation with CT imaging. *Radiol Med.* (2007) 112:195–207. doi: 10.1007/s11547-007-0135-7
136. Resnick D, Pineda C. Vertebral involvement in calcium pyrophosphate dihydrate crystal deposition disease. *Radiology.* (1984) 153:55–60. doi: 10.1148/radiology.153.1.6089266
137. Grünberg K. *Benign and Malignant Bone Tumors: Radiological Diagnosis and Imaging Features* (2013). Erlangen: Siemens Healthcare GmbH.

138. Girish G, Finlay K, Morag Y, Brandon C, Jacobson J, Jamadar D. Imaging review of skeletal tumors of the pelvis–part I: benign tumors of the pelvis. *ScientificWorldJournal.* (2012) 2012:290930. doi: 10.1100/2012/290930
139. Rodallec M, Feydy A, Larousserie F, Anract P, Campagna R, Babinet A, et al. Diagnostic imaging of solitary tumors of the spine: what to do and say. *Radiographics.* (2008) 28:1019–41. doi: 10.1148/rg.284075156
140. El Kharboutly A, El Deep D. Role of MRI in the diagnosis of bone marrow infiltrative lesions. *Tanta Med J.* (2016) 44:64–75. doi: 10.4103/1110-1415.189346
141. Long SS, Yablon CM, Eisenberg RL. Bone marrow signal alteration in the spine and sacrum. *AJR Am J Roentgenol.* (2010) 195:W178–200. doi: 10.2214/AJR.09.4134
142. Keraliya AR, Krajewski KM, Jagannathan JP, Shinagare AB, Braschi-Amirfarzan M, Tirumani SH, et al. Multimodality imaging of osseous involvement in haematological malignancies. *Br J Radiol.* (2016) 89:20150980. doi: 10.1259/bjr.20150980
143. Hwang S, Panicek DM. Magnetic resonance imaging of bone marrow in oncology, Part 2. *Skeletal Radiol.* (2007) 36:1017–27. doi: 10.1007/s00256-007-0308-4
144. Moore SG, Gooding CA, Brasch RC, Ehman RL, Ringertz HG, Ablin AR, et al. Bone marrow in children with acute lymphocytic leukemia: MR relaxation times. *Radiology.* (1986) 160:237–40. doi: 10.1148/radiology.160.1.3459212
145. Healy CF, Murray JG, Eustace SJ, Madewell J, O'Gorman PJ, O'Sullivan P. Multiple myeloma: a review of imaging features and radiological techniques. *Bone Marrow Res.* (2011) 2011:583439. doi: 10.1155/2011/583439
146. Silva JR, Jr., Hayashi D, Yonenaga T, Fukuda K, Genant HK, et al. MRI of bone marrow abnormalities in hematological malignancies. *Diagn Interv Radiol.* (2013) 19:393–9. doi: 10.5152/dir.2013.067
147. Dutoit JC, Verstraete KL. MRI in multiple myeloma: a pictorial review of diagnostic and post-treatment findings. *Insights Imaging.* (2016) 7:553–69. doi: 10.1007/s13244-016-0492-7
148. Ormond Filho AG, Carneiro BC, Pastore D, Silva IP, Yamashita SR, Consolo FD, et al. Whole-body imaging of multiple myeloma: diagnostic criteria. *Radiographics.* (2019) 39:1077–97. doi: 10.1148/rg.2019180096
149. Kocaoglu M, Frush DP. Pediatric presacral masses. *Radiographics.* (2006) 26:833–57. doi: 10.1148/rg.263055102
150. Lee D, Dahdaleh NS. Charcot spinal arthropathy. *J Craniovertebr Junction Spine.* (2018) 9:9–19. doi: 10.4103/jcvjs.JCVJS_130_17
151. Elgafy H, Tranovich M, Elsamaloty L. Charcot spine neuroarthropathy and hip heterotopic ossification. *Spine J.* (2016) 16:e443–4. doi: 10.1016/j.spinee.2016.01.001
152. Staudt MD, Bailey CS, Siddiqi F. Charcot spinal arthropathy in patients with congenital insensitivity to pain: a report of two cases and review of the literature. *Neurosurg Rev.* (2018) 41:899–908. doi: 10.1007/s10143-017-0814-3
153. Solinsky R, Donovan JM, Kirshblum SC. Charcot Spine following chronic spinal cord injury: an analysis of 201 published cases. *Spinal Cord.* (2019) 57:85–90. doi: 10.1038/s41393-018-0216-6
154. Ihde LL, Forrester DM, Gottsegen CF, Masih S, Patel DB, Vachon LA, et al. Sclerosing bone dysplasias: review and differentiation from other causes of osteosclerosis. *Radiographics.* (2011) 31:1865–82. doi: 10.1148/rg.317115093
155. Boulet C, Madani H, Lenchik L, Vanhoenacker F, Amalnath DS, de Mey J, et al. Sclerosing bone dysplasias: genetic, clinical and radiology update of hereditary and non-hereditary disorders. *Br J Radiol.* (2016) 89:20150349. doi: 10.1259/bjr.20150349
156. Kocyigit H, Turan Y, Bayram K, Gurgan A, Deveci H, Guvenc A. Coexistence of behçet's disease and ankylosing spondylitis: a case report. *Turkish J Rheumatol.* (2010) 25:217–20. doi: 10.5152/tjr.2010.32
157. Bicer A. Musculoskeletal findings in behcet's disease. *Patholog Res Int.* (2012) 2012:653806. doi: 10.1155/2012/653806
158. Canella C, Costa F, Bacchiega AB, Marchiori E. Sacroiliitis in behcet syndrome. *J Clin Rheumatol.* (2013) 19:356. doi: 10.1097/RHU.0b013e3182a2a048
159. Cobankara V. SAT0292 Clinical, imaging and laboratory variables fail to predict morphological vascular progression in takayasu arteritis. *Ann Rheum Dis.* (2014) 73 (Suppl 2):698.4-9. doi: 10.1136/annrheumdis-2014-eular.5598
160. Kim SH, Eoh W. Progressive atlanto-axial subluxation in Behcet's disease. *Skeletal Radiol.* (2010) 39:295–7. doi: 10.1007/s00256-009-0815-6
161. Ejindu V, Hine A, Mashayekhi M, Shorvon P, Misra R. Musculoskeletal manifestations of sickle cell disease. *Radiographics.* (2007) 27:1005–22. doi: 10.1148/rg.274065142
162. Ganguly A, Boswell W, Aniq H. Musculoskeletal manifestations of sickle cell anaemia: a pictorial review. *Anemia.* (2011) 2011:794283. doi: 10.1155/2011/794283
163. Kosaraju V, Harwani A, Partovi S, Bhojwani N, Garg V, Ayyappan S, et al. Imaging of musculoskeletal manifestations in sickle cell disease patients. *Br J Radiol.* (2017) 90:20160130. doi: 10.1259/bjr.20160130

Disclaimer: The views expressed are those of the authors and not necessarily those of the National Institutes of Health (NIH), (UK) National Health Service (NHS), the NIHR, or the (UK) Department of Health.

Conflict of Interest: PM has received consulting/speaker's fees from AbbVie, BMS, Celgene, Eli Lilly, Janssen, MSD, Novartis, Pfizer, Roche, and UCB all unrelated to this manuscript.

The remaining authors declare that the research was conducted in the absence of any commercial or financial relationships that could be construed as a potential conflict of interest.

Advantages of publishing in Frontiers

OPEN ACCESS
Articles are free to read for greatest visibility and readership

FAST PUBLICATION
Around 90 days from submission to decision

HIGH QUALITY PEER-REVIEW
Rigorous, collaborative, and constructive peer-review

TRANSPARENT PEER-REVIEW
Editors and reviewers acknowledged by name on published articles

Frontiers
Avenue du Tribunal-Fédéral 34
1005 Lausanne | Switzerland

Visit us: www.frontiersin.org
Contact us: frontiersin.org/about/contact

REPRODUCIBILITY OF RESEARCH
Support open data and methods to enhance research reproducibility

DIGITAL PUBLISHING
Articles designed for optimal readership across devices

FOLLOW US
@frontiersin

IMPACT METRICS
Advanced article metrics track visibility across digital media

EXTENSIVE PROMOTION
Marketing and promotion of impactful research

LOOP RESEARCH NETWORK
Our network increases your article's readership